Mariana Resener
Steffen Rebennack
Panos M. Pardalos
Sérgio Haffner   *Editors*

# Handbook of Optimization in Electric Power Distribution Systems

Springer

# Energy Systems

**Series editor**
Panos M. Pardalos, Gainesville, USA

More information about this series at http://www.springer.com/series/8368

Mariana Resener • Steffen Rebennack •
Panos M. Pardalos • Sérgio Haffner

Editors

# Handbook of Optimization in Electric Power Distribution Systems

Springer

*Editors*
Mariana Resener (iD)
Department of Electrical Systems
of Automation and Energy
Universidade Federal do Rio Grande do Sul
Porto Alegre, RS, Brazil

Steffen Rebennack (iD)
Institute for Operations Research (IOR)
Stochastic Optimization (SOP)
Karlsruhe Institute of Technology
Karlsruhe, Germany

Panos M. Pardalos (iD)
Department of Industrial
& Systems Engineering
University of Florida
Gainesville, FL, USA

Sérgio Haffner (iD)
Department of Electrical Systems
of Automation and Energy
Universidade Federal do Rio Grande do Sul
Porto Alegre, RS, Brazil

# Preface

In the recent years, the distribution systems from the substations to the customers are facing significant changes, due to the growing number of distributed and variable energy generation resources and the smart grid implementation. The distribution networks were originally designed to deliver electricity through distribution feeders and radial lines, applying traditional planning techniques, generally sufficient to offer a reliable service at affordable costs. However, the need for greater resilience, power quality, and customer participation cannot be met by this design paradigm. The abilities to dynamically optimize the operation, integrate diverse distributed generation types, and integrate demand response and energy efficiency resources are also needed in this modern power system era. As a result, significant research efforts have been dedicated to the optimal expansion and operation planning of modern distribution networks.

The smart grid implementation brings a large amount of data that can be used to better plan an energy distribution system. The concept of smart grid is related to a grid with high integration of technology information, telecommunication, sensing/measurement, and automation, seeking to enhance the operation and the ability to meet scenarios with intermittent and distributed energy resources, high reliability requirements, low impact to the environment, and adequate to new energy market regulations. The growing energy demand and limited capital for investment are making the distribution system planners look to these advances in smart grid technology in order to identify new approaches to achieve load reliability. Although challenged by methodologies, paradigms, and traditional distribution planning techniques, this "smart" scenario can lead to alternatives that result in lower investment and operational costs.

The main goal when planning a distribution system is to timely meet the demand growth in the most economical, reliable, and safe way. The planning methodology must assure that every opportunity for savings or power quality improvement are exploited. This is not a straightforward task even in traditional systems, since the distribution networks are usually large in extension, with a large amount of data to be analyzed. In addition, new regulations from authorities and the modernization of

power systems highlight the importance of a constant update and improvement of methodologies and planning techniques.

The difficulty in solving energy distribution systems planning problems, including the operation and expansion planning, relies on the combinatorial nature and the large solution space. Several models and techniques are proposed in the literature, covering the allocation of new substations, reinforcement of the existing ones, reconductoring or construction of new distribution lines, distributed generation placement, among other problems. Usually, aspects of network reliability are later considered, allocating protection and automated devices.

Since investments in the improvement of the distribution system are a constant need, the development of investment plans is a routine for power utilities. In this context, the development of models, solution techniques, and computational tools to solve power distribution systems planning problems is of great importance for power utilities. Extensive research have been made over the last decades, handling problems related to the expansion and operation planning of distribution systems. This handbook gathers the state-of-the-art research on topics related to optimization problems in energy distribution systems, covering the classical problems and the challenges introduced by distributed generation and smart grid resources. Several application examples are presented and discussed, which help to understand the importance of optimization applied to power distribution systems.

We would like to thank all the authors for their contributions, the referees for their valuable and constructive reviews, and the publisher for helping to produce this handbook. Panos M. Pardalos also thanks the support from the Humboldt Research Award.

Porto Alegre, RS, Brazil                                           Mariana Resener
Karlsruhe, Germany                                              Steffen Rebennack
Gainesville, FL, USA                                              Panos M. Pardalos
Porto Alegre, RS, Brazil                                             Sérgio Haffner

# Contents

# Contributors

**Olatunji Matthew Adeyanju** Centre of Excellence in Energy and Power System (CEESP), Federal University of Santa Maria (UFSM), Santa Maria, Brazil

**Eduardo Nobuhiro Asada** Department of Electrical and Computer Engineering, São Carlos School of Engineering—EESC, University of São Paulo—USP, São Carlos, SP, Brazil

**Aldo Bischi** Skolkovo Institute of Science and Technology, Moscow, Russia

**Aggelos S. Bouhouras** Department of Electrical and Computer Engineering, University of Western Macedonia, Kozani, Greece

**Juan Camilo Castaño** Universidad Tecnologica de Pereira, Pereira, Risaralda, Colombia

**Luciane Neves Canha** Centre of Excellence in Energy and Power System (CEESP), Federal University of Santa Maria (UFSM), Santa Maria, Brazil

**Sridhar Chouhan** Smart Grid Solutions, Leidos Engineering, Hender-sonville, TN, USA

**Javier Contreras** Escuela Técnica Superior de Ingenieros Industriales, Universidad de Castilla-La Mancha, Ciudad Real, Spain

**Analiza Dalla Costa** Post-Graduate Program in Electrical Engineering, Federal University of Rio Grande do Sul (UFRGS), Porto Alegre, Brazil

**Luiz C. P. da Silva** Department of Systems and Energy, School of Electrical and Computer Engineering, University of Campinas, Campinas, Brazil

**Ali Feliachi** Lane Dept. of Computer Science and Electrical Engineering, West Virginia Univer-sity, Morgantown, WV, USA

**Alejandro Garcés** Universidad Tecnologica de Pereira, Pereira, Colombia

**Paschalis A. Gkaidatzis** School of Electrical and Computer Engineering, Aristotle University of Thessaloniki, Thessaloniki, Greece

**Alvaro González-Castellanos**   Skolkovo Institute of Science and Technology, Moscow, Russia

**Sérgio Haffner**   Department of Electrical Systems of Automation and Energy, Universidade Federal do Rio Grande do Sul, Porto Alegre, RS, Brazil

**Milad Kabirifar**   Sharif University of Technology, Tehran, Iran

**Irfan Khan**   Marine Engineering Technology Department, Texas A&M University at Galveston, Galveston, TX, USA

**Dimitris P. Labridis**   School of Electrical and Computer Engineering, Aristotle University of Thessaloniki, Thessaloniki, Greece

**Julio López**   Electrical Engineering School, University of Cuenca, Cuenca, Ecuador

**Juan Camilo López**   University of Campinas (UNICAMP), Campinas, São Paulo, Brazil

**Moein Moeini-Aghtaie**   Faculty of Energy Engineering Department, Sharif University of Technology, Tehran, Iran

**Mashood Nasir**   Department of Electrical Engineering at LUMS, Lahore, Pakisan

**Luís Alberto Pereira**   Department of Electrical Systems of Automation and Energy, Federal University of Rio Grande do Sul (UFRGS), Porto Alegre, Brazil

**Bibiana Maitê Petry Ferraz**   Post-Graduate Program in Electrical Engineering, Federal University of Rio Grande do Sul (UFRGS), Porto Alegre, Brazil

**Niloofar Pourghaderi**   Sharif University of Technology, Tehran, Iran

**David Pozo**   Skolkovo Institute of Science and Technology, Moscow, Russia

**Ali Rajaei**   Sharif University of Technology, Tehran, Iran

**Camilo Alberto Sepúlveda Rangel**   Centre of Excellence in Energy and Power System (CEESP), Federal University of Santa Maria (UFSM), Santa Maria, Brazil

**Mariana Resener**   Department of Electrical Systems of Automation and Energy, Universidade Federal do Rio Grande do Sul, Porto Alegre, RS, Brazil

**Marcos J. Rider**   Department of Systems and Energy, School of Electrical and Computer Engineering, University of Campinas,  Campinas, Brazil

**Miguel Angel Rios**   Universidad Tecnologica de Pereira, Pereira, Risaralda, Colombia

**Amir Safdarian**   Faculty of Electrical Engineering Department, Sharif University of Technology, Tehran, Iran

**Pedro P. Vergara**   Eindhoven University of Technology, Eindhoven, Netherlands

**José Carlos de Melo Vieira Jr.** Department of Electrical and Computer Engineering, São Carlos School of Engineering—EESC, University of São Paulo—USP, São Carlos, SP, Brazil

**Tiago Soares Vítor** Department of Electrical Engineering, Federal Institute of Education, Science and Technology of São Paulo—IFSP, São João da Boa Vista, SP, Brazil

**Affaq Qamar** U.S.-Pakistan Center for Advanced Studies in Energy, UET Peshawar Pakistan, Peshawar, Pakistan

# Optimal Volt/Var Control Applied to Modern Distribution Systems

**Tiago Soares Vítor, Eduardo Nobuhiro Asada,
and José Carlos de Melo Vieira Jr.**

**Abstract** The voltage regulation in distribution systems refers to the primary objective of maintaining customers' voltages within an acceptable range under all loading conditions. This function has been accomplished by the Volt/Var control— a strategy that coordinates voltage regulating devices and reactive power controls in order to reach a suitable operation of the system. As the modernization of the distribution grid has become a reality, new intelligent and updated schemes for Volt/Var control must be developed to face the recent operating scenario challenges and to make use of the technological advances in infrastructure. Under those circumstances, Volt/Var control has the task of achieving high quality power supply and, at the same time, meeting strict performance goals on the grid operation. To tackle these problems, intelligent systems are built providing a computational efficient optimization engine. In this context, this chapter presents the Volt/Var control, from basic concepts to advanced topics, laying the foundation for a complete optimization framework and introducing the Volt/Var optimization as a determinant tool to further enhance system operation objectives.

## List of Symbols

| | |
|---|---|
| $\Delta E\%$ $(\Delta V\%)$ | Percentage of energy (voltage) reduction |
| $\Delta P$ $(\Delta Q)$ | Active (reactive) power injection estimation errors |
| $\Delta P_{CL_l}$ | Energy allocated to CL $l$ |
| $\Delta t$ | Time interval |

T. S. Vítor (✉)
Department of Electrical Engineering, Federal Institute of Education, Science and Technology of
São Paulo—IFSP, São João da Boa Vista, SP, Brazil
e-mail: tiagosvitor@ifsp.edu.br

E. N. Asada · J. C. de Melo Vieira Jr.
Department of Electrical and Computer Engineering, São Carlos School of Engineering—EESC,
University of São Paulo—USP, São Carlos, SP, Brazil
e-mail: easada@usp.br; jcarlos@sc.usp.br

| | |
|---|---|
| $\Delta U_n$ | Maximum voltage deviation from the average line voltage $U_{avg_n}$ |
| $\Delta W_L, \Delta W_U$ | Lower and upper bounds of load energy which can be used by CL |
| $\Omega_{ES_i}^{max}$ | Power capability limit of ES $i$, MVA |
| $\Omega_T$ | Set of the three-phase nodes |
| $\theta_{ij}$ | Voltage angle difference between buses $i$ and $j$ |
| $\eta_i$ | Storage charge-discharge cycle efficiency at bus $i$ |
| $C_{OLTC}$ | Cost of OLTC tap operation in \$/tap |
| $C_{OLTC}^R$ | Cost of replacing the OLTC |
| $C_{P_{dg}}$ | Cost of active power generated by DG in \$/kWh |
| $C_{ShC}$ | Purchase cost per kvar rating of shunt capacitors |
| $CVR_f$ | Conservation voltage reduction factor |
| $E_i^1 \ (E_i^2)$ | Positive-sequence (negative-sequence) voltage of bus $i$ |
| $E_{ES_{i,t}}^{max} \ (E_{ES_{i,t}}^0)$ | Maximum (initial) energy stored in ES $i$ at time $t$ |
| $E_{ES_{i,t}}$ | Energy stored in ES $i$ at time $t$ |
| $E_{ES_i}^{min}, E_{ES_i}^{max}$ | Minimum and maximum capacity of ES $i$ |
| $f_{LVUR}$ | Total line voltage unbalance rate |
| $f_{TC}$ | Number of tap changes |
| $f_{DGC}$ | Amount of MW curtailed on DG units (or the related cost) |
| $f_L$ | Total active power losses |
| $f_{EL}$ | Total electrical energy losses |
| $f_{\Delta V}$ | Total voltage deviation |
| $f_{\Delta V_{daily}}$ | Total daily voltage deviation |
| $f_{ES}$ | Energy savings |
| $G_k$ | Conductance of branch $k$ |
| $I_k^t$ | Current value of branch $k$ during time $t$ |
| $\bar{I}$ | Demand current |
| $k_p \ (k_q)$ | Voltage exponent of active (reactive) load power |
| $LS_{OLTC}^R$ | Residual lifespan of the OLTC |
| $LS_{OLTC}^T$ | Total lifespan of the OLTC |
| $N_{br}$ | Number of branches |
| $N_t$ | Number of intervals |
| $N_{bus}$ | Number of buses |
| $N_d$ | Number of voltage control devices |
| $N_d^{max}$ | Maximum allowable daily operating times of the device $d$ |
| $N_{OLTC}^R$ | Number of tap operations remaining of the OLTC |
| $N_{OLTC}^T$ | Estimated total operation times of the OLTC |
| $P_{Loss}, E_{Loss}$ | Power losses and energy losses |
| $P_{L_i} \ (Q_{L_i})$ | Active (reactive) load power at bus $i$ |
| $P_{L_{n,i}} \ (Q_{L_{n,i}})$ | Active (reactive) load power at rated voltage and frequency at bus $i$ |
| $P_{system_{base}}$ | Kilowatt power flow results for the base case (no Volt/Var control) |

| | |
|---|---|
| $P_{system_i}$ | Kilowatt power flow results for the operation $i$ (with Volt/Var control) |
| $P_{gi}^0$ $(P_{gi})$ | Current available (curtailed) active power of DG unit $i$ |
| $P_n^{spec}$ $(P_n^{calc})$ | Specified (calculated) active power injection at node $n$ |
| $P_{DG_i}^{min}$, $P_{DG_i}^{max}$ | Minimum and maximum real power components of DG $i$ |
| $P_{DG_i}^t$ $(Q_{DG_i}^t)$ | Active (reactive) power component of DG $i$ at hour $t$ |
| $P_{EV_i}^t$ | Active power of EV $i$ at time $t$ |
| $P_{CL_l}$ $(Q_{CL_l})$ | Active (reactive) power of CL $l$ |
| $P_{CL_l}^{min}$, $P_{CL_l}^{max}$ | Lower and upper bounds of active power acceptable ranges of CL $l$ |
| $P_{EV_i}^{max}$ | Maximum charging limit of EV $i$ |
| $P_{ES_{i,t}}$ | Active power produced/absorbed by ES $i$ at time $t$ |
| $P_{ES_i}^{min}$, $P_{ES_i}^{max}$ | Minimum and maximum active power rating of ES $i$ |
| $PF_{DG_i}^{min}$, $PF_{DG_i}^{max}$ | Minimum and maximum allowable power factors of DG $i$ |
| $PF_{DG_i}^t$ | Current power factor of DG $i$ at hour $t$ |
| $PF_S^{min}$, $PF_S^{max}$ | Allowable power factors of the substation |
| $PF_S^t$ | Current power factor of the substation at hour $t$ |
| $Q_{EV_i}^t$ | Reactive power injection to the grid of EV $i$ at time $t$ |
| $Q_{EV_i}^{max}$ | Capacity of maximum inverter reactive power generation of EV $i$ |
| $Q_n^{spec}$ $(Q_n^{calc})$ | Specified (calculated) reactive power injection at node $n$ |
| $Q_{CL_l}^{min}$, $Q_{CL_l}^{max}$ | Lower and upper bounds of reactive power acceptable ranges of CL $l$ |
| $Q_{ES_{i,t}}$ | Reactive power produced/absorbed by ES $i$ at time $t$ |
| $R + jX$ | Feeder impedance |
| $R_k$ | Resistance value of branch $k$ |
| $S_{DG_i}^{max}$ | Apparent power of DG $i$ |
| $S_k^t$ | Complex power flowing over the branch $k$ at hour $t$ |
| $S_k^{max}$ | Maximum allowable complex power of branch $k$ |
| $S_{TX}^t$ | Apparent power flow on substation transformer at time $t$ |
| $S_{TX}^{rat}$ | Substation transformer rating |
| $ShC^p$ | Capacitor purchase cost |
| $ShC_{Lifetime}$ | Expected lifespan of shunt capacitors |
| $T_d^t$ | Tap position (or number of capacitor banks) of the device $d$ at time $t$ |
| $T_d^{min}$, $T_d^{max}$ | Tap position limits (or capacitor banks limits) for the device $d$ |
| $THD_v^i$ | Total harmonic distortion of voltage at bus $i$ |
| $THD_v^{max}$ | Maximum distortion allowed |
| $U_{2i}$, $U_2^{max}$ | Voltage unbalance factor of bus $i$ and maximum value of $U_{2i}$ |
| $U_{avg_n}$ | Average line voltage of the three phases at node $n$ |
| $\bar{V}_G$, $\bar{V}_L$ | Generator and load voltages |
| $V_i$, $V_n$ | Voltage magnitude at bus $i$ and nominal voltage of the system |
| $V_i^*$ | Desired voltage at bus $i$ |

| | |
|---|---|
| $V_n^t$ | Voltage of node $n$ at hour $t$ |
| $V_{min}, V_{max}$ | Acceptable voltage limits |
| $V_{EV_i}^t$ | Voltage of EV $i$ at time $t$ |
| $V_{EV_i}^{min}, V_{EV,i}^{max}$ | Minimum and maximum voltage values of EV $i$ |

## 1 Introduction

Volt/Var control is one of the most important functions in the operation of distribution systems. According to [50], a proper selection and coordination of equipment for controlling voltage and reactive power are major challenges faced by power system engineering. The main objective of Volt/Var control is to keep the steady state voltage in all buses of the system within acceptable limits. However, enhanced goals have been added to this role in order to improve the overall system efficiency and performance. As a result, many researchers have concentrated efforts to develop new intelligent and advanced schemes [107]. This renewing focus opens a wide range of possibilities for applications and improvement.

To illustrate, new paradigms have demanded updated Volt/Var control strategies to face new operating challenges, which include power electronic devices (EDs) and distributed energy resources (DERs) [22], and to make use of the technological advances such as advanced metering infrastructure (AMI) and distribution management system (DMS) [66].

Volt/Var control is a process that involves multiple voltage regulating devices working in collaboration to achieve certain objectives [88]. The conventional voltage devices are on-load tap changer (OLTC), step voltage regulators (SVRs) and switchable capacitors (SCs). Essentially, the success of the Volt/Var control depends on the proper coordination among them. An enhanced strategy is obtained by formulating the Volt/Var control as an optimization problem. This problem is known as Volt/Var Optimization (VVO) [8], which aim is the definition of the system equipment control in order to reach optimized objectives such as loss minimization, better asset utilization, conservation voltage reduction and voltage profile improvement [3, 67, 82, 97]. In fact, Volt/Var control fits very well for optimization. The complete design comprises not only operating goals, modeled as objective functions, but also operating restrictions handled by the mathematical constraints.

Several problems have been treated as Volt/Var optimization. A seminal work recommended a centralized Volt/Var control algorithm for optimizing the distribution system management [91]. Since then, various methods have been proposed following this principle. In general, these methods employ different optimization procedures—which are distinguished by the formulation of the Volt/Var control problem; the modeling of the distribution system; the evaluation of such model; and the implementation of an optimization algorithm—to reach a central coordination of the voltage regulating devices. But recently, great advances were incorporated

into the centralized optimization structure enhancing its features and the capability of dealing with Volt/Var control problems.

The Volt/Var control can result in a challenging optimization problem due to inherent characteristics of the operation, for which the modeling may represent: multiple objective functions, high-dimensional variables, large number of constraints, coordination of various control devices with different time frames, and uncertainties of Distributed Generations (DGs) and load forecasts [125]. On the other hand, selecting an adequate and rapid solution for VVO problems is the main goal of integrated Volt/Var control optimization (IVVC) [87]. As the problem may result in a complex optimization problem, some research focus on specialized algorithms aiming for efficient methods and controls [65].

The aim of this chapter is to present the optimal Volt/Var control in the context of modern distribution systems. The remainder of this chapter is organized as follows: Sect. 2 provides an overview of the Volt/Var control as a key function to improve energy efficiency and quality in distribution networks; Sect. 3 presents the main approaches of Volt/Var control from traditional to advanced; Sect. 4 is devoted to detail the Volt/Var Optimization; Sect. 5 describes some computational aspects to be accounted for; Sect. 6 depicts the optimal Volt/Var control through numerical examples; and, finally, Sect. 7 concludes this chapter presenting trend challenges and open issues concerning optimal Volt/Var control in modern distribution systems.

## 2 Volt/Var Control Definition

Volt/Var control refers to the technique of using voltage regulating devices and reactive power controls to maintain steady state voltage levels within the acceptable ranges along the feeder, considering various loading conditions. Power distribution utilities are responsible for this task, who has as a goal to provide reliable high-quality power supply.

### 2.1 Volt/Var Control Objectives

Although there are many important objectives, three well-established ones are highlighted in this subsection due to their relation with quality and efficiency in the power distribution supply, namely: voltage profile improvement, loss reduction and conservation voltage reduction. Improved VVO solutions should care about these objectives [66].

### 2.1.1   Voltage Profile Improvement

Voltage is a fundamental parameter to evaluate the quality of electrical service. Standards define the voltage limits for normal and abnormal conditions (emergency, after outage, etc. for a period of time). If voltage levels are out of acceptable operating ranges, the following issues can occur [21]:

- poor operation of the power system;
- reduced performance of the equipment;
- damage to utility equipment and customer loads;
- safety hazard;
- trigger protection equipment.

To accomplish the voltage regulation, the planning and operation design of the distribution system must consider the maximum allowed voltage drops for the selection and setting of the equipment (OLTCs, SVRs and SCs). The simple two-bus power system shown in Fig. 1 will be considered to illustrate the voltage drop in a distribution system [43].

The demand current $\bar{I}$ is related to the consumed power $P_L + jQ_L$ and the voltage $\bar{V}_L$ at the load by the expression:

$$\bar{I} = \frac{P_L - jQ_L}{\bar{V}_L^*} \, , \tag{1}$$

so, by Kirchhoff's voltage law and taking the load voltage as the reference for the phase angles, the voltage drop $\Delta V$ on the feeder will be given by:

$$\begin{aligned} \bar{V}_G - \bar{V}_L &= (R + jX)\bar{I} \\ &= \frac{RP_L + XQ_L}{V_L} + j\frac{XP_L - RQ_L}{V_L} \equiv \Delta V + j\delta V \, . \end{aligned} \tag{2}$$

For a small power flow, the component in quadrature $\delta V$ is small and the voltage drop might be approximated by $\Delta V$, the component of the voltage drop in phase with the load voltage. Therefore, the voltage drop depends on the power consumed
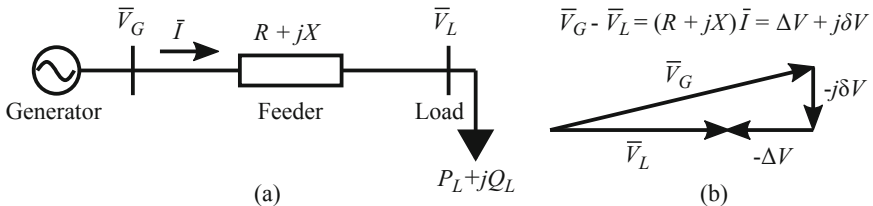


**Fig. 1** A simple two-bus power system: (**a**) one-line diagram; (**b**) components of the voltage drop along the feeder

by the loads, and the resistance and reactance of the lines, which cause active and reactive power losses. Since loads vary throughout the day and season to season, this causes voltage fluctuations [101]. During peak loading periods, the voltage along the feeder may drop significantly, and at lighter usage periods the voltage rises. Therefore, the effect of varying loads must be considered in the Volt/Var control scheme.

There are others indirect ways that improve the voltage profile (e.g., balancing of the loads on the primary feeders, using lines with increased conductor cross-section, etc.) [32]. However, the most common and economical way of improving the overall voltage regulation of the distribution system is to apply voltage regulating equipment and capacitors at the substation and along the feeders [50]. The voltage ratio of the transformers can be adjusted to enhance the voltage profile of the feeder, meanwhile capacitors can be switched to compensate the reactive power demand reducing the voltage drops.

### 2.1.2 Loss Reduction

During the process of delivering energy to customers, electrical losses happen in the system's components (lines, transformers, capacitors, etc.). In general, losses may be divided into two types: power losses and energy losses [14]. The power losses at the peak time restrict meeting the demand and causes increase on generation capacity.

The reduction of energy losses benefits both utility and customers in terms of saving costs. On the one hand, utility would purchase less amount of energy to serve customers, but on the other hand, extra energy would be available in the system to be sold by the utility. Also, loss reduction can result in better voltage profile in the feeder, which improves the quality of service.

Referring to Fig. 1 again, the line (or feeder) losses can be given as the difference between the supplied power $S_G = \bar{V}_G \bar{I}^*$ and the consumed power $S_L = \bar{V}_L \bar{I}^*$, expressed as:

$$
\begin{aligned}
S_{Loss,F} \equiv \Delta S_{G,L} &= (S_G - S_L) \\
&= (\bar{V}_G - \bar{V}_L)\bar{I}^* = (R + jX)\bar{I}\bar{I}^* \\
&= RI^2 + jXI^2 \equiv P_{Loss,F} + jQ_{Loss,F} ,
\end{aligned}
\tag{3}
$$

where $P_{Loss,F}$ and $Q_{Loss,F}$ are the active and reactive terms of the power losses.

The active power losses can also be written as:

$$
P_{Loss,F} = (I_R^2 + I_X^2)R ,
\tag{4}
$$

where $I_R$ and $I_X$ are the active and reactive components of the current.

Then, energy losses can be estimated in kilowatt-hours by using the rectangular integration method as in [34]:

$$E_{Loss} = \sum_{i=1}^{N_i} \frac{P_{Loss}^i + P_{Loss}^{i+1}}{2} \times \Delta t \, , \tag{5}$$

where $N_i$ is the number of intervals of the period of interest $T$, $P_{Loss}^i$ and $P_{Loss}^{i+1}$ are the active losses at times $i$ and $i + 1$, respectively, and $\Delta t$ is the period between the times $i$ and $i + 1$.

Based on (3), there are two ways of reducing active losses on a feeder: by replacing lines with reduced resistance and/or reducing currents in lines. The first option requires greater investments than the second one. It involves, for illustration, selecting line with larger cross-sectional area of lines, reconfiguring the network, etc. [93].

Nevertheless, the other way of reducing technical losses is to decrease the absolute value of the line current by reducing its reactive component $I_X$ in (4) [1]. This is accomplished by switching capacitors that performs the Var control part of Volt/Var control [34, 90].

### 2.1.3 Conservation Voltage Reduction

Conservation voltage reduction (CVR) is a practice of reducing the voltage levels on the network in order to promote peak demand reduction and energy savings. So, energy efficiency is the focus agreeing with Volt/Var control objectives. Successful real world applications have been reported in the literature showing a demand reduction ranging from 1 to 6% in the total demand due to CVR [3]. Therefore, CVR is a cost-effective way to save energy.

Figure 2 illustrates peak-load relief and energy savings as the response of the system with CVR implementation in a daily operation. The load demand is reduced from the reference (solid line) to a lower level (dotted line) relieving peak-load and saving energy (area enclosed by the lines).

CVR effects can be evaluated by the CVR factor ($CVR_f$), which is defined as the energy savings ($E_{saving}$) caused by 1% reduction of the voltage, as it follows [95]:

$$CVR_f = \frac{\Delta E\%}{\Delta V\%} \, , \tag{6}$$

where $\Delta E\%$ and $\Delta V\%$ are the percentage of energy and voltage reduction, respectively.

Normally the loads in medium voltage (MV) networks are modeled as voltage dependent, and the models are those that fit in the constant impedance or constant current models for CVR effectiveness. Such loads can be represented by the
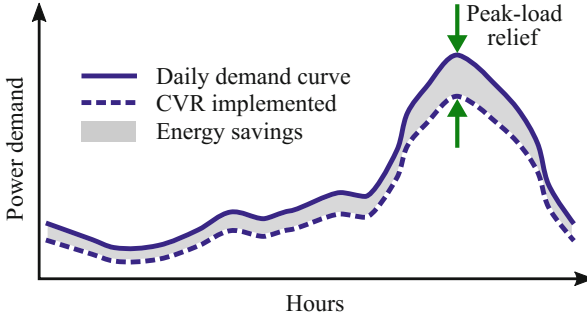
**Fig. 2** Peak demand reduction and energy savings

exponential model, which describes the voltage-dependent behavior as [82]:

$$P_{L_i} = P_{L_{n,i}} \left( \frac{V_i}{V_n} \right)^{k_p} \tag{7}$$

$$Q_{L_i} = Q_{L_{n,i}} \left( \frac{V_i}{V_n} \right)^{k_p} , \tag{8}$$

where $P_{L_i}$ and $Q_{L_i}$ are the active and reactive load power at bus number $i$, $P_{L_{n,i}}$ and $Q_{L_{n,i}}$ are the active and reactive load power at the rated voltage and frequency at bus $i$, $V_i$ is the voltage magnitude at bus $i$, $V_n$ is the nominal voltage of the system, and $k_p$ and $k_q$ are the voltage exponents of active and reactive load power.

Effective CVR implementation requires cost-benefit analyses. There are different methodologies to access CVR effects trying to simulate the energy-savings before its application. The main issue for the accurate assessment of CVR benefits is the changing behavior of the loads according to voltage variation. Additionally, load composition is not known for most of the feeders and it changes with time [95]. Moreover, a proper coordination among voltage and reactive power controls must be designed to carry out CVR with further capability of dealing with DG penetration and accommodating emerging smart monitoring and control technologies in distribution systems. For these reasons, the authors in [112] summarized the technical issues related to CVR into three aspects:

- coordination of different Volt/Var devices to reduce voltage in a reliable and optimal way;
- assessment and verification of CVR effects;
- coordination between CVR and DG.

Utilities can benefit from CVR in terms of [112]: peak-load relief, net loss reduction, and social welfare increase. However, due to the reduced energy usage by consumers, the utilities may lose revenues, as their rate structures are based on delivering a certain amount of energy [115]. Therefore, incentives are needed to

repay utilities for the lost revenue from the energy savings and to ensure return on investment in CVR.

## 2.2 Equipment

A proper coordination among the available control equipment (OLTC, SVRs and SCs) is the key for fulfilling Volt/Var objectives. Traditionally, conventional controllers operate locally these equipment to follow standards and to minimize power losses. This is case of the automatic capacitors banks operated by time or by combination of other measurements. However, in order to improve the control results, elaborated automation system must be devised.

The automatic voltage regulation is provided by equipment at the substation and along the feeders. At the substation, the core regulation is performed by the substation power transformer. Operating with an OLTC, it automatically controls the voltage levels for the secondary bus voltage and the reactive power flow through the transformer. Alternatively, voltage regulators can be installed at the substation to perform the voltage regulation of the secondary bus or at the head of the feeder. In general, the substation bus regulation provides a three-phase baseline voltage level. For the feeder voltage regulation, single-phase regulators are commonly employed to deal with the unbalanced voltages. The three-phase regulation is also possible by making connections among single-phase SVRs or using the three-phase one, which is "gang-operated" (the taps of all windings change at the same time). Capacitor banks are economical mean of supplying reactive power and minimizing system losses. They indirectly control voltage by decreasing voltage drop along the feeder.

### 2.2.1 On-Load Tap Changer Transformer

The load tap-changer (LTC) equips the transformer with tap terminals for turn-ratio control, i.e., the transformer ratio can be changed switching more or less of the transformer winding into the circuit [101]. For the on-load tap changer (OLTC) type, its mechanism permits the operation of the transformer without interruption of service. OLTC has a more complicated duty than the no-load tap changer (NLTC) type, being, accordingly, more expensive [21].

The substation transformer is a core type three-phase with gang-operated LTC—all three phases have the same tap positions and change simultaneously [21]—that typically works in the range of ±10% of the regulated voltage in discrete levels. The tap-changing can be done manually or automatically in order to maintain a consistent voltage profile to the whole network.

### 2.2.2 Step Voltage Regulator

The step voltage regulator (SVR) is a voltage control device. It consists of an autotransformer with adjustable taps (or steps) in the series winding to boost or buck the voltage at the regulated bus. The voltage change in the SVR output is obtained by changing the taps of the series winding, which can be done under load [50]. The voltage induced in this winding can be added to or subtracted from the primary voltage, depending on the reversing switch position, enabling $\pm 10\%$ regulation range in 32 steps usually, each step representing 5/8% change in voltage.

SVRs can be located at the substation bus or along the feeders. Single-phase SVRs regulate voltage per phase dealing with unbalanced voltages or when the phases are differently loaded. To obtain three-phase regulation, it is possible to make connections—wye, delta or open delta—among single-phase SVRs to form a three-phase regulator. Likewise, a three-phase SVR can be installed.

### 2.2.3 Shunt Capacitor

Shunt capacitors are widely used for Volt/Var control, being applied at various points of the distribution feeders to improve efficiency and performance. Specially, they inject reactive power into the system in order to reduce losses, free up capacity, reduce voltage drop, and correct power factor [100]. Based on **IEEE Std 1036-2010** [37], shunt capacitors represent an effective means for supplying the reactive power while minimizing system losses.

These devices are connected in parallel with the load, modifying the network characteristics by their capacitive reactance. They present low cost and flexibility of installation and operation as principal advantages [50].

Capacitor banks are controlled discretely by being switched on or off of the system [70]. The reactive power is provided locally, the inductive load is compensated bringing the power factor closer to unity, nearby the load. This decreases the total current along the feeder that flows from the substation to the load, i.e., it relieves feeder of wattless current. Accordingly, the reduced current releases feeder capacity, lowers the $I^2R$ line losses, and leads to a smaller voltage drop.

The injection of reactive power causes a reduction in the voltage drop, which results, in general, an indirectly or approximate voltage control capacity. For this reason, shunt capacitors are also used to boost the local voltage level within allowable limits as the load varies.

## 3 Main Approaches for Volt/Var Control

In general, the Volt/Var control in distribution systems can be divided into the following three main approaches [108]: Traditional Volt/Var control, SCADA-based Volt/Var control and Integrated Volt/Var control.

## 3.1 Traditional Volt/Var Control

Traditional Volt/Var control is conceptually the simplest and economical approach. It is characterized by an individual, independent, and standalone controller [32], which has a built-in intelligence that uses local measurements of voltage and current to determine the appropriate control actions for the associated device [107]. Therefore, this approach addresses to the conventional utility voltage regulation practices.

Standalone controllers make use of OLTC transformer, SVRs and switched capacitor banks to achieve basic goals of the Volt/Var control, such as maintaining feeder voltage within the acceptable range and improving power factor at load locations.

Some advantages of this approach rely on the low cost implementation, no need for field communication and the scalable feature [108]. However, traditional Volt/Var control presents some issues, specially concerning the DG penetration. Both high or low service voltage can occur due to the bidirectional power flow caused by DG, impacting the operational schemes [57]. Other disadvantages are: lack of coordination between Volt/Var devices (e.g., OLTC, SVRs and SCs), non-optimal operation, no self-monitoring (which is essential to find out if capacitors are out of service), no flexibility for handling reconfiguration of feeders, and, finally, operator cannot override the control actions whenever needed [87, 107].

### 3.1.1 OLTC Control

The OLTC is controlled automatically by the automatic voltage regulator (AVR) that senses when the regulation point is no longer within the permitted voltage range. Then, the AVR commands the tap-changing mechanism to alter its tap position to restore the voltage [101]. An adjustable time delay is used to reduce the effect of transient voltage variations, outside of the dead band, avoiding unnecessary tap position changes [102].

The line drop compensator (LDC) aids to regulate some distant bus from the OLTC by simulating the voltage drop across the feeder. Thus, it permits to boost the voltage at the output of the OLTC transformer ensuring the correct voltage at the load. More details are presented in the following item.

### 3.1.2 SVR Control

The control mechanism of the SVR provides automatic tap changing [32]. It responds to inputs from potential transformer (PT) and current transformer (CT) by means of maintaining a predetermined output voltage at the load center, which can be the output terminal of the regulator or a remote node on the feeder [45]. A typical controller includes the voltage-regulating relay (VR) and the LDC.

In the relay, the voltage set point is the desired voltage to be held at the center load. There is a bandwidth for which the voltage may vary from the set point. So, when the difference between the measured voltage and the set voltage exceeds ±one-half of the bandwidth, the regulator will change taps in order to bring the voltage back. To prevent unnecessary tap changes due to transient or short time change in current, a time delay is implemented before the actual tap operation [100].

The LDC is a procedure to boost the voltage at the regulator output to compensate the voltage drop on the feeder. Thus, it regulates the voltage at the load rather than at the regulator bus. Basically, the LDC uses an internal model with settings ($R$ and $X$) that need to be adjusted in order to match the equivalent impedance between the regulator and the load center [45].

### 3.1.3 SC Control

Switchable shunt capacitors are equipped with local controllers that switch on/off banks of capacitors based on a minimum/maximum value of a given parameter [21]. If voltage control is implemented, a voltage relay switches on the capacitor when the voltage is bellow a minimum value or switches off when the voltage is above a maximum value. Also, time delays and bandwidths are considered to prevent excessive operations. Similarly, for power factor correction or maximum reduction of losses, the load kvar (or total current) must be monitored as the means for control. Apart of the goal to be accomplished, the control systems implemented to switch automatically banks of shunt capacitors are similar. They comprise, basically, a master control relay, time-delay relays and control switches. In short, automatically controlled capacitors are switched in a similar way relative to time delays and dead bands of the OLTC and SVR equipment [83]. On feeders with typical daily load profiles, in which the need for capacitor kvar follows a fixed schedule, time controlled capacitors are especially applied [100].

## 3.2 SCADA-Based Volt/Var Control

In this approach, the Volt/Var devices are remotely monitored and controlled by the supervisory control and data acquisition (SCADA) system. The equipment settings are based on real-time substation and field measurements [106]. It is also known as rule-based Volt/Var control, because the built-in intelligence is set by predetermined rules that incorporate successful operational experiences and system studies of the distribution system operator (DSO). These rules are implemented by running a script within the SCADA system.

Typically, there are two independent systems to handle separated goals [107]. The Var dispatch system controls capacitor banks to improve power factor and reduce electrical losses, whereas the Voltage control system controls the OLTC transformer and SVRs to maintain acceptable voltage at all locations under all load-

ing conditions and to reduce demand and energy consumption, i.e., to implement the CVR. There is no integration between these systems.

The main components of the SCADA-based approach are [69]:

- substation remote terminal unit (RTU);
- voltage control and/or var dispatch processor;
- switched capacitor banks and local measurement facilities;
- OLTC transformer and/or SVRs, and local measurement facilities;
- communication facilities;
- end of line voltage feedback.

A general schematic of SCADA-based Volt/Var control, including an OLTC and a capacitor bank, is shown in Fig. 3. The substation RTU is responsible for monitoring real and reactive powers at the substation bus (or the head of the feeder). The Var dispatch processor contains rules to determine if capacitor switching is needed. It sends a signal to the capacitor bank controller, through the one-way communication link (radio), so that a command to energize or de-energize the capacitor bank may be performed. In the same way, the Voltage control processor contains rules to determine the raise or lower commands of the OLTC. It monitors the voltage at the end of the feeder, through a communication link, to ensure that voltage does not drop too much, violating the lower acceptable limit.

SCADA-based Volt/Var control is a very common approach. It improves the overall efficiency when compared to traditional approach, mainly because it provides self-monitoring, operator override capability, and enhanced measurement facilities, which permit the monitoring of strategic locations. As the visibility of remote conditions is improved, a smaller margin of safety is needed when compared to that built in traditional approach. Despite these advantages, the lack of adaptability remains for changing feeder configuration, varying operating needs, and high DG
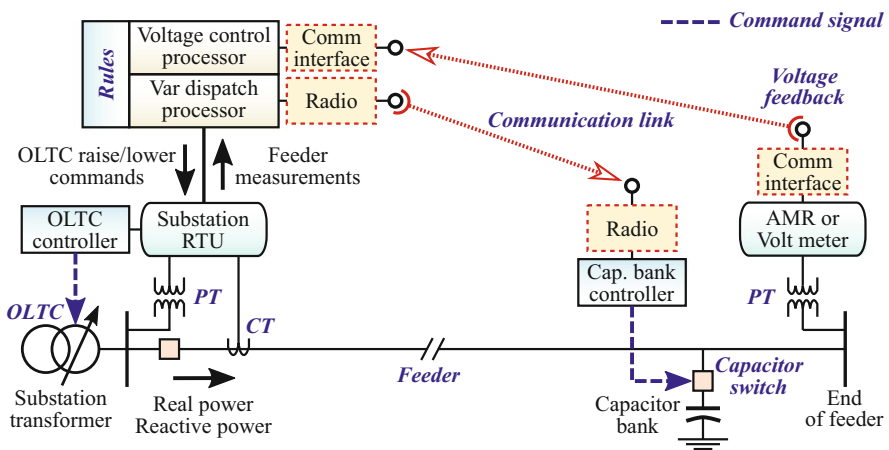


**Fig. 3** SCADA-based Volt/Var control approach [107]

penetration. Also, the devices operation are usually not coordinated to ensure optimal results. Other shortcomings are related to the less scalable feature and a more complicated deployment because of the extensive communication requirement [108].

## 3.3 Integrated Volt/Var Control: The Platform for VVO

Integrated Volt/Var control is the most advanced approach in Volt/Var control. This approach performs the Volt/Var optimization, which is the ability to determine the best set of control actions for all devices of the system (i.e., voltage regulating devices and Var control devices) to achieve one or more operating objectives of the utility without violating any of the operating constraints [107]. Thus, a proper synergy between optimization techniques and the deployment of technologies can improve the performance and efficiency of the entire distribution network operation.

Figure 4 depicts the components of the IVVC and the information exchanged between the blocks [32, 107, 108]. To execute a coordinated optimal switching plan, IVVC requires real-time monitoring and control of substation and feeder devices. Basically, a centralized control collects sensory data from the meters, then it runs Volt/Var optimization algorithms sending new setting to the Volt/Var devices in the field via SCADA system. The overall SCADA system is involved in the integration
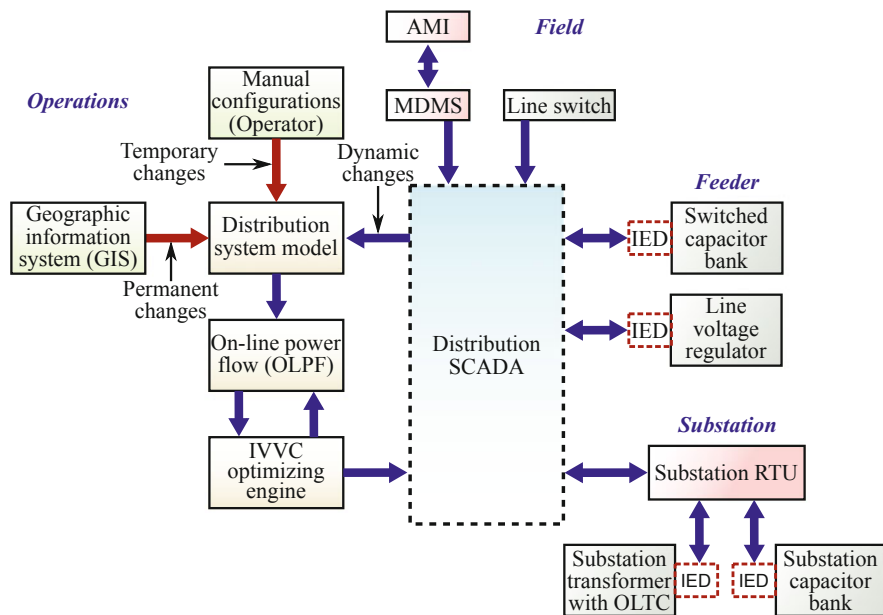


**Fig. 4** Integrated Volt/Var control approach [32, 107, 108]

of all components of the IVVC. The platform solution that supports the centralized control of these many integrated elements is the so-called distribution management system (DMS). That is why, this approach is also known as DMS-based Volt/Var control.

Advanced metering infrastructure (AMI) refers to the measurement and collection system that includes meters, communication networks and data reception. It provides real-time observability of the customer service delivery points [21]. Additionally, a meter data management system (MDMS) manages the data into the data storage and it makes analyses to extract useful information to the utility [27].

The benefit of employing a dynamic model is that the Volt/Var optimization is always dealing with the "as-operated" network state, ensuring a control that reflects the current operating configuration of the system [104]. The line switch provides switch status information to accommodate resulting scenarios of feeder reconfiguration. Also, intelligent electronic devices (IEDs) collect and transmit operating status data of the Volt/Var devices.

In the IVVC, IEDs operate as smart meters and supervisory controllers intermediating the communication between devices and coordination algorithm [57]. So, IEDs monitor voltage and status of switched capacitor banks on the feeder and perform the switch control action. IEDs also monitor and execute the tap changes of line voltage regulators and measure load voltage and load at these sites. Likewise for substation capacitor banks and substation OLTC. But, in this case, there is an important part of the SCADA system—the substation RTU—serving as a data concentrator for all substation IEDs [114].

IVVC requires an accurate and up-to-date electrical model. DMS can interface geographic information systems (GIS) to create an integrated view of the distribution network updating the distribution system model about permanent asset changes (e.g., line extension, reconductoring) [116]. Besides GIS, dynamic changes must feed the model through real-time updates via SCADA. Thus, the setting control logic are usually based on the dynamic model of the distribution system [106]. Moreover, temporary changes (e.g., line cuts, jumpers, manual switching), performed by direct operator action, must also be considered in the model.

To carry out the control of the Volt/Var equipment, IVVC requires an online power flow (OLPF) which is responsible for evaluating possible control strategies. OLPF determines the values of all relevant variables and electrical conditions of the whole network, such as: losses, voltage profile, etc. So, based on the power flow results, IVVC optimizing engine determines the optimal set of control actions to achieve the desired objectives [108]. The procedure consists in a sequence of algorithm iterations, that is, while the engine elaborates an alternative switching plan, the OLPF tests the effectiveness of such plan. Once the optimal coordination is finally elaborated, the control signals are then transmitted to the field controllers via SCADA to execute the control strategy.

Certainly, the use of a dynamic operating model in conjunction to a optimization algorithm can achieve significant performance benefits. In fact, IVVC pursues utility-specific objectives, which include [32, 90]:

- keep the system within bus voltage and line/transformer loading constrains;
- keep power factor along the feeders close to unity;
- minimize power losses in lines and transformers;
- minimize the substation transformer injected active power (energy conservation), or equivalently, minimize the sum of the power losses and the concurrent customer demand;
- maximize the service life of the equipments;
- maximize revenue that is the difference between energy sales and energy prime cost (the cost of production or the price to purchase energy from another producer).

To sum up, IVVC has several advantages over the traditional approach and SCADA-based approach [69, 107]. Because dynamic model updates automatically, IVVC can adapt well to feeder reconfiguration and handle complex feeder arrangements. Volt/Var control actions are fully coordinated reaching optimal results. IVVC can accommodate varying operating objectives and, when needed, change the control strategy. Therefore, it presents flexible operating objectives. For advanced applications, IVVC can model the dynamic effects of DG and other modern grid elements in the distribution system operation. IVVC is able to handle high penetration of distributed energy resources (DERs) and reverse power flows properly. Also, it is possible to control these devices as part of the optimal Volt/Var control strategy. In other words, IVVC potentially fulfills all the ideally characteristics for a Volt/Var control. Although IVVC presents all these advantages, in return, it could result in high cost to implement, operate and maintain. On the other hand, it is possible to reduce ownership costs through shared infrastructure with SCADA, outage management systems (OMS) and DMS applications [104].

## 4 Statement of the Volt/Var Optimization Problem

The optimization approach has received the greatest attention due to the potential to further enhance system operation. In the grid modernization initiatives, the deployment of new infrastructure and technologies are followed by the implementation of updated distribution operations [2], in which the Volt/Var control is included. Therefore, Volt/Var optimization should become much more effective than traditional approaches [82].

Although the primary definition of the Volt/Var control is related to voltage regulation, secondary benefits can also be explored as well in order to improve the overall system efficiency. This is accomplished by formulating the Volt/Var control as an optimization problem. Therefore, the voltage regulation issues become a constraint of the problem, whereas the objectives—such as minimal electrical losses, minimal electrical demand, and reduced energy consumption [107]—are included in the problem formulation. This enhanced concept opens a wide range of possibilities for the Volt/Var control.

## 4.1   Application of Optimization Approach

If more elaborated objectives are considered, better performances and improved efficiency are desired, which implies in formulating the Volt/Var control as an optimization problem. The range of possibilities for the goals to explore are wide and the constraints to be considered are critical for the problem.

Essentially, the success of the Volt/Var control depends on the proper coordination among the equipment. Different equipment settings will result in different performances of the system. So, it is possible to pursue optimal results if an optimization model, which evaluates the performance of the system from the equipment settings, is elaborated. As a necessary condition this model should comprise the power flow equations. Some characteristics that favor modeling the Volt/Var optimization are:

- objective functions can represent utility goals;
- essential limitations and requirements of the operation can be modeled as constraints;
- voltage regulating equipment and reactive controls can be handled as the control variables;
- objective functions can be evaluated by algorithms or simulation tools;
- the control variables can be encoded as continuous or discrete;
- different techniques can be used to solve the problem;
- trial and error adjusts are avoided;
- efficient algorithms can solve the problem for real-time applications;
- system optimization is part of the smart grid strategy.

## 4.2   Problem Formulation

VVO consists in a coordination problem that selects an ordered combination of the voltage and var controls so that a particular objective can be achieved optimally. This problem is usually modeled as a mixed integer nonlinear programming problem [55], which presents nonlinear objective functions and a mix of integer and continuous design variables. There are also models that use integer programming [8] and, in addition to the exact optimization methods, evolutionary computation techniques can be used to determine the control operation [34, 97].

The optimal Volt/Var control is treated in this chapter as a single-objective optimization problem. Although representing it as a multi-objective problem is more realistic, the single-objective version is often used in literature and can easily demonstrate the advantages of formulating the Volt/Var as an optimization problem.

The formal formulation of single-objective optimization problems, in the form of definition, is presented as follows [18].

**Definition 1 (General Problem)** A general single-objective optimization problem is defined as:

$$
\begin{aligned}
\text{minimize} \quad & f(\mathbf{x}) \\
\text{subject to} \quad & g_i(\mathbf{x}) \le 0, \quad i = 1, \ldots, m \\
& h_j(\mathbf{x}) = 0, \quad j = 1, \ldots, p,
\end{aligned}
\tag{9}
$$

where $\mathbf{x} = [x_1, \ldots, x_n]^T$ is a $n$-dimensional decision vector from the universe $\Omega$, which contains all possible $\mathbf{x}$ that can be used to satisfy an evaluation of $f(\mathbf{x})$ and its constraints.

The goal of an optimization problem is to search for an optimal feasible solution $\mathbf{x}^*$ (or a near optimum) that satisfies all constraints ($g$ and $h$), providing the best value (or an approximation) of the objective function ($f$) among all feasible solutions ($\mathbf{x} \in \Omega$). In what follows the VVO problem is represented as an optimization problem.

### 4.2.1 Control Variables

VVO determines the set of actions that must be implemented to achieve optimized Volt/Var control. These actions are related to the managing of the equipment and controls deployed on the grid. Classically, the following variables are considered in the problem:

- OLTC tap position;
- SVR tap position;
- Number of SC banks.

However, new proposals consider additional controls in the optimization:

- Static var compensator (SVC) [20, 97];
- Distributed static var compensator (D-STATCOM) [22];
- Shunt reactor (ShR) [97, 117];
- Operating values of automatic voltage regulator (AVR) [119];
- Voltage control at PV-buses [73, 78];
- Active power of DG [76, 77];
- Reactive power of DG [15, 76];
- Active power curtailment from DG units [71];
- Active and reactive power of microgrids [59];
- Active power injection/absorption from energy storage (ES) device [71];
- Operation state of the ES device [56];
- Reactive power injection of electric vehicle (EV) [63];
- Active and reactive power of battery energy storage system (BESS) [121, 126];
- Active and reactive power of controllable loads (CLs) [71, 126];
- Reactive power of soft open point (SOP) [52];
- Solid state transformers (SST) [98].

The control variables are represented in the optimization problem as a set of design parameters, $\mathbf{x} = x_1, x_2, \ldots, x_n$, to be evaluated through the objective function $f(\mathbf{x})$, which can be represented by discrete or continuous variables.

### 4.2.2 Objective Functions

The objective function can model an utility-specific objective that might be minimized (or maximized) throughout the optimization process. The objective function, $f$, is dependent on $\mathbf{x}$ and it represents the goal of the VVO. Some examples are:

**Minimization of Power Losses** It has a positive impact on relieving the feeders, reducing the voltage drop and presenting other environmental and economical benefits.

*Minimization of Active Power Losses [15]:*

$$\min f_L = \sum_{k=1}^{N_{br}} G_k[V_i^2 + V_j^2 - V_i V_j \cos \theta_{ij}] \tag{10}$$

where $f_L$ represents the total active power losses, $N_{br}$ is the total number of branches, $G_k$ is the conductance of branch $k$ which connects bus $i$ and bus $j$, and $V$ and $\theta$ are voltage magnitude and voltage angle ($\theta_{ij} = \theta_i - \theta_j$), respectively;

*Minimization of Electrical Energy Losses [77]:*

$$\min f_{EL} = \sum_{t=1}^{N_t} \sum_{k=1}^{N_{br}} R_k |I_k^t|^2 \Delta t \tag{11}$$

where $f_{EL}$ represents the total electrical energy losses, $N_t$ is the number of intervals, $N_{br}$ is the number of branches, $R_k$ is the resistance value of the $k$th branch, $I_k^t$ is the actual current value of the $k$th branch during time $t$, and $\Delta t$ is the time interval.

**Minimization of Voltage Deviation** Voltage deviation is one of the indexes that has been used to evaluate the stability of the system and the quality of power supply [15].

*Minimization of Total Voltage Deviation [15]:*

$$\min f_{\Delta V} = \sum_{i=1}^{N_{bus}} (V_i - V_i^*)^2 \tag{12}$$

where $f_{\Delta V}$ represents the total voltage deviation, $N_{bus}$ is the total number of buses, $V_i$ is the current voltage magnitude, and $V_i^*$ is the desired voltage at the $i$th bus;

*Minimization of Total Daily Voltage Deviation [77]:*

$$\min f_{\Delta V_{daily}} = \frac{1}{N_t} \sum_{t=1}^{N_t} \sum_{i=1}^{N_{bus}} \left| \frac{V_i^t - V_i^*}{V_i^*} \right| \tag{13}$$

where $f_{\Delta V_{daily}}$ represents the total daily voltage deviation, $N_t$ is the number of intervals, $N_{bus}$ is the total number of buses, $V_i$ is the current voltage magnitude, and $V_i^*$ is the desired voltage at the $i$th bus.

**Maximization of Energy Savings Through CVR** Energy saving is achieved by lowering the voltage along the feeder to promote a reduction in energy demand [82], with a flatter voltage profile but keeping the voltage within allowable limits [4].

*Maximization of Energy Savings [4]:*

$$\max f_{ES} = 100\% \frac{P_{system_{base}} - P_{system_i}}{P_{system_{base}}} \tag{14}$$

where $f_{ES}$ denotes the energy savings, $P_{system_{base}}$ represents the kilowatt results obtained after solving the base case power flow without Volt/Var control, and $P_{system_i}$ denotes the kilowatt power flow results obtained for each $i$th possible operation with Volt/Var control;

**Minimization of Voltage Unbalance** Practical distribution systems are unbalanced in nature—loads are unbalanced and power delivery lines are untransposed and multi-phase (a mix of single-phase, two-phase, three-phase and/or neutral lines)—and the integration of single-phase DGs makes them even more unbalanced [5]. Voltage unbalance creates negative effects causing overheating and malfunction of equipment, and power and energy losses in the distribution grid [35].

*Minimization of Total Line Voltage Unbalance Rate [110]:*

$$\min f_{LVUR} = \sum_{n \in \Omega_T} \frac{\Delta U_n}{U_{avg_n}} \tag{15}$$

where $f_{LVUR}$ represents the total line voltage unbalance rate (LVUR), $U_{avg_n}$ is the average line voltage of the three phases at node $n$, $\Delta U_n$ is the maximum voltage deviation from the average line voltage $U_{avg_n}$, and $\Omega_T$ is the set of the three-phase nodes.

**Minimization of the Number of Switching Operations** Frequent switching operations of traditional devices (OLTC, SVRs and capacitor banks) may significantly reduce the lifetime of these devices and even damage them [58]. Therefore, deterioration due to their intensive use should be prevented by minimizing the number of operations in order to prolong the lifetime of these devices [99].

*Minimization of the Number of Tap Changes [99]:*

$$\min f_{TC} = \frac{1}{N_d} \sum_{d=1}^{N_d} \sum_{t=1}^{N_t} |T_d^t - T_d^{t-1}| \tag{16}$$

where $f_{TC}$ represents the number of tap changes, $T_d^t$ is the tap position of the voltage control device $d$ at time $t$, $N_d$ is the number of devices, and $N_t$ is the number of intervals.

**Minimization of MW Curtailment on DG [11]** Generators (non-firm DG) may be accepted to be occasionally curtailed in the face of grid congestion to remove voltage constraints. Furthermore, based on real-time electricity markets, the objective looks for minimizing the distribution system operator (DSO) payments towards the owners of curtailed DG units.

*Minimization of MW Curtailed on DG Units [11]:*

$$\min f_{DGC} = \sum_{i \in G} (P_{gi}^0 - P_{gi}) \tag{17}$$

where $f_{DGC}$ represents the amount of MW curtailed on DG units or the cost of DSO payments towards the owners of curtailed DG, $P_{gi}^0$ is the current available active power of DG unit $i$, and $P_{gi}$ is the curtailed active power of DG unit $i$.

### 4.2.3 Constraints

Numerous constraints are imposed on the VVO problem. If they are not satisfied, such solutions will be infeasible, resulting in a poor operation of the distribution system or even in an impractical control. Therefore, the objective function $f(\mathbf{x})$ to be minimized (or maximized) might be subjected to a set of inequality and equality constraints. Some examples are:

**Technical and Operational Constraints** The optimization problem is subjected mainly by technical and operational constraints which ensure security, quality and reliability of the system operation. These constraints are essential in the Volt/Var optimization problem.

*Active and Reactive Power Flow Balances:*

$$\Delta P = P_n^{spec} - P_n^{calc} \tag{18}$$

$$\Delta Q = Q_n^{spec} - Q_n^{calc} , \tag{19}$$

where $\Delta P$ and $\Delta Q$ are the active and reactive power injection estimation errors, $P_n^{spec}$ and $P_n^{calc}$ are the specified and calculated active power injection at node $n$, and $Q_n^{spec}$ and $Q_n^{calc}$ are the specified and calculated reactive power injection at node $n$;

*Node Voltage Magnitude:*

$$V_{min} \leq V_n^t \leq V_{max} \ , \tag{20}$$

where $V_n^t$ is the voltage of the node $n$ at hour $t$, and $V_{min}$ and $V_{max}$ are the acceptable voltage limits;

*Thermal Capacity of Lines:*

$$|S_k^t| < S_k^{max} \ , \tag{21}$$

where $|S_k^t|$ is the absolute value of the complex power flowing over the branch $k$ at hour $t$, and $S_k^{max}$ is the maximum allowable complex power of branch $k$;

*Power Flow on Substation Transformer:*

$$S_{TX}^t \leq S_{TX}^{rat} \ , \tag{22}$$

where $S_{TX}^t$ it the apparent power flow on substation transformer at time $t$, and $S_{TX}^{rat}$ is the substation transformer rating;

*Tap Position Limits and Number of Capacitor Banks:*

$$T_d^{min} \leq T_d^t \leq T_d^{max} \ , \tag{23}$$

where $T_d^t$ is the tap position (or number of capacitor banks) for each voltage control device $d$ at hour $t$, and $T_d^{min}$ and $T_d^{max}$ are the tap position limits (or capacitor banks limits) for the device $d$.

**Ensure Performance Improvement by Using Constraints**  Some constraints can be added into the VVO problem in order to ensure a certain improvement of economy, quality and performance during the system operation.

*Substation Power Factor [91]:*

$$PF_S^{min} \leq PF_S^t \leq PF_S^{max} \ , \tag{24}$$

where $PF_S^{min}$ and $PF_S^{max}$ are the minimum and maximum allowable power factors of the substation, and $PF_S^t$ is its current power factor at hour $t$;

*Maximum Switching Operations of Devices [79]:*

$$\sum_{t=2}^{24} |T_d^t - T_d^{t-1}| \leq N_d^{max} \ , \tag{25}$$

where $T_d^t$ is the tap position of the voltage control device $d$ at hour $t$, and $N_d^{max}$ is the maximum allowable daily operating times (MADOT) [79]—or, similarly, the

maximum allowable daily switching operation number (MADSON) [55]—of the device $d$;

*Total Harmonic Distortion of Voltage [105]:*

$$THD_v^i \leq THD_v^{max} ,$$ (26)

where $THD_v^i$ and $THD_v^{max}$ are total harmonic distortion of voltage at bus $i$ and the maximum distortion allowed, respectively;

*Limit on Voltage Balance Factor for all Three-Phase Buses [20]:*

$$0 \leq U_{2i} = 100 \frac{E_i^2}{E_i^1} \leq U_2^{max}$$ (27)

where $U_{2i}$ is the voltage unbalance factor of bus $i$, $E_i^1$ and $E_i^2$ are the positive-sequence and negative-sequence voltage of bus $i$ respectively, and $U_2^{max}$ is the maximum value of $U_{2i}$.

**DER Constraints** When distributed energy resources deployed in the distribution system actively participate in the VVO, their constraints must be considered.

*Active Power and Power Factor Constraints of DGs [79]:*

$$P_{DG_i}^{min} \leq P_{DG_i}^t \leq P_{DG_i}^{max}$$ (28)

$$PF_{DG_i}^{min} \leq PF_{DG_i}^t \leq PF_{DG_i}^{max} ,$$ (29)

where $P_{DG_i}^{min}$ and $P_{DG_i}^{max}$ are the minimum and maximum real power components of the distributed generator $i$, $P_{DG_i}^t$ is its current real power at hour $t$. $PF_{DG_i}^{min}$ and $PF_{DG_i}^{max}$ are the minimum and maximum allowable power factors of the distributed generator $i$, and $PF_{DG_i}^t$ is its current power factor at hour $t$.

*Active and Reactive Power Constraints of DGs [76]:*

$$(P_{DG_i}^t)^2 + (Q_{DG_i}^t)^2 \leq (S_{DG_i}^{max})^2 ,$$ (30)

where $P_{DG_i}^t$ and $Q_{DG_i}^t$ are the active and reactive power components of the $i$th DG at hour $t$, respectively, and $S_{DG_i}^{max}$ is the apparent power of the $i$th DG.

*Electric Vehicle Constraints [63]:*

$$V_{EV_i}^{min} \leq V_{EV_i}^t \leq V_{EV_i}^{max}$$ (31)

$$0 \leq P_{EV_i}^t \leq P_{EV_i}^{max}$$ (32)

$$0 \leq -Q_{EV_i}^t \leq -Q_{EV_i}^{max} ,$$ (33)

where $V_{EV_i}^t$ is the voltage of the EV in bus $i$ at time $t$, and $V_{EV_i}^{min}$ and $V_{EV_i}^{max}$ are the minimum and maximum voltage values. $P_{EV_i}^t$ and $P_{EV_i}^{max}$ are the active power of the $i$th EV at time $t$ and the maximum charging limit of the system. $Q_{EV_i}^t$ and $Q_{EV_i}^{max}$ are the reactive power injection to the grid at time $t$ and the capacity of maximum inverter reactive power generation of the $i$th EV.

*Controllable Loads (CL) Constraints [126]:*

$$P_{CL_l}^{min} \leq P_{CL_l}(i) \leq P_{CL_l}^{max} \tag{34}$$

$$Q_{CL_l}^{min} \leq Q_{CL_l}(i) \leq Q_{CL_l}^{max} \tag{35}$$

$$\Delta W_L \leq \int_0^N \Delta P_{CL_l}(i)di \leq \Delta W_U \ , \tag{36}$$

where $P_{CL_l}$ is the active power of the $l$-th CL, $P_{CL_l}^{min}$ and $P_{CL_l}^{max}$ are the lower and upper bounds of active power acceptable ranges, $Q_{CL_l}$ is the reactive power of the $l$-th CL, $Q_{CL_l}^{min}$ and $Q_{CL_l}^{max}$ are the lower and upper bounds of reactive power acceptable ranges, $\Delta P_{CL_l}$ is the energy allocated to the $l$-th CL, $\Delta W_L$ and $\Delta W_U$ are the lower and upper bounds of load energy which can be used by CL, and $i$ and $N$ are the index and number of samples of control references.

*Energy Storage Constraints [6]:*

$$\sum_{t=1}^{24}[-\eta_i P_{ES_{i,t}} \Delta t] \leq E_{ES_{i,t}}^{max} - E_{ES_{i,t}}^0 \tag{37}$$

$$\sum_{t=1}^{24}[\eta_i P_{ES_{i,t}} \Delta t] \leq E_{ES_{i,t}}^0 \tag{38}$$

$$E_{ES_i}^{min} \leq E_{ES_{i,t}} \leq E_{ES_i}^{max} \tag{39}$$

$$P_{ES_i}^{min} \leq P_{ES_{i,t}} \leq P_{ES_i}^{max} \tag{40}$$

$$(P_{ES_{i,t}})^2 + (Q_{ES_{i,t}})^2 \leq (\Omega_{ES_i}^{max})^2 \ , \tag{41}$$

where $\eta_i$ is the storage charge-discharge cycle efficiency at bus $i$, $P_{ES_{i,t}}$ is the active power produced/absorbed by the energy storage ($ES_{i,t}$) at bus $i$ at time $t$, $\Delta t$ is 1 h time interval, and $E_{ES_{i,t}}^{max}$ and $E_{ES_{i,t}}^0$ are the maximum energy stored and the initial energy stored of the $ES_{i,t}$. The storage could be positive or negative, indicating charging or discharging cycles respectively. $E_{ES_{i,t}}$ is the energy stored, and $E_{ES_i}^{min}$ and $E_{ES_i}^{max}$ are the minimum and maximum capacity of the energy storage. $P_{ES_i}^{min}$ and $P_{ES_i}^{max}$ are the minimum and maximum active power rating. $Q_{ES_{i,t}}$ is the reactive power produced/absorbed by energy storage and $\Omega_{ES_i}^{max}$ is the power capability limit of the energy storage, MVA.

## 4.3 Dealing with Costs

Besides optimizing directly the distribution system operation, it is possible to optimize energy or operation costs through VVO. The formulation of the objective functions may have additional parameters that aggregate the costs related to the objectives. These parameters quantify economically the benefits of the optimal solutions. In general, the objective function to be optimized is as follows:

$$\min J = \sum_{i \in \Omega_o} C_i \times f_{o_i} \ , \tag{42}$$

where $J$ represents the objective function (which can be a sum of objectives), $\Omega_o$ is the set of objectives, and $C_i$ is the cost related to the $i$-th objective $f_{o_i}$.

There are several cost formulations in literature that deal with different objectives and strategies. Some examples, in the context of modern distribution systems:

- minimization of the total cost of energy purchased from the distribution substation and the dispatchable DGs [56, 76];
- minimization of the total power system operation cost which include fuel cost of generators and switching cost of equipments like tap transformers and shunt capacitors [60];
- minimization of the total costs of network losses and generation curtailment [49];
- minimization of the total cost of energy purchased from the substation and DG units, the cost of energy curtailment on electric vehicles, the cost of energy injected from the energy storage devices (ESDs), and the cost of energy curtailment on the ESDs [92].

### 4.3.1 Cost Evaluation of Distributed Generators

The cost of each kWh of electric energy generated by DG can be estimated considering: investment, operation and maintenance (O&M) cost, and fuel cost. Therefore, the hourly cost function can be expressed as [76]:

$$C_{P_{dg}}(P_{dg}) = a + b P_{dg} \ , \tag{43}$$

where $C_{P_{dg}}(P_{dg})$ is the cost of active power generated by the DG in \$/kWh and

$$a = \frac{\text{Capital cost}(\$/kW) \times \text{Capacity}(kW) \times \text{Annual rates of benefit}}{\text{Lifetime}(Year) \times 365 \times 24 \times \text{DG loading factor}} \ , \tag{44}$$

$$b = \text{Fuel Cost}(\$/kWh) + \text{O\&M Cost}(\$/kWh) \ . \tag{45}$$

### 4.3.2   Cost of the Switchable Devices

The traditional Volt/Var control devices (tap transformers and shunt capacitors) are subjected to wear-and-tear cost per adjustment. Because of the mechanical switching, a limited number of switching operations could be performed during their service life [60].

The purchase cost per kvar rating of shunt capacitors ($C_{ShC}$) can be defined based on the capacitor purchase cost ($ShC^p$) and its expected lifespan ($ShC_{Lifetime}$) [118]:

$$C_{ShC} = \frac{ShC^p}{ShC_{Lifetime}} \; .$$  (46)

OLTC control costs contain both capital investment costs and operating costs related to components wear out and maintenance [113]. So, the cost of OLTC tap operation in \$/tap can be calculated based on the cost of replacing the OLTC ($C_{OLTC}^R$) and the number of tap operations remaining ($N_{OLTC}^R$) [118]:

$$C_{OLTC} = \frac{C_{OLTC}^R}{N_{OLTC}^R} \; ,$$  (47)

where the number of tap operations remaining depends on the residual lifespan ($LS_{OLTC}^R$), the total lifespan ($LS_{OLTC}^T$), and the estimated total operation times ($N_{OLTC}^T$) of the OLTC:

$$N_{OLTC}^R = \frac{LS_{OLTC}^R}{LS_{OLTC}^T} N_{OLTC}^T \; .$$  (48)

## 5   Solving the Volt/Var Optimization Problem

The Volt/Var control problem is nondeterministic polynomial hard and combinatorial with huge solution space [75]. Traditionally, the problem is formulated as a nonconvex, mixed-integer nonlinear problem [55]. To point out, VVO has the following characteristics that challenge optimization algorithms [29]:

- integer decision variables;
- nonlinear objective being an implicit function of decision variables;
- high dimension nonlinear constraints;
- non-convex objective and solution set;
- high dimension search space.

Besides that, a major goal is to develop efficient algorithms capable to solve large problems in a real-time (or near real-time) application.

The remaining of this section is dedicated to: (1) present different algorithms commonly used to solve the VVO, (2) to detail important schemes and techniques needed to deal with the problem, and (3) to introduce real-time VVO concepts and resources.

## 5.1 Metaheuristics for VVO

The choice of the right optimizer or algorithm for a given problem is crucially important. Thus, this subsection is dedicated to present a suitable class of algorithms for VVO problems. They are often employed in literature so as to obtain good solutions in a reasonable timescale with a limited amount of resources.

### 5.1.1 Classical Methods for Optimization

Many classical methods for optimization (e.g., linear programming, mixed integer programming, quadratic programming, etc.) can be used to solve the VVO problem [77]. However, drawbacks may also accompany these methods, such as [23, 127]:

- specific knowledge of the problem may be required, which may not be available;
- convergence to a local optimal solution depends on initial solution;
- an algorithm efficient in solving one problem may not be efficient in solving another problem;
- they are not efficient for problems having discrete search space;
- most algorithms tend to get stuck at suboptimal solutions.

### 5.1.2 Characteristics of Metaheuristic Algorithms

Metaheuristics or approximated methods present several characteristics to deal with the difficulties mentioned before. They represent a class of approximate algorithms, which present a dynamic and/or stochastic search procedure that can be applied to a large number of power system problems [51]. It can be said that they are an evolution of heuristic algorithms, which normally get entrapped into poor local optimal solutions, while the metaheuristics present mechanisms to prevent those situations. One interesting characteristic is the acceptance during the search process of worsening solutions, but as an intelligent strategy to obtain better solutions.

One of the most striking characteristics is their collective (population or swarm) based nature that enables them to find multiple optimal solutions in a run. This population-based approach has a number of advantages [24]:

- it provides a parallel processing power achieving a computationally quick overall search;

- it allows to find multiple optimal solutions, facilitating the solution of multi-modal and multi-objective optimization problems;
- it provides the ability to normalize decision variables, objective and constraint functions within an evolving population using the population-best minimum and maximum values.

Besides the population-based advantages, they also present some characteristics that contribute to their robustness, such as: direct use of coding, blindness to auxiliary information, and randomized operators [31]. Most of metaheuristics work with a coding of the parameter set, not the parameters themselves. Many search techniques require auxiliary information in order to work properly, but it is not essentially required for metaheuristics. They only require an objective function or an evaluation function that translates the quality of the solution candidates to perform an effective evolving search. Some of them, such as the Evolutionary Algorithms (EA) and Simulated Annealing, use random choice (probabilistic transition rules) to guide their search. Higher probabilities are given towards regions of the search space with a perspective of improvement.

Another interesting characteristic is the best performances for multi-modal, nonlinear, non-separable, and non-convex search spaces compared to classical algorithms. This happens by virtue of the capacity to explore the search space. In the case of EA, it is possible to apply a parallel search mechanism combined with the ability to deal with a "black box optimization problem" (i.e., they only require coding and performance measure of the problem due to a set of actions). They can be readily applied to really large dimensional problems and can also show very good performance in optimizing noisy search spaces and imperfect models with uncertainties in the parameters, which are very interesting features for real world problems [31].

In short, the advantages of metaheuristics can be summarized in the following characteristics [51]:

- conceptual simplicity;
- broad applicability;
- outperform classic methods on real problems;
- potential to use knowledge and hybridize with other methods;
- parallelism;
- robust to dynamic changes;
- capability for self-optimization;
- able to solve problems that have unknown solutions.

### 5.1.3 Basic Concepts of EAs

As an illustration of a well applied metaheuristic, a very known EA, the genetic algorithms (GAs) will be described here. They are a popular class of search algorithms based on the mechanics of natural selection and natural genetics [31].
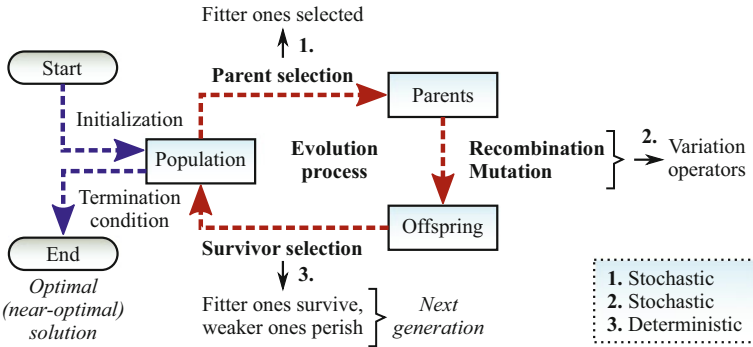
**Fig. 5** General scheme of a GA [26]

The concept of GA was developed by Holland and his students and colleagues in the 1960s and 1970s [74].

Basically, a population of individuals, which encode potential solutions to an optimization problem, evolve over multiple generations by applying natural inspired selection, recombination and mutation operators in such a way as to preserve critical information. Individuals that represent better solutions are given more chances to reproduce than those which represents poorer solutions. Thus, the degree of adaptation of the individuals, called fitness, to their artificial environment determines the probability of their survival for the next generation. As the search goes forward, the population evolves to fitter and fitter solutions, and eventually it converges [18]. The general scheme of a GA is illustrated by the flowchart in Fig. 5.

Indeed, it is important to note that Fig. 5 also outlines a general evolutionary algorithm—a category of modern heuristic search. In general, EAs differ only in technical details related to encoding mechanism, selection process and variation operators [18, 26].

### 5.1.4 Evolutionary Optimization Methods for Solving VVO Problems

Evolutionary computation have been widely employed to solve VVO problems. Some examples of EAs used to tackle such problems are:

- Genetic algorithm (GA) [34, 78, 97];
- Evolutionary particle swarm optimization (EPSO) [72];
- Differential evolutionary particle swarm optimization (DEEPSO) [71];
- Evolutionary programming (EP) [117].

Other optimization models based on recently developed metaheuristics are:

- Particle swarm optimization (PSO) [4, 126];
- Honey bee mating optimization (HBMO) [77];
- Bee swarm optimization (BSO) [123];

- Ant colony optimization (ACO) [76];
- Simulated annealing (SA) [53];
- Tabu search (TS) [96];
- Differential evolution (DE) [40];
- Memetic algorithm (MA) [54];
- Shuffled frog leaping algorithm (SFLA) [61];
- Bacterial foraging algorithm (BFA) [122];
- Teaching-learning-algorithm (TLA) [80];
- Grey wolf optimization (GWO) [13];
- Harmony search (HS) [12].

## *5.2 Volt/Var Mapping*

Volt/Var mapping is the special relation such that a given control setting is associated with a performance of the system operation. So, the VVO problem is formulated as a mapping from the design space $X_f$ to the objective space $Y$, $f_o : X_f \rightarrow Y$, where $X_f \subset X \subseteq \Omega$ represents all possible (feasible) configurations among discrete taps of the $N_D$ devices and continuous values of the $N_C$ controls for $N_H$ hours of operation, $\Omega$ is the universe $\mathbb{N}^{N_D N_H} \mathbb{R}^{N_C N_H}$, $Y \subset \mathbb{R}$ is the distribution system response represented by the performance results of the objective function $f_o$, which is performed by the power flow evaluation associated with further calculations on state variables (Sect. 4.2.2). Thus, the evaluation of the objective function on a decision vector $\mathbf{x} \in X_f$ produces an objective value $y \equiv f(\mathbf{x}) \in Y$.

For 24 h of operation and considering only traditional devices, the cardinality of the controls' combinations in the entire solution space $X$ is given by Mohapatra et al. [75]:

$$|X| = \left( \prod_{i=1}^{N_{Tap}} nt_i \prod_{j=1}^{N_{Cap}} ns_j \right)^{24} \tag{49}$$

where $N_{Tap}$ is the number of tap transformers, $N_{Cap}$ is the number of capacitor banks, $nt_i$ is the number of taps of the transformer $i$, and $ns_j$ is the number of switched units of the capacitor bank $j$.

### 5.2.1 Encoding

The solution candidates, called individuals, must be represented appropriately. Each individual is a decision vector that encodes the optimization problem's variables using a particular data structure.

In fact, the encoding mechanism can be interpreted by two points of view in VVO. On one hand, the encoding of the decision variables is part of the problem

formulation. This means that the controls must be clearly defined and modeled. On the other hand, considering the algorithm procedures, a proper data structure is required to represent the controls' settings and allow their manipulation. So, the encoding of the problem is also part of the strategy to solve the VVO problem. There are many ways to encode the decision variables. It depends on the method that is being proposed.

It is important to note that VVO can have discrete (integer or binary) and continuous control variables, as mentioned in Sect. 4.2.1. So, encoding such information requires special attention, being crucial for the performance of EAs [89]. Some algorithms can be able to deal directly with a certain nature of the variables, whereas others cannot.

**Binary Encoding** Typically in GA, the individuals are held as binary encodings (strings of ones and zeros) of the control variables. In general, the number of digits depends on the number of load levels, the number of devices, and the number of possible settings for each device.

*Example for a Capacitor Representation [105]:* The following substring, formed by two segments, permits to determine the time for switching the capacitor "on" and the duration for keeping it "on":

$$\text{turn it on} \rightarrow 00100|01100 \leftarrow \text{keep it on}$$

In this example, the capacitor is switched "on" at hour 4 and remains "on" for the next 12 h. Another way to represent the same information is to use one bit for each hour indicating the state of the capacitor. The result is capacitor "on" for hour 4 to hour 16:

$$\text{hour1} \rightarrow 000\underline{111111111111}00000000 \leftarrow \text{hour24}$$

*Representing Continuous Variables* Of course, the binary representation can also encode continuous variables. The precision depends on the number of bits used [41]:

$$\frac{(UB - LB)}{2^n - 1} \tag{50}$$

where $UB$ and $LB$ are domain bounds and $n$ is the number of bits per one element of a chromosome.

However, real representation with a binary encoding presents difficulties when dealing with continuous search space with large dimensions [124].

**Real Encoding** In evolution strategies, the solution candidates are encoded as floating point numbers instead of bit strings as in typical GA. Actually, an increasing number of GAs use real-valued (base-10) encodings to support the natural data structure of the problem [19]. This allows a straight way for representing VVO

problems that have continuous control variables. Moreover, according to the authors in [41], results showed that float point representation was faster, consistent and provided a higher degree of precision for GA. As mentioned in Sect. 4.2.1, the majority of the modern and advanced controls possess a continuous nature. This makes the real encoding very attractive for VVO.

### 5.2.2 Dealing with Discrete Variables

A conventional strategy is to treat discrete variables as continuous. This makes the problem ordinary for most of EAs [117]. Whenever the solution process requests such variables, they are rounded off to the closest discrete feasible value.

Other examples of strategies to deal with discrete variables in VVO are:

- **Gray code:** Gray code was employed to encode discrete variables in [33]. It took fewer iterations and consumes less CPU time than the binary GA;
- **Integer representation:** Discrete variables of the set of solutions were mapped through an integer representation in [82]. An integer string was used instead of binary coding to represent value of variables in [78];
- **Approximation:** The binary results for the discrete control variables are approximated considering a vector of continuous values based on their percentage distribution in the interval [0, 1] and converted to binary [4];
- **Penalty-based:** The discrete variables are treated as continuous variables by incorporating sinusoidal functions with a penalty parameter into the objective function of the problem [30].

### 5.2.3 Dealing with Multiple Objectives

Formulating real-world VVO problems may demand more than one objective to optimize. For example, a complete improvement of voltage could mean not only the reduction of the voltage deviation along the feeder, but also the reduction of the voltage unbalance [110]. In other words, there are two objectives to be accounted for.

The most intuitive approach to deal with multiple objectives is the weighted sum approach, which transforms the multi-objective optimization problem into a scalar optimization problem [18]. Basic mechanisms of metaheuristic algorithms can be applied directly without any modification.

Also known as weighted aggregation approach, the objective functions are added together using weighting coefficients in the following form:

$$\min \sum_{i=1}^{k} \omega_i f_i(\mathbf{x}) \tag{51}$$

where $\omega_i$ are the weighting coefficients, $\mathbf{x} = [x_1, x_2, \ldots, x_n]^T$ is the vector of decision variables, and $f_i : \Re^n \to \Re$, $i = 1, 2, \ldots, k$ are the objective functions.

Another very common strategy to handle multiple objectives in VVO is by using the fuzzy optimization method, devised from Fuzzy Theory [120]. In the fuzzy optimization, objective functions are modeled by membership functions and then the overall objective changes into the minimization of the combined value of all membership values. In other words, the result is a fuzzy decision value expressed by the sum of all membership values. So, Eq. (51) turns into:

$$\min \sum_{i=1}^{k} \mu_{f_i(\mathbf{x})} \tag{52}$$

where $\mu_{f_i(\mathbf{x})}$ is the membership function that models the objective $f_i(\mathbf{x})$. To illustrate, this objective can be expressed as trapezoidal membership function [77]:

$$\mu_{f_i(\mathbf{x})} = \begin{cases} 1 & f_i(\mathbf{x}) \leq f_i^{min}, \\ 0 & f_i(\mathbf{x}) \geq f_i^{max}, \\ \frac{f_i^{max} - f_i(\mathbf{x})}{f_i^{max} - f_i^{min}} & f_i^{min} \leq f_i(\mathbf{x}) \leq f_i^{max} \end{cases} \tag{53}$$

where $f_i^{min}$ and $f_i^{max}$ are the minimum and maximum values for the objective function.

Therefore, fuzzy variables can be used to describe the imprecise linguistic expressions related to the VVO objectives [53]:

- the voltage deviation on the secondary bus must be kept "as small as possible";
- the reactive power flow through the main transformer must be kept "as small as possible";
- the total real power loss on feeders must be kept "as little as possible";
- the total switching operation numbers of LTC and capacitors in a day must be kept "as few as possible".

Of course, different membership function shapes can be considered for the objectives. However, the authors in [7] concluded that the bell-shaped membership function produced the best results. Also, there are several ways to combine the single fuzzified values of the objectives. It is possible to combine them, for example, by their sum [53], their minimum (intersection) [77], or their product [7]. An advantage in fuzzy approach is that the objectives are normalized in a way that does not require the use of weighting coefficients [7].

Most solutions for VVO are based on converting the multi-objective problem into a single-objective one by using the weighted aggregation approach or fuzzy optimization method [15]. It is a simplification of the optimization process that makes the VVO easy to implement and efficient for a proper set of settings (weights or membership function parameters).

### 5.2.4 Handling Constraints

A common approach to deal with constraints is to introduce a penalty term into the objective function to penalize constraint violations [54, 80, 102]. For example, if the voltage limits in VVO are violated, the corresponding solution is punished by a penalty value. Thus, throughout the evolution process, infeasible solutions tend to be evolved or replaced by better ones (i.e., solutions that better satisfy the constraints in this case). Obviously, a feasible solution must result in no penalty at all.

VVO is naturally a constrained optimization problem (see Sect. 4.2.3). The following formulation is often used in VVO problems in order to express the complete fitness value—evaluation value of individuals—in which the penalty values are added to the objective function [5]:

$$f_{fit}(\mathbf{x}) = f_o(\mathbf{x}) + \sum_{i=1}^{q} \alpha_i f_c^i(\mathbf{x}) \tag{54}$$

where $f_c^i(\mathbf{x})$ is the $i$th constraint function, $q$ is the number of constraints, and $\alpha_i$ is the penalty weight that receives a large number if constraint is not satisfied or zero, otherwise.

Moreover, the penalty function can also be adaptive (i.e., its weight parameter changes throughout the iterations) and the constraint function term can be replaced by a function that measures the degree of constraint violation [33].

Therefore, another way to represent penalty functions is weighing down infeasible solutions by increasing their fitness values in proportion to their degree of constraint violation [6]. Several penalty functions can be used such as linear penalty functions, quadratic penalty functions or exponential penalty functions, as shown in Fig. 6 [58]. The variable to be dealt with could be a control variable, a state variable or any variable of interest.

In addition, for some VVO problems, "death penalty" is sufficient to approach feasible regions [110]. This technique is very easy to implement, and because of this it is frequently used. The algorithm rejects infeasible individuals (i.e., individuals with some constraint violation) whenever they are generated. Hence, recursive calls are made, until a feasible solution is found. The drawback of this approach is the
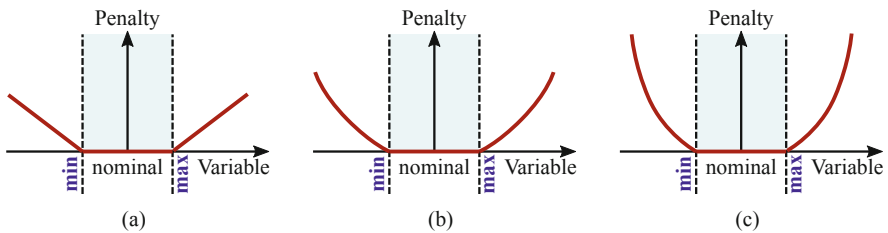


**Fig. 6** Common penalty functions for VVO [58]. (**a**) Linear. (**b**) Quadratic. (**c**) Exponential

elimination of solution candidates which may be obtained from a modification of the corresponding infeasible solution.

### 5.2.5   Stochastic Modeling of Renewable

The integration of RES-based DG—i.e., DG based on renewable energy sources (RES)—introduces uncertainties to the distribution systems due to the variable nature of the primary energy source, i.e., the stochastic variations of the weather conditions influence the generation availability, causing the variation or limiting the available generation. Due to this reason, stochastic models of renewable resources must be developed in order to represent such influence [44]. Moreover, daily load demand is also stochastic due to the heterogeneity of consumers (diverse commercial, residential and industrial consumer types) [62].

The deterministic approaches are not sufficient for this kind of analysis, once the deterministic load flow (DLF) takes into account specific values of power generations and load demands of a fixed network configuration to calculate system states and power flows [16]. In order to address the stochastic behavior of variables, probabilistic analysis can be applied to properly capture uncertainties and to provide a more realistic response of their impact on the distribution network operation [44]. The aim of the probabilistic load flow (PLF) is to take into account these uncertainties by requiring some input variables with probability density functions (PDFs), or cumulative distribution functions (CDFs), to characterize the distribution functions of output random variables, such as node voltages, line flows, etc. [16].

The different techniques applied to solve the probabilistic load flow can be classified into [61]:

- **Analytical methods:** e.g. convolution methods;
- **Approximate techniques:** e.g. First Order Second Moment (FOSM) method and Point Estimate Method (PEM);
- **Numerical methods:** e.g. Monte Carlo simulation (MCS).

Particularly, the load demand and RES generation uncertainties can be modeled through Monte Carlo sampling as a scenario-based stochastic framework. Then, EAs can be applied to solve the series of equivalent deterministic scenarios [80]. There are other examples and strategies using EAs to solve the probabilistic load flow by modeling the uncertainties via analytical methods [33] and approximate techniques [61, 62, 123].

Therefore, Volt/Var control is a complex problem that requires probabilistic analysis of distribution systems to cope with the load/generation uncertainty effects.

## 5.3   Towards the Real-Time VVO

Time considerations are essential to classify VVO schemes. Basically, time-interval and time-computing of the control strategy will determine the kind of VVO scheme.

### 5.3.1   Single Time Snapshot versus Time-Series Simulation

Power flow simulations can be carried out basically in two modes: snapshot or time-series [86]. The snapshot mode is that when the power flow is calculated for a specific operating condition at a certain time. On the other hand, time-series takes into account a series of operating conditions in time order, i.e., it performs sequential-time power flow simulations. For that, it requires more information about the system, such as: load shapes, generation curves and control functions. In general, time-series simulation is carried out as a daily simulation.

Although fixed load model, as a static snapshot problem, has been the focus of many works [48], its applicability does not correspond to practical systems. In fact, load demands vary from time to time. So, advanced applications require optimal coordination scheme considering time-varying load demand [25]. Moreover, in the context of modern distribution systems, the time-dependent nature of RES, which produces variable energy output at different timing, can also be considered in the time-interval control strategy [6].

**Daily Load Curves** The majority of applications uses load forecasting, in the form of daily load curves, for Volt/Var control. More specifically, VVO is typically associated with the optimal hourly adjustment of the Volt/Var devices based on short-term load forecasting. In general, the daily load curve is decomposed into hourly sequential of constant load levels [25]. But, it is also possible to decompose the daily load forecast into several sequential load levels so that the switching operations of OLTC at substations may be reduced [34].

Short-term load forecasting refers to the prediction of load demand in electric power systems for the time period of few hours up to 1 week. It is crucial for optimal Volt/Var control planning. All decisions rely on this forecast as it is an input for day-ahead scheduling. Modern load forecasting techniques are available to provide highly accurate forecasts [105]. They can be classified into four categories [103]:

- Statistical technique;
- Artificial intelligence (AI) technique;
- Knowledge based expert systems;
- Hybrid techniques.

    Different load profiles are obtained for a typical day in a season (winter, spring, fall and summer) [118] and for typical consumers' classes (residential, commercial and industrial) [42, 65].

    Furthermore, the daily operations of Volt/Var devices are greatly affected by different types of loads and their models [94]. EV is an example of modern devices in which the charging strategy can be defined by load profiles. The authors in [65] considered EV load curves for different consumers (residential, workplace and commercial) in a VVO engine.

**Daily RES Generation** Besides the 24-h load demand, time-varying coordination in VVO can also consider RES generation profile [52]. RES occurs mainly in the form of hourly active power output of solar photovoltaics (PV) [17, 97] and wind farm (WF) generations [62, 113].

**Daily Energy Prices** Cost-based solutions can incorporate the daily energy price variations to investigate an economic plan for the Volt/Var control problem [62, 76].

### 5.3.2 Planning and Real-Time Applications

Volt/Var control can be designed for either planning or real-time operations of power distribution systems [28]. Scheduled (or planning) operation programs day ahead schedule based on demand and renewable power generation forecasting processed by robust algorithms. Whereas, in real-time operation, actions and commands occur in short time periods based on communication signals, state-estimation algorithms and decision support systems. Both operations are supported by the IVVC framework.

**Planning Applications** Daily operation planning consists in employing day-ahead load forecast, based on processing historical records, to feed Volt/Var Optimization engine so that optimal control may be dispatched 1 day in advance. Also, if RES is deployed in the distribution system, its output generation forecast must be added as an input to the VVO engine. However, the major drawback of this approach is related to the need of accuracy for the model. In addition, as an offline solution, it lacks robustness to maintain optimal operation of the system for different scenarios (uncertainty of loads, fluctuation of RES, etc.).

**Real-Time Applications** Distribution utilities are gradually integrating the use of advanced metering, two-way communication and automation technologies into the distribution systems [84]. The result is more sensors, communication, computation, and control, transforming the conventional grid into a smart grid [9]. Consequently, the operation of the grid is evolving towards more optimization, real-time application, and intelligent algorithms.

    With this in mind, Volt/Var control has much potential to become more advanced as a smart grid-based [68]. According to [64] there is a gap between conventional

VVO with offline techniques and smart-grid-based VVO which involves real-time integrated solutions.

Besides the advanced information technologies, new control and automation techniques are required to carry out the smart distribution system management based on Volt/Var optimization. As mentioned, modern technologies for monitoring and automated control are spreading in distribution systems. The deployment of AMI has provided visibility for distribution system nodes due to its widespread communication network and system-wide smart grid sensing devices [67]. It has created considerable amount of data that can be used in optimization applications [68]. The analysis of smart meters data can provide power estimation load profile to be incorporated into the power flow model calculations [36]. In other words, real-time sample values from smart meters could be used to construct real-time load profiles [64]. Therefore, a distribution system state estimation (DSSE) assists Volt/Var control by providing an accurate on-line model [85]. Hence, advanced DMS can be responsible for finding a centralized solution that coordinates all devices in accordance to a real-time Volt/Var optimization.

Therefore, this category of control requires a higher level of distribution system automation and more hardware and software support [34]. The authors in [22] summarized the following requirements for real-time implementation of coordinated Volt/Var control:

- three-phase unbalanced power flow to optimize and validate the operation;
- centralized control system with DMS and support for SCADA;
- real-time data record of the advanced metering infrastructure (AMI) in the field equipment;
- remotely controllable devices with commutable controllers;
- efficient and modern communication system.

### 5.3.3    The Extent of the Centralized Control

Most approaches recommended by different utilities and/or literatures recently consist in a centralized control [65]. In fact, the coordinated Volt/Var control searches for a centralized solution that produces systemic optimizing effects in the distribution networks, which is not possible with only local and uncoordinated actions [22]. For this reason, a centralized control requires a widespread communication infrastructure in the system in order to make possible the implementation of the operations. The control and monitoring of the system is performed by the central controller (e.g., DMS), which receives information of termination points (from AMI and/or MDMS), execute the optimization algorithm and then transmit back the best possible settings to the Volt/Var devices in the field through existing downstream pipes, such as SCADA network [66].

It is important to mention that the centralized control has two main topologies [66, 68]:

- **Network-based:** the processing system is placed in a central controller unit, which typically resides in the so called "Utility Back-Office", and it controls the entire network of the utility;
- **Substation or feeder-based:** VVO engines are located at the medium voltage distribution substation to optimize the operation of Volt/Var components on each feeder.

The main challenge of network-based topology would be the huge amount of data that need to be transported from AMI to "back-office" and then from VVO to control devices throughout distribution network substations and feeders [65]. On the other hand, substation-based or feeder-based topology captures only required data of AMI locally leading to decrease the risk of "data tsunami" as well as to avoid high AMI cost [66]. Although this architecture works centrally in the substation, from the point of view of a wide area, it is more like a decentralized control, dealing with fewer nodes. That is why, sometimes the first topology is refereed as Centralized-VVO, whereas, the second one as Decentralized-VVO. Anyway, the VVO works very well for both topologies regardless of the degree of data centralization.

### 5.3.4 Co-Simulation

Real-time VVO inherently depends on communication networks. A fully functional real-time system integrates the VVO engine with the communication channel and the monitoring platform [67]. So, a co-simulation platform for VVO application must cover the practical integration challenges related to the communications between the field instruments and the environments where the algorithms are executed [66]. In this case, the performance of the communication system is considered into the co-simulation platform by its interaction with the VVO [36].

## 6 Numerical Example

The purpose of the following example is to illustrate the VVO's capability to improve the performance and power quality of the distribution system operation in the presence of RES-based DG.

## 6.1 Statement of the Problem

### 6.1.1 Problem Formulation

The setting of the Volt/Var equipment for optimal system operation is determined by the following formulation:

$$\text{minimize} \quad f_L^t \equiv \sum_{k=1}^{N_{br}} R_k |I_k^t|^2 \tag{55a}$$

$$\text{subject to} \quad \Delta P = P_n^{spec} - P_n^{calc} \tag{55b}$$

$$\Delta Q = Q_n^{spec} - Q_n^{calc} \tag{55c}$$

$$V_{min} \leq V_n^t \leq V_{max} \tag{55d}$$

$$PF_S^{min} \leq PF_S^t \tag{55e}$$

$$T_d^{min} \leq T_d^t \leq T_d^{max} \tag{55f}$$

where $f_L^t$ is the losses of the system at hour $t$, $N_{br}$ is the number of branches, $R_k$ is the resistance of the $k$th branch, $I_k^t$ is the current of the $k$th branch at hour $t$, $\Delta P$ and $\Delta Q$ are the active and reactive power injection estimation errors, $P_n^{spec}$ and $P_n^{calc}$ are the specified and calculated active power injection at node $n$, $Q_n^{spec}$ and $Q_n^{calc}$ are the specified and calculated reactive power injection at node $n$, $V_n^t$ is the voltage of the node $n$ at hour $t$, $V_{min}$ and $V_{max}$ are the acceptable voltage limits, $PF_S^{min}$ is the minimum allowable power factor of the substation, $PF_S^t$ is the current power factor of the substation at hour $t$, $T_d^t$ is the setting for each Vol/Var device $d$ at hour $t$, and $T_d^{min}$ and $T_d^{max}$ are the setting limits for the device $d$.

The objective function outlines the goal, per hour, designed to reduce the losses of the system (55a). Moreover, the optimization problem is subjected to constraints which ensure security, quality and reliability of the system operation. They are: active and reactive power injection balances (55b, 55c), node voltage magnitude limits (55d), minimum substation power factor (55e), and control devices capacity (55f).

### 6.1.2 Power Quality Standard

The service standard for the acceptable voltage limits is established by the Brazilian National Agency for Electric Energy (ANEEL) as $V_{min} = 0.93$ pu and $V_{max} = 1.05$ pu [10]. These bounds refer to the connecting points in which the nominal voltage is greater than 1 kV and less than 69 kV. The same standard also establishes that the PF control must be carried out by permanent measurement at these voltage levels, ensuring a PF greater than 0.92.

### 6.1.3  Solution Algorithm

The solution of the proposed optimization problem is achieved by running a GA implemented in Python. This algorithm interacts constantly with the OpenDSS for power flow evaluations throughout the optimization process.

Power balance constraints are met internally by the OpenDSS procedures. As the optimization algorithm selects only allowed values for the decision variables, the control devices capacity is also satisfied. Finally, constraint violations of voltage and PF are added as linear penalty functions weighing down infeasible solutions.

Real encoding is used in the GA. The discrete variables are treated as continuous and, whenever requested, they are rounded off to the closest discrete value. For the variation operators, the algorithm employs BLX-$\alpha$ crossover and a combination of random and Gaussian mutation.

### 6.1.4  Base System

The proposed method has been tested in the IEEE 123 node test feeder [46]. The feeder's nominal voltage is 4.16 kV. It presents unbalanced loading with all combinations of load types, totalizing 3450 kW + 1900 kvar. This system is characterized by voltage drop problems, representing a good test for the coordinated operation of the voltage regulator devices.

### 6.1.5  Distributed Generation: PV Generation

The system must accommodate the connection of a distributed generator at bus 76. A photovoltaic generation capacity of 1.2 MVA is considered with unity power factor.

### 6.1.6  Daily Curves

The daily load curve was taken from [42] and the capacity factor of photovoltaic generation was selected from persistent clear sky condition of a typical day in Brazilian Northeast region [39]. They are presented in Fig. 7a, b, respectively.

## 6.2  Case Study

### 6.2.1  Volt/Var Control Approaches

The Volt/Var control enhancement can be portrayed by different approaches as the control tends to be more centralized and coordinated. Thus, the following approaches will be considered:
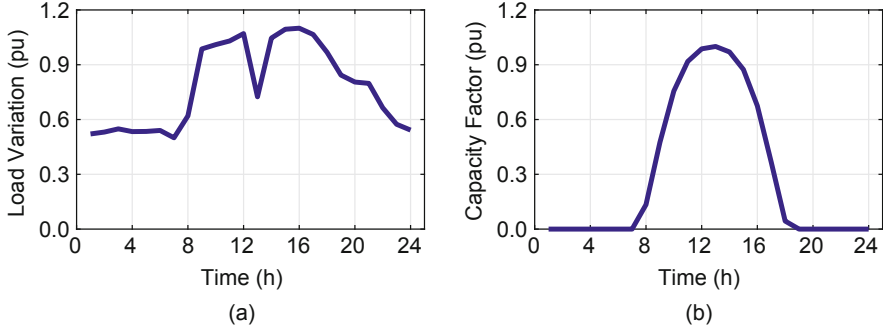
**Fig. 7** Daily curves. (**a**) Daily load. (**b**) Capacity factor of DG

1. **VVC-NC:** It is the conventional local control of the IEEE 123 with no capacitor (NC) in the substation. Only the voltage regulators perform the Volt/Var control (VVC);
2. **VVC-SC:** A 300 kvar switched capacitor is added to the substation. So, besides the voltage regulators, the VVC is also equipped with a switched capacitor (SC) typically controlled based on the PF of the utility substation;
3. **VVO-TD:** It is the Volt/Var optimization (VVO) defined in Sect. 6.1 for reducing losses and ensuring important constraints. The optimization problem presents eight decision variables, which are the following traditional devices (TD):

   - **step voltage regulators:** the tap ratio is taken from 0.90 to 1.10 pu in steps of 0.00625 pu. Specifically,

     – SVR.1 is gang-operated (the taps change at the same time);
     – SVR.2 is an individual phase regulator at phase A;
     – SVR.3 has independent tap changing at phases A and C;
     – SVR.4 has independent tap changing at all phases;

   - **switched capacitor:** the reactive power is taken from 0 to 300 kvar in modules of 150 kvar.

4. **VVO-IVC:** PV inverters can be used to absorb or inject reactive power and so to control feeder voltage [17]. Therefore, this enhanced VVO with inverter var control (IVC) considers the reactive power of PV inverters as an additional decision variable to improve the power quality of the distribution grid. The maximum injected (or absorbed) reactive power ($Q_{PV}$) depends on the active power generated by the PV plant ($P_{PV}$) and the power rating of the inverter ($S_{PV}$). Therefore, the rating of the inverter is another constraint to be satisfied by the VVO:

$$-\sqrt{S_{PV}^2 - (P_{PV}^t)^2} \leq Q_{PV}^t \leq \sqrt{S_{PV}^2 - (P_{PV}^t)^2} \tag{56}$$
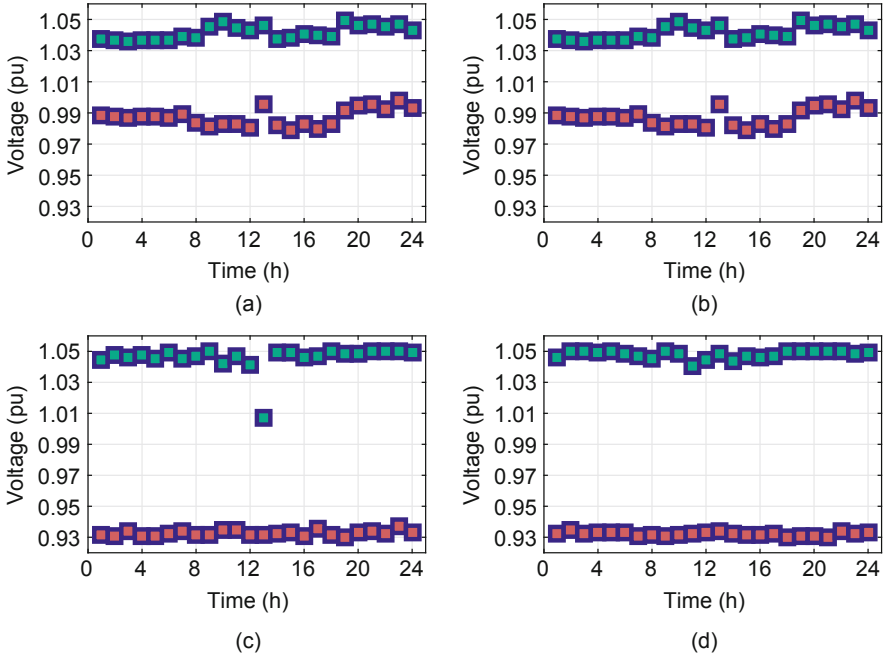
**Fig. 8** Minimum and maximum voltages among all nodes of the system for each hour. (**a**) VVC-NC. (**b**) VVC-SC. (**c**) VVO-TD. (**d**) VVO-IVC

### 6.2.2 Node Voltages

The node voltages must be within the acceptable limits. This is the basic definition of the Volt/Var control. Figure 8 shows the minimum and maximum voltages among all nodes of the system for each hour. As can be seen, all approaches are able to fulfill this fundamental requirement for the grid operation.

### 6.2.3 Substation Power Factor

Figure 9 shows the substation power factor for each control approach. In Fig. 9a, VVC-NC presents PF below the minimum allowable limit during the period of higher PV generation. By adding a switched capacitor in the substation, it is possible to correct the PF. Thus, the resulting control, VVC-SC in Fig. 9a, switches ON the capacitor when PF is below 0.92. Figure 9b proves that PF constraint are satisfied by both VVO approaches, VVO-TD and VVO-IVC. Although the formulation only shapes the constraint, the results point a greater PF along the day when the inverter var control is considered into the VVO.
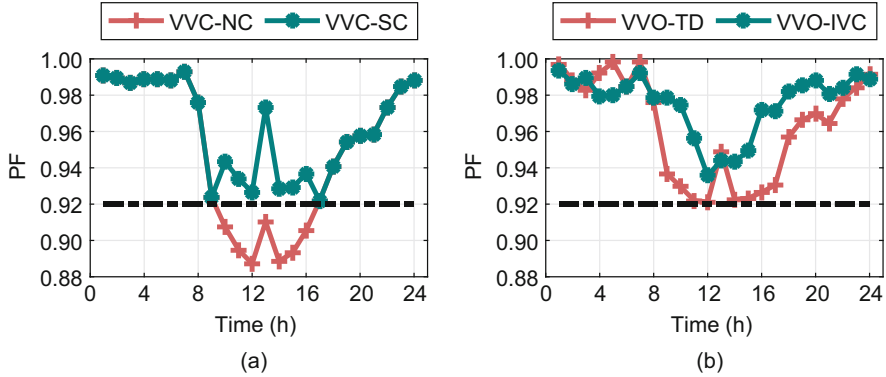
**Fig. 9** Substation power factor for each hour. (**a**) VVC. (**b**) VVO

### 6.2.4 Losses of the System

Figure 10 depicts the losses of the system for each hour. Figure 10a shows that the losses are quite similar between VVC-NC and VVC-SC. So, considering VVC as the base case, VVO is able to reduce the losses of the system for each hour. Figure 10b presents the loss reduction produced by VVO when comparing with the base case. The loss reduction of the VVO-TD is within the range of 2.37–8.65%, whereas the VVO-IVC reaches values within the range of 3.35–10.71%. Therefore, both VVO approaches reduce losses, but VVO-IVC achieves better loss reduction, mainly during the higher PV generation.

### 6.2.5 Inverter var Control

If the active power generated from the PV panels is smaller than the PV inverter rated power, the PV inverter can be controlled to inject or to absorb reactive power [17]. Figure 11 indicates this principle, showing that the constraint related to the PV inverter rated power is satisfied.

### 6.2.6 Conclusions

The results showed that modeling the Volt/Var control as an optimization problem can greatly improve the performance of the distribution system operation. An addition of a switched capacitor in the substation was needed to correct the PF, but even so the local control (VVC) was not able to reduce the losses of the system. On the other hand, the optimal coordination provided by the VVO achieved the main goal of reducing losses and ensuring important constraints of the system operation. Furthermore, the enhanced VVO, which includes the inverter var control,
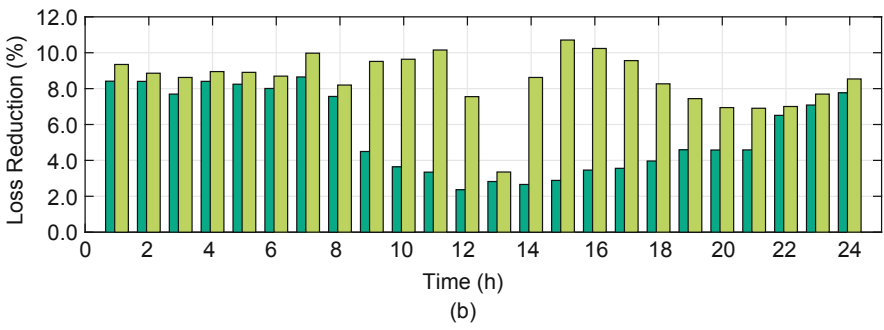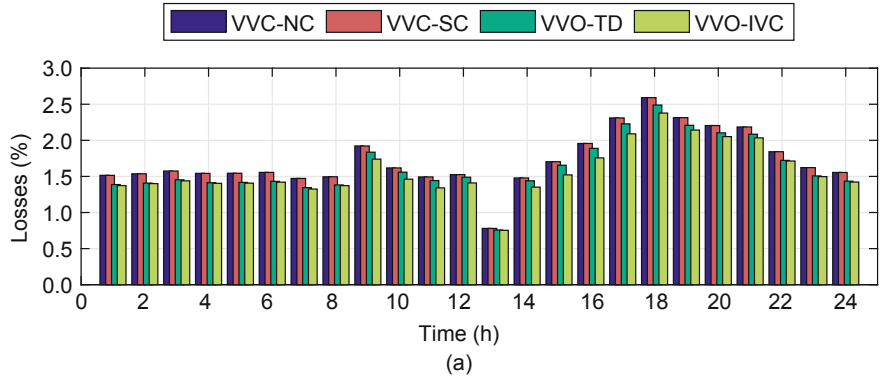
**Fig. 10** Performance for losses. (**a**) Losses of the system. (**b**) Loss reduction compared to VVC
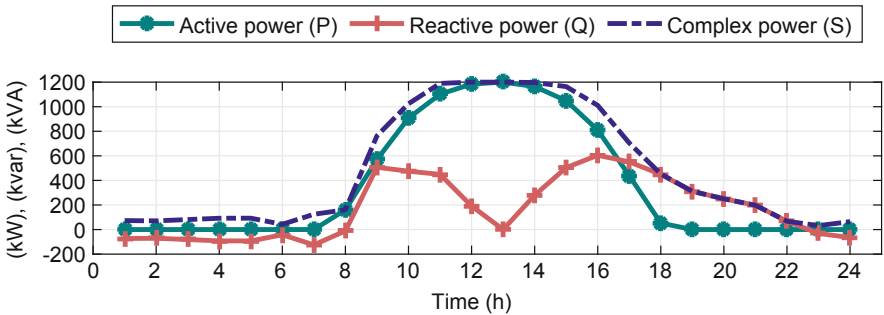


**Fig. 11** Active power, reactive power and complex power of the PV inverter

further improved the results, raising the PF close to unity and achieving better loss reduction.

This case study did not consider the switching costs of the devices, being a suggestion to be regarded in future works. Another important issue to highlight is that the average of the results was obtained for 20 executions of the algorithm. It is a common practice in the VVO to make several runs of the optimization algorithm

and then to consider the mean value of the results. This technique aids to eliminate the influence of the initial conditions of the problem in the results.

## 7 Concluding Remarks

In summary, due to the smart grid context, tackling the new paradigms on distribution management networks depends upon updated Volt/Var control strategies to face the new operating scenarios challenges and to make use of the technological advances in infrastructure. Volt/Var control trend goes beyond accommodating new smart grid features—such as ES, EV, and DER—just to minimize impacts, but further to benefit optimally from them. So, advanced and innovative solutions may take advantage of grid modernization systems to optimize the distribution system performance and accomplish a variety of business goals.

### 7.1 Trend Challenges and Open Issues

The high penetration of DERs introduces several challenges for VVO, but, from an envisioned perspective, it creates several opportunities because of the potential benefits of DER. Indeed, many works have demonstrated this. Revised IEEE 1547 allows DER to provide voltage regulation capability by varying real and reactive power [38]. Thus, the availability of DERs—generators and energy storage technologies—can make smart grid-based VVO more affordable and practical [68]. Furthermore, the DMS should take advantage of the advanced DER control capabilities for improving the reliability, efficiency, performance and overall quality of service for the electric distribution customers [109].

Studies has proven that new EV inverter technologies can enable EVs to inject reactive power to the grid while battery is under charging operation [47]. So, this feature is a potential advantage on VVO, leading to rise the distribution capacity, improvement in voltage profile, power loss reduction, and minimization of switched CBs' operation costs [63].

Therefore, VVO solutions are moving towards using new Volt/Var control devices [68], as shown in Sect. 4.2.1. In terms of optimization, these modern devices deployed in the grid means more control variables to be optimized and constraints to be met. On the one hand VVO gains more capability to accomplish its duty, but on the other hand the optimization problem becomes more complex with high dimension search space requiring more efficient algorithms to solve it.

Moreover, formulating real-world problems as reliable as possible means to consider multi-objectives which are usually in conflict with each other. This kind of formulation is known as multi-objective optimization problems (MOPs). Most MOPs do not have a single solution, but a set of solutions which are trade-offs (or good compromises) among the objectives [18]. This set, called Pareto optimal set,

could represent optimal Volt/Var control solutions taking into account two or more objectives at the same time.

A step forward towards electric utility smart grid will require advanced VVO techniques able to work dynamically in real-time applications. With the aid of AMI, real-time VVO could lead to a more accurate control and improve significantly the system level of performance and efficiency [68]. Accordingly, real-time applications demand advanced speed-up strategies for solving VVO. Besides, to achieve effective interoperability, two-way communication network must take place.

Finally, as modern distribution systems display an increasing penetration of RES-based DGs, VVO strategy must be robust enough to deal with the power fluctuations of renewable generating resources so that the operations do not result in unacceptable service levels [111]. The active outputs of renewable DGs fluctuate dramatically due to their inherent volatility and intermittency. This could demand management of power and voltage fluctuations. Furthermore, the VVO must also be able to manage voltage problems caused by reverse power due to the integration of renewables [57]. In sum, VVO has this further role of allowing increased amounts of DG without adversely impacting power quality.

Future VVO solutions are based on an automated computed-assisted decision making framework that fully coordinates and integrates a mix of traditional controls and smart grid technologies in order to accomplish a comprehensive enhancement of the grid operation. It should make progress by using grid modernization to provide more efficient and reliable energy conservation and optimization solutions towards the improvement of welfare produced by the use of electricity [81]. To achieve that, the development of advanced methods and algorithms for solving VVO should be a key challenge for distribution network planners. Although evolutionary algorithms have been highly used to solve these problems, new intelligent strategies and systems will be necessary in future distribution networks.

This chapter has addressed technical and operational aspects regarding the design of optimal Volt/Var control in a centralized framework. Regulatory and market issues have not been focused, since they could require a wider picture of the power system.

## References

1. Agüero, J.R.: Improving the efficiency of power distribution systems through technical and non-technical losses reduction. In: 2012 IEEE PES Transmission and Distribution Conference and Exposition (T&D), pp. 1–8. IEEE, Orlando (2012). https://doi.org/10.1109/TDC.2012.6281652
2. Aguero, J.R., Khodaei, A.: Grid modernization, DER integration and utility business models—trends challenges. IEEE Power Energ. Mag. **16**(2), 112–121 (2018). https://doi.org/10.1109/MPE.2018.2811817
3. Ahmadi, H., Marti, J.R., Dommel, H.W.: A framework for volt-var optimization in distribution systems. IEEE Trans. Smart Grid **6**(3), 1473–1483 (2015). https://doi.org/10.1109/TSG.2014.2374613

4. Anilkumar, R., Devriese, G., Srivastava, A.K.: Voltage and reactive power control to maximize the energy savings in power distribution system with wind energy. IEEE Trans. Ind. Appl. **54**(1), 656–664 (2018). https://doi.org/10.1109/TIA.2017.2740850
5. Anwar, A., Mahmood, A.N., Taheri, J., Tari, Z., Zomaya, A.Y.: HPC-based intelligent Volt/VAr control of unbalanced distribution smart grid in the presence of noise. IEEE Trans. Smart Grid **8**(3), 1446–1459 (2017). https://doi.org/10.1109/TSG.2017.2662229
6. Aryanezhad, M.: Management and coordination of LTC, SVR, shunt capacitor and energy storage with high PV penetration in power distribution system for voltage regulation and power loss minimization. Int. J. Electr. Power Energy Syst. **100**, 178–192 (2018). https://doi.org/10.1016/j.ijepes.2018.02.015
7. Augugliaro, A., Dusonchet, L., Favuzza, S., Sanseverino, E.R.: Voltage regulation and power losses minimization in automated distribution networks by an evolutionary multiobjective approach. IEEE Trans. Power Syst. **19**(3), 1516–1527 (2004). https://doi.org/10.1109/TPWRS.2004.825916
8. Borghetti, A., Napolitano, F., Nucci, C.A.: Volt/Var optimization of unbalanced distribution feeders via mixed integer linear programming. Int. J. Electr. Power Energy Syst. **72**, 40–47 (2015). https://doi.org/10.1016/j.ijepes.2015.02.009. The Special Issue for 18th Power Systems Computation Conference.
9. Bose, A.: Smart transmission grid applications and their supporting infrastructure. IEEE Trans. Smart Grid **1**(1), 11–19 (2010). https://doi.org/10.1109/TSG.2010.2044899
10. Brazilian Electricity Regulatory Agency (ANEEL): Procedures for Distribution of Electrical Energy in the National Electric System (PRODIST) (2018). http://www.aneel.gov.br/modulo-8 (in Portuguese)
11. Capitanescu, F., Bilibin, I., Ramos, E.R.: A comprehensive centralized approach for voltage constraints management in active distribution grid. IEEE Trans. Power Syst. **29**(2), 933–942 (2014). https://doi.org/10.1109/TPWRS.2013.2287897
12. Ceylan, O., Liu, G., Xu, Y., Tomsovic, K.: Distribution system voltage regulation by distributed energy resources. In: 2014 North American Power Symposium (NAPS), pp. 1–5. IEEE, Pullman (2014). https://doi.org/10.1109/NAPS.2014.6965466
13. Ceylan, O., Liu, G., Tomsovic, K.: Coordinated distribution network control of tap changer transformers, capacitors and PV inverters. Electr. Eng. **100**(2), 1133–1146 (2018). https://doi.org/10.1007/s00202-017-0563-x
14. Chang, N.E.: Determination of primary-feeder losses. IEEE Trans. Power Apparatus Syst. **PAS-87**(12), 1991–1994 (1968). https://doi.org/10.1109/TPAS.1968.292159
15. Cheng, S., Chen, M.Y.: Multi-objective reactive power optimization strategy for distribution system with penetration of distributed generation. Int. J. Electr. Power Energy Syst. **62**, 221–228 (2014). https://doi.org/10.1016/j.ijepes.2014.04.040
16. Chen, P., Chen, Z., Bak-Jensen, B.: Probabilistic load flow: a review. In: 2008 Third International Conference on Electric Utility Deregulation and Restructuring and Power Technologies, pp. 1586–1591. IEEE, Nanjing (2008). https://doi.org/10.1109/DRPT.2008.4523658
17. Chen, Y., Strothers, M., Benigni, A.: All-day coordinated optimal scheduling in distribution grids with PV penetration. Electr. Power Syst. Res. **164**, 112–122 (2018). https://doi.org/10.1016/j.epsr.2018.07.028
18. Coello, C.A.C., Lamont, G.B., Veldhuizen, D.A.V.: Evolutionary Algorithms for Solving Multi-Objective Problems, 2nd edn. Genetic and Evolutionary Computation Series. Springer, New York (2007). https://doi.org/10.1007/978-0-387-36797-2
19. Coley, D.A.: An Introduction to Genetic Algorithms for Scientists and Engineers. World Scientific, River Edge (1999)
20. Daratha, N., Das, B., Sharma, J.: Coordination between OLTC and SVC for voltage regulation in unbalanced distribution system distributed generation. IEEE Trans. Power Syst. **29**(1), 289–299 (2014). https://doi.org/10.1109/TPWRS.2013.2280022
21. Das, B. (ed.): Power distribution automation. In: No. 75 in IET Power and Energy Series, 1st edn. The Institution of Engineering and Technology, London (2016)

22. de Mello, A.P.C., Pfitscher, L.L., Bernardon, D.P.: Coordinated Volt/VAr control for real-time operation of smart distribution grids. Electr. Power Syst. Res. **151**, 233–242 (2017). https://doi.org/10.1016/j.epsr.2017.05.040

23. Deb, K.: Multi-Objective Optimization using Evolutionary Algorithms, 1st edn. Wiley-Interscience series in systems and optimization. Wiley, Chichester (2001)

24. Deb, K.: Multi-objective optimisation using evolutionary algorithms: an introduction. In: Wang, L., Ng, A.H.C., Deb, K. (eds.) Multi-Objective Evolutionary Optimisation for Product Design and Manufacturing, Chap. 1, pp. 3–34. Springer, London (2011). https://doi.org/10.1007/978-0-85729-652-8_1

25. Deng, Y., Ren, X., Zhao, C., Zhao, D.: A heuristic and algorithmic combined approach for reactive power optimization with time-varying load demand in distribution systems. IEEE Trans. Power Syst. **17**(4), 1068–1072 (2002). https://doi.org/10.1109/TPWRS.2002.804973

26. Eiben, A.E., Smith, J.E.: Introduction to Evolutionary Computing, 2nd edn. Natural Computer Series. Springer, Berlin (2015). https://doi.org/10.1007/978-3-662-44874-8

27. Electric Power Research Institute: Advanced Metering Infrastructure (AMI). EPRI, Palo Alto (2007). https://www.ferc.gov/CalendarFiles/20070423091846-EPRI%20-%20Advanced%20Metering.pdf

28. Evangelopoulos, V.A., Georgilakis, P.S., Hatziargyriou, N.D.: Optimal operation of smart distribution networks: A review of models, methods and future research. Electr. Power Syst. Res. **140**, 95–106 (2016). https://doi.org/10.1016/j.epsr.2016.06.035

29. Feng, X., Peterson, W., Yang, F., Wickramasekara, G.M., Finney, J.: Smarter grids are more efficient: voltage and var optimization reduces energy losses and peak demands. ABB Rev. **2009**(3), 33–37 (2009). http://search-ext.abb.com/library/Download.aspx?DocumentID=9AKK104295D7260&LanguageCode=en&DocumentPartId=&Action=Launch

30. Ferreira, E.C., Neto, M.S.I., Asada, E.N.: Metaheuristic strategies for solving the optimal reactive power dispatch with discrete variables. In: 2016 12th IEEE International Conference on Industry Applications (INDUSCON), pp. 1–6. IEEE, Curitiba (2016). https://doi.org/10.1109/INDUSCON.2016.7874516

31. Goldberg, D.E.: Genetic Algorithms in Search, Optimization, and Machine Learning, 1st edn. Addison-Wesley, Reading (1989)

32. Gonen, T.: Electric Power Distribution Engineering, 3rd edn. CRC Press, Boca Raton (2014)

33. Hong, Y., Luo, Y.: Optimal VAR control considering wind farms using probabilistic load-flow and gray-based genetic algorithms. IEEE Trans. Power Deliv. **24**(3), 1441–1449 (2009). https://doi.org/10.1109/TPWRD.2009.2016625

34. Hu, Z., Wang, X., Chen, H., Taylor, G.A.: Volt/VAr control in distribution systems using a time-interval based approach. IEE Proc. Gener. Transm. Distrib. **150**(5), 548–554 (2003). https://doi.org/10.1049/ip-gtd:20030562

35. Huda, A.S.N., Zivanovic, R.: Large-scale integration of distributed generation into distribution networks: Study objectives, review of models and computational tools. Renew. Sust. Energ. Rev. **76**, 974–988 (2017). https://doi.org/10.1016/j.rser.2017.03.069

36. Ibrahim, M., Salama, M.M.A.: Smart distribution system volt/VAR control using distributed intelligence and wireless communication. IET Gener. Transm. Distrib. **9**(4), 307–318 (2015). https://doi.org/10.1049/iet-gtd.2014.0513

37. IEEE Guide for Application of Shunt Power Capacitors. IEEE Std 1036-2010 (Revision of IEEE Std 1036-1992), pp. 1–97 (2011). https://doi.org/10.1109/IEEESTD.2011.5703189

38. IEEE Standard for Interconnection and Interoperability of Distributed Energy Resources with Associated Electric Power Systems Interfaces. IEEE Std 1547-2018 (Revision of IEEE Std 1547-2003), pp. 1–138 (2018). https://doi.org/10.1109/IEEESTD.2018.8332112

39. INPE: SONDA—Sistema Nacional de Organização de Dados Ambientais [National Organization System of Environment Data]. Instituto Nacional de Pesquisas Espaciais, São José dos (2016). http://sonda.ccst.inpe.br/index.html. In Portuguese

40. Iwata, S., Fukuyama, Y.: Verification of dependability on parallel differential evolution based voltage and reactive power control. IFAC-PapersOnLine **49**(27), 140–145 (2016). https://doi.org/10.1016/j.ifacol.2016.10.733. IFAC Workshop on Control of Transmission and Distribution Smart Grids CTDSG 2016

41. Janikow, C.Z., Michalewicz, Z.: An experimental comparison of binary and floating point representations in genetic algorithms. In: Belew, R.K., Booker, L.B. (eds.) Proceedings of the 4th International Conference on Genetic Algorithms (ICGA), pp. 31–36. Morgan Kaufmann, San Diego (1991)

42. Jardini, J.A., Tahan, C.M.V., Gouvea, M.R., Ahn, S.U., Figueiredo, F.M.: Daily load profiles for residential, commercial and industrial low voltage consumers. IEEE Trans. Power Deliv. **15**(1), 375–380 (2000). https://doi.org/10.1109/61.847276

43. Jenkins, N., Allan, R., Crossley, P., Kirschen, D., Strbac, G.: Embedded generation. In: No. 31 in IET Power and Energy Series, 1st edn. The Institution of Engineering and Technology, London (2000)

44. Keane, A., Ochoa, L.F., Borges, C.L.T., Ault, G.W., Alarcon-Rodriguez, A.D., Currie, R.A.F., Pilo, F., Dent, C., Harrison, G.P.: State-of-the-art techniques and challenges ahead for distributed generation planning and optimization. IEEE Trans. Power Syst. **28**(2), 1493–1502 (2013). https://doi.org/10.1109/TPWRS.2012.2214406

45. Kersting, W.H.: Distribution system modeling and analysis. In: The Electric Power Engineering Series, 1st edn. CRC Press, Boca Raton (2001)

46. Kersting, W.H.: Radial distribution test feeders. In: 2001 IEEE Power Engineering Society Winter Meeting. Cat. No.01CH37194, vol. 2, pp. 908–912. IEEE, Columbus (2001). https://doi.org/10.1109/PESW.2001.916993

47. Kisacikoglu, M.C., Ozpineci, B., Tolbert, L.M.: Examination of a PHEV bidirectional charger system for V2G reactive power compensation. In: 2010 Twenty-Fifth Annual IEEE Applied Power Electronics Conference and Exposition (APEC), pp. 458–465. IEEE, Palm Springs (2010). https://doi.org/10.1109/APEC.2010.5433629

48. Krok, M.J., Genc, S.: A coordinated optimization approach to Volt/VAr control for large power distribution networks. In: Proceedings of the 2011 American Control Conference, pp. 1145–1150. IEEE, San Francisco (2011). https://doi.org/10.1109/ACC.2011.5991606

49. Kulmala, A., Repo, S., Järventausta, P.: Coordinated voltage control in distribution networks including several distributed energy resources. IEEE Trans. Smart Grid **5**(4), 2010–2020 (2014). https://doi.org/10.1109/TSG.2014.2297971

50. Kundur, P.: Power System Stability and Control, 1st edn. McGraw-Hill, New York (1994)

51. Lee, K.Y., El-Sharkawi, M.A. (eds.): Modern Heuristic Optimization Techniques: Theory and Applications to Power Systems. Wiley, Hoboken (2008)

52. Li, P., Ji, H., Wang, C., Zhao, J., Song, G., Ding, F., Wu, J.: Coordinated control method of voltage and reactive power for active distribution networks based on soft open point. IEEE Trans. Sustain. Energy **8**(4), 1430–1442 (2017). https://doi.org/10.1109/TSTE.2017.2686009

53. Liang, R.H., Wang, Y.S.: Fuzzy-based reactive power and voltage control in a distribution system. IEEE Trans. Power Deliv. **18**(2), 610–618 (2003). https://doi.org/10.1109/TPWRD.2003.809740

54. Liang, R.H., Chen, Y.K., Chen, Y.T.: Volt/Var control in a distribution system by a fuzzy optimization approach. Int. J. Electr. Power Energy Syst. **33**(2), 278–287 (2011). https://doi.org/10.1016/j.ijepes.2010.08.023

55. Liu, M.B., Canizares, C.A., Huang, W.: Reactive power and voltage control in distribution systems with limited switching operations. IEEE Trans. Power Syst. **24**(2), 889–899 (2009). https://doi.org/10.1109/TPWRS.2009.2016362

56. Macedo, L.H., Franco, J.F., Rider, M.J., Romero, R.: Optimal operation of distribution networks considering energy storage devices. IEEE Trans. Smart Grid **6**(6), 2825–2836 (2015). https://doi.org/10.1109/TSG.2015.2419134

57. Madrigal, M., Uluski, R.: Practical Guidance for Defining a Smart Grid Modernization Strategy: The Case of Distribution. The World Bank, Washington (2015). https://doi.org/10.1596/978-1-4648-0410-6

58. Madureira, A.G.: Coordinated and optimized voltage management of distribution networks with multi-microgrids. Ph.D. Thesis, Department of Electrical and Computer Engineering, Faculty of Engineering, University of Porto, Portugal (2010). https://repositorio.inesctec.pt/bitstream/123456789/3180/1/PS-06923.pdf

59. Madureira, A.G., Peças Lopes, J.A.: Coordinated voltage support in distribution networks with distributed generation and microgrids. IET Renew. Power Gener. **3**(4), 439–454 (2009). https://doi.org/10.1049/iet-rpg.2008.0064

60. Malakar, T., Goswami, S.: Active and reactive dispatch with minimum control movements. Int. J. Electr. Power Energy Syst. **44**(1), 78–87 (2013). https://doi.org/10.1016/j.ijepes.2012.07.014

61. Malekpour, A.R., Niknam, T.: A probabilistic multi-objective daily Volt/Var control at distribution networks including renewable energy sources. Energy **36**(5), 3477–3488 (2011). https://doi.org/10.1016/j.energy.2011.03.052

62. Malekpour, A.R., Tabatabaei, S., Niknam, T.: Probabilistic approach to multi-objective Volt/Var control of distribution system considering hybrid fuel cell and wind energy sources using improved shuffled frog leaping algorithm. Renew. Energy **39**(1), 228–240 (2012). https://doi.org/10.1016/j.renene.2011.08.004

63. Manbachi, M., Farhangi, H., Palizban, A., Arzanpour, S.: Impact of V2G on real-time adaptive Volt/VAr optimization of distribution networks. In: 2013 IEEE Electrical Power Energy Conference, pp. 1–6. IEEE, Halifax (2013). https://doi.org/10.1109/EPEC.2013.6802909

64. Manbachi, M., Nasri, M., Shahabi, B., Farhangi, H., Palizban, A., Arzanpour, S., Moallem, M., Lee, D.C.: Real-time adaptive VVO/CVR topology using multi-agent system and IEC 61850-based communication protocol. IEEE Trans. Sustain. Energy **5**(2), 587–597 (2014). https://doi.org/10.1109/TSTE.2013.2278540

65. Manbachi, M., Farhangi, H., Palizban, A., Arzanpour, S.: A novel Volt-VAR optimization engine for smart distribution networks utilizing Vehicle to Grid dispatch. Int. J. Electr. Power Energy Syst. **74**, 238–251 (2016). https://doi.org/10.1016/j.ijepes.2015.07.030

66. Manbachi, M., Sadu, A., Farhangi, H., Monti, A., Palizban, A., Ponci, F., Arzanpour, S.: Impact of EV penetration on Volt-VAR optimization of distribution networks using real-time co-simulation monitoring platform. Appl. Energy **169**, 28–39 (2016). https://doi.org/10.1016/j.apenergy.2016.01.084

67. Manbachi, M., Sadu, A., Farhangi, H., Monti, A., Palizban, A., Ponci, F., Arzanpour, S.: Real-time co-simulation platform for smart grid Volt-VAR optimization using IEC 61850. IEEE Trans. Ind. Inf. **12**(4), 1392–1402 (2016). https://doi.org/10.1109/TII.2016.2569586

68. Manbachi, M., Farhangi, H., Palizban, A., Arzanpour, S.: Smart grid adaptive volt-VAR optimization: Challenges for sustainable future grids. Sustain. Cities Soc. **28**, 242–255 (2017). https://doi.org/10.1016/j.scs.2016.09.014

69. McGranaghan, M., Uluski, R.W.: Smart Distribution Systems Workshop. CIRED, Frankfurt (2011). http://grouper.ieee.org/groups/td/dist/da/doc/2011%20CIRED%20Panel%20Tutorial%20binder_AH.pdf. EPRI

70. Meier, A.: Electric power systems. In: Wiley survival guides in engineering and science, 1st edn. Wiley-IEEE, Hoboken, (2006)

71. Meirinhos, J.L., Rua, D.E., Carvalho, L.M., Madureira, A.G.: Multi-temporal optimal power flow for voltage control in MV networks using distributed energy resources. Electr. Power Syst. Res. **146**, 25–32 (2017). https://doi.org/10.1016/j.epsr.2017.01.016

72. Miranda, V., Fonseca, N.: EPSO-evolutionary particle swarm optimization, a new algorithm with applications in power systems. In: IEEE/PES Transmission and Distribution Conference and Exhibition, vol. 2, pp. 745–750. IEEE, Yokohama (2002). https://doi.org/10.1109/TDC.2002.1177567

73. Miranda, V., Fonseca, N.: Reactive power dispatch with EPSO-evolutionary particle swarm optimization. In: Proceedings of PMAPS - International Conference on Probabilistic Methods Applied to Power Systems, p. 6. Naples, Italy (2002)

74. Mitchell, M.: An Introduction to Genetic Algorithms, 1st edn. MIT, Cambridge (1998)

75. Mohapatra, A., Bijwe, P.R., Panigrahi, B.K.: An efficient hybrid approach for Volt/Var control in distribution systems. IEEE Trans. Power Deliv. **29**(4), 1780–1788 (2014). https://doi.org/10.1109/TPWRD.2014.2306845

76. Niknam, T.: A new approach based on ant colony optimization for daily Volt/Var control in distribution networks considering distributed generators. Energy Convers. Manag. **49**(12), 3417–3424 (2008). https://doi.org/10.1016/j.enconman.2008.08.015

77. Niknam, T.: A new HBMO algorithm for multiobjective daily Volt/Var control in distribution systems considering distributed generators. Appl. Energy **88**(3), 778–788 (2011). https://doi.org/10.1016/j.apenergy.2010.08.027

78. Niknam, T., Ranjbar, A.M., Shirani, A.R.: Impact of distributed generation on Volt/Var control in distribution networks. In: 2003 IEEE Bologna Power Tech Conference Proceedings, vol. 3, p. 7. IEEE, Bologna (2003). https://doi.org/10.1109/PTC.2003.1304390

79. Niknam, T., Firouzi, B.B., Ostadi, A.: A new fuzzy adaptive particle swarm optimization for daily Volt/Var control in distribution networks considering distributed generators. Appl. Energy **87**(6), 1919–1928 (2010). https://doi.org/10.1016/j.apenergy.2010.01.003

80. Niknam, T., Zare, M., Aghaei, J.: Scenario-based multiobjective Volt/Var control in distribution networks including renewable energy sources. IEEE Trans. Power Deliv. **27**(4), 2004–2019 (2012). https://doi.org/10.1109/TPWRD.2012.2209900

81. Oliveira, D.Q., Marujo, D., Santos, M.V., Bonatto, B.D., Arango, H., de Souza, A.C.Z., Delboni, L.F.N., Filho, J.M.C., Silveira, P.M., Felber, L.A., Braga, M.F.: Multiobjective voltage control in smart distribution power systems. In: 2015 IEEE PES Innovative Smart Grid Technologies Latin America (ISGT LATAM), pp. 7–12. IEEE, Montevideo (2015). https://doi.org/10.1109/ISGT-LA.2015.7381121

82. Padilha-Feltrin, A., Rodezno, D.A.Q., Mantovani, J.R.S.: Volt-var multiobjective optimization to peak-load relief and energy efficiency in distribution networks. IEEE Trans. Power Deliv. **30**(2), 618–626 (2015). https://doi.org/10.1109/TPWRD.2014.2336598

83. Park, J.Y., Nam, S.R., Park, J.K.: Control of a ULTC considering the dispatch schedule of capacitors in a distribution system. IEEE Trans. Power Syst. **22**(2), 755–761 (2007). https://doi.org/10.1109/TPWRS.2007.895168

84. Paudyal, S., Canizares, C.A., Bhattacharya, K.: Optimal operation of distribution feeders in smart grids. IEEE Trans. Ind. Electron. **58**(10), 4495–4503 (2011). https://doi.org/10.1109/TIE.2011.2112314

85. Primadianto, A., Lu, C.N.: A review on distribution system state estimation. IEEE Trans. Power Syst. **32**(5), 3875–3883 (2017). https://doi.org/10.1109/TPWRS.2016.2632156

86. Radatz, P., Kagan, N., Rocha, C., Smith, J., Dugan, R.C.: Assessing maximum DG penetration levels in a real distribution feeder by using OpenDSS. In: 2016 17th International Conference on Harmonics and Quality of Power (ICHQP), pp. 71–76. IEEE, Belo Horizonte (2016). https://doi.org/10.1109/ICHQP.2016.7783416

87. Rahimi, S., Marinelli, M., Silvestro, F.: Evaluation of requirements for Volt/Var control and optimization function in distribution management systems. In: 2012 IEEE International Energy Conference and Exhibition (ENERGYCON), pp. 331–336. IEEE, Florence (2012). https://doi.org/10.1109/EnergyCon.2012.6347777

88. Ranamuka, D., Agalgaonkar, A.P., Muttaqi, K.M.: Online voltage control in distribution systems with multiple voltage regulating devices. IEEE Trans. Sustain. Energy **5**(2), 617–628 (2014). https://doi.org/10.1109/TSTE.2013.2277719

89. Rothlauf, F.: Binary representations of integers and the performance of selectorecombinative genetic algorithms. In: Guervós, J.J.M., Adamidis, P., Beyer, H.G., Schwefel, H.P., Fernández-Villacañas, J.L. (eds.) Parallel Problem Solving from Nature—PPSN VII. Lecture Notes in Computer Science, vol. 2439, pp. 99–108. Springer, Berlin (2002)

90. Roytelman, I., Ganesan, V.: Coordinated local and centralized control in distribution management systems. IEEE Trans. Power Deliv. **15**(2), 718–724 (2000). https://doi.org/10.1109/61.853010

91. Roytelman, I., Wee, B.K., Lugtu, R.L.: Volt/Var control algorithm for modern distribution management system. IEEE Trans. Power Syst. **10**(3), 1454–1460 (1995). https://doi.org/10.1109/59.466504

92. Sabillon-Antunez, C., Melgar-Dominguez, O.D., Franco, J.F., Lavorato, M., Rider, M.J.: Volt-VAr control and energy storage device operation to improve the electric vehicle charging coordination in unbalanced distribution networks. IEEE Trans. Sustain. Energy **8**(4), 1560–1570 (2017). https://doi.org/10.1109/TSTE.2017.2695195

93. Sallam, A.A., Malik, O.P.: Electric distribution systems. In: No. 45 in IEEE Press Series on Power Engineering, 1st edn. Wiley-IEEE, Hoboken (2011). https://doi.org/10.1002/9780470943854

94. Satsangi, S., Kumbhar, G.B.: Effect of load models on scheduling of VVC devices in a distribution network. IET Gener. Transm. Distrib. **12**(17), 3993–4001 (2018). https://doi.org/10.1049/iet-gtd.2018.5262

95. Sen, P.K., Lee, K.H.: Conservation voltage reduction technique: an application guideline for smarter grid. IEEE Trans. Ind. Appl. **52**(3), 2122–2128 (2016). https://doi.org/10.1109/TIA.2016.2525937

96. Senjyu, T., Miyazato, Y., Touma, S., Yona, A., Funabashi, T., Kim, C.: Optimal control of distribution voltage profile by considering the number of operation of the distribution installations. In: 2008 IEEE Power and Energy Society General Meeting-Conversion and Delivery of Electrical Energy in the 21st Century, pp. 1–8. IEEE, Pittsburgh (2008). https://doi.org/10.1109/PES.2008.4596615

97. Senjyu, T., Miyazato, Y., Yona, A., Urasaki, N., Funabashi, T.: Optimal distribution voltage control and coordination with distributed generation. IEEE Trans. Power Deliv. **23**(2), 1236–1242 (2008). https://doi.org/10.1109/TPWRD.2007.908816

98. Shen, Z., Baran, M.E.: Gradient based centralized optimal Volt/Var control strategy for smart distribution system. In: 2013 IEEE PES Innovative Smart Grid Technologies Conference (ISGT), pp. 1–6. IEEE, Washington (2013). https://doi.org/10.1109/ISGT.2013.6497865

99. Shigenobu, R., Noorzad, A.S., Yona, A., Senjyu, T.: Multi-objective optimisation of step voltage regulator operation and optimal placement for distribution systems design using linkage combination update-non-dominated sorting genetic algorithm-II. IET Gener. Transm. Distrib. **12**(1), 20–30 (2018). https://doi.org/10.1049/iet-gtd.2016.1361

100. Short, T.A.: Electric power distribution handbook. In: The Electric Power Engineering Series, 1st edn. CRC Press, Boca Raton (2004)

101. Smith, C.A., Redfern, M.A., Potts, S.: Improvement in the performance of on-load tap changer transformers operating in series. In: 2003 IEEE Power Engineering Society General Meeting, vol. 3, pp. 1905–1910. IEEE, Toronto (2003). https://doi.org/10.1109/PES.2003.1267455

102. Son, K.M., Moon, K.S., Lee, S.K., Park, J.K.: Coordination of an SVC with a ULTC reserving compensation margin for emergency control. IEEE Trans. Power Deliv. **15**(4), 1193–1198 (2000). https://doi.org/10.1109/61.891502

103. Srivastava, A.K., Pandey, A.S., Singh, D.: Short-term load forecasting methods: a review. In: 2016 International Conference on Emerging Trends in Electrical Electronics Sustainable Energy Systems (ICETEESES), pp. 130–138. IEEE, Sultanpur (2016). https://doi.org/10.1109/ICETEESES.2016.7581373

104. Taylor, T.: Model behavior: using distribution models to deliver smart grid Volt/Var control. ABB Rev. **12**(3), 44–51 (2012). https://library.e.abb.com/public/0b1ca7c89a1ae491c1257a79004c4ba8/44-51%203m211_EN_72dpi.pdf

105. Ulinuha, A., Masoum, M.A.S., Islam, S.: Hybrid genetic-fuzzy algorithm for Volt/Var/total harmonic distortion control of distribution systems with high penetration of non-linear loads. IET Gener. Transm. Distrib. **5**(4), 425–439 (2011). https://doi.org/10.1049/iet-gtd.2010.0168

106. Uluski, R.W.: Volt-VAR Control Workshop. IEEE PES, Minneapolis (2010). http://grouper.ieee.org/groups/td/dist/da/doc/Uluski%20Summary%20of%20EPRI%20Volt%20VAR%20Workshop,%20Final.pdf. EPRI

107. Uluski, R.W.: VVC in the smart grid era. In: 2010 IEEE Power and Energy Society General Meeting, pp. 1–7. IEEE, Providence (2010). https://doi.org/10.1109/PES.2010.5589850

108. Uluski, R.W.: Volt/Var Control and Optimization Concepts and Issues. EPRI, [S.l.] (2011). http://cialab.ee.washington.edu/nwess/2012/talks/uluski.pdf

109. Uluski, R.: Using standards to integrate distributed energy resources with distribution management systems. In: 22nd International Conference and Exhibition on Electricity Distribution (CIRED 2013), pp. 1–3. IET, Stockholm (2013). https://doi.org/10.1049/cp.2013.1219

110. Vítor, T.S., Vieira, J.C.M.: Optimal voltage regulation in distribution systems with unbalanced loads and distributed generation. In: 2016 IEEE Innovative Smart Grid Technologies-Asia (ISGT-Asia), pp. 942–947. IEEE, Melbourne (2016). https://doi.org/10.1109/ISGT-Asia.2016.7796512

111. Vítor, T.S., Vieira, J.C.M.: A robust Volt/Var control via multi-objective optimization. In: 2018 13th IEEE International Conference on Industry Applications (INDUSCON), pp. 672–678. IEEE, São Paulo (2018). https://doi.org/10.1109/INDUSCON.2018.8627297

112. Wang, Z., Wang, J.: Review on implementation and assessment of conservation voltage reduction. IEEE Trans. Power Syst. **29**(3), 1306–1315 (2014). https://doi.org/10.1109/TPWRS.2013.2288518

113. Wang, P., Liang, D.H., Yi, J., Lyons, P.F., Davison, P.J., Taylor, P.C.: Integrating electrical energy storage into coordinated voltage control schemes for distribution networks. IEEE Trans. Smart Grid **5**(2), 1018–1032 (2014). https://doi.org/10.1109/TSG.2013.2292530

114. Wester, C., Engelman, N., Smith, T., Odetunde, K., Anderson, B., Reilly, J.: The role of the SCADA RTU in today's substation. In: 2015 68th Annual Conference for Protective Relay Engineers, pp. 622–628. IEEE, College Station (2015). https://doi.org/10.1109/CPRE.2015.7102199

115. Wilson, T.L.: Energy conservation with voltage reduction–fact or fantasy. In: 2002 Rural Electric Power Conference, pp. C3.1–C3.6. IEEE, Colorado Springs (2002). https://doi.org/10.1109/REPCON.2002.1002295

116. Xiao, Y., Tian, S., Yuan, Q., Zhang, X.: An approach to the integration of GIS and DMS. In: 1998 International Conference on Power System Technology, 1998. Proceedings. POWERCON '98, pp. 297–301. IEEE, Beijing (1998). https://doi.org/10.1109/ICPST.1998.728974

117. Yan, W., Lu, S., Yu, D.C.: A novel optimal reactive power dispatch method based on an improved hybrid evolutionary programming technique. IEEE Trans. Power Syst. **19**(2), 913–918 (2004). https://doi.org/10.1109/TPWRS.2004.826716

118. Yilmaz, M., El-Shatshat, R.: State-based Volt/VAR control strategies for active distribution networks. Int. J. Electr. Power Energy Syst. **100**, 411–421 (2018). https://doi.org/10.1016/j.ijepes.2018.02.040

119. Yoshida, H., Kawata, K., Fukuyama, Y., Takayama, S., Nakanishi, Y.: A particle swarm optimization for reactive power and voltage control considering voltage security assessment. IEEE Trans. Power Syst. **15**(4), 1232–1239 (2000). https://doi.org/10.1109/59.898095

120. Zadeh, L.A.: Fuzzy sets. Inf. Control. **8**, 338–353 (1965). http://www-bisc.cs.berkeley.edu/Zadeh-1965.pdf

121. Zafar, R., Ravishankar, J., Fletcher, J.E., Pota, H.R.: Multi-timescale model predictive control of battery energy storage system using conic relaxation in smart distribution grids. IEEE Trans. Power Syst. **33**(6), 7152–7161 (2018). https://doi.org/10.1109/TPWRS.2018.2847400

122. Zare, M., Niknam, T.: A new multi-objective for environmental and economic management of Volt/Var control considering renewable energy resources. Energy **55**, 236–252 (2013). https://doi.org/10.1016/j.energy.2013.03.058

123. Zare, M., Niknam, T., Azizipanah-Abarghooee, R., Amiri, B.: Multi-objective probabilistic reactive power and voltage control with wind site correlations. Energy **66**, 810–822 (2014). https://doi.org/10.1016/j.energy.2014.01.034

124. Zhihuan, L., Yinhong, L., Xianzhong, D.: Non-dominated sorting genetic algorithm-II for robust multi-objective optimal reactive power dispatch. IET Gener. Transm. Distrib. **4**(9), 1000–1008 (2010). https://doi.org/10.1049/iet-gtd.2010.0105

125. Zhou, B., Xu, D., Chan, K.W., Li, C., Cao, Y., Bu, S.: A two-stage framework for multiobjective energy management in distribution networks with a high penetration of wind energy. Energy **135**, 754–766 (2017). https://doi.org/10.1016/j.energy.2017.06.178

126. Ziadi, Z., Taira, S., Oshiro, M., Funabashi, T.: Optimal power scheduling for smart grids considering controllable loads and high penetration of photovoltaic generation. IEEE Trans. Smart Grid **5**(5), 2350–2359 (2014). https://doi.org/10.1109/TSG.2014.2323969

127. Zitzler, E.: Evolutionary algorithms for multiobjective optimization: methods and applications. Ph.D. in computer engineering. In: Computer Engineering and Networks Laboratory (TIK). Swiss Federal Institute of Technology Zurich (ETH Zurich), Zurich (1999). http://www.tik.ee.ethz.ch/sop/publicationListFiles/zitz1999a.pdf

# Consensus Based Distributed Optimal Reactive Power Control in Power Distribution Systems

Irfan Khan, Mashood Nasir, and Affaq Qamar

**Abstract** High penetration level of the renewable energy resources in the power distribution network is one of the main issues of the distribution system operator due to voltage deregulation, power losses and other control problems associated with intermittency of renewable energy resources. To resolve these problems following the increasing penetration level of distributed generators (DGs), appropriate reactive power control of DGs, that can lead to the voltage profile improvement and power loss minimization, should be addressed. This chapter proposes a consensus-based distributed algorithm for the optimal reactive power control (OPRC) of DGs in the power system. Proposed algorithm is found to be effective to optimize the multi-objective function including power loss, and voltage deviation of the distribution systems. The effectiveness and scalability of the proposed algorithm have been validated by testing it on 6-bus and 162-bus distribution systems and then comparing its results with the centralized control scheme.

I. Khan (✉)
Marine Engineering Technology Department in a joint appointment with Electrical and Computer Engineering Department, Texas A&M University, Galveston, TX, USA
e-mail: irfankhan@tamu.edu

M. Nasir
Department of Electrical Engineering at LUMS, Lahore, Pakistan
e-mail: 14060018@lums.edu.pk

A. Qamar
U.S.-Pakistan Center for Advanced Studies in Energy, UET Peshawar Pakistan, Peshawar, Pakistan
e-mail: affaq.qamar@uetpeshawar.edu.pk

# 1 Introduction

This section first describes the significance of this chapter and importance of reactive power control. Then it talks about various control strategies available in literature and finally proposes a new algorithm following the discussion of various control techniques.

## 1.1 Research Significance

Power loss is a major problem in utility industry all over the world. In some countries, power loss may amount to 40% of the total generation. To deal with this serious issue, optimal reactive power control can be implemented in existing power systems [1]. Optimal reactive power control can reduce power loss up to 4% in the power systems with poor efficiency. Voltage deviation is another major problem for power distribution utilities, especially on overloaded distribution feeders. Researchers have claimed that 2004 blackout in North America was due to extreme condition of voltage deviation [2]. Thus, a sophisticated optimal reactive power control is very important for a reliable and efficient operation of power system [3]. In this research, the authors include power loss, and voltage deviation in the objective function, assuming that both quantities are very important to be considered in the operation of power system.

Most of the existing reactive power control techniques are centralized in nature where information from local power system is transmitted to the central controller that computes the updated control input and sends back to the local system. This kind of control scheme may lead to single point of failure in case the central controller fails to operate [4]. Furthermore, in case of limited bandwidth of the communication channel, it may cause slow communication or even loss of important data during transmission of power system data to the central controller [5]. Due to these issues in centralized control schemes, it is important to design a more robust and efficient control that may solve the above mentioned issues. One of the possible solution is to outline a distributed control that will be able to deal with these issues.

## 1.2 Importance of Reactive Power Control

The power loss on a large power system attributes a significant part of cost of power system operation. The loss on the power line in a section of distribution between two buses is, indeed, a function of the square of current flowing on the line. Amount of current, in fact, depends on the voltage level across two buses and impedance of the line connecting them. Thus, it can be stated that power loss on the line will be substantially higher if the voltage difference between two ends of the line is not

regulated [6, 7]. There are various ways to regulate the voltage of buses. Some of the most commonly used apparatus are as follows:

1. Synchronous Condensers;
2. On-load tap changing (OLTC) transformers installed at the primary substation;
3. Voltage regulators (VR) installed along the feeders (Tap-changing auto-transformers);
4. Capacitor banks installed along the feeder.

Synchronous condensers and capacitor banks are the sources to generate reactive power in the power system. Reactive power generation can be used to improve the voltage of the buses as well as minimize the power loss in the conventional power systems [8, 9].

Today's power system is undergoing rapid changes due to the integration of renewable energy sources (RESs) and energy storage. Overall penetration of RESs mainly photo-voltaic (PV) is very high and increasing in the power system, especially, in low voltage power system [10]. As the active power generation of PV units is mostly uncontrolled, the increase in power injection from PV units can lead to a violation of nodal voltages at peak times [11]. Electric vehicles are also expected to play a major role in deterioration of nodal voltages. Thus, with the growing amount of injected power from RESs into the power system, control and stability issues become more and more severe due to the RES intermittency [12]. These control issues in modern power system need to be resolved with improved control of distributed generators.

Violation of nodal voltages can be significantly reduced if reactive power generation from generators, both conventional and renewable is controlled appropriately. Reactive power generation control is even more important in this era of connection of renewable energy sources. Thus, its control has very significant importance today.

## *1.3 Various Control Schemes for Reactive Power Control*

Optimal reactive power control is a hot research area [13] and many optimization techniques are developed for reactive power control such as linear programming [14], quadratic programming [15], mixed integer programming [16], non-linear programming [17], and computational intelligence based method [18, 19].

Recently, consensus-based control theory has been extensively analyzed in power system applications. Authors propose a decentralized control algorithm to optimize the power loss of a microgrid in [20]. They identify that the performance of proposed algorithm without communication might deteriorate significantly. In [21], authors suggest a distributed optimization technique using local communication to minimize the voltage deviations. They prove that minimizing the voltage deviation spontaneously reduce the power loss. However, minimization of the power loss is not directly considered. In [22], a similar distributed control algorithm
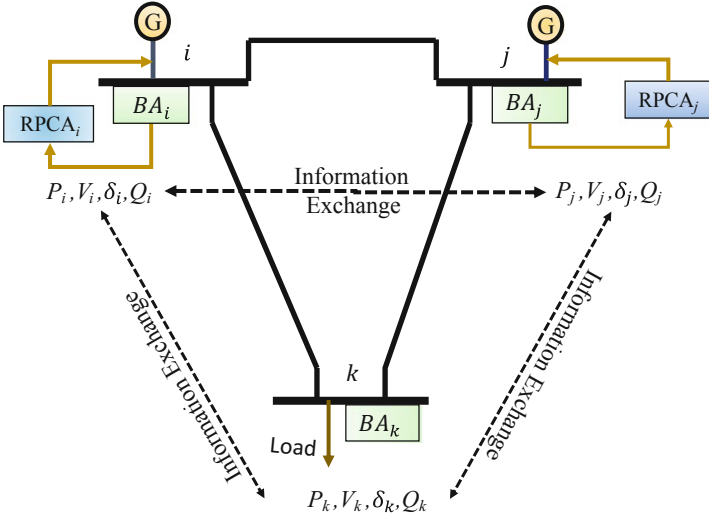
**Fig. 1** Proposed consensus based distributed algorithm

is proposed to generate the optimal reactive power from multiple generators in a power grid assuming that the power loss is affected by local voltages only [22].

In this chapter, a MAS framework based distributed algorithm is proposed to minimize the power loss, and voltage deviation, simultaneously. According to the proposed algorithm, each Distributed Generator (DG) is assigned with one agent that communicates with its neighboring agents and updates its local reactive power generation according to simple rules based on consensus algorithm as shown in Fig. 1 where a generic power system has three buses, *i, j, and k*. Each bus has a bus agent (BA) that measures its local information, $P_i$, $Q_i$, $V_i$, $\delta_i$ and share it with the neighboring buses. Each BA then sends this information to Reactive Power Control Agent (*RPCA*) that calculates optimized reactive power generation for each generator bus. In the next section, problem for power loss and voltage deviation will be formulated.

## 2 Problem Formulation

Optimal reactive power control of generators plays a crucial role in power distribution system operation. It can lead to voltage profile improvement as well as power loss minimization. Therefore, the objective function to be optimized is formulated

as Eq. (1)

$$\min_{Q_i, V_i, \delta_i} \qquad f = W_1 P_{loss} + W_2 D_v \tag{1}$$

$$s.t. \qquad \underline{P}_i \le \overline{P}_i \tag{2}$$

$$\underline{Q}_i \le \overline{Q}_i \tag{3}$$

$$\underline{V}_i \le \overline{V}_i \tag{4}$$

where $W_1$ and $W_2$ are the weight coefficients that describe the preference of the DGs suppliers. $P_{loss}$, and $D_v$ are the power loss and voltage deviation, respectively. $\overline{P}_i, \underline{P}_i, \overline{Q}_i, \underline{Q}_i, \overline{V}_i$ and $\underline{V}_i$ are the maximum and minimum active power, reactive power and voltage ratings of $i$th bus respectively.

The objective function in Eq. (1) can be minimized by optimally controlling the reactive power generation of DGs, $Q_i$.

First part of objective function, $P_{loss}$ in a distribution system is given as (5)

$$P_{loss} = \sum_{i=1}^{n} \sum_{j=1}^{n} V_i V_j Y_{ij} \cos(\theta_{ij} + \delta_{ji}) \tag{5}$$

where $Y_{ij}$ and $\theta_{ij}$ are magnitude and angle of the Y bus entry. $V_i$ and $V_j$ are voltage magnitudes of bus $i$ and bus $j$ while $\delta_{ji}$ is the angle difference between them. Voltage deviation is the sum of square of voltage difference between voltage and its reference value for all buses as given in (6)

$$D_v = \sum_{i=1}^{n} (V_i - V_i^*)^2 \tag{6}$$

The gradient of the objective function, $f$ w.r.t state variable $Q_i$ can be determined as (7)

$$\frac{\partial f}{\partial Q_i} = W_1 \frac{\partial P_{loss}}{\partial Q_i} + W_2 \frac{\partial D_v}{\partial Q_i} \tag{7}$$

Using the chain rule for the partial derivative, gradient for power loss and voltage deviation can be expanded as (8)

$$\frac{\partial f}{\partial Q_i} = W_1 \left\{ \frac{\partial P_{loss}}{\partial V_i} \frac{\partial V_i}{\partial Q_i} + \sum_{j \in N_i} \frac{\partial P_{loss}}{\partial V_j} \frac{\partial V_j}{\partial Q_i} + \frac{\partial P_{loss}}{\partial \delta_i} \frac{\partial \delta_i}{\partial Q_i} + \sum_{j \in N_i} \frac{\partial P_{loss}}{\partial \delta_j} \frac{\partial \delta_j}{\partial Q_i} \right\} + W_2 \left\{ \frac{\partial D_v}{\partial V_i} \frac{\partial V_i}{\partial Q_i} \right\} \tag{8}$$

The derivative calculation of (8) w.r.t $Q_i$ has been performed in [22, 23] and is shown in (9)

$$
\frac{\partial f}{\partial Q_i} = 2W_1 \Big\{ \frac{P_i}{Q_i - V_i^2 B_{ii}} + \sum_{j \in N_i} \frac{P_j}{-V_i V_j Y_{ij} sin(\theta_{ij} + \delta_{ji})} - \frac{Q_i + V_i^2 B_{ii}}{P_i - V_i^2 G_{ii}} +
$$

$$
\sum_{j \in N_i} \frac{Q_j + V_j^2 B_{jj}}{V_i V_j Y_{ij} \cos(\theta_{ij} + \delta_{ji})} \Big\} + \frac{2W_2 V_i (V_i - V_i^*)}{Q_i - V_i^2 B_{ii}} \tag{9}
$$

where $B_{ii}$ and $G_{ii}$ are imaginary and real part of $Y_{bus}$ elements. $N_i$ is the set of all buses connected with bus $i$.

In the next section, we will discuss the proposed consensus based algorithm to minimize power loss and voltage deviation by generating an optimal value of reactive power.

## 3   Consensus Based Distributed Algorithm

The reactive power generation from each generator in the power distribution system is calculated iteratively as given in (10)

$$
Q_i[k + 1] = \sum d_{ij} Q_i[k] - \epsilon \frac{\partial f}{\partial Q_i} \tag{10}
$$

where $\epsilon$ is the step size that can be adjusted to control the converging speed of the proposed algorithm, $d_{ij}$ is designed as (11) [24]

$$
d_{ij} = \begin{cases} \frac{2}{n_i + n_j + 1} & j \in N_i \\ 1 - \sum_{j \in N_i} \frac{2}{n_i + n_j + 1} & i = j \\ 0 & otherwise \end{cases} \tag{11}
$$

where $n_i$ and $n_j$ are the numbers of agents connected to agents $i$ and $j$, respectively. $N_i$ represents neighboring agent set of agent $i$. Reactive power generation from each generator, $Q_i$ can be updated iteratively until an optimal solution of the objective function is achieved.

Each bus is furnished with a bus agent ($BA$) and a reactive power control agent ($RPCA$). $BA$ is responsible for obtaining the local measurement and exchanging the information with its neighboring buses. The exchange of information between these $BAs$ is active power generation, reactive power generation, bus voltage magnitude and bus voltage angle. Each $BA$ then sends this information to $RCPA$ that calculates a new optimal value of reactive power generation such that the objective function may be minimized. Furthermore, communication network topology for the MAS framework is designed in such a way that two $BAs$ communicate with each other only if their corresponding buses are physically connected.

# 4   Simulation Results

In this section, couple of studies are presented to show the effectiveness of the proposed control algorithm. Case study 1 investigates the performance on 6-bus distribution system, whereas case study 2 is carried out for the 162-bus system to validate the scalability of the proposed algorithm.

## 4.1   6-Bus System

The proposed algorithm is applied to a 6 bus radial distribution system as shown in Fig. 2 where bus 1 is a slack bus and attached to the main grid. Three *RESs* are placed to bus 4, 5, and 6 and have reactive power generation ranges from −0.30 to 0.56, −0.45 to 0.75 and −0.35 to 0.60, respectively. Reactive power generation from these DGs is optimized to minimize the power loss and voltage deviation of the system. Reference voltages for 6 buses is set to 1.04, 1.03, 1, 1, 1, and 1 in an ascending order. Weight coefficients for power loss and voltage deviation were set to 5 and 500, respectively.

   Since the given 6-bus distribution system has three *RESs* on bus 4, 5 and 6, these three *RESs* will contribute to minimize the objective function by regulating their bus voltages. Optimal value of reactive power generations are achieved as shown in Fig. 3 where reactive power from bus 4, 5 and 6 rises from 0 to their optimal values to improve the voltage of their respective bus. Improved voltage
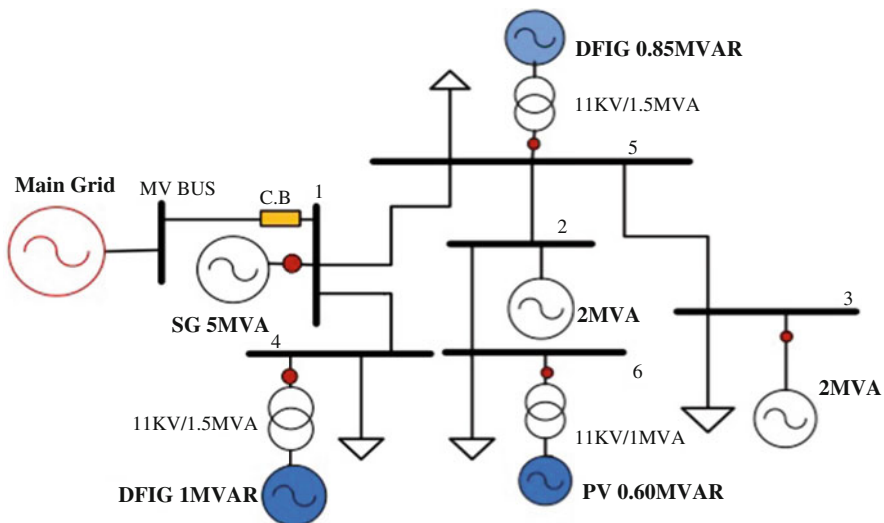


Fig. 2   6-bus radial distribution network for testing the proposed algorithm
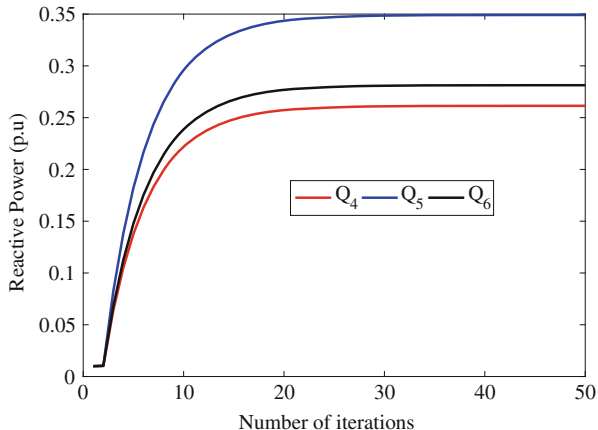
**Fig. 3** Reactive power generation update for three DGs
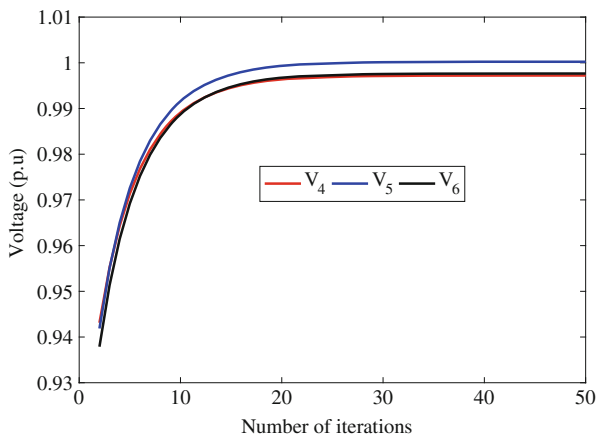


**Fig. 4** Bus voltage improvement

profile of the distribution system leads to decreasing the power loss as line current flow, $I_{ij}$ depends on voltage difference between two buses joining the line and $P_{loss} = \sum I_{ij}^2 Z$.

Furthermore, improved voltage profile of the given distribution network is shown in Fig. 4. It can be seen that voltage improves from 0.94 p.u to almost 1 p.u which is the set reference voltage value. The reference voltages can be changed to any values and the proposed distributed optimal reactive power control will generate reactive power accordingly to achieve the set reference voltages. The proposed distributed algorithm takes 20 iterations to converge to optimal value of voltage.

Finally, total objective function as well as individual sub-functions are shown in Fig. 5. In the beginning of the optimization, the voltage deviation was large that
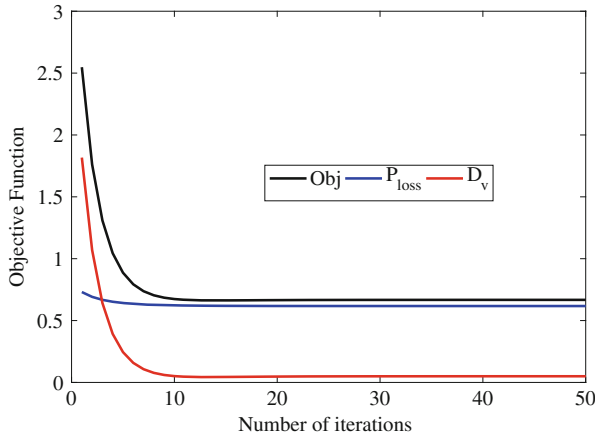
**Fig. 5** Objective function minimization with individual sub-functions

reduces to a significantly lower value after few iterations. A Similar behavior is observed for the total objective function that decreases from 2.5 p.u. to a value below 1 p.u. Thus, a significant amount of improvement in the voltage deviation and power loss is observed using proposed distributed consensus-based optimal reactive power control.

## 4.2 162-bus System

Scalability of the proposed algorithm is validated by testing it on the modified 162-bus interconnected distribution system, as given in [25]. This electrical system is modified by changing the line parameters to use it as meshed distribution network. It has 162 buses, 284 lines and 17 generators. Out of 17 generators, 16 *RESs* have participated to control the reactive power generation. This 17 generator test case system was provided courtesy of Professor Vijay Vittal and Roger Treinen of Iowa State University. More details about the system including its line and bus data is given in [25].

Reference voltages are used the same as given in [26]. The convergence of overall objective function using proposed distributed algorithm is shown in Fig. 6 which shows that objective function declined from 1.675 p.u. to 1.624 p.u by generating optimal reactive power from *RESs*. It is also important to note that our proposed algorithm converges to its optimal value within 20 iterations.

To validate the effectiveness of the proposed algorithm for a large power distribution system, 162 bus data has been applied on Particle Swarm Optimization (*PSO*) algorithm. Objective function minimization plot achieved using *PSO* is shown in Fig. 7. When comparing the result from our proposed distributed algorithm
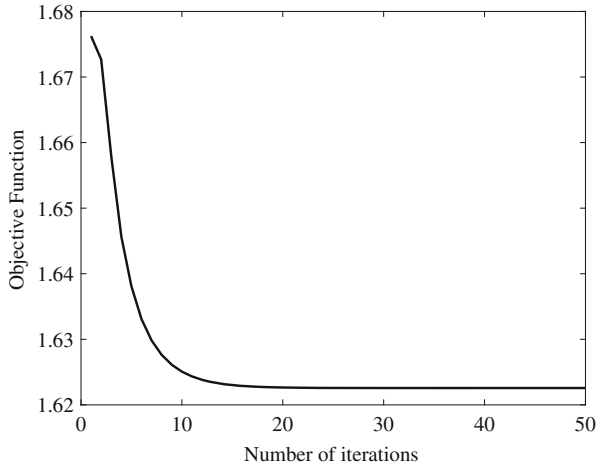
**Fig. 6**  162-bus objective function minimization using proposed distributed algorithm
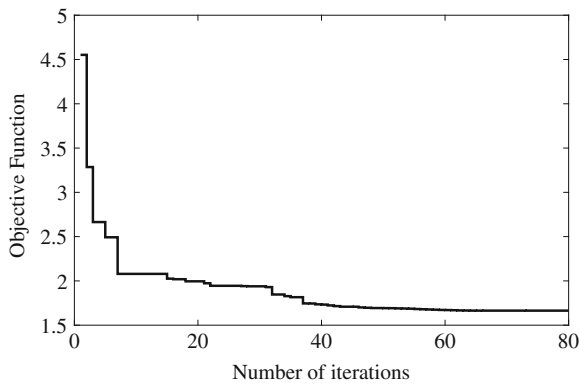


**Fig. 7**  162 bus objective function minimization using PSO

with that of the centralized $PSO$ algorithm, both algorithms converge to a uniform optimal value. However, number of iterations taken by our distributed algorithm is less than that of PSO. Thus, our proposed distributed consensus-based algorithm is observed to be faster than the centralized algorithm.

## 5   Conclusion and Future Works

This chapter presented a distributed consensus-based control algorithm for optimal reactive power control of multiple generators in a power distribution system. A multi-objective function including active power loss and voltage deviation are taken

into consideration, and the optimal reactive power control of multiple generators is formulated as a consensus based distributed problem. The proposed algorithm is distributed in a sense that only information exchange among neighboring buses is needed to achieve the optimal solution, thus, the computational and communication burden are reduced compared to the centralized algorithms.

The effectiveness and the scalability of the proposed distributed algorithm is validated by applying it on 6-bus radial system and 162-bus large interconnected distribution system. The achieved results are also compared with the centralized algorithm PSO, to validate its effectiveness.

Line flow constraints and power balance constraints are highly nonlinear equations that make the optimization problem nonconvex. In case of nonconvex constraints, gradient based consensus algorithm may not converge to an optimal solution. Therefore, for the sake of simplicity, nonlinear constraints such as line flow constraints and power balance equations are not considered in this chapter. In addition to it, the role of energy storage devices in the optimization of power loss is not considered. This may be an interesting future work.

# References

1. Electric Power Transmission and Distribution Losses (% of Output) (2018). Available via DIALOG. https://data.worldbank.org/indicator/EG.ELC.LOSS.ZS. Cited 15 Nov 2018
2. Babalola, A.A., Belkacemi, R., Zarrabian, S.: Real-time cascading failures prevention for multiple contingencies in smart grids through a multi-agent system. IEEE Trans. Smart Grid **9**, 373–385 (2018)
3. Khan, I., Xu, Y., Kar, S., Chow, M.Y., Bhattacharjee, V.: Compressive sensing and morphology singular entropy-based real-time secondary voltage control of multi-area power systems. In: IEEE Transactions on Industrial Informatics (2018)
4. Matvoz, D.; Leskovec, R.; Maksić, M.: Optimized reactive power characteristics for distributed generation sources in the low voltage network. In: 2017 IEEE Manchester PowerTech, pp. 1–6. IEEE, Manchester (2017)
5. Majumdar, A., Agalgaonkar,Y.P., Pal, B.C., Gottschalg, R.: Centralized Volt/Var optimization strategy considering malicious attack on distributed energy resources control. IEEE Trans. Sustain. Energy **9**, 148–156 (2018)
6. Li, D., Ho, C.N.M., Liu, L., Escobar, G.: Reactive power control for single-phase grid-tie inverters using quasi-sinusoidal waveform. IEEE Trans. Sustain. Energy **9**, 3–11 (2018)
7. Dong, P., Xu, L., Lin, Y., Liu, M.: Multi-objective coordinated control of reactive compensation devices among multiple substations. IEEE Trans. Power Syst. **33**(3), 2395–2403 (2018)
8. Yang, Z., Zhong, H., Bose, A., Xia, Q., Kang, C.: Optimal power flow in AC/DC grids with discrete control devices. IEEE Trans. Power Syst. **33**(2), 1461–1472 (2018)
9. Taranto, G.N., Assis, T.M., Falcao, D.M., de Carvalho, R.C.: Highlighting the importance of chronology on voltage protection and control in active distribution networks. IEEE Trans. Power Deliv. **32**(1), 361–369(2017)
10. Xu, Y., Sun, H., Gu, W., Xu, Y., Li, Z.: Optimal distributed control for secondary frequency and voltage regulation in an islanded microgrid. IEEE Trans. Ind. Inf. **15**(1), 225–235 (2018)
11. Bell, M., Berkel, F., Liu, S: Real-time distributed control of low voltage grids with dynamic optimal power dispatch of renewable energy sources. IEEE Trans. Sustain. Energy **10**(1), 417–425 (2018)

12. Wang, Q., Cheng, M., Jiang, Y., Zuo, W., Buja, G.: A simple active and reactive power control for applications of single-phase electric springs. IEEE Trans. Ind. Electron. **65**(8), 6291–6300 (2018)
13. Ansari, J., Gholami, A., Kazemi, A.: Holonic structure: a state-of-the-art control architecture based on multi-agent systems for optimal reactive power dispatch in smart grids. IET Gener. Transm. Distrib. **9**(14), 1922–1934 (2015)
14. Mantovani, J.R.S., Modesto, S.A.G., Garcia, A.V.: VAr planning using genetic algorithm and linear programming. IEE Proc. Gener. Transm. Distrib. **148**(3), 257–262 (2001)
15. Sivasubramani, S., Swarup, K.S.: Sequential quadratic programming based differential evolution algorithm for optimal power flow problem. IET Gener. Transm. Distrib. **5**(11), 1149–1154 (2011)
16. Tian, Z., Wu, W., Zhang, B., Bose, A.: Mixed-integer second-order cone programing model for VAR optimisation and network reconfiguration in active distribution networks. IET Gener. Transm. Distrib. **10**(8) 1938–1946 (2016)
17. Khan, I., Xu, Y., Kar, S., Sun, H.: Compressive sensing-based optimal reactive power control of a multi-area power system. IEEE Access **5**, 23576–23588 (2017)
18. Chen, S., Hu, W., Su, C., Zhang, X., Chen, Z.: Optimal reactive power and voltage control in distribution networks with distributed generators by fuzzy adaptive hybrid particle swarm optimisation method. IET Gener. Transm. Distrib. **9**(11), 1096–1103 (2015)
19. Srivastava, L., Singh, H.: Hybrid multi-swarm particle swarm optimisation based multi-objective reactive power dispatch. IET Gener. Transm. Distrib. **9**(8), 727–739 (2015)
20. Ahn, C., Peng, H.: Decentralized voltage control to minimize distribution power loss of microgrids. IEEE Trans. Smart Grid **4**(3), 1297–1304 (2013)
21. Maknouninejad, A., Qu, Z.: Realizing unified microgrid voltage profile and loss minimization: a cooperative distributed optimization and control approach. IEEE Trans. Smart Grid **5**(4), 1621–1630 (2014)
22. Khan, I., Li, Z., Xu, Y., Gu, W.: Distributed control algorithm for optimal reactive power control in power grids. Int. J. Electr. Power Energy Syst. **83**, 505–513 (2016)
23. Khan, I., Xu, Y., Sun, H., Bhattacharjee, V.: Distributed optimal reactive power control of power systems. IEEE Access **6**, 7100–7111 (2018)
24. Xu, Y., Liu, W.: Novel multiagent based load restoration algorithm for microgrids. IEEE Trans. Smart Grid **2**(1), 152–161 (2011)
25. 17 Generator Dynamic Test Case (162 bus system). In: Power Systems Test Case Archive. University of Washington Electrical Engineering (1993). Available via DIALOG. http://www.ee.washington.edu/research/pstca/. Cited 11 August 2018
26. Divya, P., Rao, G.S.K.: Proposed strategy for capacitor allocation in radial distribution feeders. Int. J. Res. Eng. Technol. **1**(3), 85–92 (2013)

# Linear Model to Represent Unbalanced Distribution Systems in Optimization Problems

**Analiza Dalla Costa, Sérgio Haffner ⓘ, Mariana Resener ⓘ, Luís Alberto Pereira, and Bibiana Maitê Petry Ferraz**

**Abstract** This chapter presents a linear model to determine node voltages and branch currents of unbalanced power distribution systems (PDS). The model allows to obtain approximate solutions for the load flow problem trough the solution of a system of linear equations, instead of using an iterative process as in the conventional load flow. Besides, a discussion on load modeling in PDS is presented to support the proposed model. Numerical studies are presented using a modified version of the IEEE 34-node test feeder. The agreement of results obtained with our linear model with corresponding results obtained through a conventional nonlinear load flow allowed to conclude that the proposed model is not only valid but also can give accurate results.

## 1 Introduction

Electrical energy is fundamental to the maintenance and growth of the modern society, with the main activities of the electric sector being divided into generation, transmission and distribution. The distribution system is important because it connects electrical sources to loads located in remote centers of consumption or rural areas. Since power distribution systems (PDS) are directly connected to consumers, PDS must meet quality requirements concerning the supplied energy; further, PDS are subjected to tight regulation and penalties for non-compliance with power quality standards.

Considering the planning and operation of PDS, adequate models are required to model and solve the problem of network operation under different conditions. Such

A. D. Costa (✉) · L. A. Pereira · B. M. P. Ferraz
Universidade Federal do Rio Grande do Sul, Porto Alegre, Brazil
e-mail: lpereira@ufrgs.br; bibiana.petry@ufrgs.br

S. Haffner · M. Resener
Department of Electrical Systems of Automation and Energy, Universidade Federal do Rio Grande do Sul, Porto Alegre, RS, Brazil
e-mail: haffner@ieee.org; mariana.resener@ufrgs.br

models are also fundamental to solve the expansion planning problem of PDS. To solve both types of problem, it is necessary to determine voltages and currents in all parts of the system, with the conventional load flow being usually applied to obtain these values. However, modeling a distribution system poses difficulties due to the amount of data required, unbalanced operation, uncertainties of load behavior, and the use of nonlinear equations to represent the system [23].

A further aspect to be considered when modeling distribution systems is the presence of distributed generation (DG). Nowadays, economic incentives make it attractive to include sources of electrical energy close to the potential consumers, with the possibility of selling the surplus of energy [43]. Thus, unlike large power plants, which predominantly use conventional energy resources, DGs employ several different energy resources, especially those with low environmental impact, such as wind, solar photovoltaic, and fuel cells [12]. The inclusion of DGs into the network can result in benefits such as: continuity of service during a contingency, improvements in the voltage profile, and reduction of power losses [3, 12]. On the other hand, the operation of the PDS tends to be more complex, requiring additional studies to determine the best mode of operation of DGs and their impacts on the system.

In this chapter, we present a linear model to determine voltages and currents of unbalanced distribution systems. The proposed formulation makes it possible to obtain approximate solutions for the load flow through the solution of a system of linear equations, without the need of an iterative process as in the conventional nonlinear load flow. One of the advantages of simplified models of distribution systems is that they make it easier to determine extreme operating points, with large voltage drops, for instance. A further advantage is that classical optimization techniques can be applied to solve optimization problems, thus assuring the convergence of optimal solutions. Numerical studies are carried out using a modified version of the IEEE 34-nodes test feeder. For the sake of validation, results obtained with the linear model are compared with results obtained through a conventional nonlinear load flow using the OpenDSS software [13]. Finally, operational indexes are obtained to compare differences regarding power losses and voltages.

In this chapter, we also analyze and discuss the models usually applied to represent loads in PDS; we take into account the influence of the voltage variation, which is an important aspect that is often disregarded when loads with constant power behavior are modeled. The load dependence on voltage, as well as other characteristics considered in the proposed model, justifies the representation of generation sources and loads by current injections, which further helps model the system by linear expressions and find a solution for any operation point. Moreover, using linear models, it becomes possible to determine operation points which methods based on the conventional load flow can hardly determine, generally points related to high loads and significant voltage drops. Finally, the formulation presented here can be applied to optimization problems of expansion and operation planning of PDS.

## 1.1 Bibliographic Survey

This section presents a bibliographic survey on themes related to the proposed model, where the main studies on network modeling are commented, and the load flow model is presented as the standard model used in the steady-state analysis of PDS. Loads are commonly modeled by constant power injections, resulting in a nonlinear behavior when determining voltages and currents in PDS. Modeling loads through constant current injections is presented as an alternative to the representation of loads in the conventional solution of the load flow. Additional models used for the steady-state analysis of PDS are presented considering adaptations of the conventional load flow. Besides, works which apply linear approximations for the analysis of distribution systems are discussed. Finally, this section discusses some problems of operation and expansion planning of PDS where the linear model presented in this chapter can be used.

### 1.1.1 Network Modeling

Two models are usually applied to model power systems at steady state: (1) conventional load flow (AC), which is widely used in steady state analysis, and (2) linearized load flow (DC), which is widely used in optimization models related to planning the operation and expansion of power systems. In contrast, the linearized load flow is usually applied to high voltage transmission systems; it is not suitable to PDS due to the high resistance/reactance (R/X) ratio [16].

In the load flow problem, loads are usually represented by constant power injections and transmission lines and transformers are represented by impedances. The balance equations are described by nonlinear expressions relating the power injections to the magnitudes and phase angles of the nodal voltages [28], which makes the implementation of optimization models of distribution systems more complex. This complexity comes from the need for handling nonlinear constraints relating power flows with phasors representing nodal voltages. Thus, iterative techniques are required to solve such a problem.

The sweeping method is one of the methods used to solve the load flow problem in radial distribution networks. This approach consists of two basic steps: (1) in the first step, called backward sweep step, currents are initially determined considering that all nodes have a defined voltage, usually the substation nominal voltage; (2) in the second step, called forward sweep, voltage drops are determined and used to update the voltages which are in turn used in the subsequent backward sweep step to update current flows. Step (2) is repeated until convergence is reached. Given its robustness and simplicity, the sweeping method is often used as a benchmark for comparison with other load flow methods in power distribution systems [4, 23]. The convergence of the sweeping method was improved by [7] using the linear principle of proportionality to find the relation between the real and imaginary components of the initially specified voltage, in relation to the voltage calculated at the substation

node during the forward sweep step. This method can also be modified to solve the load flow considering only magnitudes of voltages, thus eliminating the phase angle in the equations which represent the network [6].

The current injection method can also be used to solve the load flow problem in PDS. In this method, demands are represented by current injections and nodal voltages are obtained from simple matrix calculation, so that the method can be applied to balanced, unbalanced, radial, and meshed systems [9, 15, 31, 39]. However, an iterative process is necessary to update current injections. To make the differences and similarities clearer, a comparison of the three-phase current injection method (TPCIM) with the traditional Forward/Backward Sweep method (FBS) is detailed in [11]; the main aspects of this comparison are summarized in Table 1.

As shown in Table 1, one of the advantages of the sweeping method is the simple computational implementation. However, this method has disadvantages when applied to large systems heavily loaded and with consequent large voltage drops, as well as when applied to systems with meshed topology. In these cases, a large number of iterations may be required and the method may not converge. Thus, although the current injection method is comparatively more intricate, it guarantees a faster convergence for systems to which the sweeping method is difficult to apply [11].

Several authors adapted methods such as Newton-Raphson and Gauss-Seidel, generally used to solve load flow in high and extra-high voltage systems, to apply them to distribution networks too. Examples of these modifications are described in [39, 44], in which the Lower-Upper decomposition is disregarded in the solution of

**Table 1** Comparison of FBS with TCIM method according to [11]

| Characteristics | FBS | TCIM |
|---|---|---|
| Methodology | Simple | Complex |
| Method implementation | Simple | Complex |
| Extension to systems with more conductors/phases | Simple | More complicated |
| Controls (implementation) | More complicated | Simple |
| Convergence (number of iterations) | Many[a] | Few (quadratic) |
| System with controls | Considerable increase in the number of iterations | Solve without problems |
| Radial systems | Solve without problems | Solve without problems |
| Meshed systems | Problems in the solution Many loops increase the number of iterations | Solve without problems |
| Processing time | Low | Low |
| Iteration time | Low | High |
| Robustness | Medium | High |

[a] Considering a system with several nodes and heavy loaded

the load flow, thus avoiding ill-conditioning problems. In [40], a set of $3(N - 1)$ equations is proposed to describe a radial distribution system with $N$-nodes; the equations are then solved using the first-order Newton-Raphson technique. This method is applicable for constant power and constant impedance loads and uses a power injection representation.

The author of [21] treats the load flow problem as a convex optimization problem (conic optimization). According to his approach, starting from a second-order formulation and the definition of new variables, the load flow is solved using the interior point method. Using a different approach for load flow analysis, the author of [8] applied graph theory to reduce the number of equations representing the network and, consequently, also reduce the computational effort required to find the solution.

In [5], a method for load flow solution for radial and lightly meshed systems is described; the method consists of two basic steps: (1) calculating the effective power of each node during a backward sweep and (2) determination of voltages at each node and losses of each branch during a forward sweep. This model also includes closed paths along the system—arising by closing interconnection switches—to make the system change from a radial topology to a lightly meshed topology. This work takes into account the load growth,  so that it can be applied to problems concerning expansion planning of PDS, considering load models with constant impedance (Z), constant current (I), and constant power (P), as well as any combination of them (ZIP). According to the authors, the convergence of this method is guaranteed for different R/X ratios and load levels.

Ahmadi and Martí [1] proposed the use of a voltage-dependent load model and linear approximation techniques to reformulate the load flow problem. The voltage-dependent load behavior is represented by the ZIP model where the parameters are adjusted using the least squares technique. This approach results in a mixed system of equations, linear for loads and nonlinear for generation sources. According to [1], using linear approximations allows reducing the number of iterations required to determine the system solution. Compared to a nonlinear formulation in terms of accuracy, this method has a relative percent error of less than 0.1%.

Marti et al. [25] reformulated the load flow problem through a system of linear equations  whose solution does not require an iterative technique. Considering the angle of the substation voltage as a reference, it is considered that the imaginary part of the nodal voltage is much smaller than the real part and can be neglected. Furthermore, the flow equations are linearized and the load is composed of constant impedance and constant current. The tests of this model show an approximation of nodal voltages obtained with nonlinear iterative techniques. However, power losses are not discussed. Besides, [25] analyzed the suitability of the ZIP model and the proposed model to represent loads, whose behaviors were measured in laboratories considering voltage variation. The model described in [25] also includes distributed generation, but only through a node with defined active and reactive power injections. This linear model was later applied to solve problems of expansion planning and of operation of PDS, such as optimal system reconfiguration, voltage regulation, and optimal allocation of capacitor banks [2].

## 2 Load Modeling in Distribution Systems

This section discusses different load models applied to the analysis of distribution systems at steady state. Initially, the constant power model is addressed as the predominant model used in the solution of power flow. As many bibliographic sources show, the constant power load model often neglects important characteristics of loads, such as the voltage dependence. Thus, the ZIP, exponential and constant current models are discussed as alternatives to represent loads depending on the voltage. This aspect is theoretically assessed by analyzing the behavior of different types of loads when the voltage varies. Further, a typical example demonstrates the differences in the results obtained with the load flow using different load models. Finally, the load model adopted in this work is presented and discussed.

### 2.1 Initial Considerations

Studies of load models in general address the operation of the system under transient condition (dynamic models) as well as under steady state (static models) [10]. A major difficulty to accurately represent the behavior of loads in PDS resides on their inherent variable characteristics [41]. According to [30], the load parameters concerning the active power vary daily during the year. In turn, these variations are strongly influenced by the work cycle of motor-driven loads, such as air conditioning and refrigerators.

Despite the great complexity of establishing load models in distribution networks, several studies have addressed this subject. For example, among others, [27], based on a CIGRE survey made in approximately 50 countries, provided a statistical analysis of the methods used to model loads. According to [27], loads are normally represented as constant demands of active and reactive power; further, the ZIP and exponential models are also common. The ZIP model consists of a polynomial representation where the real and reactive power demands change, respectively, linearly and squarely with the voltage [19]. The coefficients of the ZIP model correspond to ratios of impedances, currents and constant powers [20, 42]. On the other hand, in the exponential model, the real and reactive power demands vary exponentially with the voltage [19, 33].

The authors of [27] determined the parameters of load models from measurements. Based on the results presented in [27], usual approaches used to identify parameters of load models can be verified; in most cases, measurements are used to determine the parameters of the models. Furthermore, 19% of the data are taken from the available literature; the data are therefore useful to model loads when few resources are available to collect the required data.

Although [27] shows a tendency to use the constant power load model, further studies also highlighted the importance of using ZIP and exponential load models to account for the influence of voltage variations on the regulation of electric loads.

Dwyer et al. [14] addressed this aspect by analyzing the load in a substation in Canada. This study demonstrates that 1% of voltage reduction at the substation node leads to a reduction of the active and reactive power of the load by 1.5% and 3.4%, respectively. The results of the mentioned study also show that the load is very sensitive to the voltage variation, a characteristic often disregarded in the constant power load model. Similar conclusions are also presented in other studies addressing different types of loads, both theoretically [24] and experimentally [36].

Hajagos and Danai [18] presented a survey on the behavior of commercial, residential, and industrial loads in distribution networks. The characteristics of the acquired data were represented by coefficients in the ZIP model. This study also compared three types of load representation taking into account voltage variation. The first type used the parameters taken from the measurements of the loads in the ZIP model. The second type represented the load as 50% constant current and 50% constant impedance for active power, and 100% constant impedance for reactive power. Finally, the third type considered the load as constant power. The results of this study showed that those loads represented using the first and second models behave in a similar way under voltage variation. On the other hand, the authors observed that representing loads as constant power lead to a reduction of 10% in the voltage when the load increased (the voltages were limited in the range of 0.8 to 1.0 pu). Thus, the constant power model proved less adequate to represent the behavior of the measured loads. For lower voltage magnitudes, the constant power model presented bigger discrepancies in the voltages compared to the other two types. However, voltage magnitudes below 0.8 pu are uncommon during normal operation of distribution systems.

Michels et al. [26] experimentally determined the parameters of the ZIP model considering the following types of loads: lighting, motors, heating, and electronic equipment. The authors experimentally determined the load parameters using a controlled voltage source and a measurement system for energy quality analysis. The results obtained proved that each load group presents a different sensitivity to voltage variation. In addition, the experimental results showed a different behavior compared to theoretical models normally used to represent some real loads.

In [32], a method for reactive power control and optimal reconfiguration is presented and applied to a 20-kV system using different load models. Table 2 summarizes the results obtained using a constant power, constant current, and mixed load models, where column 2 presents the configuration of the system, while columns 3 to 6, respectively, represent the maximum voltage drop ($\Delta V_{\max}$), the energy losses, the reduction of energy losses compared to initial configuration, and the deviation from optimum.

As shown in Table 2, assuming the optimal configuration of the system, the energy losses and the maximum voltage drop are different for each type of load model. Comparing the three load models, the constant current model exhibits the lowest energy losses and the lowest maximum voltage drop, for both the initial and the optimal configuration. In addition, the results obtained using the mixed model and the constant current model agree very well. Peponis et al. [32] also studied a case where the system has losses of 6.87 MWh in the initial configuration; in this

**Table 2** System optimization—results for different load models [32]

| Load model | Configuration | $\Delta V_{\max}$ (%) | Losses (MWh) | Reduction (%) | Deviation from optimum (%) |
|---|---|---|---|---|---|
| Constant power | Initial | 16.6 | 3.78 | 0 | 7.26 |
|  | Optimum | 12.89 | 3.53 | 6.77 | 0 |
| Mixed | Initial | 14.62 | 3.24 | 0 | 5.11 |
|  | Optimum | 11.7 | 3.087 | 4.86 | 0 |
| Constant current | Initial | 14.01 | 3.189 | 0 | 4.78 |
|  | Optimum | 11.41 | 3.044 | 4.55 | 0 |

case, a solution was possible only for the constant current model, while voltage instability occurred with other models. Thus, the constant current model almost always converges in such operating conditions.

Murty et al. [29] presented a new algorithm for load flow solution based on a sweeping method, which can be applied to unbalanced distribution systems. Loads were modeled as constant current and constant power, with a load growth being also considered. The results discussed in [29] were obtained with faster convergence and fewer iterations using the constant current load model than using the constant power model.

The works described in this Section highlighted the advantages of using voltage-dependent load models, such as the constant current load model applied in the formulation presented in this chapter.

## 2.2 Influence of Load Models on Load Flow Results

The method normally used to analyze distribution networks at steady state is the conventional load flow. Although for this method loads are represented predominately through constant power injection, several works proved that loads in effect depend on the voltage; this dependence is considered in the ZIP model. This section compares the impact on the results obtained with the load flow when using the ZIP and the constant power load models, based on the results presented in [34]. To compare the results, indices to measure the difference in voltages and power losses were applied [38]. We accordingly defined these indices as the average of the differences obtained by the models being compared. Thus, the voltage difference index is given by:

$$\varepsilon_{mV} = \frac{\sum_{k=1}^{n} \varepsilon_i^V}{n}, \tag{1}$$

**Table 3** Differences the in 70-node system with voltage perturbations

| Index | Reference voltage (pu) | | | | |
|---|---|---|---|---|---|
| | 0.8 | 0.9 | 1.0 | 1.1 | 1.2 |
| Minimum voltage (pu) | 0.68 | 0.8 | 0.91 | 1.02 | 1.13 |
| Difference in voltages (%) | 1.2 | 0.42 | – | 0.26 | 0.29 |
| Difference in power losses (%) | 49.69 | 32.06 | 12.5 | 9.15 | −29.4 |

where $n$ is the total number of nodes in the system and the relative difference is obtained for each node using:

$$\varepsilon_k^V = \left| \frac{V_k^{M1} - V_k^{M2}}{V_k^{M1}} \right|, \tag{2}$$

where $V_k^{M1}$ is the voltage magnitude at the node $k$ obtained from the solution of the conventional load flow using the contant power load model and $V_k^{M2}$ is the voltage magnitude at the node $k$ obtained from the solution of the conventional load flow using the ZIP model.

The loss difference index is defined in each system or feeder as:

$$\varepsilon_p = \frac{P_{M1}^{loss} - P_{M2}^{loss}}{P_{M1}^{loss}} \tag{3}$$

where $P_{M1}^{loss}$ and $P_{M2}^{loss}$ represent the total power losses obtained using the conventional load flow with the constant power load model and the ZIP model, respectively.

Tests were carried out considering the initial configuration—in which the reference voltage is equal to 1.0 pu—and applying perturbations to the voltage. In the ZIP load model, loads were represented as 50% constant power and 50% constant impedance. The perturbations in voltages are represented by steps of ±20% in the reference voltage. Table 3 summarizes the main results.

According to Table 3 the loss difference indices can be as high as 49% for a voltage reference of 0.8 pu. Thus, a significant difference exists between the solutions obtained with a constant power model and those with the ZIP model in the conventional load flow. Besides, the differences between voltages for each load model are smaller for each voltage perturbation compared with the difference in power losses, with voltage difference indices less than 1.2%.

In the linear model we present in this chapter, the constant current model is used. For the sake of validation, the ZIP load model was considered in the solution of the conventional load flow, since it takes into account the voltage dependence and presents a significant difference in the power losses compared to the constant power load model. Thus, we consider the constant power model less suitable for the validation of the proposed formulation.
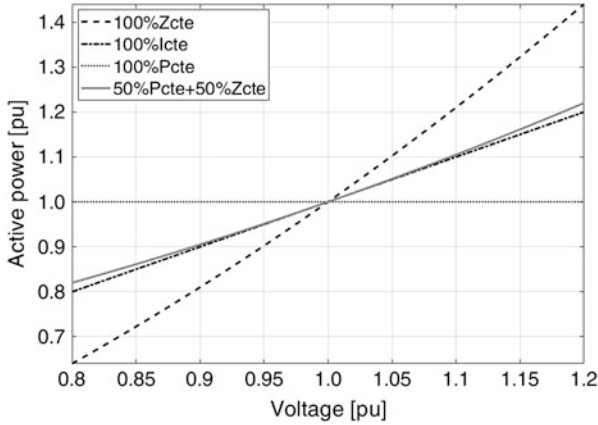
**Fig. 1** Active power *versus* voltage

The constant current model, adopted in this work, can be considered as having an intermediate behavior compared to the constant power and the constant impedance model. This intermediate behavior is illustrated in Fig. 1, where the curves of active power *versus* voltage refer to the following load models: (1) 100% constant impedance (100%Zcte); (2) 100% constant current (100%Icte); (3) 100% constant power (100%Pcte); and (4) 50% constant power and 50% constant impedance (50%Pcte + 50%Zcte). Besides, we obtained these curves by varying the voltage from 0.8 to 1.2 pu. According to Fig. 1, a good agreement can be observed between the behavior of the model with 50%Pcte + 50%Zcte and that with 100%Icte. Thus, for the range of voltage evaluated, these models can be considered as equivalent.

## 2.3 Load Representation in the Proposed Formulation

As stated in Sect. 2.2, in the conventional load flow, different load models can lead to different results for voltages and power losses. Therefore, the load model adopted in our formulation should allow a linear approximation of distribution systems and behave similarly to the ZIP model concerning the dependence on the voltage. Hence, we adopted the constant current model; this choice is based on the following characteristics:

- **possibility of linear approximations in the models of distribution systems, guaranteeing a solution for extreme operation points.** The constant current model allows an approximate representation of the system, without using an iterative process to obtain the solution for the load flow when linearizations are used [25]. Furthermore, current injections are easier to implement and guarantee a faster convergence compared with the conventional load flow when dealing

with systems with heavy loads, significant voltage drops, and also with systems with control devices and meshed topology [11].

- **good agreement with the ZIP load model.** As Sect. 2.2 demonstrates, the constant current model is similar to the ZIP model with 50% of constant impedance and 50% of constant power.
- **easy quantification and reduction of losses in models applied to the operation and the expansion planning of distribution systems.** With a linear representation of the currents, it becomes not only possible to approximate power losses (Sect. 2.2) but also to apply the constant current model to optimization problems. As a further advantage, a linear approximation assures the convergence to an optimal solution using classical optimization techniques.

Considering the characteristics above, we represent loads through constant current injections obtained from the demands of active and reactive power of each phase.

## 3 Approximate Model for Distribution Systems Representation

The model we propose here is an extension of that detailed in [35]. However, in contrast to [35], the present network model includes unbalanced networks in the presence of distributed generation (DG), capacitor banks (CBs), and voltage regulators (VRs). The formulation proposed here allows an approximate solution for the load flow through the solution of a system of linear equations; thus, no iterative process is required.

### 3.1 Loads

The current demands representing loads are obtained from the active and reactive power demands, considering that nodal voltages have nominal magnitude and zero as phase angle for all phases.[1] Hence, the current demands are defined as:

$$d_{k,ph}^{\text{Re}} + j d_{k,ph}^{\text{Im}} = \left( \frac{\overline{S}_{k,ph}^{\text{D}}}{\overline{V}_{k,ph}} \right)^* = P_{k,ph}^{\text{D}} - j Q_{k,ph}^{\text{D}}, \tag{4}$$

---

[1]The adjustment of the phase angle in nodal voltages and currents in branches is performed after the solution, as described in Sect. 8.

where $d_{k,ph}^{\text{Re}}$ and $d_{k,ph}^{\text{Im}}$ are the real and imaginary components of current demand in phase $ph$ of node $k$, $\overline{S}_{k,ph}^{\text{D}}$ is the complex power demand in phase $ph$ of node $k$, $\overline{V}_{k,ph}$ is the voltage phasor of phase $ph$ of node $k$, $P_{k,ph}^{\text{D}}$ and $Q_{k,ph}^{\text{D}}$ are the active and reactive power demand in each phase $ph$ of node $k$, given in pu.

## 3.2 Generators

We use current injections to represent generators, for which two operation modes are considered: PV and PQ; besides, generators can consist of single-phase, two-phase, or three-phase units. Similarly to the current demands, we assumed that nodal voltages have zero as phase angle for all phases. The operation modes are characterized as follows:

- generator operating as a PQ node: in this case, the active ($g_{k,ph}^{\text{Re}}$) and reactive current ($g_{k,ph}^{\text{Im}}$) injections are known and the voltage is calculated. The current injections are obtained considering that nodal voltages have nominal magnitude as follows:

$$g_{k,ph}^{\text{Re}} + j g_{k,ph}^{\text{Im}} = \left( \frac{\overline{S}_{k,ph}^{\text{G}}}{\overline{V}_{k,ph}} \right)^{*} \stackrel{\overline{V}_{k,ph}=1}{=} P_{k,ph}^{\text{G}} - j Q_{k,ph}^{\text{G}}, \tag{5}$$

where $\overline{S}_{k,ph}^{\text{G}}$ is the complex power generation in phase $ph$ of node $k$, $P_{k,ph}^{\text{G}}$ and $Q_{k,ph}^{\text{G}}$ are the active and reactive power generation in each phase $ph$ of node $k$, given in pu;
- generator operating as a PV node: in this operation mode, both the active current injection and the voltage ($V_{k}^{\text{esp}}$) are specified. Thus, the reactive current injection is calculated in order to regulate the voltage. The active current injection is obtained according to:

$$g_{k,ph}^{\text{Re}} = \frac{P_{k,ph}^{\text{G}}}{V_{k}^{\text{esp}}}, \tag{6}$$

where $P_{k,ph}^{\text{G}}$ is the active power generation in phase $ph$ of node $k$, given in pu.

## 3.3 Network Representation

The series impedance of branches and currents are represented by their real and imaginary parts. Consider the generic branch shown in Fig. 2, with a series

**Fig. 2** Generic branch of phase $ph$
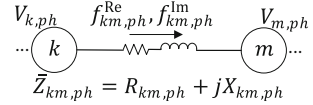


impedance defined as:

$$\overline{Z}_{km,ph} = R_{km,ph} + jX_{km,ph}, \tag{7}$$

where $R_{km,ph}$ and $X_{km,ph}$ represent the resistance and reactance of the conductor impedance in phase $ph$ of the branch connecting nodes $k$ and $m$.

The current in branch $km$ can be defined as:

$$\overline{f}_{km,ph} = f_{km,ph}^{\mathrm{Re}} + jf_{km,ph}^{\mathrm{Im}}, \tag{8}$$

where $f_{km,ph}^{\mathrm{Re}}$ and $f_{km,ph}^{\mathrm{Im}}$ are the real and the imaginary components of the current in phase $ph$ of the branch between nodes $k$ and $m$.

Using (7) and (8), the voltage drop in phase $ph$ can be obtained from:

$$\overline{V}_{km,ph} = \overline{V}_{k,ph} - \overline{V}_{m,ph} = (R_{km,ph} + jX_{km,ph})(f_{km,ph}^{\mathrm{Re}} + jf_{km,ph}^{\mathrm{Im}}), \tag{9}$$

which can be rewritten as:

$$\overline{V}_{km,ph} = R_{km,ph}f_{km,ph}^{\mathrm{Re}} - X_{km,ph}f_{km,ph}^{\mathrm{Im}} + j(R_{km,ph}f_{km,ph}^{\mathrm{Im}} + X_{km,ph}f_{km,ph}^{\mathrm{Re}}). \tag{10}$$

Neglecting the imaginary part in (10) yields:

$$V_{km,ph} = V_{k,ph} - V_{m,ph} \approx R_{km,ph}f_{km,ph}^{\mathrm{Re}} - X_{km,ph}f_{km,ph}^{\mathrm{Im}}. \tag{11}$$

An adjustment factor $K_{km,ph}$ is introduced in (11), so that the solution obtained with the approximated model equals the exact solution for a given neighborhood of the operation point [17]. The adjustment factor is obtained for the base case using a conventional load flow and is defined as:

$$K_{km,ph} = \frac{V_{km,ph}^{\mathrm{LF}} + X_{km,ph}f_{km,ph}^{\mathrm{Im}}}{R_{km,ph}f_{km,ph}^{\mathrm{Re}}}. \tag{12}$$

where $K_{km,ph}$ is the adjustment factor for the phase $ph$ of the branch $km$, and $V_{km,ph}^{\mathrm{LF}}$ is the voltage drop in branch $km$, obtained from a conventional load flow procedure.

Using (12), (11) can be rewritten as:

$$V_{km,ph} = V_{k,ph} - V_{m,ph} \approx K_{km,ph}R_{km,ph}f_{km,ph}^{\mathrm{Re}} - X_{km,ph}f_{km,ph}^{\mathrm{Im}}. \tag{13}$$

The voltage at the nodes $k$ ($V_{k,ph}$) and $m$ ($V_{m,ph}$) in each phase $ph$ can be divided in two parts, called part 1 (P1) and part 2 (P2). Thus, the following expressions can be obtained:

$$V_{k,ph} = V_{k,ph}^{P1} + V_{k,ph}^{P2}, \tag{14}$$

$$V_{m,ph} = V_{m,ph}^{P1} + V_{m,ph}^{P2}. \tag{15}$$

Considering (14) and (15), the voltage drop in branch $km$ can be defined as:

$$V_{km,ph} = V_{km,ph}^{P1} + V_{km,ph}^{P2} = V_{k,ph}^{P1} + V_{k,ph}^{P2} - \left( V_{m,ph}^{P1} + V_{m,ph}^{P2} \right). \tag{16}$$

Splitting (13) into two parts and considering (16) yields:

$$V_{km,ph}^{P1} = V_{k,ph}^{P1} - V_{m,ph}^{P1} = K_{km,ph} R_{km,ph} f_{km,ph}^{Re}, \tag{17}$$

$$V_{km,ph}^{P2} = V_{k,ph}^{P2} - V_{m,ph}^{P2} = -X_{km,ph} f_{km,ph}^{Im}. \tag{18}$$

Rearranging (17) and (18), the real and imaginary components of the currents in branches are then defined as:

$$f_{km,ph}^{Re} = \frac{V_{k,ph}^{P1} - V_{m,ph}^{P1}}{K_{km,ph} R_{km,ph}}, \tag{19}$$

$$f_{km,ph}^{Im} = \frac{V_{k,ph}^{P2} - V_{m,ph}^{P2}}{-X_{km,ph}}. \tag{20}$$

### 3.4   Capacitor Banks

Shunt capacitor banks are commonly used in distribution systems for reactive power and voltage support [23]. In the model we present here, CBs are modeled through constant impedances connected in star. This representation allows to accurately describe the behavior of these devices even under extreme conditions of operation, when the voltage is largely different from the nominal value [35].

The impedance, in pu, of a shunt CB at the node $k$ of phase $ph$ ($j X_{k,sh,ph}$) can be defined as:

$$j X_{k,ph}^{sh} = \frac{\left| \overline{V}_{k,ph} \right|^2}{(j Q_{k,ph}^{sh})^*} = \frac{\left| \overline{V}_{k,ph} \right|^2}{-j Q_{k,ph}^{sh}}, \tag{21}$$

where $j Q_{k,sh,ph}$ is the nominal reactive power per phase of the CB, and $\overline{V}_{k,sh,ph}$ is the voltage phasor, both in pu.

**Fig. 3** Phase $ph$ of a generic node with capacitor

$$V_{k,ph} = V^{P1}_{k,ph} + V^{P2}_{k,ph}$$
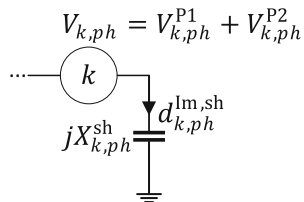


Considering $1\angle 0°$ pu as the voltage in (21) yields:

$$X^{sh}_{k,ph} = \frac{1}{Q^{sh}_{k,ph}}. \tag{22}$$

Consider now the allocation of a CB in phase $ph$ of node $k$, as illustrated in Fig. 3.

From (14), the imaginary part of the CB current ($d^{Im, sh}_{k,ph}$) at the phase $ph$ of node $k$ can be obtained as:

$$d^{Im, sh}_{k,ph} = \frac{V^{P1}_{k,ph} + V^{P2}_{k,ph}}{-X^{sh}_{k,ph}}. \tag{23}$$

### 3.5  Voltage Regulators

Voltage regulators (VRs) are basically used to control the voltage of feeders; they consist of an autotransformer equipped with an on-load tap-changing mechanism. Standard step-VRs enable voltage regulation within $\pm 10\%$, divided in 32 steps plus the neutral position, resulting in 0.625% of voltage change per step. Two types of connections are common in practice: Type A and Type B [23]. Since Type B is the most common connection for step-VRs, we derive here expressions for the voltage and current only for Type B.

Three single-phase step-VRs can be connected externally to form a three-phase VR in open-wye, grounded wye, open delta, or closed delta. In this case, the taps of each regulator are then changed separately. In this work, we assume that VRs of Type B are connected in wye; nevertheless, the formulation can be extended to include other connection types. Without loss of generality, the VR model considers that (1) the transformation is ideal (without losses); (2) the VR is of type B; and (3) the VR has 32 steps plus the neutral position. Thus, a branch $km$ with a VR is represented by an ideal autotransformer with ratio $a_{km,ph} : 1$, as shown in Fig. 4. On the other hand, the transformation ratio of the VR is
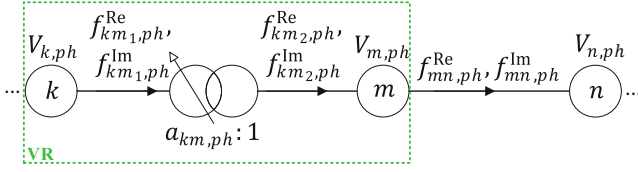
**Fig. 4** Branch with an ideal VR in phase $ph$ of the branch $km$

given by:

$$a_{km,ph} = 1 - 0.00625t_{km,ph},\tag{24}$$

where $t_{km,ph}$ is the tap position of the VR of phase $ph$, variable in the range $[-16, +16]$; thus, $a_{km,ph}$ can vary inside the interval $[1 - 10\%, 1 + 10\%]$ in discrete steps of 0.625%.

According to Fig. 4, the difference between voltages at the nodes $k$ and $m$ is given by:

$$\Delta V_{ph} = V_{m,ph} - V_{k,ph}.\tag{25}$$

From the voltage ratio of an ideal transformer, it results $V_{k,ph} = a_{km,ph}V_{m,ph}$; therefore (25) can be rewritten as:

$$\Delta V_{ph} = (1 - a_{km,ph})V_{m,ph}.\tag{26}$$

Inserting (24) into (26) yields:

$$\Delta V_{ph} = 0.00625t_{km,ph}V_{m,ph}.\tag{27}$$

Considering parts P1 and P2 of the nodal voltage, as defined in (14) and (15), (27) can be rewritten as follows:

$$\Delta V_{ph}^{\mathrm{P1}} = 0.00625t_{km,ph}V_{m,ph}^{\mathrm{P1}}.\tag{28}$$

$$\Delta V_{ph}^{\mathrm{P2}} = 0.00625t_{km,ph}V_{m,ph}^{\mathrm{P2}}.\tag{29}$$

In addition, using the relations of an ideal transformer, the currents on the primary (index 1) and on the secondary side (index 2) are defined as:

$$f_{km_2,ph}^{\mathrm{Re}} = a_{km,ph}f_{km_1,ph}^{\mathrm{Re}},\tag{30}$$

$$f_{km_2,ph}^{\mathrm{Im}} = a_{km,ph}f_{km_1,ph}^{\mathrm{Im}},\tag{31}$$

where $f^{\text{Re}}_{km_1,ph}$ and $f^{\text{Im}}_{km_1,ph}$ are the real and imaginary components of the current on the primary side of a VR installed in branch $km$, while $f^{\text{Re}}_{km_2,ph}$ and $f^{\text{Im}}_{km_2,ph}$ are the real and imaginary components of the current on the secondary side of a VR installed in branch $km$. Replacing (24) in (30) and (31) yields:

$$f^{\text{Re}}_{km_2,ph} = (1 - 0.00625t_{km,ph})f^{\text{Re}}_{km_1,ph}, \tag{32}$$

$$f^{\text{Im}}_{km_2,ph} = (1 - 0.00625t_{km,ph})f^{\text{Im}}_{km_1,ph}. \tag{33}$$

Applying the Kirchhoff's Current Law (KCL) to the node $m$ yields:

$$f^{\text{Re}}_{km_2,ph} - f^{\text{Re}}_{mn,ph} = 0, \tag{34}$$

$$f^{\text{Im}}_{km_2,ph} - f^{\text{Im}}_{mn,ph} = 0. \tag{35}$$

Inserting (32) and (33) respectively into (34) and (35), it is possible to obtain:

$$(1 - 0.00625t_{km,ph})f^{\text{Re}}_{km_1,ph} - f^{\text{Re}}_{mn,ph} = 0, \tag{36}$$

$$(1 - 0.00625t_{km,ph})f^{\text{Im}}_{km_1,ph} - f^{\text{Im}}_{mn,ph} = 0. \tag{37}$$

Rearranging the terms in (36) and (37), then the effect of a VR on the currents can be represented as loads at the node $m$ according to:

$$\Delta f^{\text{Re}}_{ph} = f^{\text{Re}}_{km_1,ph} - f^{\text{Re}}_{mn,ph} = 0.00625t_{km,ph}f^{\text{Re}}_{km_1,ph}, \tag{38}$$

$$\Delta f^{\text{Im}}_{ph} = f^{\text{Im}}_{km_1,ph} - f^{\text{Im}}_{mn,ph} = 0.00625t_{km,ph}f^{\text{Im}}_{km_1,ph}. \tag{39}$$

Considering the equations thus far derived, ideal VRs can be represented through ideal voltage sources with amplitude depending on their tap position, plus current demands which also depend on the tap position of the device. Therefore, the branch presented in Fig. 4 can be represented as Fig. 5 shows. Due to the inclusion of an ideal VR in the circuit $km$, $\Delta V_{ph}$ represents the voltage variation in phase $ph$ of node $m$ with respect to the node $k$, while $\Delta f^{\text{Re}}_{ph}$ and $\Delta f^{\text{Im}}_{ph}$ represent, respectively, the variation in the real and imaginary part of the current in phase $ph$.

**Fig. 5** Modified branch $km$ with an ideal VR in phase $ph$
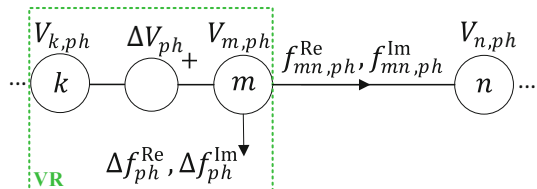
### 3.5.1 Non-ideal Voltage Regulators

Non-ideal VRs (with losses) can be represented by a series impedance and an ideal VR, as shown in Fig. 6. $R_{kp,ph}$ and $X_{kp,ph}$ represent series impedance of the phase $ph$ where the VR is installed, while node $p$ is an auxiliary node, internal to the VR.

## 4 Nodal Equations for a 5-Node System

To exemplify the application of the proposed linearized model, this section uses the distribution system with five nodes and four circuits presented in Fig. 7. The circuit between nodes 4 and 5 is a single-phase circuit (phase $A$). In addition, node 2 has a three-phase capacitor bank installed, while node 5 has a single-phase capacitor connected in phase $A$.
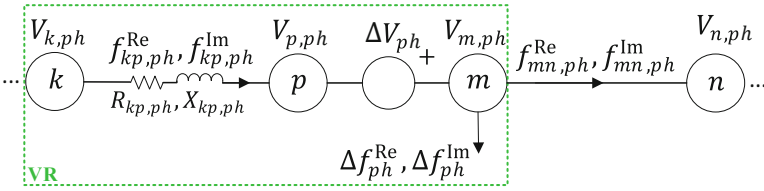


**Fig. 6** Modified branch $km$ with non-ideal VR in phase $ph$
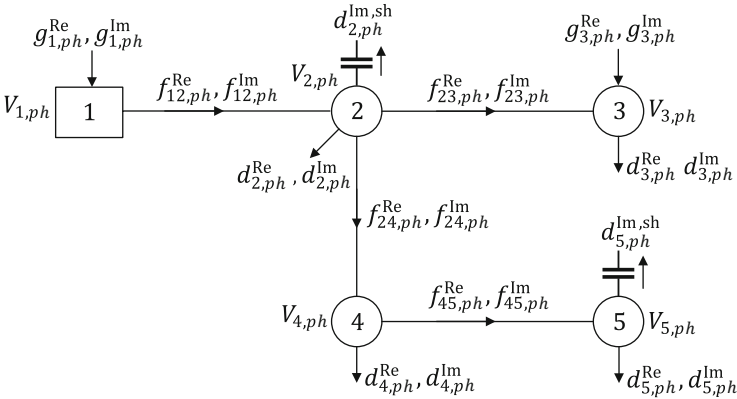


**Fig. 7** 5-Node distribution system

In what follows, the equations corresponding to the application of the Kirchhoff's Laws to the 5-node system are presented. Applying the KCL, the left side will be the sum of the currents leaving the node and the right side will be the net current injection (generation minus demand).

### 4.1   Equations for Node 1

The current balance equation for node 1 (phase $A$) is given by:

$$f_{12,A}^{\text{Re}} + jf_{12,A}^{\text{Im}} = g_{1,A}^{\text{Re}} + jg_{1,A}^{\text{Im}}. \tag{40}$$

Separating the real and imaginary parts yields:

$$f_{12,A}^{\text{Re}} = g_{1,A}^{\text{Re}}, \tag{41}$$

$$f_{12,A}^{\text{Im}} = g_{1,A}^{\text{Im}}. \tag{42}$$

Inserting (19) and (20), respectively, into (41) and (42), the following expressions result:

$$\frac{1}{K_{12,A}R_{12,A}}V_{1,A}^{\text{P1}} + \frac{-1}{K_{12,A}R_{12,A}}V_{2,A}^{\text{P1}} = g_{1,A}^{\text{Re}}, \tag{43}$$

$$\frac{-1}{X_{12,A}}V_{1,A}^{\text{P2}} + \frac{1}{X_{12,A}}V_{2,A}^{\text{P2}} = g_{1,A}^{\text{Im}}. \tag{44}$$

The expressions for phases $B$ and $C$ can be analogously obtained.

### 4.2   Equations for Node 2

The current balance equation for node 2 (phase $A$) is given by:

$$-f_{12,A}^{\text{Re}} - jf_{12,A}^{\text{Im}} + f_{23,A}^{\text{Re}} + jf_{23,A}^{\text{Im}} + f_{24,A}^{\text{Re}} + jf_{24,A}^{\text{Im}} + jd_{2,A}^{\text{Im, sh}} = -d_{2,A}^{\text{Re}} - jd_{2,A}^{\text{Im}}. \tag{45}$$

Separating the real and imaginary parts yields:

$$-f_{12,A}^{\text{Re}} + f_{23,A}^{\text{Re}} + f_{24,A}^{\text{Re}} = -d_{2,A}^{\text{Re}}, \tag{46}$$

$$-f_{12,A}^{\text{Im}} + f_{23,A}^{\text{Im}} + f_{24,A}^{\text{Im}} + d_{2,A}^{\text{Im, sh}} = -d_{2,A}^{\text{Im}}. \tag{47}$$

Inserting (19) and (20), respectively, into (46) and (47) yields:

$$\frac{-1}{K_{12,A}R_{12,A}} V_{1,A}^{P1} + \left( \frac{1}{K_{12,A}R_{12,A}} + \frac{1}{K_{23,A}R_{23,A}} + \frac{1}{K_{24,A}R_{24,A}} \right) V_{2,A}^{P1} +$$
$$+ \frac{-1}{K_{23,A}R_{23,A}} V_{3,A}^{P1} + \frac{-1}{K_{24,A}R_{24,A}} V_{4,A}^{P1} = -d_{2,A}^{Re},$$

(48)

$$\frac{1}{X_{12,A}} V_{1,A}^{P2} + \left( \frac{-1}{X_{12,A}} + \frac{-1}{X_{23,A}} + \frac{-1}{X_{24,A}} + \frac{-1}{X_{2,A}^{sh}} \right) V_{2,A}^{P2} +$$
$$+ \frac{1}{X_{23,A}} V_{3,A}^{P2} + \frac{1}{X_{24,A}} V_{4,A}^{P2} + \frac{-1}{X_{2,A}^{sh}} V_{2,A}^{P1} = -d_{2,A}^{Im}.$$

(49)

The expressions for phases $B$ and $C$ are analogous to (48) and (49).

## 4.3  Equations for Node 3

The current balance equation for node 3 (phase $A$) is given by:

$$- f_{23,A}^{Re} - j f_{23,A}^{Im} = g_{3,A}^{Re} + j g_{3,A}^{Im} - d_{3,A}^{Re} - j d_{3,A}^{Im},$$

(50)

which can be splitted into its real and imaginary part as follows:

$$- f_{23,A}^{Re} = g_{3,A}^{Re} - d_{3,A}^{Re},$$

(51)

$$- f_{23,A}^{Im} = g_{3,A}^{Im} - d_{3,A}^{Im}.$$

(52)

Equations (19) and (20), respectively, can be inserted into (51) and (52), resulting in the following expressions:

$$\frac{-1}{K_{23,A}R_{23,A}} V_{2,A}^{P1} + \frac{1}{K_{23,A}R_{23,A}} V_{3,A}^{P1} = g_{3,A}^{Re} - d_{3,A}^{Re},$$

(53)

$$\frac{1}{X_{23,A}} V_{2,A}^{P2} + \frac{-1}{X_{23,A}} V_{3,A}^{P2} = g_{3,A}^{Im} - d_{3,A}^{Im}.$$

(54)

The expressions for phases $B$ and $C$ are analogous to (53) and (54).

## 4.4 Equations for Node 4

The current balance equation of node 4 (phase $A$) is given by:

$$-f_{24,A}^{\text{Re}} - jf_{24,A}^{\text{Im}} + f_{45,A}^{\text{Re}} + jf_{45,A}^{\text{Im}} = -d_{4,A}^{\text{Re}} - jd_{4,A}^{\text{Im}}. \tag{55}$$

Splitting (55) into its real and imaginary components, there results:

$$-f_{24,A}^{\text{Re}} + f_{45,A}^{\text{Re}} = -d_{4,A}^{\text{Re}}, \tag{56}$$

$$-f_{24,A}^{\text{Im}} + f_{45,A}^{\text{Im}} = -d_{4,A}^{\text{Im}}. \tag{57}$$

Introducing (19) and (20) into (56) and (57), respectively, the following expressions are obtained:

$$\frac{-1}{K_{24,A}R_{24,A}}V_{2,A}^{\text{P1}} + \left(\frac{1}{K_{24,A}R_{24,A}} + \frac{1}{K_{45,A}R_{45,A}}\right)V_{4,A}^{\text{P1}} + \frac{-1}{K_{45,A}R_{45,A}}V_{5,A}^{\text{P1}} = -d_{4,A}^{\text{Re}}, \tag{58}$$

$$\frac{1}{X_{24,A}}V_{2,A}^{\text{P2}} + \left(\frac{-1}{X_{24,A}} + \frac{-1}{X_{45,A}}\right)V_{4,A}^{\text{P2}} + \frac{1}{X_{45,A}}V_{5,A}^{\text{P2}} = -d_{4,A}^{\text{Im}}. \tag{59}$$

Due to the unbalance caused by the presence of only phase $A$ in the circuit connecting nodes 4 and 5, the expressions for phase $A$ of node 4 are different from the expressions of phases $B$ and $C$. The expressions for phase $B$ are presented in what follows:

$$-f_{24,B}^{\text{Re}} - jf_{24,B}^{\text{Im}} = -d_{4,B}^{\text{Re}} - jd_{4,B}^{\text{Im}}. \tag{60}$$

Splitting (60) into its real and imaginary components yields:

$$-f_{24,B}^{\text{Re}} = -d_{4,B}^{\text{Re}}, \tag{61}$$

$$-f_{24,B}^{\text{Im}} = -d_{4,B}^{\text{Im}}. \tag{62}$$

Using (19) and (20), the expressions (61) and (62) can be rewritten as:

$$\frac{-1}{K_{24,B}R_{24,B}}V_{2,B}^{\text{P1}} + \frac{1}{K_{24,B}R_{24,B}}V_{4,B}^{\text{P1}} = -d_{4,B}^{\text{Re}}, \tag{63}$$

$$\frac{1}{X_{24,B}}V_{2,B}^{\text{P2}} + \frac{-1}{X_{24,B}}V_{4,B}^{\text{P2}} = -d_{4,B}^{\text{Im}}. \tag{64}$$

The expressions for phase $C$ of node 4 are analogous to (63) and (64).

## 4.5   Equations for Node 5

The current balance equation for node 5 (phase $A$) is given by:

$$- f_{45,A}^{\text{Re}} - j f_{45,A}^{\text{Im}} + j d_{5,A}^{\text{Im, sh}} = -d_{5,A}^{\text{Re}} - j d_{5,A}^{\text{Im}}. \tag{65}$$

Splitting (65) into its real and imaginary parts results:

$$- f_{45,A}^{\text{Re}} = -d_{5,A}^{\text{Re}}, \tag{66}$$

$$- f_{45,A}^{\text{Im}} + d_{5,A}^{\text{Im, sh}} = -d_{5,A}^{\text{Im}}. \tag{67}$$

Replacing (19) and (20), respectively, in (66) and (67) yields:

$$\frac{-1}{K_{45,A} R_{45,A}} V_{4,A}^{\text{P1}} + \frac{1}{K_{45,A} R_{45,A}} V_{5,A}^{\text{P1}} = -d_{5,A}^{\text{Re}}, \tag{68}$$

$$\frac{1}{X_{45,A}} V_{4,A}^{\text{P2}} + \left( \frac{-1}{X_{45,A}} + \frac{-1}{X_{5,A}^{\text{sh}}} \right) V_{5,A}^{\text{P2}} + \frac{-1}{X_{5,A}^{\text{sh}}} V_{5,A}^{\text{P1}} = -d_{5,A}^{\text{Im}}. \tag{69}$$

The expressions for phases $B$ and $C$ are not presented since node 5 has only the phase $A$.

## 4.6   Matrix Formulation

In Sects. 4.1–4.5 two expressions were presented for each phase $ph$ of each node: the first relates the part 1 (P1) of nodal voltages to the real part of nodal current injections; the second relates the part 2 (P2) of nodal voltages to the imaginary part of nodal current injections. In this section we introduce a matrix formulation for the equations previously presented.

The system of nodal equations can be described by the following linear system, with one of such system being required for each phase of the feeder:

$$\mathbf{M}_{ph} \mathbf{V}_{ph} = \mathbf{I}_{ph}, \tag{70}$$

where $\mathbf{M}_{ph}$ is a matrix formed by submatrices of nodal modified admittances, $\mathbf{V}_{ph}$ is the vector of parts 1 and 2 of nodal voltages, and $\mathbf{I}_{ph}$ is the vector of the real and imaginary parts of the net current injections.

The matrix $\mathbf{M}_{ph}$ is composed of four submatrices:

$$\mathbf{M}_{ph} = \begin{bmatrix} \mathbf{E}_{ph} & \mathbf{0}_{ph} \\ \mathbf{F}_{ph} & \mathbf{H}_{ph} \end{bmatrix}, \tag{71}$$

and the vector $\mathbf{V}_{ph}$ is composed of two subvectors defined as:

$$\mathbf{V}_{ph} = \begin{bmatrix} \mathbf{V}_{ph}^{\mathrm{P1}} \\ \mathbf{V}_{ph}^{\mathrm{P2}} \end{bmatrix}, \tag{72}$$

while the vector $\mathbf{I}_{ph}$ is also composed of two subvectors:

$$\mathbf{I}_{ph} = \begin{bmatrix} \mathbf{g}_{ph}^{\mathrm{Re}} - \mathbf{d}_{ph}^{\mathrm{Re}} \\ \mathbf{g}_{ph}^{\mathrm{Im}} - \mathbf{d}_{ph}^{\mathrm{Im}} \end{bmatrix}. \tag{73}$$

In what follows, the expressions of the components of Eqs. (71)–(73) are presented.

### 4.6.1 Equations for Phase A

For phase $A$, the submatrices of (71) are of $5 \times 5$ dimension, as this phase is present in all nodes of the feeder. The submatrix $\mathbf{0}_A$ formed by zeros and the submatrix $\mathbf{E}_A$ is given by:

$$\mathbf{E}_A = \begin{bmatrix} \frac{1}{K_{12,A}R_{12,A}} & \frac{-1}{K_{12,A}R_{12,A}} & 0 & 0 & 0 \\ \frac{-1}{K_{12,A}R_{12,A}} & E_{22,A} & \frac{-1}{K_{23,A}R_{23,A}} & \frac{-1}{K_{24,A}R_{24,A}} & 0 \\ 0 & \frac{-1}{K_{23,A}R_{23,A}} & \frac{1}{K_{23,A}R_{23,A}} & 0 & 0 \\ 0 & \frac{-1}{K_{24,A}R_{24,A}} & 0 & E_{44,A} & \frac{-1}{K_{45,A}R_{45,A}} \\ 0 & 0 & 0 & \frac{-1}{K_{45,A}R_{45,A}} & \frac{1}{K_{45,A}R_{45,A}} \end{bmatrix}, \tag{74}$$

the elements of the diagonal $E_{22,A}$ and $E_{44,A}$ being defined as:

$$E_{22,A} = \frac{1}{K_{12,A}R_{12,A}} + \frac{1}{K_{23,A}R_{23,A}} + \frac{1}{K_{24,A}R_{24,A}}, \tag{75}$$

$$E_{44,A} = \frac{1}{K_{24,A}R_{24,A}} + \frac{1}{K_{45,A}R_{45,A}}. \tag{76}$$

The submatrix $\mathbf{F}_A$ is given by:

$$\mathbf{F}_A = \begin{bmatrix} 0 & 0 & 0 & 0 & 0 \\ 0 & \frac{-1}{X_{2,A}^{\mathrm{sh}}} & 0 & 0 & 0 \\ 0 & 0 & 0 & 0 & 0 \\ 0 & 0 & 0 & 0 & 0 \\ 0 & 0 & 0 & 0 & \frac{-1}{X_{5,A}^{\mathrm{sh}}} \end{bmatrix}. \tag{77}$$

Submatrix $\mathbf{H}_A$ is defined as:

$$\mathbf{H}_A = \begin{bmatrix} \frac{-1}{X_{12,A}} & \frac{1}{X_{12,A}} & 0 & 0 & 0 \\ \frac{1}{X_{12,A}} & H_{22,A} & \frac{1}{X_{23,A}} & \frac{1}{X_{24,A}} & 0 \\ 0 & \frac{1}{X_{23,A}} & \frac{-1}{X_{23,A}} & 0 & 0 \\ 0 & \frac{1}{X_{24,A}} & 0 & H_{44,A} & \frac{1}{X_{45,A}} \\ 0 & 0 & 0 & \frac{1}{X_{45,A}} & \frac{-1}{X_{45,A}} + \frac{-1}{X_{5,A}^{\mathrm{sh}}} \end{bmatrix}, \tag{78}$$

where:

$$H_{22,A} = \frac{-1}{X_{12,A}} + \frac{-1}{X_{23,A}} + \frac{-1}{X_{24,A}} + \frac{-1}{X_{2,A}^{\mathrm{sh}}}, \tag{79}$$

$$H_{44,A} = \frac{-1}{X_{24,A}} + \frac{-1}{X_{45,A}}. \tag{80}$$

The subvectors in (72) are of $5 \times 1$ dimension. The subvectors $\mathbf{V}_A^{\mathrm{P1}}$ and $\mathbf{V}_A^{\mathrm{P2}}$ are given by:

$$\mathbf{V}_A^{\mathrm{P1}} = \begin{bmatrix} V_{1,A}^{\mathrm{P1}} \\ V_{2,A}^{\mathrm{P1}} \\ V_{3,A}^{\mathrm{P1}} \\ V_{4,A}^{\mathrm{P1}} \\ V_{5,A}^{\mathrm{P1}} \end{bmatrix}, \tag{81a}$$

$$\mathbf{V}_A^{\mathrm{P2}} = \begin{bmatrix} V_{1,A}^{\mathrm{P2}} \\ V_{2,A}^{\mathrm{P2}} \\ V_{3,A}^{\mathrm{P2}} \\ V_{4,A}^{\mathrm{P2}} \\ V_{5,A}^{\mathrm{P2}} \end{bmatrix}. \tag{81b}$$

The subvectors in (73) are $5 \times 1$. The subvectors $\mathbf{g}_A^{\text{Re}} - \mathbf{d}_A^{\text{Re}}$ and $\mathbf{g}_A^{\text{Im}} - \mathbf{d}_A^{\text{Im}}$ are defined as:

$$\mathbf{g}_A^{\text{Re}} - \mathbf{d}_A^{\text{Re}} = \begin{bmatrix} g_{1,A}^{\text{Re}} \\ -d_{2,A}^{\text{Re}} \\ g_{3,A}^{\text{Re}} - d_{3,A}^{\text{Re}} \\ -d_{4,A}^{\text{Re}} \\ -d_{5,A}^{\text{Re}} \end{bmatrix}, \tag{82a}$$

$$\mathbf{g}_A^{\text{Im}} - \mathbf{d}_A^{\text{Im}} = \begin{bmatrix} g_{1,A}^{\text{Im}} \\ -d_{2,A}^{\text{Im}} \\ g_{3,A}^{\text{Im}} - d_{3,A}^{\text{Im}} \\ -d_{4,A}^{\text{Im}} \\ -d_{5,A}^{\text{Im}} \end{bmatrix}. \tag{82b}$$

### 4.6.2 Equations for Phases $B$ e $C$

Regarding phases $B$ and $C$, the submatrices of (71) are $4 \times 4$, since phases $B$ and $C$ are not present at node 5. Thus, the submatrix $\mathbf{E}_B$ is defined as:

$$\mathbf{E}_B = \begin{bmatrix} \frac{1}{K_{12,A}R_{12,B}} & \frac{-1}{K_{12,B}R_{12,B}} & 0 & 0 \\ \frac{-1}{K_{12,A}R_{12,B}} & E_{22,B} & \frac{-1}{K_{23,B}R_{23,B}} & \frac{-1}{K_{24,B}R_{24,B}} \\ 0 & \frac{-1}{K_{23,A}R_{23,A}} & \frac{1}{K_{23,A}R_{23,A}} & 0 \\ 0 & \frac{-1}{K_{24,B}R_{24,B}} & 0 & \frac{1}{K_{24,B}R_{24,B}} \end{bmatrix}, \tag{83}$$

where:

$$E_{22,B} = \frac{1}{K_{12,B}R_{12,B}} + \frac{1}{K_{23,B}R_{23,B}} + \frac{1}{K_{24,B}R_{24,B}}. \tag{84}$$

The submatrix $\mathbf{0}_B$ is formed by zeros, while submatrix $\mathbf{F}_B$ is given by:

$$\mathbf{F}_B = \begin{bmatrix} 0 & 0 & 0 & 0 \\ 0 & \frac{-1}{X_{2,B}^{\text{sh}}} & 0 & 0 \\ 0 & 0 & 0 & 0 \\ 0 & 0 & 0 & 0 \end{bmatrix}. \tag{85}$$

The elements of the submatrix $\mathbf{H}_B$ are defined as:

$$
\mathbf{H}_B =
\begin{bmatrix}
\frac{-1}{X_{12,B}} & \frac{1}{X_{12,B}} & 0 & 0 \\
\frac{1}{X_{12,B}} & \frac{-1}{X_{12,B}} + \frac{-1}{X_{23,B}} + \frac{-1}{X_{24,B}} + \frac{-1}{X_{2,B}^{\text{sh}}} & \frac{1}{X_{23,B}} & \frac{1}{X_{24,B}} \\
0 & \frac{1}{X_{23,B}} & \frac{-1}{X_{23,B}} & 0 \\
0 & \frac{1}{X_{24,B}} & 0 & \frac{-1}{X_{24,B}}
\end{bmatrix}.
\tag{86}
$$

The subvectors of (72) for phase $B$ have dimension $4 \times 1$. Besides, the subvectors $\mathbf{V}_B^{\text{P1}}$ and $\mathbf{V}_B^{\text{P2}}$ are given by:

$$
\mathbf{V}_B^{\text{P1}} =
\begin{bmatrix}
V_{1,B}^{\text{P1}} \\
V_{2,B}^{\text{P1}} \\
V_{3,B}^{\text{P1}} \\
V_{4,B}^{\text{P1}}
\end{bmatrix},
\tag{87a}
$$

$$
\mathbf{V}_B^{\text{P2}} =
\begin{bmatrix}
V_{1,B}^{\text{P2}} \\
V_{2,B}^{\text{P2}} \\
V_{3,B}^{\text{P2}} \\
V_{4,B}^{\text{P2}}
\end{bmatrix}.
\tag{87b}
$$

The subvectors in (73) are of $4 \times 1$ dimension. The subvectors $\mathbf{g}_B^{\text{Re}} - \mathbf{d}_B^{\text{Re}}$ and $\mathbf{g}_B^{\text{Im}} - \mathbf{d}_B^{\text{Im}}$ are given by:

$$
\mathbf{g}_B^{\text{Re}} - \mathbf{d}_B^{\text{Re}} =
\begin{bmatrix}
g_{1,B}^{\text{Re}} \\
-d_{2,B}^{\text{Re}} \\
g_{3,B}^{\text{Re}} - d_{3,B}^{\text{Re}} \\
-d_{4,B}^{\text{Re}}
\end{bmatrix},
\tag{88a}
$$

$$
\mathbf{g}_B^{\text{Im}} - \mathbf{d}_B^{\text{Im}} =
\begin{bmatrix}
g_{1,B}^{\text{Im}} \\
-d_{2,B}^{\text{Im}} \\
g_{3,B}^{\text{Im}} - d_{3,B}^{\text{Im}} \\
-d_{4,B}^{\text{Im}}
\end{bmatrix}.
\tag{88b}
$$

The expression for phase $C$ are analogous to (83)–(88b).

## 5 Matrix Nodal Formulation

Using the equations presented in Sects. 4.6.1 and 4.6.2, it is possible to establish a general rule for the formation of the submatrices in (71) and subvectors in (72)–(73). Considering these equations, the application of nodal analysis leads to the following linear system of equations to be written for each phase of the

network:

$$\begin{bmatrix} \mathbf{E}_{ph} & \mathbf{0}_{ph} \\ \mathbf{F}_{ph} & \mathbf{H}_{ph} \end{bmatrix} \begin{bmatrix} \mathbf{V}_{ph}^{P1} \\ \mathbf{V}_{ph}^{P2} \end{bmatrix} = \begin{bmatrix} \mathbf{g}_{ph}^{Re} - \mathbf{d}_{ph}^{Re} \\ \mathbf{g}_{ph}^{Im} - \mathbf{d}_{ph}^{Im}. \end{bmatrix} \tag{89}$$

The system of Eq. (89) can be solved in two steps. In the first step, $\mathbf{V}_{ph}^{P1}$ is determined using:

$$\mathbf{E}_{ph} \mathbf{V}_{ph}^{P1} = \mathbf{g}_{ph}^{Re} - \mathbf{d}_{ph}^{Re}. \tag{90}$$

In the second step, $\mathbf{V}_{ph}^{P1}$ is known and $\mathbf{V}_{ph}^{P2}$ is obtained through the following expression:

$$\mathbf{H}_{ph} \mathbf{V}_{ph}^{P2} = \mathbf{g}_{ph}^{Im} - \mathbf{d}_{ph}^{Im} - \mathbf{F}_{ph} \mathbf{V}_{ph}^{P1}. \tag{91}$$

The equations for the submatrices $\mathbf{E}_{ph}$, $\mathbf{F}_{ph}$, and $\mathbf{H}_{ph}$ in (89) are presented in what follows. The submatrix $\mathbf{0}_{ph}$ is a square $n \times n$ matrix, where $n$ is the number of nodes in the feeder which contains phase $ph$, with all elements in $\mathbf{0}_{ph}$ being zero.

## 5.1 Submatrix $\mathbf{E}_{ph}$

The submatrix $\mathbf{E}_{ph}$ is square and $n \times n$, being $n$ the number of nodes in the system containing phase $ph$. Thus, this submatrix can be defined as:

$$\mathbf{E}_{ph} = \begin{bmatrix} E_{11,ph} & E_{12,ph} & \cdots & E_{1n,ph} \\ E_{21,ph} & E_{22,ph} & \cdots & E_{2n,ph} \\ \vdots & \vdots & \ddots & \vdots \\ E_{n1,ph} & E_{n2,ph} & \cdots & E_{nn,ph} \end{bmatrix}, \tag{92}$$

in which the diagonal elements are given by:

$$E_{ii,ph} = \sum_{j \in \Omega_{i,ph}} \frac{1}{K_{ij,ph} R_{ij,ph}}, \tag{93}$$

where $\Omega_{i,ph}$ is the set of all nodes connected to node $i$ through phase $ph$. On the other hand, the off-diagonal elements in (92) are given by:

$$E_{ij,ph} = \begin{cases} \frac{-1}{K_{ij,ph} R_{ij,ph}}, & \text{if } j \in \Omega_{i,ph} \\ 0, & \text{otherwise.} \end{cases} \tag{94}$$

## 5.2 Submatrix $\mathbf{F}_{ph}$

The submatrix $\mathbf{F}_{ph}$ is diagonal with dimension $n \times n$, where $n$ is the number of nodes in which phase $ph$ is present; $\mathbf{F}_{ph}$ is defined as:

$$\mathbf{F}_{ph} = \begin{bmatrix} F_{11,ph} & 0 & \cdots & 0 \\ 0 & F_{22,ph} & \cdots & 0 \\ \vdots & \vdots & \ddots & \vdots \\ 0 & 0 & \cdots & F_{nn,ph} \end{bmatrix}, \tag{95}$$

where:

$$F_{ii,ph} = \begin{cases} \frac{-1}{X_{i,ph}^{\text{sh}}}, & \text{if } X_{i,ph}^{\text{sh}} \neq 0 \\ 0, & \text{otherwise.} \end{cases} \tag{96}$$

## 5.3 Submatrix $\mathbf{H}_{ph}$

The submatrix $\mathbf{H}_{ph}$ is square and its order is equal to the number of nodes in which phase $ph$ is present. This submatrix is given by:

$$\mathbf{H}_{ph} = \begin{bmatrix} H_{11,ph} & H_{12,ph} & \cdots & H_{1n,ph} \\ H_{21,ph} & H_{22,ph} & \cdots & H_{2n,ph} \\ \vdots & \vdots & \ddots & \vdots \\ H_{n1,ph} & H_{n2,ph} & \cdots & H_{nn,ph} \end{bmatrix}, \tag{97}$$

where the diagonal elements are given by:

$$H_{ii,ph} = \sum_{j \in \Omega_{i,ph}} \frac{1}{X_{ij,ph}}. \tag{98}$$

On the other hand, the elements outside the main diagonal of (97) are given by:

$$H_{ij,ph} = \begin{cases} \frac{-1}{X_{ij,ph}}, & \text{if } j \in \Omega_{i,ph} \\ 0, & \text{otherwise.} \end{cases} \tag{99}$$

## 5.4 Subvectors of $\mathbf{V}_{ph}$

The dimension of the subvectors $\mathbf{V}_{ph}^{P1}$ and $\mathbf{V}_{ph}^{P2}$ is equal to the number of nodes in which phase $ph$ is present and are defined as:

$$\mathbf{V}_{ph}^{P1} = \begin{bmatrix} V_{1,ph}^{P1} \\ V_{2,ph}^{P1} \\ \vdots \\ V_{n,ph}^{P1} \end{bmatrix}, \tag{100a}$$

$$\mathbf{V}_{ph}^{P2} = \begin{bmatrix} V_{1,ph}^{P2} \\ V_{2,ph}^{P2} \\ \vdots \\ V_{n,ph}^{P2} \end{bmatrix}. \tag{100b}$$

## 5.5 Subvectors of $\mathbf{I}_{ph}$

The subvectors $\mathbf{g}_{ph}^{Re} - \mathbf{d}_{ph}^{Re}$ and $\mathbf{g}_{ph}^{Im} - \mathbf{d}_{ph}^{Im}$ have dimension $n \times 1$, where $n$ is the number of nodes in which phase $ph$ is present. These subvectors can be defined as:

$$\mathbf{g}_{ph}^{Re} - \mathbf{d}_{ph}^{Re} = \begin{bmatrix} g_{1,ph}^{Re} - d_{1,ph}^{Re} \\ g_{2,ph}^{Re} - d_{2,ph}^{Re} \\ \vdots \\ g_{n,ph}^{Re} - d_{n,ph}^{Re} \end{bmatrix}, \tag{101a}$$

$$\mathbf{g}_{ph}^{Im} - \mathbf{d}_{ph}^{Im} = \begin{bmatrix} g_{1,ph}^{Im} - d_{1,ph}^{Im} \\ g_{2,ph}^{Im} - d_{2,ph}^{Im} \\ \vdots \\ g_{n,ph}^{Im} - d_{n,ph}^{Im} \end{bmatrix}. \tag{101b}$$

## 6 Nodal Equations for the 6-Node System with Ideal VR

To illustrate the application of the proposed linearized model to a feeder with VR, one node (node 6) and one ideal VR have been included into the system in Fig. 7, thus resulting the system illustrated in Fig. 8, which has now six nodes.

Considering the VR model discussed in Sect. 3.5, the system in Fig. 8 can be represented as Fig. 9 shows.
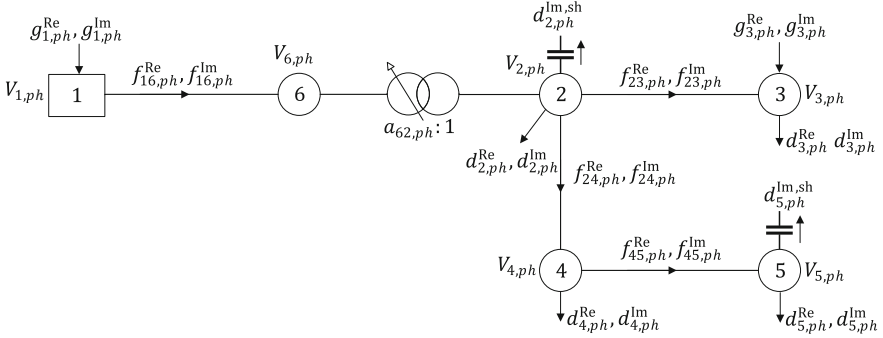
**Fig. 8** Distribution system with 6 nodes and an ideal VR
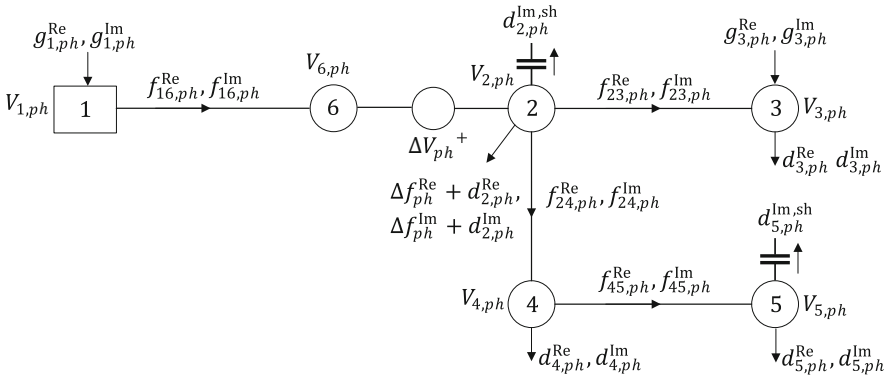


**Fig. 9** Modified 6-node distribution system with ideal VR

Since equations for nodes 3 to 5 are analogous to those already presented in Sects. 4.3 to 4.5, we do not present them here. In addition, equations for node 1 and super node $6 - 2$ are presented only for phase $A$; equations for phases $B$ and $C$ can be analogously obtained.

## 6.1 Equations for Node 1

The current balance equation for node 1 is given by:

$$f_{16,A}^{\text{Re}} + j f_{16,A}^{\text{Im}} = g_{1,A}^{\text{Re}} + j g_{1,A}^{\text{Im}}. \tag{102}$$

Splitting (102) into its real and imaginary parts yields:

$$f_{16,A}^{\text{Re}} = g_{1,A}^{\text{Re}}, \tag{103}$$

$$f_{16,A}^{\text{Im}} = g_{1,A}^{\text{Im}}. \tag{104}$$

After inserting (19) and (20) into (103) and (104), the following expressions result:

$$\frac{1}{K_{16,A}R_{16,A}}V_{1,A}^{\text{P1}} + \frac{-1}{K_{16,A}R_{16,A}}V_{6,A}^{\text{P1}} = g_{1,A}^{\text{Re}}, \tag{105}$$

$$\frac{-1}{X_{16,A}}V_{1,A}^{\text{P2}} + \frac{1}{X_{16,A}}V_{6,A}^{\text{P2}} = g_{1,A}^{\text{Im}}. \tag{106}$$

For phases $B$ and $C$, the expressions are analogous to the expressions developed for phase $A$.

## 6.2 Equations for Super Node $6 - 2$

The current balance for super node $6 - 2$ is given by:

$$\Delta f_A^{\text{Re}} + j\Delta f_A^{\text{Im}} - f_{16,A}^{\text{Re}} - jf_{16,A}^{\text{Im}} + f_{23,A}^{\text{Re}} + jf_{23,A}^{\text{Im}} + f_{24,A}^{\text{Re}} + jf_{24,A}^{\text{Im}} + jd_{2,A}^{\text{Im, sh}} =$$
$$= -d_{2,A}^{\text{Re}} - jd_{2,A}^{\text{Im}}. \tag{107}$$

which, splitted into its real and imaginary parts, results in:

$$\Delta f_A^{\text{Re}} - f_{16,A}^{\text{Re}} + f_{23,A}^{\text{Re}} + f_{24,A}^{\text{Re}} = -d_{2,A}^{\text{Re}}, \tag{108}$$

$$\Delta f_A^{\text{Im}} - f_{16,A}^{\text{Im}} + f_{23,A}^{\text{Im}} + f_{24,A}^{\text{Im}} + d_{2,A}^{\text{Im, sh}} = -d_{2,A}^{\text{Im}}, \tag{109}$$

where $\Delta f_A^{\text{Re}}$ and $\Delta f_A^{\text{Im}}$ are given by:

$$\Delta f_A^{\text{Re}} = 0.00625 t_{62,\,ph} f_{16,A}^{\text{Re}}, \tag{110}$$

$$\Delta f_A^{\text{Im}} = 0.00625 t_{62,A} f_{16,A}^{\text{Im}}. \tag{111}$$

Inserting (110) and (111), respectively, into (108) and (109) yields:

$$0.00625 t_{62,A} f_{16,A}^{\text{Re}} - f_{16,A}^{\text{Re}} + f_{23,A}^{\text{Re}} + f_{24,A}^{\text{Re}} = -d_{2,A}^{\text{Re}}, \tag{112}$$

$$0.00625 t_{62,A} f_{16,A}^{\text{Im}} - f_{16,A}^{\text{Im}} + f_{23,A}^{\text{Im}} + f_{24,A}^{\text{Im}} + d_{2,A}^{\text{Im, sh}} = -d_{2,A}^{\text{Im}}. \tag{113}$$

Putting (19) into (112), and (20) and (23) into (113), the following expressions are obtained:

$$\left( \frac{-1}{K_{16,A} R_{16,A}} + \frac{0.00625 t_{62,A}}{K_{16,A} R_{16,A}} \right) V_{1,A}^{\text{P1}} + \left( \frac{1}{K_{16,A} R_{16,A}} + \frac{-0.00625 t_{62,A}}{K_{16,A} R_{16,A}} \right) V_{6,A}^{\text{P1}} +$$

$$+ \left( \frac{1}{K_{23,A} R_{23,A}} + \frac{1}{K_{24,A} R_{24,A}} \right) V_{2,A}^{\text{P1}} + \frac{-1}{K_{23,A} R_{23,A}} V_{3,A}^{\text{P1}} + \frac{-1}{K_{24,A} R_{24,A}} V_{4,A}^{\text{P1}} =$$

$$= -d_{2,A}^{\text{Re}}, \tag{114}$$

$$\left( \frac{1}{X_{16,A}} + \frac{-0.00625 t_{62,A}}{X_{16,A}} \right) V_{1,A}^{\text{P2}} + \left( \frac{-1}{X_{16,A}} + \frac{0.00625 t_{62,A}}{X_{16,A}} \right) V_{6,A}^{\text{P2}} +$$

$$+ \left( \frac{-1}{X_{23,A}} + \frac{-1}{X_{24,A}} + \frac{-1}{X_{2,A}^{\text{sh}}} \right) V_{2,A}^{\text{P2}} + \frac{1}{X_{23,A}} V_{3,A}^{\text{P2}} + \frac{1}{X_{24,A}} V_{4,A}^{\text{P2}} + \frac{-1}{X_{2,A}^{\text{sh}}} V_{2,A}^{\text{P1}} =$$

$$= -d_{2,A}^{\text{Im}}. \tag{115}$$

The voltage equation for the super node $6 - 2$ can now be written as:

$$\Delta V_A^{\text{P1}} + \Delta V_A^{\text{P2}} = V_{2,A}^{\text{P1}} + V_{2,A}^{\text{P2}} - (V_{6,A}^{\text{P1}} + V_{6,A}^{\text{P2}}), \tag{116}$$

and splitting (116) into parts P1 and P2 yields:

$$\Delta V_A^{\text{P1}} = V_{2,A}^{\text{P1}} - V_{6,A}^{\text{P1}}, \tag{117}$$

$$\Delta V_A^{\text{P2}} = V_{2,A}^{\text{P2}} - V_{6,A}^{\text{P2}}, \tag{118}$$

where $\Delta V_A^{\text{P1}}$ and $\Delta V_A^{\text{P2}}$ are given by:

$$\Delta V_A^{\text{P1}} = 0.00625 t_{62,A} V_{2,A}^{\text{P1}}, \tag{119}$$

$$\Delta V_A^{\text{P2}} = 0.00625 t_{62,A} V_{2,A}^{\text{P2}}. \tag{120}$$

Putting (119) and (120), respectively, into (117) and (118) and rearranging these two expressions, the following can be obtained:

$$V_{6,A}^{P1} + V_{2,A}^{P1}(0.00625t_{62,A} - 1) = 0, \tag{121}$$

$$V_{6,A}^{P2} + V_{2,A}^{P2}(0.00625t_{62,A} - 1) = 0. \tag{122}$$

For phases $B$ and $C$ of super node $6 - 2$, the expressions are analogous to those developed for phase $A$.

## 6.3  Matrix Formulation

The previous sections outlined a nodal analysis of the 6-node system in Fig. 9. On the other hand, concerning the system in Fig. 7, two equations for each phase of the nodes 1, 3, 4 and 5 were defined: the first connects the part 1 (P1) of nodal voltages with the real part of the nodal net current injection, while the second connects part 2 (P2) of nodal voltages with the imaginary part of the nodal net current injection.

Moreover, two voltage equations were obtained for each phase $ph$, (121) and (122), and two balance equations for super node $6 - 2$, these being analogous to the balance equations for other nodes of the system. In the matrix formulation, the voltage equation for the super node $6 - 2$ appears in the line corresponding to the balance equation of node 6; in contrast, the balance equation for the super node $6-2$ appears in the line corresponding to the balance equation of node 2.

### 6.3.1  Equations for Phase $A$

The submatrices $\mathbf{E}_A$, $\mathbf{0}_A$, $\mathbf{F}_A$ and $\mathbf{H}_A$ in (89) are $6 \times 6$, since phase $A$ is present in all nodes of the system. Due to the VR, the equations presented in Sect. 4.6 have to be modified according to:

$$\mathbf{E}_A = \begin{bmatrix} \frac{1}{K_{16,A}R_{16,A}} & \frac{-1}{K_{16,A}R_{16,A}} & 0 & 0 & 0 & 0 \\ 0 & 1 & E_{23,A} & 0 & 0 & 0 \\ E_{31,A} & E_{32,A} & E_{33,A} & \frac{-1}{K_{23,A}R_{23,A}} & \frac{-1}{K_{24,A}R_{24,A}} & 0 \\ 0 & 0 & \frac{-1}{K_{23,A}R_{23,A}} & \frac{1}{K_{23,A}R_{23,A}} & 0 & 0 \\ 0 & 0 & \frac{-1}{K_{24,A}R_{24,A}} & 0 & E_{55,A} & E_{56,A} \\ 0 & 0 & 0 & 0 & \frac{-1}{K_{45,A}R_{45,A}} & E_{66,A} \end{bmatrix}, \tag{123}$$

where the diagonal elements $E_{33,A}$, $E_{55,A}$ and $E_{66,A}$ are given by:

$$E_{33,A} = \frac{1}{K_{23,A}R_{23,A}} + \frac{1}{K_{24,A}R_{24,A}}, \tag{124}$$

$$E_{55,A} = \frac{1}{K_{24,A}R_{24,A}} + \frac{1}{K_{45,A}R_{45,A}}, \tag{125}$$

$$E_{66,A} = \frac{1}{K_{45,A}R_{45,A}}, \tag{126}$$

and the elements $E_{23,A}$, $E_{31,A}$, $E_{32,A}$ and $E_{56,A}$ are given by:

$$E_{23,A} = 0.00625t_{62,A} - 1, \tag{127}$$

$$E_{31,A} = \frac{-1}{K_{16,A}R_{16,A}} + \frac{0.00625t_{62,A}}{K_{16,A}R_{16,A}}, \tag{128}$$

$$E_{32,A} = \frac{1}{K_{16,A}R_{16,A}} + \frac{-0.00625t_{62,A}}{K_{16,A}R_{16,A}}, \tag{129}$$

$$E_{56,A} = \frac{-1}{K_{45,A}R_{45,A}}. \tag{130}$$

The submatrix $\mathbf{0}_A$ is consists of only zeros. In addition, the submatrix $\mathbf{F}_A$ is given by:

$$\mathbf{F}_A = \begin{bmatrix} 0 & 0 & 0 & 0 & 0 & 0 \\ 0 & 0 & 0 & 0 & 0 & 0 \\ 0 & 0 & \frac{-1}{X_{2,A}^{sh}} & 0 & 0 & 0 \\ 0 & 0 & 0 & 0 & 0 & 0 \\ 0 & 0 & 0 & 0 & 0 & 0 \\ 0 & 0 & 0 & 0 & 0 & \frac{-1}{X_{5,A}^{sh}} \end{bmatrix}. \tag{131}$$

The elements of submatrix $\mathbf{H}_A$ are given by:

$$\mathbf{H}_A = \begin{bmatrix} \frac{-1}{X_{16,A}} & \frac{1}{X_{16,A}} & 0 & 0 & 0 & 0 \\ 0 & 1 & 0.00625t_{62,A} - 1 & 0 & 0 & 0 \\ H_{31,A} & H_{32,A} & H_{33,A} & \frac{1}{X_{23,A}} & \frac{1}{X_{24,A}} & 0 \\ 0 & 0 & \frac{1}{X_{23,A}} & \frac{-1}{X_{23,A}} & 0 & 0 \\ 0 & 0 & \frac{1}{X_{24,A}} & 0 & H_{55,A} & \frac{1}{X_{45,A}} \\ 0 & 0 & 0 & 0 & \frac{1}{X_{45,A}} & \frac{-1}{X_{45,A}} + \frac{-1}{X_{5,A}^{\text{sh}}} \end{bmatrix}, \quad (132)$$

where:

$$H_{31,A} = \frac{1}{X_{16,A}} + \frac{-0.00625t_{62,A}}{X_{16,A}}, \quad (133)$$

$$H_{32,A} = \frac{-1}{X_{16,A}} + \frac{0.00625t_{62,A}}{X_{16,A}}, \quad (134)$$

$$H_{33,A} = \frac{-1}{X_{23,A}} + \frac{-1}{X_{24,A}} + \frac{-1}{X_{2,A}^{\text{sh}}}, \quad (135)$$

$$H_{55,A} = \frac{-1}{X_{24,A}} + \frac{-1}{X_{45,A}}. \quad (136)$$

The subvectors $\mathbf{V}_A^{\text{P1}}$ and $\mathbf{V}_A^{\text{P2}}$ in (89) are $6 \times 1$ and are given by:

$$\mathbf{V}_A^{\text{P1}} = \begin{bmatrix} V_{1,A}^{\text{P1}} \\ V_{6,A}^{\text{P1}} \\ V_{2,A}^{\text{P1}} \\ V_{3,A}^{\text{P1}} \\ V_{4,A}^{\text{P1}} \\ V_{5,A}^{\text{P1}} \end{bmatrix}, \quad (137a)$$

$$\mathbf{V}_A^{\text{P2}} = \begin{bmatrix} V_{1,A}^{\text{P2}} \\ V_{6,A}^{\text{P2}} \\ V_{2,A}^{\text{P2}} \\ V_{3,A}^{\text{P2}} \\ V_{4,A}^{\text{P2}} \\ V_{5,A}^{\text{P2}} \end{bmatrix}. \quad (137b)$$

The subvectors $\mathbf{g}_A^{\text{Re}} - \mathbf{d}_A^{\text{Re}}$ and $\mathbf{g}_A^{\text{Im}} - \mathbf{d}_A^{\text{Im}}$ in (89) are $6 \times 1$ and defined as:

$$
\mathbf{g}_A^{\text{Re}} - \mathbf{d}_A^{\text{Re}} =
\begin{bmatrix}
g_{1,A}^{\text{Re}} \\
0 \\
-d_{2,A}^{\text{Re}} \\
g_{3,A}^{\text{Re}} - d_{3,A}^{\text{Re}} \\
-d_{4,A}^{\text{Re}} \\
-d_{5,A}^{\text{Re}}
\end{bmatrix},
\tag{138a}
$$

$$
\mathbf{g}_A^{\text{Im}} - \mathbf{d}_A^{\text{Im}} =
\begin{bmatrix}
g_{1,A}^{\text{Im}} \\
0 \\
-d_{2,A}^{\text{Im}} \\
g_{3,A}^{\text{Im}} - d_{3,A}^{\text{Im}} \\
-d_{4,A}^{\text{Im}} \\
-d_{5,A}^{\text{Im}}
\end{bmatrix}.
\tag{138b}
$$

### 6.3.2   Equations for Phases $B$ and $C$

For phases $B$ and $C$, the submatrices $\mathbf{E}_{ph}$, $\mathbf{0}_{ph}$, $\mathbf{F}_{ph}$ and $\mathbf{H}_{ph}$ in (89) are $5 \times 5$, since phases $B$ and $C$ are not connected to node 5, but only to nodes 1 to 4. The main modifications in the equations presented in Sect. 4.6, which are necessary due to the inclusion of the VR. The submatrix $\mathbf{E}_B$ is given by:

$$
\mathbf{E}_B =
\begin{bmatrix}
\frac{1}{K_{16,B} R_{16,B}} & \frac{-1}{K_{16,B} R_{16,B}} & 0 & 0 & 0 \\
0 & 1 & 0.00625 t_{62,B} - 1 & 0 & 0 \\
E_{31,B} & E_{32,B} & E_{33,B} & \frac{-1}{K_{23,B} R_{23,B}} & \frac{-1}{K_{24,B} R_{24,B}} \\
0 & 0 & \frac{-1}{K_{23,A} R_{23,A}} & \frac{1}{K_{23,A} R_{23,A}} & 0 \\
0 & 0 & \frac{-1}{K_{24,B} R_{24,B}} & 0 & \frac{1}{K_{24,B} R_{24,B}}
\end{bmatrix},
\tag{139}
$$

where the elements $E_{31,B}$, $E_{32,B}$ and $E_{33,B}$ are given by:

$$
E_{31,B} = \frac{-1}{K_{16,B} R_{16,B}} + \frac{0.00625 t_{62,B}}{K_{16,B} R_{16,B}},
\tag{140}
$$

$$
E_{32,B} = \frac{1}{K_{16,B} R_{16,B}} + \frac{-0.00625 t_{62,B}}{K_{16,B} R_{16,B}},
\tag{141}
$$

$$
E_{33,B} = \frac{1}{K_{23,B} R_{23,B}} + \frac{1}{K_{24,B} R_{24,B}}.
\tag{142}
$$

The submatrix $\mathbf{0}_B$ is composed of zeros. In addition, the submatrix $\mathbf{F}_B$ is given by:

$$\mathbf{F}_B = \begin{bmatrix} 0 & 0 & 0 & 0 & 0 \\ 0 & 0 & 0 & 0 & 0 \\ 0 & 0 & \frac{-1}{X_{2,B}^{\text{sh}}} & 0 & 0 \\ 0 & 0 & 0 & 0 & 0 \\ 0 & 0 & 0 & 0 & 0 \end{bmatrix}. \tag{143}$$

The elements of submatrix $\mathbf{H}_B$ are defined as:

$$\mathbf{H}_B = \begin{bmatrix} \frac{-1}{X_{16,B}} & \frac{1}{X_{16,B}} & 0 & 0 & 0 \\ 0 & 1 & 0.00625t_{62,B} - 1 & 0 & 0 \\ H_{31,B} & H_{32,B} & H_{33,B} & \frac{1}{X_{23,B}} & \frac{1}{X_{24,B}} \\ 0 & 0 & \frac{1}{X_{23,B}} & \frac{-1}{X_{23,B}} & 0 \\ 0 & 0 & \frac{1}{X_{24,B}} & 0 & \frac{-1}{X_{24,B}} \end{bmatrix}. \tag{144}$$

where:

$$H_{31,B} = \frac{1}{X_{16,B}} + \frac{-0.00625t_{62,B}}{X_{16,B}}, \tag{145}$$

$$H_{32,B} = \frac{-1}{X_{16,B}} + \frac{0.00625t_{62,B}}{X_{16,B}}, \tag{146}$$

$$H_{33,B} = \frac{-1}{X_{23,B}} + \frac{-1}{X_{24,B}} + \frac{-1}{X_{2,B}^{\text{sh}}}. \tag{147}$$

The subvectors $\mathbf{V}_B^{\text{P1}}$ and $\mathbf{V}_B^{\text{P2}}$ in (89), for phase $B$, have dimension $5 \times 1$ and are given by:

$$\mathbf{V}_B^{\text{P1}} = \begin{bmatrix} V_{1,B}^{\text{P1}} \\ V_{6,B}^{\text{P1}} \\ V_{2,B}^{\text{P1}} \\ V_{3,B}^{\text{P1}} \\ V_{4,B}^{\text{P1}} \end{bmatrix}, \tag{148a}$$

$$\mathbf{V}_B^{\mathrm{P2}} = \begin{bmatrix} V_{1,B}^{\mathrm{P2}} \\ V_{6,B}^{\mathrm{P2}} \\ V_{2,B}^{\mathrm{P2}} \\ V_{3,B}^{\mathrm{P2}} \\ V_{4,B}^{\mathrm{P2}} \end{bmatrix}. \tag{148b}$$

The subvectors $\mathbf{g}_B^{\mathrm{Re}} - \mathbf{d}_B^{\mathrm{Re}}$ and $\mathbf{g}_B^{\mathrm{Im}} - \mathbf{d}_B^{\mathrm{Im}}$ in (89) are $5 \times 1$ and given by:

$$\mathbf{g}_B^{\mathrm{Re}} - \mathbf{d}_B^{\mathrm{Re}} = \begin{bmatrix} g_{1,B}^{\mathrm{Re}} \\ 0 \\ -d_{2,B}^{\mathrm{Re}} \\ g_{3,B}^{\mathrm{Re}} - d_{3,B}^{\mathrm{Re}} \\ -d_{4,B}^{\mathrm{Re}} \end{bmatrix}, \tag{149a}$$

$$\mathbf{g}_B^{\mathrm{Im}} - \mathbf{d}_B^{\mathrm{Im}} = \begin{bmatrix} g_{1,B}^{\mathrm{Im}} \\ 0 \\ -d_{2,B}^{\mathrm{Im}} \\ g_{3,B}^{\mathrm{Im}} - d_{3,B}^{\mathrm{Im}} \\ -d_{4,B}^{\mathrm{Im}} \end{bmatrix}. \tag{149b}$$

The expressions for phase $C$ are analogous to the expressions developed for phase $B$.

# 7 Modifications to Consider Nodes with Controlled Voltage

In order to consider nodes with controlled voltage, the submatrices and subvectors previously presented have to be modified. Special attention is given to nodes where the voltage is regulated by a three-phase synchronous generator, as in this case, the power injections of all phases should be as balanced as possible.[2]

## 7.1 Modifications to Consider the Reference Node

In the model we present in this chapter, one of the nodes is chosen to close the current balance, similarly to the conventional load flow where a node is chosen

---

[2]Current imbalances in the phases of synchronous generators can cause additional losses in the stator and rotor leading to excessive temperature rise and thus potential damage to the windings; besides, imbalances can increase mechanical stress and produce vibrations in the structural parts. Therefore, in practice, protection devices limit imbalances to 5%.

to close the power balance. For medium voltage feeders, the substation node is usually chosen. To consider the known voltage at the reference node, for each phase $ph$, the specified voltage is assigned to part 1 $\left( V_{k,ph}^{\text{P1}} = V_k^{\text{esp}} \right)$ and zero to part 2 $\left( V_{k,ph}^{\text{P2}} = 0 \right)$. This modification is done before the solution of (90) and (91) is found.

For the system in Fig. 7, node 1 is chosen to close the current balance. Thus, in what follows, the modifications in the elements in the line corresponding to node 1 of submatrices and subvectors in (89), given in Sect. 4.6, are described. The submatrices $\mathbf{0}_{ph}$ and $\mathbf{F}_{ph}$ are not modified. For phase $A$, the submatrix $\mathbf{E}_A$ defined in (74) becomes:

$$\mathbf{E}_A = \begin{bmatrix} 1 & 0 & 0 & 0 & 0 \\ \frac{-1}{K_{12,A}R_{12,A}} & E_{22,A} & \frac{-1}{K_{23,A}R_{23,A}} & \frac{-1}{K_{24,A}R_{24,A}} & 0 \\ 0 & \frac{-1}{K_{23,A}R_{23,A}} & \frac{1}{K_{23,A}R_{23,A}} & 0 & 0 \\ 0 & \frac{-1}{K_{24,A}R_{24,A}} & 0 & E_{44,A} & \frac{-1}{K_{45,A}R_{45,A}} \\ 0 & 0 & 0 & \frac{-1}{K_{45,A}R_{45,A}} & \frac{1}{K_{45,A}R_{45,A}} \end{bmatrix}, \tag{150}$$

where the elements of the diagonal $E_{22,A}$ e $E_{44,A}$ are given by:

$$E_{22,A} = \frac{1}{K_{12,A}R_{12,A}} + \frac{1}{K_{23,A}R_{23,A}} + \frac{1}{K_{24,A}R_{24,A}}, \tag{151}$$

$$E_{44,A} = \frac{1}{K_{24,A}R_{24,A}} + \frac{1}{K_{45,A}R_{45,A}}. \tag{152}$$

For phase $A$, (78) becomes:

$$\mathbf{H}_A = \begin{bmatrix} 1 & 0 & 0 & 0 & 0 \\ \frac{1}{X_{12,A}} & H_{22,A} & \frac{1}{X_{23,A}} & \frac{1}{X_{24,A}} & 0 \\ 0 & \frac{1}{X_{23,A}} & \frac{-1}{X_{23,A}} & 0 & 0 \\ 0 & \frac{1}{X_{24,A}} & 0 & H_{44,A} & \frac{1}{X_{45,A}} \\ 0 & 0 & 0 & \frac{1}{X_{45,A}} & \frac{-1}{X_{45,A}} + \frac{-1}{X_{5,A}^{\text{sh}}} \end{bmatrix}, \tag{153}$$

where:

$$H_{22,A} = \frac{-1}{X_{12,A}} + \frac{-1}{X_{23,A}} + \frac{-1}{X_{24,A}} + \frac{-1}{X_{2,A}^{\text{sh}}}, \tag{154}$$

$$H_{44,A} = \frac{-1}{X_{24,A}} + \frac{-1}{X_{45,A}}. \tag{155}$$

The submatrices $\mathbf{E}_{ph}$ and $\mathbf{H}_{ph}$ of phases $B$ and $C$ are modified analogously to phase $A$.

The subvectors $\mathbf{g}_A^{\text{Re}} - \mathbf{d}_A^{\text{Re}}$ and $\mathbf{g}_A^{\text{Im}} - \mathbf{d}_A^{\text{Im}}$ are given by:

$$\mathbf{g}_A^{\text{Re}} - \mathbf{d}_A^{\text{Re}} = \begin{bmatrix} V_1^{\text{esp}} \\ -d_{2,A}^{\text{Re}} \\ g_{3,A}^{\text{Re}} - d_{3,A}^{\text{Re}} \\ -d_{4,A}^{\text{Re}} \\ -d_{5,A}^{\text{Re}} \end{bmatrix}, \tag{156a}$$

$$\mathbf{g}_A^{\text{Im}} - \mathbf{d}_A^{\text{Im}} = \begin{bmatrix} 0 \\ -d_{2,A}^{\text{Im}} \\ g_{3,A}^{\text{Im}} - d_{3,A}^{\text{Im}} \\ -d_{4,A}^{\text{Im}} \\ -d_{5,A}^{\text{Im}} \end{bmatrix}. \tag{156b}$$

The subvectors $\mathbf{g}_{ph}^{\text{Re}} - \mathbf{d}_{ph}^{\text{Re}}$ and $\mathbf{g}_{ph}^{\text{Im}} - \mathbf{d}_{ph}^{\text{Im}}$ of phases $B$ and $C$ are analogously modified.

## 7.2 Modifications to Consider Voltage-Controlled Generation Nodes

For DGs to control the voltage at the node to which they are connected (PV node), part 1 of nodal voltage is determined $\left( V_{k,ph}^{\text{P1}} \right)$ through (90). When the part 1 for the PV node is determined, part 2 $\left( V_{k,ph}^{\text{P2}} \right)$ can then be calculated by subtracting the part 1 of the nodal voltage from the specified voltage, that is $V_{k,ph}^{\text{P2}} = V_k^{\text{esp}} - V_{k,ph}^{\text{P1}}$. This modification is undertaken before solving (91).

The system in Fig. 7 has one DG connected at the node 3. Considering this DG operating as a PV node, modifications are necessary in the elements in the line corresponding to the node 3 of the submatrices and subvectors in (91), given in Sect. 4.6. For phase $A$, (78) becomes:

$$\mathbf{H}_A = \begin{bmatrix} 1 & 0 & 0 & 0 & 0 \\ \frac{1}{X_{12,A}} & H_{22,A} & \frac{1}{X_{23,A}} & \frac{1}{X_{24,A}} & 0 \\ 0 & 0 & 1 & 0 & 0 \\ 0 & \frac{1}{X_{24,A}} & 0 & H_{44,A} & \frac{1}{X_{45,A}} \\ 0 & 0 & 0 & \frac{1}{X_{45,A}} & \frac{-1}{X_{45,A}} + \frac{-1}{X_{5,A}^{\text{sh}}} \end{bmatrix}, \tag{157}$$

where:

$$H_{22,A} = \frac{-1}{X_{12,A}} + \frac{-1}{X_{23,A}} + \frac{-1}{X_{24,A}} + \frac{-1}{X_{2,A}^{sh}}, \tag{158}$$

$$H_{44,A} = \frac{-1}{X_{24,A}} + \frac{-1}{X_{45,A}}. \tag{159}$$

For the submatrix $\mathbf{H}_{ph}$ related to phases $B$ and $C$, the modifications are the same. The submatrix $\mathbf{F}_{ph}$ needs no modifications.

The subvector $\mathbf{g}_A^{Im} - \mathbf{d}_A^{Im}$ is given by:

$$\mathbf{g}_A^{Im} - \mathbf{d}_A^{Im} = \begin{bmatrix} 0 \\ -d_{2,A}^{Im} \\ V_3^{esp} - V_{3,A}^{P1} \\ -d_{4,A}^{Im} \\ -d_{5,A}^{Im} \end{bmatrix}. \tag{160}$$

For the subvectors $\mathbf{g}_{ph}^{Im} - \mathbf{d}_{ph}^{Im}$ of phases $B$ and $C$ the same modifications apply.

It is worth mentioning that, after obtaining the nodal voltages, the current injections (real and imaginary parts) of the reference node and PV nodes can be easily obtained.

## 7.3 Modifications to Consider Nodes with Synchronous Generators

When a synchronous generator is connected to an unbalanced three-phase system, the injected or absorbed reactive power is different in each phase. However, the automatic voltage regulators (AVRs) of the generator usually monitors only a single voltage, which can be the voltage of one of the phases, or a function of the voltages of all phases, such as the average phase voltage, or the positive sequence voltage [37]. Therefore, AVRs do not regulate each phase voltage individually; they rather act to maintain the specified terminal voltage by injecting or absorbing the same reactive power into each phase of the synchronous generator.

In the proposed model, voltages are initially obtained considering that the imaginary part of current injections at the PV node is different in each phase. Thus, the imaginary part of current injection is obtained for each phase of the node where the DG is connected; these current injections, which can be different for each phase, lead to the specified voltage ($V_k^{esp}$) for all phases at this node. In a second step, the imaginary part of current injections at the PV node is modified to be equal to the mean value of the imaginary current injections previously obtained for each phase; this mean value is then assigned to all three phases. Subsequently, voltages are once

again calculated considering this information. Different voltages may result for each phase, however they will be close to the specified voltage ($V_k^{\text{esp}}$).

## 8    Three-Phase Voltages and Currents Calculation

In the formulation presented so far, we assumed that nodal voltages have zero as phase angle. Thus, after the solution is obtained for all phases, the nodal voltages and the currents in branches have to be adjusted. This adjustment in nodal voltages is done considering the operator a $= 1 \angle 120^o$ through the following equations:

$$\overline{V}_{k,A} = V_{k,A}^{\text{P1}} + V_{k,A}^{\text{P2}}, \tag{161}$$

$$\overline{V}_{k,B} = \text{a}^2 \left( V_{k,B}^{\text{P1}} + V_{k,B}^{\text{P2}} \right), \tag{162}$$

$$\overline{V}_{k,C} = \text{a} \left( V_{k,C}^{\text{P1}} + V_{k,C}^{\text{P2}} \right). \tag{163}$$

The currents in branches are adjusted using the following equations:

$$\overline{f}_{km,A} = f_{km,A}^{\text{Re}} + j f_{km,A}^{\text{Im}}, \tag{164}$$

$$\overline{f}_{km,B} = \text{a}^2 \left( f_{km,B}^{\text{Re}} + j f_{km,B}^{\text{Im}} \right), \tag{165}$$

$$\overline{f}_{km,C} = \text{a} \left( f_{km,C}^{\text{Re}} + j f_{km,C}^{\text{Im}} \right). \tag{166}$$

## 9    Tests and Results

This Section presents numerical studies obtained using a modified version of the IEEE 34-node test feeder [22]. The proposed model was implemented in MATLAB and the results obtained with the proposed linear model (LM) have been compared with the solution of the nonlinear load flow (LF) obtained using the OpenDSS software [13]. To compare the results, indices to measure the difference in voltages and power losses are used. The voltage difference index is defined as:

$$\bar{\varepsilon}_{ph}^{V}(\%) = \frac{\sum_{k=1}^{n} \varepsilon_{k,ph}^{V}}{n} 100, \tag{167}$$

where $n$ is the total number of nodes of the system and $\varepsilon_{k,ph}^{V}$ is the relative difference in voltages, determined for each phase $ph$ and each node $k$ through the following

expression:

$$\varepsilon_{k,ph}^V = \left| \frac{V_{k,ph} - V_{k,ph}^{\mathrm{LF}}}{V_{k,ph}^{\mathrm{LF}}} \right|, \tag{168}$$

where $V_{k,ph}^{\mathrm{LF}}$ is the voltage of phase $ph$ at the node $k$ obtained from the solution of the LF; $V_{k,ph}$ is the voltage of phase $ph$ at the node $k$ obtained using the LM.

The difference in power losses is obtained comparing the total power losses of the system obtained using the LF and the LM; this difference in percentage is given by:

$$\varepsilon_{loss}(\%) = \frac{P_{loss} - P_{loss}^{\mathrm{LF}}}{P_{loss}^{\mathrm{LF}}} 100, \tag{169}$$

where $P_{loss}^{\mathrm{LF}}$ are the total power losses obtained from the solution of the LF and $P_{loss}$ are the total power losses obtained from the solution of the LM; $P_{loss}$ is determined as follows:

$$P_{loss} = P_{loss,A} + P_{loss,B} + P_{loss,C}, \tag{170}$$

where the power losses $P_{loss,ph}$ of each phase $ph$ are obtained from:

$$P_{loss,ph} = \sum_{km=1}^{nb} P_{loss,km,ph}, \tag{171}$$

with $nb$ being the number of branches in the system. The power losses $P_{loss,km,ph}$ of each phase $ph$ of each branch $km$ are obtained from:

$$P_{loss,km,ph} = R_{km,ph}(f_{km,ph}^{\mathrm{Re}})^2 + R_{km,ph}(f_{km,ph}^{\mathrm{Im}})^2. \tag{172}$$

## 9.1 Modified IEEE 34-Nodes Test Feeder

Figure 10 illustrates the modified IEEE 34-node test feeder. This three-phase unbalanced system operates at 24.9 kV with a nominal load of 1.77 MW and 1.07 Mvar. Furthermore, in the solution of the LF using OpenDSS, loads were modeled as defined in [22]; it is worth mentioning that the test feeder contains loads modeled as constant impedance, as constant current, and also as constant power. The modifications we implemented are:
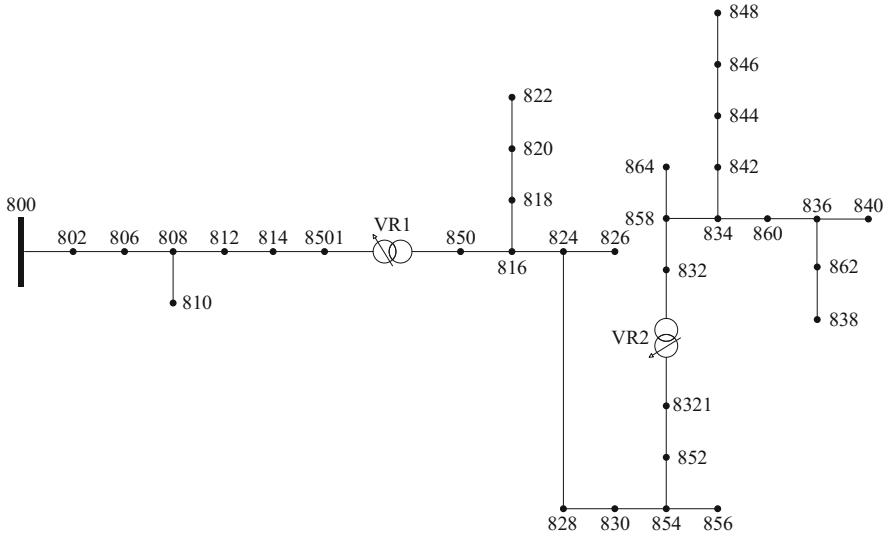
**Fig. 10** 34-Node system

- loads connected between phases have been transformed into equivalent loads connected between phase and ground;
- branches downstream node 832 have been modeled as an equivalent load at the node 832;
- loads distributed along a given branch have been reconnected at the terminals of the branch, with each terminal receiving half of the load.
- line capacitances have been neglected;
- each VR is replaced by an ideal VR and a branch with impedance of $0.001 + j0.01$ pu.

In the linear model we present in this chapter, the series impedance of the branches are approximated by the difference between the self impedance and the mutual impedances of the respective phases according to:

$$\overline{Z}_{km,A} = \overline{Z}_{km,AA} - \frac{\overline{Z}_{km,AB} + \overline{Z}_{km,AC}}{2}, \tag{173}$$

$$\overline{Z}_{km,B} = \overline{Z}_{km,BB} - \frac{\overline{Z}_{km,AB} + \overline{Z}_{km,BC}}{2}, \tag{174}$$

$$\overline{Z}_{km,C} = \overline{Z}_{km,CC} - \frac{\overline{Z}_{km,BC} + \overline{Z}_{km,AC}}{2}, \tag{175}$$

where $\overline{Z}_{km,A}$, $\overline{Z}_{km,B}$ and $\overline{Z}_{km,C}$ are the approximations of the series impedances of phases $A$, $B$, and $C$ of the branch $km$, which are used in the linear model

**Table 4** Series impedances of each phase of the branches of the 34-node feeder used in the linear model

| Configuration | $\overline{Z}_{km,A}[\frac{\Omega}{km}]$ | $\overline{Z}_{km,B}[\frac{\Omega}{km}]$ | $\overline{Z}_{km,C}[\frac{\Omega}{km}]$ |
|---|---|---|---|
| 300 | $0.6992 + j0.4937$ | $0.6931 + j0.5210$ | $0.6957 + j0.5386$ |
| 301 | $1.0537 + j0.5001$ | $1.0470 + j0.5245$ | $1.0498 + j0.5434$ |
| 302 | $1.7395 + j0.9230$ | – | – |
| 303 | – | $1.7395 + j0.9230$ | – |
| 304 | – | $1.1941 + j0.8831$ | – |

to represent the network. For the modified 34-node test feeder, the approximate impedances are presented in Table 4. The line configurations 302, 303 and 304 [22] have no mutual impedances as they are single-phase lines, thus $\overline{Z}_{km,A} = \overline{Z}_{km,AA}$, $\overline{Z}_{km,B} = \overline{Z}_{km,BB}$, and $\overline{Z}_{km,C} = \overline{Z}_{km,CC}$.

The base case was defined assuming that no CB or DG is installed and that the voltage regulators VR1 and VR2 operate at the neutral tap position in all three phases. For this base case, we obtained the adjustment factors $K_{km,ph}$ using (12) for each phase of each branch. These adjustment factors are then used in the subsequent tests.

To validate the proposed model, it was tested under different operation points, with new devices being added to modify the base case. The following test cases were considered:

- **Case I:** VR1 is operating with taps 12, 5 and 5 in phases $A$, $B$, and $C$, respectively; VR2 is operating with taps 13, 11, and 12 in phases $A$, $B$, and $C$, respectively; a 300-kvar three-phase CB at the node 844 and a 450 kvar three-phase CB at the node 848 were included. In this case, the reactive power compensation and VR taps are those suggested in [22].
- **Case II:** both VRs are operating at the neutral tap position in all three phases, and eight three-phase CBs distributed in the system, each one with 133.85 kvar, were included at the following nodes: 808, 816, 828, 854, 858, 844, 848, and 836. In this case, the reactive power compensation is approximately equivalent to the total reactive power demanded by the loads.
- **Case III:** both VRs are operating at the neutral tap position in all three phases. In this case, a DG was connected at the node 830 and is operating in the PQ mode, with a maximum active power generation of 1 MW and unity power factor. In addition, three-phase CBs of 300 kvar and 450 kvar were included at nodes 844 and 848, respectively.
- **Case IV:** both VRs are operating at the neutral tap position in all phases. In addition, a synchronous DG was connected at the node 830 operating in the PV mode, with a maximum active power generation of 1 MW and specified voltage of 1.0 pu. Three-phase CBs of 300 and 450 kvar were included at nodes 844 and 848, respectively.

The parameters used in the base case and the four test cases are summarized in Table 5.

**Table 5** Summary of the test cases

| Base case | | |
|---|---|---|
| VRs | $t_{8501\_850,A}$ $= t_{8501\_850,B} = t_{8501\_850,C} = 0$ | $t_{8321\_832,A} = t_{8321\_832,B}$ $= t_{8321\_832,C} = 0$ |
| CBs (kvar) | | |
| DG (kW) | | |
| Case I | | |
| VRs | $t_{8501\_850,A} = 12$ $t_{8501\_850,B} = 5$ $t_{8501\_850,C} = 5$ | $t_{8321\_832,A} = 13$ $t_{8321\_832,B} = 11$ $t_{8321\_832,C} = 12$ |
| CBs (kvar) | $Q_{844,A}^{\mathrm{sh}} = Q_{844,B}^{\mathrm{sh}} = Q_{844,C}^{\mathrm{sh}} = -100$ | $Q_{848,A}^{\mathrm{sh}} = Q_{848,B}^{\mathrm{sh}} = Q_{848,C}^{\mathrm{sh}} = -150$ |
| DG (kW) | | |
| Case II | | |
| VRs | $t_{8501\_850,A} = t_{8501\_850,B} =$ $t_{8501\_850,C} = 0$ | $t_{8321\_832,A} = t_{8321\_832,B} =$ $t_{8321\_832,C} = 0$ |
| CBs (kvar) | $Q_{k,A}^{\mathrm{sh}} = Q_{k,B}^{\mathrm{sh}} = Q_{k,C}^{\mathrm{sh}} = -44.62$ | where $k =$ 808, 816, 828, 854, 858, 844, 848, 836 |
| DG (kW) | | |
| Case III | | |
| VRs | $t_{8501\_850,A} = t_{8501\_850,B} =$ $t_{8501\_850,C} = 0$ | $t_{8321\_832,A} = t_{8321\_832,B} =$ $t_{8321\_832,C} = 0$ |
| CBs (kvar) | $Q_{844,A}^{\mathrm{sh}} = Q_{844,B}^{\mathrm{sh}} = Q_{844,C}^{\mathrm{sh}} = -100$ | $Q_{848,A}^{\mathrm{sh}} = Q_{848,B}^{\mathrm{sh}} = Q_{848,C}^{\mathrm{sh}} = -150$ |
| DG (kW) | $P_{830,A}^{\mathrm{G}} = P_{830,B}^{\mathrm{G}} = P_{830,C}^{\mathrm{G}} = 333.33$ $\quad pf = 1$ | |
| Case IV | | |
| VRs | $t_{8501\_850,A} = t_{8501\_850,B} =$ $t_{8501\_850,C} = 0$ | $t_{8321\_832,A} = t_{8321\_832,B} =$ $t_{8321\_832,C} = 0$ |
| CBs (kvar) | $Q_{844,A}^{\mathrm{sh}} = Q_{844,B}^{\mathrm{sh}} = Q_{844,C}^{\mathrm{sh}} = -100$ | $Q_{848,A}^{\mathrm{sh}} = Q_{848,B}^{\mathrm{sh}} = Q_{848,C}^{\mathrm{sh}} = -150$ |
| GD (kW) | $P_{830,A}^{\mathrm{G}} = P_{830,B}^{\mathrm{G}} = P_{830,C}^{\mathrm{G}} = 333.33$ | $V_{830}^{\mathrm{esp}} = 1.00\,\mathrm{pu}$ |

## 9.2 Comparison of Results

To further investigate the accuracy of the proposed linear model, we compared the results obtained with our model with results obtained with the conventional load flow using the OpenDSS software [13]. The results for the voltage difference indices (167) and power losses difference indices (169) are summarized in Table 6. In this table, columns 2 to 4 show the voltage difference indices for phases $A$, $B$, and $C$, respectively, while column 5 presents the loss difference index.

In the base case, the nodal voltages obtained using the linear model (LM) and the load flow (LF) are equal because the linearization was done around the same operation point as in the base case.[3] From the results in Table 6, a very good agreement emerges between the results obtained using the LM and using the LF. For

---

[3]The difference is zero since the adjustment factor $K_{km,ph}$ is obtained for the same operation point.

**Table 6** Differences in indices $\bar{\varepsilon}_{ph}^{V}(\%)$ and $\varepsilon_{loss}(\%)$ for the modified 34-node test feeder

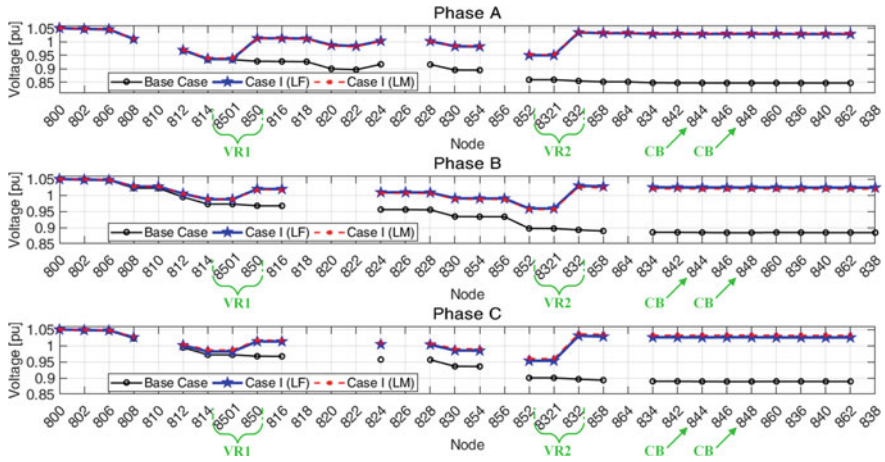| Case | $\bar{\varepsilon}_{A}^{V}(\%)$ | $\bar{\varepsilon}_{B}^{V}(\%)$ | $\bar{\varepsilon}_{C}^{V}(\%)$ | $\varepsilon_{loss}(\%)$ |
|---|---|---|---|---|
| **Base** | 0.000 | 0.000 | 0.000 | −3.469 |
| **I** | 0.532 | 0.067 | 0.720 | −3.763 |
| **II** | 0.203 | 0.181 | 0.199 | −0.098 |
| **III** | 0.593 | 0.216 | 0.237 | −6.737 |
| **IV** | 0.330 | 0.045 | 0.033 | −3.372 |



**Fig. 11** Voltage profiles—Case I

instance, the voltage difference indices are less than 0.7% and the biggest difference in power losses is approximately −6.7%.

An analysis of the results in Table 6 reveals that, even in the base, differences can be observed in the power losses.[4] In general, the LM underestimates the power losses. The fact that the losses obtained through both models are close indicates that currents in branches are also close, even though the load models are different in the LM and LF.

To better illustrate the quality of the solutions achieved, we compared the voltage profiles obtained with the proposed model with those obtained through the nonlinear load flow. Figures 11, 12, 13 and 14 show the voltage profiles for the test cases I, II, III, and IV, respectively. The voltages of the base case are also shown, to demonstrate the improvements in the voltage profile when VRs, CBs, and DGs are included in the system. The gaps in the voltage profiles indicate that the node in the gap has no branch in the respective phase.

---

[4]Note that the adjustment factors $K_{km,ph}$ are calculated so that no differences arise in the voltage magnitudes of the base case; yet the power losses are not corrected.
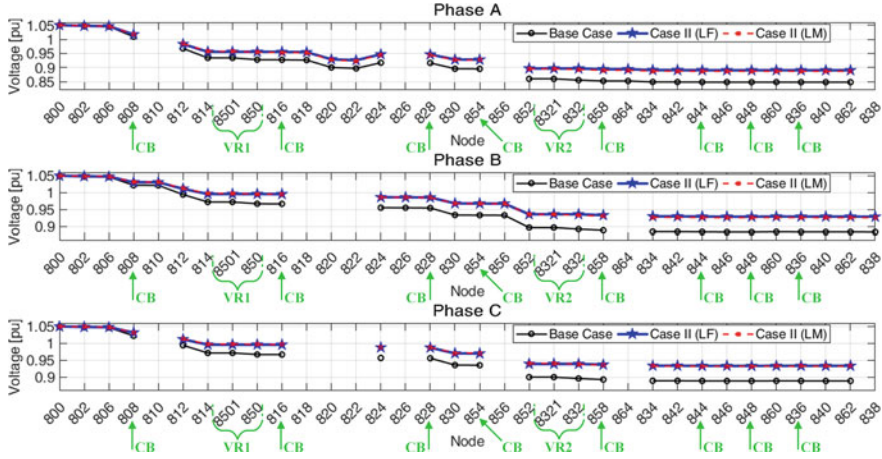
**Fig. 12** Voltage profiles—Case II
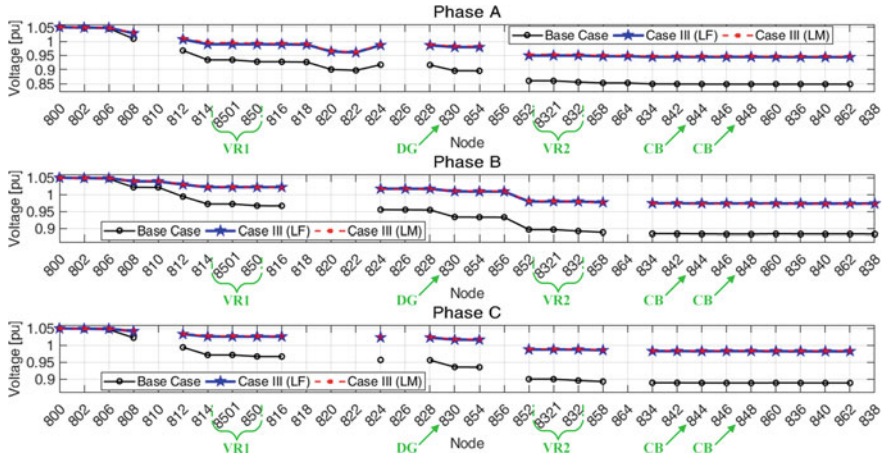


**Fig. 13** Voltage profiles—Case III

The profile of node voltages when VRs operate at different taps can be observed in Fig. 11. This figure confirms the importance of VRs to the voltage regulation of distribution systems, since a significant improvement in voltage magnitudes can be achieved. In addition, small divergences between voltages obtained using the LM and the LF can be seen, the indices of voltage difference for Case I being less than 1.03%, for example.

The impacts of the inclusion of CBs in the magnitudes of node voltages can be observed in Fig. 12. In this case, the total reactive power of CBs approximately equals the reactive power demanded by the loads. Also in this case, a very good agreement can be observed between the voltages obtained using the LM and those

**Fig. 14** Voltage profiles—Case IV

obtained with the LF. According to Table 6, the indices for the voltage difference is lower than 0.3%.

Regarding Case III, where a DG at the node 830 operate in the PQ mode, the voltage difference index for this node resulted in 0.6% for phase $A$, 0.3% for phase $B$, and 0.2% for phase $C$. On the other hand, in Case IV, the DG operates in the PV mode with specified voltage of 1.0 pu at the node 830 (where the DG is connected), as can be 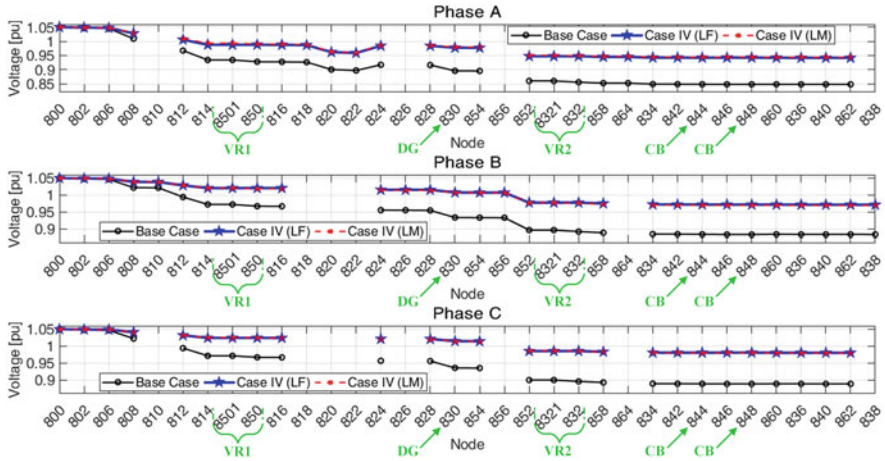confirmed in Fig. 14. The voltage magnitudes at the node 830 obtained using the LM were 0.9794 (phase $A$), 1.0075 (phase $B$), and 1.0145 (phase $C$), while using the LF, the voltage magnitudes are 0.9765 (phase $A$), 1.0078 (phase $B$), and 1.0157 (phase $C$). The resulting reactive power of the DG is 79.1 kvar (absorbing) using the LM, and 1.3 kvar (injecting) using the LF. Thus, the results of both models agree very well.

The results presented so far confirm that the proposed model can appropriately predict the system response to the imposed disturbances. Further, the results are very close to those obtained using the OpenDSS, in which different load models are considered. It is worth mentioning that the operation points in all cases considered are quite different from the operation point of the base case, which is the operation point around which the LM was developed.

## 10  Conclusions

This chapter presented a linear load flow formulation for unbalanced distribution systems. The proposed model can solve the load flow problem considering the presence of voltage regulators, capacitor banks, and distributed generation. Using a linear model, a solution for the load flow problem is guaranteed even for extreme

operation points, in which conventional load flow may not converge. In addition, the proposed formulation can be applied to optimization models to solve expansion planning problems of power distribution systems. Using a linear formulation, the convergence to the optimal solution is guaranteed using classical optimization techniques.

To assess and validate the proposed formulation, we used a modified version of the IEEE 34-node test feeder. A comparison of results obtained using the proposed linear model with corresponding results obtained using the nonlinear load flow confirmed that the model is not only valid but also able to give accurate results.

# References

1. Ahmadi, H., Martí, J.R.: Power flow formulation based on a mixed-linear and nonlinear system of equations. In: 2013 13th International Conference on Environment and Electrical Engineering (EEEIC), pp. 27–32 (2013). https://doi.org/10.1109/EEEIC-2.2013.6737877
2. Ahmadi, H., Martí, J.R.: Distribution system optimization based on a linear power-flow formulation. IEEE Trans. Power Delivery **30**(1), 25–33 (2015). https://doi.org/10.1109/TPWRD.2014.2300854
3. Anwar, A., Mahmood, A.N.: CF-PSO based loss sensitivity clustering technique to identify optimal DG allocation nodes for energy efficient smart grid operation. In: 2014 9th IEEE Conference on Industrial Electronics and Applications, pp. 1130–1135 (2014), https://doi.org/10.1109/ICIEA.2014.6931335
4. Berg, R., Hawkins, E.S., Pleines, W.W.: Mechanized calculation of unbalanced load flow on radial distribution circuits. IEEE Trans. Power Syst. **PAS-86**(4), 415–421 (1967). https://doi.org/10.1109/TPAS.1967.291849
5. Bhimarasetti, R.T., Kumar, A.: A new contribution to distribution load flow analysis for radial and mesh distribution systems. In: 2014 International Conference on Computational Intelligence and Communication Networks, pp. 1229–1236 (2014). https://doi.org/10.1109/CICN.2014.255
6. Cespedes, R.G.: New method for the analysis of distribution networks. IEEE Trans. Power Delivery **5**(1), 391–396 (1990). https://doi.org/10.1109/61.107303
7. Chang, G.W., Chu, S.Y., Wang, H.L.: An improved backward/forward sweep load flow algorithm for radial distribution systems. IEEE Trans. Power Syst. **22**(2), 882–884 (2007). https://doi.org/10.1109/TPWRS.2007.894848
8. Chen, T., Yang, N.: Three-phase power-flow by direct ZBR method for unbalanced radial distribution systems. IET Gener. Transm. Distrib. **3**(10), 903–910 (2009). https://doi.org/10.1049/iet-gtd.2008.0616
9. Chen, T., Chen, M., Hwang, K., Kotas, P., Chebli, E.A.: Distribution system power flow analysis-a rigid approach. IEEE Trans. Power Delivery **6**(3), 1146–1152 (1991). https://doi.org/10.1109/61.85860
10. Concordia, C., Ihara, S.: Load representation in power system stability studies. IEEE Trans. Power Syst. **PAS-101**(4), 969–977 (1982). https://doi.org/10.1109/TPAS.1982.317163
11. de Araújo, L.R., Penido, D.R.R., Júnior, S.C., Pereira, J.L.R., Garcia, P.A.N.: Comparisons between the three-phase current injection method and the forward/backward sweep method. Int. J. Electr. Power Energy Syst. **32**(7), 825–833 (2010). https://doi.org/10.1016/j.ijepes.2010.01.020

12. Driesen, J., Katiraei, F.: Design for distributed energy resources. IEEE Power Energ. Mag. **6**(3), 30–40 (2008). https://doi.org/10.1109/MPE.2008.918703
13. Dugan, R.C.: Software OpenDSS (version 7.6.5.52). (2018). http://smartgrid.epri.com/SimulationTool.aspx
14. Dwyer, A., Nielsen, R.E., Stangl, J., Markushevich, N.S.: Load to voltage dependency tests at B.C. Hydro. IEEE Trans. Power Syst. **10**(2), 709–715 (1995). https://doi.org/10.1109/59.387907
15. Garcia, P.A.N., Pereira, J.L.R., Carneiro, S., da Costa, V.M., Martins, N.: Three-phase power flow calculations using the current injection method. IEEE Trans. Power Syst. **15**(2), 508–514 (2000). https://doi.org/10.1109/59.867133
16. Gasperin, L.V.: Optimal capacitor bank allocation in power distribution networks (in portuguese). Thesis (Master's degree in Electrical Engineering), Pontifília Universidade Católica do Rio Grande do Sul, Brazil (2008)
17. Haffner, S., Alves, M.: Optimal allocation of capacitor banks and voltage regulators in radial power distribution networks (in portuguese). In: 6th Latin-American Congress: Electricity Generation and Transmission, Mar del Plata, Argentina, pp. 1–6 (2005)
18. Hajagos, L.M., Danai, B.: Laboratory measurements and models of modern loads and their effect on voltage stability studies. IEEE Trans. Power Syst. **13**(2), 584–592 (1998). https://doi.org/10.1109/59.667386
19. IEEE: Load representation for dynamic performance analysis (of power systems). IEEE Trans. Power Syst. **8**(2), 472–482 (1993). https://doi.org/10.1109/59.260837
20. IEEE: Standard load models for power flow and dynamic performance simulation. IEEE Trans. Power Syst. **10**(3), 1302–1313 (1995). https://doi.org/10.1109/59.466523
21. Jabr, R.A.: Radial distribution load flow using conic programming. IEEE Trans. Power Syst. **21**(3), 1458–1459 (2006). https://doi.org/10.1109/TPWRS.2006.879234
22. Kersting, W.H.: Radial distribution test feeders. IEEE Trans. Power Syst. **6**(3), 975–985 (1991)
23. Kersting, W.H.: Distribution System Modeling and Analysis. CRC Press, Boca Ratón (2002)
24. Louie, K.W.: Aggregation of voltage and frequency dependent electrical loads. Thesis (doctor of philosophy), University of British Columbia, Canada (1999)
25. Marti, J., Ahmadi, H., Bashualdo, L.: Linear power-flow formulation based on a voltage-dependent load model. IEEE Trans. Power Delivery **28**(3), 1682–1690 (2013)
26. Michels, L., Julião, T.A.N., Ferigollo, C., Rech, C., Mezaroba, M., Haffner, S.: Analysis and modeling of typical power distribution network loads (in portuguese). In: 8th Latin American Congress on Electricity Generation and Transmission, Ubatuba, pp. 1–8 (2009)
27. Milanovic, J.V., Yamashita, K., Martínez Villanueva, S., Djokic, S., Korunović, L.M.: International industry practice on power system load modeling. IEEE Trans. Power Syst. **28**(3), 3038–3046 (2013). https://doi.org/10.1109/TPWRS.2012.2231969
28. Monticelli, A., Garcia, A.: Introduction to Electric Power Systems (in Portuguese). Unicamp, Campinas (2011)
29. Murty, V.V.S.N., Teja, B.R., Kumar, A.: A contribution to load flow in radial distribution system and comparison of different load flow methods. In: 2014 International Conference on Power Signals Control and Computations (EPSCICON), pp. 1–6 (2014). https://doi.org/10.1109/EPSCICON.2014.6887494
30. Ohyama, T., Watanabe, A., Nishimura, K., Tsuruta, S.: Voltage dependence of composite loads in power systems. IEEE Trans. Power Syst. **PAS-104**(11), 3064–3073 (1985). https://doi.org/10.1109/TPAS.1985.318814
31. Penido, D.R.R., de Araujo, L.R., Carneiro, S., Pereira, J.L.R., Garcia, P.A.N.: Three-phase power flow based on four-conductor current injection method for unbalanced distribution networks. IEEE Trans. Power Syst. **23**(2), 494–503 (2008). https://doi.org/10.1109/TPWRS.2008.919423
32. Peponis, G.J., Papadopoulos, M.P., Hatziargyriou, N.D.: Distribution network reconfiguration to minimize resistive line losses. IEEE Trans. Power Delivery **10**(3), 1338–1342 (1995). https://doi.org/10.1109/61.400914

33. Ranade, Sagi, Adapa: Load understanding and model development. In: 2005/2006 IEEE/PES Transmission and Distribution Conference and Exhibition, pp. 1315–1319 (2006). https://doi.org/10.1109/TDC.2006.1668701

34. Rangel, C.A.S.: Approximate model of distribution systems considering distributed generation and the effect of voltage on load (in portuguese). Thesis (Master's degree in Electrical Engineering), Universidade Federal do Rio Grande do Sul, Porto Alegre (2015)

35. Resener, M., Haffner, S., Pereira, L.A., Pardalos, P.M.: Mixed-integer LP model for volt/var control and energy losses minimization in distribution systems. Electr. Power Syst. Res. **140**, 895–905 (2016). https://doi.org/10.1016/j.epsr.2016.04.015

36. Rios, L.M.V.: Local voltage stability assessment for variable load characteristics. Thesis (Master of applied science), University of British Columbia, Vancouver (2009)

37. Salim, R.H.: A new approach to the analysis of small signal stability in power distribution systems with distributed synchronous generators (in Portuguese). Ph.D. Thesis, Universidade de São Paulo (2011)

38. Sepúlveda, C., Resener, M., Haffner, S., Pereira, L.A.: Computational model for the analysis of distributed generation in systems including smart grids (in portuguese). In: 2015 IEEE PES Innovative Smart Grid Technologies Latin America (ISGT LATAM), pp. 405–410 (2015). https://doi.org/10.1109/ISGT-LA.2015.7381189

39. Teng, J.-H.: A direct approach for distribution system load flow solutions. IEEE Trans. Power Delivery **18**(3), 882–887 (2003). https://doi.org/10.1109/TPWRD.2003.813818

40. Venkatesh, B., Dukpa, A., Chang, L.: An accurate voltage solution method for radial distribution systems. Can. J. Electr. Comput. Eng. **34**(1/2), 69–74 (2009). https://doi.org/10.1109/CJECE.2009.5291210

41. Villalba, S.A., Bel, C.A.: Hybrid demand model for load estimation and short term load forecasting in distribution electric systems. IEEE Trans. Power Delivery **15**(2), 764–769 (2000). https://doi.org/10.1109/61.853017

42. Wang, K., Huang, H., Zang, C.: Research on time-sharing zip load modeling based on linear bp network. In: 2013 5th International Conference on Intelligent Human-Machine Systems and Cybernetics, vol. 1, pp. 37–41 (2013). https://doi.org/10.1109/IHMSC.2013.16

43. Willis, H.: Power Distribution Planning Reference Book, 2nd edn. Taylor & Francis Group, Didcot (2009)

44. Zhang, F., Cheng, C.S.: A modified newton method for radial distribution system power flow analysis. IEEE Trans. Power Syst. **12**(1), 389–397 (1997). https://doi.org/10.1109/59.575728

# Convex Optimization for the Optimal Power Flow on DC Distribution Systems

**Alejandro Garcés**

**Abstract** Most of renewable energy technologies and energy storage devices are operated in dc. Indeed, solar photovoltaic generation and batteries require a dc/ac converter in order to be integrated into a conventional ac distribution grid. Dc distribution emerges a suitable alternative that reduces the losses and increases reliability in modern smartgrids. Classical methodologies such as the optimal power flow require to be adapted to this new scenario. However, just as in the case of ac grids, the power flow in dc distribution grids is non-linear non-convex. Therefore, convex approximations are required in order to guarantee convergence and global optimality. Several approximations can be proposed including second order cone optimization, semidefinite programming and linealization. These approximations are analyzed theoretically and numerically in this chapter.

## 1 Introduction

DC-microgrids and dc-distribution are emerging technologies that promise to change the form as we conceive medium and low voltage networks [1]. They have well documented advantages in terms of efficiency, controlability and reliability [2]. In addition, they can integrate efficiently renewable energy resources and energy storage devices that are intrinsically dc; for example, batteries, super magnetic energy storage, super capacitors and solar energy [3]. All these devices are integrated to the grid by using power electronic converters which are controlled as constant power devices. A constant power generate a non-linear behavior since the current is given by $i = p/v$, this type of relation is non-linear but also non-convex and require a judicious analysis.

Here, we use the name dc-grid for both, dc-microgrids and dc-distribution since both share similar features from the operative point of view [4]. Dc-grids are usually

A. Garcés (✉)
Universidad Tecnologica de Pereira, Pereira, Colombia
e-mail: alejandro.garces@utp.edu.co

operated in hierarchical structures with a primary, secondary and tertiary control [5]. Primary control is local and search for stability while secondary control, which can be local, distributed or centralized, tries to maintain a suitable voltage profile. Tertiary control [6] is a usually centralized algorithm, which search for the optimal operation of the grid. This control is also known as *optimal power flow* (OPF) and is the methodology to be studied in this chapter.

Dc-grids can be operated in grid connected operation or island operation. In this chapter, we are interested in the grid mode in which there is a slack node which maintains a constant voltage. As aforementioned, each nodal element is integrated by a power electronic converter which maintains a fixed power defined by the OPF. However, this power can be changed between well defined limits such that $p_{min} \leq p_k \leq p_{max}$. These limits are given by technical characteristics of the distributed resource (generation, load or storage). For example, a solar panel can have a constraint such as $0 \leq p \leq p_{max}$ where $p_{max}$ is given by the actual solar radiation in a particular time. Controlled loads can also have these type of constraints [7]. Our objective is therefore to determine the optimal values of the power $p_k$ for each node in order to minimize the power loss and fulfilling physical constrains.

It is important to emphasize that optimal power flow in dc grids is different from the well known dc power flow in ac systems [8]. The latter is a linearization of the ac equations whereas the problem studied in this chapter, is related to grids that are actually dc and non-linear due to the constant power terminals. However, the optimal power flow problem in dc grids has similar challenges to the problem in ac grids, because the model is non-convex and quadratic. The problem in ac grids has been investigated for decades in the power systems community and recently, it has attracted the attention of the control and mathematical communities due to its practical importance and mathematical complexity. In [9] and [10] a complete revision of the problem for ac grids was presented, including theoretical and practical challenges.

## 1.1 Why Convexity Matters

As aforementioned, the OPF is a non-linear optimization model that acts as tertiary control in dc-grids. Being a control, we expect two main features of the optimization algorithm: convergence and global optimality. The former refers to the capability of the algorithm to achieve an optimal solution in a finite and well defined lapse of time; the latter refers to the capability to obtain global optimum.

There are many results related to the convergence of the gradient method as well as the interior point methods for convex optimization problems [11]. Perhaps the most famous result is the Nesterov's proof of convergence for the gradient method [12] and for minimizing self-concordant functions guaranteing the convergence of the interior point methods in convex problems. Therefore, convex optimization problems can be solved efficiently in practice allowing real-time operation [13].

On the other hand, global optimum is important in real-time operation in which it is desired to reduce the human intervention. There is a strong theoretical background that guarantees global optimality in convex optimization problems. Uniqueness can be also guarantee in strictly-convex optimization problems. This aspect will be discussed later in this chapter.

Most of the non-linear programming problems in power systems applications are non-convex. However, it is possible to define convex approximations to the original problem. In this chapter, we study three convex approximations namely: linearization of the power flow equations, semidefinite programming and second order cone optimization.

## *1.2   Outline of the Chapter*

The rest of the chapter is organized as follows: in Sect. 2, the model of the OPF for dc-grid is presented. We call this model as the non-linear OPF. The main results of convex optimization methods are briefly presented in Sect. 3. After that, a linear approximation as well as semidefinite programming and second order cone approximations are presented in Sects. 4, 5 and 6 respectively. Numerical results are analyzed in Sect. 7 followed by conclusions and relevant references.

## 2   Brief Review of Convex Optimization

Before presenting the model for the optimal power flow in dc-grids, let us review some basic concepts related to convex optimization. This review is far to be complete but gives the main elements for understanding the approximations presented latter in this chapter. Interested reader is refer to [13] for a more complete review of convex optimization theory.

**Definition 1**  We say that a set $\Omega \subset \mathbb{R}^n$ is convex if for any $x, y \in \Omega$ we have that

$$(1 - \lambda)x + \lambda y \in \Omega \tag{1}$$

for all $\lambda \in \mathbb{R}, \ 0 \leq \lambda \leq 1$.

Intuitively, this means that all points in line segments inside the set, belong to the set. Figure 1 shows examples of convex and non-convex sets.

Some optimization problems may seem simple but in reality hide a high mathematical complexity. This complexity is closely related to the geometry of the feasible set. Therefore, we must be very careful when defining whether a set is convex or not. Consider the following examples
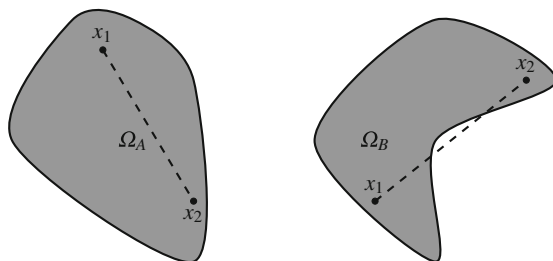
**Fig. 1** Example of a convex set $\Omega_A$ and a non-convex set $\Omega_B$. In the second case, there are points in the line segment $x_1$–$x_2$ which are outside the set
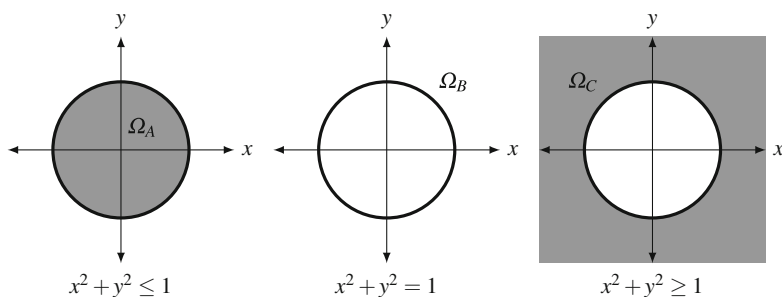


**Fig. 2** Example of three different sets defined in $\mathbb{R}^2$. $\Omega_A$ is convex while $\Omega_B$ and $\Omega_C$ are not

*Example 1* Convex and not convex sets: Consider the following sets in the plane:

$$\Omega_A = \left\{ (x, y) : \sqrt{x^2 + y^2} \leq 1 \right\} \tag{2}$$

$$\Omega_B = \left\{ (x, y) : \sqrt{x^2 + y^2} = 1 \right\} \tag{3}$$

$$\Omega_C = \left\{ (x, y) : \sqrt{x^2 + y^2} \geq 1 \right\} \tag{4}$$

In this case, $\Omega_A$ is convex while $\Omega_B$ and $\Omega_C$ are non-convex. This can be easily concluded by a simple inspection on the corresponding plot (see Fig. 2). However, in a more general case we need to resort to the definition. Consider two different points $\mathbf{a} = (x_a, y_a)$ and $\mathbf{b} = (x_b, y_b)$ which belongs to $\Omega_A$, this means:

$$\sqrt{x_a^2 + y_a^2} \leq 1 \tag{5}$$

$$\sqrt{x_b^2 + y_b^2} \leq 1 \tag{6}$$

notice that these constraints can be represented as function of the Eucldean norm, as follows:

$$\|\mathbf{a}\| \leq 1 \tag{7}$$

$$\|\mathbf{b}\| \leq 1 \tag{8}$$

therefore, we can use the triangular inequality given by (9):

$$\|\mathbf{a} + \mathbf{b}\| \leq \|\mathbf{a}\| + \|\mathbf{b}\| \tag{9}$$

now consider an intermediate point $\mathbf{c} = \lambda\mathbf{a} + (1 - \lambda)\mathbf{b}$ which fulfills the following conditions:

$$\|\mathbf{c}\| = \|\lambda\mathbf{a} + (1 - \lambda)\mathbf{b}\| \tag{10}$$

$$\leq \lambda \|\mathbf{a}\| + (1 - \lambda) \|\mathbf{b}\| \tag{11}$$

$$\leq \lambda(1) + (1 - \lambda)(1) \tag{12}$$

$$= 1 \tag{13}$$

consequently, $\mathbf{c} \in \Omega_A$ and the set is convex.

For demonstrating that $\Omega_B$ and $\Omega_C$ are not convex, is enough to generate a numerical counter example, for instance $\mathbf{a} = (\sqrt{2}/2, \sqrt{2}/2)$ and $\mathbf{b} = (\sqrt{2}/2, \sqrt{2}/2)$.

*Example 2* In general, quadratic equalities are not convex. Consider the set $\mathscr{B} = \{x(x - 1) = 0\}$ which consists in only two points $\mathscr{B} = \{0, 1\}$. This is a binary set and hence, it is non-convex.

Our objective is to study problems whose feasible domain is a convex set. This domain is given by several constrains, therefore, it is useful to consider the following lemma

**Lemma 1 (see [14])** *The intersection of convex sets is also a convex set*

Therefore, it is enough to check that each constraint define a convex set. However, we can have equality and inequality constraints and the former requires a more strict condition, namely to be an affine space defined as[1]

$$\Omega = \left\{x \in \mathbb{R}^n : Ax = b\right\} \tag{14}$$

where $A$ is a constant matrix and $b$ a vector with suitable dimensions. Notice the difference between a linear space and a affine space. $\Omega$ in (14) is a linear space

---

[1]There are more general definitions of affine spaces, however, this simple definition is enough for our purposes.
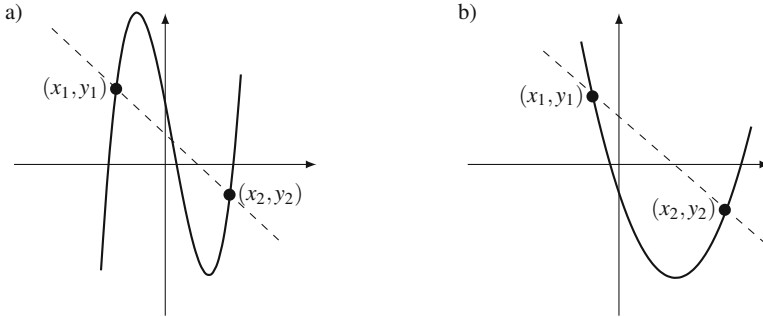
**Fig. 3** Comparison between a convex and a non-convex function. In the case (**a**) we can draw a line between point $(x_1, y_1)$ and the point $(x_2, y_2)$ but there are some parts of the function which are above the line segment (i.e the function is non-convex). In the case (**b**) we can see that every point in the line segment is below the function itself (i.e the function is convex)

if and only if $b = 0$. As a consequence of that, all linear space are affine, but the opposite is not true. Let us analyze now the convexity of real valued functions

**Definition 2** A real-valued function $f : \mathbb{R}^n \to \mathbb{R}$ is convex if its domain is convex and for any two points $x, y \in \mathbb{R}^n$ we have that

$$f(\lambda x + (1 - \lambda)y) \leq \lambda f(x) + (1 - \lambda) f(y) \tag{15}$$

for all $\lambda \in \mathbb{R}$ such that $0 \leq \lambda \leq 1$.

Graphically, a convex function is a real valued function in which it is possible to draw a line above the function for a given interval as depicted in Fig. 3

Convex functions and convex sets are related by the epigraph defined by

$$\mathcal{E}_g(x, y) = \left\{ (x, t) \in \mathbb{R}^n \times \mathbb{R} : g(x) \leq t \right\} \tag{16}$$

This set allows us to check convexity in an optimization model by checking the convexity of the inequality constraints thanks to the following lemma

**Lemma 2 (see [13])** *A function g is convex if and only if its epigraph is convex.*

As a consequence of this, we can ensure a constraint of the form $g(x) \leq 0$ generates a convex set $\mathcal{E}_g(x, y)$; with these simple definitions, we are ready for the formal definition of convex optimization model:

**Definition 3** A convex optimization model is defined as

$$\text{Minimize } f(x) \tag{17}$$

$$x \in \Omega \tag{18}$$
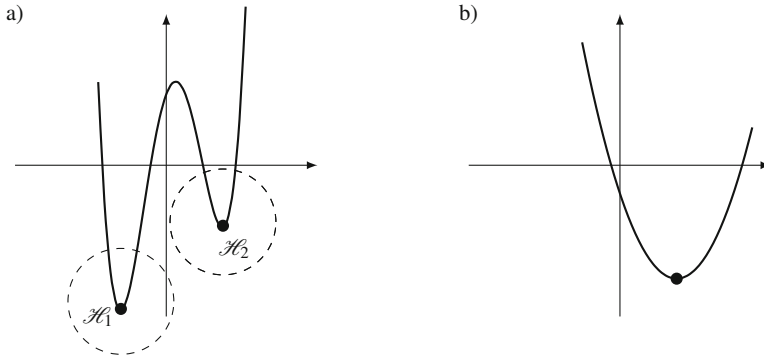
where $f$ is a convex functions and $\Omega$ is a convex set.

**Fig. 4** Example of functions with global or local optima: (**a**) function with local optima $\mathscr{H}$, (**b**) function with a global optimum

As aforementioned, convex optimization models have many theoretical and practical features which are suitable for optimization in power distribution grids. One of this important features is the guarantee of the global optimum.

**Definition 4** A point $\tilde{x}$ is a local optimum of a minimization problem if there exist an open set $\mathscr{H}$ such that $\tilde{x} \in \mathscr{H}$ and $f(x) \geq f(\tilde{x}), \forall x \in \mathscr{H}$. If $\mathscr{H}$ includes the complete feasible space then the optimum is global.

Figure 4 shows the case of a non-convex function which has two minimum points. The convex case however, have a global minimum. This is because the second function is convex.

**Theorem 1 (see [13])** *Consider a convex function $f : \mathbb{R}^n \rightarrow \mathbb{R}$ defined in a convex domain $\Omega$. In this case, every local minimum is also global.*

From the numerical point of view, there are many results about the convergence of the algorithms for convex optimization. These algorithms include the gradient method, Newton's method and interior point. Fortunately, there are many available software and toolboxes that solves efficiently convex optimization models. Readers interested in the convergence of the algorithms for convex optimization models, can consult [11] and [14].

## 3 Modelling the Optimal Power Flow Problem

Let us consider a dc-grid with different distributed resources and controlled loads as shown in Fig. 5. Define 0 as the slack node (i.e the node that maintains a constant voltage $v_0$) and $k = \{1, 2, \ldots, N\}$ the rest of the nodes, corresponding to distributed resources integrated with power electronic converters, which maintain a constant power $p_k$. The nodal admittance matrix is defined as $g_{km}$, where step nodes (such as
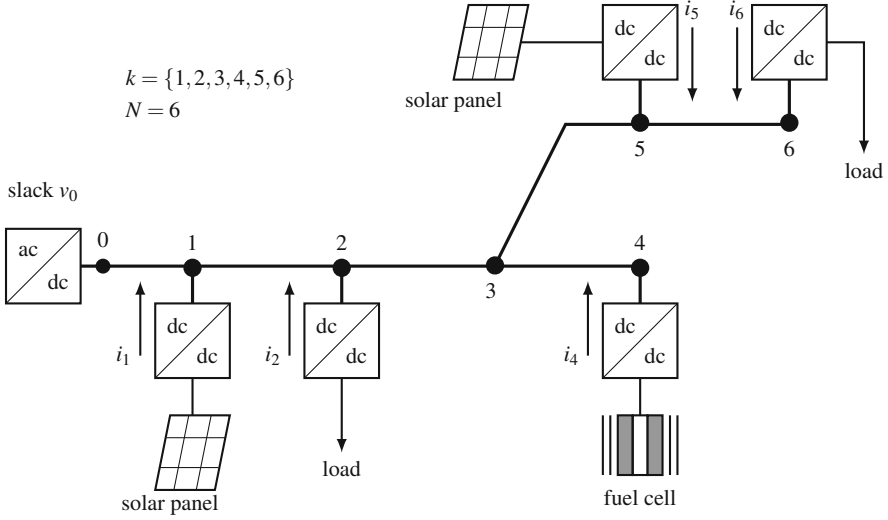
**Fig. 5** Schematic representation of a dc-grid. All components are integrated through a power electronic converter which controls $p_k$. Currents are entering to the node

3 in the figure) can be eliminated by a Kron's reduction [15]. We do not make any assumption about the radiality of the grid allowing meshed dc-grids. However, the graph that represents the grid must be connected in order to guarantee the admittance matrix is non-singular.

Under these considerations, nodal currents have a non-linear relation given by

$$\frac{p_k}{v_k} = g_{k0}v_0 + \sum_{m=1}^{N} g_{km}v_m \tag{19}$$

where $g_{km}$ represents the corresponding entries in the admittance matrix and $v_k$, $p_k$ are the voltage and power respectively.

Each distributed resource (load or generation) has some degree of flexibility that allows to optimize the operation point. For example, the solar panel connected in Node 1 could inject power in an interval given by $0 \leq p_1 \leq p_{1max}$ where $p_{1max}$ is the maximum power given by the available solar radiation (the same can be said for the panel connected to Node 5). The fuel cell however, have physical constraints in both, the minimum and the maximum power $p_{4min} \leq p_4 \leq p_{4max}$. Finally, controlled loads have a negative power that can be limited by the same type of constraint. In conclusion, any distributed resource can be modeled as a box constraint $p_{k(min)} \leq p_k \leq p_{k(max)}$.

Our objective is to minimize power loss in the grid by the following non-linear optimization model

**Model 1 (Optimal Power Flow in DC-Grids)**

$$\text{Minimize } P_L = g_{00}v_0^2 + 2\sum_{m=1}^{N} g_{0m}v_0v_m + \sum_{k=1}^{N}\sum_{m=1}^{N} g_{km}v_kv_m \tag{20}$$

$$\text{subject to } \frac{p_k}{v_k} = g_{k0}v_0 + \sum_{m=1}^{N} g_{km}v_m \qquad \forall k \in \{1,\dots,N\} \tag{21}$$

$$|v_k - 1| \leq \delta \qquad \forall k \in \{1,\dots,N\} \tag{22}$$

$$p_{k(min)} \leq p_k \leq p_{k(max)} \qquad \forall k \in \{1,\dots,N\} \tag{23}$$

where $P_L$ is the power loss, $\delta$ is the maximum deviation of the nodal voltages and $p_{k(max)}$, $p_{k(min)}$ are the maximum and minimum capability of distributed resources which includes distributed generation (solar or wind), controlled loads and storage.

Notice that the objective function (20) is convex since $g_{km}$ forms a symmetric positive definite matrix. Inequality constraints are also convex, including (22) which can be reformulated as a linear inequality.[2] Nevertheless, Constraint (21) is a non-affine equality equation that makes the problem non-convex. This constraint cannot be transformed into a quadratically constrainted quadratic optimization model due to the presence of constant power loads. Therefore, the model remains non-convex even for the case of only one load (See the examples in Sect. 2).

Different approximations have been presented to solve this problem. In the next sections, we study three main approaches, namely: Second order cone optimization [16], semi-definite programming [17] and linearization [18].

## 4 Second Order Cone Approximation

Second order cone optimization is an active research area in power systems applications after the seminal paper of Low [19] for dc grids. This methodology has demonstrated to be very efficient in the case of dc-distribution. In some cases, it can lead to the optimum of the original problem. In other cases, it gives a very close

---

[2]we maintain the absolute value representation for the sake of simplicity. Notice also that any software for disciplined convex programming, such as cvx and cvxpy, allows to include effortless norm constraints.

approximation which is valid for practical applications. Let us start by some basic definitions taken from [16].

**Definition 5 (SOC)**  A second order cone optimization model is a convex optimization problem that can be represented as

$$\text{Minimize} c^T x$$

$$\|A_i x + b_i\| \le \alpha_i^T x + \beta_i \ \forall i \tag{24}$$

where $\|\cdot\|$ is the Euclidean norm, $A_i$ are real matrices, $c, b_i, \alpha_i$ are vectors and $\beta_i$ are scalars.

Many problems can be represented as SOC, a particular case is the hyperbolic constraint defined as follows:

$$xy \ge w^T w \tag{25}$$

$$x \ge 0 \tag{26}$$

$$y \ge 0 \tag{27}$$

where $w$ is a decision vector and $x, y$ are decision variables. This constraint is equivalent to:

$$\left\| \begin{pmatrix} 2w \\ x - y \end{pmatrix} \right\| \le x + y \tag{28}$$

let's see the step-by-step procedure

$$\begin{pmatrix} 2w \\ x - y \end{pmatrix}^T \begin{pmatrix} 2w \\ x - y \end{pmatrix} \le (x + y)^2 \tag{29}$$

$$4w^T w + (x - y)^2 \le (x + y)^2 \tag{30}$$

$$4w^T w + x^2 - 2xy + y^2 \le x^2 + 2xy + y^2 \tag{31}$$

$$4w^T w \le 4xy \tag{32}$$

$$w^T w \le xy \tag{33}$$

With this in mind, it is possible to obtain a SOC approximation to the load flow equations. Consider Equation (21) and define a new variable $w_{km} = v_m v_k$ which

transforms this equation in an affine space in variables $w_{km}$, as follows:

$$p_k = g_{k0}v_k v_0 + \sum_{m=1}^{N} g_{km}v_k v_m \tag{34}$$

$$p_k = g_{k0}w_{k0} + \sum_{m=1}^{N} g_{km}w_{km} \tag{35}$$

Now, the non-convexity is in the definition of $w_{km}$ which can be squared as follows

$$w_{km} = v_m v_k \tag{36}$$

$$w_{km}w_{km} = v_m v_k v_m v_k \tag{37}$$

$$\|w_{km}\|^2 = w_{kk}w_{mm} \tag{38}$$

now we relax this hyperbolic constraint in order to obtain SOC constrains

$$\|w_{km}\|^2 \leq w_{kk}w_{mm} \tag{39}$$

$$\left\| \begin{pmatrix} 2w_{km} \\ w_{kk} - w_{mm} \end{pmatrix} \right\| \leq w_{kk} + w_{mm} \tag{40}$$

Therefore, the optimal power flow (Model 1) can be represented as the following convex model:

**Model 2 (SOC Approximation)** *Second order cone approximation for the power flow in dc-distribution*

$$\text{Minimize } P_L = g_{00}w_{00} + 2\sum_{m=1}^{N} g_{0m}w_{0m} + \sum_{k=1}^{N}\sum_{m=1}^{N} g_{km}w_{km} \tag{41}$$

$$\text{subject to } p_k = g_{k0}w_{k0} + \sum_{m=1}^{N} g_{km}w_{km} \qquad \forall k \in \{1, \ldots, N\} \tag{42}$$

$$|w_{kk} - 1| \leq \delta_s \qquad \forall k \in \{1, \ldots, N\} \tag{43}$$

$$p_{k(min)} \leq p_k \leq p_{k(max)} \qquad \forall k \in \{1, \ldots, N\} \tag{44}$$

$$\left\| \begin{pmatrix} 2w_{km} \\ w_{kk} - w_{mm} \end{pmatrix} \right\| \leq w_{kk} + w_{mm} \qquad \forall k \in \{1, \ldots, N\} \tag{45}$$

This approximated model is completely formulated in terms of new variables $w_{km}$, however, it is straightforward to recuperate the original voltages by using the definition. Section 7 will compare the results.

## 5 Semidefinite Approximation

Semidefinite programming (SDP) is another possibility for convexification of Model 1. In this approach, we change from the space of the vectors $\mathbb{R}^n$ to a bigger linear space, namely, the space of the matrices. This space have better geometric characteristics that allow a semidefinite approximation. However, this change has as a disadvantage, a higher computational requirements for the new problem (this will be discussed latter in Sect. 7). Let us start with some basic definitions

**Definition 6** A semidefinite programming model is represented as follows:

$$
\begin{aligned}
&\text{Minimize } \text{Tr}(CX) \\
&\text{subjetto}: AX = B \\
&\quad\quad\quad X \succeq 0
\end{aligned}
\tag{46}
$$

where $\succeq$ represents the Loewner partial order defined by the convex cone of positive semi-definite matrices and $Tr$ is the trace of the corresponding matrix.

It is easy to see that a constraint $X \succeq 0$ is convex and $AX = B$ is affine which makes the entire problem convex.

Now for the optimal power flow problem, we define a new variable $w_{km} = v_k v_m$ just as in the case of SOC transforming the problem as follows

$$
p_k = g_{k0} w_{k0} + \sum_{m=1}^{N} g_{km} w_{km}
\tag{47}
$$

$$
w_{km} = v_k v_m
\tag{48}
$$

Now, the second constraint can be represented as a matrix $W = vv^T$. Notice this matrix is possitive definite and has rank = 1. Therefore, the constraint can be represented as

$$
W \succeq 0
\tag{49}
$$

$$
rank(W) = 1
\tag{50}
$$

at this point, the problem is completely equivalent to Model 1 and hence, non-convex. However, by relaxing the last constraint $rank(W) = 1$ we obtain a convex optimization model with semidefinite constraints.

**Model 3 (SDP Approximation)** *Semidefinite approximation for the power flow in dc-distribution*

$$\text{Minimize } P_L = Trace(G \cdot W) \tag{51}$$

$$\text{subject to } p_k = diag(G \cdot W) \tag{52}$$

$$|w_{kk} - 1| \leq \delta_s \tag{53}$$

$$p_{k(min)} \leq p_k \leq p_{k(max)} \ \forall k \in \{1, \cdots, N\} \tag{54}$$

$$W \succeq 0 \tag{55}$$

This type of models can be solved efficiently by different toolboxes for convex optimization, such as cvx [20]. The original variables can be obtained by a simple eigenvalue decomposition as follows

$$v \approx \sqrt{\sigma_m}\phi_m \tag{56}$$

were $\sigma_m$ is the maximum eigenvalue associated to $W$ and $\phi_m$ is the corresponding eigenvector. In most of the practical cases, the eigenvalues are all close to zero except $\sigma_m$. The accuracy of the approximation depends on this characteristics since all-except one eigenvalues must be equal to zero in order to be a rank 1 matrix. More details in Sect. 7.

## 6 Linearization

A simple but effective way to convexify Model 1 is through linearization. Equation (21) can be seen as a Manifold $\mathscr{M}$ represented by a set of algebraic equations. The tangent space $T_v\mathscr{M}$ around 1p.u is given by the following affine space

$$p_k = g_{k0}v_0 + \sum_{m=1}^{N} g_{km}(v_k + v_m - 1) \tag{57}$$

this approximation is unique (see [21] page 270 for more details about manifold theory and linearizations).

*Example 3* Consider a simple dc distribution system with two terminals shown in Fig. 6a. The non-linear representation of the grid is given by Eq. (21) which is a non-linear space as depicted in Fig. 6. This equation can be linearized around $1\,pu$ using a simple Taylor expansion. In this case, the manifold $\mathscr{M}$ is only one equation but the idea is easily generalized to the n-dimensional case.

This simple approximation leads the following convex quadratic model
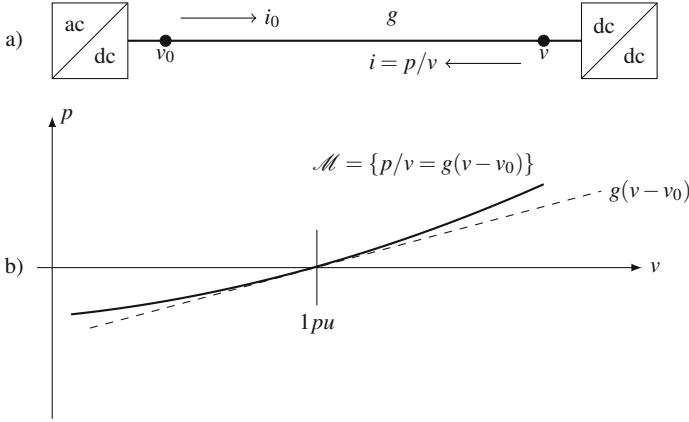
**Fig. 6** Schematic example of a linearization. (**a**) dc power distribution with two nodes. (**b**) Linearization of the equations that represents the power flow

**Model 4 (Linear Approximation)** *Linear approximation of the power flow for dc distribution systems.*

$$\text{Minimize } P_L = g_{00}v_0^2 + 2\sum_{m=1}^{N} g_{0m}v_0v_m + \sum_{k=1}^{N}\sum_{m=1}^{N} g_{km}v_kv_m \tag{58}$$

$$\text{subject to } p_k = g_{k0}v_0 + \sum_{m=1}^{N} g_{km}(v_k + v_m - 1) \qquad \forall k \in \{1,\ldots,N\} \tag{59}$$

$$|v_k - 1| \le \delta \qquad \forall k \in \{1,\ldots,N\} \tag{60}$$

$$p_{k(min)} \le p_k \le p_{k(max)} \qquad \forall k \in \{1,\ldots,N\} \tag{61}$$

This model is also convex and in fact easier to solve compared to previous models. However, its accuracy is reduced compared to these models.

## 7 Results

A 10-nodes dc-distribution system is used for evaluate each of the studied approximations. The grid is depicted in Fig. 7 and parameters are given in Table 1.

Models 2, 3 and 4 were evaluated using cvx, a package for specifying and solving convex programs [20]; the source code can be obtained in [22]. Results are

**Fig. 7** Graph of the studied microgrid
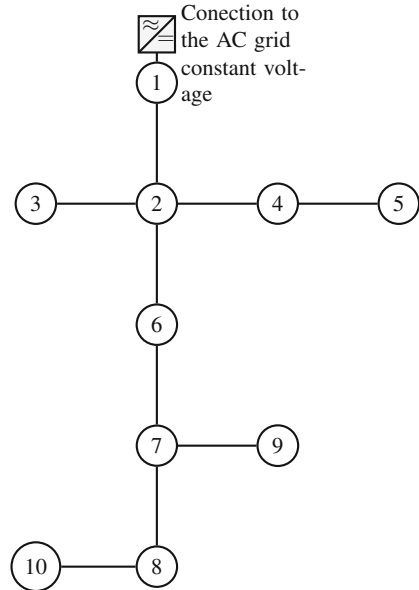


**Table 1** Parameters of the test microgrid

| Node 1 | Node 2 | $r_{km}(pu)$ | $P_{min}(pu)$ | $P_{max}(pu)$ |
|--------|--------|--------------|---------------|---------------|
| 1 | 2 | 0.0050 | 0.00 | 0.30 |
| 2 | 3 | 0.0015 | −1.80 | −1.00 |
| 2 | 4 | 0.0020 | −2.30 | −2.00 |
| 4 | 5 | 0.0018 | 0.00 | 3.00 |
| 2 | 6 | 0.0023 | 0.00 | 2.00 |
| 6 | 7 | 0.0017 | 0.00 | 0.50 |
| 7 | 8 | 0.0021 | 0.00 | 1.30 |
| 7 | 9 | 0.0013 | −3.00 | −1.00 |
| 3 | 10 | 0.0015 | 0.00 | 2.25 |

summarized in Table 2. Since the models are convex, these results does not depend on the software used.

Performance of each model is compared in Table 3. In terms of speed, the linear approximation (Model 4) is the fastest while semidefinite programming (Model 3) is the slowest. The average elapsed time for Model 4 was 0.31 s while for Model 3 was 2.7 s. Model 2 had an intermediate performance with an average time of 0.40 s. This performance is expected due to the complexity and number of variables of each Model.

A way to evaluate the accuracy of each Model consist in using the obtained voltages and calculate the nodal powers. The difference between these power and the power given by the model is a measure of accuracy. For Model 2 this error was $4 \times 10^{-4}$ while for linearization it was 0.0050. In general, all models exhibit good performance, however, second order cone optimization has the best

**Table 2** Results for each approximation

| Node | $V_{SOC}$ | $V_{SDP}$ | $V_{LIN}$ | $P_{SOC}$ | $P_{SDP}$ | $P_{LIN}$ |
|------|-----------|-----------|-----------|-----------|-----------|-----------|
| 1 | 1.0000 | 1.0000 | 1.0000 | 0.1851 | 0.2325 | 0.1716 |
| 2 | 0.9991 | 0.9988 | 0.9991 | 0.2997 | 0.2804 | 0.2900 |
| 3 | 0.9988 | 0.9985 | 0.9989 | −1.0002 | −1.0129 | −1.0051 |
| 4 | 0.9977 | 0.9974 | 0.9977 | −2.0002 | −2.0074 | −2.0024 |
| 5 | 1.0000 | 0.9998 | 1.0001 | 1.3070 | 1.3047 | 1.3042 |
| 6 | 1.0000 | 0.9997 | 1.0001 | 0.6855 | 0.6903 | 0.7018 |
| 7 | 0.9995 | 0.9992 | 0.9996 | 0.4997 | 0.4622 | 0.4887 |
| 8 | 0.9999 | 0.9998 | 1.0001 | 0.2125 | 0.2484 | 0.2385 |
| 9 | 0.9982 | 0.9979 | 0.9983 | −1.0002 | −1.0061 | −1.0055 |
| 10 | 1.0000 | 0.9998 | 1.0001 | 0.8172 | 0.8122 | 0.8182 |

**Table 3** Comparison of performance for each convex approximation

| Parameter | Model 2 | Model 3 | Model 4 |
|-----------|---------|---------|---------|
| Elapsed time | 0.45 s | 2.7 s | 0.31 s |
| Error | $4 \times 10^{-4}$ | 0.0012 | 0.0050 |

tradeoff between accuracy and speed. However, the linear model is enough for many practical applications with a error less than 5% and a very fast calculation which can be suitable for real time operation problems.

## 8 Conclusions

This chapter presented some basic introduction to convex optimization with applications to the optimal power flow in dc-distribution. Three different convex approximations were analyzed, namely: second order cone optimization, semidefinite programming and Linearization. The three models demonstrated to be highly accurate with low computational time. Linearization shown to be faster although it was less accurate compared to the other two models. Semidefinite programming was the most accurate with a high computational effort. Second order cone optimization was less accurate with a moderate computational cost. As a general conclusion, SOC is the most suitable alternative when accuracy is an issue, but a simple linearization allowed a faster implementation with a reasonable error (less than 5%).

# References

1. Patterson, B.T.: Dc, come home: Dc microgrids and the birth of the "enernet". IEEE Power Energ. Mag. **10**(6), 60–69 (2012)
2. Meng, L., Shafiee, Q., Trecate, G.F., Karimi, H., Fulwani, D., Lu, X., Guerrero, J.M.: Review on control of dc microgrids and multiple microgrid clusters. IEEE J. Emerging Sel. Top. Power Electron. **5**(3), 928–948 (2017)
3. Dragicevic, T., Lu, X., Vasquez, J.C., Guerrero, J.M.: DC microgrids part i: A review of control strategies and stabilization technique. IEEE Trans. Power Electron. **31**(7), 4876–4891 (2015)
4. Prabhala, V.A.K., Baddipadiga, B.P., Ferdowsi, M.: DC distribution systems - an overview. In: 2014 International Conference on Renewable Energy Research and Application (ICRERA), pp. 307–312 (2014)
5. Jin, C., Wang, P., Xiao, J., Tang, Y., Choo, F.H.: Implementation of hierarchical control in DC microgrids. IEEE Trans. Ind. Electron. **61**(8), 4032–4042 (2014)
6. Che, L., Shahidehpour, M.: DC microgrids: economic operation and enhancement of resilience by hierarchical control. IEEE Trans. Smart Grid **5**(5), 2517–2526 (2014)
7. Frank, S.M., Rebennack, S.: Optimal design of mixed ac-dc distribution systems for commercial buildings: a nonconvex generalized benders decomposition approach. Eur. J. Oper. Res. **242**(3), 710–729 (2015)
8. Stott, B., Jardim, J., Alsac, O.: DC power flow revisited. IEEE Trans. Power Syst. **24**(3), 1290–1300 (2009)
9. Frank, S., Rebennack, S.: An introduction to optimal power flow: Theory, formulation, and examples. IIE Trans. **48**(12), 1172–1197 (2016)
10. Krasko, V., Rebennack, S.: Chapter 15: Global Optimization: Optimal Power Flow Problem, pp. 187–205
11. Nesterov, Y.: Introductory Lectures on Convex Programming Volume I: Basic course. Springer, Berlin (2008)
12. Nesterov, Y., Nemirovskii, A.: Interior Point Polynomial Algorithms in Convex Programming, vol. 1, p. 10, 1st edn. SIAM, Philadelphia (1994)
13. Boyd, S., Vandenberghe, L.: Convex Optimization. Cambridge University, New York (2004)
14. Luenberger, D.: Optimization by Vector Space Methods. Wiley, New York (1969)
15. Kron, G.: Tensors for Circuits. Dover, United States (1942)
16. Lobo, M.S., Vandenberghe, L., Boyd, S., Lebret, H.: Applications of second-order cone programming. Linear Algebra Appl. **284**(1), 193–228 (1998). International Linear Algebra Society (ILAS) Symposium on Fast Algorithms for Control, Signals and Image Processing
17. Vancenberghet, L., Boyd, S.: Semidefinite programming. SIAM Rev. **38**(1), 49–95 (1996)
18. Montoya, O.D., Grisales-Noreña, L.F., González-Montoya, D., Ramos-Paja, C.A., Garces, A.: Linear power flow formulation for low-voltage dc power grids. Electr. Pow. Syst. Res. **163**, 375–381 (2018)
19. Gan, L., Low, S.H.: Optimal power flow in direct current networks. IEEE Trans. Power Syst. **29**(6), 2892–2904 (2014)
20. Inc. CVX Research. CVX: Matlab Software for Disciplined Convex Programming, version 2.0 (2012). http://cvxr.com/cvx
21. Hubbard, J.H., Hubbard, B.B.: Vector Calculus, Linear Algebra, and Differential Forms a Unified Approach. Prentice Hall, Upper Saddle River (1999)
22. Garces A.: Matlab Exchage web page. https://www.mathworks.com/matlabcentral/profile/authors/3009175-alejandro-garces. Accessed 30 Sept 2018

# Energy Storage System Sitting and Sizing for Renewable Support

**Luciane Neves Canha, Camilo Alberto Sepúlveda Rangel, and Olatunji Matthew Adeyanju**

**Abstract** This chapter addresses the Energy Storage System (ESS) sitting and sizing problem for renewable support. It is divided into four major subtitles in order to give the reader an introduction of the issue by providing fundamental information and theorical background to show the basic concepts for solving the intended problem, and discusses perspectives to encourage the reader for further research. Also, it solves two practical examples using specific optimization tools. In the first part of the chapter, ESS applications for Renewable Support is presented with general introduction to renewable energy system and its limitations. Subsequently, the ESS technologies with different characteristics are described and possible applications of ESS are presented from the perspective of the utility, medium and large-business, and off and micro-grid scale applications. The second part presents the optimization methods that is used in ESS sizing and sitting problems. These methods consider heuristic and meta-heuristic approaches with a major focus on evolutionary algorithms. An optimization formulation and ESS modelling for given power system application considering specific objective function and constraints are also presented. In the third part, future applications of the ESS, together with set of possible subjects that can expand the ESS field of research are presented. Finally, the fourth part presents two practical examples of ESS support problem using HOMER proprietary software and a Genetic Algorithms, respectively. Based on the ESS specifications and types, performance is examined for selected scenarios of network architecture. In both solution procedures, the algorithms established the size of ESS for optimal technical and economic performance for the distribution system.

L. N. Canha (✉) · C. A. S. Rangel · O. M. Adeyanju
Centre of Excellence in Energy and Power System (CEESP), Federal University of Santa Maria, Santa Maria, Brazil
e-mail: lucianecanha@ufsm.br

# 1    ESS Applications for Renewable Support

## 1.1    What Is Renewable Energy?

Renewable energy is energy from any source that has natural replenishing ability but are generally limited in quantity per unit time. Figure 1 presents common renewable energy sources that are been explored for mankind benefit today.

Most of the renewable energy shown in Fig. 1 depend on sunlight, directly or indirectly. For example, air movement occurs because of the differential heating of the sun on the Earth's surface and it causes precipitation to be formed as the air is lifted, resulting into wind and hydro energy production. Also, solar energy is the direct energy from the sun which is usually harnessed using solar panels or collectors. Generally, plants depend on sunlight to produce their foods—a process known as photosynthesis. The energy stored in these plants because of their interaction with sunlight is known as Biomass energy. An example of renewable source which does not depend on sunlight is the geothermal energy. It occurs due to the radioactive decomposition due to heat reactions in the earth's crust. Another example is the tidal energy which is formed due to a conversion of gravitational energy—mainly found in the surge of ocean waters when there is rise and fall of tides. In [1], several forms of renewable energy and their production processes are well detailed.

Renewable energy or energy from renewable sources may be deployed in different scales (domestic, commercial, industrial and utility-scales) whether as a stand-alone or as grid-connected forms. In today's power grid development and operation planning, high integration of renewable energy is in perspective and are considered based on benefits such as safety and cleaner environment, reduction of greenhouse effect and carbon-emission, reduction of energy cost, voltage stabilization and loss reduction among others [2].

### 1.1.1    Limitations of Energy from Renewables Sources

Even with the attractive benefits that renewable energy presents, its increasing level in the power grid may result into unstable and unreliable operation. This is because, renewable sources are characterized with intermittent and fluctuating features which increases its production uncertainties. It may be possible to generate large amount of useful energy from a renewable source but may be impossible to generate that amount when and how it is needed. For example, large amount of wind energy can result in unpredictable variability and power imbalance in order of GW. This is a major challenge to maintaining stable power grid operation (See Fig. 2). Generation-



**Fig. 1**  Renewable energy sources [1]

load imbalance will lead to variation in voltage level especially, at the location where the wind source is connected, and in a major way, load voltage fluctuation affects power system voltage stability [3].

To address these challenges, Energy Storage Systems (ESS) are considered an important option to support power grid with significant level of renewable energy inclusion [4, 5]. In the following section, an overview of ESS technology is briefly discussed.

## 1.2 Introduction to ESS Technology

EES technology works by transforming electrical energy to an electro-potential energy in storable form using storage devices. The stored energy can be transformed back into electricity and used when required [6, 7]. Regardless of the conversion process involved, typical ESS system can be arranged according to the block presented in Fig. 3.
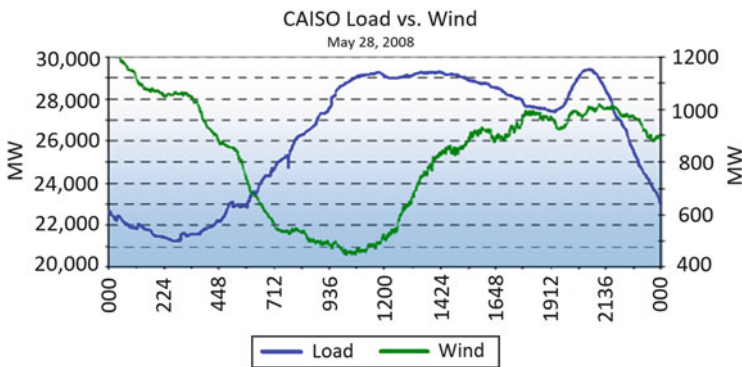


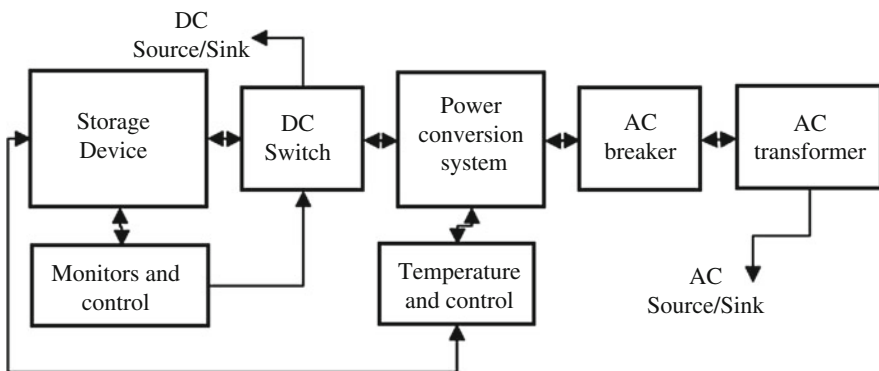**Fig. 2** Comparison of wind generation to load demand [3]



**Fig. 3** Typical energy storage system and primary power components [8]

In Fig. 3, the ESS follows three main bi-directional processes which are; the source, converter and storage components. Depending on the supply source (e.g., AC or DC), energy is stored and reserved when power flows from the AC source through the power conversion system (if AC) and to the storage device, and vice versa when energy is needed for use. A generic battery storage system is made up of key components which include power conversion system, control and monitoring system, and the battery itself. Monitoring and control systems manages and ensures safe and maximum performance of the entire storage system. Another function is that it prevents the batteries from either overcharging or over drained (i.e., it controls the charge and discharge of the battery). For the grid use, the DC power from the Battery is transformed into AC power using power converter [8]. Some common ESS types and their parameters are presented in the following section.

### 1.2.1 Types and Parameters of ESS Technology

Today, several ESS technologies have been designed and used for power system applications (See Fig. 4) [9–11]. A brief discussion on each is presented as follows.

**Flow Battery (FB)** It utilizes a non-toxic and non-hazardous recyclable electrolyte that provides thousands of cycles of power with little maintenance. It is characterized with high energy storage and flexible control capability when compared to typical fixed cell storages.

**Lead Acid Batteries (LA)** They are made from a lead alloy. Compared with nickel- and lithium-based systems, lead acid is weightier, and is less durable when deep cycled due to its rapid ageing characteristic at increased operating temperature and high discharge currents.

**Lithium-Ion Batteries (LI)** They have relatively high efficiency, light weight and energy density. They are suitable for home use and Electric Vehicle systems.

**Flywheels (FW)** In this type of ESS, the kinetic energy is stored in rotating discs which in turn rotates a generator to produce electricity. However, because of huge losses due to friction, its discharge current is high, and as a result are only efficient for short-duration applications.
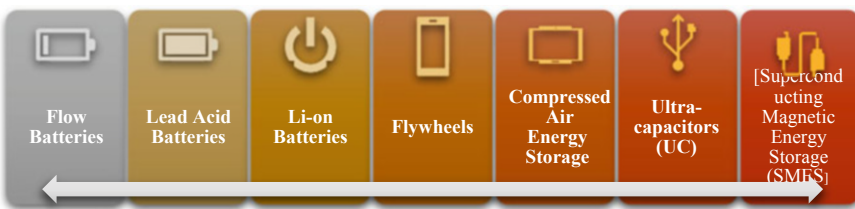


**Fig. 4** Types of ESS technology [9–11]

**Compressed Air Energy Storage (CAES)** They are based on technology which uses compressed air to power a generator that produces electricity. These types of system require large space, such as underground tanks.

**Ultra-Capacitors (UC)** They are operated in similar manner with electrostatic capacitors but can hold significantly more energy like that of conventional capacitors. They are good as large uninterruptible power supply systems (UPS).

**Superconducting Magnetic Energy Storage (SMES)** In this device, the magnetic field of a coil made up of a superconducting wire with minimum loss is used for storing electricity from the grid. Its advantage is that it can emit bulk power within a fraction of time to maintain grid balancing especially after a dip or loss of line power event.

### 1.2.2 Key Properties of ESS Technology

While the technical performance capability can help determine an ESS for a given application, the choice should be based on specific application need. This is because an ESS which performed best in Time-shifting application may perform worse in Off-grid or microgrid operation. From both technical and economic point of view, combination of two or more EES technologies may be required for a given power system application [12], however, in general, viable ESS technology choice should meet the following key properties: economics, durability, environmental safety, and long-duration storage capability for that application [13]. The key properties for selecting ESS system for any application is presented in Fig. 5.

- **Performance:** A technical suitability factor for choosing ESS technology in distribution network is its performance in terms of high efficiency and high operating temperature range.
- **Economics:** A major requirement for ESS consideration and usage in any power applications is its cost-effectiveness. Its acquisition, operating and maintenance costs are expected to be minimal. Also, its proliferation and wider usage in power systems will largely depend on the market situation.

**Fig. 5** Key properties of ESS system [13]
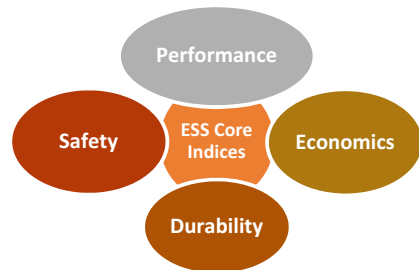
- **Durability:** Durability of an ESS is a measure of its ability to withstand long-term usage fading, minimum performance loss and highly competitive cycle life, for any given application.
- **Safety:** Safety of personnel and environment are important factors in the selection and deployment of ESS technology. Hence, ESS technology should be inherently safe and non-flammable in all applications.

## 1.3 The Need for ESS in Power Systems

The primary reason for ESS adoption in power systems is the underlying characteristics of electricity, high penetration of intermittent renewable resources and need to reduce fossil-fueled energy consumption [7]. ESS is considered to influence the system technical and economic performance and thought to shift energy market horizon. One, based on the principle of energy reservation, energy produced if not used immediately will become wasted. However, during power imbalance situation when there is surplus electricity and low load, or vice-versa, system voltage or frequency may be jeopardized. Two, ESS is deployed considering the short coming of the long-distance link between generation and load where huge energy loss and congestion occur arising from system adequacy issue. The generation-load link also witnesses occasional fault events whose occurrence may not be easily predicted at any given time [7]. This uncertainty can create some level of economic risk for the power system stakeholders (include the operators, utilities and consumers), and the impact created may be large or small depending on the level and or duration of fault sustained. Consequent upon these reasons, ESS is deployed to improve system security, reliability and continuity, since it is sited closely to the load center and does not depend on long-distance transmission need. In this case, ESS inclusion will permit more flexible operation including energy arbitraging, which will largely influence the evolving Smart grid and or Electric Vehicle future.

## 1.4 Power System Operation and the Roles of ESS Technology

Demand Response program was primarily designed to reduce peak demand. As a result, consumers were provided with flexibility to shift their load between peak and off-peak situations for economic advantage. However, because this provision suffers certain set back due to its inefficiency, a new alternative evolved with energy storage facility where load shifting is made possible by storing energy in the off-peak state and using it when the load is at peak. In most recent times, ESS have been used in homes to reduce consumer's energy bill in a time-varying energy pricing situation [9]. In many cases, selecting the appropriate EES technologies have been an important and challenging issues in some countries. For instance, a specific storage system with a capacity of 27.6 GWh exists in the UK network

and even though the technology has gained more market recognition, it has strict restrictions on usage due to its environmental limitation [6]. Thus, it is necessary to select storage technology in combination that is best suitable for both economic and environmental needs.

Generally, ESS can assume specific roles considering the following application situations [10, 14]:

- Time-shifting and energy arbitraging application.
- Demand or Time-Of-Use (TOU) tariff management.
- Renewable intermittency smoothing.
- Cost reduction and fuel efficiency for remote areas.
- Peak demand reduction
- Ancillary Services including backup for power supply
- Off-grid and microgrid stabilization
- Frequency regulation
- Support for voltage control, etc.

With consideration for ESS technology, a sustainable ESS is scalable and easily transportable, clean and possesses longer-duration storage capability. Currently, there exist several scalable ESS technologies being deployed for on-grid, off-grid and microgrid applications [6]. They are selected with the confidence that power system will become more flexibility and energy cost will become cheaper. As such, ESS technology is expected to be resilient, cheap, and environmentally friendly. The advantages of a given ESS technology lies in its durability, and the possibility for recycling with appreciable number of power cycles and relatively low maintenance cost. In any case, ESS technology with more storage capacity could be more reliable than storages with shorter-duration solutions for efficient energy management reasons. In addition, some ESS has been considered with an in-built power electronics to respond to voltage and frequency variations in microgrids, off-grids, medium and large-business and utility scale applications [13].

## 1.5 Opportunities for ESS in Low and Medium Voltage Systems

The potential of ESS technologies to reduce costs has been examined in [12]. Besides, several opportunities exist for ESS deployment in the power system. For example, deploying appropriate ESS technology gives utilities options to manage the operation of their networks more efficiently. The alternative which ESS provides has completely downplayed the need to upgrade the distribution infrastructures which usually incur huge investment burdens. The need to construct extra transmission lines to meet demands is no longer necessary while significant utilities have seen real power loss reduction in their daily operations and have had more control of the system [9]. However, in some countries, there are policies and regulations that guide the use of ESS systems. Certain requirements may have to be met before ESS is permitted for deployment [15].

The ESS application at the utility, medium and large-business and off-grid and microgrid scales are illustrated using specific application cases in the following section.

## 1.6  Specific ESS Application Cases with Illustrations

As mentioned earlier, ESS can be deployed in different scales. However, this section discusses specific ESS application cases from the utility, medium and large-business, and off and micro-grid scale applications perspectives.

### 1.6.1  From the Utility Perspective

ESS deployment is dictated by the degree of renewable energy penetration in the network. Utilities are using ESS having long operating life to time-shift major investments on distribution system such as the construction of new circuits and installations of additional transformers, overload sensors, etc. Time shifting is the process of storing electrical energy when demand is low, or supply is in excess, and using it during demand peaks [14]. This process requires an established communication link between the utilities and ESS systems for necessary observability and controllability reasons. As a result, energy consumption can be managed in response to energy supplies, and energy stored during excess renewables generation can be used when they have greater economic values [16]. Practical energy shifting case considering ESS deployment are depicted in Figs. 6 and 7, respectively.

In Fig. 6, the utility depends on the energy from the generator (or electricity supply from the transmission company) and PV systems to meet its time-varying
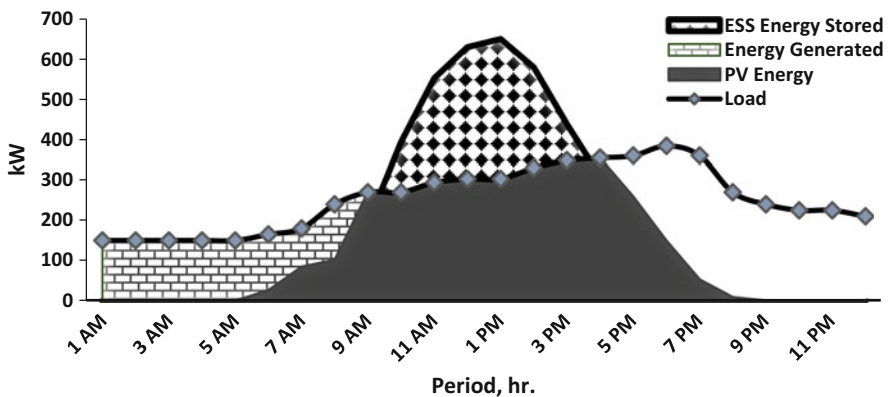


**Fig. 6**  Storing excess PV energy in ESS from 9 AM to 4 PM [14]
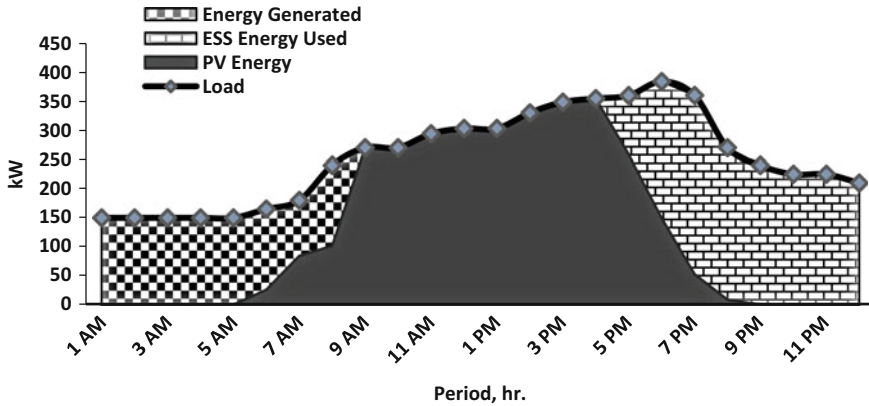
**Fig. 7** Using ESS energy from 5 PM to 12 AM [14]

load across 24-h of the day. However, with the ESS system, excess energy produced by the PV is stored and re-used later. As seen in Fig. 7, the energy stored in ESS was re-used between 5 PM and 12 AM. After 9 PM for instance, there is no longer production from the PV and a no longer necessary to depend on energy from the generator. The excess or un-used energy have been successfully shifted to the later time and used to supply the demands for the rest of the day. In this way, utility will save significant energy cost because of the ESS deployment. However, ESS deployed must be sized according to the load demand for those hours.

### 1.6.2 From the Company or Large Business (Such as Medium and Large Industries) Perspective

High energy consumption can result in increasing operation cost and expenses. Minimizing this cost is the concern of most business and enterprise for profits. For companies that utilize renewable energy, ESS can become a solution for reducing operating costs and energy charges and tariffs from the utilities. This will also enhance supply during outages of electricity from the utility [16, 17]. The following figures illustrate the demand charges reduction situation with ESS support from R\$1200 to R\$900, saving R\$300 per month.

Usually, demand charges consider the demand peak rather than the actual energy consumed. By deploying ESS however, the demand peak can be shaved thereby reducing the demand charges. Given the demand charge of R\$3/kW, Fig. 8 shows the demand charges before peak shaving at a total cost of R\$1.200 per month. After the deployment of ESS, as shown in Fig. 9, the peak was shaved (where the shaved load is met using the ESS energy) to 300 kW which resulted into saving R\$300 per month.
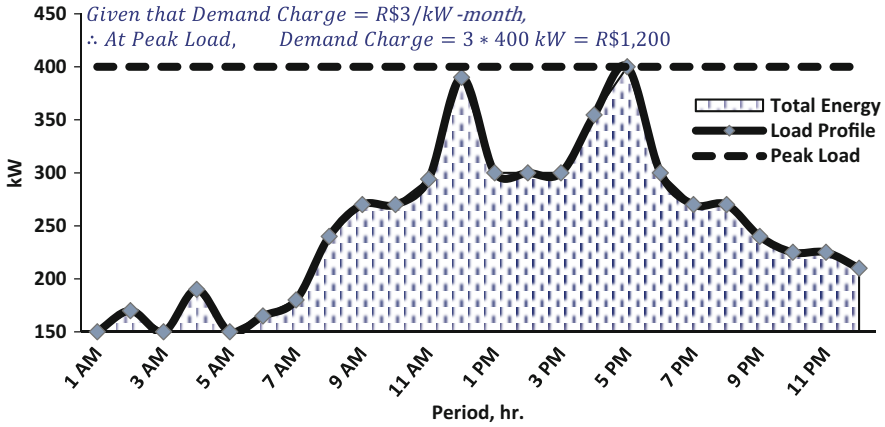
**Fig. 8** Demand charge before peak shaving [16]
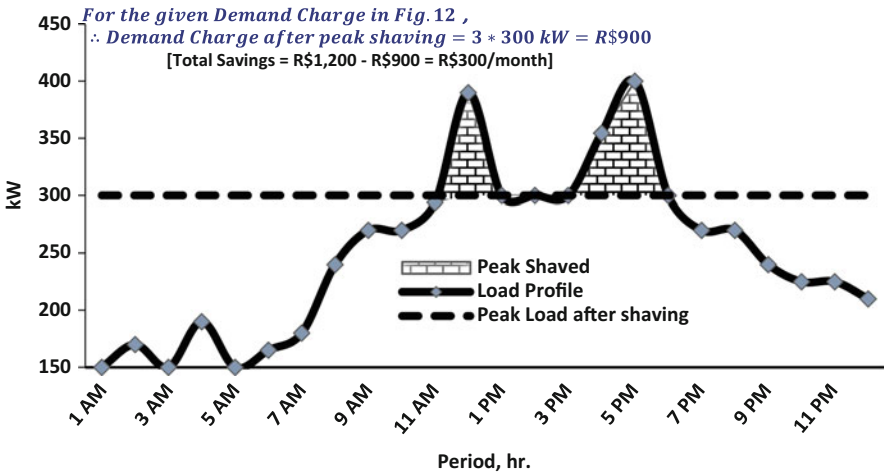


**Fig. 9** Demand charge reduction after peak shaving [16]

### 1.6.3 From the Off-Grid and Microgrid Perspective

Electricity supply may be short and inadequate in most remote areas and many users may seek to get energy from alternative sources such as diesel generators which are costly and have high negative environmental disadvantages. With the development of off-grid and microgrid with renewable energy resource mix, remote areas can rely on independent, cheap and environmentally friendly energy supply. In this case, ESS acts as a baseload energy source where cost of fossil fuel generator can drastically reduce to minimum [18]. Specific case of limiting diesel generator reliance in remote areas are presented in Figs. 10 and 11. The examples show the
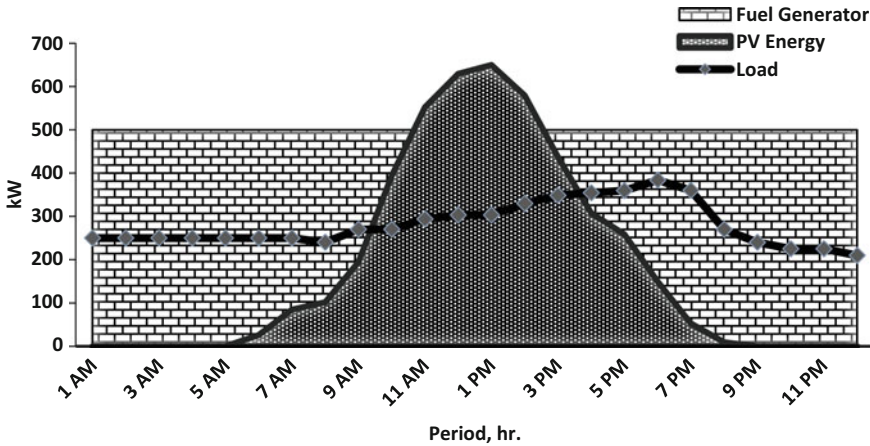
**Fig. 10** Charging ESS with fuel-generator and excess PV energy ($1^0$ 24 h) [18]
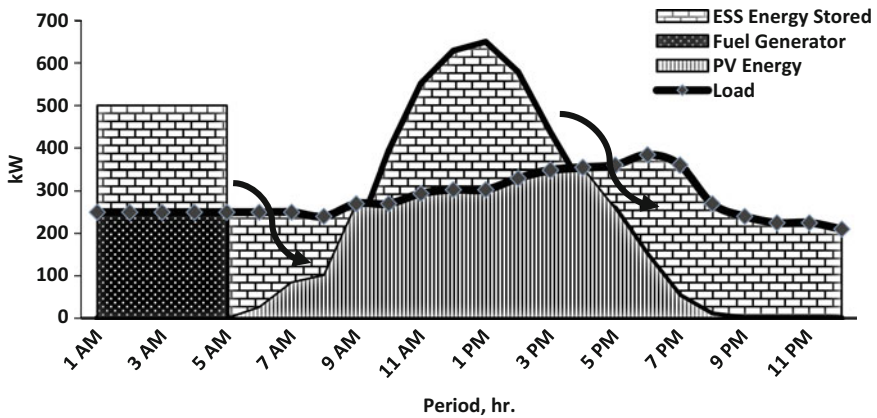


**Fig. 11** Switching-off fuel-generator and using ESS energy from 5 to 8 AM and 5 PM to 12 AM ($2^0$ 24 h) [18]

case of ESS acting as load-varying source where generator is only used when ESS is needed to be recharged. The advantages of this is related to the fact that the generator operates at its peak efficiency and the costs of fuels and maintenance are minimized.

During the first 24-h, both generator and PV are used to meet the demand and to fully charge the ESS systems as depicted in Fig. 10. For the next 24-h, only the PV and ESS supply most part of the load as seen in Fig. 11. However, to determine the overall benefit of the ESS, thorough economic analysis is needed. In the following section, ways to understand and evaluate the economic worth of ESS are discussed.

## 1.7  Evaluating the Economic Worth of ESS

Cost is a key factor when choosing ESS for a given application to meet economic goals. In most cases, capital cost has been used to determine and justify the economic worth of deploying ESS. However, while capital cost may be a major factor when choosing ESS technology, Levelized Cost of ESS (LCOE) is currently been used for evaluating long-term benefits of ESS acquisition in a period of 25 years. The advantage of this method is that the recurring cost of maintenance, operation and replacement in a long-period situation are easily evaluated and compared with the cumulative savings that is being generated by ESS deployment. Several models exist in literature according to specific need. A model for calculating LCOE is given in [14] and presented in Eq. (1).

$$LCOE = \frac{\sum (C_t + OM_t + Ch_t) . (1 + rd)^{-t}}{\sum E_t . (1 + rd)^{-t}} \tag{1}$$

where;

- $C_t$ = *Total capital expenditures*
- $OM_t$ = *Operation and maintenance costs,*
- $Ch_t$ = *Charging cost,*
- $E_t$ = *Discharged electricity in MWh, and*
- $(1+rd)_t$ = *Discount factor, in year t.*

Since determining the right choice of ESS may be quite challenging, the factors in the following sections can help in choosing most appropriate ESS technology for given application in addition to the ESS specifications mentioned earlier. In Fig. 5, key parameters which represents the ESS technology suitability for power application are presented [9]. However, since these parameters vary significantly across technologies, the need to obtain the best choice becomes evident considering the technical and economic values of ESS for different power system applications. Generally, how to minimize cost, energy lost and maximize profit is the baseline for ESS consideration in systems with high renewable energy resources.

## 1.8  ESS Sitting and Sizing and Need for Optimization

Several questions will likely arise if planning for ESS for either small scale or large-scale applications, such as:

- The cost and type of ESS storage to apply
- Timeframe to deploy ESS storage system (ranging from hours to years)
- The sizing of the ESS (in kWh or MWh)

- ESS peak instantaneous power provision (in kW or MWh)
- ESS cycling frequency (in multiple times, daily or infrequently)
- Consideration for renewable energy support (Solar or Wind or Solar-Wind or None)
- Type of application where the ESS will apply
- The ESS location in the system

In principle, such questions can be addressed by evaluating all individual storage application alternatives, one by one. In practice however, the number of storage application options can be very large. In distribution system, this number will depend on the number of system buses and ESS to be installed, making the alternative evaluation process time consuming. As a result, optimization methods are essential and can be adopted to solve similar complex problems. Rather than evaluating every possible storage alternative, the optimization tool produces storage alternatives itself, where the evolution of a new group of options is constructed based on the evaluation results of previous sets, thereby producing an optimal storage alternative for given optimization objectives and constraints. The following section provides a basic introduction to optimization techniques and algorithms used in power system applications [6, 19].

## 2 Optimization Methods

Figure 12 shows the optimization methods that exist in literature and its classifications according to [20]. The two major group are deterministic and stochastic methods. The stochastic method deals with uncertainty and perform probabilistic solutions based on scenarios. The deterministic method is normally based on real data and does not deal with uncertainty and risk.

### 2.1 Stochastic Optimization

As presented in Fig. 12, stochastic optimization is divided into two major groups—heuristic and meta-heuristic methods, which are closely related but with little differences [20, 21]. Meta-heuristic (also known as modern heuristic) optimization have been widely applied to power systems [22]. The following section briefly discusses the heuristic method and provide a detail optimization approach of meta-heuristic optimization in the subsequent.

#### 2.1.1 Heuristic Optimization

According to [21], heuristics solution method is based on trial and error approach. This technique is useful to solve complex optimization problems with the possibility
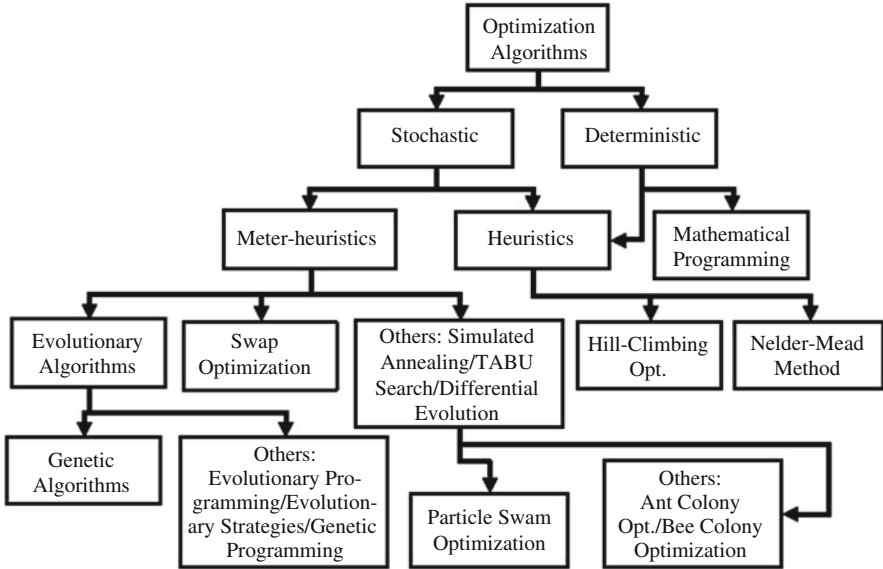
**Fig. 12** Optimization methods and classifications [20]

of need a comparative short time, although might not guarantee an optimal solution. The low processing times make these methods advantageous to many engineers. Sometimes, this technique may not perform well especially while trying to find optimal points to a complex combinatorial optimization problem, however some good solution points can be easily and quickly reached. In other words, an approximate solution may be found for any complex optimization problem. Its main objective is to generate some quick and good solution for a given problem in a reasonable time. The best solution may not be met, or the solution algorithm may just approximate the exact solution. Superior and more robust to the heuristics are the Meta-heuristics which have been developed in recent times. In literatures, both heuristics and meta-heuristics have been used interchangeably but it is important to note their differences, practical use and application limitations.

### 2.1.2 Meta-heuristic Optimization

Meta-heuristics are optimization algorithms or techniques that are developed with more robustness for solving complex optimization problems. The solution provided by this method is more satisfactory since it can meet optimal solution points though in significant time scale. According to [21], meta-heuristics generally performs better than ordinary heuristics. The meta-heuristic approach adopts specific randomization trade-offs and local search. With randomization, transiting from the local to global search can be realized. As highlighted in Fig. 17, Evolutionary Algorithms (EAs) are one of the methods considered as meta-heuristic methods. They are discussed in the following section.

Evolutionary Algorithms (EAs)

According to [23], an evolutionary algorithm (EA) is a genetic population-based algorithm characterized by fitness function. It is also be defined as a variation-driven meta-heuristic optimization algorithm governed by the theory of biological evolution, (e.g., reproduction, mutation, recombination, and selection). EAs aim to optimize a given process so that better or new solutions are generated from existing or old candidate solutions. EAs are associated with a fitness function which also determines the quality of the solutions. If there exist several solutions, the best solution among many others is determined by the fitness value associated with the individual solution as obtained from a fitness function. Variation is usually introduced into the fitness function to ensure that acceptable solution is found in the current population [23]. In this way, a better solution is generated as individual solution undergoes several changes. EAs exist in various types, and they differ in their genetic representation, nature of the problem and details of the implementation approach applied. An example is genetic algorithms presented in the following section [24].

*Genetic Algorithms*

According to most ideologists, GA was formulated to solve optimization problems based on the theory of natural evolution [24]. By definition, GAs are adaptive heuristic search algorithms that are based on the evolutionary and genetic theory. In GAs, the ideas of genetics and natural selection are employed using some intelligent random search processes to provide solution to given optimization problems. They adopt historical data sample to find better solution within the candidate solutions or search space. This process involves simulation of natural systems according to Charles Darwin theory of the fittest survival. GAs are robust and performs better compared to other stochastic [25]. Unlike the conventional AI solution, they are not affected with slight change in the input parameters or with significant noise level.

Unique characteristics that defines GAs are as follows:

- There is competition among individuals in a population for the purpose of mating.
- Parents with better genes have more likelihood to produce more and better offspring than parents with poor genes.
- Successive generations become more suitable in their environment.

As soon as the population has converged and offspring with conspicuous differences evolved from the population in initial generations, the solution algorithm converges, giving rise to set of solutions that meet the optimization problem.

**Solution Search Space**
Individuals in the population represent chromosomes and their variables represent genes, thus the solution is a chromosome which has a set of variables or genes (See Fig. 13). By assigning fitness values to each solution space which represent the ability of the individual member to compete, individual with the fitness value closest
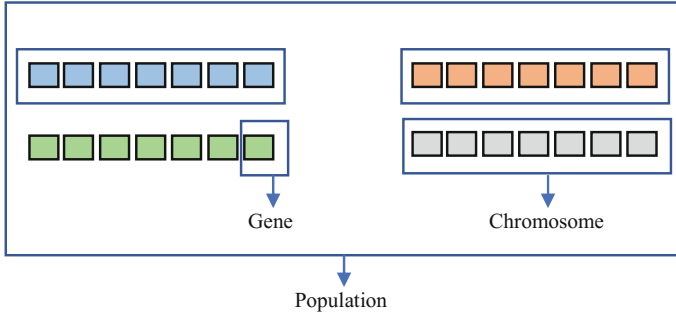
**Fig. 13** Gene, chromosome and population
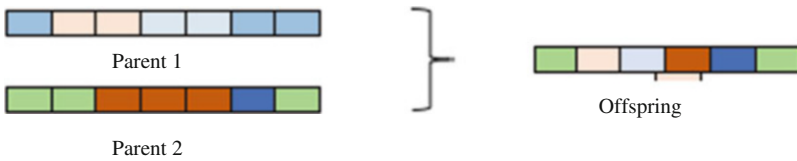


**Fig. 14** Offspring vs. parents



**Fig. 15** Pre and post mutation situations

to the optimal solution is sought. This solution selection or breeding produces offspring that are better than the parents by combining or manipulating their chromosomes [24] (See Figs. 13, 14 and 15).

GA based on natural selection, are implemented through three major processes. which is selection, crossover, and mutation processes.

**Selection Process**

Selection process performs as follow;

- it permits better individuals to replicate their genes in the next generation.
- the better the function of the individual fitness is, the better the individual.
- Fitness can be defined by a specific or multiple objective function.

**Crossover Process**

Crossover process analogous to mating between individuals is described as follow;

- random selection operation is used to select set of individuals to produce set of new offspring.
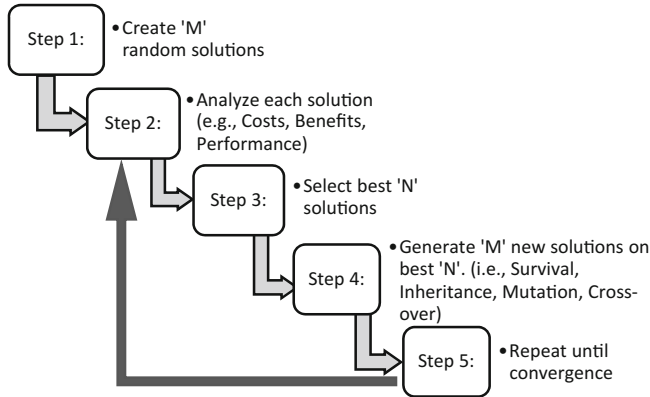
**Fig. 16** The GA algorithm [25]

- the set of new offspring produced are transferred into the population of the next generation where new and better generations are produced by recombination as shown in Fig. 14.

**Mutation Process**

Mutation is the process of introducing random modifications. Figure 15 presents the pre and post mutation situations where the set of new individuals have their colours flipped.

The processes of implementing the genetic algorithm is presented in the GA algorithm flowchart presented in Fig. 16.

Swarm Optimization

Swarm optimization takes its initiative from the behavioral concept of flock of bird or swarms of fish. The optimization problem consists of a population of swarms that flow in trajectories driven by self and neighbors' best abilities. This exchange or flow of information among particles takes place through the local neighborhood or the entire global swarm initiative [26]. In the following section, particle swarm optimization concept is discussed.

*The Particle Swarm Optimization (PSO)*

Particle swarm optimization (PSO) is a meta-heuristic global optimization method which is based on swarm intelligence concept [27]. The candidate solutions in PSO are called "particles". From a given h particles, the position of the $i_{th}$ particle in the h particles can be defined by vector $u_i$ as;

$$u_i = [u_{i1}u_{i2}u_{i3}u_{i4}\ldots u_{is}] \tag{2}$$

The swarm is a population of h candidate solutions and can be represented as:

$$u = \{u_1, u_2, u_3, u_4, \ldots, u_L\} \tag{3}$$

To search and find the optimal solution in the search space (or in an iterative sequence), the particles trajectories will be dependent on the equation of motion as given in Eq. (4) to update their given positions.

$$u_i\,(n+1) = u_i\,(n) + v_i\,(n+1) \tag{4}$$

where $n$ and $n+1$ are successive iterations of the optimization algorithms and $v_i$ is the velocity components of the $i_{th}$ particle in the q-dimensions. The movement pattern of individual particles is dictated by the velocity vector. The particle movement is governed by its inertia, cognitive and social components. The inertia keeps the particle from an erratic motion such that it keeps track of its previous direction of flow. The cognitive component explains the willingness of the particle to remain to its initial best position, whereas, social component is the tendency of the particle to migrate towards the best position of a local neighbourhood or the entire swarm. Thus, the $i_{th}$ particle has a velocity described as Eq. (5).

$$v_i\,(n+1) = v_i\,(n) + c_1\left(p_i - u_i\,(t)\right)r_1 + c_2\left(g - u_i\,(t)\right)r_2 \tag{5}$$

where $p_i$ refers to the particle personal best which is the coordinates of the existing best solution obtained, and $g$ is the global best. $c_1$ and $c_2$ are the cognitive coefficient and social coefficient, respectively. They also refer as acceleration constants. $r_1$ and $r_2$ are diagonal matrices of random numbers with a uniform distribution of [0,1]. These meta-parameters (e.g., $c_1$ and $c_2$) have great influence on the final result and thus are key factors in designing efficient optimization algorithms [28, 29]. Equations (4) and (5) follow an iterative process that are repeated until an ending condition is reached. The basic PSO algorithm can be represented by the following process:

1. Initialization

    For the h particle;

    - Initialize the particle position $u_i(0)\ \forall\ i \in 1:h$
    - Initialize the particle's best position $p_i(0) = u_i(0)$
    - Evaluate the fitness function such that if $f(u_j(0)) \geq f(u_i(0))\ \forall\ i \neq j$, then initialize the global best as $g = u_j(0)$

2. To meet the stopping criterion, the following steps are repeated;

    - Update the particle velocity;

    $$v_i\,(n+1) = v_i(n) + c_1\,(p_i - u_i(t))\,r_1 + c_2\,(g - u_i(t))\,r_2$$

- Update the particle position $u_i(n + 1) = u_i(n) + v_i(n + 1)$
- Evaluate the fitness function $f(u_i(n + 1))$
- If $f(u_i(n + 1)) \geq f(p_i)$, update personal best at $p_i = u_i(n + 1)$
- If $f(u_i(n + 1)) \geq f(g)$, update global best at $g = u_i(n + 1)$

3. End the iteration process and present the final best solution as $g$

**Initialization of the particle's position and velocity**

The initialization process determines the probability of the particles travelling within the search space boundaries. This property has an influence on the solution convergence of the optimization problem. According to literatures, the particles' positions initialization can be governed by the following equation [30].

$$u_{ij}(0) \in R\left(u_{j,min}, u_{j,max}\right) \tag{6}$$

where $u_{j,min}$ and $u_{j,max}$ determines the lower and upper limits of the $j_{th}$ size of the solution space, respectively, and $R$ is a random number generator function. Its main function is that it increases the convergence speed of the optimization algorithm [31]. However, caution must be taken as this may lead to the particles violating the solution space limits, leading to the non-convergence of the algorithms, the phenomenon known as velocity explosion [30, 32]. The initial positions are guaranteed by making the initial velocities as small random numbers [30].

**Determination of the acceleration coefficients**

According to Eq. (5), the acceleration coefficients $c_1$ and $c_2$ determines the tendency of the particles to migrate towards the self and global best and increasing the social and cognitive terms. The effect of these coefficients has been investigated in [26] relating to the convergence capability of the method and it showed that high acceleration coefficients increases the particle's oscillation frequency around the optimum and low values lead to sinusoidal behaviour. The conditions to obtain the best solution is defined as: $c_1 = c_2 = 2$.

**Preventing particle's velocity explosion**

Different methods are proposed in the literatures to damp the particle's oscillations across the search space and enhance easy convergence. The most common methods include velocity clamping and inertia weight inclusion concepts [28].

*Velocity Clamping Concept*

The velocity clamping imposes a boundary on the maximum velocity of the particle in the search space limits. By introducing a velocity limits into the algorithm, the following parameters are adjusted based on the following criteria;

$$If\ v_{ij}(n + 1) > v_j^{max},\ then\ v_{ij}(n + 1) = v_j^{max} \tag{7}$$

$$If\ v_{ij}(n + 1) < -v_j^{max},\quad then\ v_{ij}(n + 1) = -v_j^{max} \tag{8}$$

where $v_{ij}(n + 1)$ is the velocity component of the $i_{th}$ particle in the $j_{th}$ direction during $(n + 1)_{th}$ iteration and $v_j^{max}$ is the maximum velocity. The best value of $v_j^{max}$ could be chosen as in [28] considering the difficulty to find the best value.

$$v_j^{max} = \sigma \cdot \frac{\left(u_{j,max} - u_{j,min}\right)}{2} \quad \sigma \in (0, 1) \tag{9}$$

where $\sigma$ is a constant that assumes any value between 0 and 1.

**Initial Weight Rule Concept**

The second method that is used to prevent the explosion of the velocity is by introducing inertia weight $\omega(n + 1)$ to update the particle velocity [33]. The inertia weight introduced in [33] is a constant. Studies showed that its dynamic changes significantly influence the convergence properties of PSO. Choosing the inertia weight greater than 1 favour global search and a value less than 1 favours local search [34]. The velocity update rule concept is governed by the following equation:

$$v_i(n + 1) = \omega(n + 1) \cdot v_i(n) + c_1\left(p_i - u_i(t)\right)r_1 + c_2(g - u_i(t))r_2 \tag{10}$$

The dynamic adjustment approaches adopted in literatures for evaluating inertia weight for a given optimization problem are presented as follows [29–31, 35].

- Chaotic descending inertia weight:

$$\omega(n) = \omega(0) - \omega(n_{max})) \left(\frac{n_{max} - n}{n_{max}}\right) + \omega(n_{max})z; z = 4r(1 - r); r \in R(0, 1) \tag{11}$$

- Chaotic random inertia weight:

$$\omega(n) = 0.5r_1 + 0.5z; z = 4r_2(1 - r_2); r_1, r_2 \in R(0, 1) \tag{12}$$

- Inertia weight of the global-local best:

$$\omega_{ij}(n) = 1.1 - \left(\frac{p_{ij}(n)}{g_j(n)}\right) \tag{13}$$

- Random inertia weight:

$$\omega(n) = 0.5 + \frac{r}{2}; r \in R(0, 1) \tag{14}$$

- Constant inertia weight:

$$\omega(n) = \omega = constant \tag{15}$$

- Linear decreasing inertia weight:

$$\omega(n) = \omega_{max} - \left( \frac{\omega_{max} - \omega_{min}}{n_{max}} \right) n \tag{16}$$

The linearly decreasing inertia weight proved superior in many practical applications, adopting $\omega_{max} = 0.9$ and $\omega_{min} = 0.4$ [35]. In [34], a set of benchmark functions for optimization showed a faster convergence situation with random inertia weight, and, the chaotic descending inertia weight showed consistency in terms of lowest average error for over 25 repeated simulations. Both constant and linearly decreasing inertia weight strategies also lead to total lowest errors [30].

## 2.2 Optimization Formulation Representation for ESS Problems

### 2.2.1 ESS Modelling

Solving ESS sitting and sizing problem for DG support depends on the objective function to minimize or maximize. Since renewable energy like solar or wind are subject to climate variations, it is difficult to precisely determine the timescale solar or wind generation, and to predict changes in their behavior. Consequently, energy generation by these sources are evaluated based on probabilistic approach. Thus, stochastic optimization considers the DG and load uncertainties and determines where ESS should be included and managed to support DG. There are several kinds of stochastic approaches to determine ESS site and size, but mostly they are based on the following formulation.

### 2.2.2 Objective Functions and Control Variables

Depending on the problem to consider, several approaches of the ESS size and allocation can be. In this case the control variable would be the ESS size and location, with the "best" value that must be determined subject to the objective formulated. Some of the objectives which can be considered in the ESS sitting and sizing problem are minimization of power losses, operational cost, voltage variation, Expected Energy Not Supplied (EENS), and or maximization of voltage limits satisfaction, Consumer benefit and Utility's profits, among others.

These objectives affect consumers, distribution companies, DG owners among others. Depending on the affected group, some objectives that are good for one group could have negative impact on another. For example: consumers are more focused on electricity cost reduction but maybe unconcerned with the network behavior especially during high system loading. Considering these aspects, an

objective function can be defined as in Eq. (17).

$$\text{Min } Fo; \qquad \text{Max } Fo \qquad (17)$$

where *Fo* is the objective function, and its defined in relation to the ESS use.

The objective function can be the energy cost (Cost for energy production), losses cost (Cost related to system losses), DG cost (Cost for installation and operation of DG), and **ESS cost** (Cost for installation and operation of the ESS).

### 2.2.3  ESS Constraints

First, a major consideration for ESS is its charging and discharging capacities. Both State of Charge (SOC) and Depth of Discharge (DoD) are parameters usually used for limiting the ESS power injection. The SOC is calculated by [5, 36]:

$$SOC_{i,t} = \frac{C_{ESS,t}}{C_{ESS,max}} \qquad (18)$$

$$DOD_{i,t} = 1 - SOC_{i,t} \qquad (19)$$

$$0 \leq \left| P_{ESSi,t} \right| \leq P_{ESS,max} \qquad (20)$$

$$C_{ESS,min} \leq C_{ESS,t} \leq C_{ESS,max} \qquad (21)$$

$$C_{ESS,t} = C_{ESS,t-1} + \left( P_{ESS,t} eff \right) \Delta t \qquad (22)$$

where $SOC_{i,t}$ is the SOC for the ith ESS; $C_{ESS,max}$ a the rated energy capacity (usually in MWh or kWh, and $C_{ESS,t}$ the energy capacity for the time *t*); $DOD_{i,t}$ is the DOD for the ith ESS; the power injection/consumption made by the ith ESS is $P_{ESSi,t}$, and the rated power capacity of the ESS is $P_{ESS,max}$ (Usually in MW or kW); the minimum and maximum energy allowed in each state of time are $C_{ESS,min}$ and $C_{ESS,max}$, respectively and the energy capacity of the ESS is $C_{ESS,t}$; eff is the efficiency of charging or discharge of the ESS, and the time step of each time interval is $\Delta t$ (in seconds, minutes, or hours)

### 2.2.4  Network Constraints

**Power Flow Formulation**
A power flow analysis calculates the current injections and voltages in the distribution system, and consequently helps to quantify system loses, and voltage

deviations. The inclusion of this formulation is important if the method considers network constraints for ESS planning. Some methods that focus on economic approach only (Market arbitrage and prizes) may not need a power flow formulation [37], but for a more detailed analyses with technical impacts this maybe important. The balance load equation considering DG and ESS is [38]:

$$\sum_{j=1}^{A} P_{Dj,t} + P_{loss,t} = \sum_{i=1}^{B} P_{DGi,t} + \sum_{i=1}^{C} P_{ESSi,t} \tag{23}$$

where $A$, $B$ and $C$, are the total number of nodes, DG units and ESS units respectively. $P_{Dj,t}$ is the load demand for the bus $j$, $P_{loss,t}$ is the network losses for each time step $P_{DGi,t}$ is the DG power injection located at node j, and $P_{ESSi,t}$ is the power input/output by the ESS at node $i$ at time $t$.

Usually, for the $P_{ESSi,t}$, as positive value indicates discharging (power injection) and $P_{ESSi,t}$, as a negative value indicates that the ESS is charging. Considering these conditions, the real and reactive parts of the power flow equations are [37, 38]:

$$\sum_{i=1}^{B} P_{DGi,t} + \sum_{i=1}^{C} P_{ESSi,t} - \sum_{j=1}^{A} P_{Dj,t} = U_i \sum U_j \left( G_{ij} cos\theta_{ij} + B_{ij} sin\theta_{ij} \right) \tag{24}$$

$$\sum_{i=1}^{B} Q_{DGi,t} + \sum_{i=1}^{C} Q_{ESSi,t} - \sum_{j=1}^{A} Q_{Dj,t} = U_i \sum U_j \left( G_{ij} cos\theta_{ij} + B_{ij} sin\theta_{ij} \right) \tag{25}$$

where the real and imaginary parts are the bus admittance matrix are $G_{ij}$ and $B_{ij}$ and the angle difference between the i-th and the j-th buses is $\theta_{ij}$, the active and reactive parts are $P$ and $Q$, and $U_i$ and $U_j$ are the voltage at bus $i$ and is $j$ respectively. For simplicity purposes in the calculation, the reactive injection/consumption of the ESS and DG can be disregard.

To model the network impact, it is considered current and voltage limits in each bus of the distribution system. The line current and voltage at the buses are constrained by [37, 38]:

$$I_{min} \leq I_{ij,t} < I_{max} \tag{26}$$

$$V_{min} \leq V_{j,t} \leq V_{max} \tag{27}$$

where $I_{min}$ is the minimum allowed current, $I_{ij,t}$, is the current for the line $ij$, and $I_{max}$ is the maximum allowed current, $V_{min}$ the minimum allowed voltage, $V_{ij,t}$ the voltage at bus $j$ and $V_{max}$ the maximum allowed voltage.

The network constraints can be modelled as a linear model, which requires some approximation, or as a nonlinear model, which requires nonlinear optimization techniques or heuristic techniques to be solved. The power flow problem can be solved by licensed software like, OpenDSS, DIgSilent, and other available

proprietary power analysis software. Computer solutions are often sought based on robustness and speed, and extra coding involving power flow can be totally avoided.

### 2.2.5 Forecasting Uncertainties

Considering the random behavior of renewable sources and load, the stochastic optimization makes a probabilistic solution to forecast the uncertain and give a possible solution. Consequently, some models create different scenarios of the system to have critical and expected responses. These scenarios are considered for optimization problems usually applied in planning horizons of days or years [39].

### 2.2.6 Load Forecasting

Gaussian cumulative distribution function can be useful in order to predict the load behavior. The formulation is given by [39]:

$$f_L(L) = \frac{1}{\sqrt{2\pi\sigma_L^2}} exp\left[-\frac{(L-\mu_L)^2}{2\pi\sigma_L^2}\right]_{l_c}^{u_c} \tag{28}$$

where the mean and standard deviation of the load are $\sigma_L$ and $\mu_L$, respectively, and maximum and minimum values of the load are $l_c$ and $u_c$, respectively

After this formulation a curve fitting method is used for estimating the distribution parameters for simulation of the load demand on timescale basis.

### 2.2.7 Wind Generation

In order to represent the random characteristic of wind speed, a Weibull probability distribution function is used. The probability density function, before and after performing a linear transformation for the wind power, is given by [40, 41]:

$$f_u(u) = \frac{k_u}{C_u}\left[\frac{u}{C_u}\right]^{k_u-1} exp\left[-\left(\frac{u}{C_u}\right)^{k_u}\right] \tag{29}$$

$$f_w(u) = f_u\left(\frac{w-b_w}{a_w}\right)\left[\frac{1}{a_w}\right] \tag{30}$$

where the forecast error probability density function of wind speed is $f_u(u)$ and for the wind power is $f_w(u)$, the wind speed, and wind power are defined as $u$ and $w$ and $k_u$, $C_u$, $a_w$ and $b_w$ are used for the probability function parameters.

### 2.2.8 Representation of Solar Power

Solar radiation uncertainty depends strongly on weather conditions. As a result, a clearness index is used in order to consider this parameter. The stochastic behavior of the clearness index can be defined by a Beta distribution function as given in Eq. (31) [42]:

$$f_{cl}(k_t) = \frac{\Gamma(a_k + b_k)}{\Gamma(a_k)\,\Gamma(b_k)} k_t^{a_k - 1} * (1 - k_t)^{b-1} \tag{31}$$

where the forecast error probability density function used for the clearness index $k_t$, is $f_{cl}(k_t)$ is, $a_k$ and $b_k$ are the Beta distribution function parameters, respectively.

## 3 Perspectives and Future Works

The proliferation and market penetration of ESS may be gradual, then there are many possibilities for new studies and applications. Some studies have already been done to investigate the potential of ESS application in distribution systems, showing excellent performance in terms of reliability, losses, voltage regulation, and profit/cost reduction. Nevertheless, ESS support for high DG implementation in distribution system may require a lot of time to be fully integrated in most countries. Some countries are currently evaluating ESS use but mostly on a laboratory and not used on consumer or utility scale [36]. Also, the development of different types of ESS for smart grid technologies, demand side approach, and electric vehicle use introduces researchers in power systems to more challenges which will create new opportunities for investigating wider and future applications. In the following section current studies and perspectives for ESS application are presented and discussed.

### 3.1 Smart Grids vs. Transmission Reinforcements

The conversion of the distribution networks to fully automated infrastructure may become costly but will delay some investment in network reinforcement. The migration to a more distributed system with less transmission lines may happen considering large ESS systems like CAES, to guarantee energy availability all the time [43–45]. With these two contradictory perspectives, there is need for studies on the costs of ESS projects and select the best alternative. Thus, multi-objective models are prior to new investigation of ESS use in distribution systems.

## 3.2 Dynamic Pricing Response and Real Time Operation with DG Generation Prediction

With the DG behavior and demand response policies, dynamic pricing will affect consumer and its decisions [39, 46, 47]. In this context, ESS optimization is an approach to manage consumer behavior and match prices for generation considering risk reductions (for DG stochastic behavior) and capacity limits. Also, the need to reduce stochastic behavior of DG is evident as Wind and Solar Photovoltaic generation grow around the world. Stochastic models are used to predict the random behavior of DG to precisely determine energy available and uncertainties. The accuracy for the real time measuring is also important in order to determine the load behavior exactly as it is needed [43]. Thus, models with ESS for real time control and consideration for error measurement will be interesting.

## 3.3 Multiple ESS System Control and Type Selection

Most studies attempt to optimize distribution systems considering a small number of ESS units [4, 36, 43, 48]. However, considering a bigger participation of DG and ESS units, new robust optimization models are required for ESS energy management in order to reduce operational costs. This could be useful if the DISCO has the control of the ESS and regulate each operation in order to guarantee a more efficient energy supply. As suggested in literature, there are several types of ESS, and each one has specific characteristic in terms of power capacity, costs, energy capacity, depth of discharge, self-discharge rate, lifetime among others [36, 49, 50]. In this way, ESS type selection could be useful to consider the suitable technology for each application in the distribution system. With the correct type selection, costs of projects installment and operational costs may reduce.

## 3.4 Reconfiguration and Reliability

ESS concept can ensure system reconfiguration in order to guarantee a better reliability [5, 48, 51]. In this case, it is important to analyze how ESS can improve SAIFI and SAIDI indices with DG penetration, and to ensure that its use will reduce further investment requirements for lines, switches and other protection devices.

## 3.5 Voltage Regulation and Ancillary Services

ESS units can be used to improve voltage profile. Recent studies carried out optimal voltage and/or frequency control with ESS [52–55]. In this case, comparison

of advertence of replacement or support of voltage regulator devices with ESS was presented. Also, studies on economic incentives for frequency regulation and regulatory framework to determine the ESS best operational use can emerge.

## 3.6 ESS Environmental Impact

Optimizing the ESS capacity and also selecting the best technology, considering CO2 emissions/reductions, and other environmental impacts that may have ESS use in the system can also become a major focus [4, 42, 56]. Environmental concern also considers the grow of solar and wind generation, and the comparison with coal-based technologies use. Studies also must investigate if consumer behavior match with DISCO interests, and how economic incentives could be used to satisfy each part involved considering systems efficiency, consumer needs, and environment.

## 3.7 Electric Vehicle Station and Mobility

With the growth of electric vehicles and electric vehicle stations (ESV), the ESS potential also could be coordinated with the ESV but it must consider consumer behavior in terms of charging and discharging, mobility interests and costs implications [40, 57, 58]. The optimal location of ESS could be affected as the ESV grow considering that the optimal point for generation and charging could change as the vehicle demand for energy and supply varies in a dynamic way and could be in different points along the days. Stochastic optimization models to predict this behavior could be useful but it is important to have historical data to investigate the consumer perspectives.

# 4 Practical Examples

## 4.1 Example One

In the following example, a few ESS storage is proposed to be deployed at a given distribution bus to support its installed PV system. A Hybrid Optimization Model for Multiple Energy Resources (HOMER) proprietary software is used to find the solution. HOMER has the capacity to simulate hybrid renewable electric generation systems on hourly basis [59]. The ESS type and specification for the PV support are given in [60] as presented in Table 1.

**Table 1** ESS type and specifications for PV support [60]

| Description | ESS type (Surrette 4KS25P) |
|---|---|
| Manufacturer | Rolls/Surrette |
| Nominal ESS capacity | 1900 Ah |
| Nominal ESS voltage | 4 V |
| ESS round trip efficiency | 80% |
| ESS min. state of charge | 40% |
| Float life of ESS | 12 years |
| ESS max. charge current | 67.5 A |
| ESS max. charge rate | 1 A/Ah |
| ESS lifetime throughput | 10,569 kWh |
| Suggested value | 10,494 kWh |
| Capacity ratio | 0.254 |
| Rate constant | 0.528 1/h |
| ESS charge voltage range | 2.45–2.5 V/cell @ 25 °C (77 °F) |
| ESS float voltage range | 2.25 V/cell @ 25 °C (77 °F) |
| ESS self-discharge rate | 5–10% per month at 25 °C (77 °F) |

**Table 2** Search space and possible combination of ESS for PV support

| ESS search space | 1 | 2 | 3 | 4 | 5 | 6 | 7 |
|---|---|---|---|---|---|---|---|
| Battery strings | 0 | 4 | 32 | 64 | 128 | 256 | 512 |
| Battery per string | 3 | 3 | 3 | 3 | 3 | 3 | 3 |
| Possible combination | 0 | 12 | 96 | 192 | 384 | 768 | 1536 |

The HOMER optimization algorithm searched the optimal size of the ESS to support both technical and economic performance of the distribution bus. Table 2 shows the search space and possible combination of ESS for the PV support.

In Table 2, the system performance was evaluated by including and testing each possible combination of ESS (from space 1 to 7) on the distribution bus to determine the actual number of ESS that will result into optimal benefit.

The performance characteristic of the ESS in terms of its capacity and discharge current is presented in Fig. 17.

Figure 17 shows how the ESS capacity decreases with the increase in the discharge current. Literally, this information is important to determine the number of ESS that will be needed for the PV support depending on the load to be fed; the higher the load the higher the capacity of the ESS. To support this point, the relationship between ESS capacity and discharge current is presented as a function of hour rate in Fig. 18.

In Fig. 18, a load of 19.04 A can be fed by ESS capacity of 1904 Ah for up to 100 h, while a load of 456 A will be met by ESS of 459 Ah capacity for only 1 h before the ESS reaches its discharge limit. Therefore, ESS capacity is chosen based on the amount of load and number of hours of electricity supply. The Failure cycles and Lifetime throughput in relation with Depth of discharge are presented in Fig. 19.
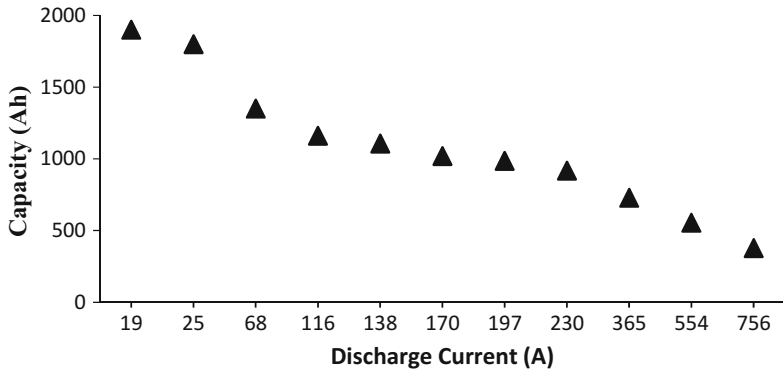
**Fig. 17** ESS capacity and discharge current relationship
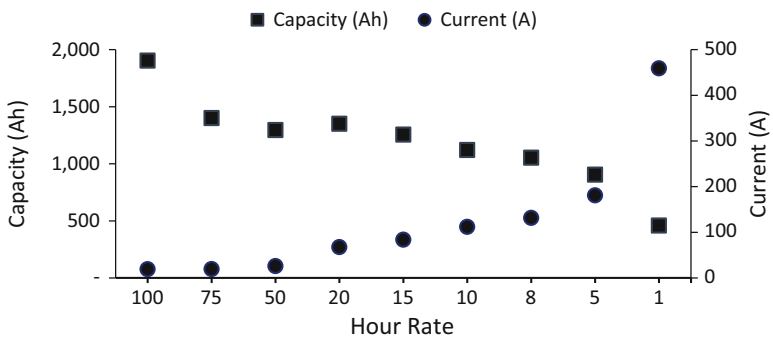


**Fig. 18** ESS capacity and discharge current as a function of hour rate
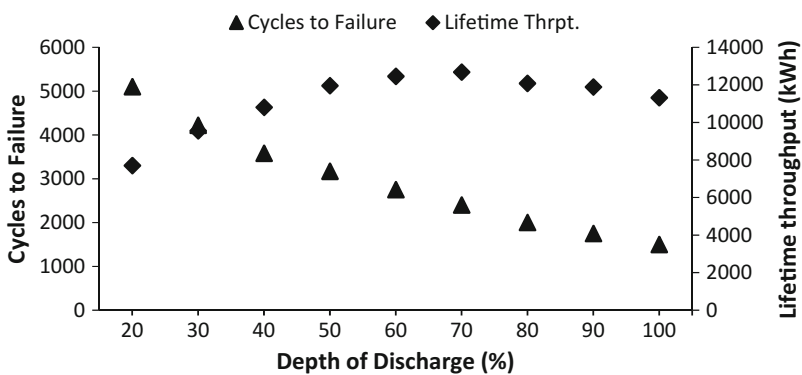


**Fig. 19** Failure cycles and lifetime throughput in relation with depth of discharge
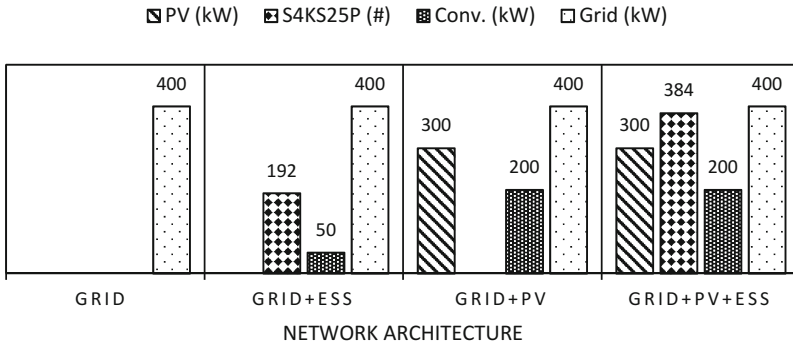
**Fig. 20** Network architecture of ESS optimization for PV support
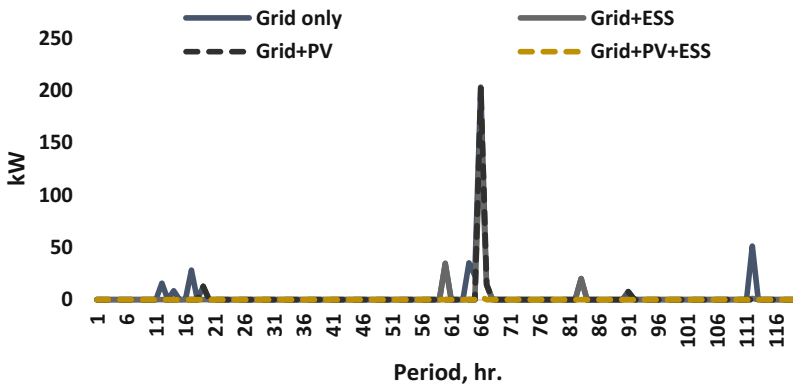


**Fig. 21** Network unmet load

As shown in Fig. 19, as the ESS percentage depth of discharge increases, its failure cycles decrease but increases its lifetime throughput. For this reason, ESS charging and discharging should stay within appropriate thresholds to enhance its total lifespan.

Based on the ESS specifications, the network architecture for different operational scenarios is examined. Figure 20 shows the network architecture of ESS optimization for PV support.

According to the optimization algorithms and selection, four scenarios of network architecture which include: Grid only, Grid plus ESS, Grid plus PV and Grid plus PV plus ESS were considered, and their performances were examined. Under these conditions, Fig. 21 shows the unmet load for each network architecture.

As shown in Fig. 21, there were situations where significant amount of load was not met due to capacity shortage as presented in Fig. 22. The largest unmet load was observed with Grid plus PV architecture. There were no unmet load considering the Grid plus PV plus ESS architecture, adding that ESS can support Grid/PV systems to enhance supply reliability (i.e., availability and adequacy).
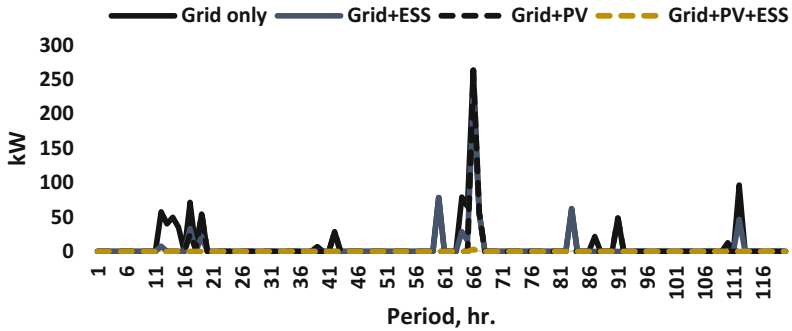
**Fig. 22** Network capacity shortage
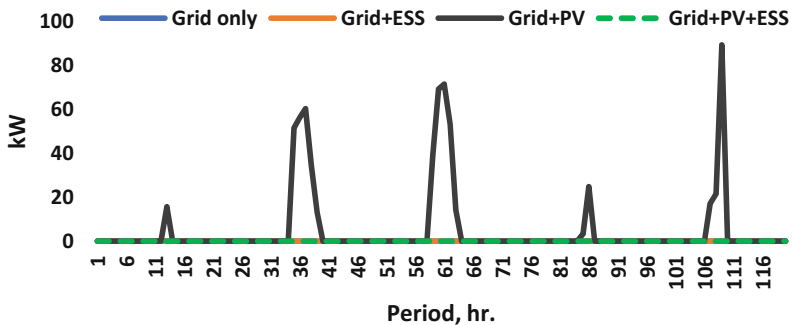


**Fig. 23** Network excess energy

Figure 22 shows that the Grid plus PV plus ESS has no capacity shortage limitations. It is also worth noting that the Grid plus ESS architecture will present capacity shortage limitation while charging the ESS and meeting the entire system load at same time. This is because, the total power purchased from the grid is limited to 400 kW only. However, as observed in the 66th hour, the Grid plus PV architecture has the largest capacity shortage limitation since the maximum grid power purchase is limited to 300 kW and PV supply at this hour is too low to meet the total system load. Considering the intermittent nature of the PV supply, its tendency to produce excess power in the system during low load situation is examined as presented in Fig. 23.

Figure 23 shows that only the Grid plus PV architecture produces power in excess in the period of 116 h. Consequently, considering the limitation of each network architecture, only Grid plus PV plus ESS architecture satisfies all technical performance and best economic benefit as presented in Figs. 25–28. The operation situation of the Grid plus PV plus ESS architecture for a period of 72 h is presented in Fig. 24.

Figure 25 presents the initial capital and total net present cost for each architecture.
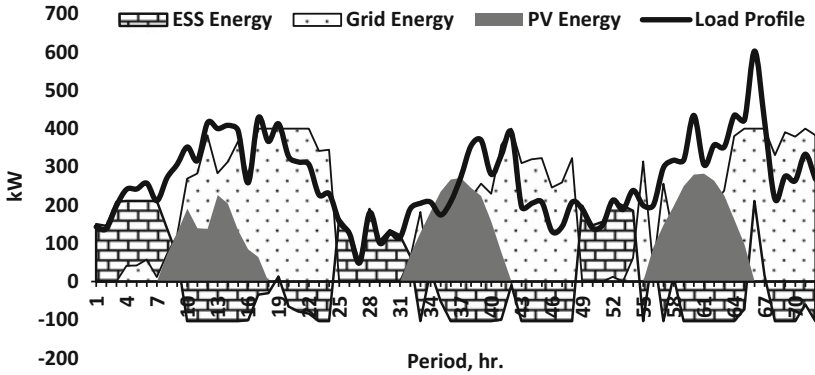
**Fig. 24** Grid plus PV plus ESS architecture performance in 72 h
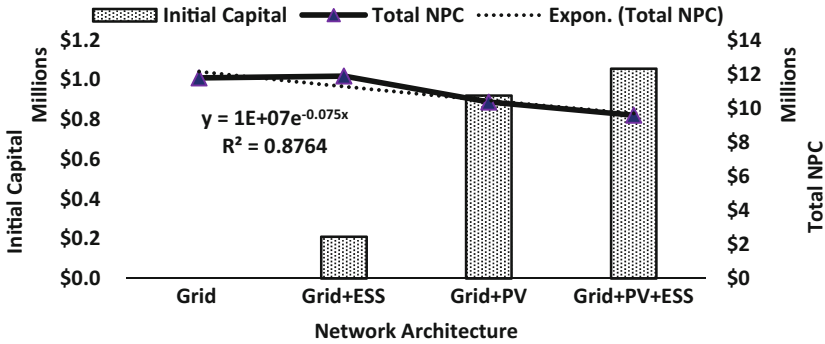


**Fig. 25** Capital cost and total net present cost

In Fig. 25, the Grid plus PV plus ESS architecture has the highest initial capital cost, however, its total net present cost is lower compared to other architectures. This shows that in term of cost, Grid plus PV plus ESS architecture is more economical for the period of 25 years considered in this case study. The energy cost per hour is presented in Fig. 26.

By defining the hourly grid power price and grid sellback rate, ESS energy cost fluctuates around $0.30/kWh for the Grid plus PV plus ESS architecture. In addition, as presented in Fig. 27, the architecture possesses lowest levelized cost of energy.

Table 3 compares the Grid plus PV plus ESS with other architectures in terms of present value, annual worth, return on investment, internal rate of return, simple payback and discounted payback values

In conclusion, the optimization and deployment of ESS to support (control and regulate) high renewable resources in the distribution system is necessary for technical and economic reasons, and the results presented in this study has proven so.
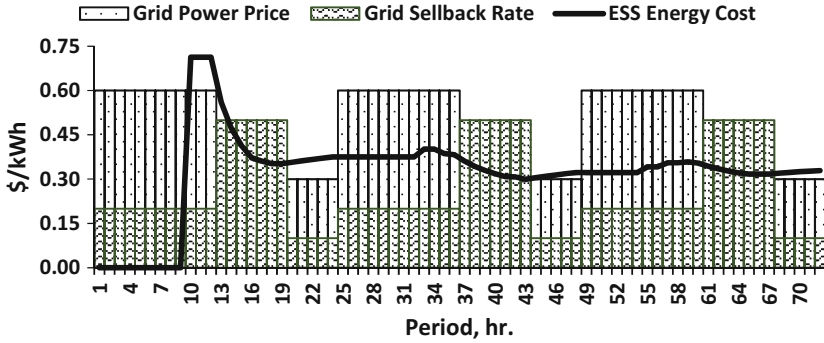
**Fig. 26** Energy cost per hour
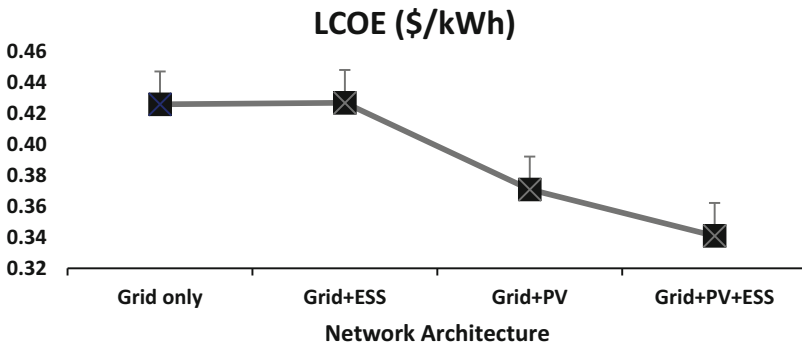


**Fig. 27** Levelized cost of energy

## 4.2 Example Two

The following example attempts to reduce the cost of operation and losses of a substation considering ESS deployment in 1 day of operation in a distribution system with penetration of DG sources based on the ideas presented in Sect. 2. The objective is defined by a fitness function *Fit* given in the following equation [55]:

$$Fit = CE^{HD} + CE^{Loss} + CV^{Pen} \tag{32}$$

where $CE^{HD}$ is the total cost of energy for the substation, $CE^{Loss}$ are the total loss cost for the period under study, and $CV^{Pen}$ are the penalties applied for violation of voltage levels.

To determine the ESS operation, a nonlinear optimization problem is solved considering the ESS capacity and electrical restrictions. The substation objective
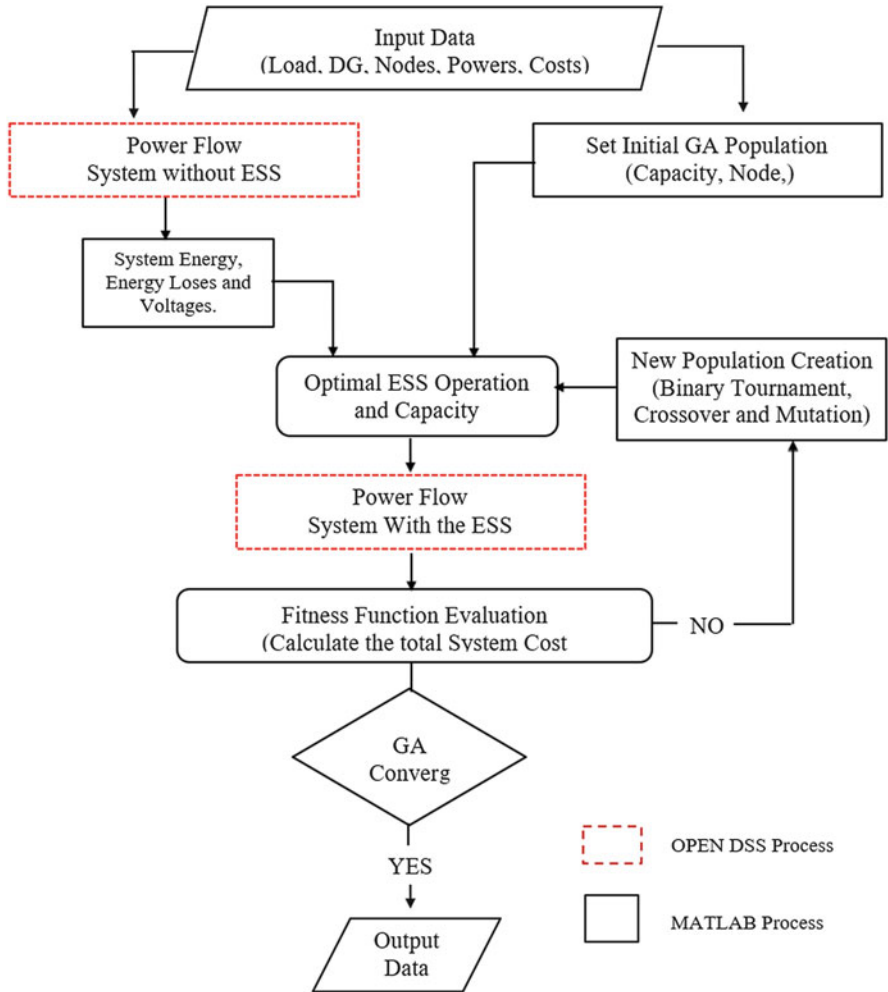
**Fig. 28** Flowchart of the methodology based on [61]

**Table 3** Grid plus PV plus ESS architecture comparison with others

| Metric | With Grid only | With Grid+ESS | With Grid+PV |
|---|---|---|---|
| Present worth | $2,185,881 | $2,294,889 | $771,388 |
| Annual worth | $170,994/year | $179,522/year | $60,343/year |
| Return on investment | 24.00% | 29.10% | 52.60% |
| Internal rate of return | 25.60% | 30.80% | 58.70% |
| Simple payback | 3.75 years | 3.17 years | 1.68 years |
| Discounted payback | 4.38 years | 3.63 years | 1.83 years |

is a capacity minimization problem defined in Eq. (1) [61]:

$$min\ CE^{HD} = min \sum_{j=1}^{24} C_j P_j^{HD} \Delta t_j \qquad (33)$$

where $C_j$ is the kWh cost for hour $j$, $\Delta t_j$ represents the time variation for the case study and $P_j^{HD}$ is the substation capacity.

The substation capacity is defined for the ESS discharging and charging as in Eqs. (2) and (3) respectively:

$$P_j^{HD} = P_j^L - P_j^{DG} - P_j^{ESS} - P_j^{Loss} \quad j = 1.....24 \qquad (34)$$

$$P_{ij}^{HD} = P_{ij}^L - P_{ij}^{DG} + P_{ij}^{ESS} - P_{ij}^{Loss} \quad j = 1.....24 \qquad (35)$$

where $P_{ij}^L$ is the load, $P_{ij}^{DG}$ is the DG power injection, $P_{ij}^{ESS}$ is the ESS power, and $P_{ij}^{Loss}$ is the power losses in the hour $i$ and the day $j$.

The ESS constraints are formulated as presented in Eqs. (36)–(43) [61]:

$$0, 2\ PC^{ESS} < P_{ij}^{ESS} < PC^{ESS} \qquad (36)$$

$$E_{ij}^{ESS} + P_{j+1}^{ESS} \Delta t_{j+1} > 0.2 E_j^{ESS} \quad j = 1....24 \qquad (37)$$

$$E_j^{ESS} + P_{j+1}^{ESS} \Delta t_{j+1} \le EC^{ESS} \quad j = 1....24 \qquad (38)$$

$$\sum_{j=1}^{24} \left| \left( P_{ij}^{ESS} \right) \right| = 0 \quad j = 1.....24, \ i = 1...365 \qquad (39)$$

$$PC^{ESS} = \frac{EC^{ESS}}{t_{dn}} \qquad (40)$$

$$\sigma \left( P_{ij}^{HD} \right) < Desv1 \quad j = 1....8 \qquad (41)$$

$$\sigma \left( P_{ij}^{HD} \right) < Desv2 \quad j = 8....16 \qquad (42)$$

$$\sigma \left( P_{ij}^{HD} \right) < Desv3 \quad j = 16....24 \qquad (43)$$

The ESS type is a NaS battery and constraint (36) is used to ensure that the ESS State of Charge (SOC) remains at least in 20% after discharging or charging, as in [41], and constraint (37) is used to limit the capacity and power injection of the ESS. Constraint (38) affords that the ESS does not exceed its capacity of charging, where the maximum capacity is $EC^{ESS}$. The standard deviation of the resulting power at the

substation is denoted as $\sigma\left(P_{ij}^{HD}\right)$. The constraint (39) was added to ensure that ESS SOC final state remain the same as the initial state that started in the day (zero for this case). Constraint (40) defines the power capacity of the ESS as the energy ESS divided by the maximum duration of discharge/charge for the Battery (40 h for this case). Constraints (41)–(42) were used to divide the power of the substation in three levels during the day, in order to reduce abrupt demand variations. The time-levels were divided into three groups, each one with a duration of 8 h. It should be noted that the number of levels could be different in order to approximate the behavior of the demand to a line, but for this case three levels was a good approximation. Finally, *Desv*1, *Desv*2, *Desv*3 were assumed as the maximum allowable deviations for the time-levels under consideration [61].

In a line, adapting the genetic algorithm and model based on [61], the provisioned ESS are randomly allocated into the system until it reaches the best fitness value for the project. The solution method determines the bus location, capacity, and operation for the ESS. The power flow is solved using the OPENDSS software [62] and is used COM interface with MATLAB for the Genetic algorithm solution [63]. A flowchart from Fig. 28 explain the method.

### 4.2.1 Test Case

The methodology is tested on the 33-node system in [64] and showed in Fig. 29. The DG location also is the same as in [64] defined in Table 4 considering solar and wind generation.

The real power/rated power indices for both Load and DG, are presented in Fig. 30.

A DG participation of up to 50% is considered with a power factor of 1, and the load is reduced to 50% of its capacity as a result. Energy price is divided in times as in [64], from 9:00 to 21:00, 0:00 to 7:00, 23:00 to 24:00, 7:00 to 9:00, 21:00 to 23:00, at 0.1876 $/kWh, 0.0608 $/kWh, 0.0608 $/kWh, and 0.1224 $/kWh,
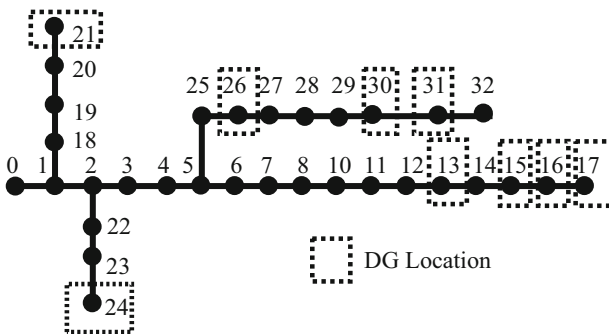


**Fig. 29** Test system based on [64]

**Table 4** Location and Size for the DG [64]

| DG type | Node location | Rated active power (kW) |
|---------|---------------|-------------------------|
| Wind    | 13            | 200                     |
| Wind    | 15            | 100                     |
| Solar   | 16            | 250                     |
| Wind    | 17            | 200                     |
| Solar   | 21            | 300                     |
| Solar   | 24            | 200                     |
| Solar   | 26            | 350                     |
| Wind    | 30            | 200                     |
| Wind    | 31            | 100                     |
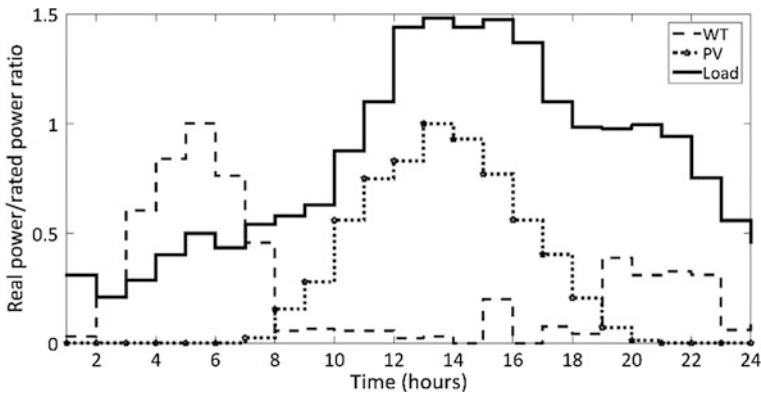


**Fig. 30** Power/rated power relation for Load and DG [64]

respectively. The installed ESS energy capacity is bounded within 500 kWh and 2000 kWh.

The ESS capacity is deployed and tested on each system node—(from node 1 to node 32), using sweeping process given a step of 15 kW and the total costs for each case is evaluated. The results for the total costs for each node are shown in Fig. 31.

As presented in Fig. 31, the costs of the project reduce as the energy capacity of the ESS increases. This is due to a reduction of the substation capacity with the ESS use. Also, the ESS performed better for nodes that are nearest to the substation or at the end of the feeder. In Fig. 32, the performance in terms of system energy loses is shown.

Figure 32 shows that the nearest node (node 30) to the ESS system presented the best performance in terms of loss reduction for ESS with the highest energy capacity 2000 kWh. It can be deduced therefore that the node closest to the ESS system will yield the best performance in terms of cost and loss reduction as shown in Figs. 31 and 32 respectively.

Figures 33 and 34 show the performance in terms of the maximum and minimum voltage, where the node voltages are bounded from 0.95 pu to 1.05 pu.
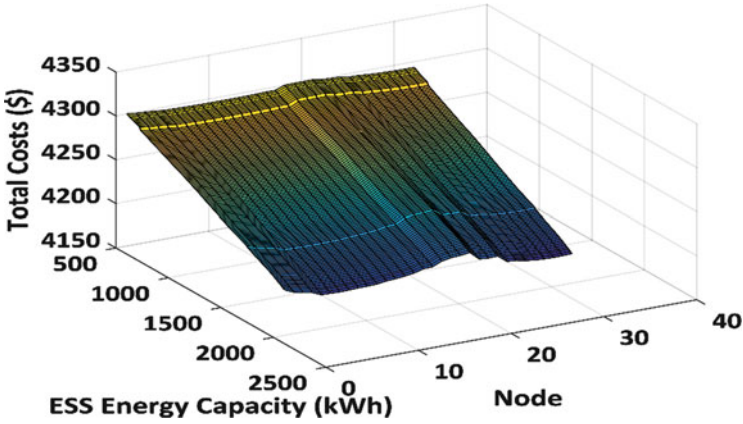
**Fig. 31** Estimated region of costs for the swept
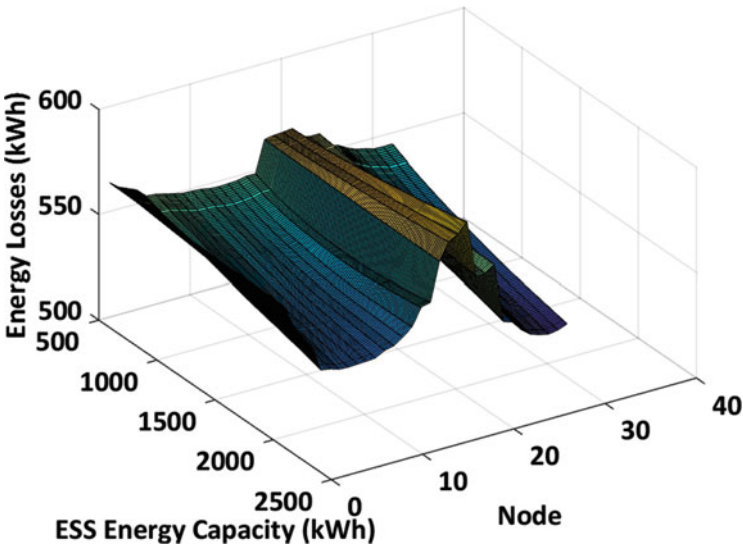


**Fig. 32** Estimated region of energy losses for the swept

Figure 33 shows that each case keep below the maximum 1.05 pu voltage allowed. Nevertheless, as the ESS capacity increases and its position changes between nodes 10 and 20, the maximum voltage was reduced.

In Fig. 34 the minimum voltage remain close to the critical value as the storage is located close to buses 10–20. However, it should be noted that the case without ESS presents a more critical behavior in terms of voltage (this will be presented later). The minimum voltage approaches 1.0 pu while the ESS capacity increases and its position changes to bus 30. Consequently, considering these performance trends, ESS selection and deployment with highest capacity of 200 kWh favors node 30.
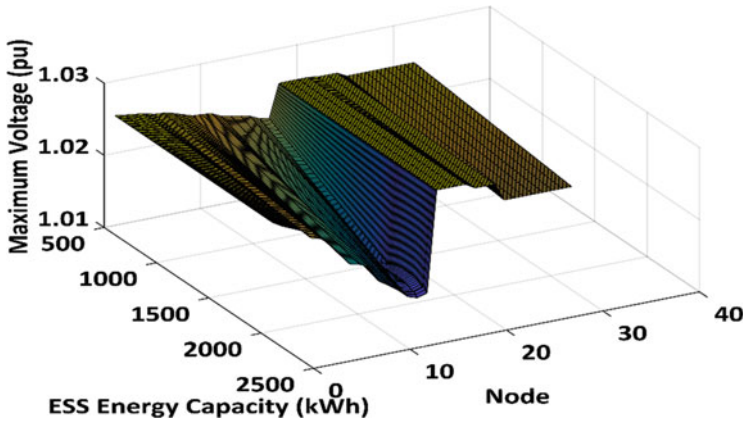
**Fig. 33** Estimated region of maximum voltage (pu) for the swept
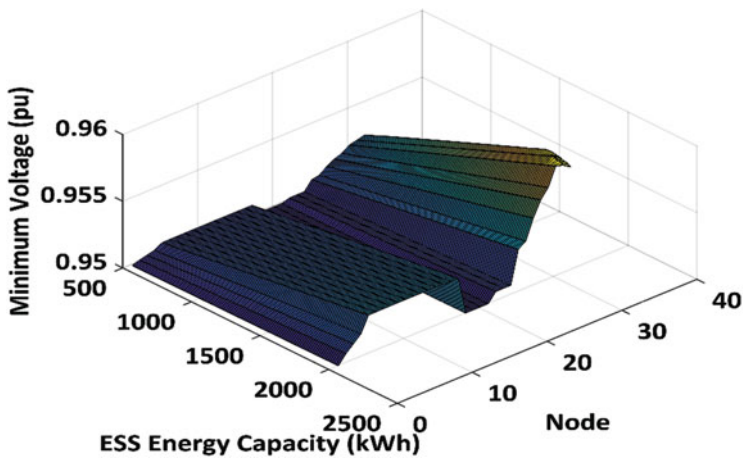


**Fig. 34** Estimated region of minimum voltage (pu) for the swept

In the following section, the results of the heuristic methodology considering the GA method for ESS selection is analyzed. In this case, an elitism rate of 0.4, with maximum of 80 generations for a population composed of 500 individuals with a mutation rate of 1.5% are considered. After 28 generations, the solution emerged. The solution determines the ESS with 1998 kWh of capacity to be located at bus 30. The result is like the ones obtained using the swept process previously presented, showing also that the GA successfully finds a good result. The selection results are showed in Table 5. The cases considered are:

- **Base Case:** It is the original network without DG and ESS inclusions.
- **Case A:** It is the original network with DG inclusion.
- **Case B:** It is the original network with DG and ESS inclusions.

**Table 5** Results of the methodology

| Case | $V_{min}$ (pu) | $V_{max}$ (pu) | Total energy loss (kWh) | Total cost ($) | % Energy loss reduction compared with Base Case | % Reduction in total cost compared with Base Case |
|---|---|---|---|---|---|---|
| Base Case | 0.9360 | 0.9998 | 967.0 | 5829.4 | – | – |
| Case A | 0.9499 | 1.0256 | 566.8 | 4136.5 | 41.4 | 29.0 |
| Case B | 0.9583 | 1.0220 | 514.7 | 4010.9 | 46.8 | 31.2 |
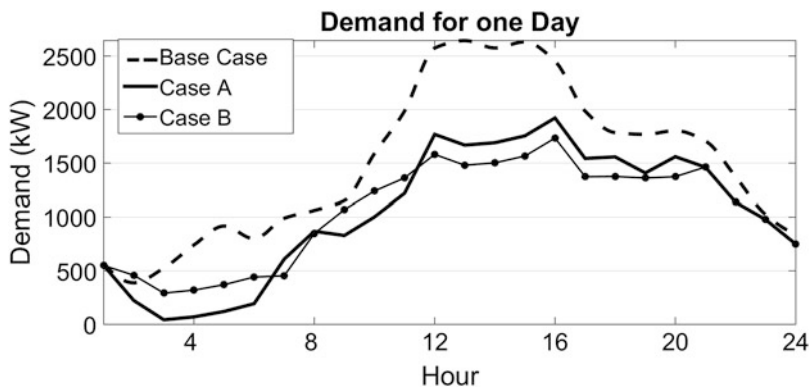


**Fig. 35** Demand for the studied day

As shown in Table 5, the minimum voltage increases to 0.9583 pu with the ESS inclusion, a higher value when compared with Case A and the Base Case in which minimum voltage values remained at 0.936 pu and 0.9499 pu, respectively. In terms of energy loss and cost reduction, Case B which included the ESS use performed better than the Case Base and Case A, reducing the energy loss by 46.8% and total cost by 31.2%. Consequently, the solution method of the GA for optimally selecting the ESS capacity and location was able to minimize energy costs, losses and voltage deviations.

Figure 35 shows the system daily demand for the three cases and improvement in the substation behavior with the ESS use. In this case, the peak demands reduce, and the curve trends have less variations. This is due to the reduction in the reverse flows by the DG.

In conclusion, the results of the two given examples show the importance of ESS selection and its performance for DG support in terms of losses, voltage, substation capacity regulation, and operational costs reductions, by selecting accurately the discharging/charging times for ESS operation considering capacity restrictions and DG behavior. The results also show that heuristic methods like GA is a robust solution method for solving optimization problems with ESS inclusion. It should be noted, however, that the ESS installation, replacement, and operation costs, are important aspects of the projects which were not considered in the second example.

Also, a battery degradation model and type selection approach are important to accurately model DG and ESS problems for a better possible outcome. Finally, the information here presented are intended to encourage the readers to expand their knowledge in optimization methods in power systems and increase their research in ESS for renewable energy support.

# References

1. U.S. Department of Energy: Renewable Energy Explained. U.S. Energy Information Administration, 13 July. [Online]. https://www.eia.gov/energyexplained/?page=renewable_home (2018). Accessed 11 Aug 2018
2. National Renewable Energy Laboratory: VOICES of Experiences | Integrating Intermittent Resources | What Utilities are Learning. US Department of Energy (2017)
3. Petinrin, J.O., Shaaban, M.: Overcoming challenges of renewable energy on future smart grid. TELKOMNIKA. **10**(2), 229–234 (2012)
4. Beaudin, M., Zareipour, H., Schellenberglabe, A., Rosehart, W.: Energy storage for mitigating the variability of renewable electricity sources: an updated review. Energy Sustain. Dev. | ScienceDirect.com. **14**(4), 302–314 (2010)
5. Farrokhifar, M.: Optimal operation of energy storage devices with RESs to improve efficiency of distribution grids; Technical and economical assessment. Int. J. Electr. Power Energy Syst. **74**, 153–161 (2016)
6. ESS Inc.: The ESS Energy Warehouse. ESS Inc. [Online]. https://www.essinc.com/energy-storage-products/ (2018). Accessed 8 Aug 2018
7. International Electrotechnical Commission: Electrical Energy Storage. IEC, Geneva (2017)
8. Battery Energy Storage Systems. AMDC Energy Limited [Online]. http://www.amdcenergy.com/battery-energy-storage-system.html. Accessed 24 Oct 2018
9. Mishra, A., Sitaraman, R., Irwin, D., Zhuz, T., Shenoy, P., Dalvix, B., Lee, S.: Integrating Energy Storage in Electricity Distribution Networks, pp. 1–10. ACM, New York (2015)
10. Zhao, H., Wua, Q., Hu, S., Xu, H., Rasmussen, C.N.: Review of energy storage system for wind power integration support. Elsevier Appl Energy. 1–9 (2014)
11. Tixador, P.: Superconducting magnetic energy storage (SMES) systems. In: Electricity Transmission, Distribution and Storage Systems, France, Woodhead Publishing Series in Energy, pp. 442–477 (2013)
12. Energy Storage Panel, EAC Meeting: Energy Storage Cost Effectiveness Evaluation DNV KEMA Modeling for CPUC Energy Storage Proceeding. DNV KEMA (2013)
13. ESS Tech Inc.: Cleanest, Lowest-Cost Long-Duration Storage with No Capacity Degradation. ESS, Inc., Wilsonville (2017)

14. ESS Inc.: Helping Utilities Reap the Rewards of Renewable Energy. ESS Inc. [Online]. https://www.essinc.com/energy-storage-applications/utility/ (2018). Accessed 8 Aug 2018
15. Independent Pricing and Regulatory Tribunal (IPART): Application Guide for ESS Accreditation. IPART, New South Wales, 2016.
16. ESS Inc.: Clean Energy Storage Shifts the Power Into Your Hands. Catalizing a cleaner future [Online]. https://www.essinc.com/energy-storage-applications/commercial-industrial/ (2018). Accessed 8 Aug 2018
17. Sproull, B.: Sonoma Microgrid Proves Ideal Fit for Long-Duration, All-Iron Flow Battery. North American Clean Energy: ESS Inc., Sonoma, CA (2017)
18. Wood, E.: The Life and Death Value of Energy Storage in Military Microgrids. microgridknowledge.com, 1 October [Online]. https://www.essinc.com/wp-content/uploads/2017/01/The-Life-and-Death-Value-of-Energy-Storage-in-Military-Microgrids.pdf (2017). Accessed 8 Aug 2018
19. Cremers, R., Bloemhof, G.: Storage optimization in distribution systems. In: 21st International Conference on Electricity Distribution, Frankfurt (2011)
20. Pospíšilová, A.: Modern Optimization Methods. CTU, Prague (2015)
21. Kunche, P., Reddy, K.: Heuristic and meta-heuristic optimization. In: Metaheuristic Applications to Speech Enhancement, pp. 17–24. Springer, New Jersey (2016)
22. Niu, M., Wan, C., Xu, Z.: A review on applications of heuristic optimization algorithms for optimal power flow in modern power systems. J. Mod. Power Syst. Clean Energy. **2**(4), 289–297 (2014)
23. Vikhar, P.A.: Evolutionary algorithms: a critical review and its future prospects. In: Proceedings of the 2016 International Conference on Global Trends in Signal Processing, Information Computing and Communication (ICGTSPICC), Jalgaon, (2016)
24. Melanie, M.: An Introduction to Genetic Algorithms. MIT Press, London (1999)
25. Rojas, R.: Genetic algorithms. In: Neural Networks, pp. 429–450. Springer, Berlin (1996)
26. Kennedy, J., Eberhart, R.C.: Particle swarm optimization international conference on neural networks. In: Proceedings of the IEEE, New York, NY (1995)
27. Kennedy, J., Eberhart, R.C.: Particle swarm optimization. In: Proceedings of the IEEE International Conference on Neural Networks, vol. 4, pp. 1942–1948. IEEE Press, New York, NY (1995)
28. Eberhart, R.C., Shi, Y., Kennedy, J.: Swarm Intelligence. Morgan Kaufmann, Burlington, MA (2001)
29. Porto, V.W., Saravanan, N., Waagen, D., Eiben, A.E.: Evolutionary programming. In: Proceedings of the 7th International Conference EP98, Heidelberg (1998)
30. Engelbrecht, A.: Particle swarm optimization: velocity initialization. In: Proceedings of the IEEE Congress on Evolutionary Computation 2012, pp. 1–8. IEEE Press, New York, NY (2012)
31. Clerc, M., Kennedy, J.: The particle swarm: explosion stability and convergence in a multidimensional complex space. IEEE Trans. Evol. Comput. **6**, 58–73 (2002)
32. Van Den Bergh, F.: An analysis of particle swarm optimizers. Ph.D. thesis, University of Pretoria, South Africa (2002)
33. Shi, Y., Eberhart, R.C.: A modified particle swarm optimizer. In: Proceedings of IEEE 1998 International Conference on Evolutionary Computation, New York, NY (1998)
34. Bansal, J.C., Singh, P.K., Saraswat, M., Verma, A., Singh, J.S., Abraham, A.: Inertia weight strategies in particle swarm optimization. In: Proceedings of the 2011 Third World Congress on Nature and Biologically Inspired Computing, New York, NY, (2011)
35. Dagli, C.H., Akay, M., Buczak, A.L., Ersoy, O., Bernandez, B.R.: Intelligent engineering systems through artificial neural networks. In: Proceedings of the Artificial Neural Networks in Engineering Conference (ANNIE 98), New York, NY (1998)
36. Luo, X., Wang, J., Dooner, M., Clarke, J.: Overview of current development in electrical energy storage technologies and the application potential in power system operation. Appl. Energy. **137**, 511–536 (2015)

37. Zheng, Y., Hill, D.J., Dong, Z.Y.: Multi-agent optimal allocation of energy storage systems in distribution systems. IEEE Trans. Sustain. Energy (2017)
38. Zhang, Y., Dong, Z.Y., Luo, F., Zheng, Y., Meng, K., Wong, K.P.: Optimal allocation of battery energy storage systems in distribution networks with high wind power penetration. IET Renew. Power Gener. **10**(8), 1105–1113 (2016)
39. Zheng, Y., Dong, Z.Y., Luo, F.J., Meng, K., Qiu, J., Wong, K.P.: Optimal allocation of energy storage system for risk mitigation of discos with high renewable penetrations. IEEE Trans. Power Syst. **29**(1), 212–220 (2014)
40. Aly, M.M., Abdelkarim, E., Abdel-Akher, M.: Mitigation of photovoltaic power generation fluctuations using plug-in hybrid electric vehicles storage batteries. Int. Trans. Electr. Energy Syst. **25**(12), 3720–3737 (2015)
41. Atwa, Y.M., El-Saadany, E.F.: Optimal allocation of ESS in distribution systems with a high penetration of wind energy. IEEE Trans. Power Syst. **25**(4), 1815–1822 (2010)
42. ElNozahy, M.S., Abdel-Galil, T.K., Salama, M.M.A.: Probabilistic ESS sizing and scheduling for improved integration of PHEVs and PV systems in residential distribution systems. Electr. Power Syst. Res. **125**, 55–66 (2015)
43. Evangelopoulos, V.A., Georgilakis, P.S., Hatziargyriou, N.D.: Optimal operation of smart distribution networks: a review of models, methods and future research. Electr. Power Syst. Res. **140**, 95–106 (2016)
44. Mohamed, A., Mohammed, O.: Real-time energy management scheme for hybrid renewable energy systems in smart grid applications. Electr. Power Syst. Res. **96**, 133–143 (2013)
45. Motalleb, M., Reihani, E., Ghorbani, R.: Optimal placement and sizing of the storage supporting transmission and distribution networks. Renew. Energy **94**, 651–659 (2016)
46. Mohsenian-Rad, A.H., Leon-Garcia, A.: Optimal residential load control with price prediction in real-time electricity pricing environments. IEEE Trans. Smart Grid. **1**(2), 120–133 (2010)
47. Morais, H., Faria, P., Vale, Z.: Demand response design and use based on network locational marginal prices. Int. J. Electr. Power Energy Syst. **61**, 180–191 (2014)
48. Zhao, H., Wu, Q., Hu, S., Xu, H., Rasmussen, C.N.: Review of energy storage system for wind power integration support. Appl. Energy. **137**, 545–553 (2015)
49. Divya, K.C., Østergaard, J.: Battery energy storage technology for power systems-an overview. Electr. Power Syst. Res. **79**(4), 511–520 (2009)
50. Hill, C.A., Such, M.C., Chen, D., Gonzalez, J., Grady, W.M.K.: Battery energy storage for enabling integration of distributed solar power generation. IEEE Trans. Smart Grid. **3**(2), 850–857 (2012)
51. Mohamed, A.E.M., Sarah, A., Bekdache, K., Barrios, L.A.: Optimal sizing for a hybrid power system with wind/energy storage based in stochastic environment. Renew. Sust. Energ. Rev. **59**, 1149–1158 (2016)
52. Aryanezhad, M.: Management and coordination of LTC, SVR, shunt capacitor and energy storage with high PV penetration in power distribution system for voltage regulation and power loss minimization. Int. J. Electr. Power Energy Syst. **100**, 178–192 (2018)
53. Lucas, A., Chondrogiannis, S.: Smart grid energy storage controller for frequency regulation and peak shaving, using a vanadium redox flow battery. Int. J. Electr. Power Energy Syst. **80**, 26–36 (2016)
54. Olival, P.C., Madureira, A.G., Matos, M.: Advanced voltage control for smart microgrids using distributed energy resources. Electr. Power Syst. Res. **146**, 132–140 (2017)
55. Sebastián, R.: Application of a battery energy storage for frequency regulation and peak shaving in a wind diesel power system. IET Gener. Transm. Distrib. **10**(3), 764–770 (2016)
56. Zhang, L., Tang, W., Liu, Y., Li, T.: Multiobjective optimization and decision-making for DG planning considering benefits between distribution company and DGs owner. Int. J. Electr. Power Energy Syst. **73**, 465–474 (2015)
57. Khederzadeh, M., Maleki, H.: Coordinating storage devices, distributed energy sources, responsive loads and electric vehicles for microgrid autonomous operation. Int. Trans. Electr. Energy Syst. **25**(10), 2482–2498 (2015)

58. Littler, T., Zhou, B.: Local storage meets local demand: a technical solution to future power distribution system. IET Gener. Transm. Distrib. **10**(3), 704–711 (2016)
59. HOMER Energy LLC: HOMER Energy [Online]. https://www.homerenergy.com/products/pro/index.html (2014–2018). Accessed 6 Nov 2018
60. Rolls Surrette: Rolls Surrette 4KS25P (4-KS-25P/4KS-25P) Battery [Online]. https://www.dcbattery.com/rollssurrette_4ks25ps.html (2018). Accessed 9 Aug 2018
61. Sepulveda, C., Luciane, C., Mauricio, S., Railson, S.: Methodology for ESS-type selection and optimal energy management in distribution system with DG considering reverse flow limitations and cost penalties. IET Gener. Transm. Distrib. **12**(5), 1164–1170 (2018)
62. Dugan, R.C., McDermott, T.E.: An open source platform for collaborating on smart grid research. In: IEEE Power and Energy Society General Meeting (2011)
63. The MathWorks, Inc.: MATLAB. United State Patent 7,051,338 (2016)
64. Xiao, J., Bai, L., Zhang, Z., Liang, H.: Determination of the optimal installation site and capacity of battery energy storage system in distribution network integrated with distributed generation. IET Gener. Transm. Distrib. **10**(3), 601–607 (2016)

# Distribution System Operation with Energy Storage and Renewable Generation Uncertainty

**Alvaro González-Castellanos, David Pozo, and Aldo Bischi**

**Abstract** The need for secure and flexible operation of distributed power systems and the decline in prices for Li-ion batteries have made energy storage deployment a viable option. The electric energy storage units' characterization (including Li-ion batteries) currently utilized for power system operation and planning models relies on two major assumptions: the charge and discharge efficiencies are constant during such processes, and the maximum charge and discharge rates are independent of the system's state of charge. This approach can lead to an over- or underestimation of the available power and energy for supporting services such as frequency response and load balancing; thus, threatening the overall system reliability. In this chapter, we introduce an optimal stochastic operation model for distribution systems with energy storage. We, firstly, present the power flow formulation for distribution networks and derive its equivalent second-order conic reformulation. Secondly, we introduce an ideal energy storage model and a new detailed linear model for the state-dependent characterization of the unit's charge and discharge processes. Finally, we integrate the proposed model into a deterministic and stochastic economic operation model of a distribution power grid to illustrate the benefits of a detailed battery characterization, in comparison with the existing constant efficiency approach. The proposed energy storage models are computationally compared on a modified IEEE 33-bus electric distribution system.

## 1 Introduction

Electric distribution grids are moving from passive systems toward active ones due to their digitization, the increase on renewable energy sources (RES) and distributed generation (DG). Since the existing distribution systems were designed to operate with the power flowing from the main substation to the users, the use of RES and

A. González-Castellanos (✉) · D. Pozo · A. Bischi
Skolkovo Institute of Science and Technology, Moscow, Russia
e-mail: alvaro.gonzalez@skolkovotech.ru; alvaro.gonzalez@skoltech.ru; d.pozo@skoltech.ru; a.bischi@skoltech.ru

DG risks violating the systems' operating constraints via reserve flow direction [21]. Therefore, the installation of new RES in distribution systems requires an increase in the systems' generation flexibility to compensate for the variable nature of the RES [25]. Additionally, non-controllable RES not only introduce stochastic load unbalance but also voltage fluctuation issues in distribution networks [28]. Such volatility experienced in the system forces to reserve capacity in the day-ahead market for real-time load balancing [20].

The installation and proper use of energy storage systems would allow compensating the intermittence and daily variability of RES generation by providing to electric distribution grids, among others, the following services: minimization of operational costs, provision of reserve capacity, peak shaving, and voltage stabilization [29]. Energy storage systems also provide benefits for the long-term system planning, like deferring grid reinforcements [5] and other associated compensation technologies [24], e.g., flexible generation and reactive compensation.

To obtain the optimal economic operation of the system, it is necessary, in addition to the above mentioned deterministic problem, to model and quantify the uncertainty in the system's management model. The distribution system operation can be modeled through the use of probabilistic scenario-based stochastic programming, where the scenarios represent the forecasted RES generation samples [27]. The first (day-ahead/scheduling) stage represents the purchase/sell of energy to the electricity market and allocation of reserve capacity, as well as the commitment of the distributed generation. The second (real-time/operation) stage depicts the realization of the reserves (bounded by the allocated reserve capacity), and the operation of the generation and energy storage units based on the forecasted RES generation for the associated scenario.

The main contribution of this chapter is to outline the operation of a distribution power network with renewable generation uncertainty and non-ideal energy storage system while participating in the day-ahead energy and reserve market, and the real-time market. This chapter describes the modeling of the main components of the distribution system operation in a logical and modular way:

- Section 2 describes the power flow formulation, starting with the complete non-convex alternating current (AC) model, followed by its second-order conic programming approximation.
- Section 3 presents the ideal energy storage formulation and introduces the main limitations for its application in real-time operation, deriving in a linear non-ideal model for energy storage systems.
- Section 4 describes the deterministic unit commitment (UC) formulation for the participation in the day-ahead market, including generation and storage operation.
- Section 5 introduces to the unit commitment formulation the use of stochastic information. The stochastic UC is modeled as a two-stage stochastic programming model including the reserve allocation and realization. Each of the

above-listed Sects. 2–5 conclude with a brief revisit to the introduced model and its main characteristics.

- Section 6 applies the developed model to a test network, evaluating the impact of the model selection on the optimal operation strategy (deterministic *vs.* stochastic, ideal storage *vs.* non-ideal storage).
- Section 7 provides the main conclusions of this chapter.

## 2 Power Flow on a Radial Distribution Network

To describe the state of the electric distribution system in an accurate way, it is necessary to efficiently model its power flow and capture not only the load balance but also the voltage variation in its nodes. The set of equations that describes them is known as the *power flow equations*, that in essence are the Kirchhoff laws generalized to power grids. They are also called *alternating current power flow* (AC-PF). AC-PF is a non-convex set of constraints, but it has a particular structure in distribution networks due to their operation as a radial (tree-like) grids.

There exist many reformulations of the AC-PF that attempt to find useful mathematical properties on this set of equations. The classic approach is a linearization of the AC-PF called, with an unfortunate name, linearized *direct current* (DC) approximation.[1] The linearized DC approximation is the most widely employed for techno-economic studies and in electricity market applications [10]. The DC approximation allows for a fast, albeit inaccurate, solution of the power flow problem. However, since it does not consider the reactive power flow and voltage drop in the network, the DC model becomes unsuitable for the study of distribution networks.

During the last years, there has been increasing attention to new approaches based on convexification, i.e. relaxation, of the power flow problem. A rich literature of approximations based on convexification techniques tries to address the characterization of the power system operation while maintaining convexity and high computational efficiency [7], e.g., semi-definite programming (SDP) [19], second-order conic programming (SOCP) [15] and quadratic convex (QC) [8] relaxations, among others. Even though the SOCP relaxation is less accurate than the SDP [18] and QC models [8], the SOCP model provides significantly faster results than the SDP one, while providing the same lower bound on radial networks [18], and a more intuitive formulation and interpretation of the results than its counterparts. Therefore, the SOCP relaxation would present a stronger case for its application in the economic operation in radial distribution networks.

---

[1]This formulation is not named in this manner because it is based on the direct (non-alternating) type of current, but rather by the fact that its assumptions lead to the exclusion of reactive power. Additionally, the DC approximation assumes a flat voltage profile, i.e., voltages fixed at 1 p.u., and small differences between voltage angles.

This section describes the full formulation of the electric power flow in distribution networks. Section 2.1 introduces the general AC power flow equations, with Sect. 2.2 deriving the second-order conic programming approximation of the power flow in a distribution network. Finally, Sect. 2.3 points out the main inaccuracies introduced by the convexified model when applied to radial networks.

## 2.1 AC Power Flow in Electric Networks

The power flowing in an electric network can be derived from the *Kirchhoff's Voltage Law* and the *Kirchhoff's Current Law*. Consider the power line equivalent circuit presented in Fig. 1.

The impedance $G_{nm} - jB_{nm}$ represents the series impedance of the power line, while $jb_{nm}^{\text{cha}}$ its charging susceptance. The active and reactive power flowing through the line, in *per unit* (p.u.) can be calculated by [12]

$$p_{nm} = G_{nm}V_{nn}^2 + V_nV_m\left(-G_{nm}\cos\theta_{nm} + B_{nm}\sin\theta_{nm}\right), \tag{1a}$$

$$q_{nm} = (B_{nm} - b_{nm}^{\text{cha}})V_n^2 - V_nV_m\left(B_{nm}\cos\theta_{nm} + G_{nm}\sin\theta_{nm}\right), \tag{1b}$$

where $\theta_{nm} = \theta_n - \theta_m$. The net power injected in a node $n$, generated minus consumed, is equal to the power leaving the node through the adjacent power lines

$$\sum_{m\in\mathcal{N}(n)} p_{nm} = \sum_{g\in\mathcal{G}(n)} p_g - P_n^{\text{D}}, \tag{1c}$$

$$\sum_{m\in\mathcal{N}(n)} q_{nm} = \sum_{g\in\mathcal{G}(n)} q_g - Q_n^{\text{D}}, \tag{1d}$$

where $m \in \mathcal{N}(n)$ are the nodes directly connected with $n$. The power generated by generator $g$, active and reactive, are respectively given by $p_g$ and $q_g$, while $g \in \mathcal{G}(n)$
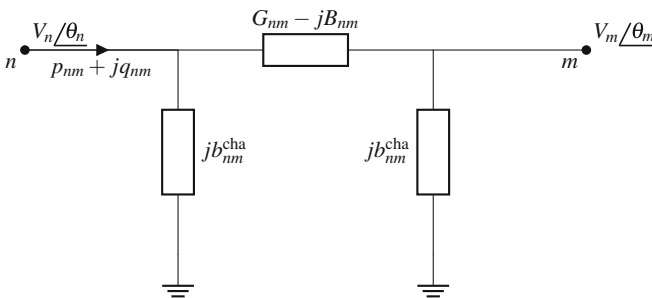


**Fig. 1** Power line $\pi$–model

are the generators connected at $n$. $P_n^D$ and $Q_n^D$ represent the active and reactive power consumed by the demand at node $n$, respectively. The power flowing through an electric network can be calculated by employing (1). However, due to the non-convex nature of the trigonometric functions in (1a) and (1b), in many occasions it is preferable to express the power flow equations with convex functions that allow calculating the optimal network operation in a computationally efficient manner, although the approximation may not be exact.

## 2.2 Second-Order Conic Programming Approximation

The power flow on a radial distribution network can be exactly reformulated by introducing the variables $c_{nm}$ and $s_{nm}$ in the rectangular formulation provided in (1) by [11]

$$c_{nm} = V_n V_m \cos \theta_{nm} \tag{2a}$$

$$s_{nm} = V_n V_m \sin \theta_{nm}. \tag{2b}$$

Replacing $c_{nm}$ and $s_{nm}$ in (1a) and (1b)[2]

$$p_{nm} = G_{nm} c_{nn} - G_{nm} c_{nm} + B_{nm} s_{nm}, \tag{3a}$$

$$q_{nm} = (B_{nm} - b_{nm}^{cha}) c_{nn} - G_{nm} s_{nm} - B_{nm} c_{nm}. \tag{3b}$$

Equations (3a) and (3b) linearize the expressions for the power flowing through the lines, but in order to represent the underlying trigonometric nature of the AC power flow it is necessary to impose additional constraints on $c_{nm}$ and $s_{nm}$. By applying the Pythagorean identity $\sin^2 \theta + \cos^2 \theta = 1$ to (2), constraint (3c) for $c_{nm}$ and $s_{nm}$ is obtained,[3] while the symmetries of the cosine and sine respectively result in (3d) and (3e).

$$c_{nm}^2 + s_{nm}^2 = c_{nn} c_{mm} \tag{3c}$$

$$c_{nm} = c_{mn}, \tag{3d}$$

$$s_{nm} = -s_{mn}. \tag{3e}$$

---

[2] For the same node $n$: $c_{nn} = V_n V_n \cos \theta_{nn} = V_n^2 \underbrace{\cos(\theta_n - \theta_n)}_{1} = V_n^2$.

[3] By the Pythagorean identity: $\cos^2 \theta_{nm} + \sin^2 \theta_{nm} = 1 \rightarrow V_n^2 V_m^2 \cos^2 \theta_{nm} + V_n^2 V_m^2 \sin^2 \theta_{nm} = V_n^2 V_m^2 \rightarrow c_{nm}^2 + s_{nm}^2 = c_{nn} c_{mm}$.

**Fig. 2** Application of the SOCP relaxation (3g), to the Pythagorean identity (3c)
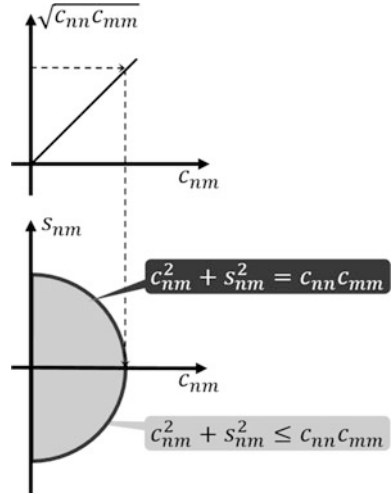


Given that (3c) represents a non-convex region, it is possible to approximate it by replacing it with the second-order cone given by [15]

$$c_{nm}^2 + s_{nm}^2 \leq c_{nn}c_{mm}, \tag{3f}$$

which is equivalent to

$$c_{nm}^2 + s_{nm}^2 + \left(\frac{c_{nn} - c_{mm}}{2}\right)^2 \leq \left(\frac{c_{nn} + c_{mm}}{2}\right)^2. \tag{3g}$$

Figure 2 represents the approximation introduced by (3g). Where the solid line represents the non-convex region defined by (3c) and the shaded area the convex range of (3g).

Once the values of $c_{nm}$ and $s_{nm}$ are obtained, the voltage magnitude and phase angle at the different nodes can be recovered by

$$V_n = \sqrt{c_{nn}} \tag{4a}$$

$$\tan \theta_{nm} = \frac{s_{nm}}{c_{nm}}, \tag{4b}$$

where the phase angle $\theta_n$ at the substation of the radial network can be conveniently set equal to zero to ease the calculation of the angles at the remaining nodes.

The replacement of (3c) by (3g), together with Eqs. (1c)–(1d), (3a)–(3b), and (3d)–(3e), represent the second-order conic programming relaxation of the power flow firstly introduced in [15]. The SOCP approximation is condensed in Model 1.

In Model 1, the active and reactive power balance at the nodes are presented by (5a) and (5b). The demanded and generated active and reactive powers, as well as

**MODEL 1** SOCP power flow

**Indexes:**

| | |
|---|---|
| $n, m$ | Node index |
| $g$ | Conventional generation unit index |

**Sets:**

| | |
|---|---|
| $\mathscr{L}$ | Set containing every existing line $(n, m)$ |
| $\mathscr{G}(n)$ | Set containing the generators connected at $n$ |
| $\mathscr{N}(n)$ | Set containing the nodes $m$ connected to $n$ |

**Parameters:**

| | |
|---|---|
| $b_{nm}^{\text{cha}}$ | Line charging susceptance of branch $(n, m)$ [p.u.] |
| $G_{nm}, B_{nm}$ | Conductance and susceptance of line $(n, m)$ [p.u.] |
| $P_n^{\text{D}}, Q_n^{\text{D}}$ | Demanded active and reactive power at $n$ [MW, MVAr] |
| $S_{base}$ | Base value for the apparent power [MVA] |

**Variables:**

| | |
|---|---|
| $p_g, q_g$ | Generated active and reactive power by unit $g$ [MW, MVAr] |
| $p_{nm}, q_{nm}$ | Active and reactive power flow through line $(n, m)$ [MW, MVAr] |
| $c_{nm}$ | $V_n V_m \cos(\theta_n - \theta_m)$ [p.u.] |
| $s_{nm}$ | $V_n V_m \sin(\theta_n - \theta_m)$ [p.u.] |

**Constraints:**

$$P_n^{\text{D}} = \sum_{g\in\mathscr{G}(n)} p_g - \sum_{m\in\mathscr{N}(n)} p_{nm}, \qquad \forall n \tag{5a}$$

$$Q_n^{\text{D}} = \sum_{g\in\mathscr{G}(n)} q_g - \sum_{m\in\mathscr{N}(n)} q_{nm}, \qquad \forall n \tag{5b}$$

$$p_{nm} = S_{base}\big[G_{nm}c_{nn} - G_{nm}c_{nm} + B_{nm}s_{nm}\big], \qquad \forall(n,m)\in\mathscr{L} \tag{5c}$$

$$q_{nm} = S_{base}\big[(B_{nm} - b_{nm}^{\text{cha}})c_{nn} - G_{nm}s_{nm} - B_{nm}c_{nm}\big], \qquad \forall(n,m)\in\mathscr{L} \tag{5d}$$

$$c_{nm}^2 + s_{nm}^2 + \left(\frac{c_{nn} - c_{mm}}{2}\right)^2 \leq \left(\frac{c_{nn} + c_{mm}}{2}\right)^2, \qquad \forall(n,m)\in\mathscr{L} \tag{5e}$$

$$c_{nm} = c_{mn}, \qquad \forall(n,m)\in\mathscr{L} \tag{5f}$$

$$s_{nm} = -s_{mn}, \qquad \forall(n,m)\in\mathscr{L}. \tag{5g}$$

the power flowing through the lines, are respectively given in MWand MVAr rather than in p.u.. This change of units is done to reflect the common practice in the economic operation of power systems with regard to the given data units [16].

The active power flowing through the line $(n, m)$ is given in terms of its conductance $G_{n,m}$ and susceptance $B_{n,m}$ by Eq. (5c), where $c_{nm}$ and $s_{nm}$ are the pair variables used to respectively represent the branch relationships $V_n V_m \cos(\theta_n - \theta_m)$ and $V_n V_m \sin(\theta_n - \theta_m)$. Analogously, Eq. (5d) provides the reactive power flowing through lines in terms of their conductance, susceptance and line charging

susceptance $b_{n,m}^{\text{cha}}$. To keep the dimensional equivalence between both sides of expressions (5c) and (5d), the right-hand sides are multiplied by the base value of the apparent power $S_{base}$ in MVA. The SOCP relaxation of the expression $c_{nm}^2 + s_{nm}^2 = c_{nn}c_{mm}$ is given by (5e), while the trigonometric symmetries of $c_{nm}$ and $s_{nm}$ are presented in (5f) and (5g), respectively.

## 2.3   Limitations of the SOCP Model

By being a relaxation of the complete AC power flow formulation, the SOCP approximation introduces a degree of error when compared to the original formulation. This error becomes especially evident in the domain of variables $c_{nm}$ and $s_{nm}$ after the conic relaxation, (3f), is introduced. In Fig. 2 it can be seen how the values that $c_{nm}$ and $s_{nm}$ can take, could greatly differ from the equality $c_{nm}^2 + s_{nm}^2 = c_{nn}c_{mm}$.

As noted in Sect. 2.2, the SOCP presents an exact reformulation of the power flow in a radial network for normal operating conditions. However, the exactness of the formulation has been proved to be invalid under stressed network conditions such as tight reactive generation bounds and deviations from the nominal network demand. To overcome the inexactness of the SOCP model under high demand operation, it is possible to introduce tightening inequalities as proposed by Kocuk et al. [18].

## 3   Energy Storage Model

The variability of the RES generation requires the use of energy storage to ensure the flexible operation of the power system. An accurate model of the storage system is necessary, not only to properly asses the flexibility gains but also to preserve its lifetime, by operating within its technical limits. Section 3.1 describes the modeling of an ideal energy storage system, while Sect. 3.2 introduces the expressions for defining the technical limits and efficiencies of the non-ideal storage system, followed by their convexification in a linear model.

## 3.1   Ideal Energy Storage

Electric energy storage can be modeled based on two features: the characterization of its charging and discharging processes, and the establishing of its operational limits. The power limits are usually given by the manufacturer concerning maximum charging and discharging currents as a function of the *C-rate*. The *C-rate* provides an inverse relationship with the amount of time needed for the charge and discharge

of a battery. A battery is fully discharged in 1 h at a rate of 1C (1A of discharging current in a battery with 1Ah capacity), while at 5C (5A/1Ah) a battery is discharged in 12 min. 1C and 5C have been respectively selected as common charge and discharge limits for a Li-ion battery [3]. Hence, by setting $\overline{E}$ as the battery capacity in Ah and at constant operating voltage, the operational limits for the battery can be set by

$$0 \le p_t^{\text{dis}} \le \overline{P}^{\text{dis}}, \tag{6a}$$

$$0 \le p_t^{\text{cha}} \le \overline{P}^{\text{cha}}, \tag{6b}$$

$$0 \le e_t \le \overline{E}. \tag{6c}$$

where $e_t$ is the energy level at time $t$, while $p_t^{\text{cha}}$ and $p_t^{\text{dis}}$ are the powers transferred from and to the electric grid, respectively. The discharge and charge power limits are respectively set by $\overline{P}^{\text{dis}}$ and $\overline{P}^{\text{cha}}$.

The energy accumulated at each period in the battery is related with the charging and discharging power and can be modeled through a linear energy balance [23]:

$$e_t = e_{t-1} + \Delta \cdot \left[ \eta^{\text{cha}} \cdot p_{t-1}^{\text{cha}} - \frac{1}{\eta^{\text{dis}}} \cdot p_{t-1}^{\text{dis}} \right], \tag{6d}$$

where the charge and discharge efficiencies are respectively given by $\eta^{\text{cha}}$ and $\eta^{\text{dis}}$. The parameter $\Delta$ provides the size of time discretization (in hours).

## 3.2 Non-ideal Energy Storage: A Li-ion Battery Model

The model mentioned above for ideal storage is a generalization of complex storage processes, such as: electrochemical (e.g., Li-ion batteries), electromechanical (e.g., flywheels), or electro-thermo-mechanical (e.g., compressed air energy storage systems). The limits of the rated power for charge and discharge, as well as the efficiencies, cannot be considered independent values as in the ideal storage model. For the particular case of Li-ion batteries, the maximum discharging and charging powers are limited by the charge transfer at the battery cells, Fig. 3a and b, which is dependent on the state-of-charge ($SOC$) [13]. The maximum discharging power is limited for low $SOCs$ by the high losses inside the cell, resulting in a voltage drop below the cutoff value. The limitations on the charging power for higher values of $SOC$ correspond to cell saturation in the charge absorption process. From Fig. 3a and b it is clear that it is not easy to choose a single value for the maximum rate of charge and discharge.

Additionally, the energy balance presented in (6d) assumes constant efficiencies for the charge and discharge processes. As with the power limits, the efficiencies in electrochemical storage systems are not constant and are a function of the $SOC$
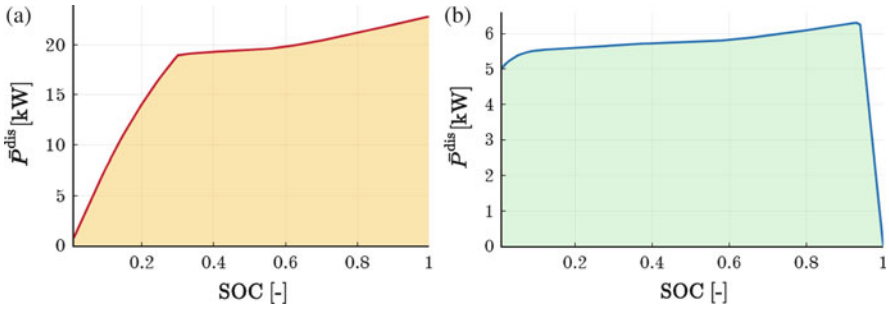
**Fig. 3** Maximum discharging (**a**) and charging (**b**) power, as a function of the $SOC$. Shadowed areas represent feasible operation [13]
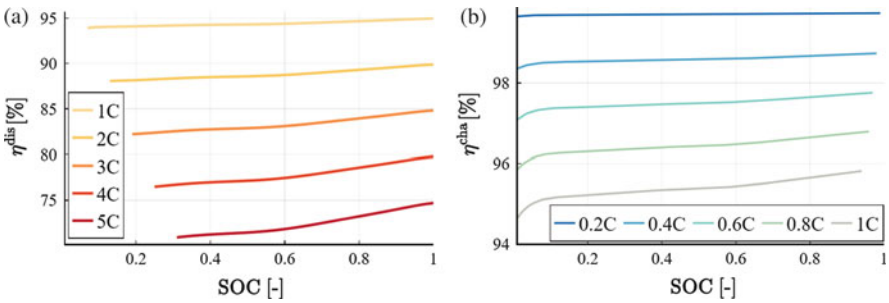


**Fig. 4** Discharging (**a**) and charging (**b**) efficiencies as a function of the SOC and discharging and charging current rate [13]
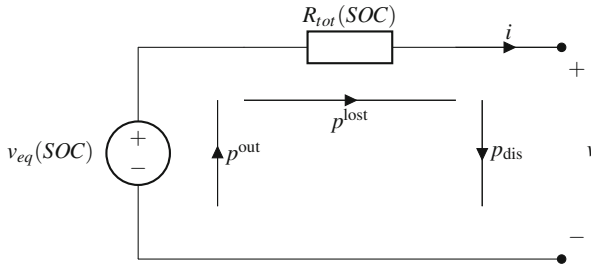


**Fig. 5** Power flows during discharge in a battery-equivalent electric circuit

and the discharged/charged power [13]. The efficiency for both the discharging and charging processes, Fig. 4a and b, increase for greater values of $SOC$ and lower power requests.

A battery can be represented as an equivalent resistive circuit, Fig. 5, during its steady-state operation, i.e., charging/discharging processes longer than its time constants. By considering the power flowing from the battery cell, $p^{out}$, power lost in its equivalent resistance, $p^{lost}$, and the power ultimately delivered to the grid, $p^{dis}$,

it is possible to obtain the following expression for the discharging efficiency $\eta^{\text{dis}}$

$$\eta^{\text{dis}} = \frac{p^{\text{dis}}}{p^{\text{out}}}, \tag{7}$$

Observe that the discharging efficiency is dependent on $p^{\text{dis}}$ and $p^{\text{out}}$. The voltage $v_{eq}$ changes with the $SOC$ and with it the losses through $R_{tot}$; effectively affecting the value of $p^{\text{out}}$ needed to supply the requested demand $p^{\text{dis}}$. Consequently, $p^{\text{dis}}$ is dependent of the $SOC$. Therefore, we could replace $\eta^{\text{dis}}$ by (7) to express $p^{\text{dis}}$ (the value of importance at the electric grid level) as a function of the $SOC$ and the $p^{\text{out}}$, only. It is possible to derive the non-linear analytical expression linking the three variables, $[p^{\text{dis}}, SOC, p^{\text{out}}]^{\top}$, but instead of it, we propose a data-driven approach.

The values $[p^{\text{dis}}, SOC, p^{\text{out}}]^{\top}$ can be represented as a linear combination of selected sampling points $[\widehat{P}_i^{\text{dis}}, \widehat{SOC}_i, \widehat{P}_i^{\text{out}}]^{\top}$ in the characteristic convex envelope. This relationship can be seen in Fig. 6. Every point forming the envelope could be obtained by using laboratory experiments or computational simulations. It is important to observe from Fig. 6 that the non-linear relationship between the three variables is quite similar to the proposed convex approach. In this way, the storage discharging process can be characterized by

$$p^{\text{out}} \quad = \sum_i \widehat{P}_i^{\text{out}} x_i \tag{8a}$$

$$p^{\text{dis}} \quad = \sum_j \widehat{P}_i^{\text{dis}} x_i \tag{8b}$$

$$SOC = \sum_i \widehat{SOC}_i x_i \tag{8c}$$

$$1 \quad = \sum_i x_i \tag{8d}$$

$$0 \quad \le x_i, \qquad \forall i, \tag{8e}$$

where $x_i$ is an auxiliary variable related to each point.

An analogous expression to (8) can be found for representing the power entering the cell $p^{\text{in}}$, in terms of the charging efficiency $\eta^{\text{cha}}$ and the power charged from the grid $p^{\text{cha}}$, transforming the energy balance (6d) into

$$e_t = e_{t-1} + \Delta \cdot \left[ p_{t-1}^{\text{in}} - p_{t-1}^{\text{out}} \right], \tag{9}$$

The storage operation with non-constant efficiency can be described in a linear way by Model 2 [13]. The energy balance is given by (10a), where $p_t^{\text{batt}}$ is the net power delivered to the battery cell (positive if charging, negative if discharging), and defined in (10b). The discharging and charging powers are respectively described by
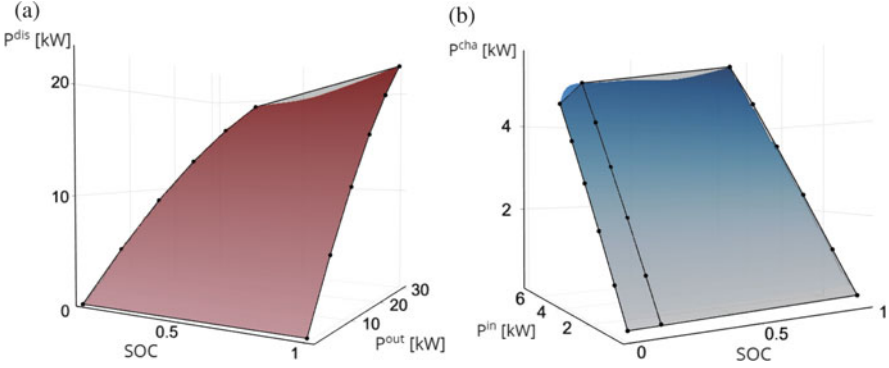
**Fig. 6** Operating region of a Li-ion battery for (**a**) discharging, and (**b**) charging processes. The surface represents the non-linear dependence, black dots are sampled points, and the lines between them define the convex envelope of the sampled points [13]

Eqs. (10c)–(10d) and (10e)–(10f). The $SOC$ as a linear combination of the sampling points is presented by (10g), while its definition is stated in (10h). The linear combination of the characteristic points during discharge and charge is ensured by (10i)–(10l).

---

**MODEL 2** Linear Li-ion battery model

**Indexes:**

| | |
|---|---|
| $i, j$ | Sampling indexes for the charging and discharging operation points |
| $t$ | Time step index |

**Parameters:**

| | |
|---|---|
| $\Delta$ | Duration of time step in hours [h] |
| $\overline{E}$ | Battery capacity [MWh] |
| $\widehat{P}_i^{\text{out}}, \widehat{P}_j^{\text{in}}$ | Sample points for the power leaving and entering the battery cell [MW] |
| $\widehat{P}_i^{\text{dis}}, \widehat{P}_j^{\text{cha}}$ | Sample points for the power discharged to and charged from the electric grid [MW] |
| $\widehat{SOC}_i, \widehat{SOC}_j$ | State-of-charge sample points for the discharging and charging processes |

**Variables:**

| | |
|---|---|
| $e_t, SOC_t$ | Battery energy level (absolute and relative values) on $t$ [MWh, −] |
| $p_t^{\text{batt}}$ | Net power charged/discharge by the battery during $t$ [MW] |
| $p_t^{\text{dis}}, p_t^{\text{cha}}$ | Discharging and charging power on $t$ [MW] |
| $p_t^{\text{out}}, p_t^{\text{in}}$ | Power outgoing and incoming at the cells on $t$ [MW] |
| $x_{jt}, y_{kt}$ | Auxiliary variables for the sample sets $J$ and $K$ |

(continued)

**MODEL 2** (continued)

**Constraints:**

$$e_t = e_{t-1} + \Delta \cdot p_{t-1}^{\text{batt}}, \qquad\qquad \forall t \qquad (10\text{a})$$

$$p_t^{\text{batt}} = p_t^{\text{in}} - p_t^{\text{out}}, \qquad\qquad \forall t \qquad (10\text{b})$$

$$p_t^{\text{out}} = \sum_i \widehat{P}_i^{\text{out}} x_{it}, \qquad\qquad \forall t \qquad (10\text{c})$$

$$p_t^{\text{dis}} = \sum_i \widehat{P}_i^{\text{dis}} x_{it}, \qquad\qquad \forall t \qquad (10\text{d})$$

$$p^{\text{in}} = \sum_j \widehat{P}_j^{\text{in}} y_{jt}, \qquad\qquad \forall t \qquad (10\text{e})$$

$$p^{\text{cha}} = \sum_j \widehat{P}_j^{\text{cha}} y_{jt}, \qquad\qquad \forall t \qquad (10\text{f})$$

$$SOC_t = \sum_i \left( \widehat{SOC}_i \cdot x_{it} + \sum_j \widehat{SOC}_j \cdot y_{jt} \right), \qquad \forall t \qquad (10\text{g})$$

$$SOC_t = e_t / \overline{E}, \qquad\qquad \forall t \qquad (10\text{h})$$

$$1 = \sum_i x_{it}, \qquad\qquad \forall t \qquad (10\text{i})$$

$$1 = \sum_j y_{jt}, \qquad\qquad \forall t \qquad (10\text{j})$$

$$0 \leq x_{it}, \qquad\qquad \forall i, t \qquad (10\text{k})$$

$$0 \leq y_{jt}, \qquad\qquad \forall j, t. \qquad (10\text{l})$$

# 4 Deterministic Distribution Unit Commitment with Battery Storage System

For the optimal economic operation of an electric power system, it is necessary to schedule the production of the different generation plants and the power exchange with adjacent systems. The unit commitment (UC) problem replicates the power system operation scheduling, where the *committed* units are those which generate electricity during a time period, i.e., they are *online* [1]. For a distribution system, with distributed generation and energy storage, the general formulation of the unit

commitment, with cost minimization, can be expressed as:

$$\text{min.} \qquad \sum_t \left[ \sum_g \Phi\left(p_{g,t}, z_{g,t}\right) + K\left(p_t^{\text{grid}}\right) \right] \qquad (11)$$

$$\text{subject to} \qquad \text{Power Flow}(t), \qquad \forall t \qquad (11\text{a})$$

$$\text{Energy Storage Model}(t), \qquad \forall t \qquad (11\text{b})$$

$$\text{Generation Limits}(t), \qquad \forall t \qquad (11\text{c})$$

$$\text{Power System Limits}(t), \qquad \forall t. \qquad (11\text{d})$$

In the above model, the objective (11) is to minimize, over the time horizon of interest, the cost function for the generators operation $\Phi$, and the economic exchange with the main grid $K$. The power produced by generator $g$ during $t$ is denoted by $p_{g,t}$ and its online status (*on/off*) by $z_{g,t}$. The net power exchanged with the grid, imported minus exported, is given by $p_t^{\text{grid}}$. The main constraints of the UC model are the power flow equations (Sect. 2), the energy storage model (Sect. 3), and the technical constraints on the generation units and power system.

This section addresses the deterministic formulation of the UC for a distribution network. In this context, the demand and RES generation is assumed to be known/forecasted with enough accuracy. In the next Sect. 5, this formulation will be expanded upon to include the variability of the users' electricity demand and RES.

## 4.1 Objective Function

The objective of the UC on a distribution network is the satisfaction of the users' demand at the minimum operational cost. This operational cost can be divided into two: the cost of operating the distributed generation, and the cost of purchasing/selling electricity to the main grid through the interconnection substation.

### 4.1.1 Cost of Energy Exchange

The day-ahead electricity market usually operates with hourly time steps, during which, the purchase/sale of electricity is done at constant power. Nonetheless, the actual technical power system operation must balance the generation and the demand in a prompt manner, result of the variation in demand and RES generation. In order to provide better scheduling of the system operation, it is advisable to solve the UC in time steps shorter than an hour [23], while maintaining the interaction with the main grid (through the day-ahead electricity market) in the traditional

**Fig. 7** Representation of market ($h$: hourly) and operational ($t$: intra-hour) time steps
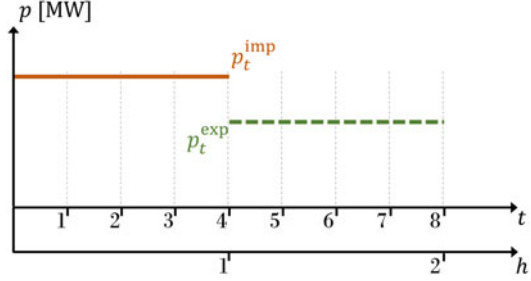


hourly segments. For this purpose, an additional index $h$ will be introduced to represent an hourly time step, and the notation $h(t)$ will be used to denote the hour to which the time step $t$ belongs. For instance, as seen in Fig. 7, the time step $t = 1$ belongs to $h = 1$, $h(t = 1) = 1$; whereas, $h(t = 5) = 2$. Additionally, since the market operation assumes a constant power exchange, $p_t^{\text{imp}}$ and $p_t^{\text{exp}}$ remain at the same value during the hourly interval, i.e.,

$$p_t^{\text{imp/exp}} = p_{t'}^{\text{imp/exp}}, \qquad \forall (t,t') \in h(t) \tag{12}$$

The economic interaction with the main grid depends on two factors: the power imported/exported, $p_t^{\text{imp/exp}}$, during time $t$, and the price of purchase/sell, $K_{h(t)}^{\text{imp/exp}}$. Thus, if the electricity cost, for purchase and sell, is known for each time step, the economic exchange with the grid can be calculated by:

$$K = \Delta \cdot \sum_t \left[ K_{h(t)}^{\text{imp}} p_t^{\text{imp}} + K_{h(t)}^{\text{exp}} p_t^{\text{exp}} \right], \tag{13}$$

where the cost of importing and exporting electricity during the hour $h(t)$ are respectively denoted by $K_{h(t)}^{\text{imp}}$ and $K_{h(t)}^{\text{exp}}$. In order to preserve the relationship between the prices in MWh and the exchanged power, the size of the time step ($\Delta$) is used to transform the imported/exported power from MW into MWh. This dimensional transformation assumes a constant power exchange for the duration of each time step $t$.

### 4.1.2 Cost of Generation

The cost of operating fuel-based generation units is typically composed by the cost of fuel consumption, the startup cost and the shutdown cost [6], given by:

$$\Phi = \sum_{g,t} \left[ \Delta \Phi_g^{\text{fuel}} p_{g,t} + \phi_{g,t}^{\text{su}} + \phi_{g,t}^{\text{sd}} \right], \tag{14}$$

where $\Phi_g^{\text{fuel}}$ is the fuel cost for the unit $g$, and $\phi_{g,t}^{\text{su}}$ and $\phi_{g,t}^{\text{sd}}$ are respectively the startup and shutdown costs incurred by $g$ during the time step $t$, defined by:

$$0 \le \phi_{g,t}^{\text{su}} \ge \Phi_g^{\text{su}}[z_{g,t} - z_{g,t-1}], \ \forall g, t \tag{14a}$$

$$0 \le \phi_{g,t}^{\text{sd}} \ge \Phi_g^{\text{sd}}[z_{g,t-1} - z_{g,t}], \qquad \forall g, t. \tag{14b}$$

It is straightforward to verify that $\phi_{g,t}^{\text{su}}$ and $\phi_{g,t}^{\text{sd}}$ can only take values greater than zero when the respective startup and shutdown processes are undergone.

## 4.2 Power Flow with Energy Storage and Renewable Generation

Given the introduction of RES and energy storage in the system, the power flow equations must reflect their influence in the system. The contribution of the RES is to reduce the total load served in the power system, whereas the storage system $s$ can act as generator by discharging energy into the system ($p_{s,t}^{\text{batt}} > 0$), or as a load when it is charging ($p_{s,t}^{\text{batt}} < 0$). The power contributions of these resources are included in the power balance presented in (5a), resulting in:

$$P_{n,t}^{\text{D}} = \Gamma_n^{\text{grid}} \cdot p_t^{\text{grid}} + \sum_{g \in \mathcal{G}(n)} p_{g,t} + \sum_{s \in \mathcal{S}(n)} p_{s,t}^{\text{batt}} + \Gamma_n^{\text{RES}} \cdot P_{n,t}^{\text{RES}} - \sum_{m \in \mathcal{N}(n)} p_{nm,t}, \qquad \forall n, t. \tag{15}$$

In the previous nodal power balance, the set $\mathcal{S}(n)$ represents the storage units connected at node $n$; while binary matrix parameters, $\Gamma_n^{\text{grid}}$ and $\Gamma_n^{\text{RES}}$, indicate if in the node $n$ there is a connection of the distribution grid with the main grid, and if there is RES generation, respectively.

## 4.3 Energy Storage Model

The set of equations characterizing the energy storage, (11b), is the same as described in Sect. 3.2. The use of the storage system in the deterministic UC is to allow arbitraging, i.e., to purchase and store electricity from the grid at low prices, and discharge the stored energy when the prices increase [9].

## 4.4 Generation Limits

Fuel-based generation units are constrained in the amount of power that they can change their power production between consecutive hours. This type of limits are referred to as *ramp rates*. The maximum power increase between hours for a unit $g$ is known as the ramp-up rate, $RU_g$ in MWh, while its maximum power reduction as ramp-down rate, $RD_g$ also in MWh. In addition, the power plants have upper and lower bounds for their electricity production. These limits depend on the generation unit's capacity. The lower and upper capacity bounds for the active power are respectively given by $\underline{P}_g$ and $\overline{P}_g$, while the limits for reactive power generation are denoted by $\underline{Q}_g$ and $\overline{Q}_g$. The ramp rates and capacity limits are then given by:

$$p_{g,t} \leq p_{g,t-1} + \Delta z_{g,t} RU_g, \quad \forall g, t \tag{16a}$$

$$p_{g,t} \geq p_{g,t-1} - \Delta z_{g,t} RD_g, \quad \forall g, t \tag{16b}$$

$$z_{g,t} \underline{P}_g \leq p_{g,t} \leq z_{g,t} \overline{P}_g, \quad \forall g, t \tag{16c}$$

$$z_{g,t} \underline{Q}_g \leq q_{g,t} \leq z_{g,t} \overline{Q}_g, \quad \forall g, t. \tag{16d}$$

It must be noted that the ramp rates and the capacity limits only affect the generation unit $g$ when it is operating, i.e., $z_{g,t} = 1$. Furthermore, the up and down ramp rates are scaled to the size of the intra hour time step $t$, by multiplying them by the parameter $\Delta$. The scaling of the ramp rates follows the assumption that the power generation is constant during the time step. Hence, if the time step were to have the duration of an hour, the scaling would be of factor 1.

## 4.5 Power System Limits

For a secure operation of the power system, technical limits are imposed in the transmission of electricity though the power lines. Thermal limits (ampacity), measured in Amperes (A), are the main constraint in distribution networks [26]. The ampacity states the maximum current that can flow through the conductor without damaging the insulation or the conductor itself. The current limit in a power line $(n, m) \in \mathscr{L}$ as a function of $c_{nm,t}$ at each time step $t$ is given in (17a) [17]. Here, the set $\mathscr{L}$ is introduced to represent all the existing power lines $(n, m)$, while the parameter $\overline{F}_{nm,t}$ represents the thermal limit in A. Additionally, the voltage at node $n$ is limited in (17b).

$$\overline{F}_{nm,t}^2 \geq (B_{nm}^2 + G_{nm}^2) \cdot (c_{nn,t} - 2c_{nm,t} + c_{mm,t}), \quad \forall (n, m) \in \mathscr{L}, t \tag{17a}$$

$$\underline{V}_n^2 \leq c_{nn,t} \leq \overline{V}_n^2, \quad \forall n, t \tag{17b}$$

### *4.6   Summary for the Deterministic Unit Commitment Formulation*

As previously introduced, the objective of the UC in a distribution network is to operate the existing distributed generation and electricity exchange with the main grid at a minimum cost, while satisfying the users' demand and system constraints. The complete formulation of the deterministic unit commitment is given in Model 3.

The minimization of the generation operational cost and the economic exchange with the main grid is stated in (18), whereas these costs are respectively defined in (18a) and (18b). Constraint (18c) sets the constant power exchange with the main electric grid is defined, while (18d) defines the net power exchange. The startup and shutdown costs associated with the unit $g$ are respectively given by (18e) and (18f). Equation (18g) represents the nodal power balance for each time step $t$, including the RES generation and storage usage. Unit $g$'s ramp constraints are given by (18h) and (18i), whereas its capacity limits are set by (18j) and (18k). The voltage limits at the nodes and the thermal rates for the power lines are given by (18l) and (18m), respectively.

The power flow equations are included in (18n) by the addition of Model 1's constraints (5b)–(5g). Constraint (5a) has been replaced by (18g) to include the storage system and the RES. The reader must notice that the power flow equations represent the state of the system at any time. The sub-index $t$ is included to the Model 1 to represent this fact. Similarly, the energy storage model, Model 2, has been included in its entirety in constraint (18o).

---

**MODEL 3** Unit commitment with battery storage system

**Indexes:**

| | |
|---|---|
| $s$ | Index for the battery storage system |

**Sets:**

| | |
|---|---|
| $h(t)$ | Hour containing time step $t$ |

**Parameters:**

| | |
|---|---|
| $\overline{F}_{nm}$ | Current limit for line $(n, m)$ [p.u.] |
| $K_h^{\mathrm{imp}}, K_h^{\mathrm{exp}}$ | Import and export cost during $h$ [€/MWh] |
| $P_{n,t}^{\mathrm{RES}}$ | Active power generated by the RES resource at $n$ during $t$ [MW] |
| $\underline{P}_g, \overline{P}_g$ | Active power generation limits for $g$ [MW] |
| $RU_g, RD_g$ | Ramp-up and ramp-down limits for $g$ [MWh] |
| $\underline{Q}_g, \overline{Q}_g$ | Reactive power limits for $g$ [MVAr] |
| $\underline{V}_n, \overline{V}_n$ | Voltage limits at $n$ [p.u.] |
| $\Gamma_n^{\mathrm{grid}}, \Gamma_n^{\mathrm{RES}}$ | Binary indicator of connection to the main grid and the RES resources at $n$ |
| $\Phi^{\mathrm{fuel}}$ | Fuel consumption costs of $g$ [€/MWh,€] |
| $\Phi_g^{\mathrm{su}}, \Phi_g^{\mathrm{sd}}$ | Costs related to $g$'s start-up & shut-down [€] |

(continued)

**MODEL 3** (continued)

**Variables:**

| | |
|---|---|
| $K$ | Total economic exchange with the grid [€] |
| $\Phi$ | Total operational costs of generators [€] |
| $\phi_{g,t}^{su}, \phi_{g,t}^{sd}$ | Start-up and shut-down cost for $g$ on $t$ [€] |
| $p_t^{grid}$ | Net power exchanged with the main grid during $t$ [MW] |
| $p_t^{imp}, p_t^{exp}$ | Imported and exported power on $t$ [MW] |
| $z_{g,t} \in \{0, 1\}$ | On/off status of generating unit $g$ on $t$ |

**Objective:**

$$\min. \Phi + K \tag{18}$$

**Constraints:**

$$\Phi = \sum_{g,t} \left[ \Delta \Phi_g^{fuel} p_{g,t} + \phi_{g,t}^{su} + \phi_{g,t}^{sd} \right], \tag{18a}$$

$$K = \Delta \cdot \sum_t \left[ K_{h(t)}^{imp} p_t^{imp} + K_{h(t)}^{exp} p_t^{exp} \right] \tag{18b}$$

$$p_t^{imp/exp} = p_{t'}^{imp/exp}, \qquad \forall (t,t') \in h(t) \tag{18c}$$

$$p_t^{grid} = p_t^{imp} - p_t^{exp}, \qquad \forall t \tag{18d}$$

$$0 \le \phi_{g,t}^{su} \ge \Phi_g^{su} \left[ z_{g,t} - z_{g,t-1} \right], \qquad \forall g,t \tag{18e}$$

$$0 \le \phi_{g,t}^{sd} \ge \Phi_g^{sd} \left[ z_{g,t-1} - z_{g,t} \right], \qquad \forall g,t \tag{18f}$$

$$P_{n,t}^D = \Gamma_n^{grid} \cdot p_t^{grid} + \sum_{g \in \mathscr{G}(n)} p_{g,t} + \sum_{s \in \mathscr{S}(n)} p_{s,t}^{batt} + \Gamma_n^{RES} \cdot P_{n,t}^{RES} - \sum_{m \in \mathscr{N}(n)} p_{nm,t}, \qquad \forall n,t \tag{18g}$$

$$p_{g,t} \le p_{g,t-1} + \Delta z_{g,t} RU_g, \qquad \forall g,t \tag{18h}$$

$$p_{g,t} \ge p_{g,t-1} - \Delta z_{g,t} RD_g, \qquad \forall g,t \tag{18i}$$

$$z_{g,t} \underline{P}_g \le p_{g,t} \le z_{g,t} \overline{P}_g, \qquad \forall g,t \tag{18j}$$

$$z_{g,t} \underline{Q}_g \le q_{g,t} \le z_{g,t} \overline{Q}_g, \qquad \forall g,t \tag{18k}$$

$$\underline{V}_n^2 \le c_{nn,t} \le \overline{V}_n^2, \qquad \forall n,t \tag{18l}$$

$$\overline{F}_{l,t}^2 \ge (B_{nm}^2 + G_{nm}^2) \cdot (c_{nn,t} - 2c_{nm,t} + c_{mm,t}), \qquad \forall (n,m) \in \mathscr{L}, t \tag{18m}$$

SOCP power flow (Model 1($t$)) : (5b)–(5g), $\qquad \forall t \tag{18n}$

Battery model (Model 2). $\tag{18o}$

# 5 Stochastic Unit Commitment

In order to supply the users' demanded energy reliably and securely, the system operator must be able to react to variations in the forecasted load and RES generation [16]. The random nature of the demand and RES generation correspond to stochastic processes, i.e., randomly generated. Such flexible operation can be guaranteed by (1) purchasing reserve generation capacity from the main grid and scheduling the commitment of the generation units, and (2) setting the operation for the generation units and energy storage in a manner that would allow them to respond, within their technical limits, to load and RES fluctuations.

Section 5.1 describes the general formulation of a two-stage optimization problem considering stochastic parameters. Whereas, Sect. 5.2 outlines the formulation of the distribution UC under the two-stage stochastic optimization framework. Sections 5.2.1 and 5.2.2 respectively define the scheduling and operational aspects of purchasing reserve capacity from the main grid and flexibly operating the generation resources. The power flow and energy storage models' adaptation to the stochastic framework is described in Sects. 5.2.3 and 5.2.4, respectively. Finally, Sect. 5.3 provides a summary of the full formulation for the stochastic UC of a distribution system.

## 5.1 Two-Stage Stochastic Optimization

An optimization problem containing random parameters, such as RES generation, can be modelled as a deterministic problem in which the stochastic parameters are represented by scenarios indexed by $\omega$ with an associated realization probability $\rho_\omega$. For the optimization model, some decisions must be made before the random event realizes, e.g., a backup generator is committed before the RES generation is known. These decisions are known as first-stage decisions. Whereas the second-stage decisions are the correcting or real-time actions that respond to the stochastic realization, e.g., how much power must the backup generator produce in real time based on the RES generation. A representation of a two-stage stochastic model is presented in Fig. 8.

The first-stage decisions are made for each time step $t$ and affect each of the operative decisions made to react to the scenario realizations $\omega$ evaluated on the different time steps. A general formulation for the two-stage stochastic optimization model can be represented by:

$$\min_{x} \quad c^T x + \mathbb{E}[Q(x, \omega)] \tag{19a}$$

$$\text{subject to :} \quad Ax \leq b, \tag{19b}$$

$$x \geq 0. \tag{19c}$$
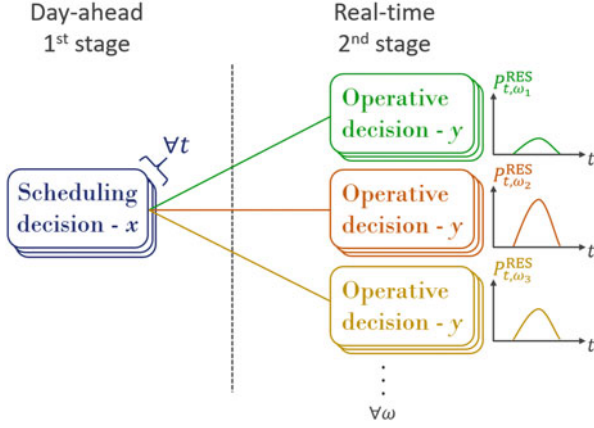
**Fig. 8** First-stage scheduling decisions. Second-stage: operative decisions

where $Q(x, \omega)$ is the second-stage optimal solution of the problem (20) parameterized in the first-stage decision and scenario.

$$\min_{y} \quad q^T(\omega)y \tag{20a}$$

$$\text{subject to}: \quad T(\omega)x + D(\omega)y \leq h(\omega), \tag{20b}$$

$$y \geq 0. \tag{20c}$$

The objective function (19a) is composed of the first-stage decisions' cost $c^T x$, plus the expected value of the second-stage $Q(x, \omega)$ costs. The second stage problem (20) minimizes the cost of corrective/real-time actions, $y$, taken once we have observed the RES scenario realization $\omega$, and for a given first-stage decision $x$. Similarly to the first-stage problem, we could have a set of constraints, (20b), that define the feasibility space for second-stage decisions $y$, whereas the first-stage constraints are defined by (19b). The positivity in the general model of $x$ and $y$ is set by (19c) and (20c).

Both problems (19) and (20) can be recast into a single deterministic model that can be easily solved with off-the-shelf commercial solvers.

$$\min_{x, y_\omega} \quad c^T x + \sum_{\omega} \rho_\omega \left( q_\omega^T y_\omega \right) \tag{21a}$$

$$\text{subject to}: \quad Ax \leq b, \tag{21b}$$

$$T_\omega x + D_\omega y_\omega \leq h_\omega, \forall \omega \tag{21c}$$

$$x, y_\omega \geq 0. \tag{21d}$$

where $\rho_\omega$ is the probability of occurrence of the scenario $\omega$, and parameters such as $T(\omega)$, are not anymore a probability distribution function of $\omega$, but rather a sample was taken from it, $T_\omega$. It must be noted that each operative decision $y$ must be solved for each scenario, increasing accordingly the complexity of the model. However, the model would result to have better performance than a deterministic model where uncertainty is important. We refer to the monograph [4] for further details in stochastic programming theory.

## 5.2 Stochastic Unit Commitment Formulation

In order to transform the deterministic UC model presented in Model 3 into one that allows the allocation and use of reserves under uncertainties, it is necessary to determine which decision variables will belong to the scheduling and which to the operation stages. The following sections will cover the two-stage stochastic formulation for the interaction with the main grid, generation operation, power flow, and energy storage models.

### 5.2.1 Reserves Allocation and Realization

The purchase and use of reserve generation capacity from the main grid follows a two-step process, Fig. 9. In the first step, day-ahead, the quantified needs for upward $r_t^{\text{up}}$ and downward $r_t^{\text{dw}}$ reserves are purchased. In case of an increase of the demand $P_{n,t,\omega}^{\text{D}}$ or decrease in RES generation $P_{n,t,\omega}^{\text{RES}}$ during the real-time operation (scenario $\omega$) and without the possibility of the generation to respond in a promptly manner, the system operator can increase its power consumption from the purchased quantity $p_t^{\text{imp}}$ up to the allocated amount of reserve capacity $r_t^{\text{up}}$. The increased power import corresponds to the *reserve realization* $\hat{r}_{t,\omega}^{\text{up}}$. Unlike the reserves capacity allocation, their realization can and must change with each scenario. Thus, they are not bound to the hourly time steps $h$ and are only bounded by the allocated reserved capacity. In case of a decrease of the demand or increase of the RES generation, the downward reserve realization $\hat{r}_{t,\omega}^{\text{dw}}$ can reduce the power import $p_t^{\text{imp}}$ up to $r_t^{\text{dw}}$.

Figure 10 represents the relationship between the hourly upward reserves allocation and their scenario-based realization.[4]

The constraints modeling the power exchange in the day-ahead (first-stage) and during the operation stage (second-stage) are presented in (22). The total reserve allocation cost $\Upsilon$, (22a), is given by the sum of the requested capacity $r_t^{\text{up/dw}}$ and the cost associated to it $K_{h(t)}^{\text{up/dw}}$. Increasing the power output by $\hat{r}_{t,\omega}^{\text{up}}$ during the

---

[4]The downward reserve realization and allocation process is analog to that presented in Fig. 10, but is omitted to allow better figure readability.
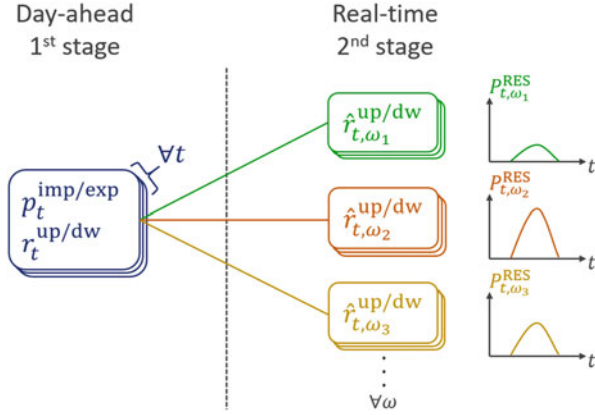
**Fig. 9** First-stage import/export scheduling and upward/downward reserve allocation, second-stage upward reserve realization process
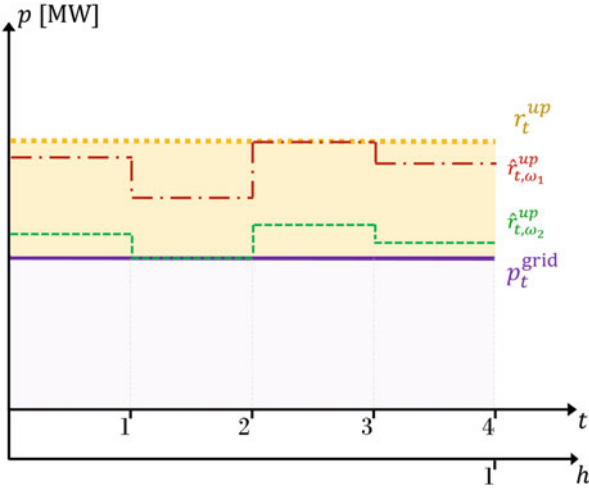


**Fig. 10** First-stage energy and upward reserve allocation, second-stage upward reserve realization process

operation stage will incur the system operator in an additional marginal cost of $\hat{K}_{h(t)}^{\text{up}}$, in €/MWh, whereas reducing its consumption will provide him a marginal revenue of $\hat{K}_{h(t)}^{\text{dw}}$. The reserve realization cost is given by (22b).

Equation (22c) defines the net power exchanged with the grid during the operation stage by the sum of the scheduled import and export, plus the realized reserves. Constraints (22d) and (22e) respectively determine the upper bound for the allocation of upward and downward reserves in terms of the scheduled power import $p_t^{\text{imp}}$ and the maximum import capacity $\overline{P}^{\text{imp}}$. The bounds for reserve allocation

based on the market rules are presented in (22f) and (22g). The limits for the reserves realization during the operational stage are set by (22h) and (22i). Finally, the hourly market nature for the reserve allocation is guaranteed by (22j).

$$\Upsilon = \Delta \cdot \sum_t \left( K_{h(t)}^{\mathrm{r,\, up}} r_t^{\mathrm{up}} + K_{h(t)}^{\mathrm{r,\, dw}} r_t^{\mathrm{dw}} \right), \tag{22a}$$

$$\Theta_\omega = \Delta \cdot \sum_t \left[ \hat{K}_{h(t)}^{\mathrm{r,\, up}} \hat{r}_{t,\omega}^{\mathrm{up}} + \hat{K}_{h(t)}^{\mathrm{r,\, dw}} \hat{r}_{t,\omega}^{\mathrm{dw}} \right], \qquad \forall \omega \tag{22b}$$

$$p_{t,\omega}^{\mathrm{grid}} = p_t^{\mathrm{imp}} - p_t^{\mathrm{exp}} + \hat{r}_{t,\omega}^{\mathrm{up}} - \hat{r}_{t,\omega}^{\mathrm{dw}}, \qquad \forall t, \omega \tag{22c}$$

$$\overline{P}^{\mathrm{imp}} \geq p_t^{\mathrm{imp}} + r_t^{\mathrm{up}}, \qquad \forall t \tag{22d}$$

$$0 \leq p_t^{\mathrm{imp}} - r_t^{\mathrm{dw}}, \qquad \forall t \tag{22e}$$

$$0 \leq r_t^{\mathrm{up}} \leq \overline{R}^{\mathrm{up}}, \qquad \forall t \tag{22f}$$

$$0 \leq r_t^{\mathrm{dw}} \leq \overline{R}^{\mathrm{dw}}, \qquad \forall t \tag{22g}$$

$$0 \leq \hat{r}_{t,\omega}^{\mathrm{up}} \leq r_t^{\mathrm{up}}, \qquad \forall t, \omega \tag{22h}$$

$$0 \leq \hat{r}_{t,\omega}^{\mathrm{dw}} \leq r_t^{\mathrm{dw}}, \qquad \forall t, \omega \tag{22i}$$

$$r_t^{\mathrm{up/dw}} = r_{t'}^{\mathrm{up/dw}}, \qquad \forall (t,t') \in h(t). \tag{22j}$$

### 5.2.2 Generation Commitment and Operation

As the power exchange with the main grid, the use of generation resources can be divided into a two-stage process: scheduling and operation. Figure 11 illustrates how the scheduling (first) stage of the units is done by determining their on/off state $z_{g,t}$ for the considered time horizon. Based on their status, the generation units will be operated, together with the energy storage system, to produce the power ($p_{g,t,\omega}$, $q_{g,t,\omega}$) required for balancing the load and the RES generation [1].

### 5.2.3 Power Flow Model

The power flow equations characterize the operational stage of the stochastic UC. Consequently, the power flow equations must be considered in the second stage of the formulation and be indexed by each probabilistic scenario. This fact is represented in Model 4 by stating that Model 3 is a function of the scenarios $\omega$ and in the definition of the model's variables.
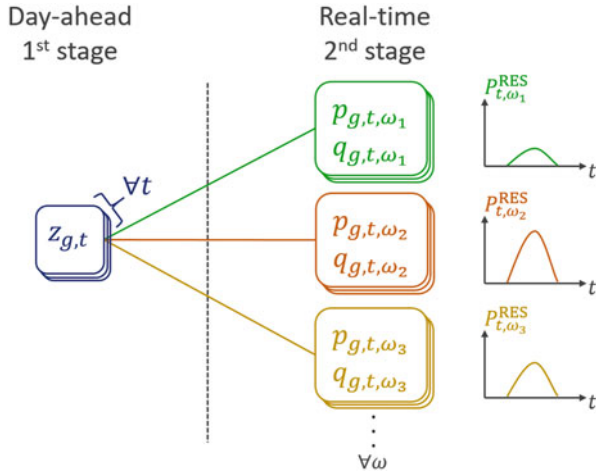
**Fig. 11** Generation stages: first-stage turned on/off during $t$, second-stage active and reactive power production

### 5.2.4 Energy Storage Model

The energy storage model described in Sect. 3.2 is the base for the operation of the storage system in the second stage of the stochastic UC. Therefore, the operating variables of the storage system must be indexed not only for each time $t$ but also for every scenario $\omega$, as presented in Model 4.

## 5.3 Summary for the Stochastic Unit Commitment Formulation

Figure 12 presents how the different introduced models are related. As described in Sect. 5.2, the main differences between the Model 3 and the UC stochastic model is the allocation and use of reserves for the system operation under the different probabilistic scenarios, as well as the differentiation of the scheduling and operating stage for the generation units. The reserves allocation and unit commitment occur in the first stage of the model, while the reserves realization and power production of the generation units occur in the second stage. The power flow and energy storage operation also take place in the second stage. Model 4 presents the two-stage stochastic formulation of the unit commitment. The first- and second-stage variables have been differentiated in the model. For the sake of simplicity, only the new constraints describing the allocation and realization of reserves have been explicitly presented. The Model 3 has been indexed by scenarios $\omega$ to represent the fact that its constraints must consider the second stage when required.
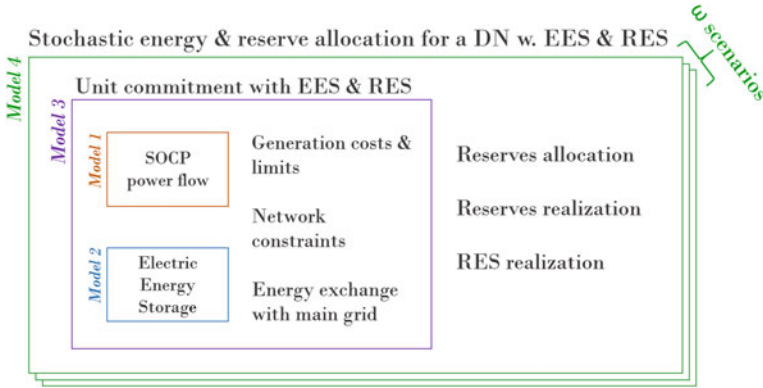
**Fig. 12** Relationship between the presented models

---

**MODEL 4** Stochastic distribution unit commitment with BSS

**Indexes:**

$\omega$                 Index for probabilistic scenarios

**Parameters:**

| | |
|---|---|
| $K_h^{\mathrm{r,\,up}}$, $K_h^{\mathrm{r,\,dw}}$ | Up and down reserve allocation cost during $h$ [€/MWh] |
| $\hat{K}_h^{\mathrm{r,\,up}}$, $\hat{K}_h^{\mathrm{r,\,dw}}$ | Up and down reserve deployment cost during $h$ [€/MWh] |
| $\overline{P}^{\mathrm{imp}}$ | Power import limits [MWh] |
| $\overline{R}^{\mathrm{up}}$, $\overline{R}^{\mathrm{dw}}$ | Up and down reserve power limits [MWh] |

**First-stage variables:**

| | |
|---|---|
| $\Phi$ | Total scheduling costs of generators [€] |
| $K$ | Total economic exchange with the grid [€] |
| $p_t^{\mathrm{imp}}$, $p_t^{\mathrm{exp}}$ | Imported and exported power committed day-ahead [MW] |
| $r_t^{\mathrm{up}}$, $r_t^{\mathrm{dw}}$ | Allocated up/down reserve during $t$ [MWh] |
| $\Upsilon$ | Total reserve allocation cost [€] |
| $z_{g,t} \in \{0, 1\}$ | On/off status of generating unit $g$ on $t$ |

**Second-stage variables:**

| | |
|---|---|
| $c_{nm,t,\omega}$ | $\lvert V_{n,t,\omega} \rvert \lvert V_{m,t,\omega} \rvert \cos(\theta_{n,t,\omega} - \theta_{m,t,\omega})$ [p.u.] |
| $e_{t,\omega}$, $SOC_{t,\omega}$ | Battery energy level (absolute and relative values) during $t$ and scenario $\omega$ [MWh, −] |
| $\phi_{g,t,\omega}^{\mathrm{su}}$, $\phi_{g,t,\omega}^{\mathrm{sd}}$ | Start-up and shut-down cost for $g$ on $t$ and scenario $\omega$ [€] |
| $p_{g,t,\omega}$, $q_{g,t,\omega}$ | Generated active and reactive power by unit $g$ during $t$ and scenario $\omega$ [MW, MVAr] |
| $p_{nm,t,\omega}$, $q_{nm,t,\omega}$ | Active and reactive power flow through line $(n, m)$ during $t$ and scenario $\omega$ [MW, MVAr] |
| $p_{t,\omega}^{\mathrm{batt}}$ | Net power charged/discharge by the battery during $t$ and scenario $\omega$ [MW] |

(continued)

## MODEL 4 (continued)

| | |
|---|---|
| $p_{t,\omega}^{\mathrm{dis}}, p_{t,\omega}^{\mathrm{cha}}$ | Discharging and charging power during $t$ and scenario $\omega$ [MW] |
| $p_{t,\omega}^{\mathrm{grid}}$ | Net power exchanged with the main grid during $t$ and scenario $\omega$ [MW] |
| $p_{t,\omega}^{\mathrm{out}}, p_{t,\omega}^{\mathrm{in}}$ | Power outgoing and incoming at the cells during $t$ and scenario $\omega$ [MW] |
| $\hat{r}_{t,\omega}^{\mathrm{up}}, \hat{r}_{t,\omega}^{\mathrm{dw}}$ | Real-time deployed up/down reserve during $t$ and scenario $\omega$ [MWh] |
| $s_{nm,t,\omega}$ | $|V_{n,t,\omega}||V_{m,t,\omega}| \sin(\theta_{n,t,\omega} - \theta_{m,t,\omega})$ [p.u.] |
| $\Theta_\omega$ | Total real-time reserves deployment cost for scenario $\omega$ [€] |
| $x_{j,t,\omega}, y_{k,t,\omega}$ | Auxiliary variables for the sample sets $J$ and $K$ during $t$ and scenario $\omega$ |
| $W_\omega$ | Total operational costs of generators for scenario $\omega$ [€] |

**Objective**:

$$\text{min.} \quad K + \Upsilon + \Phi + \mathbb{E}\left[\Theta_\omega + W_\omega\right] \tag{23}$$

**Constraints:**

$$\Phi = \sum_{g,t} \phi_{g,t}^{\mathrm{su}} + \phi_{g,t}^{\mathrm{sd}} \tag{23a}$$

$$W_\omega = \Delta \cdot \Phi_g^{\mathrm{fuel}} \sum_{g,t,\omega} p_{g,t,\omega} \tag{23b}$$

$$\Upsilon = \Delta \cdot \sum_t \left(K_{h(t)}^{\mathrm{r,\,up}} r_t^{\mathrm{up}} + K_{h(t)}^{\mathrm{r,\,dw}} r_t^{\mathrm{dw}}\right), \tag{23c}$$

$$\Theta_\omega = \Delta \cdot \sum_t \left[\hat{K}_{h(t)}^{\mathrm{r,\,up}} \hat{r}_{t,\omega}^{\mathrm{up}} + \hat{K}_{h(t)}^{\mathrm{r,\,dw}} \hat{r}_{t,\omega}^{\mathrm{dw}}\right], \qquad \forall \omega \tag{23d}$$

$$p_{t,\omega}^{\mathrm{grid}} = p_t^{\mathrm{imp}} - p_t^{\mathrm{exp}} + \hat{r}_{t,\omega}^{\mathrm{up}} - \hat{r}_{t,\omega}^{\mathrm{dw}}, \qquad \forall t, \omega \tag{23e}$$

$$\overline{P}^{\mathrm{imp}} \geq p_t^{\mathrm{imp}} + r_t^{\mathrm{up}}, \qquad \forall t \tag{23f}$$

$$0 \leq p_t^{\mathrm{imp}} - r_t^{\mathrm{dw}}, \qquad \forall t \tag{23g}$$

$$0 \leq r_t^{\mathrm{up}} \leq \overline{R}^{\mathrm{up}}, \qquad \forall t \tag{23h}$$

$$0 \leq r_t^{\mathrm{dw}} \leq \overline{R}^{\mathrm{dw}}, \qquad \forall t \tag{23i}$$

$$0 \leq \hat{r}_{t,\omega}^{\mathrm{up}} \leq r_t^{\mathrm{up}}, \qquad \forall t, \omega \tag{23j}$$

$$0 \leq \hat{r}_{t,\omega}^{\mathrm{dw}} \leq r_t^{\mathrm{dw}}, \qquad \forall t, \omega \tag{23k}$$

$$r_t^{\mathrm{up/dw}} = r_{t'}^{\mathrm{up/dw}} \qquad \forall (t,t') \in h(t) \tag{23l}$$

$$\text{Stochastic Real-Time UC-BSS } \big(\text{Model } 3(\omega)\big), \qquad \forall \omega. \tag{23m}$$

# 6 Numerical Example

A modified IEEE 33-bus system is used to test different aspects of the distribution system operation [2]. The radial distribution system, represented in Fig. 13, operates at 12.66 kV, with an aggregated peak demand of 4.37 MVA. The system counts with a connection to the main transmission grid at node 1, two fuel-based generators at nodes 22 and 33, and a photovoltaic system of 1.5 MW at node 18. The capacity of the generators 1 and 2 are respectively 1.5 and 3 MW, and their marginal cost of generation $\Phi_g^{\text{fuel}}$ is 150 and 120 €/MWh. A lithium-ion energy storage system with a 3 MWh capacity (power rate of 3MW, 15MW at 5C) has been placed at node 18. The network, generation and demand data, as well as the sampling points for the storage system, are available in the online appendix [14]. Prices for the energy exchange with the network are also available in the online appendix [14].

In order to simplify the analysis, only three scenarios for the stochastic RES generation will be considered. The scenarios were generated through a forecast using a seasonal ARIMA model based on surface radiation data corresponding to the first month of the year 2017 on Desert Rock, Nevada, USA [22]. The ARIMA method was chosen to produce a more accurate forecast, resulting in a non-smooth generation curve for the 24 h of study (see in Fig. 14). The probabilities associated with scenarios 1, 2, and 3 have been manually set respectively at 25, 50, and 25%.

We have tested the proposed electric distribution operation with energy storage models in four cases described as follows:

- CASE 1–D: optimal system's operation is solved by adopting an ideal energy storage model (6) in a deterministic unit commitment (Model 3). The RES generation is taken as the average forecast, i.e., the mean value between the three scenarios. The average discharge and charge battery efficiencies are set to 86.8% and 97.2%, respectively.
- CASE 1–S: an ideal energy storage model (6), and a stochastic unit commitment model (Model 4) are employed.
- CASE 2–D: the solution is based on a non-ideal energy storage model (Model 2) while using the deterministic unit commitment version for optimal operation model of the distribution grid (Model 3).
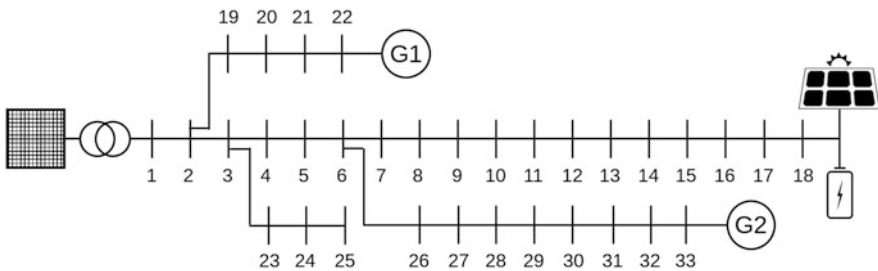


**Fig. 13** 33-Bus test system
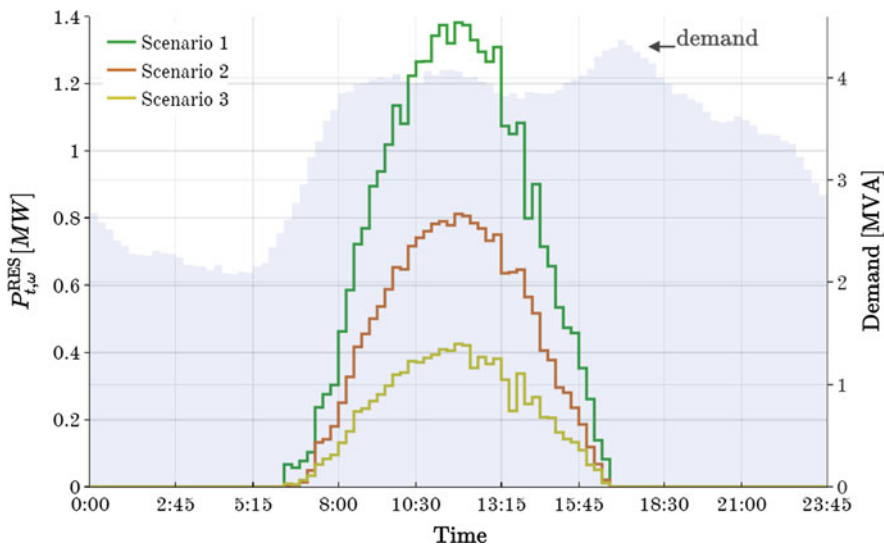
**Fig. 14** Total demand per time step and scenario of solar energy generation

- CASE 2–S: the system is optimized with the developed a non-ideal energy storage (Model 2), and a stochastic unit commitment model (Model 4).

The results summary for the different test cases is presented in Table 1. As seen in the table, the total costs remained almost the same for all the cases. However, it is important to note that there is also a slight reduction in cost by using a detailed battery model instead of the ideal one; explained by the use of the battery in regions of higher efficiency.

**Table 1** Results summary for computational test cases

|  | CASE 1–D | CASE 1–S | CASE 2–D | CASE 2–S |
|---|---|---|---|---|
| Battery model | Ideal | | Non-ideal | |
| Type | Deterministic | Stochastic | Deterministic | Stochastic |
| Total costs [€] | 7909.5 | 7954.4 | 7906.2 | 7952.6 |
| Computational time [s] | 141.6 | 501.8 | 119.7 | 733.2 |
| Total imports [MWh] | 19.0 | 16.6 | 19.0 | 16.7 |
| Total export [MWh] | 0.0 | 0.0 | 0.0 | 0.0 |
| Total realized up-reserve ($\omega_1$) [MWh] | – | 0.64 | – | 0.44 |
| Total realized up-reserve ($\omega_2$) [MWh] | – | 3.0 | – | 3.0 |
| Total realized up-reserve ($\omega_3$) [MWh] | – | 3.1 | – | 3.1 |
| Total realized down-reserve ($\omega_1$) [MWh] | – | 0.5 | – | 0.4 |
| Total realized down-reserve ($\omega_2$) [MWh] | – | 0.0 | – | 0.1 |
| Total realized down-reserve ($\omega_3$) [MWh] | – | 0.0 | – | 0.1 |
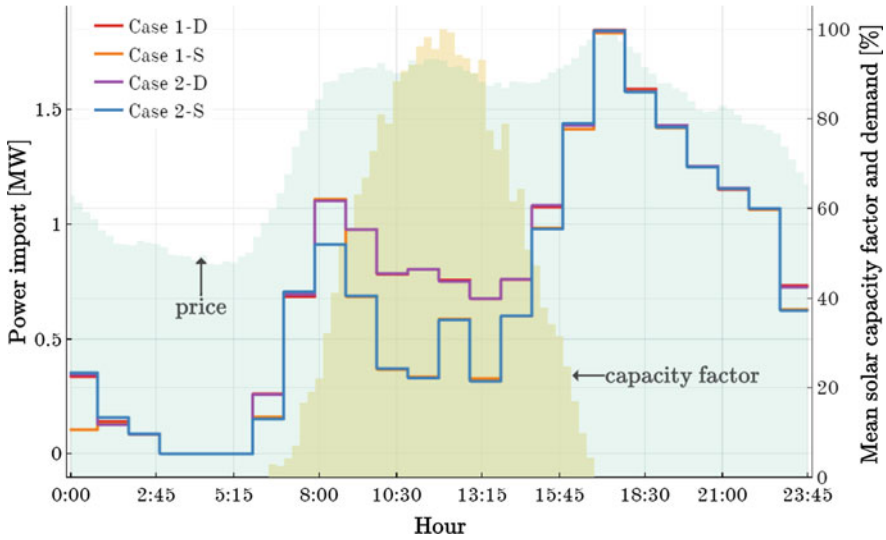
**Fig. 15** Power import per case, in comparison with the normalized solar radiation and energy import price

The purchase of energy from the main grid for the four test cases is displayed in Fig. 15. The solar production is presented normalized to its maximum value, i.e., its capacity factor. Similarly, energy import prices are represented in the background. As it can be seen from the figure, the import of energy for the test cases follows the demand throughout the day. The presence of higher radiation between 10:00 and 15:00 allows to complement the use of the fuel-based generation, reducing the need for energy import. The import reduction around the noon hours is greater for the test cases that considered the probabilistic scenarios, CASE 1–S and CASE 2–S; given their consideration of the weighted effect from higher RES generation.

Figure 16 presents the energy storage operation for CASE 2–S. The use of the storage system for each scenario follows a similar pattern, except around the noon hours. During this time frame, the use of the storage has a direct relationship with the amount of RES generation of each scenario; for scenario 1 there is an intense storage usage, greater than, for instance, scenario 2. Whereas around the noon hours, the energy storage is discharged at (almost zero) constant power in scenario 3. The difference in the storage usage between the scenarios highlights the importance of pairing RES with energy storage systems since they allow to balance the power generation from RES sources.
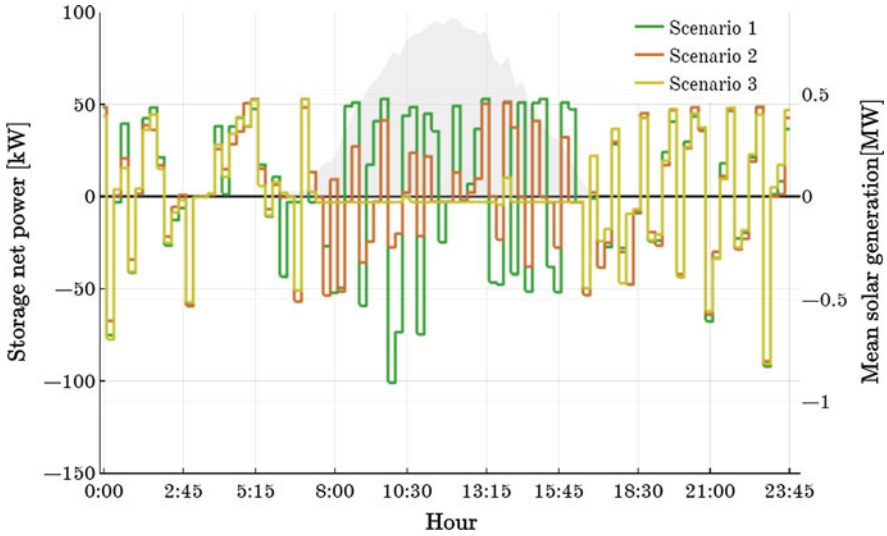
**Fig. 16** Storage usage for CASE 2–S. Each trace represents the operation of the energy storage system for a different stochastic scenario. In the background, average solar generation

## 6.1 Operation Reliability

Even though the total cost obtained, the amount of imported energy and employed reserves are similar through the four test cases, the ideal energy storage model employed in CASE 1–D and CASE 1–S does not take into account the variation of the maximum power that a storage system can charge and discharge as a function of its state of charge. The use of constant power limits could lead to infeasible battery operation, resulting in situations where the scheduled power falls outside the feasible operating region. Figure 17 presents the differences between the scheduled battery energy level for each scenario and the corrected operation, i.e., with the requested power being limited by the control system when the scheduled storage usage surpasses the technical limits presented in Sect. 3.2. The energy deviation (scheduled minus corrected) for scenarios 1 to 3 was of 78.8, 113.4, and 24.7 kWh, respectively representing 3.6, 6.2, and 1.0% of the scheduled energy to be stored with the battery. Such scheduling imbalances could produce violations of the system constraints and must be covered by the distribution system operator through the purchase of more energy in the real-time market or utilizing the backup generation, incurring in additional operating expenses. Therefore, it becomes of the utmost importance the accurate modeling of the energy storage system that provides additional flexibility and reserve for supporting reliable operation under uncertain and intermittent RES generation.
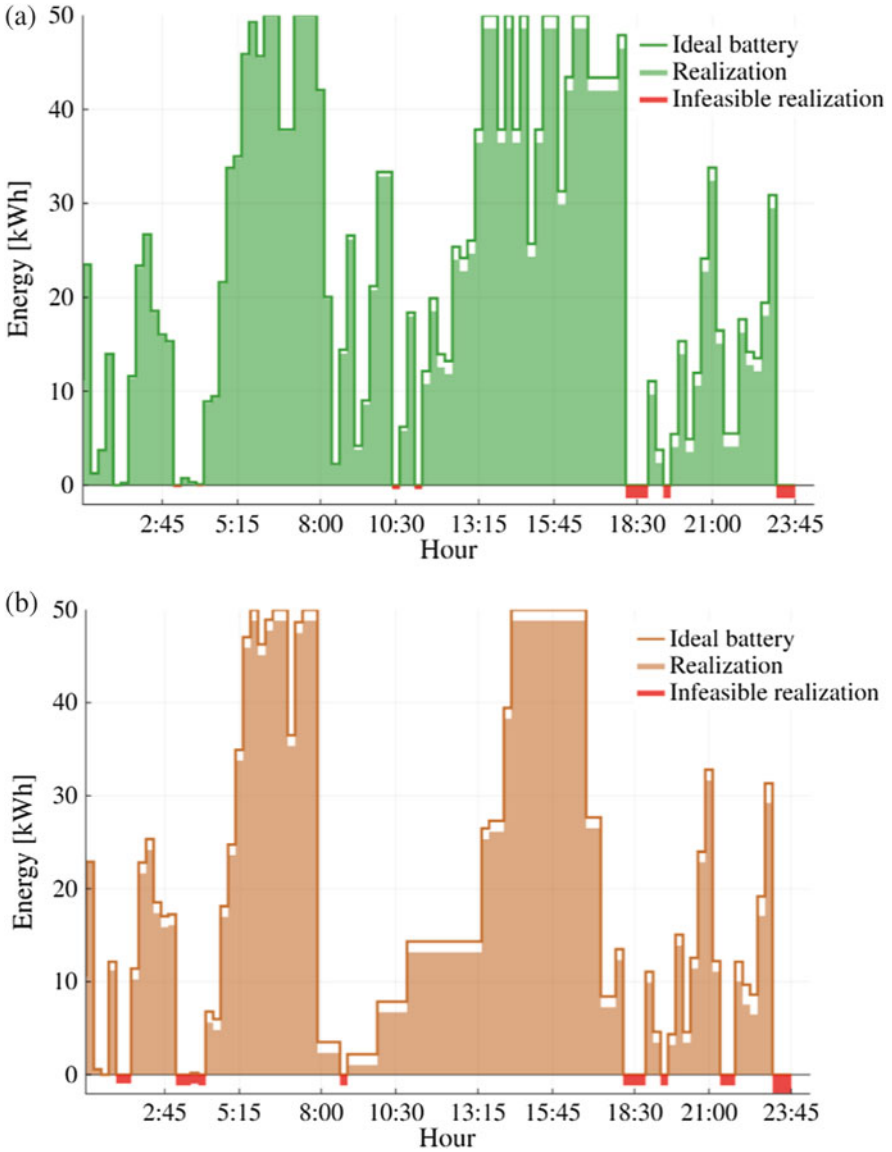
**Fig. 17** Storage energy level for CASE 1−S. The solid line represents the scheduled level, while the shaded area displays the realized energy level after accounting for operation infeasibilities, i.e., limiting the power discharge to a function of the $SOC$. The red area represents negative realized values. (**a**) Storage energy level in scenario 1. (**b**) Storage energy level in scenario 2. (**c**) Storage energy level in scenario 3
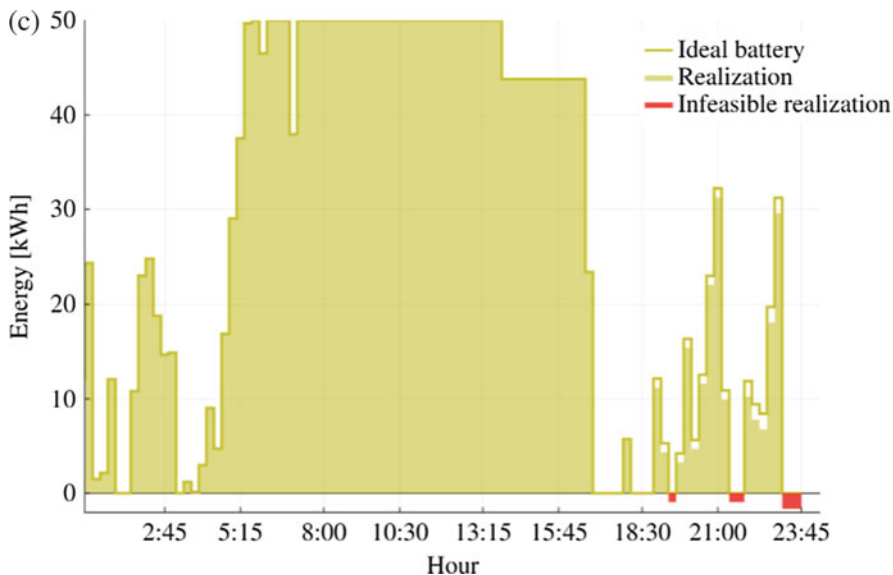
**Fig. 17** (continued)

## 6.2 Value of the Stochastic Solution

Despite the fact that the obtained total costs for the deterministic test cases and their stochastic counterparts were similar, there exist great differences in the solutions, e.g., the amount of imported energy around the noon hours. Such operative differences would come with unfavorable costs increase for the distribution system operator if it were to optimize the system based on a deterministic approach by considering the averaged value of the forecast, and the realized RES generation deviated greatly from it. In order to illustrate and quantify the benefits of using a stochastic model instead of a deterministic one, we compute the value of the stochastic solution (*VSS*) for CASE 2–D. The VSS is calculated as the difference between the expected and realized costs [4]:

1. The CASE 2–D is solved with the averaged RES forecasted and the value of its first-stage decisions will be saved, i.e., power import/export and generation commitment. The total cost obtained will also saved as $z^*_{EV}$ and its called *expected value solution (EV)*.
2. Next, the distribution system is optimized as a two-stage stochastic optimization problem, Model 4, with the forecasted value of $P^{RES}_{t,\omega}$ changing for each scenario, but with the first-stage decisions fixed obtained in 1. The optimal cost for each problem will be stored as $z^*_{EEV}$, known as the *expected result of using the EV solution*. This step is equivalent to quantifying the performance of the first-stage decisions from step 1 in the three scenarios of RES generation.

3. Finally, the value of the stochastic solution is calculated as the difference between the EEV and the EV: $VSS = z^*_{EEV} - z^*_{EV}$.

Based on these steps, $z^*_{EV} = 7906.2€$ and $z^*_{EEV} = 8000.2€$. The calculated value of the stochastic solution for the case with non-ideal energy storage is $94€$ (1.2 % of the total expected cost). This additional cost is the cost paid for ignoring the probabilistic nature of the RES generation during the decision making process. The cost difference can be explained by the inflexibility of the scheduled energy import in the hourly time scale since it does not allow for the deployment of reserves for the balancing of RES generation fluctuations in intra hour time steps.

# 7 Conclusions

In this chapter, we have presented a mixed-integer second-order cone programming (MISOCP) formulation for the optimal operation of distribution systems with energy storage systems and renewable generation. We have recalled to the most conventional model of energy storage in power system literature: a generic and ideal model. Then, we have introduced a detailed formulation of a non-ideal storage model that capture its parameters dependence with the battery's state-of-charge. Although it was mainly based on electrochemical energy storage, the model is general enough to cope with a variety of different technologies. The energy storage model is convexified providing an accurate and simple set of linear constraints that models the storage behavior with no compromise of the computational time. Then, the deterministic operational model is extended to a two-stage stochastic model to consider the uncertainty of renewable generation. Four cases are simulated based on a 33-bus distribution network. Simulation results show that ideal modeling of energy storage could lead to infeasible operation of the energy storage compromising the reliability of the system. The proposed stochastic model with non-ideal energy storage systems appears to be particularly appropriate for distribution networks operation with uncertain RES generation.

# References

1. Anjos, M.F., Conejo, A.J.: Unit commitment in electric energy systems. Foundations and trends in electric energy systems **1**(4), 220–310 (2017)
2. Baran, M., Wu, F.: Network reconfiguration in distribution systems for loss reduction and load balancing. IEEE Trans. Power Delivery **4**(2), 1401–1407 (1989)
3. Berrueta, A., Urtasun, A., Ursúa, A., Sanchis, P.: A comprehensive model for lithium-ion batteries: from the physical principles to an electrical model. Energy **144**, 286–300 (2018)
4. Birge, J.R., Louveaux, F.: Introduction to stochastic programming. Springer Series in Operations Research and Financial Engineering. Springer, New York (2011)
5. Bustos, C., Sauma, E., de la Torre, S., Aguado, J.A., Contreras, J., Pozo, D.: Energy storage and transmission expansion planning: substitutes or complements?. IET Gen. Trans. Distrib. **12**(8), 1738–1746 (2018)

6. Carrion, M., Arroyo, J.M.: A computationally efficient mixed-integer linear formulation for the thermal unit commitment problem. IEEE Trans. Power Syst. **21**(3), 1371–1378 (2006)
7. Castillo, A., O'Neill, R.P.: History of optimal power flow and formulations (2013). https://www.ferc.gov/industries/electric/indus-act/market-planning/opf-papers/acopf-4-solution-techniques-survey.pdf
8. Coffrin, C., Hijazi, H.L., Van Hentenryck, P., The QC relaxation: a theoretical and computational study on optimal power flow. IEEE Trans. Power Syst. **31**(4), 3008–3018 (2016)
9. Fares, R.L., Webber, M.E.: A flexible model for economic operational management of grid battery energy storage. Energy **78**, 768–776 (2014)
10. Federal Energy Regulatory Commission (FERC): Recent ISO Software Enhancements and Future Software and Modeling Plans (2011). https://www.ferc.gov/industries/electric/indus-act/rto/rto-iso-soft-2011.pdf
11. Gómez-Expósito, A., Ramos, E.R.: Reliable load flow technique for radial distribution networks. IEEE Trans. Power Syst. **14**(3), 1063–1069 (1999)
12. Gómez-Expósito, A., Conejo, A.J., Cañizares, C. (eds.): Electric Energy Systems: Analysis and Operation, ser. The Electric Power Engineering Series. CRC Press, Boca Raton (2009)
13. Gonzalez-Castellanos, A.J., Pozo, D., Bischi, A.: Non-ideal linear operation model for Li-ion batteries. IEEE Trans. Power Syst. 1–1 (2019)
14. Gonzalez-Castellanos, A., Pozo, D., Bischi, A.: Online appendix for book chapter: distribution system operation with energy storage and renewable generation uncertainty. Zenodo (2019). Available at: https://zenodo.org/record/2540789
15. Jabr, R.A.: Radial distribution load flow using conic programming. IEEE Trans. Power Syst. **21**(3), 1458–1459 (2006)
16. Kirschen, D.S., Strbac, G.: Fundamentals of Power System Economics. John Wiley & Sons, Hoboken (2004)
17. Kocuk, B., Dey, S.S., Sun, X.A.: Strong SOCP relaxations for the optimal power flow problem. Oper. Res. **64**(6), 1177–1196 (2016)
18. Kocuk, B., Dey, S.S., Sun, X.A.: Inexactness of SDP relaxation and valid inequalities for optimal power flow. IEEE Trans. Power Syst. **31**(1), 642–651 (2016)
19. Lavaei, J., Low, S.H.: Zero duality gap in optimal power flow problem. IEEE Trans. Power Syst. **27**(1), 92–107 (2012)
20. Nasrolahpour, E., Kazempour, J., Zareipour, H., Rosehart, W.D.: A bilevel model for participation of a storage system in energy and reserve markets. IEEE Trans. Sustainable Energy **9**(2), 582–598 (2018)
21. Nick, M., Cherkaoui, R., Paolone, M.: Optimal allocation of dispersed energy storage systems in active distribution networks for energy balance and grid support. IEEE Trans. Power Syst. **29**(5), 2300–2310 (2014)
22. NOAA Earth System Research Laboratory: ESRL Global Monitoring Division – GRAD – Surface Radiation Budget Network (SURFRAD). https://www.esrl.noaa.gov/gmd/grad/surfrad/dataplot.html
23. Pozo, D., Contreras, J., Sauma, E.E.: Unit commitment with ideal and generic energy storage units. IEEE Trans. Power Syst. **29**(6), 2974–2984 (2014)
24. Pudjianto, D., Aunedi, M., Djapic, P., Strbac, G.: Whole-systems assessment of the value of energy storage in low-carbon electricity systems. IEEE Trans. Smart Grid **5**(2), 1098–1109 (2014)
25. Qadrdan, M., Jenkins, N., Wu, J.: Smart grid and energy storage. In: McEvoy's Handbook of Photovoltaics, pp. 915–928. Elsevier, Amsterdam (2018)
26. Sabillón, C.F., Franco, J.F., Rider, M.J., Romero, R.: Mathematical optimization of unbalanced networks with smart grid devices. In: Shahnia, F., Arefi, A., Ledwich, G. (eds.) Electric Distribution Network Planning, pp. 65–114. Springer, Singapore (2018)
27. Safdarian, A., Fotuhi-Firuzabad, M., Lehtonen, M.: A stochastic framework for short-term operation of a distribution company. IEEE Trans. Power Syst. **28**(4), 4712–4721 (2013)

28. Sugihara, H., Yokoyama, K., Saeki, O., Tsuji, K., Funaki, T.: Economic and efficient voltage management using customer – owned energy storage systems in a distribution network with high penetration of photovoltaic systems. IEEE Trans. Power Syst. **28**(1), 102–111 (2013)
29. Zidar, M., Georgilakis, P.S., Hatziargyriou, N.D., Capuder, T., Škrlec, D.: Review of energy storage allocation in power distribution networks: applications, methods and future research. Transm. Distrib. IET Gen. **10**(3), 645–652 (2016)

# Network Reconfiguration in Modern Power Distribution Networks

**Aggelos S. Bouhouras, Paschalis A. Gkaidatzis, and Dimitris P. Labridis**

**Abstract** This chapter introduces the Network Reconfiguration (NR) concept in Distribution Networks (DNs) as an efficient scheme to face various operational issues like reliability improvement and loss reduction. Furthermore, the potential for utilizing NR to perform voltage profile improvement under high DG or Renewable Energy Sources (RESs) penetration is presented. Finally, the coordination of the NR along with the optimal siting and sizing of DG units aiming to maximize their impact on loss reduction is also analyzed. The basic aim of this chapter is to demonstrate how specific automation upgrade in modern DNs regarding the replacement of manual switching equipment by automated controlled sectionalizers or tie-switches could allow Distribution System Operators (DSOs) to integrate real time management techniques of the DN under relatively low investment plans. Specific examples regarding both real and benchmarked DNs are included and the proposed algorithms are explained in detail.

## 1 Introduction

Modern power Distribution Networks (DNs) are experiencing significant alternations regarding both their structural and infrastructural aspects. The implementation of the Smart Grid concept, along with the high Distributed Generation (DG) and Renewable Energy Sources (RESs) penetration, have facilitated in upgrading the automation level in DNs and in establishing a more de-centralised generation model. On the one hand the installation of remote controlled elements [24], e.g. automatic

A. S. Bouhouras
Department of Electrical and Computer Engineering, University of Western Macedonia, Kozani, Greece
e-mail: abouchou@teiwm.gr

P. A. Gkaidatzis (✉) · D. P. Labridis
School of Electrical and Computer Engineering, Aristotle University of Thessaloniki, Thessaloniki, Greece
e-mail: pgkaidat@ece.auth.gr; labridis@ece.auth.gr

reclosers and remote controlled circuit breakers, the enhanced metering capabilities under the Advanced Metering Infrastructure (AMI) and Phasor Measurements Units (PMUs) integration [29], as well as the upgraded Information and Communication Technology (ICT) capabilities [13] have radically changed the conventional form of the DNs by enabling the transition of their traditional passive profile to a more active one. In this latter context, all entities interact with each other in order to optimize their goals but at the same time they improve several operational aspects of the network with economic benefits for all parts. On the other hand, DG and RES penetration has reached or even exceeded saturation level in many parts of the DN, causing unexpected issues such as overvoltage and reverse power flow [1, 12]. Under these operating conditions, DNs undergo bidirectional power flow and its impact on protection schemes, e.g. one direction fault indicators and fault relays, should be faced properly to prevent the reliability level to be reduced. Additionally, the rapid penetration of Electric Vehicles (EVs) [35], the required charging lots that are scheduled to be installed, as well as the Battery Energy Storage Systems (BESSs) that are promoted as efficient storage solutions, in both distributed and centralized form, add complexity on the DN design, operation and management.

The DSOs are responsible for maintaining uninterruptible power supply via a reliable and robust DN under the minimum cost for both themselves and the consumers. Usually, the load growth demand along with mid or long term interferences to the grid are faced with respective investment plans regarding the reinforcement or the expansion of the DN [17]. Moreover, emergency situations like short circuit faults or other kind of outages have already been studied within a scenario case framework and based on simulations, emergency plans and guided actions have been developed. The problem is that the intermittent behavior of the RES generation and the time varying load demand along with the complexity added by EVs and BESS regarding the power control in the grid, render an imperative need for real time interventions. One of the most efficient ways to rearrange the power flow in the DN relies on exploiting its topology. DNs operate as radial networks, but they are designed as meshed ones. The concept here is that all main lines have at least two feeding points, but under normal operation conditions they are fed only by one. The other one plays the role of a standby alternative feeding source that is ready to supply the loads, all or some of them depending on the available capacity of the respective feeder, mainly in cases of outages. In these latter cases, appropriate switching operations could enable the line to be fed by two feeders and still preserve its radial structure. This intervention scheme is called Network Reconfiguration (NR) and it has initially been performed for reliability improvement during outages.

The implementation of NR has soon attracted a lot of interest, since it was found out that the layout alteration of the DN could change the loading level of the network's branches and yield voltage profile improvement and loss reduction. This potential is further enhanced by the fact that a great number of tie-switches in DNs enables numerous possible configurations and thus, it increases the possibility of yielding the best needed one under various loading and operational conditions of the network. Therefore, it could be found rational to believe that instead of adjusting the demand and generation power uncertainties of the current modern and rather

complex DN to the network's fixed topology, the opposite could more efficiently serve the Smart Grid concept towards the implementation of a more active and self-healing grid. For example, under high RES generation and reverse power flow, appropriate NR could mitigate the congestion of the DN and relief the branches overloading that cause overvoltage and loss reduction. Therefore, in this case, NR could contribute in increasing RES penetration in DNs. The same concept could also be implemented under the high load demand during the EVs charging while it could also be combined with the BESS operation to further exploit these potentials.

This chapter presents the concept of NR in DNs towards reliability improvement and loss reduction. Initially, reliability in DNs is analyzed along with its performance metrics, namely the reliability indices. Subsequently, the idea of NR in order to perform fault isolation and power restoration during an outage is described and some examples are presented. Some of the most widely utilized heuristic and metaheuristic based approaches are in turn discussed in order to highlight both the problem complexity and these aforementioned algorithms' contribution to solving the problem with less computational burden and within acceptable computational times. Next, the potential of NR to power and energy loss reduction is explained. Firstly, the respective section distinguishes power loss reduction from energy loss reduction by analyzing the problem's dependency from load variations for the latter case. Secondly, the problem formulation along with the respective NR scheme are analyzed for both cases and examples are given on benchmarked DNs. Finally, in the last section the idea of applying the NR scheme in modern DNs with high DG is examined in order to face new arising issues like reverse power flow and overvoltage and also to analyze the schemes of NR and optimal sizing and siting of DG units for loss reduction. At the end of the chapter the basic conclusions derived are discussed.

## 2 Reliability Improvement

### 2.1 Reliability in Distribution Networks

One of the earliest references in the reliability concept for DNs is presented by L.B Crann in [15], where the key role of the sectionalizing switches in DNs towards reliability improvement is explained for the first time. Moreover, reliability is directly related to the average time for which a consumer experiences an outage. Later on, other approaches pointed out that fault occurrence in DN follow a Marcov chain [16] and that outages should not be considered independent to each other [18], because under such an approach the reliability level could be underestimated. Billinton [6, 7] was the first who tried to develop formulas to quantify both the frequency and the duration of the interruptions, which in turn led to the formulation of the reliability indices [34]. Reliability improvement refers to either the reduction of the interruption frequency in a DN or to the interruption time minimization after an outage. Obviously, the former has an impact on the latter but in order

**(a)**



**(b)**
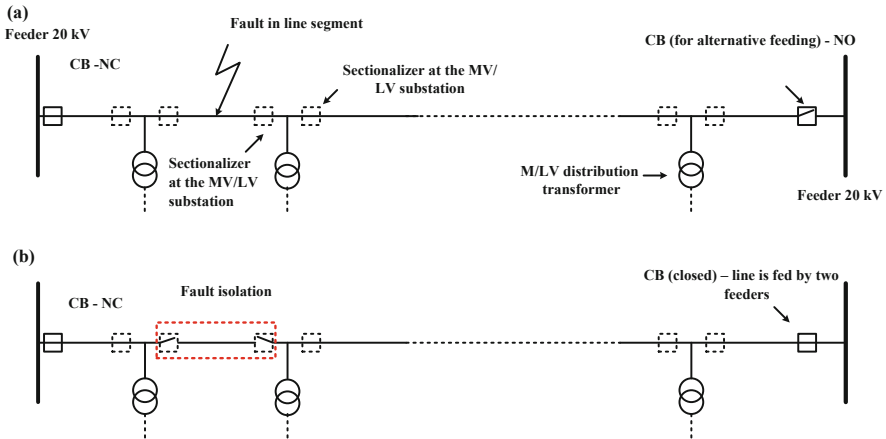


**Fig. 1** Fault isolation and power restoration scheme in MV line

to efficiently manage the power restoration scheme, automation upgrade in DN switching equipment is necessary. This is due to the fact that the largest number of both sectionalizers and tie-switches is manually operated and thus the appropriate switching operations for fault isolation and power restoration could be very time consuming. Additionally, the guideline regarding the proper switching operation sequence has a vital role towards reliability improvement and several on/off real time methodologies have been presented [3, 21, 31]. In Fig. 1 a simple example referring to the fault isolation and power restoration scheme for a single radial MV feeder is presented, where CB refers to Circuit Breaker, NC to Normally Closed status, NO to Normally Open status and LV to Low Voltage.

In Fig. 1a a simple representation of the DN layout for a single line is illustrated where it is obvious that although the DN operates as a radial one it is actually designed as a meshed one since the line has the capability for simultaneous feeding by two respective MV feeders. In Fig. 1b the fault isolation and power restoration scheme are presented. The idea here is to locate the fault within the shortest possible line segment, i.e. between two adjacent MV/LV transformers, by opening the respective sectionalizers at these respective line edges. Then, the upstream part of the line will continue its feeding by the left MV feeder, while the loads of the downstream part of the line will be delivered (given that the capacity of the feeder is adequate) by the right MV feeder. In the case where the right-alternative MV feeder lacks of enough capacity to deliver all load of the downstream line part then some MV/LV transformers will inevitably be disconnected and their consumers will be out of service. In this latter case, these consumers will experience an outage and for them reliability issues will be raised.

The example shown in Fig. 1 is quite simple and the fault isolation and power restoration scheme is quite straightforward. In most MV DNs having numerous sectionalizers and many tie-switches the layout is more complex and therefore

many alternative configurations of the DN could perform the power restoration for the loads after the fault isolation. In these cases, the complexity of the problem regarding the optimal configuration that could efficiently restore power to the maximum possible number of consumers within the shortest time period is quite challenging, due to the numerous possible switching operations. Usually, such dynamic combinatorial problems with topology and operational constraints are described as Nondeterministic Polynomial time (NP) complexity class problems and they can be addressed by either real time operational schedules regarding the switching operations or by distributed advanced monitoring and operational schemes, like Multi-Agent systems [5]. Another alternative is to utilize heuristic and metaheuristic based methodologies [2, 32], in order to come up with a relatively efficient solution within acceptable computational time under a near-real time approach.

## 2.2 Reliability Assessment in DNs

The reliability level of a DN constitutes a performance indicator on the services provided to the consumers and thus within the liberalized energy market the customers are expected to have choices regarding not only the energy provider preferred but also the DSO. Thus, DSOs invest on automation upgrade and on advanced monitoring schemes in order to be able to respond to outages and to achieve power restoration as soon as possible. Alternatively, network reinforcements aim in reducing the interruption frequency across the network, causing a high reliability level that benefits both the operator and the consumers. Reliability cost is the cost for the DSO in order to reach a predefined reliability level via investments related to the two aforementioned approaches, while reliability worth is the benefit for the DSO by the obtained reliability improvement. From the economic point of view, we usually refer to cost of unreliability [20], which defines that the reliability worth should be matched with the customers' cost during an outage. Based on this clarification, the feasibility study of a DSO regarding potential investment should consider (a) the revenue after reliability improvement by the energy not supplied and (b) the benefit due to the fact that customer interruption cost would be reduced. In Fig. 2 the cost for both the DSO and the consumers in respect to reliability level is presented.

From Fig. 2 it is evident that for the consumers the higher the reliability the lower the interruption cost, since the outage time is lower, while for the DSO the case is completely the opposite, since investments are required in order to increase the reliability level of the DN. Still, the point where these two lines intersect, i.e. point A in Fig. 2, indicates the minimum of the total cost curve for both the DSO and the consumers in terms of the best tradeoff between the individual costs. In this context, the corresponding cost indicated by point A should be considered feasible by the DSO in order to perform investment plans for reliability improvement.
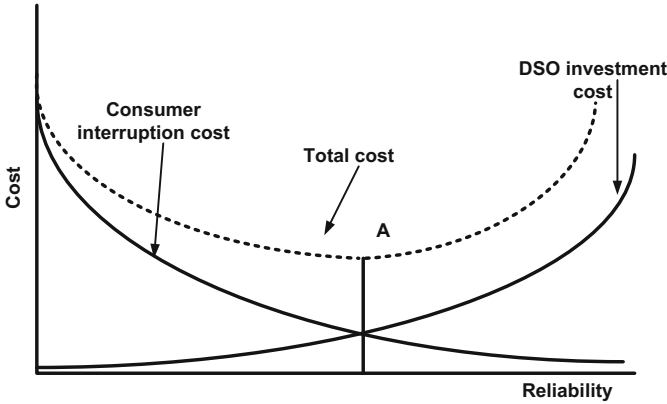
**Fig. 2** Cost vs. reliability for both the DSO and the consumers

## 2.3 Reliability Indices

The most widely utilized indices for the evaluation of the reliability level for a DN
are summarized as follows [34]:

- System Average Interruption Duration Index—$SAIDI$

$$SAIDI = \frac{\sum Customer\ Interruption\ duration}{Total\ number\ of\ Customers\ served} \tag{1}$$

For the computation of the index value, the following formulae is used:

$$SAIDI = \frac{\sum r_i N_i}{N_T} = \frac{CMI}{N_T} \tag{2}$$

where:
- $r_i$: is the time needed for power restoration for each consumer,
- $N_i$: is the number of consumers that experience an outage during the examined
  time period,
- $N_T$: the total number of consumers served by the examined DN
- $CMI$: outage duration for the consumer that experience the interruption
- System Average Interruption Frequency Index—$SAIFI$

$$SAIFI = \frac{\sum Customers\ interrupted}{Total\ number\ of\ customers\ served} \tag{3}$$

For the computation of the index value, the following formulae is used:

$$SAIFI = \frac{\sum N_i}{N_T} = \frac{CI}{N_T} \qquad (4)$$

where:
– $CI$: is the number of customers that experience an outage
• Customer Average Interruption Durations Index—$CAIDI$

$$CAIDI = \frac{\sum Customer\ Interruption\ Duration}{Total\ number\ of\ customers\ interrupted} = \frac{SAIDI}{SAIFI} \qquad (5)$$

For the computation of the index value, the following formulae is used:

$$CAIDI = \frac{\sum r_i N_i}{N_i} \qquad (6)$$

• Average Energy Not Supplied Index—$AENS$, or Expected Energy Not Supplied—$EENS$
This index expresses the amount of energy that the consumer will fail to be provided due to the outage. Usually it is computed as the product of the average loading of the consumer during the outage to the duration of the outage and is expressed in kWh/year.

## 2.4 Selective Automation Upgrade for Reliability Improvement

In order to highlight the impact of automation upgrade in DNs towards reliability improvement, a simple example regarding the replacement of a small targeted number of manual sectionalizers with automated ones will be briefly presented. The examined real urban DN consists of five MV underground 3-phase cables and they all feed in total 62 MV/LV (20/0.4 kV) distribution transformers, as illustrated in Fig. 3. There are also four tie-switches at the ends of the lines in order to allow NR in cases of outages.

In order to keep the investment cost as lower as possible, only the case of upgrading the minimum possible number of sectionalizers will be examined and the impact on the reliability indices will be evaluated [10]. Therefore, it is considered that only the sectionalizers of the middle MV/LV transformer of each line are replaced with automated ones. Under this approach, it will be possible to immediately isolate the fault either to the first or to the second half of the faulted line, without the need for time delays caused by manual switching operations that
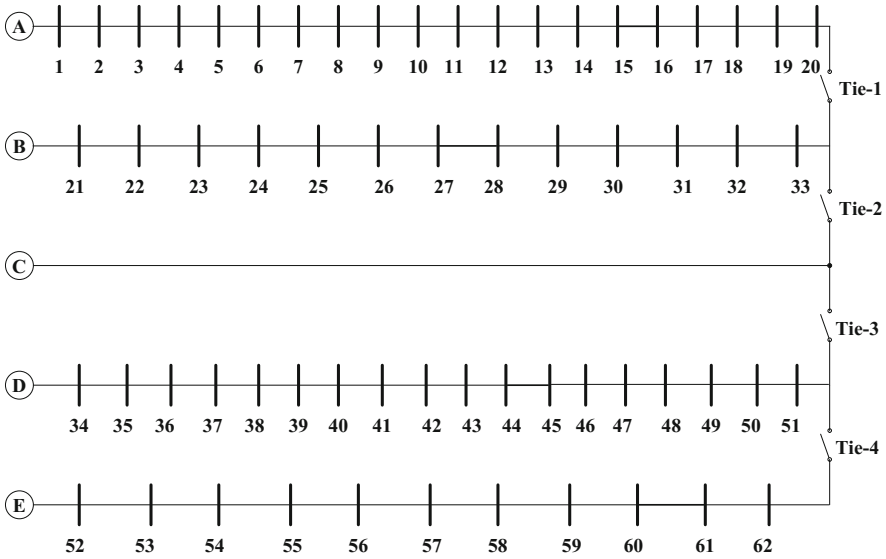
**Fig. 3** DN with manual sectionalizers

require human interference. After the isolation of the fault, the remaining manual switching operations have to be performed to only the half segment of the line, meaning that (a) almost half consumers will experience almost immediate power restoration (the healthy part of the line will be fed by an alternative feeder) and (b) the power restoration for the faulted line segment will be performed within a very short time period. In Fig. 4 the DN with the selected manual switches to be upgraded is presented, while in Table 1 the input data regarding the performed simulations for the reliability assessment are shown.

In Table 2 the simulation results (performed in Neplan$^{©}$ software package) [10] regarding the reliability improvement after the targeted automation upgrade are presented. It should be clarified that for the presented analysis only first order faults, i.e. only one fault at line segment, have been considered. It is observed that even under the examined limited automation upgrade with only two sectionalizers to be replaced by automated ones, the reliability improvement is significant for all lines. The latter is evident in both terms of SAIDI and EENS indices reduction. It should also be clarified that, as presented in Table 1, the initial CAIDI index value coincides with the considered time for power restoration in the initial state of the DN.
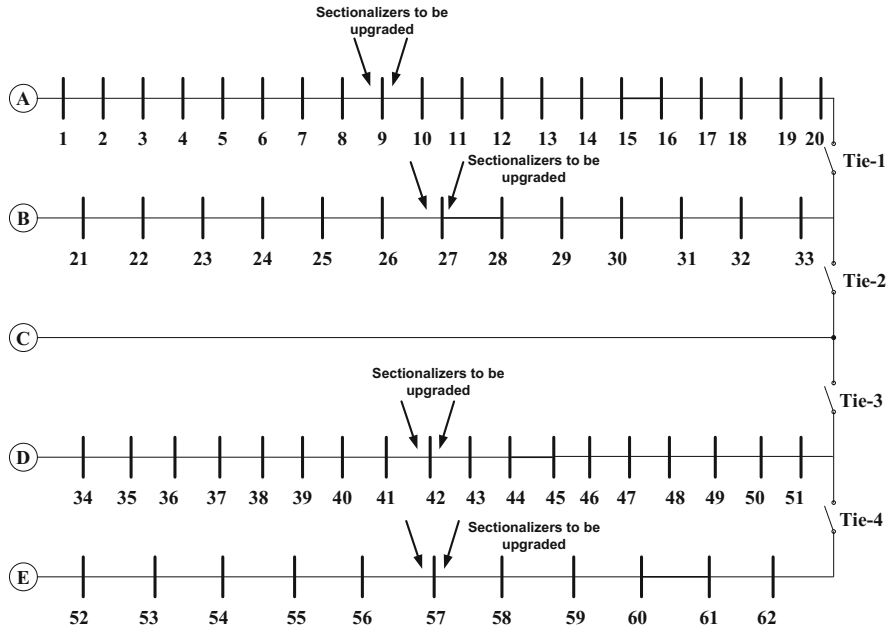
**Fig. 4** Selected automation upgrade to targeted sectionalizers

**Table 1** Reliability
assessment input data

| | |
|---|---|
| Number of MV/LV transformer | 62 |
| DN nominal capacity (kVA) | 42.44 |
| Total line length of DN (km) | 20.743 |
| Annual fault frequency (1/km/yr) | 0.1 |
| Average time for power restoration (h) | 2 |

**Table 2** Reliability improvement after targeted automation upgrade

| Reliability | Initial State | | | | Automation upgrade state | | | |
|---|---|---|---|---|---|---|---|---|
| | Manual sectionalizers only | | | | Targeted sectionalizer replacement 2 sectionalizers at the middle of the line (see Fig. 4) | | | |
| Indices | Line A | Line B | Line D | Line E | Line A | Line B | Line D | Line E |
| SAIFI (1/yr) | 0.63 | 0.49 | 0.53 | 0.436 | 0.63 | 0.49 | 0.53 | 0.43 |
| SAIDI (min/yr) | 74.77 | 58.95 | 64.13 | 51.07 | 45.73 | 28.39 | 34.65 | 38.05 |
| CAIDI (h) | 2 | 2 | 2 | 2 | 1.22 | 0.96 | 1.02 | 1.49 |
| EENS (MWh) | 3.41 | 1.288 | 2.60 | 1.12 | 2.10 | 0.66 | 1.335 | 0.85 |

# 3   Loss Reduction via Heuristic and Metaheuristic Algorithms for Network Reconfiguration

## 3.1   *Loss Reduction in DNs*

The NR scheme that was initially utilized for reliability purposes was soon found to be an efficient technique towards loss reduction/minimization in DNs [27]. As in reliability improvement, the core concept here also relies on load transferring among feeders via tie-switches. The main idea behind this approach is that under a more efficient distribution of the network's loads to the available feeders, the loading of most lines could, as uniformly as possible, be also distributed among the feeders. Thus, since the power losses are in direct relationship with the square of the lines' current, even a small reduction of the lines' loading could yield significant loss reduction. The problem of loss reduction via NR is a mixed integer nonlinear programming problem (MINLP) with both binary and integer variables. An objective function $OF$ could be formed as:

$$OF = \min \sum_{z=1}^{n_l} R_z I_z^2 \tag{7}$$

where:

- $n_l$: is the total number of lines of the DN,
- $R_z$: is the resistance of line $z$,
- $I_z$: is the rms current of line $z$.

The $OF$ shown in Eq. (7) could be formed based only on the voltage values of the DN nodes, as presented in Eq. (8):

$$OF = \min \sum_{\substack{i,j=1 \\ i \neq j}}^{n_b} g_{i,j}(V_i^2 + V_j^2 - 2V_i V_j \cos(\theta_i - \theta_j)) \tag{8}$$

where:

- $n_b$: is the total number of buses of the DN,
- $g_{i,j}$ is the conductance between buses $i$ and $j$,
- $V_i$, $V_j$ are the voltage magnitudes of buses $i$ and $j$,
- $\theta_i$, $\theta_j$ are the voltage angles of buses $i$ and $j$.

Both of the $OF$ variants presented in Eqs. (7) and (8) are subject to the following constraints under the NR scheme:

- equality constraints referring to the power flow equations, as in Eqs. (9) and (10):

$$\sum_{i=1}^{n_b} \left\{ P_{G,i} - P_{D,i} - \sum_{\substack{j=1 \\ i \neq j}}^{n_b} |V_i||V_j||Y_{i,j}| \cos(\delta_{i,j} - \theta_i + \theta_j) \right\}^2 = 0 \qquad (9)$$

$$\sum_{i=1}^{n_b} \left\{ Q_{G,i} - Q_{D,i} + \sum_{\substack{j=1 \\ i \neq j}}^{n_b} |V_i||V_j||Y_{i,j}| \sin(\delta_{i,j} - \theta_i + \theta_j) \right\}^2 = 0 \qquad (10)$$

where:
- $P_{G,i}$ is the real power generation on bus $i$,
- $Q_{G,i}$ is the reactive power generation on bus $i$,
- $P_{D,i}$ is the real power demand on bus $i$,
- $Q_{D,i}$ is the reactive power demand on bus $i$,
- $Y_{i,j}$ is the magnitude of bus admittance element $i, j$,
- $\delta_{i,j}$ is the angle of bus admittance element $i, j$.
- upper and lower voltage limits for the DN as defined by inequality constraint in Eq. (11):

$$V_i^{min} \leq V_i \leq V_i^{max} \qquad (11)$$

where:
- $V_i^{min}$: the lower voltage limit of bus $i$,
- $V_i^{max}$: the upper voltage limit of bus $i$.
- Loading level of each branch lower than its ampacity level as defined in inequality constraint in Eq. (12):

$$I_z \leq I_z^{max} \qquad (12)$$

where:
- $I_z$: is the maximum thermal line limit of line $z$.
- DN radial structure. The switching operation of an initially open tie-switch is expected to form a loop across the DN and thus at least one sectionalizer should open within the loop in order to reestablish the radial structure of the DN. The simplest formulation of this constraint is presented in Eq. (13):

$$n_l = n_b - 1 \qquad (13)$$

## 3.2 Network Reconfiguration for Loss Reduction Based on Heuristics

The optimal solution for the loss minimization problem via NR refers to the identification of the proper switching operations in terms of closing a number of initially open tie-switches and of opening a respective number of sectionalizers, while all the constraints described earlier are satisfied. The problem here is that, given the number of switches for a DN is $m$, then the possible switching operations to be investigated are equal to $2^m$. The latter means that for a real DN with numerous sectionalizers the computational burden becomes very high and the problem cannot be solved within acceptable computational time. This is due to the fact that after a switching operation, a load flow analysis should be performed in order to evaluate the value of the $OF$ and examine whether all constraints are satisfied. In Table 3 the required time for the load flows calculations regarding three small sized DNs are presented. It should be clarified that the time for a single load flow is approximately 25 ms, as derived by a load flow analysis software on an average PC.

Based on the data in Table 3 it is quite evident that the exhaustive search of the solution space is very time consuming for this kind of problem. Even if the computational time for each load flow simulation may fall down to 1/1000 of the value utilized here, i.e. 25 μs, it is clear again that the final solution could not be reached within a reasonable time period. This is where heuristics mechanisms come up to give the solution.

A heuristic mechanism is a solution search strategy that relies on prior knowledge about the problem which is used in order to facilitate the solution. Usually, this knowledge is matched with practical judgment that is ruled by common sense and is called heuristic rule. In general, the solution of problem by heuristics is faced as a form of mapping the definition space $D$ of the problem to its solution space $S$. As stated earlier, the number of possible solutions for the NR problem is enormous and thus the exhaustive search of the solution space is time consuming. Heuristics mechanisms guide this search to specific parts of the solution space in order to speed up the solution procedure. In Fig. 5 a graphical representation of this scheme is illustrated.

The basic advantage of the heuristic algorithms is highlighted in Fig. 5, where it is obvious that through the heuristic rules the solution space search is limited to specific parts. The point though in this case is that since some parts are excluded,

**Table 3** Indicative simulation time for load flow simulations regarding a pair of switching operations

| Number of sectionalizers for DN | Number of required load flow simulations | Total simulation time (s) |
|---|---|---|
| 13 | $2^{13}$ | 203 |
| 29 | $2^{29}$ | $1.33E + 07$ |
| 58 | $2^{58}$ | $7.2E + 15$ |
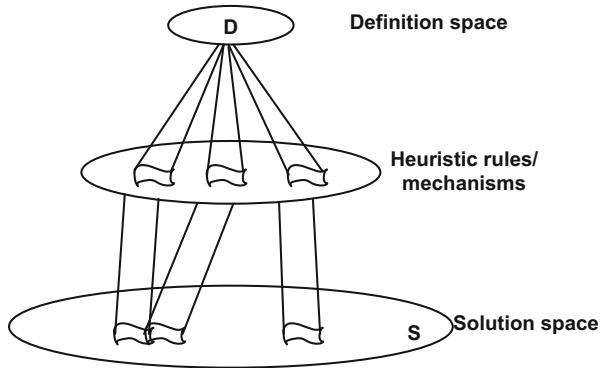
**Fig. 5** Graphical representation of heuristic mechanism

the algorithm cannot guarantee the global optimal regardless the performance of the heuristic rules. Moreover, since the heuristic rules constitute decision making rules that depend on prior knowledge about the problem, usually named as "knowledge of engineer", they are case dependent and their efficiency in not ensured for all possible cases. Nevertheless, heuristics have been widely utilized for the NR problem, either as the sole solution algorithm or by acting as subsidiary subroutine to analytical or other optimization methodologies.

One of the first attempts to deal with the NR problems towards loss minimization was based on two simple heuristic rules [14] that aimed to guideline NR procedure in a specific manner that could perform both efficient loss reduction and minimum switching operations. The first heuristic rule prioritizes the closing of the initially open tie-switches based on the voltage difference across them, because the highest voltage difference indicates that the respective feeders at the low and high dynamic edges of the tie-switch experience low and heavy loading conditions respectively. Therefore, since the NR scheme basically aims in uniformly distributing the network's loads to the available feeders, a good start could be the transferring of loads between feeders with low and high loading. The second heuristic rule indicates the sectionalizer to open across the formed loop after the tie-switch is closed, in order to regain the radial structure of the DN. Based on this rule the branch to open is the one carrying the minimum current within the loop, since the respective sectionalizer opening would cause the lowest transient interruption with the minimum impact on the DN. The implementation of the NR scheme based on these heuristic rules is summarized in the flowchart presented in Fig. 6.

It should be noted that the threshold $\epsilon$ in Fig. 6 plays the role of the convergence criterion for the algorithm implementation: a low value for this threshold indicates that the respective feeders at the edges of the tie-switch are almost equally loaded and thus, no load transfer between them could lead to further loss reduction. Alternatively, the value of $\epsilon$ could be set to zero and in this case all tie-switches of the DN will be examined, regarding their potential to contribute to further loss reduction performing further NR.

**Fig. 6** Flowchart for NR
with heuristic rules
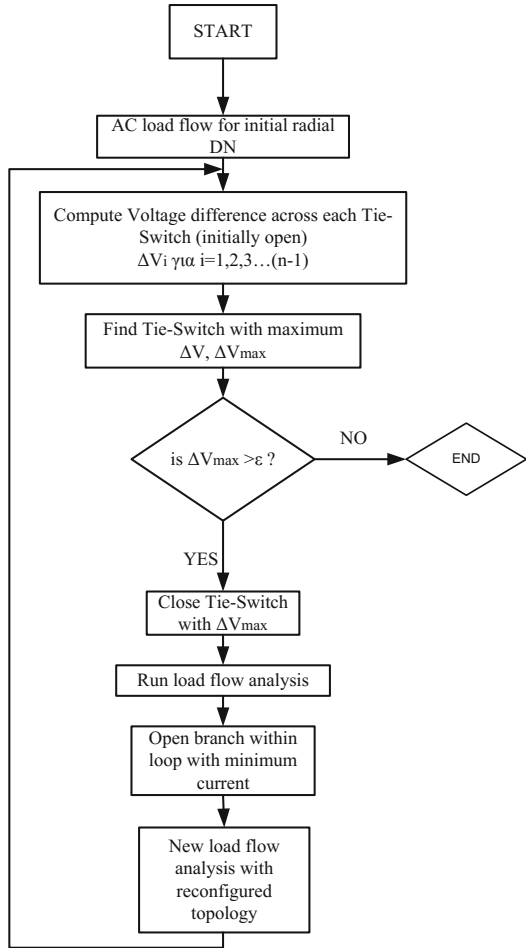


The presented algorithm in Fig. 6 is applied on the benchmarked 33 bus system
[23]. The layout of the DN is illustrated in Fig. 7 and the switching operations
that implement the NR scheme are presented in Table 4. The reconfigured DN is
presented in Fig. 8, in which the red circles indicate the open sectionalizers at the
respective branches. The application of the proposed NR scheme yields 33.65%
loss reduction (from 211 kW to 139.98 kW), which is the same found in other
methodologies in literature [23]. It should be stated though that under the presented
heuristic approach, only 11 load flow analyses are required instead of $2^{33}$ that would
be needed if the solution space had to be exhaustively searched for the optimal
solution.
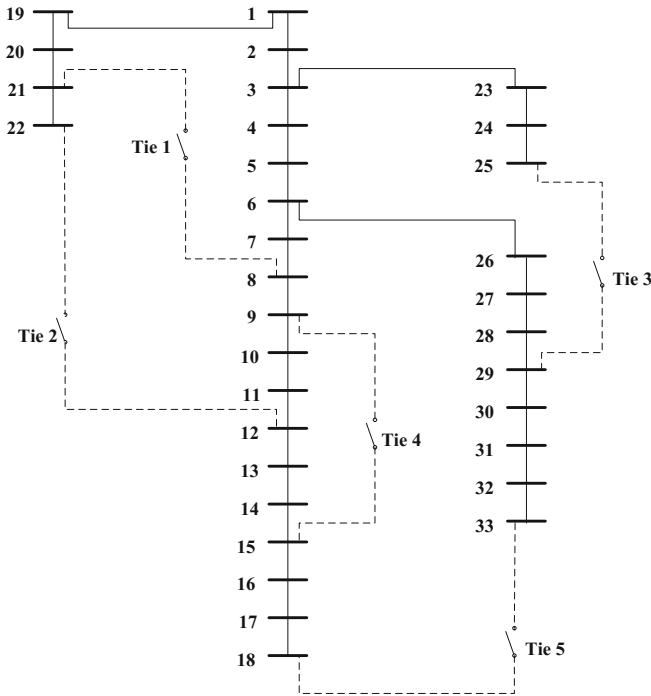
**Fig. 7** 33 bus system

## 3.3 Network Reconfiguration for Loss Reduction Based on Metaheuristics

The proposed technique presented in the previous section is a knowledge-based heuristic methodology that performs NR in compliance with specific rules that are formed based on system experience [33] and is considered to be the more straightforward of the relating techniques with the basic drawback to be the weakness to guarantee the optimal solution for large and complex DNs. The latter is faced by the so called meta-heuristic algorithms which are utilized for complex optimization problems since due to their structure and formulation they solve the problem iteratively without derivative information about the problem itself [33]. The basic advantage of the metaheuristic algorithms is that the possibility for local minima entrapment is less than the heuristic based algorithms and under proper parametrization they perform well providing efficient solutions. Figure 9 summarizes the NR classification methods with emphasis on metaheuristic ones [33].

In this section the binary Particle Swarm Optimization (PSO) is presented with the $OF$ shown in Eq. (8). PSO is a population based algorithm initially proposed in [22]. In PSO a swarm of particles is designated to explore the solution space.

**Table 4** Switching operations for NR based on heuristics—33 bus system

| $\Delta V$ across tie-switches (kV) | Closing tie-switch with maximum $\Delta V$ | Formed loop after closing tie-switch | Branch within formed loop to open |
|---|---|---|---|
| *1st step* | | | |
| (Tie 1) 0.64427 | No | * | * |
| **(Tie 2) 0.81897** | Yes | 2-19-20-21-22-12-11-10-9-8-7-6-5-4-3-2 | **9–10** |
| (Tie 3) 0.55514 | No | * | * |
| (Tie 4) 0.22737 | No | * | * |
| (Tie 5) 0.44180 | No | * | * |
| *2nd step* | | | |
| (Tie 1) 0.27206 | No | * | * |
| **(Tie 3) 0.4374** | Yes | 3-23-24-25-29-28-27-26-6-5-4-3 | **28–29** |
| (Tie 4) 0.5773 | No | * | * |
| (Tie 5) 0.26459 | No | * | * |
| *3rd step* | | | |
| (Tie 1) 0.08963 | No | * | * |
| **(Tie 4) 0.24029** | Yes | 2-19-20-21-22-12-13-14-15-9-8-7-6-5-4-3-2 | **14–15** |
| (Tie 5) 0.16382 | No | * | * |
| *4th step* | | | |
| (Tie 1) 0.23699 | No | * | * |
| **(Tie 5) 0.24649** | Yes | 3-23-24-25-29-30-31-32-33-18-17-16-15-9-8-7-6-5-4-3 | **32–33** |
| *5th step* | | | |
| **(Tie 1) 0.23699** | Yes | 2-19-20-21-8-7-6-5-4-3-2 | **7–8** |

The asterisk shows that no particular loop has been formed, since no tie-switch has closed
Bold values indicate the best solution reached at every step of the solving method

The particles' position changes depending on their personal experience (personal best—pbest), that of either the whole swarm (global best—gbest) in the case of Global PSO (GPSO), or that of their neighbors' (local best—lbest), in the case of Local PSO (LPSO), and finally that of their previously obtained velocity, as shown in Fig. 10.

In Eqs. (14) and (15) the expressions describing the velocity and the position alteration of each particle are presented [22].

$$v_i(t+1) = \chi\left[v_i(t) + c_1 R_1\Big(P_i(t) - X_i(t)\Big) + c_2 R_2\Big(P_g(t) + X_i(t)\Big)\right] \quad (14)$$

$$X_i(t+1) = X_i(t) + v_i(t+1) \quad (15)$$
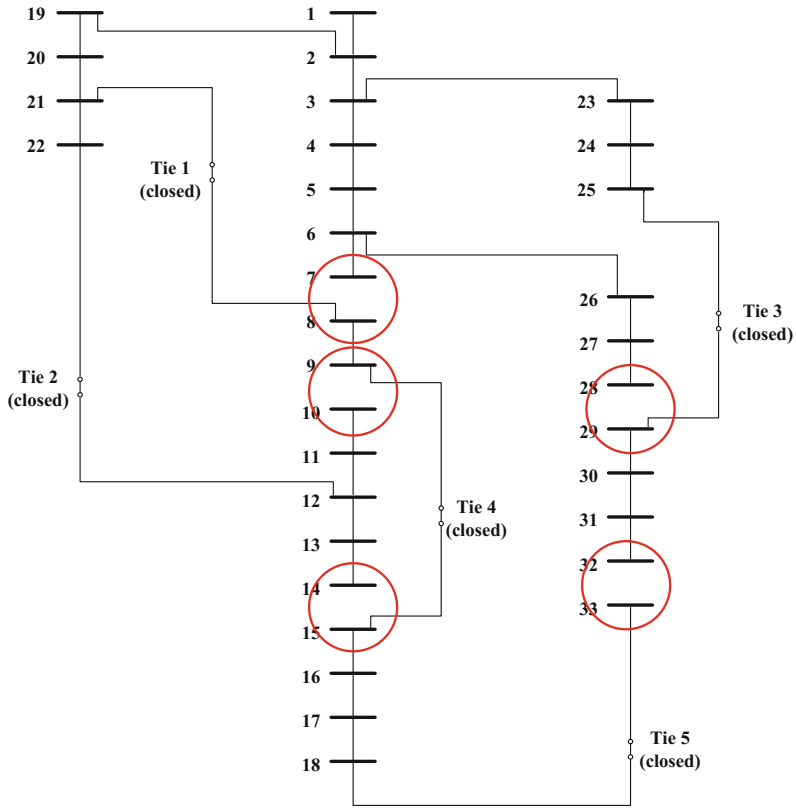
**Fig. 8** Reconfigured topology for the 33 bus system via heuristic rules

where:

- $i = 1, 2, \ldots, N$ and $N$: is the number of particles,
- $X_i(t)$: the current position of particle $i$,
- $X_i(t + 1)$: its future position,
- $v_i(t)$: its current velocity,
- $v_i(t + 1)$: its future velocity,
- $P_i(t)$: its personal best, pbest,
- $P_g(t)$: gbest or lbest,
- $c_i$: weighting factors, also called the cognitive and social parameters, respectively,
- $R_i, i \in [1, 2]$: random variables uniformly distributed within $[0, 1]$,
- $\chi$: the constriction coefficient or factor, formulated as:

$$\chi = \frac{2}{|2 - (c_1 + c_2) - \sqrt{(c_1 + c_2)^2 - 4(c_1 + c_2)}|} \tag{16}$$
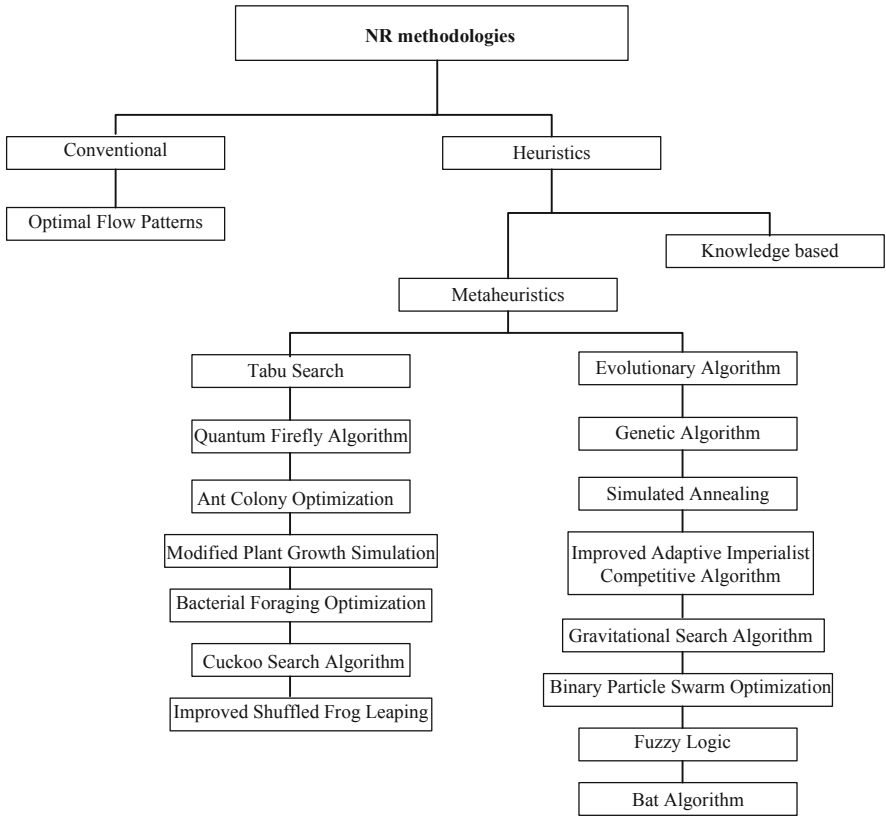
**Fig. 9** NR classification methodologies
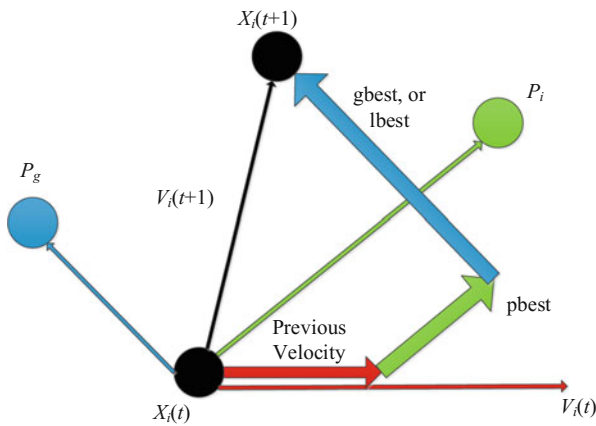


**Fig. 10** Factors determining particle's motion within solution space

The GPSO and LPSO constitute two PSO variants with advantages and drawbacks since they either promote exploration or exploitation of the solution space. In order to harness their aforementioned merits while neutralizing their flaws the Unified PSO (UPSO) variant has been proposed [28]. For UPSO in Eqs. (17) and (18), the global and local velocities of the particles are calculated using the GPSO, Eq. (17), and the LPSO versions, Eq. (18), respectively, while in Eqs. (19a) and (19b) the unified velocity is given. The particle position equation remains as in Eq. (15).

$$GV_i(t + 1) = \chi\left[v_i(t) + c_1 R_1\left(P_i(t) - X_i(t)\right) + c_2 R_2\left(P_g(t) - X_i(t)\right)\right] \quad (17)$$

$$LV_i(t + 1) = \chi\left[v_i(t) + c_1 R_1\left(P_i(t) - X_i(t)\right) + c_2 R_2\left(P_l(t) - X_i(t)\right)\right] \quad (18)$$

for $u \leq 0.5$:

$$v_i(t + 1) = u R_3 GV_i(t + 1) + (1 - u) LV_i(t + 1) \quad (19a)$$

for $u > 0.5$:

$$v_i(t + 1) = u GV_i(t + 1) + (1 - u) R_3 LV_i(t + 1) \quad (19b)$$

where:

– $u \in [0, 1]$: is a parameter, called unification factor, and controls the influence of the global and local velocity update. Evidently, lower values of $u$ correspond to distributions biased towards the LPSO, i.e. exploration, and higher values of $u$ towards GPSO, i.e. exploitation.
– $R_3$: is a random variable uniformly distributed within $[0, 1]$, is applied either to the global, or the local velocity, depending on the value of $u$, infusing partial stochasticity and enhancing in this way even further the exploration capabilities of the technique.

As for assigning value to the unification factor, there are a lot of schemes. One of them, called swarm partitioning, is a particle-level scheme, where the swarm is divided in partitions consisting of a predefined number of particles. All particles in the same partition share the same $u$, while each partition has a different value, i.e. a value from the set $W = \{0, 0.1, \ldots, 0.9, 1\}$. In order to avoid any search bias of the swarm, due to the entanglement of neighborhoods and partitions, particles of the same partitions are spread in different ring neighborhoods, by assigning particles to partitions in a non-sequential order, such that the $i$-th particle is assigned to the $(1+(i-1)\mathrm{mod}k)$-th partition. For example, the first $k$ particles are assigned to partitions 1 to $k$, respectively, one particle per partition. Then, it starts over by assigning $x_{(k+1)}$ to partition 1, $x_{(k+2)}$ to partition 2, and so on.

The particle formulation for the UPSO is a vector with its dimension to be equal to the sum of the sectionalizers and the tie-switches as presented in Eq. (20). For each dimension a binary variable is considered with values 0 or 1 to denote the

**Table 5** NR under UPSO for 33 and 69 bus systems

| | NR under UPSO algorithm | | | | |
|---|---|---|---|---|---|
| | Initial losses (kW) | Sectionalizers open | Tie-switches closed | Loss reduction reduction (%) | Final losses (kW) |
| 33 bus system | 211.0 | 7, 9, 14, 28, 32 | All | 33.65 | 140.0 |
| 69 bus system | 229.8 | 14, 58, 62 | Tie 3, Tie4, Tie5 | 54.70 | 104.1 |

status of the respective switch, either open or closed.

$$X = \left[ S_1, S_2, \ldots, S_{n_b}, T_1, T_2, \ldots, T_w \right] \tag{20}$$

where:

- $S_i$: refers to sectionalizer,
- $n_b$: the number of buses of the DN,
- $T_j$: refers to tie-switch,
- $w$: is the number of tie-switches of the DN.

The results after the UPSO application for NR for both 33 bus system and 69 bus system [4] are presented in Table 5 and the initial layout of the 69 bus system in Fig. 11 [19].

## 4  Power and Energy Loss Minimization under Network Reconfiguration

### 4.1  Load Variation Consideration

The application of the NR scheme for loss reduction refers to seeking for the optimal network reconfiguration given specific operating conditions for the DN in terms of active and reactive load demand. The latter is the case of the so called snapshot of the DN's operation and it constitutes a reference case with fixed load composition of the network, that allows the concept of load transferring among feeders to be implemented. The problem though is that the final solution depends directly on the load composition, since the solution algorithm will determine the required switching operations to perform the NR based on load level differences among feeders and on the layout of the network. Given an altered load composition for the DN, it is rational to accept that the final reconfigured topology after NR could also alter. An issue is raised here regarding the definition of the optimal solution under load variations: if for any different operating snapshot of the DN with altered load composition a possibility for a different optimal solution exists, then under real load variations the topology should be continuously being reconfigured. Fortunately, this is not the case due to the reason that, under smooth load variations, the optimal reconfigured
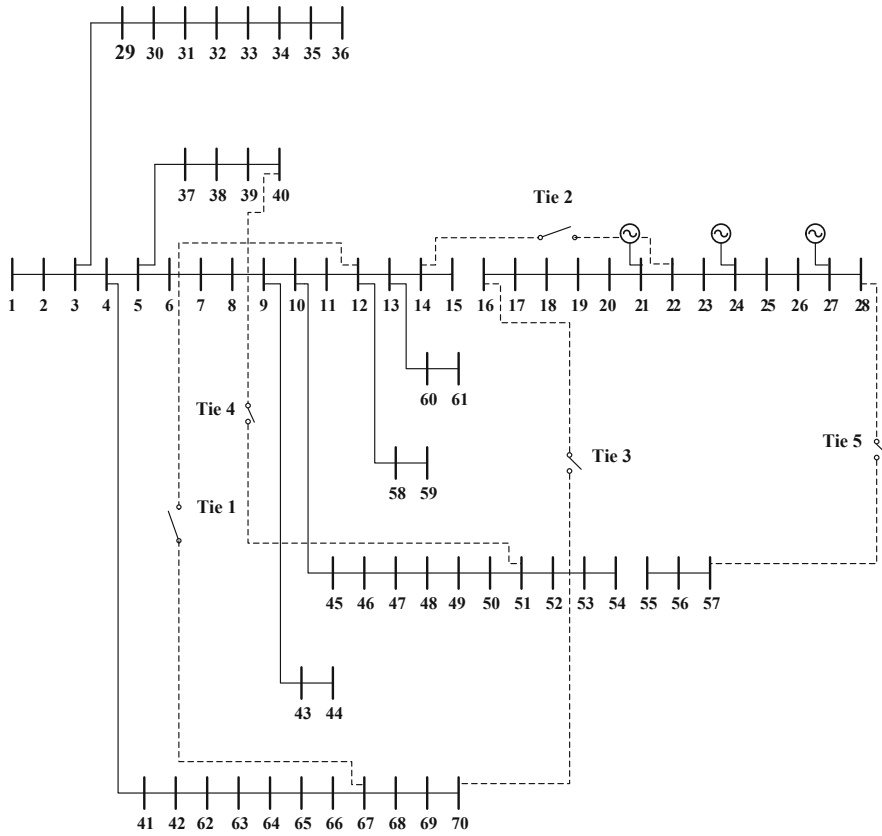
**Fig. 11** Layout of the 69 bus system

topology proves to be quite fixed. Also, under more intense load variations, a fixed reconfigured topology can be efficient enough regarding the loss reduction, even if it is not the optimal one for every single snapshot with different load composition. Given these clarifications, the problem under load variations is known as energy loss reduction via NR and a simple formation of the $OF$ is presented in Eq. (21).

$$OF = \min \sum_{\Delta t=1}^{T} \sum_{z=1}^{n_l} R_z I_z^2 \tag{21}$$

where:

- $\Delta t$: is the time interval for which a fixed load composition is considered
- $T$: is the time period for which energy loss minimization is examined

The number of $\Delta t$ intervals in Eq. (21) has a great impact on the problem's computational burden. For example, if $T$ is equal to 1 day, then it is possible to break down the problem to 24 sequential sub-problems when $\Delta t = 1$ h or even to 3600 sequential sub-problems when $\Delta t = 1$ min. Given the problem's complexity for a single snapshot, it becomes obvious that special attention about the assumed number of the $\Delta t$ intervals should be given.

If the load alterations between sequential time intervals, corresponding to at least two consecutive snapshots, are considered to be performed equally and uniformly for all loads of the DN, then the final solution concerning the reconfigured topology is not affected. The latter means that for a different load composition with all loads uniformly increased or reduced, the same switching operations are required to perform the optimal NR scheme. In order to investigate the impact of load variations to the optimal NR problem, the 33 bus system is again examined under a series of different loading conditions regarding its load composition. The load alterations are performed randomly because the probabilistic modelling of loads, especially the residential ones, is well justified by the fact that electricity demand is largely a stochastic process exhibiting diversity [25, 26]. Therefore, the load variations for the examined DN are assumed to follow a uniform distribution [8] and the corresponding lower and upper limits are computed as in Eqs. (22) and (23):

$$P_i^{lower} = \overline{P_i}\Big(1 - \frac{l_u}{100}\Big) \tag{22}$$

$$P_i^{upper} = \overline{P_i}\Big(1 + \frac{l_u}{100}\Big) \tag{23}$$

where:

- $P_i^{lower}$: is the lower limit of the uniform distribution interval of bus $i$
- $P_i^{upper}$: is the upper limit of the uniform distribution interval of bus $i$
- $\overline{P_i}$: is the mean load value of node n (initial snapshot of the DN)
- $l_u$: is the number defining the length of the uniformly distribution interval

The flowchart of the methodology that performs optimal NR under load variations is illustrated in Fig. 12. It should be clarified that the NR scheme is based on the heuristic rules that have been presented previously in this chapter. The proposed algorithm considers for each new scenario different load composition for the DN and applies the heuristic rules to perform optimal NR for loss minimization. Furthermore, the algorithm examines the performance of the optimal reconfigured topology resulted for the initial load composition of the DN (mean load values), regardless the actual load composition. The latter means that the algorithm computes the loss reduction that the initial reconfigured topology yields for every different snapshot formed by the uniform distribution. The goal here is to investigate whether it is actually necessary to apply the NR scheme under load variations. For example, if the initial optimal NR with the mean load values performs well concerning the loss reduction regardless the load variations, then this solution could be considered

```
                          ┌─────────────┐
                          │    START    │
                          └──────┬──────┘
                          ┌──────┴──────┐
                          │ Counter j=1 │
                          └──────┬──────┘
                   ┌─────────────┴─────────────┐
                   │ Run ac load flow for radial│
                   │       configuration        │
                   └─────────────┬─────────────┘
          ┌──────────────────────┴──────────────────────┐
          │  Compute voltage drop across open tie-switches│
          │          ΔVi για i=1,2,3...n-1                │
          └──────────────────────┬──────────────────────┘
               ┌──────────────────┴──────────────────┐
               │  Find tie-switch with maximum         │
               │       voltage drop, ΔVmax            │
               └──────────────────┬──────────────────┘
```
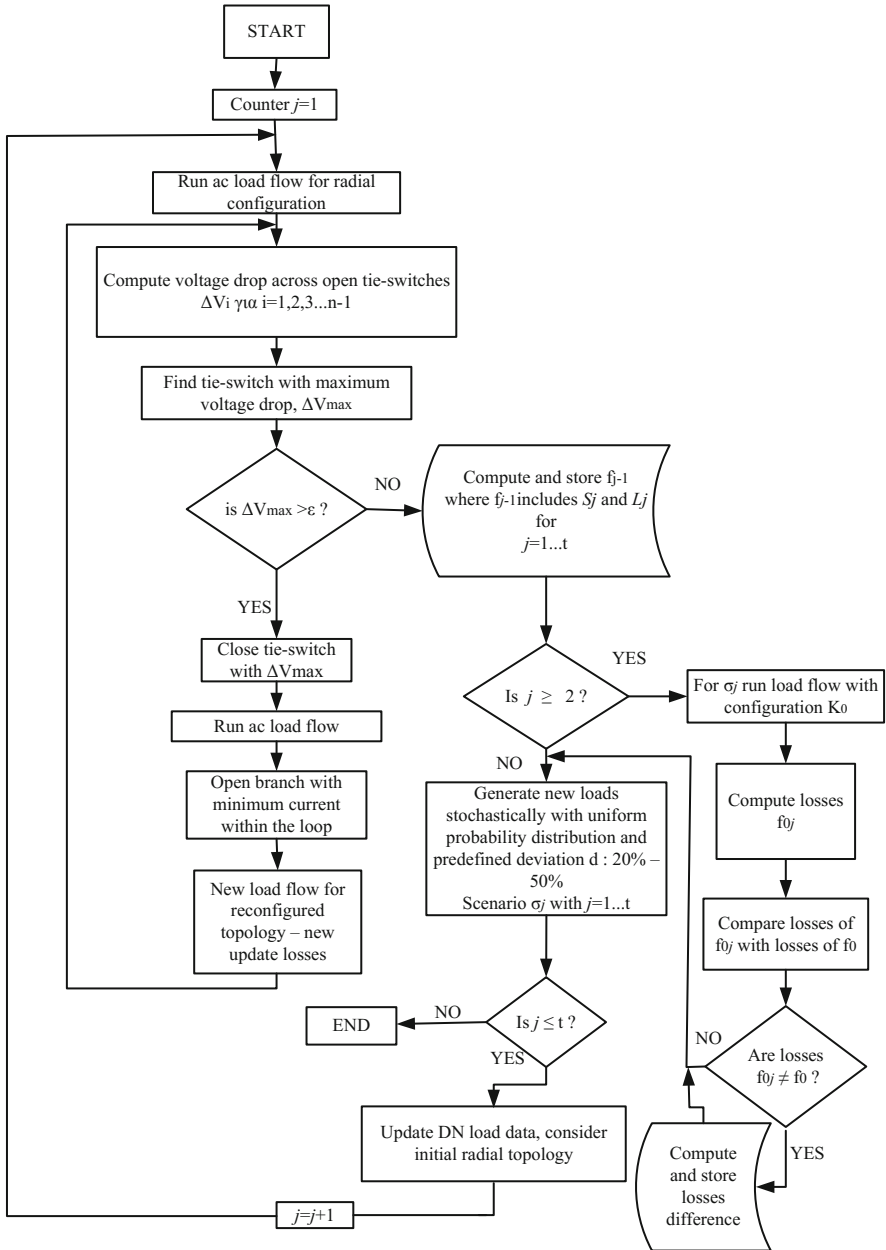


**Fig. 12** NR algorithm with load variations consideration

**Table 6** Sectionalizers operation for NR under smooth load variations for 33 bus system

| Close tie-switch | Open branch | $l_u = \pm20\%$ participation frequency of branch (%) to 10,000 scenarios | Open branch | $l_u = \pm30\%$ participation frequency of branch (%) to to 10,000 scenarios |
|---|---|---|---|---|
| Tie 1 | 7–8 | 100 | 7–8 | 100 |
|  | 8–9 | 100 | 8–9 | 6.46 |
| Tie 2 | 9–10 | 81.44 | 9–10 | 66.78 |
|  | 10–11 | 17.49 | 10–11 | 26.76 |
| Tie 3 | 28–29 | 100 | 28–29 | 100 |
| Tie 4 | 14–15 | 100 | 14–15 | 100 |
|  | 32–33 | 99.98 | 17–18 | 0.48 |
| Tie 5 | 17–18 | 0.02 | 31–32 | 0.42 |
|  |  |  | 32–33 | 99.1 |

**Table 7** Sectionalizers operation for NR under intense load variations for 33 bus system

| Close tie-switch | Open branch | $l_u = \pm40\%$ participation frequency of branch (%) to 10,000 scenarios | Open branch | $l_u = \pm50\%$ participation frequency of branch (%) to 10,000 scenarios |
|---|---|---|---|---|
| Tie 1 | 7–8 | 100 | 7–8 | 100 |
|  | 8–9 | 14.44 | 8–9 | 19.82 |
| Tie 2 | 9–10 | 55.59 | 9–10 | 46.85 |
|  | 10–11 | 29.85 | 10–11 | 32.28 |
|  | 11–12 | 0.12 | 11–12 | 1.05 |
| Tie 3 | 28–29 | 100 | 28–29 | 100 |
| Tie 4 | 14–15 | 100 | 14–15 | 100 |
|  | 16–17 | 0.01 | 16–17 | 0.05 |
| Tie 5 | 17–18 | 2.13 | 17–18 | 5.37 |
|  | 31–32 | 1.40 | 31–32 | 2.52 |
|  | 32–33 | 96.46 | 32–33 | 92.06 |

fixed and assumed to be the near optimal under load variations. In Tables 6 and 7 the results regarding 4 values for $l_u$, i.e. 20, 30, 40, 50, are presented. The latter means that all loads have been considered to randomly alter within $\pm20\%$, $\pm30\%$, $\pm40\%$, $\pm50\%$ from their mean initial values respectively. For each $l_u$ value 10,000 scenarios with different load composition for the 33 bus system have been produced and for each one of them the NR scheme under the heuristic based approach has been applied.

The results in Table 6 indicate that for smooth load variations, i.e. within $\pm30\%$ from the mean load value, and regardless the load composition the sectionalizers that have to be operated for the initial NR with the mean load values seem to also participate in the vast majority of the solutions for all other snapshots. Even under more intense load variations, as the results in Table 7 show, these sectionalizers still keep high participation frequency to the reconfigured topology. Nevertheless, the

**Fig. 13** Schematic representation of corresponding sectionalizers to open for each tie-switch regardless load composition for 33 bus system

analysis shows that from the 32 available sectionalizers of the 33 bus system, only 11 of them (33%) should be expected to participate in the NR scheme, regardless the load composition of the DN. Moreover, this number could be considered further reduced since for some of them the probability to be operated is quite low. In Fig. 13 the layout of the 33 bus system with all participated sectionalizes for all possible NRs is illustrated in order to highlight that, for each tie-switch, the expected sectionalizers to open after the tie-switch operation are sectionalizers within specific neighborhoods of the DN. Based on these results, it is up to the DSO to proceed with selective automation upgrade to targeted sectionalizers in order to exploit the benefits for real time NR towards energy loss reduction under relatively low investment cost.
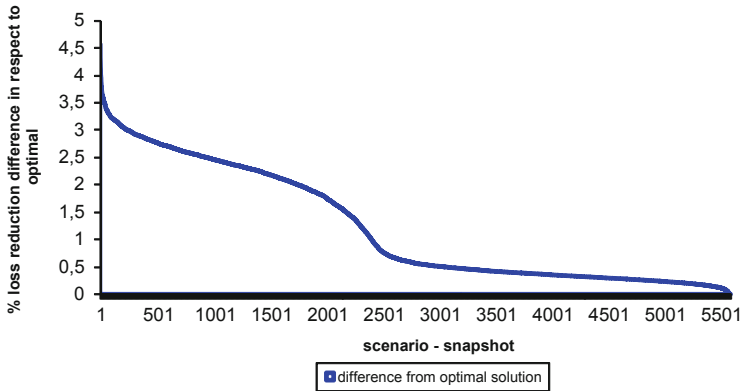
**Fig. 14** Loss reduction difference yielded by fixed NR in regard to optimal one for each snapshot

Finally, in Fig. 14 the performance evaluation of the fixed NR derived by the initial load composition with mean load values, regardless the load variations, is presented. More specifically, for each snapshot the aforementioned NR is applied and the difference in loss reduction in respect to the optimal NR for this snapshot is computed. All these differences are placed in descending order and as clearly presented the worst case refers to a difference of approximately 4.5% by the optimal NR for this snapshot. Thus, it is rational to consider that for time periods within which the load variations of the network's loads are not intense, a fixed reconfigured topology could be assumed as an efficient solution for energy loss reduction due to low investment cost for the DSO, regarding the automation upgrade of the DN in terms of replacing manual sectionalizers with automated ones.

The results corresponding to the 69 bus system are presented in Tables 8 and 9 and are schematically summarized in Fig. 15, in which the blue dotted frames indicate the sectionalizers to be operated after the respective tie-switch is closed.

## 5 Network Reconfiguration Under DG Penetration in DNs

### 5.1 Overloading Mitigation in DNs due to High DG Penetration

In general, it is expected that DG penetration in power systems has shifted power generation to a more decentralized model, which could benefit the grid in terms of improving the voltage profile and alleviating the lines' loading. The increased and without proper guideline installation of DG units has driven parts of the DNs in saturation conditions, in which overvoltage and reverse power flow issues cause

**Table 8** Sectionalizers operation for NR under smooth load variations for 69 bus system

| Close tie-switch | Open branch | $l_u = \pm20\%$ participation frequency of branch (%) to 10,000 scenarios | Open branch | $l_u = \pm30\%$ participation frequency of branch (%) to 10,000 scenarios |
|---|---|---|---|---|
| Tie 1 | 12–67 | 100 | 12–67 | 100 |
| Tie 2 | 14–22 | 100 | 14–22 | 100 |
| Tie 3 | 15–16 | 100 | 14–15 | 0.01 |
| | | | 15–16 | 99.99 |
| | 47–48 | 57.23 | 47–48 | 45.32 |
| Tie 4 | 48–49 | 12.20 | 48–49 | 13.78 |
| | 49–50 | 14.42 | 49–50 | 17.16 |
| | 50–51 | 16.15 | 50–51 | 23.74 |
| | 53–54 | 28.26 | 53–54 | 34.63 |
| | 54–55 | 37.52 | 54–55 | 29.48 |
| Tie 5 | 55–56 | 33.92 | 55–56 | 35.39 |
| | | | 56–57 | 0.05 |

**Table 9** Sectionalizers operation for NR under intense load variations for 69 bus system

| Close tie-switch | Open branch | $l_u = \pm40\%$ participation frequency of branch (%) to 10,000 scenarios | Open branch | $l_u = \pm50\%$ participation frequency of branch (%) to 10,000 scenarios |
|---|---|---|---|---|
| Tie 1 | 12–67 | 100 | 12–67 | 100 |
| Tie 2 | 14–22 | 99.96 | 14–22 | 99.26 |
| | 21–22 | 0.04 | 21–22 | 0.74 |
| | 13–14 | 0.22 | 13–14 | 1.09 |
| Tie 3 | 14–15 | 0.35 | 14–15 | 1.31 |
| | 15–16 | 99.43 | 15–16 | 97.60 |
| | 47–48 | 38.12 | 47–48 | 34.02 |
| Tie 4 | 48–49 | 13.80 | 48–49 | 15.08 |
| | 49–50 | 19.33 | 49–50 | 19.15 |
| | 50–51 | 28.75 | 50–51 | 31.75 |
| | 53–54 | 38.73 | 53–54 | 42.47 |
| Tie 5 | 54–55 | 24.42 | 54–55 | 20.71 |
| | 55–56 | 33.74 | 55–56 | 31.28 |
| | 56–57 | 3.11 | 56–57 | 5.54 |

power quality problems and increased power losses. The latter is usually the case in DN with increased RES penetration either during midday and night, when the Photovoltaic (PV) and the Wind Generation (WG) power units, respectively, are active. Since these effects are present for specific lines-parts of the DN, it is possible to face them by NR due to the fact that power flow allocation within the DN could more efficiently exploit the power surplus by the DG or RES units. In Fig. 16 the 69 bus system is presented, in which the carrying capacity for branches 1-9 is 400
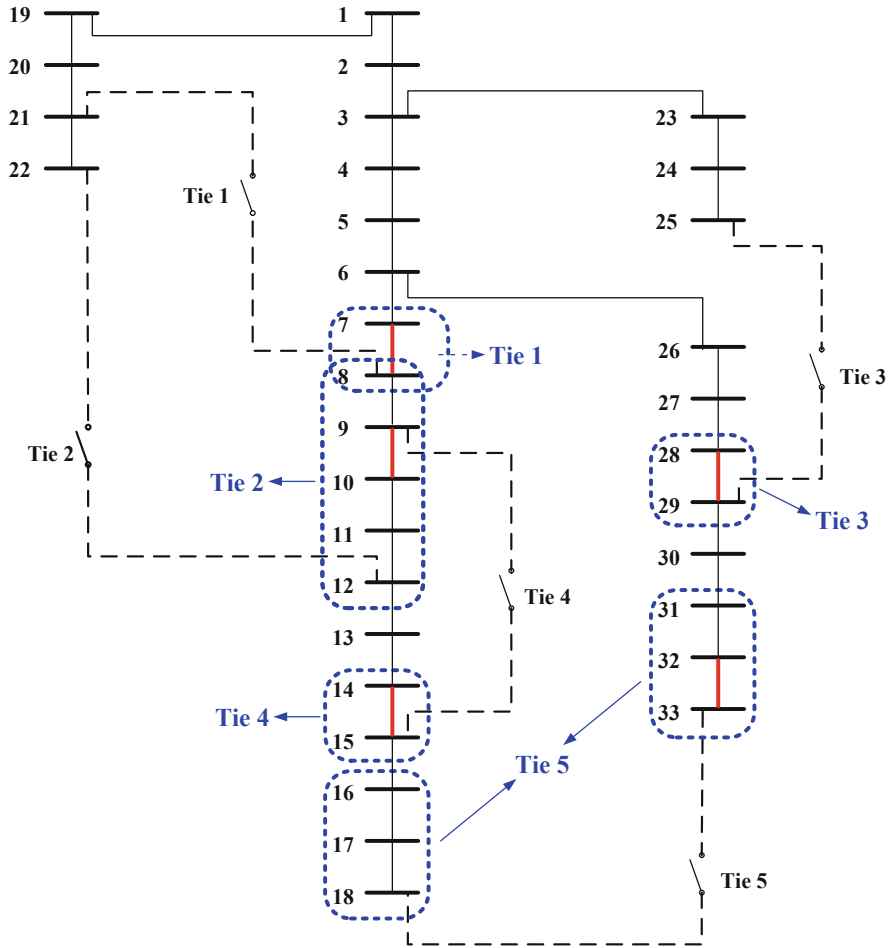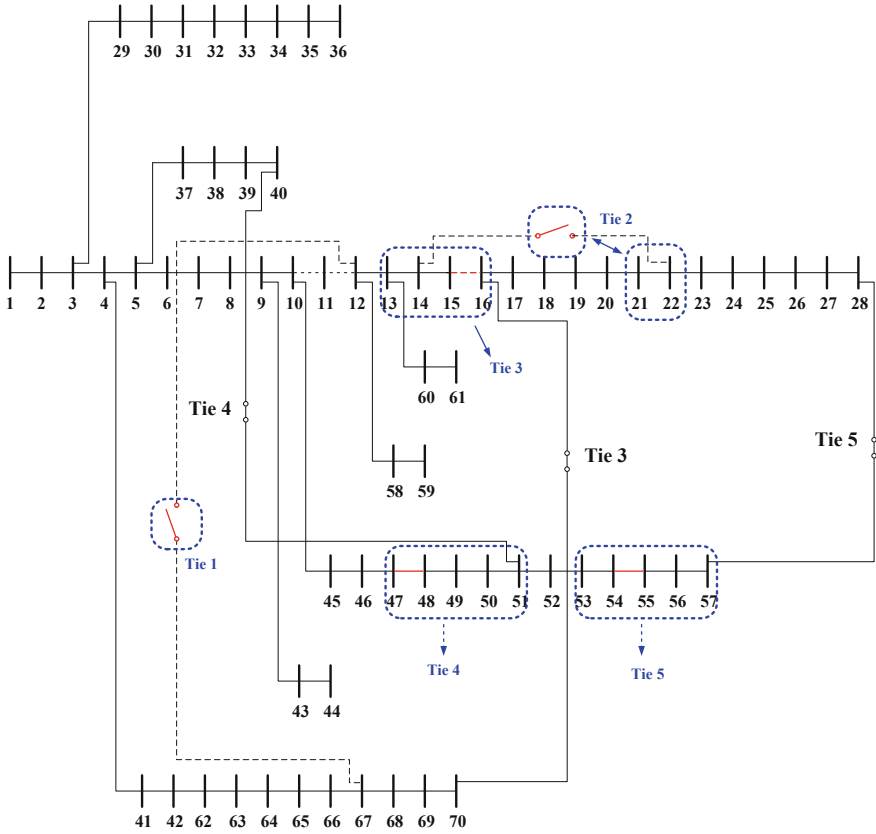
**Fig. 15** Schematic representation of corresponding sectionalizers to open for each tie-switch regardless load composition for the 69 bus system

A, for branches 46–49 and 52–64 is 300 A and for all the remaining the ampacity is 200 A [30]. It is considered that three DG units, with 500 kW and 300 kVAr active and reactive power generation respectively, are installed as shown in Fig. 16 and thus a low DG penetration scenario is examined [11]. In Fig. 17 the carrying current for each branch normalized to its ampacity level for the cases before and after the DG installation is illustrated. It is observed that the DG power generation causes for some branches reduction of their current flow, while for some other the opposite happens. The results in Fig. 17 show no constraint violations for the branches' loading, but this is due to the low penetration level of the DG. Still, the trend is evident since for high DG penetration it is high possible to experience heavy loading conditions subject to reverse power flow. Therefore, NR could prove to be an efficient scheme to mitigate both possible overvoltage and reverse power flow conditions.
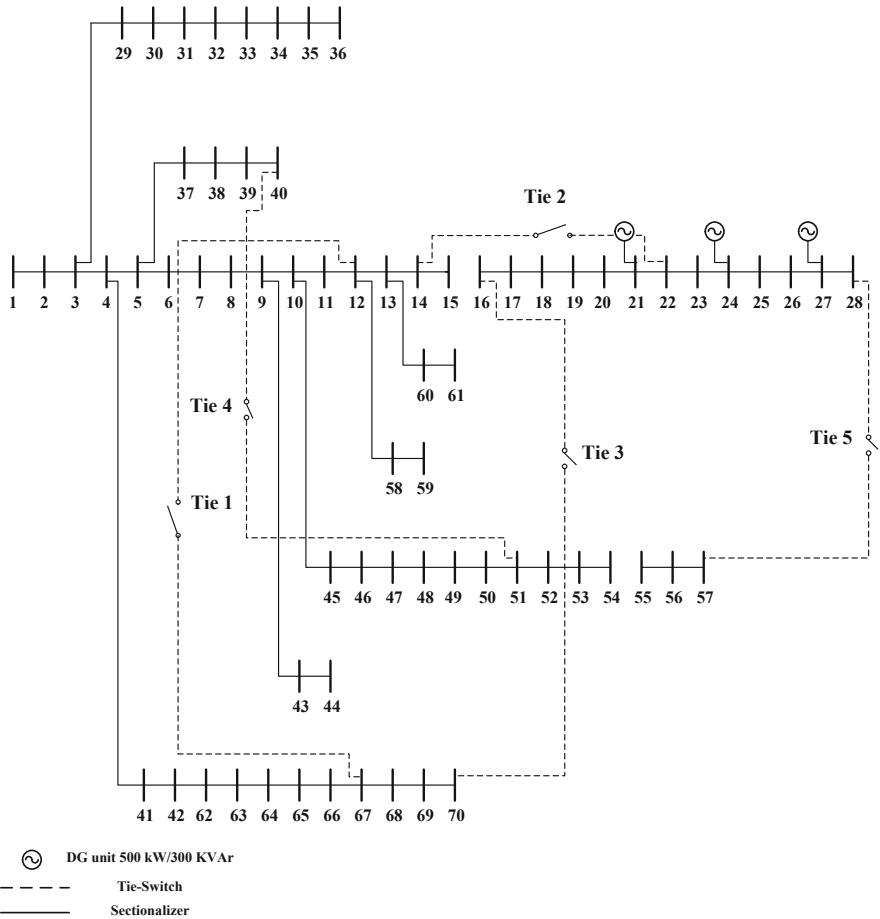
**Fig. 16** The 69 bus system with low DG penetration

The problem is addressed through a linear $OF$ that is formed based on the indices shown in Eqs. (24) and (25) [11]:

$$CCIF = \frac{\sum_{z=1}^{[(n_b-1+t)]} \frac{I_{b_z}^k}{I_{a_z}}}{[(n_b - 1 + t)]} \tag{24}$$

where:

- $CCIF$: is the current index,
- $n_b$: is the number of buses of the DN,
- $t$: is the number of tie-switches of the DN
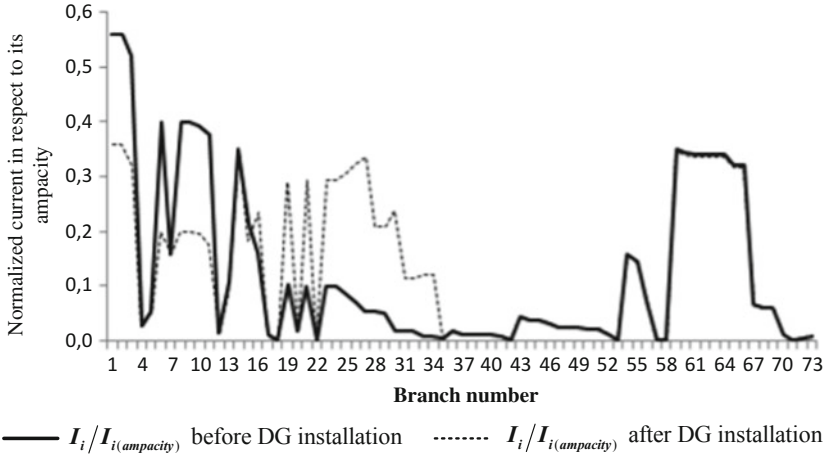
**Fig. 17** The 69 bus system branch currents before and after DG installation

– $k$: is the operation state of the DN, i.e. the load and generation composition for the snapshot solved,
– $z$: is the line $z$, with $i = 1, 2, \ldots, [(n-1)+t]$,
– $I_{b_z}^k$: is the current (rms value) of line $z$,
– $I_{a_z}$: is the ampacity level of line $z$.

$$VCIF = \frac{\sum_{i=1}^{n_b} \frac{V_i^k}{V_r}}{n_b} \tag{25}$$

where:

– $VCIF$: is the voltage index,
– $V_i^k$: is the voltage of bus $i$ for state $k$,
– $V_r$: is the nominal voltage of the DN.

The proposed algorithm performs the NR scheme based on the simple heuristic rules that explained earlier in this chapter in order to optimize either the $CCIF$ or the $VCIF$ index under a weighted factor approach. The flowchart of the proposed algorithm is shown in Fig. 18. Initially the algorithm checks whether the DG penetration has increased either the $CCIF$ or the $VCIF$ index and then based on the index optimization prioritization, NR is applied. The results for 100 scenarios concerning random allocation of 15 DG units with random power generation between 100–850 kW (with a fixed power factor equal to 0.9) are presented in
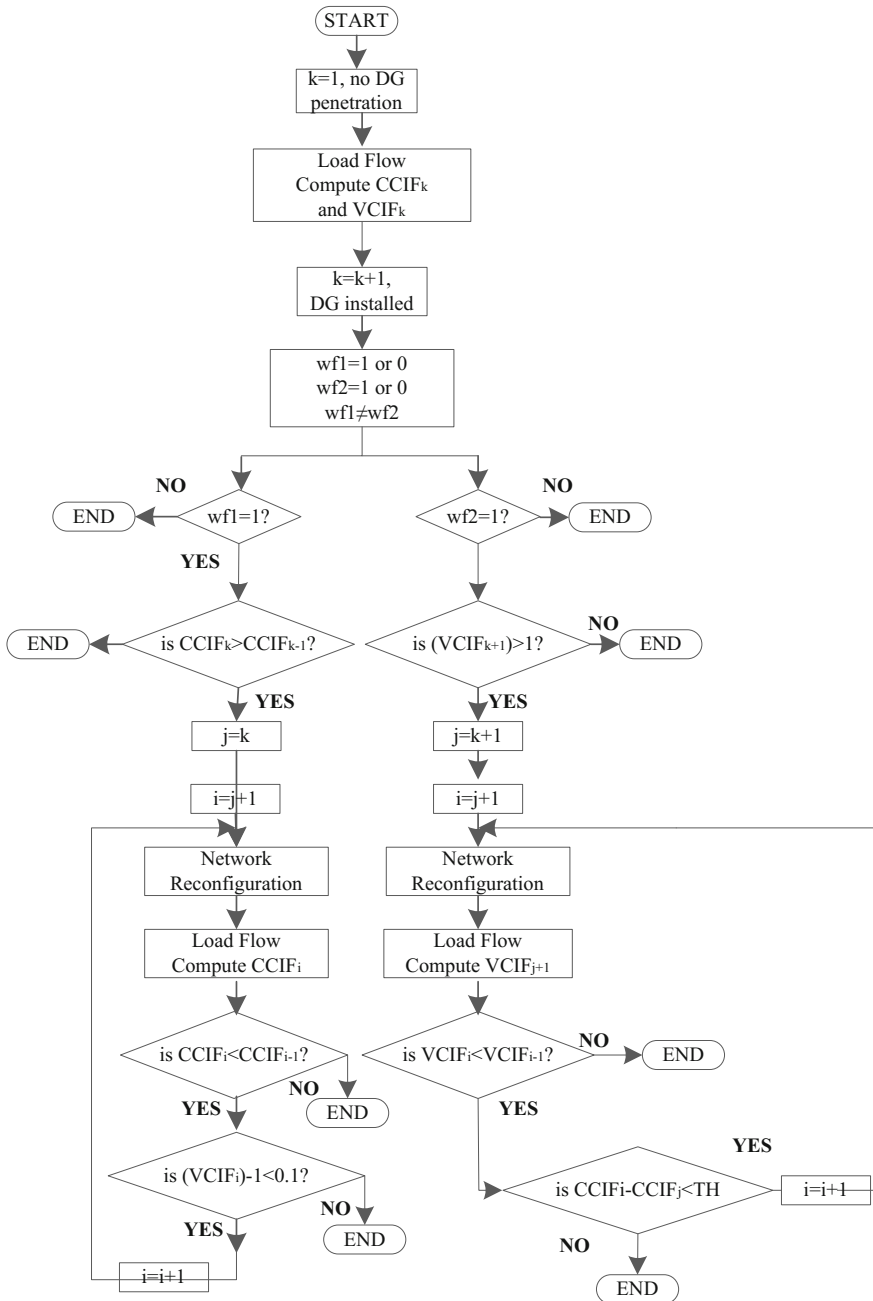
**Fig. 18** Flowchart for NR towards CCIF and VCIF optimization due to DG penetration
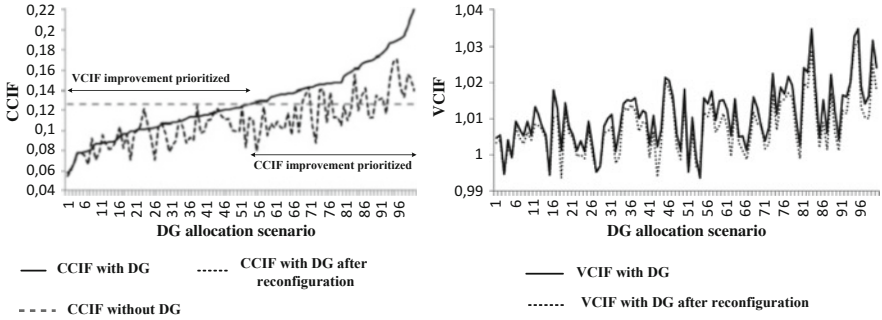
**Fig. 19** CCIF and VCIF values for 100 scenarios with DG penetration after NR
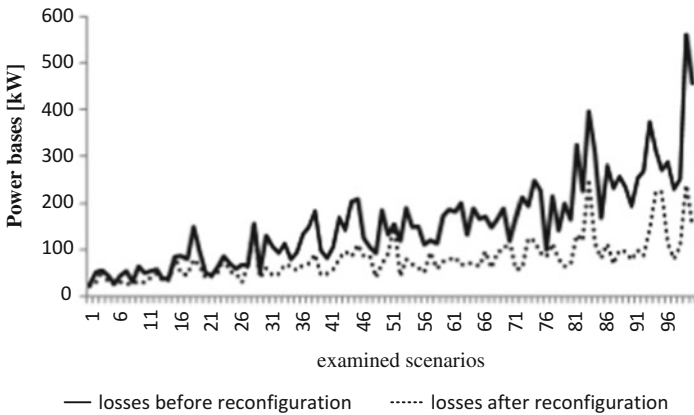


**Fig. 20** Loss reduction under DG penetration via NR

Fig. 19 [11]. At the left graph of Fig. 19 the NR is performed aiming to optimize the *VCIF* index but as observed this scheme leads also to *CCIF* improvement in most examined scenarios. When *CCIF* is prioritized, the algorithm applies the NR scheme and in all cases the index is reduced yielding by this way more balanced branch loading across the DN. For the right part of Fig. 19 the results presented show that the voltage profile of the DN has been improved under the NR scheme for all cases with DG penetration. Finally, the impact of improving the voltage profile and of mitigating the branch loading is also reflected on the network's power loss, as presented in Fig. 20, where in all cases the reconfigured topology caused loss reduction. The latter is important since the *OF* is not formed directly to express the power loss for the DN but to reduce the branch current across the DN, that is a linear simplified and approximating approach of the loss reduction *OF*.

## 5.2 Optimal Siting and Sizing of DG and NR Towards Loss Reduction in DNs

In the previous section the NR scheme is applied in DNs given the penetration of DG in terms of siting and sizing of the DG units. In this section, the application order of NR and the so called Optimal Distributed Generation Placement (ODGP) problem for loss reduction is examined. The basic concept is to investigate whether it is more efficient, in terms of higher loss reduction, to apply the NR scheme and then the ODGP or vice versa. Both schemes are implemented by the UPSO algorithm that has been explained in section 3.3 but for the ODGP problem the particle's formulation is different [12] and is presented in Fig. 21. Each particle is a nine dimension vector for the 33 bus system, since the first 3 dimensions refer to the 3 candidate nodes of the DN for DG installation, the other 3 dimensions concern the active power generation of each DG unit and the remaining 3 dimensions refer to the reactive power of each DG unit. Using this approach, it becomes evident that only three nodes of the DN are considered as candidates for DG installation and moreover, the algorithm will determine the power generation for each installed unit.

In Table 10 the UPSO parameters are presented and they are the same either for the ODGP or the NR scheme implementation. Using the OF shown in Eq. (8), the NR scheme is initially applied first and then the ODGP scheme is applied in order to further reduce power losses by defining the optimal siting and sizing of three DG units. The concept here is to firstly exploit the current structure of the DN by NR for potential loss reduction and then proceed in optimal DG penetration. The alternative application order of these schemes refers to firstly perform optimal DG penetration and then examine whether the NR could further reduce power losses. The results of these two approaches are presented in Table 11 [9].

$$X_i = \left[ a_1, a_2, ..., a_{n_g}, b_{n_g+1}, b_{n_g+2}, ..., b_{2n_g}, c_{2n_g+1}, c_{2n_g+1}, ..., c_{3n_g} \right]$$

a refers to DG (or node)
b refers to active power generation at respective node
c refers to reactive power generation at respective node
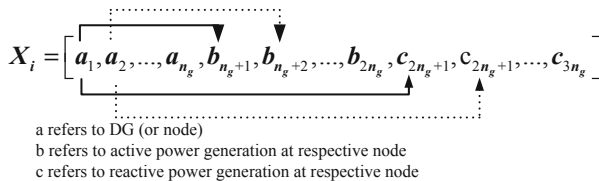
**Fig. 21** Particle formulation in ODGP for UPSO algorithm

**Table 10** UPSO parameters

| Parameter | Value |
| --- | --- |
| Cognitive and social coefficient $c_i$ | 2.05 |
| Number of particles $N$ | 50 |
| Neighborhood radius $r$ | 2 |
| Maximum iteration number $T_{max}$ | 500 |
| Convergence tolerance | $10^{-7}$ |

**Table 11** NR and ODGP for loss reduction

| | NR scheme applied 1st and ODGP scheme applied 2nd | | | | |
|---|---|---|---|---|---|
| | Initial losses (kW) | Sectionalizers open | Tie-switches closed | – | Loss reduction (%) and final losses (kW) |
| NR applied | 211 | 7, 9, 14, 28, 32 | All | – | 33.65% |
| | | | | – | 140 |
| | Initial Losses (kW) | Nodes to host DG units | Active power of each DG unit (kW) | Reactive power of each DG unit (kVAr) | Loss reduction (%) and final losses (kW) |
| ODGP applied | 140 | 6 | 681.7 | 317.8 | 87.36% |
| | | 8 | 933.2 | 435.5 | 17.7 |
| | | 30 | 1234.3 | 1108.3 | |
| | ODGP scheme applied 1st and NR scheme applied 2nd | | | | |
| | Initial Losses (kW) | Nodes to host DG units | Active power of each DG unit (kW) | Reactive power of each DG unit (kVAr) | Loss reduction (%) and final losses (kW) |
| ODGP applied | 211 | 3 | 1633.3 | 800.2 | 91.37% |
| | | 14 | 741.4 | 346.9 | 19.2 |
| | | 30 | 987.4 | 990.4 | |
| | Initial Losses (kW) | Sectionalizers open | Tie-switches closed | – | Loss reduction (%) and final losses (kW) |
| NR applied | 19.2 | 7, 8, 9, 28 | Tie 1, Tie 2, Tie 3, Tie 4 | – | 15.38% |
| | | | | – | 15.4 |

The basic observation from the results shown in Table 11 is that, although both approaches regarding the application order for the NR and ODGP schemes yield almost the same final loss reduction, the application order of the schemes has an individual impact on them. More specifically, if the NR scheme is applied firstly, the aggregated DG penetration is approximately 2.85 GW, while if it is applied secondly then the total DG capacity is close to 3.36 GW. The obtained difference of approximately 500 kW could have a great impact on the total investment cost regarding the DG penetration, thus it seems that the ODGP should be applied on the most efficient network topology, i.e. the one after NR, in order to minimize the installation cost.

## 6   Conclusions

In this chapter, the NR scheme in DNs is examined related mainly to reliability improvement and loss reduction issues. NR is based on changing the layout of the DN by appropriate switching operations. These operations concern the closing of normally open tie-switches and the opening of normally closed sectionalizers within

the performed loops. The idea behind these switching operations relies on allocating the network's load within its feeders in order to somehow balance overall network's loading level. It is expected that under a more balanced load profile both loss reduction and voltage improvement could be achieved. Moreover, the NR technique also enables fault isolation and power restoration after an outage in DNs which in turn contributes in reliability improvement.

The first part of the chapter describes the importance of establishing a high automation level in DNs in order to be able to remotely perform the required switching operations during an outage aiming to isolate the fault within the shortest possible line segment of the network and restore power to the maximum number of consumers within the shortest possible time framework. A brief presentation of the reliability assessment in DNs is presented based on the respective reliability indices and a simple approach concerning targeted automation upgrade is analyzed. This approach refers to limited investment interventions subject to guided switching replacement in order to yield efficient reliability improvement subject to low cost. An example of a real urban DN is illustrated where it is shown that the claimed scheme is possible.

The second part of the chapter analyzes the loss reduction problem under NR via heuristic and metaheuristic based algorithms. The distinction between these two aforementioned algorithms is highlighted and their application on benchmarked DNs is presented. For heuristic approaches two well established and widely utilized heuristic rules are described while for the metaheuristic approaches a binary PSO variant, namely the Unified PSO, is presented along with the respective results. Subsequently, the problem of energy loss reduction is presented by explaining how load alterations are expected to influence the NR implementation. An analysis regarding numerous load compositions is shown in order to explain how the problem of energy loss minimization under NR is actually faced. The results presented indicate that even under intense load variations the expected switching operations in order to perform optimal NR could be considered somehow previously known based on prior knowledge for their participation frequency to the NR scheme.

Finally, the chapter also examines the potential for utilizing the NR concept with DG penetration. On the one hand, the NR is applied under high RES or DG penetration in order to mitigate branch overloading, reduce the current flow and improve voltage profile via the optimization of proposed indices. On the other hand, NR along with ODGP are treated as effective schemes for loss minimization in DNs and their application order is investigated. It has been proven to be more efficient to apply NR firstly, and then the optimal siting and sizing of DG units scheme, since in this way the aggregated DG or RES capacity is lower, while the loss reduction percentage is not affected.

The chapter succeeds to highlight the contribution of the NR scheme on several operational issues especially within the current smart grid concept, where immediate decisions have to be made and respective responses of the DN layout to several challenges related with load and generation uncertainties have to be faced.

# References

1. Alyami, S., Wang, Y., Wang, C., Zhao, J., Zhao, B.: Adaptive real power capping method for fair overvoltage regulation of distribution networks with high penetration of pv systems. IEEE Trans. Smart Grid **5**(6), 2729–2738 (2014). https://doi.org/10.1109/TSG.2014.2330345
2. Atteya, I.I., Ashour, H.A., Fahmi, N., Strickland, D.: Distribution network reconfiguration in smart grid system using modified particle swarm optimization. In: 2016 IEEE International Conference on Renewable Energy Research and Applications (ICRERA), pp. 305–313 (2016). https://doi.org/10.1109/ICRERA.2016.7884556
3. Atteya, I.I., Ashour, H., Fahmi, N., Strickland, D.: Radial distribution network reconfiguration for power losses reduction using a modified particle swarm optimisation. CIRED—Open Access Proc. J. **2017**(1), 2505–2508 (2017). https://doi.org/10.1049/oap-cired.2017.1286
4. Baran, M.E., Wu, F.F.: Optimal capacitor placement on radial distribution systems. IEEE Trans. Power Delivery **4**(1), 725–734 (1989). https://doi.org/10.1109/61.19265
5. Baxevanos, I.S., Labridis, D.P.: Implementing multiagent systems technology for power distribution network control and protection management. IEEE Trans. Power Delivery **22**(1), 433–443 (2007). https://doi.org/10.1109/TPWRD.2006.877085
6. Billinton, R., Grover, M.S.: Quantitative evaluation of permanent outages in distribution systems. IEEE Trans. Power Syst. **94**(3), 733–741 (1975). https://doi.org/10.1109/T-PAS.1975.31901
7. Billinton, R., Grover, M.S.: Reliability assessment of transmission and distribution schemes. IEEE Trans. Power Syst. **94**(3), 724–732 (1975). https://doi.org/10.1109/T-PAS.1975.31900
8. Bouhouras, A.S., Labridis, D.P.: Influence of load alterations to optimal network configuration for loss reduction. Electr. Power Syst. Res. **86**, 17–27 (2012). https://doi.org/10.1016/j.epsr.2011.11.023
9. Bouhouras, A.S., Gkaidatzis, P.A., Labridis, D.P.: Optimal application order of network reconfiguration and odgp for loss reduction in distribution networks. In: 2017 IEEE International Conference on Environment and Electrical Engineering and 2017 IEEE Industrial and Commercial Power Systems Europe (EEEIC/ICPS Europe), pp. 1–6 (2017). https://doi.org/10.1109/EEEIC.2017.7977443
10. Bouhouras, A.S., Andreou, G.T., Labridis, D.P., Bakirtzis, A.G.: Selective automation upgrade in distribution networks towards a smarter grid. IEEE Trans. Smart Grid **1**(3), 278–285 (2010). https://doi.org/10.1109/TSG.2010.2080294
11. Bouhouras, A.S., Iraklis, C., Evmiridis, G., Labridis, D.P.: Mitigating distribution network congestion due to high dg penetration. In: MedPower 2014, pp. 1–6 (2014). https://doi.org/10.1049/cp.2014.1638
12. Bouhouras, A.S., Sgouras, K.I., Gkaidatzis, P.A., Labridis, D.P.: Optimal active and reactive nodal power requirements towards loss minimization under reverse power flow constraint defining dg type. Int. J. Electr. Power Energy Syst. **78**, 445–454 (2016). https://doi.org/10.1016/j.ijepes.2015.12.014
13. Celli, G., Garau, M., Ghiani, E., Pilo, F., Corti, S.: Co-simulation of ICT technologies for smart distribution networks. In: CIRED Workshop 2016, pp. 1–5 (2016). https://doi.org/10.1049/cp.2016.0745
14. Civanlar, S., Grainger, J.J., Yin, H., Lee, S.S.H.: Distribution feeder reconfiguration for loss reduction. IEEE Trans. Power Delivery **3**(3), 1217–1223 (1988). https://doi.org/10.1109/61.193906
15. Crann, L.B.: Service reliability on rural distribution systems. Trans. Am. Inst. Electr. Eng. Part 3 **77**(3), 761–764 (1958). https://doi.org/10.1109/AIEEPAS.1958.4500021
16. DeSieno, C.F., Stine, L.L.: A probability method for determining the reliability of electric power systems. IEEE Trans. Power Syst. **83**(2), 174–181 (1964). https://doi.org/10.1109/TPAS.1964.4765983
17. Feng, C., Liu, W., Wen, F., Li, Z., Shahidehpour, M., Shen, X.: Expansion planning for active distribution networks considering deployment of smart management technologies. IET Gener. Transm. Distrib. **12**(20), 4605–4614 (2018). https://doi.org/10.1049/iet-gtd.2018.5882

18. Gaver, D.P., Montmeat, F.E., Patton, A.D.: Power system reliability i-measures of reliability and methods of calculation. IEEE Trans. Power Syst. **83**(7), 727–737 (1964). https://doi.org/10.1109/TPAS.1964.4766068

19. Hamouda, A., Zehar, K.: Efficient load flow method for radial distribution feeders. J. Appl. Sci. **6**, 2741–2748 (2006)

20. Kariuki, K.K., Allan, R.N.: Factors affecting customer outage costs due to electric service interruptions. IEE Proc. Gener. Transm. Distrib. **143**(6), 521–528 (1996). https://doi.org/10.1049/ip-gtd:19960623

21. Kavousi-Fard, A., Niknam, T.: Optimal distribution feeder reconfiguration for reliability improvement considering uncertainty. IEEE Trans. Power Delivery **29**(3), 1344–1353 (2014). https://doi.org/10.1109/TPWRD.2013.2292951

22. Kennedy, J., Eberhart, R.: Particle swarm optimization. In: Proceedings of ICNN'95—International Conference on Neural Networks, vol. 4, pp. 1942–1948 (1995). https://doi.org/10.1109/ICNN.1995.488968

23. Kumar, G.S., Kumar, S.S., Kumar, S.V.J.: Reconfiguration of electrical distribution network for loss reduction and voltage enhancement. In: 2017 IEEE International Conference on Power, Control, Signals and Instrumentation Engineering (ICPCSI), pp. 1387–1392 (2017). https://doi.org/10.1109/ICPCSI.2017.8391939

24. Lei, S., Hou, Y., Qiu, F., Yan, J.: Identification of critical switches for integrating renewable distributed generation by dynamic network reconfiguration. IEEE Trans. Sustainable Energy **9**(1), 420–432 (2018). https://doi.org/10.1109/TSTE.2017.2738014

25. Meliopoulos, A.P., Chao, X., Cokkinides, G.J., Monsalvatge, R.: Transmission loss evaluation based on probabilistic power flow. IEEE Power Eng. Rev. **11**(2), 73– (1991). https://doi.org/10.1109/MPER.1991.88755

26. Meliopoulos, A.P.S., Cokkinides, G.J., Chao, X.Y.: A new probabilistic power flow analysis method. IEEE Trans. Power Syst. **5**(1), 182–190 (1990). https://doi.org/10.1109/59.49104

27. Merlin, A.: Search for a minimal-loss operating spanning tree configuration for an urban power distribution system. In: Proceedings of 5th PSCC, vol. 1, pp. 1–18 (1975)

28. Parsopoulos, K.E.: Particle Swarm Optimization and Intelligence: Advances and Applications: Advances and Applications. IGI Global, Pennsylvania (2010)

29. Ramesh, V., Khanz, U., Ilićx, M.D.: Data aggregation strategies for aligning PMU and ami measurements in electric power distribution networks. In: 2011 North American Power Symposium, pp. 1–7 (2011). https://doi.org/10.1109/NAPS.2011.6025198

30. Rugthaicharoencheep, N., Sirisumrannukul, S.: Feeder reconfiguration for loss reduction in distribution system with distributed generators by tabu search. GMSARN Int. J. **3**, 47–54 (2009)

31. Sarma, N.D.R., Ghosh, S., Rao, K.S.P., Srinivas, M.: Real time service restoration in distribution networks-a practical approach. IEEE Trans. Power Delivery **9**(4), 2064–2070 (1994). https://doi.org/10.1109/61.329539

32. Shirmohammadi, D.: Service restoration in distribution networks via network reconfiguration. In: Proceedings of the 1991 IEEE Power Engineering Society Transmission and Distribution Conference, pp. 626–632 (1991). https://doi.org/10.1109/TDC.1991.169571

33. Sultana, B., Mustafa, M., Sultana, U., Bhatti, A.R.: Review on reliability improvement and power loss reduction in distribution system via network reconfiguration. Renew. Sust. Energ. Rev. **66**, 297–310 (2016). https://doi.org/10.1016/j.rser.2016.08.011

34. Transmission and Distribution Committee: IEEE Guide for Electric Power Distribution Reliability Indices. IEEE Std 1366™-2003 (2003)

35. Veldman, E., Verzijlbergh, R.A.: Distribution grid impacts of smart electric vehicle charging from different perspectives. IEEE Trans. Smart Grid **6**(1), 333–342 (2015). https://doi.org/10.1109/TSG.2014.2355494

# Switch Optimization for Smart Grid Distribution Automation

S. Chouhan and A. Feliachi

**Abstract** It is a daunting task to find optimum number and placement of sectionalizing switches in Distribution Automation (DA) feeders. Switch optimization is the most essential component of evaluating economic feasibility of a DA project and one has to consider the trade-off between reliability and economics to arrive at the answer. This chapter presents a novel iterative algorithm for the optimal switch number and placement problem. The proposed iterative algorithm can determine the solution faster compared to traditional switch optimization techniques by minimizing the total interruption costs at each step of the analysis. The proposed algorithm does not rely on varying switch capital investment and customer interruption cost data that are usually based on outdated utility surveys. The proposed method has been successfully implemented on Mon Power's, a FirstEnergy company, distribution system as part of the US Department of Energy (DOE) funded project, West Virginia Super Circuit (WVSC). The proposed method is also validated using IEEE 34-bus and 123-bus test feeders to demonstrate the effectiveness of the proposed approach. The mathematical model is developed in Matlab and the results show that the proposed iterative algorithm can drastically reduce the search space, and can find optimal number and placement of the switches with minimum computational effort.

## 1 Introduction

Improvement of the system reliability is one of the main drivers of Distribution Automation (DA) technologies. It is one of the most effective strategies in distribution networks to increase reliability by reducing the duration of

S. Chouhan (✉)
Smart Grid Solutions, Leidos Engineering, Hendersonville, TN, USA

A. Feliachi
Lane Department of Computer Science and Electrical Engineering, West Virginia University, Morgantown, WV, USA
e-mail: alfeliachi@mail.wvu.edu

the interruptions and the number of affected customers. The key aspect of DA project is to install automated sectionalizing switches on distribution feeders to divide them into multiple zones. The sectionalization of the feeder helps improving reliability by isolating the faulted zone, and serving the un-faulted zones by adjacent feeders. The first step in economic feasibility evaluation process of DA project is the determination of number and placement of sectionalizing switches.

The problem of determining optimal number and placement of switches has been studied by several authors with different approaches. Many works in literature formulated the problem as an optimization problem with objective functions such as reliability improvement and minimization of investment cost of switches. The reliability improvement is modeled as minimization of interruption costs. These methods are heavily reliant on the data pertaining to interruption costs and switch investment costs. The main problem with such data is the fact that it is not openly available, and even if it is available, seldom the data represent the present market conditions. Therefore, implementation of switch optimization problem using the actual values of interruption costs and investment costs might not always result in the correct answer.

Authors in [1] defined the problem using a combined cost function that includes investment, maintenance, and outage costs to determine the optimal number and location of switches using a Simulated Annealing (SA) approach. A polynomial-time partitioning algorithm is presented in [2] that can decompose the problem into a set of convex independent sub-problems to aid in reducing the problem complexity. A binary array is provided as a solution of optimal locations for deploying automated switches in the distribution feeders. A Genetic Algorithm (GA) based approach to solve the switch optimization problem using a binary representation model and System Average Interruption Duration Index (SAIDI) is presented in [3]. The same authors in [3] presented a solution to determine optimal location of switches, reclosers, and fuses by using a non-linear integer programming method with an objective function to minimize System Average Interruption Frequency Index (SAIFI).

An immune algorithm based approach to solve the optimal location of automated switches is presented in [4]. The proposed approach is utilized in designing a DA system for a real distribution system in Taiwan Power Company. The optimization problem is modeled with an objective of minimizing sum of the customer interruption cost and the switch capital costs. Authors in [5] solved the problem of optimal device allocation using reactive tabu search that has an objective to minimize estimated interruption costs.

A Simulated Annealing algorithm based approach using cost/worth analysis is proposed in [6] to find best locations to install switches in distribution system. A relative analysis was used in the solution that compared switch capital costs and reliability worth. Authors in [7] used a Particle Swarm optimization approach to solve switch optimization problem for sectionalizing switches and circuit breakers in radial distribution systems. The work in [8] proposed a solution for locating optimal location of automated sectionalizing switches in distribution

systems with DG penetration. The optimization problem was formulated using a fuzzy multi-objective function and solved using Ant Colony optimization technique.

A unique iterative algorithm is presented in this chapter that can find optimal switch number and placement based on relative reduction in normalized customer interruption costs. The proposed algorithm minimizes the total interruption costs at each step of the analysis to find the solution faster compared to traditional switch optimization techniques. This methodology greatly reduces the search space of the problem to aid in reducing the problem complexity.

The underlying problem with many of the switch optimization methods mentioned above is the reliance on varying customer outage cost and switch capital investment cost data. This could make the switch optimization solution very subjective and unrealistic. The switch capital investment costs vary greatly based on several factors such as manufacturer, country of deployment, and type of switch. Therefore, the proposed economic approach isolates switch capital costs to make it a generalized switch optimization model that can be applied to variety of switches such as reclosers, load break switches, circuit breakers, etc., with different levels of automation including manually operated, motor operated, and remotely operated. The customer interruption costs are derived from customer damage functions given in various utility surveys. The main problem with the survey data is that they are usually outdated and sensitive to the estimation methodology used in the survey. Thus, the usage of absolute customer interruption cost data makes determination of optimal switch number and placement very subjective and unrealistic. In order to solve this issue, the proposed iterative algorithm uses normalized customer interruption costs instead.

## 2 Mathematical Problem Formulation

The customer interruption cost *(CIC)* [4] represents the outage costs incurred by customers due to grid outages, and can be calculated using Eq. (1). The proposed iterative algorithm makes use of *CIC* as it considers interruption duration, system topology, load variations, and device random failures. It also accounts for various customer types and associated nonlinear customer damage functions.

The initial step in the analysis is to divide the distribution feeder into a set of Super Sections (SS). SS are also referred to as zones that can be isolated using automated switches during a grid outage. Therefore, each SS is considered as a potential automated switch location in the analysis. SS are formed by logically combining a number of consecutive feeder line segments. Each SS has a load point to represent the equivalent load of SS which is obtained by summing up individual loads in the SS. SS must be strategically selected in a way that the created zones of the feeder will have the ability to restore the power from adjacent feeders in the event of outages. The restoration of the power must not violate the system constraints such as thermal capacity constraints (conductor or equipment loading limits) and voltage
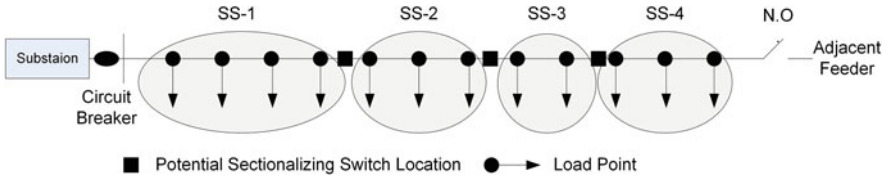
**Fig. 1** Typical radial distribution feeder

constraints (low and high voltage issues). DA feeders can be divided into SS with un-equal circuit lengths and loadings. A typical distribution feeder that is divided into several SS is shown in Fig. 1.

$$CIC = \sum_{y=1}^{k} OC_y = \sum_{y=1}^{k} \xi_y l_y \left( \sum_{z=1}^{k} C_{yz} P_z \right) \tag{1}$$

$$C_{yz} = \left( \mathrm{Re}\, s_z \times f_R \left( r_{yz} \right) + Com_z \times f_C \left( r_{yz} \right) + Ind_z \times f_I \left( r_{yz} \right) \right) \tag{2}$$

Where,

| | |
|---|---|
| $kk$ | Total number of Super Sections |
| $OC_y$ | Interruption cost per year due to outages in SS-y |
| $\xi_y$ | Outage rate (failure/mile-year) of SS-y |
| $l_y$ | Circuit length in miles of SS-y |
| $C_{yz}$ | Interruption cost of load (residential, commercial and industrial customers) in \$/kW at SS-z due to an outage at SS-y |
| $P_z$ | Total load in kW of SS-z |
| $Res_z$ | Load percentage of residential customers at SS-z |
| $Com_z$ | Load percentage of commercial customers at SS-z |
| $Ind_z$ | Load percentage of industrial customers at SS-z |
| $f_R$ | Interruption cost function of residential customers |
| $f_C$ | Interruption cost function of commercial customers |
| $f_I$ | Interruption cost function of industrial customers |
| $r_{yz}$ | Duration of service interruption of SS-z due to an outage at SS-y |

Equation (2) represents the integrated interruption cost framework which can be expanded to include other types of customers given the customer damage functions are known. Customer interruption costs are mainly dependent on customer type and outage duration. For example, the interruption cost of residential customers is far less compared to commercial customers. The customers with high service priorities such as hospitals, police stations, fire stations, and tele-communication data centers have high interruption costs.

# 3   Switch Optimization Iterative Algorithm

In a switch optimization problem for a distribution feeder with "n" number of SS with "r" number of automated switch placements, the total number of possible combinations for which the *CIC* is calculated is given by Eq. (3). *CIC* needs to be calculated for all possible combinations of switch placements to arrive at a global optimal solution. In the proposed iterative algorithm, the search space of *CIC* calculations is significantly reduced by minimizing the total interruption cost at each step of the analysis.

$$\sum_{r=1}^{(n-1)} C_r^{(n-1)} = \sum_{r=1}^{(n-1)} \frac{(n-1)!}{r!\,(n-1-r)!} \tag{3}$$

The determination of optimal switch number and location is achieved by the switch optimization iterative algorithm [9] shown in Fig. 2. The steps involved in the process are explained below,

- Step 1: Divide the DA feeder into "n" number of SS.
- Step 2: Calculate *CIC* for the base case feeder with zero automated switches *(CICb)*. Normalize this interruption cost to find cost index *(CICmi_0)*.
- Step 3: Start the iterative process with one automated switch "r" = 1.
- Step 4: Calculate *CIC* for all possible switch configurations with "r" switches. The number of possible combinations is given by Eq. (3).
- Step 5: Find the lowest *CIC* among all the possible switch configurations *(CICm_r)* with "r" switches.
- Step 6: Normalize *CICm_r* to find cost index *(CICmi_r)*.
- Step 7: Calculate reduction in *CICmi_r* relative to *CICmi_{(r-1)}* *(CICDmi_r)*.
- Step 8: Check if *CICDmi_r* is lower than the iterative threshold *(CICDmi_{limit})*. Although this is a configurable parameter, a value of "8" is used as the threshold in this study.
- Step 9: If the condition is FALSE, then increment the number of switches "r" by one and repeat the process from Step 4.
- Step 10: If the condition is TRUE, then the iterative process has identified the optimal number and placement of switches. The optimal number of switches is "r". The optimal placement is the placement corresponding to *CICm_r*.

# 4   Test Systems

The proposed iterative algorithm for optimal switch number and placement is tested on IEEE 34-bus and IEEE 123-bus test feeders, and Mon Power's real distribution network involved in the WVSC project.
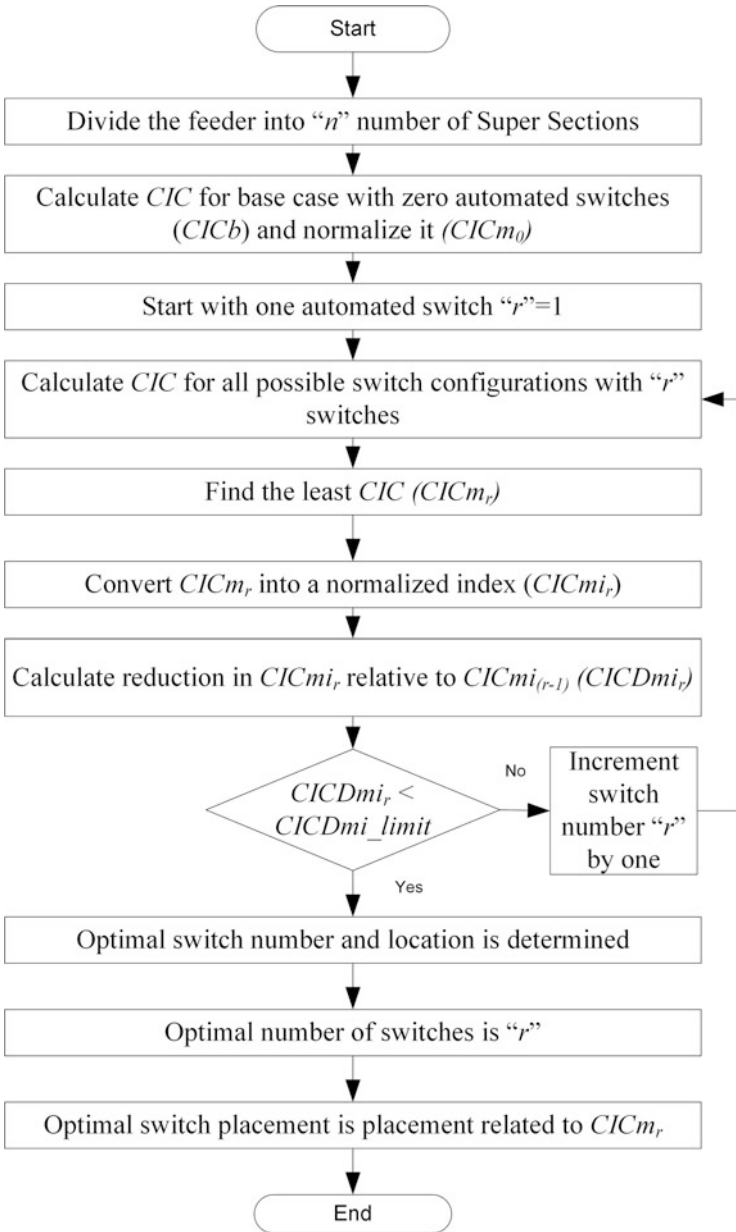
**Fig. 2** Switch optimization iterative algorithm

## 4.1 IEEE 34-Bus System

The IEEE 34-bus system is a perfect candidate to test the proposed algorithm as it is a lengthy feeder and assumed to have a poor reliability. The IEEE 34-bus system represents a real distribution feeder located in Arizona USA. The nominal voltage is 24.9 kV and it has 33 line segments, 6 spot loads, and 19 distributed loads. The feeder data such as spot loads, distributed loads, overhead and underground line segment information, and equipment locations are taken from [10]. Reliability and customer mix data are not available for this feeder. Typical values of reliability data in terms of failure rates are used in the analysis. The customer mix is assumed as 50% residential, 25% commercial, and 25% industrial customers for each line segment.

Circuit topology, switch locations, tie points to adjacent feeders, and customer distribution were taken into consideration to divide the IEEE 34-bus feeder into seven (7) SS as shown in Fig. 3. Table 1 presents data pertaining to all the SS including circuit length, load, and failure rate per annum per mile. It is important to note that circuit length is different from actual feeder length. The circuit length is calculated by summing up individual phase lengths so that the failure rate can be applied to individual phases of the circuit. For example, a three phase line segment's circuit length would be three times the actual line segment's length.

## 4.2 IEEE 123-Bus System

The proposed switch optimization solution is tested on the IEEE 123-bus system to evaluate computational efficacy. The IEEE 123-bus system is the most compre-
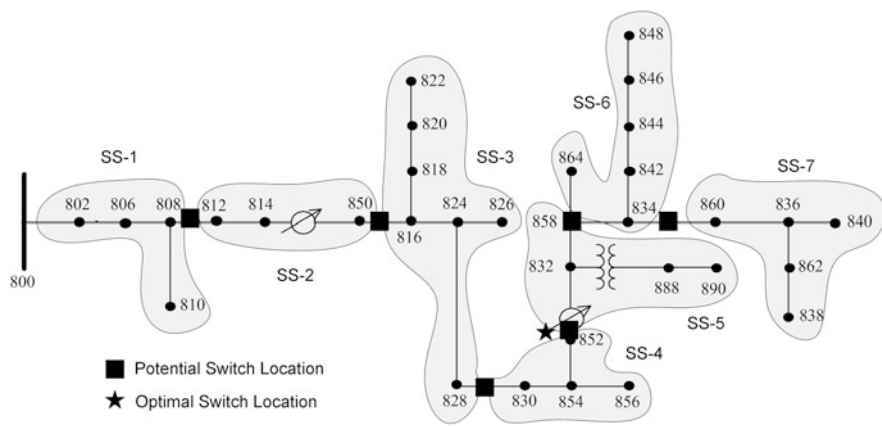


**Fig. 3** IEEE 34-bus test feeder

**Table 1** IEEE 34-bus and IEEE 123-bus test feeder SS data

| Super section ID | IEEE 34-bus system | | | IEEE 123-bus system | | |
|---|---|---|---|---|---|---|
| | Circuit length (miles) | Load (kVA) | Failure rate/year-mile | Circuit length (miles) | Load (kVA) | Failure rate/year-mile |
| SS-1 | 21.86 | 80.1 | 0.06 | 1.17 | 335.4 | 0.59 |
| SS-2 | 38.20 | 0.0 | 0.06 | 4.67 | 1406.2 | 0.59 |
| SS-3 | 19.07 | 244.7 | 0.06 | 1.02 | 178.9 | 0.59 |
| SS-4 | 37.25 | 61.3 | 0.06 | 1.23 | 449.4 | 0.59 |
| SS-5 | 9.10 | 521.9 | 0.06 | 3.47 | 626.1 | 0.59 |
| SS-6 | 6.61 | 712.5 | 0.06 | 0.31 | 438.2 | 0.59 |
| SS-7 | 4.24 | 442.9 | 0.06 | 1.85 | 290.7 | 0.59 |
| SS-8 | N/A | N/A | N/A | 1.06 | 268.3 | 0.59 |
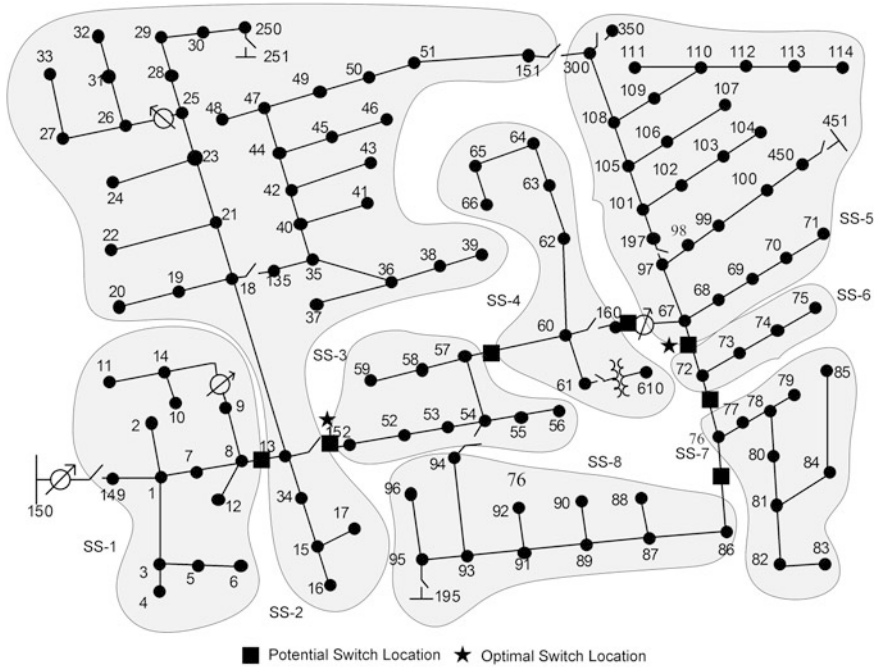
**Fig. 4** IEEE 123-bus test feeder

hensive test feeder which operates at a nominal voltage of 4.16 kV. The feeder has overhead and underground line segments, unbalanced loading, voltage regulators, and shunt capacitor banks. This test feeder is logically divided into eight (8) SS as shown in Fig. 4. The SS data [10] used in the analysis is presented in Table 1. Similar data assumptions are used for this test system as the IEEE 34-bus test system.

## 4.3 WVSC Distribution System

The proposed switch optimization algorithm was successfully implemented on two distribution circuits in Morgantown, West Virginia in USA that were part of the WVSC project. The geographic view of the target distribution system for the WVSC project is illustrated in Fig. 5. The two circuits are the West Run #3 (WR#3) Stewarts Street and the West Run #4 (WR#4) Pine View Circuits. The WR#3 circuit has five (5) normally open tie points with adjacent circuits. Likewise, WR#4 has five (5) normally open tie points with adjacent circuits. Therefore, both circuits have many alternative circuits which can be utilized to provide service after a fault condition has been successfully isolated.
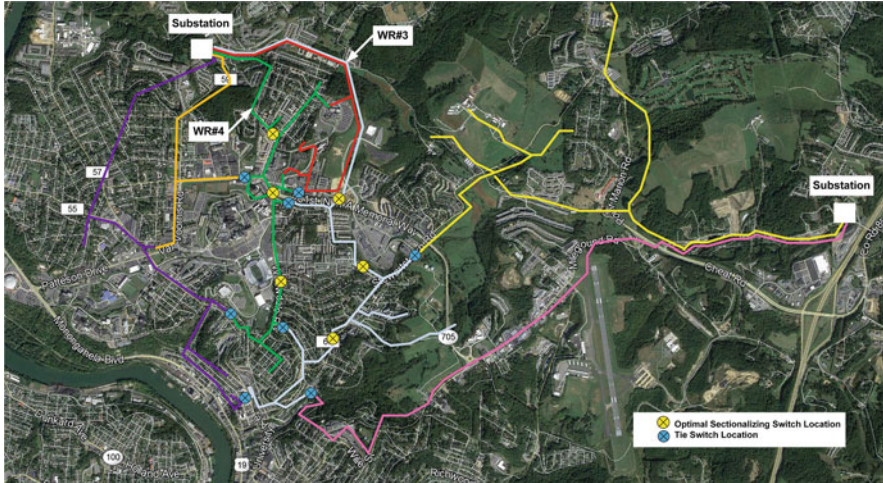
**Fig. 5** Geographic view of WVSC distribution system

The West Run substation has two 138/12.5 kV transformers, each with an installed capacity of 33.6 MVA. The Pierpont substation has two 138/12.5 kV transformers with each having a capacity of 22.4 MVA. There are 327 distribution transformers installed on the WR#3 circuit and 341 distribution transformers installed on the WR#4 circuit. The sum of the capacities of the distribution transformers installed on the WR#3 circuit is 12,942 kVA, while the sum of the capacities of the distribution transformers installed on the WR#4 circuit is 16,670 kVA. The number of transformers, according to their installed capacities, is illustrated in Fig. 6.

The WR#3 circuit has 5.85 miles of 3-phase, 1.28 miles of open-wye circuits and 7.39 miles of single phase circuits. The WR#4 circuit has 6.02 miles of 3-phase, 0.22 miles of open-wye circuits and 10.08 miles of single phase circuits. Both the circuits are dominated by residential type loads. The WR#3 circuit has 2452 customers (2336 residential, 111 commercial and 5 industrial). Similarly, the WR#4 circuit has 3032 customers (2804 residential, 219 commercial and 9 industrial).

The circuits are protected by Cooper Electronic Reclosers with Form-6 controllers at the West Run substation. There are no other reclosers on the main line or on the tap lines on either circuit. Table 2 presents historic reliability data in the form of reliability indices SAIDI, Customer Average Interruption Duration Index (CAIDI), and SAIFI for WR#3 and WR#4 circuits.
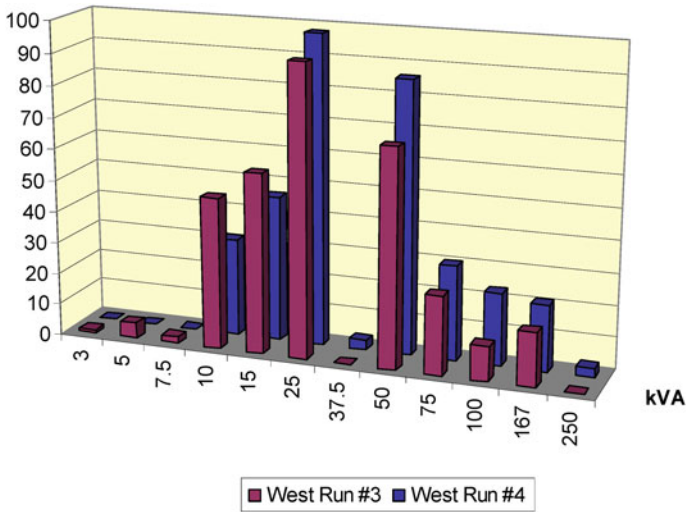
**Fig. 6** WR#3 and WR#4 distribution transformer data

**Table 2** Reliability indices of WVSC circuits (major events included)

|       | 2003 | 2004 | 2005 | 2006 | 2007 | 2008 |
|-------|------|------|------|------|------|------|
| CAIDI |      |      |      |      |      |      |
| WR#3  | 149.00 | 655.48 | 1387.33 | 138.15 | 105.63 | 84.88 |
| WR#4  | 177.41 | 285.23 | 1847.76 | 85.10 | 132.74 | 78.66 |
| SAIDI |      |      |      |      |      |      |
| WR#3  | 192.65 | 198.01 | 2193.16 | 36.21 | 24.13 | 182.80 |
| WR#4  | 53.81 | 102.58 | 929.50 | 11.11 | 17.89 | 277.28 |
| SAIFI |      |      |      |      |      |      |
| WR#3  | 1.2892 | 0.3031 | 1.5807 | 0.2620 | 0.2484 | 2.1538 |
| WR#4  | 0.3032 | 0.3594 | 0.5079 | 0.1305 | 0.1347 | 3.5252 |

The WR#3 and WR#4 circuits are strategically divided into 16 SS and 15 SS respectively. Each SS location is considered to be a potential location for sectionalizing switch. The information relevant to each SS is furnished in Table 3. The load data is only available at the substation transformer in 15-min intervals. Therefore, it is assumed that transformer load is distributed to the feeders evenly proportional with the feeders' distribution transformer installed capacities. It is assumed that customer load percentages at all SS are equal to each other, and the customer mix at the feeder level are used as the input data. The customer load percentages $(Res_z, Com_z, Ind_z)$ for WR#3 and WR#4 feeder used in the analysis are (0.95, 0.04, 0.01) and (0.92, 0.07, 0.00) respectively.

**Table 3** WVSC WR#3 and WR#4 SS data

| Super section ID | WR#3 feeder | | | WR#4 feeder | | |
|---|---|---|---|---|---|---|
| | Circuit length (miles) | Load (kVA) | Failure rate/year-mile | Circuit length (miles) | Load (kVA) | Failure rate/year-mile |
| SS-1 | 0.95 | 463 | 0.0356 | 0.82 | 651 | 0.0364 |
| SS-2 | 1.20 | 274 | 0.0356 | 1.03 | 385 | 0.0364 |
| SS-3 | 1.19 | 89 | 0.0356 | 1.03 | 125 | 0.0364 |
| SS-4 | 0.98 | 164 | 0.0356 | 0.84 | 230 | 0.0364 |
| SS-5 | 1.35 | 1249 | 0.0356 | 1.16 | 1755 | 0.0364 |
| SS-6 | 2.94 | 1309 | 0.0356 | 5.06 | 3681 | 0.0364 |
| SS-7 | 2.94 | 1309 | 0.0356 | 0.36 | 482 | 0.0364 |
| SS-8 | 0.41 | 343 | 0.0356 | 1.30 | 960 | 0.0364 |
| SS-9 | 1.50 | 683 | 0.0356 | 1.48 | 1307 | 0.0364 |
| SS-10 | 1.72 | 930 | 0.0356 | 1.56 | 1240 | 0.0364 |
| SS-11 | 1.81 | 882 | 0.0356 | 1.76 | 1875 | 0.0364 |
| SS-12 | 2.04 | 1334 | 0.0356 | 1.55 | 2599 | 0.0364 |
| SS-13 | 1.80 | 1849 | 0.0356 | 1.36 | 1132 | 0.0364 |
| SS-14 | 1.58 | 806 | 0.0356 | 1.86 | 610 | 0.0364 |
| SS-15 | 2.16 | 434 | 0.0356 | 2.38 | 1155 | 0.0364 |
| SS-16 | 2.76 | 822 | 0.0356 | N/A | N/A | N/A |

## 5  Switch Optimization Results

The customer interruption costs can be derived from the customer damage functions. The customer damage functions for different types of customers used in the analysis are shown in Fig. 7. The analysis assumes average service duration of 240 min to repair the fault and bring back the system to normal condition. Restoration of power to un-faulted zones with the help of automated switches is assumed to take 1 min. Another underlying assumption is that every SS has a back feed capability from an adjacent feeder for power restoration during a grid outage.

The optimal switch number and placement results for IEEE 34-bus, 123-bus, WR#3, and WR#4 test systems are presented in Fig. 8, Tables 4 and 5. The optimal switch solution for IEEE 34-bus system is "1" and "SS-4". The optimal switch solution for IEEE 123-bus system is "2" and "SS-2, SS-5". The optimal switch solution for WR#3 feeder is "3" and "SS-6, SS-10, SS-13". The optimal switch solution for WR#4 feeder is "3" and "SS-5, SS-7, SS-11". The least normalized customer interruption cost index *CICmi* and relative reduction in normalized customer cost interruption index *CICDmi* for a number of switch placements from "0" to "6" are presented in Tables 4 and 5. Each row in Tables 4 and 5 represents a single iteration of the proposed algorithm, and the iterations stop as soon as the *CICDmi* index goes below the predefined threshold of "8". All iterations from a number of switch placements "0" to "6" are shown even beyond the optimal solution to illustrate the working mechanism of the proposed algorithm. Increasing
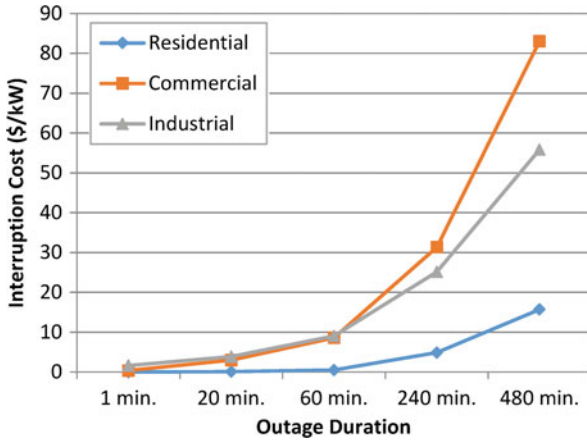
**Fig. 7** Customer damage functions [1]
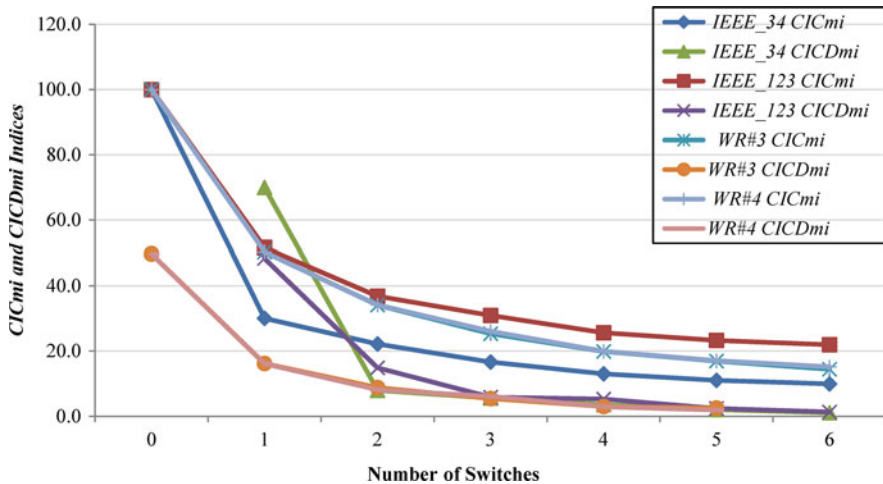


**Fig. 8** Calculated indices for test systems

the number of switches beyond the optimal number would return minimal reduction in total customer interruption cost as shown in Fig. 8 and is not worth exploring.

As per the solution provided by the proposed algorithm, installing one sectionalizing switch at SS-4 on IEEE 34-bus test feeder would reduce the total interruption cost by 69.9% compared to the base case with no switches. Similarly, installing three sectionalizing switches at SS-6, SS-10, and SS-13 on WR#3 feeder would reduce the total interruption cost by 74.7% compared to the base case. Increasing the number of sectionalizing switches beyond the optimal number would result in relative reduction of interruption costs less than 8%. Figures 3, 4, and 5 mark optimal placement of switches for IEEE 34-bus, IEEE-123 bus, WR#3, and WR#4 feeders respectively.

**Table 4** Switch optimization results (IEEE 34-bus and 123-bus feeders)

| | IEEE 34-bus feeder | | | IEEE 123-bus feeder | | |
|---|---|---|---|---|---|---|
| # of switches | $CICmi$ | $CICDmi$ | Optimal switch location | $CICmi$ | $CICDmi$ | Optimal switch location |
| 0 | 100.0 | N/A | N/A | 100.0 | N/A | N/A |
| 1 | 30.1 | 69.9 | SS4[a] | 51.6 | 48.4 | SS3 |
| 2 | 22.2 | 7.9 | SS2, SS4 | 36.8 | 14.8 | SS2, SS5[a] |
| 3 | 16.6 | 5.6 | SS2, SS4, SS5 | 30.9 | 5.9 | SS2, SS4, SS5 |
| 4 | 13.0 | 3.5 | SS2, SS3, SS4, SS5 | 25.6 | 5.3 | SS1, SS2, SS4, SS5 |
| 5 | 11.0 | 2.0 | SS2, SS3, SS4, SS5, SS6 | 23.3 | 2.4 | SS1, SS2, SS4, SS5, SS6 |
| 6 | 9.9 | 1.1 | SS1, SS2, SS3, SS4, SS5, SS6 | 21.9 | 1.3 | SS1, SS2, SS4, SS5, SS6, SS7 |

[a]Optimal switch location determined by the proposed iterative algorithm

**Table 5** Switch optimization results (WVSC WR#3 and WR#4 feeders)

| | WR#3 feeder | | | WR#4 feeder | | |
|---|---|---|---|---|---|---|
| # of switches | $CICmi$ | $CICDmi$ | Optimal switch location | $CICmi$ | $CICDmi$ | Optimal switch location |
| 0 | 100.0 | N/A | N/A | 100.0 | N/A | N/A |
| 1 | 50.3 | 49.7 | SS9 | 50.3 | 49.7 | SS8 |
| 2 | 34.1 | 16.2 | SS6, SS11 | 34.2 | 16.1 | SS6, SS11 |
| 3 | 25.3 | 8.8 | SS6, SS10, SS13[a] | 26.1 | 8.1 | SS5, SS7, SS11[a] |
| 4 | 19.9 | 5.4 | SS5, SS7, SS11, SS13 | 19.9 | 6.1 | SS5, SS6, SS10, SS12 |
| 5 | 16.9 | 3.0 | SS4, SS6, SS9, SS11, SS13 | 17.0 | 2.9 | SS5, SS6, SS9, SS11, SS13 |
| 6 | 14.4 | 2.5 | SS4, SS6, SS8, SS10, SS12, SS14 | 15.2 | 1.9 | SS4, SS5, SS6, SS9, SS11, SS13 |

[a]Optimal switch location determined by the proposed iterative algorithm

The number of *CIC* computations increases as the number of switches "r" value increases. The "r" = 1 scenario incurs the lowest processing time as it requires a lower number of *CIC* computations compared to other "r" > 1 scenarios. Therefore, the proposed iterative algorithm starts with "r" = 1 scenario and stops as soon as the desired solution is achieved. This strategy helps reducing the search space of the problem. According to Eq. (3), there would be 63, 127, 32,767, and 16,383 possible combinations of switch placements on IEEE 34-bus, IEEE-123 bus, WR#3, and WR#4 feeders respectively. The customer interruption cost *CIC* needs to be computed for all the possible combinations to arrive at a global optimal solution. However, the proposed approach cuts down the search space drastically to 21, 63, 1940, and 1470 possible combinations for these test systems and arrives at a solution that satisfies the defined criteria for minimum reduction in customer interruption costs. This greatly simplifies computational complexity of the problem and shows efficacy of the proposed solution. Figure 9 shows the comparison of search space
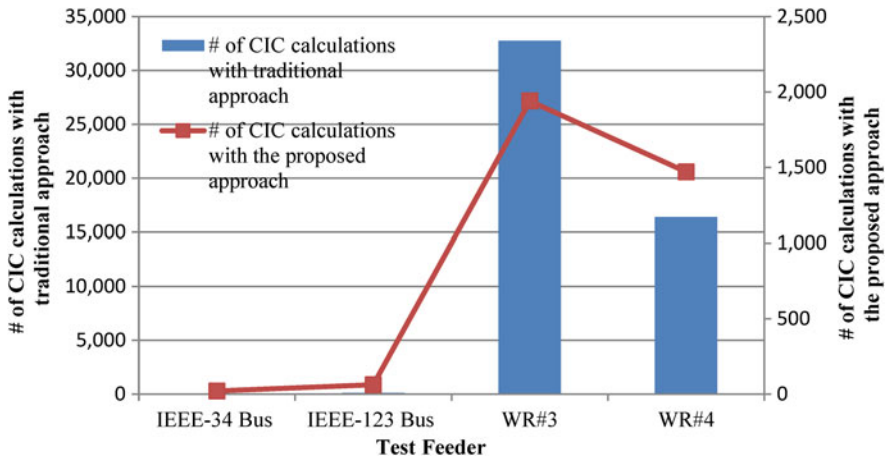
**Fig. 9** Comparison of *CIC* calculations between traditional [4] and proposed switch optimization techniques

in terms of number of *CIC* computations needed for traditional switch optimization approach [4] and the proposed iterative algorithm.

# 6 Conclusions

An innovative iterative algorithm is presented for the optimum switch number and placement problem pertaining to DA projects. The switch optimization is a daunting and crucial step in the economic feasibility evaluation process of DA project. The proposed iterative algorithm can determine the solution faster compared to traditional switch optimization techniques by minimizing the total interruption costs at each step of the analysis. The proposed algorithm does not rely on varying switch capital investment and customer interruption cost data that are usually based on outdated utility surveys. The proposed method is implemented on IEEE 34-bus, 123-bus, and WVSC test feeders. The mathematical model is developed in Matlab and the results show the computational robustness and efficacy of the solution. The proposed technique significantly scales down the search space and simplifies problem complexity that requires minimal computational effort and time.

# References

1. Billinton, R., Jonnavithula, S.: Optimal switching device placement in radial distribution systems. IEEE Trans. Power Deliv. **11**(3), 1646–1651 (1996)
2. Carvalho, P.M., Ferreira, L.A., Da Silva, A.C.: A decomposition approach to optimal remote controlled switch allocation in distribution systems. IEEE Trans. Power Deliv. **20**(2), 1031–1036 (2005)
3. Levitin, G., Mazal-Tov, S., Elmakis, D.: Genetic algorithm for optimal sectionalizing in radial distribution systems with alternative supply. Electr. Power Syst. Res. **35**(3), 149–155 (1995)
4. Chen, C.S., Lin, C.H., Chuang, H.J., et al.: Optimal placement of line switches for distribution automation systems using immune algorithm. IEEE Trans. Power Syst. **21**(3), 1209–1217 (2006)
5. da Silva, L.G., Pereira, R.A., Abbad, J.R., et al.: Optimised placement of control and protective devices in electric distribution systems through reactive tabu search algorithm. Electr. Power Syst. Res. **78**(3), 372–381 (2008)
6. Moradi, A., Fotuhi-Firuzabad, M., Rashidi-Nejad, M.: A reliability cost/worth approach to determine optimum switching placement in distribution systems. In: IEEE Transmission and Distribution Conference and Exhibition: Asia and Pacific, pp. 1–5 (2005)
7. Moradi, A., Fotuhi-Firuzabad, M.: Optimal switch placement in distribution systems using trinary particle swarm optimization algorithm. IEEE Trans. Power Deliv. **23**(1), 271–279 (2008)
8. Falaghi, H., Haghifam, M.R., Singh, C.: Ant colony optimization-based method for placement of sectionalizing switches in distribution networks using a fuzzy multiobjective approach. IEEE Trans. Power Deliv. **24**(1), 268–276 (2009)
9. Chouhan, S., Inan, H., Feliachi, A.: Optimal number and placement of automated sectionalizing switches for smart grid distribution automation. In: IEEE Power and Energy Society General Meeting (PESGM), pp. 1–5 (2016)
10. Kersting, W.H.: Radial distribution test feeders. IEEE Trans. Power Syst. **6**(3), 975–985 (1991)

# Optimal Restoration of Electrical Distribution Systems Considering Switching Sequence

**Juan Camilo López, Pedro P. Vergara, Marcos J. Rider, and Luiz C. P. da Silva**

**Abstract** A short literature review on optimal restoration methods applied to electrical distribution systems (EDS) was presented in chapter one. On that context, this chapter presents a mixed-integer linear programming (MILP) model for the optimal restoration of electrical distribution systems, considering switching sequence. After a permanent fault has been identified, the optimal service restoration determines the status of the remote-controlled switches and the operation of the dispatchable distributed generation (DG) units, in order to isolate the faulty zone and supply as many customers as possible. The proposed mathematical approach considers the switching sequence over a horizon of $S$ discrete steps, guaranteeing that the operational constraints of the system are not violated in every step. By considering the switching sequence in the optimization model, the restoration time and the number of switching operations can be controlled. Thus, the reliability and the power quality of the system are enhanced. The use of a MILP model guarantees convergence to the optimal solution by applying convex optimization techniques. Tests are run using a 136-node distribution system with 28 remote controlled switches, and dispatchable DG. Finally, a comparative analysis is used to establish the relationship between the total un-supplied demand and the number of switching actions along the sequence horizon.

J. C. López (✉) · M. J. Rider · L. C. P. da Silva
UNICAMP - University of Campinas, Campinas, São Paulo, Brazil
e-mail: jclopeza@dsee.fee.unicamp.br; mjrider@dsee.fee.unicamp.br; lui@dsee.fee.unicamp.br

P. P. Vergara
Eindhoven University of Technology, Eindhoven, Netherlands
e-mail: p.p.vergara.barrios@tue.nl

# Notation

The main notations are reproduced below for reference.

*Sets*

| | |
|---|---|
| $\Omega_b$ | Set of nodes |
| $\Omega_g$ | Set of dispatchable DG units |
| $\Omega_s$ | Set of discrete steps of the switching sequence |
| $\Omega_l$ | Set of circuits |
| $\Omega_{\mathrm{sw}}$ | Set of switches |
| $\Omega_z$ | Set of load zones |
| $\Omega_z^{\mathrm{S}}$ | Set of substations |

*Parameters*

| | |
|---|---|
| $c_{z,s}^{\mathrm{U}}$ | Cost of de-energizing zone $z$ during the $s$ |
| $\overline{I}_{ij}$ | Current capacity of circuit $ij$ |
| $\overline{I}_{ij}^{\mathrm{sw}}$ | Current capacity of switch $ij$ |
| $\hat{n}_g$ | Node in which the DG unit $g$ is allocated |
| $\hat{n}_z$ | Initial node of zone $z$ |
| $P_i^{\mathrm{D}}$ | Active demand at node $i$ |
| $\overline{P}_g^{\mathrm{DG}}$ | Active power capacity of DG unit $g$ |
| $\mathrm{pf}_g$ | Power factor limit of DG unit $g$ |
| $Q_i^{\mathrm{D}}$ | Reactive power demanded at node $i$ |
| $\overline{Q}_g^{\mathrm{DG}}$ | Upper reactive power capacity of DG unit $g$ |
| $\underline{Q}_g^{\mathrm{DG}}$ | Lower reactive power capacity of DG unit $g$ |
| $R_{ij}$ | Resistance of circuit $ij$ |
| $\overline{S}_i$ | kVA capacity of substation at node $\hat{z}_i \in \Omega_z^{\mathrm{S}}$ |
| $s_{ij}^{\mathrm{INI}}$ | Initial status of switch $ij$ |
| $s^{\mathrm{MAX}}$ | Maximum discrete step of the switching sequence |
| $\overline{V}$ | Upper voltage limit |
| $\underline{V}$ | Lower voltage limit |
| $V_{\mathrm{nom}}$ | Nominal voltage of the system |
| $X_{ij}$ | Reactance of circuit $ij$ |
| $\hat{z}_i$ | Zone of node $i$ |
| $\hat{z}_{ij}$ | Zone of circuit $ij$ |
| $z_f$ | Faulty zone $z_f \in \Omega_z$ |

*Continuous Variables*

| | |
|---|---|
| $I_{ij,s}$ | Current through circuit $ij$ at discrete step $s$ |
| $I_{ij,s}^{\mathrm{sqr}}$ | Square of $I_{ij,s}$ |
| $I_{ij,s}^{\mathrm{sw}}$ | Current through switch $ij$ at discrete step $s$ |
| $I_{ij,s}^{\mathrm{sw,sqr}}$ | Square of $I_{ij,s}^{\mathrm{sw}}$ |
| $P_{i,s}^{\mathrm{S}}$ | Active generation at node $i$ at discrete step $s$ |

| $P_{g,s}^{DG}$ | Active generation of DG unit $g$ at discrete step $s$ |
| $P_{z_f}^{U}$ | Total un-supplied demand, computed after the restoration due to the isolation of zone $z_f \in \Omega_z$ |
| $P_{ij,s}$ | Active flow at circuit $ij$ at discrete step $s$ |
| $P_{ij,s}^{sw}$ | Active flow at switch $ij$ at discrete step $s$ |
| $Q_{i,s}^{S}$ | Reactive generation at node $i$ at discrete step $s$ |
| $Q_{g,s}^{DG}$ | Reactive generation of DG unit $g$ at discrete step $s$ |
| $Q_{ij,s}$ | Reactive flow through circuit $ij$ at discrete step $s$ |
| $Q_{ij,s}^{sw}$ | Reactive flow through switch $ij$ at discrete step $s$ |
| $V_{i,s}$ | Voltage magnitude at node $i$ at discrete step $s$ |
| $V_{i,s}^{sqr}$ | Square of $V_{i,s}$ |

*Binary Variables*

| $y_{ij,s}$ | Status of switch $ij$ at discrete step $s$, where $y_{ij,s} = 1$ if switch $ij$ is closed at discrete step $s$, or $y_{ij,s} = 0$ otherwise |
| $x_{z,s}$ | Status of zone $z$ at discrete step $s$, where $x_{z,s} = 1$ if zone $z$ is energized, or $x_{z,s} = 0$ otherwise |
| $\Delta y_{ij,s}^{+}$ | Opening of switch $ij$ at discrete step $s$, where $\Delta y_{ij,s}^{+} = 1$ if switch $ij$ has been opened if compared with discrete step $s-1$, or $\Delta y_{ij,s}^{+} = 0$ otherwise |
| $\Delta y_{ij,s}^{-}$ | Closing of switch $ij$ at discrete step $s$, where $\Delta y_{ij,s}^{-} = 1$ if switch $ij$ has been closed if compared with discrete step $s-1$, or $\Delta y_{ij,s}^{-} = 0$ otherwise. |

# 1  Introduction

After a permanent fault has been properly identified and located by the protection scheme, the optimal restoration of electrical distribution systems (EDS) determines the set of sequenced operations that isolates the faulty zone and minimizes the total unsupplied demand. The solution must satisfy a set of operational constraints, related to the electrical and topological limits of the EDS, such as the current and voltage magnitude limits, the operational constraints of the dispatchable DG units, the feeder capacities, and radiality [1].

The optimal restoration of the EDS is a combinatorial optimization problem because the remote controlled switches can be represented using binary decision variables. Furthermore, the optimal restoration is also a non-linear programming problem, due to the non-convex nature of the equations that represent the operation of AC electrical networks [2].

The first computational methodologies used for solving the optimal restoration problem relied on the operator's experience, and step-by-step procedures [3, 4]. Further works considered the operational and topological constraints of the system, using power flow simulations and heuristic approaches to provide restoration sched-

ules in a reasonable computational time [5–7]. With the advent of modern heuristics (a.k.a. meta-heuristics), these techniques have been widely used to provide quality solutions to the restoration problem. Meta-heuristics have been used to deal with conflicting objective functions [8], comparative studies [9], unbalanced systems [10], large distribution networks [11] and robust approaches [12]. Fuzzy logic has also been used in order to enhance the decision making process [13, 14].

Recently, in the context of distribution automation and smart grids, new and more sophisticated approaches have been proposed. A specialized service restoration algorithm is presented in [15], considering direct load control and demand response. Authors in [16] also present a specialized restoration scheme, based on the smart-grid infrastructure. Distributed alternatives are presented in [17–19], via multi-agent systems. A spanning-tree search algorithm is proposed in [20] in order to restore microgrid-based networks after a fault, considering DG and islanded operation. The main drawback of the former methodologies is that none of them guarantee optimality, and none of them are either flexible or easy to develop and adapt in case of new, unexpected, network conditions (i.e., different objective functions, new constraints or topologies).

The use of classical optimization methods—also called exact methods—has also been studied by specialized literature. Authors in [21] have presented a mixed-integer linear programming (MILP) model, based on a DC power flow, used to restore critical shipboard power feeders in case of a contingency (e.g., during battle). Furthermore, authors in [22] formulated a mixed-integer non-linear programming (MINLP) model, with the aim of restoring unbalanced EDS. Authors in [22] have applied an optimization solver to obtain the solution for their proposed MINLP formulation; since the mathematical model is non-convex, the optimization solver cannot guarantee optimality, even for small instances. Authors in [23] present an mixed integer second-order cone programming model to solve the optimal restoration. The model in [23] is convex and can be solved efficiently using classical optimization techniques. Finally, a novel MILP model for the optimal restoration of three-phase unbalanced EDS considering switching sequence and DG units was proposed in [24]. A comprehensive review on optimal restoration methods applied to EDS can be found in [25].

This chapter presents a MILP model used to solve the restoration problem in EDS, which considers switching sequence and operational constraints. The solution of the proposed MILP model determines the operation of the remote controlled switches and dispatchable DG units in each step of the sequence horizon, in order to isolate the faulty zone, and minimize the total un-supplied demand, while guaranteeing a feasible operation and a final radial topology. In each step of the sequence, a single switch would be allowed to change its status. Thus, the proposed MILP model can be used by the system operators to efficiently restore the electrical service after a permanent fault, or to isolate a section of the network, e.g. for maintenance, while supplying most of the demand. Despite other enumerating, heuristic or metaheuristic approaches, MILP models are flexible, easy to reproduce and represent using modeling languages for mathematical programming, such

as AMPL [26]; convergence to optimality is guaranteed by convex optimization solvers, such are as CPLEX [27].

The main objectives of this chapter are as follows:

1. To present a precise and flexible MILP model for the optimal restoration of EDS, considering switching sequence, operational constraints and dispatchable DG resources. The proposed formulation has an efficient computational behavior, and its convergence to optimality is guaranteed by convex optimization techniques.
2. To perform a comparative analysis that demonstrate the conflicting relationship between the total un-supplied demand and the number of switching operations along the sequenced restoration horizon.

## 2  Optimal Restoration of EDS Considering Switching Sequence

After a permanent fault, the optimal restoration problem is solved to determine the best switching sequence, with the double aim of isolating the faulty section of the network and minimizing the un-supplied demand. Meanwhile, all the operational constraints must be guaranteed in every step of the sequence.

The 16-node test system, shown in Fig. 1, is used to explain the proposed sequenced restoration process. During the pre-fault status, the EDS is totally energized, having two radial feeders (associated with sources F1 and F2), five load zones (wherein each load zone is an interconnected section of the system, delimited by switches), and eight remotely-controlled switches, represented by black-colored squares, if closed; white-colored squares are used if open. If a permanent fault occurs in any component of Zone 2, then a basic protection scheme would open the circuit-breaker S2 in order to extinguish the fault (Step 0). However, the opening of S2 also de-energizes zone 5 and increases the amount of un-supplied demand. Eventually, an optimized restoration scheme determines that the demand in Zone 5 can be transferred to the feeder F1, by opening the switch S6 (step 1), followed by the closing of the switch S8 (step 2). This load transference is carried out taking into account the electrical and topological constraints of the system, and considering one switch operation at a time [12].

In addition to the load transference and the switching operation, the optimal restoration process can be enhanced by considering the contribution of the dispatchable DG resources at the end of the switching sequence. Finally, if none of the aforementioned strategies are sufficient, the restoration process can de-energize other zones of the system if necessary in order to maintain the system constraints within their operational limits.

**Fig. 1** Sequenced restoration after a fault in Zone 2: Step 0, open switch S2 to extinguish the faulty zone. Step 1, open switch S6. Step 2, close switch S8 in order to transfer the demand in Zone 5 to the feeder supplied by F1
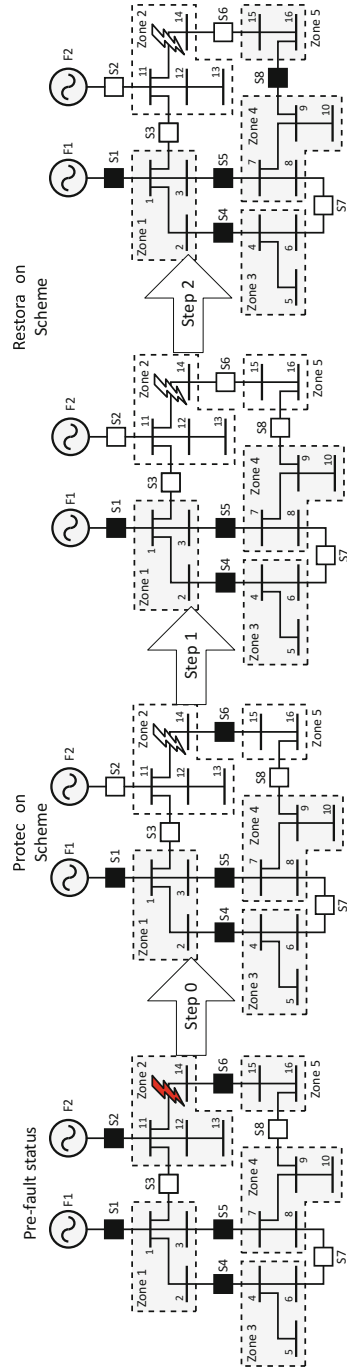
# 3 Mathematical Programming Approach

This section discusses the assumptions and the proposed mathematical model used to represent the optimal restoration problem of EDS, considering switching sequence and DG operation.

## 3.1 Assumptions

The mathematical functions used to calculate the steady-state operating point of the EDS are based on the analytical equations of the backward/forward sweep AC load flow algorithm presented in [28], and first used by authors in [29, 30] to solve other related EDS planning problems. In order to formulate the optimization model the following hypotheses are made:

1. Electrical loads in the EDS are represented as constant active and reactive power loads.
2. The system is assumed to be balanced and represented by its single-phase equivalent circuit.
3. All switches are considered short-length circuits with negligible impedance and limited current capacity.
4. The sequence of switching operations is performed over a horizon of $S$ discrete steps.

## 3.2 Mixed-Integer Non-linear Programming Model

The MINLP model that represents the optimal restoration of balanced EDS, considering the optimal switching sequence is shown in (1)–(20). Note that every node and circuit of the network belongs to a unique zone $z \in \Omega_z$, wherein each zone is a portion of the network delimited by the switching devices.

$$\min \quad \sum_{s \in \Omega_s} \sum_{z \in \Omega_z} c_{z,s}^{\mathrm{U}} \left(1 - x_{z,s}\right) \tag{1}$$

subject to:

$$P_{i,s}^{\mathrm{S}} + \sum_{\substack{g \in \Omega_g| \\ \hat{n}_g = i}} P_{g,s}^{\mathrm{DG}} + \sum_{ji \in \Omega_l} P_{ji,s} - \sum_{ij \in \Omega_l} \left(P_{ij,s} + R_{ij} I_{ij,s}^2\right) +$$

$$\sum_{ji \in \Omega_{\mathrm{sw}}} P_{ji,s}^{\mathrm{sw}} - \sum_{ij \in \Omega_{\mathrm{sw}}} P_{ij,s}^{\mathrm{sw}} = P_i^{\mathrm{D}} x_{\hat{z}_i,s} \quad \forall i \in \Omega_b, s \in \Omega_s \tag{2}$$

$$Q_{i,s}^{\text{S}} + \sum_{\substack{g \in \Omega_g| \\ \hat{n}_g = i}} Q_{g,s}^{\text{DG}} + \sum_{ji \in \Omega_l} Q_{ji,s} - \sum_{ij \in \Omega_l} \left( Q_{ij,s} + X_{ij} I_{ij,s}^2 \right) +$$

$$\sum_{ji \in \Omega_{\text{sw}}} Q_{ji,s}^{\text{sw}} - \sum_{ij \in \Omega_{\text{sw}}} Q_{ij,s}^{\text{sw}} = Q_i^{\text{D}} x_{\hat{z}_i,s} \quad \forall i \in \Omega_b, s \in \Omega_s \quad (3)$$

$$V_{i,s}^2 - V_{j,s}^2 = 2(R_{ij} P_{ij,s} + X_{ij} Q_{ij,s}) + \left( R_{ij}^2 + X_{ij}^2 \right) I_{ij,s}^2 \quad \forall ij \in \Omega_l, s \in \Omega_s \quad (4)$$

$$I_{ij,s}^2 = \frac{P_{ij,s}^2 + Q_{ij,s}^2}{V_{j,s}^2} \quad \forall ij \in \Omega_l, s \in \Omega_s \quad (5)$$

$$\left| V_{i,s}^2 - V_{j,s}^2 \right| \leq \overline{V}^2 \left( 1 - y_{ij,s} \right) \quad \forall ij \in \Omega_{\text{sw}}, s \in \Omega_s \quad (6)$$

$$\left( I_{ij,s}^{\text{sw}} \right)^2 = \frac{\left( P_{ij,s}^{\text{sw}} \right)^2 + \left( Q_{ij,s}^{\text{sw}} \right)^2}{V_{j,s}^2} \quad \forall ij \in \Omega_{\text{sw}}, s \in \Omega_s \quad (7)$$

$$0 \leq I_{ij,s}^2 \leq \overline{T}_{ij}^2 x_{\hat{z}_{ij},s} \quad \forall ij \in \Omega_l, s \in \Omega_s \quad (8)$$

$$\underline{V}^2 x_{\hat{z}_i,s} \leq V_{i,s}^2 \leq \overline{V}^2 x_{\hat{z}_i,s} \quad \forall i \in \Omega_b, s \in \Omega_s \quad (9)$$

$$0 \leq \left( I_{ij}^{\text{sw},s} \right)^2 \leq \left( \overline{T}_{ij}^{\text{sw}} \right)^2 y_{ij,s} \quad \forall ij \in \Omega_{\text{sw}}, s \in \Omega_s \quad (10)$$

$$\left( P_{i,s}^{\text{S}} \right)^2 + \left( Q_{i,s}^{\text{S}} \right)^2 \leq \overline{S}_i^2 \quad \forall i \in \Omega_b^{\text{S}}, s \in \Omega_s \quad (11)$$

$$0 \leq P_{g,s\text{MAX}}^{\text{DG}} \leq \overline{P}_g^{\text{DG}} \quad \forall g \in \Omega_g \quad (12)$$

$$\underline{Q}_g^{\text{DG}} \leq Q_{g,s\text{MAX}}^{\text{DG}} \leq \overline{Q}_g^{\text{DG}} \quad \forall g \in \Omega_g \quad (13)$$

$$\left| Q_{g,s\text{MAX}}^{\text{DG}} \right| \leq P_{g,s\text{MAX}}^{\text{DG}} \tan \left( \arccos \left( \text{pf}_g \right) \right) \quad \forall g \in \Omega_g \quad (14)$$

$$y_{ij,1} - s_{ij}^{\text{INI}} = \Delta y_{ij,1}^+ - \Delta y_{ij,1}^- \quad \forall ij \in \Omega_{\text{sw}} \quad (15)$$

$$y_{ij,s} - y_{ij,s-1} = \Delta y_{ij,s}^+ - \Delta y_{ij,s}^- \quad \forall ij \in \Omega_{\text{sw}}, s \in \Omega_s | s > 1 \quad (16)$$

$$\sum_{ij \in \Omega_{\text{sw}}} \left( \Delta y_{ij,s}^+ + \Delta y_{ij,s}^- \right) \leq 1 \quad \forall s \in \Omega_s \quad (17)$$

$$\left| x_{\hat{z}_i,s} - x_{\hat{z}_j,s} \right| \leq 1 - y_{ij,s} \quad \forall ij \in \Omega_{\text{sw}}, s \in \Omega_s \quad (18)$$

$$\sum_{ij \in \Omega_{\text{sw}}} \left( y_{ij,s\text{MAX}} \cdot x_{\hat{z}_i,s\text{MAX}} \right) = \sum_{z \in (\Omega_z \setminus \Omega_z^{\text{S}})} \left( x_{z,s\text{MAX}} \right) \quad (19)$$

$$y_{ij,s}, x_{z,s}, \Delta y_{ij,s}^{+,-} \in \{0, 1\} \quad \forall ij \in \Omega_{\text{sw}}, z \in \Omega_z, s \in \Omega_s \quad (20)$$

The objective function in (1) aims at minimizing the total cost of the un-supplied demand, computed after deploying the restoration process. If a given zone $z \in \Omega_z$ is de-energized during discrete step $s \in \Omega_s$, then $x_{z,s} = 0$, and the objective function in (1) will increase according to the cost of de-energizing Zone $z$ during discrete step $s$, given by parameter $c_{z,s}^{\mathrm{U}}$.

Constraints (2) and (3) represent the active and reactive power flow balance equations, defined for each node $i \in \Omega_b$ and discrete step $s \in \Omega_s$; these equations considers the DG power injections. Constraint (4) and (5) represent the application of Kirchhoff's voltage law for each circuit of the EDS [28]. Since the impedance of the switches is negligible, constraint (6) guarantees that the voltage drop of a closed switch ($y_{ij,s} = 1$) is equal to zero. Otherwise, if the switch is open ($y_{ij,d} = 0$), both nodal voltages can vary freely within their limits. Constraint (7) calculates the current magnitude of each switch, while constraint (8) limits the current magnitude of the energized circuits. If circuit $ij \in \Omega_{ij}$ is not energized, i.e., if $x_{\hat{z}_{ij},s} = 0$, then (8) guarantees that no current will flow through it. Similarly, constraint (9) limits the voltage magnitude in the energized nodes. If node $i \in \Omega_b$ is not energized, i.e., if $x_{\hat{z}_i,s} = 0$, then no voltage will be set on it. The current limit for the switches is given by (10). If a switch $ij \in \Omega_{\mathrm{sw}}$ is open ($y_{ij,s} = 0$), then no current will flow through it. Otherwise, if $y_{ij,s} = 1$, the square current magnitude will be limited by the switch current capacity. Constraint (11) limits the magnitude of the apparent power generated at each substation $i \in \Omega_b^{\mathrm{S}}$.

The operation of the DG units is represented by constraints (12)–(14). The active and reactive generation capacity of each DG unit is limited by (12) and (13), respectively. As shown by (14), each DG unit is also limited by the nominal power factor, $\mathrm{pf}_g$. Note that all DGs can only operate in the final step of the restoration process ($s^{\mathrm{MAX}}$), since they are not meant to be operated during the switching sequence, unless the model is used to isolate a zone for maintenance.

Equations (15)–(17) represent the sequence operation of the switching devices. Both binary auxiliary variables, $\Delta y_{ij,s}^{+}$ and $\Delta y_{ij,s}^{-}$, represent a switching transition from open-to-closed and closed-to-open, respectively. Constraint (17) guarantees that no more than one transition will be made in each step of the switching horizon. Equation (18) defines the relationship between the switch status $y_{ij,s}$ and zone status $x_{z,s}$. If a switch $ij \in \Omega_{\mathrm{sw}}$ is closed, then both zones must share the same status, since an energized zone cannot be connected to a de-energized zone, and vice versa.

At the final step of the restoration process, it is desired that the energized portion of the system has a radial topology. Radiality is made possible by (19) and the power flow balance equations (2) and (3). As shown by [31], in order to produce a radial graph, the number of energized branches must be equal to the number of energized load nodes. In this particular case, (19) guarantees that the number of closed and energize switches (hence the "·" operator), must be equal to the number of energized load zones. Finally, the binary nature of the decision variables is established by (20).

## 3.3 Linearizations and Approximations

The optimization model shown in (1)–(20) is a MINLP problem due to the non-linear relationships between the variables. MINLP problems are non-convex and optimality can neither be guaranteed by classical optimization techniques nor by modern heuristic approaches. Thus, in order to provide quality solutions using convex optimization tools, such as CPLEX [27], the original MINLP is transformed into a precise, flexible, MILP model, by using the following linearization strategies and approximations:

### 3.3.1 Approximation of the Voltage Magnitude

The squared voltage magnitudes ($V_j^2$) in (5) and (7) are replaced by the squared nominal voltage of the system ($V_{\text{nom}}^2$), as indicated in (21) and (22).

$$I_{ij}^2 \approx \frac{P_{ij}^2 + Q_{ij}^2}{V_{\text{nom}}^2} \qquad\qquad\qquad \forall ij \in \Omega_l \quad (21)$$

$$\left(I_{ij}^{\text{sw}}\right)^2 \approx \frac{\left(P_{ij}^{\text{sw}}\right)^2 + \left(Q_{ij}^{\text{sw}}\right)^2}{V_{\text{nom}}^2} \qquad\qquad \forall ij \in \Omega_{\text{sw}} \quad (22)$$

This approximation produces a relatively low error because the voltage magnitude at each node is limited by a narrow interval, given by $\underline{V}^2 \leq V_{j,s}^2 \leq \overline{V}^2$, if the node is energized.

### 3.3.2 Substitution of Variables

Since the current and voltage magnitudes appear as squared variables in (2)–(10), the following substitutions are applied without loss of generality:

$$I_{ij,s}^{\text{sqr}} = I_{ij,s}^2 \qquad\qquad\qquad \forall ij \in \Omega_l, s \in \Omega_s \quad (23)$$

$$I_{ij,s}^{\text{sw, sqr}} = \left(I_{ij,s}^{\text{sw}}\right)^2 \qquad\qquad \forall ij \in \Omega_{\text{sw}}, s \in \Omega_s \quad (24)$$

$$V_{i,s}^{\text{sqr}} = V_{i,s}^2 \qquad\qquad\qquad \forall i \in \Omega_b, s \in \Omega_s \quad (25)$$

$$I_{ij,s}^{\text{sqr}}, I_{ij,s}^{\text{sw, sqr}}, V_{i,s}^{\text{sqr}} \geq 0 \qquad \forall ij \in \Omega_l, i \in \Omega_b, s \in \Omega_s \quad (26)$$

### 3.3.3 Piece-Wise Linearization

In order to linearize the quadratic terms $P_{ij}^2$ and $Q_{ij}^2$ in (5), $\left(P_{ij}^{\mathrm{sw}}\right)^2$ and $\left(Q_{ij}^{\mathrm{sw}}\right)^2$ in (7), and $\left(P_i^{\mathrm{S}}\right)^2$ and $\left(Q_i^{\mathrm{S}}\right)^2$ in (11), a piecewise linear approximation function is used to linearize each of them. The piece-wise linearization is an adjustable, well-established procedure, similar to the linear approximations used in [32–34] for other EDS optimization problems. An illustration of the piece-wise linearization function of $x^2$ using $\Lambda$ blocks is shonw in Fig. 2.

### 3.3.4 Absolute Value Linear Equivalent

Considering that the inequality $|y| \leq x$ is identical to the combined linear expressions $-x \leq y$ and $y \leq x$, then the absolute values in (6), (14) and (18) are replaced by their linear equivalents.
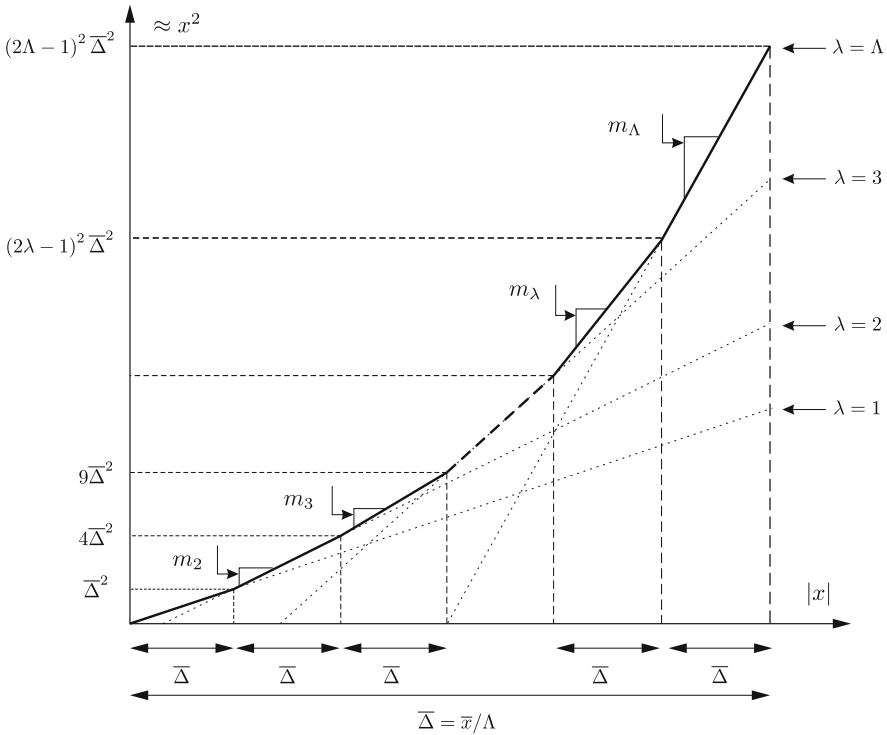


**Fig. 2** Piece-wise linearization function of $x^2$ using $\Lambda$ blocks

### 3.3.5 Binary Product Equivalent

The product between two binary variables in (19) can be assumed by the continuous auxiliary variable $b_{ij,s}$ and calculated using the following linear equivalent equations:

$$y_{ij,s} + x_{\hat{z}_i,s} - 1 \leq b_{ij,s} \leq 1 \qquad\qquad \forall ij \in \Omega_{\text{sw}}, s \in \Omega_s \quad (27)$$

$$0 \leq b_{ij,s} \leq y_{ij,s} \qquad\qquad\qquad \forall ij \in \Omega_{\text{sw}}, s \in \Omega_s \quad (28)$$

$$0 \leq b_{ij,s} \leq x_{\hat{z}_i,s} \qquad\qquad\qquad \forall ij \in \Omega_{\text{sw}}, s \in \Omega_s \quad (29)$$

## 4 Optimization Process

This section presents the proposed step-by-step procedure used to efficiently solve the optimal restoration of EDS, considering switching sequence and DG operation. The following procedure was programmed using the mathematical programming language AMPL [26].

**Step 1:** Let $s^{\text{MAX}}$ be the maximum number of discretized steps. Define the faulty zone $z_f \in \Omega_z$ and fix the zone status $x_{z_f,s} = 0$. Define the initial configuration of the system using the parameter $s_{ij}^{\text{INI}} \in \{0, 1\}$.

**Step 2:** Solve the restoration problem given by (1)–(20), considering the linearizations and simplifications in Sect. 3.3. If feasible, continue. Otherwise, stop.

**Step 3:** Save the switching sequence and neglect redundant operations, i.e., if the a given switch operation does not influence the value of the objetive function, then it is redundant and it should be neglected. Save the total cost of the un-supplied demand (objective function (1)), and the total de-energized demand at the final step of the restoration process, using (30).

$$P_{z_f}^{\text{U}} = \sum_{i \in \Omega_b} P_i^{\text{D}} \left(1 - x_{\hat{z}_i, s^{\text{MAX}}}\right) \qquad (30)$$

## 5 Tests and Results

The 136-node test system shown in Fig. 3 is used to demonstrate the performance of the proposed restoration process. Circuit parameters and node demands can be obtained in [35]. The nominal voltage is $V_{\text{nom}} = 13.2\,\text{kV}$. For simplicity, the cost of de-energizing a given zone during the switching sequence is $c_{z,s}^{\text{U}} = 1 \cdot 10^3\,\text{\$US}$ for $s < s^{\text{MAX}}$, and the cost of de-energizing a zone at the end of the restoration process is $c_{z,s^{\text{MAX}}}^{\text{U}} = 10 \cdot 10^3\,\text{\$US}$. The system has two substations (source nodes
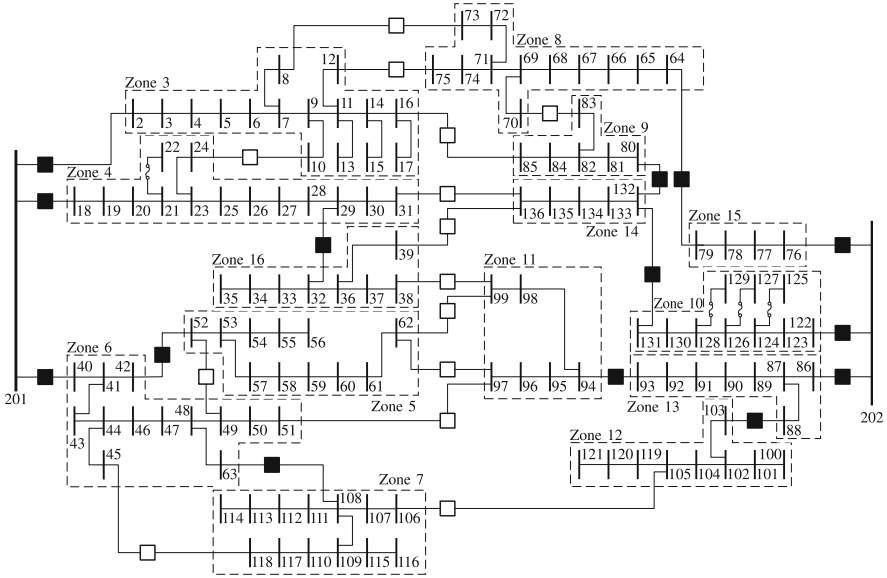
**Fig. 3** 136-node real system with 16 load zones

201 and 202), 16 radial load zones, and 28 remote-controlled switches, indicated with black-colored squares, if initially closed; and if initially open, white-colored squares. The topology shown in Fig. 3 corresponds to the pre-fault state of the EDS. All load zones are energized with a minimum voltage magnitude of 0.9031 p.u., at node 75 (zone 8).

Two case studies are used to demonstrate the adaptability of the proposed restoration process for different operative scenarios. In Case 1, the objective is to isolate a faulty zone and maximize the supplied demand; as soon as the protective scheme has located the fault, i.e., the faulty zone must be de-energized during the entire restoration sequence. In contrast, the objective of Case 2 is to de-energize a given zone for scheduled maintenance, i.e., the EDS operator would like to de-energize a zone in the last step of the switching sequence while reducing the number of de-energized customers in the process. In summary, for Case 1, $x_{z_f,s} = 0 \; \forall s \in \Omega_s$, and for Case 2, $x_{z_f,s^{\text{MAX}}} = 0$. The last column of Table 1 indicates the objective of each case study.

In Case 1, there are no DG units, and the voltage deviation limits are wider, if compared with Case 2. Furthermore, as shown in Table 1, four dispatchable DG units with $\bar{P}_g^{\text{DG}} = 500 \, \text{kW}$, $\bar{Q}_g^{\text{DG}} = 300 \, \text{kVAr}$ and $\text{pf}_g = 0.9$, are available in Case 2, and the generation capacities for both substations are lower. The DG units are located at nodes 35, 56, 83, and 74.

The optimization process in Sect. 4 was implemented using AMPL [26], and the linearized restoration problem was solved via CPLEX [27], with a maximum gap

**Table 1** Features of the proposed case studies

|  | $V_{\min}$ [p.u.] | $V_{\max}$ [p.u.] | $\overline{S}_{201}$ [MVA] | $\overline{S}_{202}$ [MVA] | #DG | Objective |
|---|---|---|---|---|---|---|
| Case 1 | 0.90 | 1.05 | 15.0 | 12.0 | 0 | Restoration |
| Case 2 | 0.93 | 1.05 | 12.0 | 10.0 | 4 | Maintenance |

of 1% as the optimality criterion, on a workstation with an Intel Core i7-4510U (2.60 GHz) processor.

## 5.1 Analysis of Results

Table 2 summarizes the results of the proposed restoration process. Each line in Table 2 indicates the simulated faulty zone ($z_f$), and each column represents the maximum number of discrete steps ($s^{\text{MAX}}$) used for each case study. The first number in each row is the total de-energized demand in kW, calculated using (30), and the second (in parenthesis) is the cost of the un-supplied demand of the restoration process in $10^3$U\$, namely the value of the objective function (1).

In both cases, the total de-energized demand calculated after the isolation of Zones 3, 5, 7, 8, 9, 11, and 12 are identical for all possible values of $s^{\text{MAX}}$. This is expected, because as shown in Fig. 3, the isolation of those zones is made possible by opening only one switch without de-energizing another zone. Thus, the optimal restoration policy after a fault in Zones 3, 5, 7, 8, 9, 11, and 12 is trivial and can be achieved with only one step ($s^{\text{MAX}} = 1$). If more than one discretized step is used ($s^{\text{MAX}} > 1$), then the cost of the un-supplied demand in Case 1 increases because the same zone remains de-energized during all the sequence horizon. However, the cost of the un-supplied demand in Case 2 remains unchanged because the optimization process only de-energizes the specified zone at the last step of the switching sequence.

The proposed restoration process shows that the isolation of Zone 6 can be reached without de-energizing the Zone 5, if the number of discrete steps in Case 1 is set to $s^{\text{MAX}} \geq 5$, or if the number of discrete steps in Case 2 is set to $s^{\text{MAX}} \geq 3$.

The proposed restoration process shows that the isolation of Zone 4 cannot be deployed without de-energizing Zone 16 in Case 1, due to the voltage limits. However, if the number of discrete steps in Case 2 is set to $s^{\text{MAX}} \geq 3$, then the DG resources increase the voltage profile and make it possible to transfer the load in Zone 16 to another neighboring feeder by closing switch 38-99 and opening switch 29-32. The switching sequence used to isolate Zone 4 is shown in Table 3 for both case studies. The symbols "↑" and "↓" represent the "opening" and "closure" of the specified switch, and "–" indicates no switching action required.

Another interesting result is the isolation of Zone 6. In both cases, the proposed restoration process minimizes the total un-supplied demand by transferring Zone

**Table 2** Total de-energized demand ($P^{U}_{z_f}$) in kW, and the cost of the un-supplied demand in $10^3$ \$US, calculated using (1)

| | Case 1 | | | | Case 2 | | | |
|---|---|---|---|---|---|---|---|---|
| Zone | $s^{MAX}=1$ | $s^{MAX}=3$ | $s^{MAX}=5$ | $s^{MAX}=7$ | $s^{MAX}=1$ | $s^{MAX}=3$ | $s^{MAX}=5$ | $s^{MAX}=7$ |
| 3 | 2578.41 | 2578.41 | 2578.41 | 2578.41 | 2578.41 | 2578.41 | 2578.41 | 2578.41 |
| | (10.0) | (12.0) | (14.0) | (16.0) | (10.0) | (10.0) | (10.0) | (10.0) |
| 4 | 2256.98 | 2256.98 | 2256.98 | 2256.98 | 2256.98 | 1276.12 | 1276.12 | 1276.12 |
| | (20.0) | (24.0) | (28.0) | (32.0) | (20.0) | (10.0) | (10.0) | (10.0) |
| 5 | 906.44 | 906.44 | 906.44 | 906.44 | 906.44 | 906.44 | 906.44 | 906.44 |
| | (10.0) | (12.0) | (14.0) | (16.0) | (10.0) | (10.0) | (10.0) | (10.0) |
| 6 | 5226.77 | 5226.77 | 4320.33 | 4320.33 | 5226.77 | 4320.33 | 4320.33 | 4320.33 |
| | (30.0) | (36.0) | (31.0) | (35.0) | (30.0) | (20.0) | (20.0) | (20.0) |
| 7 | 2666.77 | 2666.77 | 2666.77 | 2666.77 | 2666.77 | 2666.77 | 2666.77 | 2666.77 |
| | (10.0) | (12.0) | (14.0) | (16.0) | (10.0) | (10.0) | (10.0) | (10.0) |
| 8 | 1548.18 | 1548.18 | 1548.18 | 1548.18 | 1548.18 | 1548.18 | 1548.18 | 1548.18 |
| | (10.0) | (12.0) | (14.0) | (16.0) | (10.0) | (10.0) | (10.0) | (10.0) |
| 9 | 1300.45 | 1300.45 | 1300.45 | 1300.45 | 1300.45 | 1300.45 | 1300.45 | 1300.45 |
| | (10.0) | (12.0) | (14.0) | (16.0) | (10.0) | (10.0) | (10.0) | (10.0) |
| 10 | 3300.74 | 2000.29 | 851.17 | 851.17 | 3300.74 | 2000.29 | 2000.29 | 2000.29 |
| | (30.0) | (26.0) | (20.0) | (22.0) | (30.0) | (20.0) | (20.0) | (20.0) |
| 11 | 524.32 | 524.32 | 524.32 | 524.32 | 524.32 | 524.32 | 524.32 | 524.32 |
| | (10.0) | (12.0) | (14.0) | (16.0) | (10.0) | (10.0) | (10.0) | (10.0) |
| 12 | 301.03 | 301.03 | 301.03 | 301.03 | 301.03 | 301.03 | 301.03 | 301.03 |
| | (10.0) | (12.0) | (14.0) | (16.0) | (10.0) | (10.0) | (10.0) | (10.0) |
| 13 | 3063.00 | 2538.67 | 2237.64 | 2237.64 | 3063.00 | 2538.67 | 2237.64 | 2237.64 |
| | (30.0) | (26.0) | (20.0) | (22.0) | (30.0) | (20.0) | (10.0) | (10.0) |
| 14 | 2449.57 | 1149.12 | 1149.12 | 1149.12 | 2449.57 | 1149.12 | 1149.12 | 1149.12 |
| | (20.0) | (14.0) | (16.0) | (18.0) | (20.0) | (10.0) | (10.0) | (10.0) |
| 15 | 1886.92 | 1886.92 | 1886.92 | 1886.92 | 1886.92 | 338.74 | 338.74 | 338.74 |
| | (20.0) | (24.0) | (28.0) | (30.0) | (20.0) | (10.0) | (10.0) | (10.0) |
| 16 | 980.85 | 980.85 | 980.85 | 980.85 | 980.85 | 980.85 | 980.85 | 980.85 |
| | (10.0) | (12.0) | (14.0) | (16.0) | (10.0) | (10.0) | (10.0) | (10.0) |
| Total | 28990 | 25865 | 23506 | 23506 | 28990 | 22430 | 22129 | 22129 |
| | (230) | (246) | (255) | (287) | (230) | (170) | (160) | (160) |

**Table 3** All switching sequences used to isolate Zone 4 for every case study

| | Case 1 | | | | | | | Case 2 | | | | | | |
|---|---|---|---|---|---|---|---|---|---|---|---|---|---|---|
| $s^{MAX}$ | $s=1$ | $s=2$ | $s=3$ | $s=4$ | $s=5$ | $s=6$ | $s=7$ | $s=1$ | $s=2$ | $s=3$ | $s=4$ | $s=5$ | $s=6$ | $s=7$ |
| 1 | 201-18↑ | | | | | | | 201-40↑ | | | | | | |
| 3 | 201-18↑ | — | — | | | | | 38-99↓ | 32-29↑ | 201-18↑ | | | | |
| 5 | 201-18↑ | — | — | — | — | | | — | — | 38-99↓ | 32-29↑ | 201-18↑ | | |
| 7 | 201-18↑ | — | — | — | — | — | — | — | — | — | — | 38-99↑ | 32-29↑ | 201-40↑ |

**Table 4** All switching sequences used to isolate Zone 6 for every case study

| $s^{MAX}$ | Case 1 | | | | | | | Case 2 | | | | | | |
|---|---|---|---|---|---|---|---|---|---|---|---|---|---|---|
| | $s=1$ | $s=2$ | $s=3$ | $s=4$ | $s=5$ | $s=6$ | $s=7$ | $s=1$ | $s=2$ | $s=3$ | $s=4$ | $s=5$ | $s=6$ | $s=7$ |
| 1 | 201-40↑ | | | | | | | 201-40↑ | | | | | | |
| 3 | 201-40↑ | — | — | | | | | 62-99↓ | 42-52↑ | 201-40↑ | | | | |
| 5 | 201-40↑ | 42-52↑ | 38-99↓ | 62-99↓ | 93-94↑ | | | — | — | 62-99↓ | 42-52↑ | 201-40↑ | | |
| 7 | 201-40↑ | 42-52↑ | 38-99↓ | 62-99↓ | 93-94↑ | — | — | — | — | — | — | 62-99↑ | 42-52↑ | 201-40↑ |

5 to another neighboring feeder. However, as shown in Table 4, this restoration is only possible in Case 1 if $s^{MAX} \geq 5$, while it only takes three steps in Case 2; this difference is due to the contribution of the DG units. Note that in Case 2, the proposed restoration process generates a temporary loop before isolating Zone 6; since the loop is only set for two steps, the protection scheme should not be triggered or adjusted.

Finally, the contribution of the DG resources can be seen by comparing the values of the last row in Table 2. In spite of the narrow voltage and generation limits, the sums of the total un-supplied demands in Case 2 are lower than the ones in Case 1 for $s^{MAX} \geq 3$. This is because the dispatchable DG resources increases the voltage profile of the system and enhances the restoration capacity of the feeders.

As shown in Table 2, the absence of DGs in Case 1 prevents Zone 16 from being transferred to other feeders, thus the total un-supplied demand is 2256.98 kW. On the other hand, the use of DGs in case 3, makes possible to transfer the load in Zone 16 to the Zone 11, if $s^{MAX} \geq 3$, and reduces the total un-supplied demand to 1276.12 kW in those instances.

## 6 Applicability

Centralized methods, such as the one shown in this chapter, are very flexible and they provide cost efficient restoration solutions. However, they require powerful centralized processors and expensive communication infrastructure. Note that computational complexity grows significantly with the increasing number of switches. Thus, a good pre-processing procedure is recommended to select only the most convenient and reliable switches available at each restoration scenario.

The main challenge of the proposed method relies on the computational performance when deployed in real world applications. The computational complexity of the method can be improved by increasing the processing capacity of the computer being used to run the solver, by reducing the number of linearization blocks $\Lambda$, or by solving the model in two stages or trough decomposition techniques.

# 7 Conclusions

In this chapter, a MILP model for the optimal restoration of EDS has been presented, considering a discretized switching sequence horizon and the contribution of the DG resources. The proposed optimization methodology isolates the zone wherein a permanent fault has been identified (or for maintenance issues) and minimizes the total un-supplied demand after the restoration process. In order to reduce the un-supplied demand, and guarantee the operational limits of the system, the proposed MILP model establishes the sequence of switch operations, one at a each step, and DG outputs, along the switching horizon.

As demonstrated by the results, if the number of discrete steps is increased, more demand can be energized at the end of the restoration process. However, the number of switching operations and the complexity of the problem are also increased. The proposed MILP model can be used to efficiently isolate load zones, e.g., for maintenance, considering the use of temporary loops in order to transfer load to neighboring feeders. Finally, some applicability issues and implementation challenges of the proposed approach have been discussed.

# References

1. Willis, H.L.: Power Distribution Planning Reference Book, 2nd edn. New York, Marcel Dekker (2004)
2. Cavalcante, P.L., et al.: Centralized self-healing scheme for electrical distribution systems. IEEE Trans. Smart Grid **7**, 145–155 (2016)
3. Liu, C.-C., Lee, S.-J. , Venkata, S.: An expert system operational aid for restoration and loss reduction of distribution systems. IEEE Trans. Power Syst. **3**, 619–626 (1988)
4. Hsu, Y.-Y., et al.: Distribution system service restoration using a heuristic search approach. IEEE Trans. Power Delivery **7**, 734–740 (1992)
5. Aoki, K., Nara, K., Itoh, M., Satoh, T., Kuwabara, H.: A new algorithm for service restoration in distribution systems. IEEE Trans. Power Delivery **4**, 1832–1839 (1989)
6. Morelato, A.L., Monticelli, A.: Heuristic search approach to distribution system restoration. IEEE Trans. Power Delivery **4**, 2235–2241 (1989)
7. Sarma, N., Ghosh, S., Rao, K., Srinivas, M.: Real time service restoration in distribution networks-a practical approach. IEEE Trans. Power Delivery **9**, 2064–2070 (1994)
8. Kumar, Y., Das, B., Sharma, J.: Multiobjective, multiconstraint service restoration of electric power distribution system with priority customers. IEEE Trans. Power Delivery **23**, 261–270 (2008)
9. Toune, S., Fudo, H., Genji, T., Fukuyama, Y., Nakanishi, Y.: Comparative study of modern heuristic algorithms to service restoration in distribution systems. IEEE Trans. Power Delivery **17**, 173–181 (2002).
10. Manjunath, K., Mohan, M.: A new hybrid multi-objective quick service restoration technique for electric power distribution systems. Int. J. Electr. Power Energy Syst. **29**, 51–64 (2007)
11. Sanches, D.S., et al.: Multiobjective evolutionary algorithm with a discrete differential mutation operator developed for service restoration in distribution systems. Int. J. Electr. Power Energy Syst. **62**, 700–711 (2014)

12. López, J.C., Rider, M.J., Wu, Q.: Parsimonious short-term load forecasting for optimal operation planning of electrical distribution systems. IEEE Trans. Power Syst. **34**, 1427–1437 (2019)
13. Huang, C.-M. Multiobjective service restoration of distribution systems using fuzzy cause-effect networks. IEEE Trans. Power Syst. **18**, 867–874 (2003)
14. Chen, W.-H.: Quantitative decision-making model for distribution system restoration. IEEE Trans. Power Syst. **25**, 313–321 (2010)
15. Kleinberg, M., Miu, K., Chiang, H.-D.: Improving service restoration of power distribution systems through load curtailment of in-service customers. IEEE Trans. Power Syst. **26**, 1110–1117 (2011)
16. Song, I.-K., et al.: Operation schemes of smart distribution networks with distributed energy resources for loss reduction and service restoration. IEEE Trans. Smart Grid **4**, 367–374 (2013)
17. Solanki, J., Khushalani, S., Schulz, N.: A multi-agent solution to distribution systems restoration. IEEE Trans. Power Syst. **22**, 1026–1034 (2007)
18. Nguyen, C., Flueck, A.: Agent based restoration with distributed energy storage support in smart grids. IEEE Trans. Smart Grid **3**, 1029–1038 (2012)
19. Eriksson, M., Armendariz, M., Vasilenko, O., Saleem, A., Nordstrom, L.: Multiagent-based distribution automation solution for self-healing grids. IEEE Trans. Ind. Electron. **62**, 2620–2628 (2015)
20. Li, J., Ma, X.-Y., Liu, C.-C., Schneider, K.: Distribution system restoration with microgrids using spanning tree search. IEEE Trans. Power Syst. **29**, 3021–3029 (2014)
21. Butler, K., Sarma, N., Ragendra Prasad, V.: Network reconfiguration for service restoration in shipboard power distribution systems. IEEE Trans. Power Syst. **16**, 653–661 (2001)
22. Khushalani, S., Solanki, J., Schulz, N.: Optimized restoration of unbalanced distribution systems. IEEE Trans. Power Syst. **22**, 624–630 (2007)
23. Romero, R., Franco, J.F., Leão, F.B., Rider, M.J., de Souza, E.S.: A new mathematical model for the restoration problem in balanced radial distribution systems. IEEE Trans. Power Syst. **31**(2), 1259–1268 (2016)
24. López, J.C., Franco, J.F., Rider, M.J., Romero, R.: Optimal restoration/maintenance switching sequence of unbalanced three-phase distribution systems. IEEE Trans. Smart Grid **9**, 6058–6068 (2018)
25. Shen, F., et al.: Review of service restoration methods in distribution networks. In: 2018 IEEE PES Innovative Smart Grid Technologies Conference Europe (ISGT-Europe), Sarajevo (2018)
26. Fourer, R., Gay, D.M., Kernighan, B.W.: AMPL: A Modeling Language for Mathematical Programming, 2nd edn. Brooks/Cole-Thomson Learning, Pacific Grove (2003)
27. ILOG Inc., Incline Village, NV: CPLEX Optimization Subroutine Library Guide and Reference. CPLEX division edn. (2008)
28. Cespedes, R.: New method for the analysis of distribution networks. IEEE Trans. Power Delivery **5**, 391–396 (1990)
29. Baran, M., Wu, F.: Optimal capacitor placement on radial distribution systems. IEEE Trans. Power Delivery **4**, 725–734 (1989)
30. Baran, M., Wu, F.: Network reconfiguration in distribution systems for loss reduction and load balancing. IEEE Trans. Power Delivery **4**, 1401–1407 (1989)
31. Lavorato, M., Franco, J.F., Rider, M.J., Romero, R.: Imposing radiality constraints in distribution system optimization problems. IEEE Trans. Power Syst. **27**, 172–180 (2012)
32. Franco, J.F., Rider, M.J., Lavorato, M., Romero, R.: Optimal conductor size selection and reconductoring in radial distribution systems using a mixed-integer LP approach. IEEE Trans. Power Syst. **28**, 10–20 (2013)
33. Zhang, H., Vittal, V., Heydt, G., Quintero, J.: A mixed-integer linear programming approach for multi-stage security-constrained transmission expansion planning. IEEE Trans. Power Syst. **27**, 1125–1133 (2012)

34. Gonçalves, R.R., Alves, R.P., Franco, J.F., Rider, M.J.: Operation planning of electrical distribution systems using a mixed integer linear model. J. Control Autom. Electr. Syst. **24**, 668–679 (2013)
35. Sistemas Testes. Laboratorio de Planejamento de Sistemas de Energia Elétrica (LaPSEE). 136 Buses, 156 Branches Medium City Real Distribution System for Network Reconfiguration. http://www.feis.unesp.br/#!/departamentos/engenharia-eletrica/pesquisas-e-projetos/lapsee/downloads/

# Electric Distribution Network Planning Under Uncertainty

**Julio López, Marcos J. Rider, and Javier Contreras**

**Abstract** This chapter presents a deterministic and an adaptive robust model for the short-term network expansion planning in electric distribution networks, considering siting and sizing of voltage regulators, capacitor banks, renewable energy generation, energy storage systems, and existing overloaded feeders reinforcement. The objective function to be minimized consists of investment and operation costs. Conventional expansion models in distribution networks are stated as a mixed-integer non-linear mathematical programs. In this chapter, we introduce the standard formulation and transform it into a mixed-integer linear programming form. This formulation is used to solve a deterministic short-term electric distribution network expansion planning case. Based on the deterministic formulation, we expand the formulation to a two-stage tri-level adaptive robust problem for considering load consumption and renewable-based DG uncertainties. By using Karush–Kuhn–Tucker conditions, this model is transformed into a two-stage bi-level adaptive robust optimization problem. A column and constraint generation framework is used to solve the problem. Computational results are obtained from a 123-node distribution system under different conditions to assess the performance of the proposed approach. Results show the effectiveness of the proposed methodology.

J. López (✉)
Electrical Engineering School, University of Cuenca, Cuenca, Ecuador
e-mail: julio.lopez@ucuenca.edu.ec

M. J. Rider
Department of Systems and Energy, School of Electrical and Computer Engineering, University of Campinas, Campinas, SP, Brazil
e-mail: mjrider@dsee.fee.unicamp.br

J. Contreras
Escuela Técnica Superior de Ingenieros Industriales, Universidad de Castilla-La Mancha, Ciudad Real, Spain
e-mail: Javier.Contreras@uclm.es

# 1    Introduction

Nowadays, distribution companies (DISCOs) are facing multiple challenges to meet the new needs and preferences of the consumers. DISCOs are moving from operating passive networks to dealing with active elements such as distributed energy resources (DERs) (e.g. microturbines, wind turbines, photovoltaic systems, and battery energy storage systems), electric vehicles (EVs) and demand-side management. The future electric distribution networks (EDNs) will need to deal with these challenges in the operation of EDNs. However, we need to start to carefully envisage future EDNs in order to consider them in the short-term planning decisions.

DERs play an essential role in EDNs because of their potential techno-economic advantages [17]. But the uncertainty and intermittency of DERs, as well as the stochastic characteristics of certain types of load consumption such as plug-in EVs, are new challenges to be faced by the EDN operators and planners, which have never existed before.

Thus, it is indispensable to consider the uncertainty of those DERs in EDN planning when a lot of renewable energy resources are incorporated into those networks [23]. In this context, EDN planners need to take into consideration the existing uncertainties in DERs. In [6], stochastic programming is used to deal with these uncertainties. In the stochastic programming approach, Monte Carlo strategies are frequently used to generate the necessary number of scenarios for the sources of uncertainty such as photovoltaic generation (PVG), turbine generation (WTG), demand consumption, energy price and EV impact based on specified probabilities [60]. It is important to know that probability density functions are necessary for the stochastic methods [25]. However, it is difficult to obtain the precise probability values of those sources of uncertainty in real-world applications. Stochastic programming techniques have been successfully applied in many fields. However, in practice, one may not always have sufficient data to estimate the probability density functions [56]. In comparison with stochastic optimization, robust optimization has become a powerful approach because of its efficiency [8–11, 13, 14, 31, 57]. In the robust optimization framework, an uncertainty set scheme is used to represent the uncertain parameters of the stochastic sources [53] instead of the probability density functions. The most significant advantages of the robust approach are: i) an exact probability density function is not required and ii) the obtained optimal solution can be maintained for all the realizations within the uncertainty set [54].

Solutions from a single-stage robust optimization model have a tendency to be extremely conservative. To deal with this issue, two-stage optimization, also known as *adjustable* or *adaptable* robust optimization, has been extensively studied [12], where the second-stage problem is associated with the decision-making after the first-stage decisions are made and the uncertainty revealed.

According to [12], two-stage robust optimization based problems are hard to compute, because, even the simplest ones, could be NP-hard. Three solution

strategies have been studied. The first one consists of the use of algorithms, which assume that second-stage decisions are affine functions of the uncertainty [15]. The second type is based on Benders decomposition, where the function values of the first-stage decisions are established in a gradual way, using the dual solutions of the second-stage problem [16, 35, 51, 58]. These are the well-known Benders-dual cutting plane algorithms. The third type of algorithm is a different cutting plane strategy. This algorithm uses a master problem and a subproblem; it is based on the fact that the algorithm iteratively adds the variables that correspond to the decision variables of the second-stage problem and the constraints are added to from the uncertainty parameters considering the worst-case scenario in the second stage. This algorithm is known as the column-and-constraint generation (C&CG) method.

Traditional short-term EDN planning mainly seeks to decrease the power loss by sitting and sizing voltage magnitude control devices, such as voltage regulators (VRs), reactive power compensators such as capacitor banks (CBs), as well as conductor replacement and network reconfiguration [26]. In this context, since renewable-based DG is subject to uncertainty, integrating these DGs into EDNs can have an impact on its operation [5]. Therefore, it is important to characterize the uncertainty appropriately to find a robust integration scheme for the renewable-based DG.

Stochastic programming has been extensively used to face renewable-based DG uncertainties. In [40, 43], PVG or WTG generation power outputs are studied. In [2], a voltage control methodology stochastic-based optimization, considering PVG uncertainties is proposed. A scenario-based stochastic programming methodology, taking into account the renewable sources and load consumption uncertainties, is presented in [41] to solve the distribution system expansion planning problem considering both cost and reliability functions. In [52], the sitting and sizing of both dispatchable DG and renewable-based DG in microgrids are studied by a two-stage robust optimization problem, which is solved using a C&CG-based algorithm. The multi-period EDN expansion planning problem, considering load consumption and electricity price as uncertain, is solved in [3] by a robust framework. In [49], a multi-period and stochastic programming has been implemented for DER integration, minimizing the emissions level, operation and maintenance costs.

According to [5], robust optimization could be more practical and manageable in planning problems considering DERs than stochastic programming because of the nature of the uncertainty sources. The reasons are: (1) robust optimization needs only the variation of an uncertainty parameter to create the uncertainty set, while stochastic optimization needs the probability distribution functions of the uncertain parameters, (2) the optimal solution obtained from the robust optimization problem is feasible for all the realizations within the uncertainty set, while the optimal solution obtained from the stochastic optimization problem may be feasible only for the scenarios considered in this problem, and (3) the solution space of a robust optimization problem depends on the number of uncertainty parameters, while the solution space of a stochastic optimization problem depends on the number of uncertainty parameters and the number of scenarios [15, 19]. As stated, uncertainty in EDNs considering renewable-based DG creates problems that are

computationally challenging. According to literature, all authors agree that robust optimization is an efficient method to deal with uncertainties compared with scenario-based stochastic optimization.

Furthermore, the non-linear and non-convex framework of the AC optimal power flow equations adds a notable challenge to the solution of this problem. Some authors have been dealing with these features for the expansion planning problems, e.g., [30]. However, the non-convex AC-OPF problem cannot guarantee optimal global solutions [1]. Fortunately, the AC-OPF has a special formulation in distribution grids that are operated in a tree-shaped network. For instance, a second-order conic relaxation (SOCR) of the original nonconvex and nonlinear programming can employed resulting in a second-order conic programming (SOCP) model that can be efficiently solved [34]. Though, this is a relaxation (not exactly the same problem), SOCP can guarantee a global solution making it appealing to use as alternative to the nonconvex AC-OPF.

Based on the aforementioned issues, we propose an adaptive robust optimization model for short-term EDN planning problem that considers sitting and sizing of renewable-based DG units, particularly PV and WT units, ESSs, conductor replacement of overloaded circuits, voltage control equipment, such as VRs, and reactive power compensators, such as CBs, characterizing the uncertainty of load consumption and power generation of PV and WT by an adjustable polyhedral uncertainty set. Besides, as a result of the incorporation this adjustable polyhedral uncertainty set, a two-stage three-level robust optimization mathematical model is formulated, which is transformed into a two-stage two-level adaptive robust optimization problem by using Karush–Kuhn–Tucker (KKT) conditions and solved by employing a C&CG algorithm. The nonlinear AC power flow equations are convexified, resulting in a mixed integer linear programming (MILP) model [5, 7, 50, 52].

The rest of this chapter is organized as follows. Section 2 introduces a detailed deterministic model for EDN operation. The power flow formulation is presented in Sect. 2.1. In Sect. 2.2, VR equations are modeled. In Sect. 2.3, fixed and switchable CB equations are modeled. Equations for ESSs are presented in Sect. 2.4. Section 2.5 presents the WTG and PVG modeling equations. In Sect. 2.6, the mathematical formulation for conductor replacement of overload feeders is presented. The objective function for the proposed deterministic model is formulated in Sect. 2.7. The overall formulation of the deterministic model is presented in Sect. 2.8. Numerical results for the deterministic approach are presented and discussed in Sect. 2.9. An adaptive robust optimization framework is addressed in Sect. 3. The definition of the uncertainty parameters for the robust problem is presented in Sect. 3.1. Section 3.1.1 presents the uncertainty set characterization. The adaptive robust formulation for the proposed problem is presented in Sect. 3.2. The solution framework, numerical results and discussions are presented in Sect. 3.3. Finally, some conclusions and remarks are presented in Sect. 4.

## 2 Deterministic Formulation for Short-Term EDN Expansion Planning

### 2.1 Power Flow Formulation

Contrary to transmission networks, EDNs have a radial topology and are operated radially. The analysis of an EDN requires the solution of the power flow problem to establish the state of the system that is determined by voltage magnitudes in nodes, current flows in feeders, energy losses and other variables of interest [37]. In this work, the equations that represent the multi-period steady-state power flow problem of radial networks are obtained from the "DistFlow" equations [7, 27], and can be used to calculate the power flows at each node as follows:

$$\sum_{(jk)\in\mathbf{B}} p_{jk,t} - \sum_{(km)\in\mathbf{B}} (p_{km,t} + R_{km}i_{km,t}^2) + p_{k,t}^S - P_{k,t}^D = 0 \qquad \forall k \in \mathbf{N},\ \forall t \in \mathbf{P} \tag{1}$$

$$\sum_{(jk)\in\mathbf{B}} q_{jk,t} - \sum_{(km)\in\mathbf{B}} (q_{km,t} + X_{km}i_{km,t}^2) + q_{k,t}^S - Q_{k,t}^D = 0 \qquad \forall k \in \mathbf{N},\ \forall t \in \mathbf{P} \tag{2}$$

$$v_{k,t}^2 - v_{m,t}^2 = 2(R_{km}p_{km,t} + X_{km}q_{km,t}) + (R_{km}^2 + X_{km}^2)i_{km,t}^2 \quad \forall(km) \in \mathbf{B},\ \forall t \in \mathbf{P} \tag{3}$$

$$i_{km,t}^2 = \frac{p_{km,t}^2 + q_{km,t}^2}{v_{m,t}^2} \qquad \forall(km) \in \mathbf{B},\ \forall t \in \mathbf{P} \tag{4}$$

The "DistFlow" equations are used by removing the nonlinear terms from constraints (1), (2), (3) and (4), resulting in a linear equation set for the power flow in radial EDNs as follows:

$$\sum_{(jk)\in\mathbf{B}} p_{jk,t} - \sum_{(km)\in\mathbf{B}} p_{km,t} + p_{k,t}^S - P_{k,t}^D = 0 \qquad \forall k \in \mathbf{N},\ \forall t \in \mathbf{P} \tag{5}$$

$$\sum_{(jk)\in\mathbf{B}} q_{jk,t} - \sum_{(km)\in\mathbf{B}} q_{km,t} + q_{k,t}^S - Q_{k,t}^D = 0 \qquad \forall k \in \mathbf{N},\ \forall t \in \mathbf{P} \tag{6}$$

$$v_{k,t} - v_{m,t} = \frac{2(R_{km}p_{km,t} + X_{km}q_{km,t})}{v_0} \qquad \forall(km) \in \mathbf{B},\ \forall t \in \mathbf{P} \tag{7}$$

Thus, constraints (5)–(7) represent the convexified form of the nonlinear constraints (1)–(4).

The total active power losses on the EDN are calculated as follows:

$$TPL = \sum_{t \in \mathbf{P}} \sum_{(km) \in \mathbf{B}} R_{km} \left( \frac{p_{km,t}^2 + q_{km,t}^2}{v_{m,t}^2} \right) \tag{8}$$

## 2.2 Voltage Regulator Model

Basically, a voltage regulator (VR) is an autotransformer with an automatic changing mechanism of the tap position inside of the winding that allows us to maintain a predetermined level of output voltage magnitude in case of load variations, and can be operated under loading conditions.

Figure 1 shows a VR located at node $m$ of branch $km$, where node $m$ is the non-regulated voltage magnitude node.

As observed in Fig. 1, the VR in branch $km$ can be divided into two branches, where one of the branches includes the tap changer and the other the VR impedance. Note that $v_m$ is the non-regulated voltage magnitude (before the VR) and $a_{km}$ varies within the range $[(1 - R_{km}^\%), (1 + R_{km}^\%)]$, allowing regulation of $\pm R_{km}^\%$. On the other hand, taking into account the multi-period short-term characteristic of the EDN problem planning, the tap position ($a_{km}$) of the VR can be computed approximately [29]. In this work, the tap position of the VR is assumed to be a continuous variable. With these considerations, the linear equations (9) and (10) represent the mathematical formulation to the operation and allocation of VRs in the EDNs, where (9) allows us to compute the regulating voltage in node $m$ (after the VR) and (10) limits the voltage magnitude varying within the range of regulation. Finally, $\alpha_{km,t}^{vr}$ variable is introduced to indicate the installation of a new VR. If $\alpha_{km,t}^{vr} = 1$, a VR must be installed at node $k$.

$$(1 - R_{km}^\%)v_{m,t} \leq \tilde{v}_{m,t} \leq (1 + R_{km}^\%)v_{m,t} \qquad \forall (km) \in \mathbf{VR}, \ \forall t \in \mathbf{P} \tag{9}$$

$$\tilde{v}_{m,t} - v_{m,t} \leq \left| V_m^{\max} - V_m^{\min} \right| \alpha_{km,t}^{vr} \qquad \forall (km) \in \mathbf{VR}, \ \forall t \in \mathbf{P} \tag{10}$$

$$\alpha_{km,t}^{vr} \in \{0, 1\} \qquad \forall k \in \mathbf{VR}, \ \forall t \in \mathbf{P} \tag{11}$$



**Fig. 1** Voltage regulator model
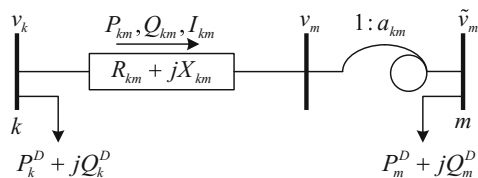
## 2.3 Capacitor Bank Model

With the aim of improving the EDNs overall efficiency and power delivery, it is essential to reduce the total losses of the system. Total losses can be reduced by the optimal sizing and placing of capacitor banks (CBs) at EDNs [42]. Usually, two types of CBs are available to be installed in EDNs: (1) Fixed Capacitor Banks (FCBs) and (2) Switchable Capacitor Banks (SCBs) [38]. FCBs are formed by units that are always connected to the EDN, as shown in Fig. 2, whereas SCBs are conformed by units that may be totally or partially connected to the EDN depending on the load variability, as shown in Fig. 3.

In this work, the allocation of fixed and switchable capacitor banks is formulated according to [39], where the reactive capacitive power injected by each installed CB is formulated in (12) and its capacity is formulated in (13). Constraints (14) and (15) define the type of CB (fixed or switchable) to be installed, when $n_{k,t}^{cb} = n_k^{max}$ is fixed and when $n_{k,t}^{cb} < n_k^{max}$ is switchable. Constraint (16) guarantees that only one type of CB (fixed or switchable) can be installed at node $k$. Constraints (17) and (18) define the capacity of the fixed or switchable CBs to be installed at node $k$. Equations (19) and (20) represent the binary and integer installation decision variables.

$$q_{k,t}^{CB} = n_{k,t}^{cb} Q_b^{sp} \qquad \forall k \in \mathbf{R}, \ \forall t \in \mathbf{P}, \ \forall b \in \mathbf{CB} \qquad (12)$$

$$0 \le n_k^{max} \le \sum_{b \in \mathbf{CB}} b\alpha_{k,b,t}^{fx} + \sum_{b \in \mathbf{CB}} b\alpha_{k,b,t}^{sw} \qquad \forall k \in \mathbf{R}, \ \forall t \in \mathbf{P} \qquad (13)$$
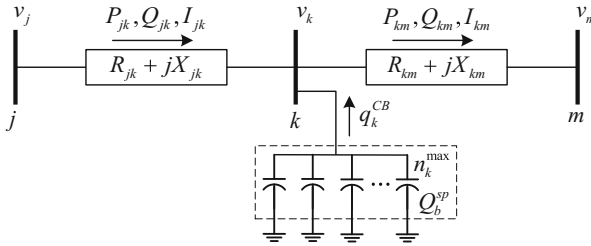


**Fig. 2** Fixed capacitor model
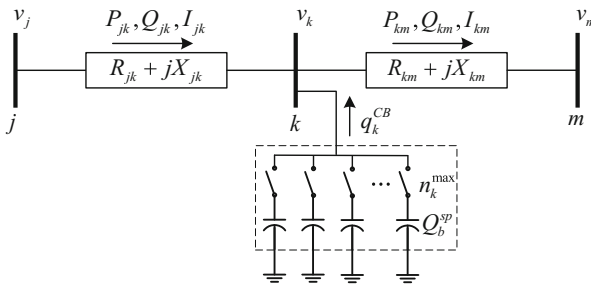


**Fig. 3** Switchable capacitor model

$$n_k^{\max} \leq n_{k,t}^{cb} + \sum_{b \in \mathbf{CB}} b\alpha_{k,b,t}^{sw} \qquad \forall k \in \mathbf{R}, \ \forall b \in \mathbf{CB}, \ \forall t \in \mathbf{P} \qquad (14)$$

$$0 \leq n_{k,t}^{cb} \leq n_k^{\max} \qquad \forall k \in \mathbf{R}, \ \forall t \in \mathbf{P} \qquad (15)$$

$$\sum_{b \in \mathbf{CB}} b\alpha_{k,b,t}^{fx} + \sum_{b \in \mathbf{CB}} b\alpha_{k,b,t}^{sw} \leq 1 \qquad \forall k \in \mathbf{R}, \ \forall t \in \mathbf{P} \qquad (16)$$

$$\sum_{b \in \mathbf{CB}} b\alpha_{k,b,t}^{fx} \leq 1 \qquad \forall k \in \mathbf{R}, \ \forall t \in \mathbf{P} \qquad (17)$$

$$\sum_{b \in \mathbf{CB}} b\alpha_{k,b,t}^{sw} \leq 1 \qquad \forall k \in \mathbf{R}, \ \forall t \in \mathbf{P} \qquad (18)$$

$$\alpha_{k,b,t}^{fx}, \alpha_{k,b,t}^{sw} \in \{0, 1\} \qquad \forall k \in \mathbf{R}, \ \forall b \in \mathbf{CB}, \ \forall t \in \mathbf{P} \qquad (19)$$

$$n_{k,t}^{cb}, n_k^{\max} \in \mathbf{Z} \qquad \forall k \in \mathbf{R}, \ \forall t \in \mathbf{P} \qquad (20)$$

## 2.4 Energy Storage System Model

By integrating renewable energy sources and ESSs into the EDN, the reliability indexes and the capacity of the network are improved. Therefore, the EDNs are anticipated to play an important role in fulfilling the aims of future smart grids [48]. ESSs are considered to be the best alternatives to deal with the challenges imposed by renewable energy sources, improving the EDN reliability indexes and reducing the EDN operation cost at the same time. Energy storage can store the excess of renewable energy source generation to be used when this is advantageous from either an economic or a technical perspective [4]. Figure 4 shows a diagram of the model of an ESS connected at node $k$.

ESSs have been implemented on a large scale in centralized systems using technologies such as pumped hydro, compressed air, and megawatt-hour batteries [21]. ESSs are adequate tools to accomplish the network support functions related to centralized generation units and transmission infrastructure constraints [20]. The stored energy can be consumed during peak hours, when energy is expensive and load demand is high [36, 47]. ESSs power is defined according to the generator



**Fig. 4** Energy storage system model
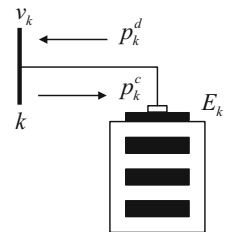
convention, i.e. the storage power is positive during discharge periods and negative during charge periods. ESS's characteristics such as capacity, charge/discharge rate limits and allocation are represented in the proposed problem by Eqs. (21)–(32).

$$p_{k,t}^{ESS} = pd_{k,t} - pc_{k,t} \qquad \forall k \in \mathbf{E}, \ \forall t \in \mathbf{P} \tag{21}$$

$$Pc_k^{\min}\alpha c_{k,t} \leq pc_{k,t} \leq Pc_k^{\max}\alpha c_{k,t} \qquad \forall k \in \mathbf{E}, \ \forall t \in \mathbf{P} \tag{22}$$

$$Pd_k^{\min}\alpha d_{k,t} \leq pd_{k,t} \leq Pd_k^{\max}\alpha d_{k,t} \qquad \forall k \in \mathbf{E}, \ \forall t \in \mathbf{P} \tag{23}$$

$$es_{k,t} = es_{k,t-1} + \left(\eta c_k pc_{k,t} - \frac{1}{\eta d_k}pd_{k,t}\right)\Delta_t \quad \forall k \in \mathbf{E}, \ \forall t \in \mathbf{P} : 1 < t < \text{card}(\mathbf{P}) \tag{24}$$

$$es_{k,t} = ES_{k,0} + \left(\eta c_k pc_{k,t} - \frac{1}{\eta d_k}pd_{k,t}\right)\Delta_t \qquad \forall k \in \mathbf{E}, \ \forall t \in \mathbf{P} : t = 1 \tag{25}$$

$$es_{k,t} = ES_{k,0} \qquad \forall k \in \mathbf{E}, \ t = \text{card}(\mathbf{P}) \tag{26}$$

$$ES_k^{\min}\alpha_{k,t}^{es} \leq es_{k,t} \leq ES_k^{\max}\alpha_{k,t}^{es} \qquad \forall k \in \mathbf{E}, \ \forall t \in \mathbf{P} \tag{27}$$

$$\alpha c_{k,t} + \alpha d_{k,t} \leq \alpha_{k,t}^{es} \qquad \forall k \in \mathbf{E}, \ \forall t \in \mathbf{P} \tag{28}$$

$$0 \leq \alpha_{k,t}^{es} \leq 1 \qquad \forall k \in \mathbf{E} \tag{29}$$

$$\sum_{t \in \mathbf{P}} \alpha_{k,t}^{es} \leq 1 \qquad \forall k \in \mathbf{E} \tag{30}$$

$$\sum_{t \in \mathbf{P}} \sum_{k \in \mathbf{E}} \alpha_{k,t}^{es} \leq N_{ES} \tag{31}$$

$$\alpha c_{k,t}, \alpha d_{k,t} \in \{0, 1\} \qquad \forall k \in \mathbf{E}, \ \forall t \in \mathbf{P} \tag{32}$$

Constraint (21) captures the charging and discharging cycles of the ESS separately. Constraints (22)–(23) limit extraction/injection power from the ESS respectively. Equation (24) determines the stored energy of the ESS connected at node $k$ at period $t$, which depends on the previous $(t - 1)$ state of charge and the injected/extracted power for the time interval multiplied by their respective effi-

ciencies. Equation (25) considers the initial stored energy, and the charge/discharge storage efficiencies. Equation (26) is used for setting the final value of the stored energy to a pre-specified value, which is considered equal to the initial value $ES_{k,0}$. Constraint (27) represents the maximum and minimum energy capacity that can be stored in the ESS. This constraint includes the binary variable $\alpha_k^{es}$ in its formulation, which indicates where and when the ESS is installed, if $\alpha_k^{es} = 1$, otherwise $\alpha_k^{es} = 0$. Constraint (30) indicates that only one ESS can be allocated at each node. The maximum number of ESSs to be allocated in the EDN is defined by constraint (31). No simultaneous charging and discharging is guaranteed by constraints (28)–(32). A simultaneous charging and discharging process is unrealistic for most storage technologies [33].

## 2.5  WTG and PVG Models

Installation of distributed generation (DG) in EDNs increases the overall reliability of the networks in general. The higher the penetration of distributed generation in the utilities, the lower the amount of power transmitted over long distances and the lower the transmission losses [22]. When scheduling the maintenance of the transmission and distribution systems with high penetration of distributed generation, it is possible to perform this maintenance without loss of service in many parts of the system. Hence, apart from distributed generation serving as a backup power supply, it may as well be used to provide clean, cost-effective and reliable power that will contribute to reserve margins, reduced transmission losses, VAr support for voltage profile improvements, deferral of addition of transmission and distribution lines and the alleviation of transmission bottlenecks is assumed [45].

In this work, PVG and WTG unit sitting and sizing are included in the proposed short-term EDN planning problem by the mathematical formulation in (33)–(40).

$$p_{k,t}^{PV} = \sum_{v \in \mathbf{PV}} PV_v^{\max} \alpha_{k,v,t}^{pv} \qquad\qquad \forall k \in \mathbf{V},\ \forall t \in \mathbf{P} \qquad (33)$$

$$\sum_{t \in \mathbf{P}} \sum_{v \in \mathbf{PV}} \sum_{k \in \mathbf{V}} \alpha_{k,v,t}^{pv} \leq N_{PV} \qquad\qquad\qquad (34)$$

$$\sum_{v \in \mathbf{PV}} \alpha_{k,v,t}^{pv} \leq 1 \qquad\qquad\qquad \forall k \in \mathbf{V},\ \forall t \in \mathbf{P} \qquad (35)$$

$$p_{k,t}^{WT} = \sum_{w \in \mathbf{WT}} WT_w^{\max} \alpha_{k,w,t}^{wt} \qquad\qquad \forall k \in \mathbf{W},\ \forall t \in \mathbf{P} \qquad (36)$$

$$\sum_{t \in \mathbf{P}} \sum_{w \in \mathbf{WT}} \sum_{k \in \mathbf{W}} \alpha_{k,w,t}^{wt} \leq N_{WT} \qquad\qquad\qquad (37)$$

$$\sum_{w \in \mathbf{WT}} \alpha^{wt}_{k,w,t} \leq 1 \qquad\qquad \forall k \in \mathbf{W}, \ \forall t \in \mathbf{P} \qquad (38)$$

$$\alpha^{pv}_{k,v,t} \in \{0, 1\} \qquad\qquad \forall k \in \mathbf{V}, \ \forall v \in \mathbf{PV}, \ \forall t \in \mathbf{P} \qquad (39)$$

$$\alpha^{wt}_{k,w,t} \in \{0, 1\} \qquad\qquad \forall k \in \mathbf{W}, \ \forall w \in \mathbf{WT}, \ \forall t \in \mathbf{P} \qquad (40)$$

where Eqs. (33) and (36) define the allocation of PVG and WTG units respectively, which depends on the modules to be installed. Constraints (34) and (37) limit the number of PVG and WTG units allocated at the EDN, respectively. Constraints (35) and (38) define the size of the PVG and WTG plants to be allocated, respectively, and guarantee that the model can only choose one type of module. Finally, the binary nature of the decision variables is represented by (39) and (40).

## 2.6   Conductor Replacement Modeling

In our short-term EDN planning model, conductor replacement of overloaded feeders is considered without changing the EDN topology [55]. Therefore, the convexified mathematical model that represents it is formulated in (41)–(45).

$$\sum_{c \in \mathbf{C}} \sum_{(jk) \in \mathbf{B}} p_{jk,c,t} - \sum_{c \in \mathbf{C}} \sum_{(km) \in \mathbf{B}} p_{km,c,t} + p^{S}_{k,t} +$$

$$p^{PV}_{k,t} + p^{WT}_{k,t} + p^{ESS}_{k,t} - P^{D}_{k,t} = 0 \qquad\qquad \forall k \in \mathbf{N}, \ \forall t \in \mathbf{P} \qquad (41)$$

$$\sum_{(jk) \in \mathbf{B}} q_{jk,c,t} - \sum_{c \in \mathbf{C}} \sum_{(km) \in \mathbf{B}} q_{km,c,t} + q^{S}_{k,t} +$$

$$q^{CB}_{k,t} - Q^{D}_{k,t} = 0 \qquad\qquad \forall k \in \mathbf{N}, \ \forall t \in \mathbf{P} \qquad (42)$$

$$v_{k,t} - v_{m,t} = \frac{2}{v_0} \sum_{c \in \mathbf{C}} (R_c L_{km} p_{km,c,t} + X_c L_{km} q_{km,c,t}) \qquad\qquad \forall (km) \in \mathbf{B}, \ \forall t \in \mathbf{P} \qquad (43)$$

$$\left| p_{km,c,t} \right| \leq P^{\max}_c \alpha^{cr}_{km,c,t} \qquad\qquad \forall (km) \in \mathbf{B}, \ \forall c \in \mathbf{C}, \ \forall t \in \mathbf{P} \qquad (44)$$

$$\left| q_{km,c,t} \right| \leq Q^{\max}_c \alpha^{cr}_{km,c,t} \qquad\qquad \forall (km) \in \mathbf{B}, \ \forall c \in \mathbf{C}, \ \forall t \in \mathbf{P} \qquad (45)$$

$$\sum_{t \in \mathbf{P}} \alpha^{cr}_{km,c,t} \leq 1 \qquad\qquad \forall (km) \in \mathbf{B} \qquad (46)$$

$$\alpha^{cr}_{km,c,t} \in \{0, 1\} \qquad\qquad \forall (km) \in \mathbf{B}, \ \forall c \in \mathbf{C}, \ \forall t \in \mathbf{P} \qquad (47)$$

where (41) and (42) represent the active and reactive power balance of the reinforced feeder $c$ in branch $km$, respectively. Constraint (43) represents the voltage magnitude drop in branch $km$ for the reinforced feeder $c$. The active and reactive power flow limits of the reinforced feeders are shown in (44) and (45), respectively. Constraint (46) imposes that only one conductor type is selected for each feeder. The decision variable in (47) indicates the need of a feeder to be reinforced, which can take values of 0 or 1 for each case, respectively.

### 2.7 Objective Function

The objective function consists of investment and operation costs. Investment costs indicated by $C_{INV}$ in (48) include VR allocation (first term), fixed and switchable CB allocation (second and third terms), ESS allocation (fourth therm), DG unit PVG- and WTG-based allocation (fifth and sixth terms) and conductor replacement of overloaded feeders (seventh term).

$$
\begin{aligned}
C_{INV} = &\sum_{t \in \mathbf{P}} \frac{1}{(1+r)^t} \sum_{(km) \in \mathbf{VR}} \Gamma_{km}^{vr} \left( \alpha_{km,t}^{vr} - \alpha_{km,t-1}^{vr} \right) + \\
&\sum_{t \in \mathbf{P}} \frac{1}{(1+r)^t} \sum_{b \in \mathbf{CB}} \sum_{k \in \mathbf{R}} \Gamma_b^{cbfx} \left( \alpha_{k,b,t}^{fx} - \alpha_{k,b,t-1}^{fx} \right) + \\
&\sum_{t \in \mathbf{P}} \frac{1}{(1+r)^t} \sum_{b \in \mathbf{CB}} \sum_{k \in \mathbf{R}} \Gamma_b^{cbsw} \left( \alpha_{k,b,t}^{sw} - \alpha_{k,b,t-1}^{sw} \right) + \\
&\sum_{t \in \mathbf{P}} \frac{1}{(1+r)^t} \sum_{k \in \mathbf{E}} \Gamma_k^{es} \left( \alpha_{k,t}^{es} - \alpha_{k,t-1}^{es} \right) + \\
&\sum_{t \in \mathbf{P}} \frac{1}{(1+r)^t} \sum_{v \in \mathbf{PV}} \sum_{k \in \mathbf{V}} \Gamma_v^{pv} \left( \alpha_{k,v,t}^{pv} - \alpha_{k,v,t-1}^{pv} \right) + \\
&\sum_{t \in \mathbf{P}} \frac{1}{(1+r)^t} \sum_{w \in \mathbf{WT}} \sum_{k \in \mathbf{W}} \Gamma_w^{wt} \left( \alpha_{k,w,t}^{wt} - \alpha_{k,w,t-1}^{wt} \right) + \\
&\sum_{t \in \mathbf{P}} \frac{1}{(1+r)^t} \sum_{c \in \mathbf{C}} \sum_{(km) \in \mathbf{B}} \Gamma_c^{cr} \left( \alpha_{km,c,t}^{cr} - \alpha_{km,c,t-1}^{cr} \right)
\end{aligned}
\tag{48}
$$

On the other hand, the operation costs indicated by $C_{OP}$ in (49) include devices such as: ESS (first term) and DG units PVG- and WTG-based allocation (second and third terms). The operation costs in these devices can be evaluated based on

their sizes per hour of operation [52].

$$C_{OP} = \sum_{t \in \mathbf{P}} \frac{1}{(1+r)^t} \sum_{k \in \mathbf{E}} H_t \Pi_k^{es} \alpha_{k,t}^{es} +$$

$$\sum_{t \in \mathbf{P}} \frac{1}{(1+r)^t} \sum_{v \in \mathbf{PV}} \sum_{k \in \mathbf{V}} H_t \Pi_v^{pv} \alpha_{k,v,t}^{pv} +$$

$$\sum_{t \in \mathbf{P}} \frac{1}{(1+r)^t} \sum_{w \in \mathbf{WT}} \sum_{k \in \mathbf{W}} H_t \Pi_w^{wt} \alpha_{k,w,t}^{wt} +$$

$$\sum_{t \in \mathbf{P}} \sum_{k \in \mathbf{S}} \Pi_{k,t}^s p_{k,t}^S \tag{49}$$

## 2.8  Deterministic Formulation

In this section, a short-term EDN planning deterministic optimization model is presented, which is aimed at the minimization of investment and operation costs by conductor replacement of overloaded feeders, installing VRs, CBs, PVGs, WTGs and ESSs. Equations related to each device considered have been developed to determine its performance in the network. Then, a convexified formulation is obtained to build an MILP optimization problem that can be solved using commercial MILP solvers, which guarantees a global optimal solution of the problem.

The proposed MILP model in (50)–(57) defines an economic approach to obtain the best short-term plan for an EDN, where constraint (56) represents the active/reactive power of substation limits, controlled by the power factor. The voltage magnitude limits are represented by (57).

$$\min\ C_{INV} + C_{OP} \tag{50}$$

s.t.:

Conductor replacement:  (41)−(47)                                              (51)

WTG and PVG:  (33)−(40)                                                        (52)

ESS:  (21)−(32)                                                                (53)

CBs:  (12)−(20)                                                                (54)

VRs:  (9)−(11)                                                                 (55)

$$-\sum_{t \in \mathbf{P}} p_{k,t}^S \tan(\cos^{-1} \underline{\phi}^S) \le \sum_{t \in \mathbf{P}} q_{k,t}^S \le \sum_{t \in \mathbf{P}} p_{k,t}^S \tan(\cos^{-1} \overline{\phi}^S) \quad \forall k \in \mathbf{SE},\ \forall t \in \mathbf{P} \tag{56}$$

$$V_k^{\min} \le v_{k,t} \le V_k^{\max} \qquad\qquad\qquad\qquad \forall k \in \mathbf{N},\ \forall t \in \mathbf{P} \tag{57}$$

## 2.9 Numerical Results

### 2.9.1 Data Specifications

The effectiveness and efficiency of the proposed deterministic model is illustrated using a 123-bus distribution test system, whose data has been taken from [44]. In this case, the expected values of the renewable energy sources generation and load consumption are used. The annual increase rate of load consumption is 3%. The lower and upper voltage limits are 0.95 and 1.05 p.u., respectively. The substation lower and upper power factor limits are 0.95 and 1.0, respectively, and the reactive power depends on the power factor and the supplied active power. The regulation range and installation cost of VRs are assumed to be $\pm 10\%$ and $26,400, respectively. The annual discount rate is set to be 5%. The planning horizon considered is 3 years. All buses were assumed to be candidates for VRs, CBs, ESSs, PV and WT plants placement.

Installing costs and power of CBs are reported in Table 1.

Conductors' data and conductors' replacement costs are shown in Table 2, which are adapted from [46].

**Table 1** Installing costs and power of CBs

| $Q^{sp}$ [kVAr] | $CB^{fx}$ [$] | $CB^{sw}$ [$] |
|---|---|---|
| 300 | 4950 | 7450 |
| 600 | 5150 | 7650 |
| 900 | 6550 | 9550 |
| 1200 | 7500 | 10,150 |
| 1500 | 8075 | 10,950 |

**Table 2** Technical and economic information about conductor replacement

| Data of conductors | | | | |
|---|---|---|---|---|
| Type | Name | $R(\Omega/km)$ | $X(\Omega/km)$ | $I^{max}(A)$ |
| 1 | $C_1$ | 1.1140 | 0.8762 | 130 |
| 2 | $C_2$ | 0.9963 | 0.7133 | 175 |
| 3 | $C_3$ | 0.7618 | 0.7077 | 235 |
| 4 | $C_4$ | 0.5995 | 0.6610 | 365 |
| 5 | $C_5$ | 0.3692 | 0.4150 | 495 |
| 6 | $C_6$ | 0.3209 | 0.3554 | 615 |

| Conductor replacement costs [$] | | | | | | |
|---|---|---|---|---|---|---|
| Type | $C_1$ | $C_2$ | $C_3$ | $C_4$ | $C_5$ | $C_6$ |
| 1 | – | 7500 | 13,500 | 21,500 | 29,500 | 37,500 |
| 2 | – | – | 11,000 | 18,500 | 25,500 | 34,000 |
| 3 | – | – | – | 14,000 | 22,000 | 29,000 |
| 4 | – | – | – | – | 17,500 | 25,000 |
| 5 | – | – | – | – | – | 20,500 |

Generation capacities of 150 and 50 kW are assumed for each WT unit and PV module, respectively. The maximum number of WT units and PV modules that can be installed at node $k$ is set to 5 and 15, respectively. The maximum number of WT units and PV modules that can be installed in the EDN is set to 300 for each. Investment costs of $200 \times 10^3$ and $50 \times 10^3$ and operation costs of \$300 and \$400 are contemplated for each WT unit and PV module, respectively.

Investment and operation costs of \$106 and \$220 for each kWh are considered for each energy storage device. The available storage is assumed to be in multiples of 32 kWh storage capacity, with charge/discharge maximum powers set at 25% of this capacity. The efficiencies for charging and discharging are considered to be 90% each [33]. The maximum number of ESSs that can be installed in the EDN is set to 10.

### 2.9.2 Simulation Results

The proposed mathematical model has been implemented in the AMPL mathematical language [28] and the solution framework has been obtained using the optimization solver CPLEX 12.7 [32], in a Dell PowerEdge R910x64, 512 GB of RAM and 3.3 GHz.

This case has been solved in 7 min 23 s. The objective function is \$,1212,908. Two VRs are allocated at nodes 109 in $t = 2$ and 44 in $t = 3$ with an investment cost of \$46,750. Three fixed CBs are allocated at nodes 11 (600 kVAr), 27 (900 kVAr) and 43 (900 kVAr) in $t = 2$ with an investment cost of \$16,553. Two PV-based DG units are sized and sited at nodes 102 (150 kW) and 117 (100 kW) in $t = 3$ with investment and operation costs of \$43,192 and \$1728, respectively. Two WT-based DG units are sized and sited at nodes 53 (300 kW) and 90 (450 kW) in $t = 3$ with investment and operation costs of \$863,838 and \$1296, respectively. There are no ESSs allocated in the EDN. The lowest voltage magnitude value is 0.95 p.u., till the end of the planning horizon.

Table 3 shows the proposal for conductor replacement with an investment cost of \$105,551.

In summary, the proposed deterministic model provides appropriate solutions for the short-term EDN planning problem, where some devices are installed in the EDN to meet the objectives under the implemented constraints.

**Table 3** Conductor replacement

| Branch $k-m$ | Initial conductor | New conductor | Stage $t$ |
|---|---|---|---|
| 0–1 | $C_3$ | $C_5$ | 1 |
| 1–7 | $C_3$ | $C_5$ | 1 |
| 7–8 | $C_3$ | $C_5$ | 2 |
| 8–14 | $C_3$ | $C_5$ | 2 |
| 14–55 | $C_3$ | $C_5$ | 2 |
| 55–56 | $C_3$ | $C_5$ | 2 |
| 56–57 | $C_3$ | $C_5$ | 2 |
| 57–58 | $C_3$ | $C_5$ | 2 |
| 58–61 | $C_3$ | $C_5$ | 2 |
| 61–64 | $C_3$ | $C_5$ | 2 |
| 64–67 | $C_3$ | $C_5$ | 3 |
| 67–68 | $C_3$ | $C_5$ | 3 |

# 3 Adaptive Robust Formulation for Long-Term EDN Expansion Planning

## 3.1 Robust Optimization

Real-word decision-making problems in operation and planning of electric energy systems are highly affected by uncertainties, which are associated to energy price, demand, intermittent generation sources, equipment availability, etc. [18]. In the proposed robust optimization model, load consumption and power output of renewable-based DG are considered as uncertain parameters. In this context, parameters $\mu_t^D$ (load consumption), $\mu_t^{pv}$ (PVG) and $\mu_t^{wt}$ (WTG), are uncertain parameters representing the uncertainty of the capacity factor (taking values from 0 to 1) for each case. Therefore, terms from Eqs. (33)–(40) and (41)–(42) containing the aforementioned uncertainties are formulated considering those parameters as follows:

$$\sum_{c\in\mathbf{C}}\sum_{(jk)\in\mathbf{B}} p_{jk,c,t} - \sum_{c\in\mathbf{C}}\sum_{(km)\in\mathbf{B}} p_{km,c,t} + p_{k,t}^{S} +$$

$$p_{k,t}^{PV} + p_{k,t}^{WT} + p_{k,t}^{ESS} - P_{k,t}^{D}\mu_t^{D} = 0 \qquad \forall k\in\mathbf{N},\ \forall t\in\mathbf{P} \qquad (58)$$

$$\sum_{(jk)\in\mathbf{B}} q_{jk,c,t} - \sum_{c\in\mathbf{C}}\sum_{(km)\in\mathbf{B}} q_{km,c,t} + q_{k,t}^{S} +$$

$$q_{k,t}^{CB} - Q_{k,t}^{D}\mu_t^{D} = 0 \qquad \forall k\in\mathbf{N},\ \forall t\in\mathbf{P} \qquad (59)$$

$$p_{k,t}^{PV} = \sum_{v\in\mathbf{PV}} PV_v^{\max}\alpha_{k,v,t}^{pv}\mu_t^{pv} \qquad \forall k\in\mathbf{V},\ \forall t\in\mathbf{P} \qquad (60)$$

$$p_{k,t}^{WT} = \sum_{w\in\mathbf{WT}} WT_w^{\max}\alpha_{k,w,t}^{wt}\mu_t^{wt} \qquad \forall k\in\mathbf{W},\ \forall t\in\mathbf{P} \qquad (61)$$

### 3.1.1 Uncertainty Characterization

It is important to take into account a clear definition of the uncertainty set $\mathbf{U}$ for an effective representation of the uncertainty involved. In this context, to define uncertainty set $\mathbf{U}$, a polyhedral uncertainty set similar to the one used in [13, 14] is considered for WTG and PVG, as well as load consumption. This uncertainty set at each time period in the specified planning horizon is described by the following constraints:

$$\mathbf{U}_t^D = \left\{ \mu_t^D \in \mathbb{R}^{n_D} : \underline{\Upsilon}^D \leq \sum_{t \in \mathbf{P}} \frac{\mu_t^D}{\hat{\mu}_t^D} \leq \overline{\Upsilon}^D \; ; \quad \mu_t^D \in \left[ \underline{\mu}_t^D, \overline{\mu}_t^D \right] \right\} \tag{62}$$

$$\mathbf{U}_t^{pv} = \left\{ \mu_t^{pv} \in \mathbb{R}^{n_{pv}} : \underline{\Upsilon}^{pv} \leq \sum_{t \in \mathbf{P}} \frac{\mu_t^{pv}}{\hat{\mu}_t^{pv}} \leq \overline{\Upsilon}^{pv} \; ; \quad \mu_t^{pv} \in \left[ \underline{\mu}_t^{pv}, \overline{\mu}_t^{pv} \right] \right\} \tag{63}$$

$$\mathbf{U}_t^{wt} = \left\{ \mu_t^{wt} \in \mathbb{R}^{n_{wt}} : \underline{\Upsilon}^{wt} \leq \sum_{t \in \mathbf{P}} \frac{\mu_t^{wt}}{\hat{\mu}_t^{wt}} \leq \overline{\Upsilon}^{wt} \; ; \quad \mu_t^{wt} \in \left[ \underline{\mu}_t^{wt}, \overline{\mu}_t^{wt} \right] \right\} \tag{64}$$

The range of the load consumption at each time period is described by the interval $\left[ \underline{\mu}_t^D, \overline{\mu}_t^D \right]$ in (62). The added load in all consumption nodes at each time period is constrained by the "budget of uncertainty", $\underline{\Upsilon}^D$ and $\overline{\Upsilon}^D$. Thus, a conservative level can be achieved by these adjustable parameters. Similar uncertainty sets are defined for the PVG in (63) and for the WTG in (64).

## 3.2 Adaptive Robust Optimization Problem Formulation

We assume that the uncertainty parameters in the proposed short-term EDN planning problem (50)–(57) are associated to: (1) load consumption ($\mu_t^D$) and (2) renewable-based DG ($\mu_t^{PV}$ and $\mu_t^{WT}$), respectively. Once this is specified, the optimal short-term EDN planning can be determined for the optimal values of variable $\alpha$, considering the worst possible realizations of the uncertainty parameters. To obtain this, an adaptive robust optimization (ARO) problem is formulated with the following characteristics:

1. The optimal short-term EDN planning solution is obtained by minimizing investment and operation costs for the worst-case scenario of uncertainty (65).
2. This optimal short-term EDN planning is determined by anticipating that, once short-term EDN planning decisions are made, the worst-case uncertainty will occur, i.e., considering a given short-term EDN planning, uncertainty parameters will take the values that maximize operational costs given the new network changes (66).
3. The worst-case realization of the uncertainty parameters is contemplated once the worst case is realized in advance, so the system adapts to it. That is, considering

that the short-term EDN planning decision variables and uncertainty parameters are fixed, the optimal values of the remaining variables are selected so that the objective function is minimized (67).

The aforementioned decision sequence is realistic for the short-term EDN planning problem solution. First, the EDN planner decides the short-term expansion plan to be implemented. Then, the worst-case uncertainty occurs (e.g., an unexpected peak load consumption and/or the unavailability of some renewable resources). Finally, the EDN operator, based on previous events, decides the most appropriate actions in order to minimize the operation costs. The hierarchical structure previously explained can be represented using the tri-level optimization problem as follows:

$$\min_{\boldsymbol{\alpha}} \ C^{INV} + \delta \tag{65}$$

s.t.: (11), (13)–(20), (28)–(32), (34), (35), (37)–(40), (46), (47)

$$\delta = \left\{ \max_{\boldsymbol{\mu} \in \mathbf{U}} \varphi \right\} \tag{66}$$

s.t.: (62)–(64)

$$\varphi = \left\{ \min_{\boldsymbol{y} \in \Omega(\boldsymbol{\alpha}, \boldsymbol{\mu})} C^{OP} \right\} \tag{67}$$

s.t.: (9), (10), (12), (21)–(27), (43)–(45), (56)–(61)

In this tri-level optimization problem (65)–(67), set $\mathbf{U}$ is included, which defines the uncertainty set and also set $\Omega(\boldsymbol{\alpha}, \boldsymbol{\mu})$, which guarantees the feasibility of the operation decision variables given the short-term EDN planning decisions and the realizations of the uncertainty parameters.

The proposed adaptive robust optimization formulation in (65)–(67) can be reformulated in matrix form as follows:

$$\min_{\mathbf{x} \in \mathbf{X}} c^T x + \delta \tag{68}$$

$$\text{s.t.:} Ax \leq b \tag{69}$$

$$x \in \{0, 1\} \tag{70}$$

$$\delta = \left\{ \max_{\boldsymbol{\mu} \in \mathbf{U}} \varphi \right\} \tag{71}$$

$$\text{s.t.:} \quad I_\mu = \mu \tag{72}$$

$$\varphi = \left\{ \min_{\boldsymbol{y} \in \Omega(\boldsymbol{\alpha}, \boldsymbol{\mu})} d^T y \right\} \tag{73}$$

$$\text{s.t.:} \quad Gy \leq h \tag{74}$$

$$Tx + Qy \leq r \tag{75}$$

where the upper level is represented by (68)–(70), the middle level by (71) and (72) and the lower level by (73)–(75). Vector **x** includes all binary variables and vector **y** all continuous variables.

In the matrix form formulation, the objective function (50) is split into two parts: (68) and (73). The upper level (68)–(70) is associated with the investment decision constraints and the specification of binary variables ((11), (13)–(20), (28)–(32), (34), (35), (37)–(40), (46),(47)). The middle level (71) and (72) selects the components that are considered as uncertain, such as, load consumption and renewable-based DG units ((62)–(64)). The lower level (73), (74) and (75) is equivalent to the reaction of the EDN, taking into account the planning decisions and uncertainty realization. Equation (73) selects the objective function part associated with the operation costs (49), (74) collects all constraints of the problem that include only continuous variables ((9), (12), (21), (24)–(26) (27), (43), (56)–(59)), whereas (75) considers the constraints with both binary and continuous variables ((10), (22), (23), (27), (44) (45) (60) (61)).

## 3.3  Solution Framework

Vector $\boldsymbol{\mu} \in \mathbf{U}$ in (68)–(75) represents the uncertainty parameters. In this context, the variables can be grouped into two sets: (1) $\mathbf{x} \in \mathbf{X}$, which represents the vector of first-stage binary decision variables whose optimal value is not subject to any adjustment after the realization of the uncertainty parameters. The variables in vector **x** define the investment decision plan and are known as the unadjustable decision variables of the "here-and-now" decisions and (2) $\boldsymbol{y} \in \Omega(\boldsymbol{\alpha}, \boldsymbol{\mu})$ which describes the vector of second-stage continuous variables whose optimal value is conditioned by the realization of the uncertainty parameters and the optimal value of the first-stage variables. The variables in vector *y* include the adjustable decision variables of the "wait-and-see" decisions. Therefore, if the vector of unadjustable binary variables is known, then, the vector of adjustable variables can be calculated for any realization of the uncertain parameters using linear programming ((68)–(75) with fixed binary variables). This linear program, also known as the second-stage problem, is feasible for any realization of the uncertain parameters [33].

The proposed tri-level (min-max-min) adaptive robust optimization model (68)–(75) represents the actions of a planner, uncertainty realizations and an operator for the short-term EDN planning problem, which is difficult to solve, since its multilevel structure makes it an NP-hard problem and cannot be solved using existing classical optimization techniques.

To solve this type of problem, several algorithms exist in technical literature, mainly based on Benders decomposition and on constraint-and-column generation (C&CG) methods [24, 59]. In Benders decomposition-based methods, the problem is separated into two parts: a so-called master problem (MP) and a so-called subproblem (SP). In the solution process, dual information from the so-called subproblem is used to compute the objective function of the so-called master pro-

blem sequentially [16]. Moreover, the C&CG generation method uses cutting plane approaches based on primal cuts that include only primal decision variables. C&CG creates primal cuts that are generally more effective than the dual cuts used in Benders decomposition, therefore, compared with the Benders decomposition-based methods, the C&CG needs fewer iterations to converge, developing a better computational performance [59].

In order to show in detail the C&CG algorithm, the proposed two-stage adaptive robust optimization problem (68)–(75) that represents the short-term EDN planning problem is rewritten in a compact matrix form:

$$\min_{\mathbf{x} \in \mathbf{X}} \quad \left\{ c^T x + \max_{\boldsymbol{\mu} \in \mathbf{U}} \min_{\mathbf{y} \in \Omega(\boldsymbol{\alpha}, \boldsymbol{\mu})} d^T y \right\} \tag{76}$$

s.t.:

$$Ax \leq b \tag{77}$$

$$x \in \{0, 1\} \tag{78}$$

where

$$\Omega(\mu, x) = \left\{ y \, : \, Gy \leq h, \qquad Qy \leq r - Tx, \qquad I_\mu y = \mu \right\} \tag{79}$$

To apply CC&G in the short-term EDN planning problem, the formulation in (76)–(79) needs to be reformulated in a hierarchical framework as an MP and a SP. The MP can be defined as follows:

$$\min_{\mathbf{x} \in \mathbf{X}} \quad c^T x + \eta \tag{80}$$

s.t.:

$$\eta \geq d^T y \tag{81}$$

$$Ax \leq b \tag{82}$$

$$x \in \{0, 1\} \tag{83}$$

$$I_\mu = \mu \tag{84}$$

$$Gy \leq h \tag{85}$$

$$Tx + Qy \leq r \tag{86}$$

This MP is a relaxation of the proposed adaptive robust problem, where the variables in vector $\mathbf{y}$ are dependent on the uncertainty realizations $\boldsymbol{\mu}$, which are fixed. The solution of the MP is defined for the variables in vector $\mathbf{x}$, yielding a lower bound. Thus, the MP solutions are fixed in the SP solution defined

by (87)–(90).

$$\max_{\boldsymbol{\mu} \in \mathbf{U}} \min_{y \in \Omega(\boldsymbol{\alpha}, \boldsymbol{\mu})} \quad d^T y \tag{87}$$

s.t.:

$$I_\mu = \mu : \qquad \lambda \tag{88}$$

$$Gy \leq h : \qquad \gamma_1 \tag{89}$$

$$Tx + Qy \leq r : \quad \gamma_2 \tag{90}$$

SP (87)–(90) is a bi-level optimization problem that can be transformed into an equivalent single-level optimization problem. In this work, Karush–Kuhn–Tucker (KKT) conditions are used to transform the bi-level problem (87)–(90) into an equivalent single-level problem. KKT conditions are necessary and sufficient for optimality. Thus, we consider the Lagrangian function in (91) associated with the bi-level (87)–(90) optimization problem for a given upper-level solution in $x^*$.

$$\mathscr{L}(x^*, y, \gamma_1, \gamma_2) = d^T y - \lambda^T (I_\mu - \mu) - \gamma_1^T (Gy - h) - \gamma_2^T (Tx^* + Qy - r) \tag{91}$$

The optimal solution to (87)–(90) must satisfy the KKT necessary optimality conditions, as shown in (92)–(97).

$$\nabla_y \mathscr{L}(x^*, y, \gamma_1, \gamma_2) = d - G\gamma_1 - Q\gamma_2 = 0 \tag{92}$$

$$I_\mu = \mu \tag{93}$$

$$Gy \leq h \tag{94}$$

$$Tx + Qy \leq r \tag{95}$$

$$0 \leq h - Gy \perp \gamma_1 \geq 0 \tag{96}$$

$$0 \leq r - Tx^* - Qy \perp \gamma_2 \geq 0 \tag{97}$$

where (92) is the dual feasibility constraint, (93)–(95) are the primal feasibility constraints and (96), and (97) are the complementarity constraints. $\gamma_1$ and $\gamma_2$ are the dual variables of the problem in (87)–(90). Complementarity constraints in (96) and (97) can be convexified to be an exact equivalent mixed-integer linear expressions using the Big-M method, as shown in (98)–(101).

$$0 \leq h - Gy \leq M\sigma \tag{98}$$

$$0 \leq \gamma_1 \leq M(1 - \sigma) \tag{99}$$

$$0 \leq r - Tx^* - Qy \leq K(1 - \rho) \tag{100}$$

$$0 \leq \gamma_2 \leq K(1 - \rho) \tag{101}$$

where $M$ and $K$ are large values and $\sigma$ and $\rho$ are binary variables. Thus, the constraints of the SP become (92)–(95) and (98)–(101), which is an MILP.

KKT conditions in (92)–(95) and (98)–(101) are included as constraints of the bi-level SP in (87)–(90), obtaining a single-level SP as follows:

$$\max_{\boldsymbol{\mu}, \boldsymbol{y}} \ d^T y \tag{102}$$

s.t.:

$$d - G\gamma_1 - Q\gamma_2 = 0 \tag{103}$$

$$I_\mu = \mu \tag{104}$$

$$Gy \leq h \tag{105}$$

$$Tx^* + Qy \leq r \tag{106}$$

$$0 \leq h - Gy \leq M\sigma \tag{107}$$

$$0 \leq \gamma_1 \leq M(1 - \sigma) \tag{108}$$

$$0 \leq r - Tx^* - Qy \leq K(1 - \rho) \tag{109}$$

$$0 \leq \gamma_2 \leq K(1 - \rho) \tag{110}$$

### 3.3.1 Algorithm

By taking into account the defined MP in (80)–(86) and the SP in (102)–(110), the C&CG algorithm considered is described as follows:

**Step 0**  Fix the Lower Bound (LB) to LB = $-\infty$, the Upper Bound (UB) to UB = $+\infty$, define the tolerance ($\epsilon$), define the initial value of $\mu_i \in [\underline{\mu}, \overline{\mu}]$, and set the iteration counter $i = 0$.

**Step 1**  Solve the MP (80)–(86). Obtain the optimal solution $(x^*, \eta^*)$ and update the LB:

$$\text{LB} = c^T x^* + \eta^*$$

**Step 2**  Solve the SP (102)–(110) by considering the optimal value $x^*$, obtained in Step 1 as a parameter. Obtain the optimal solution $(\mu^*, y^*)$ and update the UB:

$$\text{UB} = \min \left\{ UB, c^T x^* + d^T y^* \right\} \tag{111}$$

**Step 3**  if (UB - UL)/UM $\leq \epsilon$ then end, otherwise update $i = i + 1$ and $\mu_i^* = \mu_{i-1}$. Continue with Step 1.

## 3.4  Numerical Results

### 3.4.1  Data Specifications

The effectiveness of the proposed adaptive robust optimization problem to solve the short-term EDN planning problem is illustrated using the 123-bus distribution test system. Technical and economic information about this test system were specified in Sect. 2.9.1. The tolerance ($\epsilon$) is set to 0.5%. Finally, the adjustment of constants $M$ and $K$ must be taken into account considering the physical nature of the bounded variables, so that values that are too large do not complicate the solution of the problem.

### 3.4.2  Simulation Results

The proposed adaptive robust mathematical model is implemented in the AMPL mathematical language [28] and the solution framework is obtained using the optimization solver CPLEX 12.7 [32], in a Dell PowerEdge R910x64, 512 GB of RAM and 3.3 GHz.

In this case study, different robustness parameters are assumed, since they cannot have the same values in all periods in a realistic model.

Tables 4 and 5 show the decision planning considering different instances of the robustness parameters. The lowest voltage magnitude value is 0.97 p.u., till the end of the planning horizon. This case is solved in an average time of 28 min 12 s. in four iterations.

**Table 4** Uncertainty levels and plans

| Uncertainty $\mu, \overline{\mu}$ | VRs | CBs | PVG | WTG | ESSs |
|---|---|---|---|---|---|
| [0.5, 1.0] | Two VRs at nodes 57 and 42 | Three FCBs (2×600 kVA, 1×300 kVA) at nodes 49 and 69 | Two PV plants (2×100 kW) at nodes 83 and 104 | None | One ESS (1×64 kW) at node 151 |
| Costs | $48,700 | $13,370 | $843,000 | – | $233,700 |
| [0.7, 1.2] | Two VRs at nodes 57 and 42 | Three FCBs (2×600 kVA, 1×300 kVA) at nodes 49 and 69 | Two PV plants (2×50 kW) at nodes 83 and 104 | None | One ESS (1×64 kW) at node 151 |
| Costs | $48,700 | $13,370 | $430,000 | – | $233,700 |
| [0.9, 1.1] | Two VRs at nodes 57 and 42 | Three FCBs (3×600 kVA) at nodes 49 and 69 | Two PV plants (2×150 kW) at nodes 83 and 104 | None | One ESS (1×96 kW) at node 151 |
| Costs | $48,700 | $19,577 | $1,112,650 | – | $378,300 |

**Table 5** Conductor
replacement

| Branch $k - m$ | Initial conductor | New conductor |
|---|---|---|
| 0–1 | $C_3$ | $C_5$ |
| 1–7 | $C_3$ | $C_5$ |
| 7–8 | $C_3$ | $C_5$ |
| 8–14 | $C_3$ | $C_5$ |
| 14–55 | $C_3$ | $C_5$ |
| 55–56 | $C_3$ | $C_5$ |
| 56–57 | $C_3$ | $C_5$ |
| 57–58 | $C_3$ | $C_5$ |
| 58–61 | $C_3$ | $C_5$ |
| 61–64 | $C_3$ | $C_5$ |

All the solutions found by the proposed deterministic and robust models present plans with a main difference to highlight: the ESSs allocated by the robust model for all instances of the robustness parameters. The total costs for each model are $1,338,770, $997,450 and $1,638,705. Comparing these costs with the deterministic ones, it is observed that they are similar, but the proposed robust model shows an enhancement in the system voltage profile compared with the deterministic one, which explains the ESS allocations and the different capacities of the devices.

For all instances of the robustness parameters, VRs, CBs, PVG plants and ESSs are allocated in the EDN to meet the system operational requirements, such as voltage profiles. It can be seen that the locations are the same for all instances of the robustness parameters, but the equipment sizes associated with each location are relatively different. The locations of the installations are similar, since the EDN topology remains the same for all instances of the robustness parameters. However, load consumption, wind speeds and solar irradiances vary from one occurrence to another, which results in different sizes of the installed equipment. Conductor reinforcements are the same for all instances, as shown in Table 5.

## 4   Conclusions

In this work, deterministic and two-stage adaptive robust models are proposed to address the short-term EDN planing problem, considering VRs, CBs, WTG and PVG based-DG, ESSs, and conductor replacement of overloaded feeders. The main objective of the optimization is to minimize investment and operation costs, while maximizing EDN profits along the planning horizon. The proposed deterministic approach is based on a convexified multi-period MILP that guarantees a global optimal solution. The proposed adjustable robust optimization-based approach is formulated as a three-level programming problem. In order to solve the resulting mixed-integer linear three-level program, a C&CG technique is applied. The proposed methodology comprises the iterative resolution of an MP and an SP. Both

problems are formulated with a suitable MILP that can be solved using commercial solvers. The proposed adaptive robust method for the short-term EDN planning problem solution is subject to an uncertainty set associated with the load consumptions and intermittent power output of renewable-based DG. Thus, this robust model takes into account these uncertainties defined through a polyhedral uncertainty set. The uncertainty level can be adjusted by the planner to develop a tradeoff between the robustness and conservativeness of the solutions. Numerical results show that the adjustable robust approach is able to attain optimal or high-quality solutions with a reasonable computational effort. Therefore, the proposed short-term EDN planning methods are more suitable to be used in practice.

Further research will explore a convex formulation without linearizations together with a robust planning framework tool for distribution company planners, allowing them the optimal management of distribution networks, guaranteeing security, reliability and quality in the service to the consumers.

# Appendix

The notations used throughout this chapter are listed below.

## *Acronym*

AMPL     A Modeling Language for Mathematical Programming.

## *Indexes*

$b$     Index of installed CB sizes.
$c$     Index of conductor types.
$k$     Index of buses of the system.
$km$     Index of branches of the system.
$t$     Index of periods of planning.
$\mu$     Index of uncertain parameters.

## *Sets*

| | |
|---|---|
| **B** | Set of branches of the system. |
| **C** | Set of conductor types. |
| **CB** | Set of CBs. |
| **E** | Set of candidate buses to install ESSs. |
| **N** | Set of buses of the system. |
| **P** | Set of periods. |
| **R** | Set of candidate buses to install CBs. |
| **SE** | Set of substations of the system. |
| **U** | Set of uncertainties. |
| **V** | Set of candidate buses to install PV plants. |
| **VR** | Set of voltage regulators. |
| **W** | Set of candidate buses to install WP plants. |
| **Z** | Set of integer numbers. |

## *Constants*

| | |
|---|---|
| $ES_{k,0}$, $ES_{k,T}$ | Initial/final stored energy in the storage unit at node $k$. |
| $ES_k^{\min}$, $ES_k^{\max}$ | Minimum/maximum storage capacity of the unit at node $k$. |
| $L_{km}$ | Length of circuit $km$. |
| $N_{ES}$ | Maximum number of storage units to be installed in the EDN. |
| $N_{PV}$, $N_{WT}$ | Maximum number of PV/WT plants to be installed in the EDN. |
| $PV_v^{\max}$, $WT_w^{\max}$ | Active power capacity of PV module/WT unit. |
| $Pc_k^{\min}$, $Pc_k^{\max}$ | Minimum/maximum charging power rate of the storage unit at node $k$. |
| $P_c^{\max}$, $Q_c^{\max}$ | Minimum/maximum active/reactive power through conductor $c$. |
| $Pd_k^{\min}$, $Pd_k^{\max}$ | Minimum/maximum discharging power rate of the storage unit at node $k$. |
| $P_{Dk}$, $Q_{Dk}$ | Active/reactive load demand in bus $k$. |
| $Q_b^{sp}$ | Specified reactive power capacity of CB $b$. |
| $R_c$, $X_c$ | Resistance/reactance of conductor $c$. |
| $R_{km}^{\%}$ | Regulation % of the VR to be installed in $km$. |
| $r$ | Discount rate. |
| $V_k^{\min}$, $V_k^{\max}$ | Minimum/maximum voltage magnitude limit in bus $k$. |
| $\eta c_k$, $\eta d_k$ | Charging/discharging storage efficiency of the storage unit at node $k$. |
| $\Delta_t$ | Time slot. |
| $\Gamma_{km}^{vr}$ | Installation cost of VR at node $km$. |
| $\Gamma_b^{cb^{fx/sw}}$ | Installation cost of FCB/SCB with capacity type $b$. |
| $\Gamma_{v/w}^{pv/wt}$ | Installation cost of PV modules/WT units. |
| $\Gamma_k^{es}$ | Installation cost of storage unit at node $k$. |

| | |
|---|---|
| $\Gamma_{km,c}^{cr}$ | Replacement cost of overloaded conductor in branch $km$ by a conductor $c$. |
| $\Pi_k^{es}$ | Operation cost of storage unit at node $k$. |
| $\Pi_{v/w}^{pv/wt}$ | Operation cost of PV modules/WT units. |
| $\Pi_k^{s}$ | Cost of energy supply by the substation at node $k$. |
| $\underline{\phi}^S, \overline{\phi}^S$ | Minimum/maximum power factor at substation. |
| $\underline{\Upsilon}^D, \overline{\Upsilon}^D$ | Load demand uncertainty budget. |
| $\underline{\Upsilon}^{pv}, \overline{\Upsilon}^{pv}$ | PVG uncertainty budget. |
| $\underline{\Upsilon}^{wt}, \overline{\Upsilon}^{wt}$ | WTG uncertainty budget. |
| $\underline{\mu}_t^D, \overline{\mu}_t^D$ | Minimum/maximum limits for load demand factor in period $t$. |
| $\underline{\mu}_t^{pv}, \overline{\mu}_t^{pv}$ | Minimum/maximum limits for PVG factor in period $t$. |
| $\underline{\mu}_t^{wt}, \overline{\mu}_t^{wt}$ | Minimum/maximum limits for WTG factor in period $t$. |

## *Continuous Variables*

| | |
|---|---|
| $p_{km,c,t}, q_{km,c,t}$ | Active/reactive power flow through replaced circuit $c$ in branch $km$ in period $t$. |
| $p_{k,t}^S, q_{k,}^S$ | Active/reactive power in substation $k$ in period $t$. |
| $v_{k,t}, \tilde{v}_{k,t}$ | Non regulated/regulated voltage magnitude in bus $k$ in period $t$. |
| $q_{k,t}^{CB}$ | Reactive capacitive power injected by the CB in bus $k$ in period $t$. |
| $p_{k,t}^{ESS}$ | Active power injected or absorbed to/from the system by storage unit $k$ in period $t$. |
| $pd_{k,t}, pc_{k,t}$ | Charging/discharging active power of storage unit $k$ in period $t$. |
| $es_{k,t}$ | Stored energy in storage unit $k$ in period $t$. |
| $p_{k,t}^{PV}, p_{k,t}^{PV}$ | PV/WT active power generation at node $k$ in period $t$. |
| $\mu_t^D, \mu_t^{pv}, \mu_t^{wt}$ | Uncertainty parameters for load demand, PV and WT power output in period $t$. |

## *Binary and Integer Variables*

| | |
|---|---|
| $\alpha_{km}^{vr}$ | Binary variable, $\alpha_{km}^{vr} = 1$ if the VR is installed in branch $km$ in period $t$, $\alpha_{km}^{vr} = 0$ otherwise. |
| $\alpha_{k,b,t}^{fx/sw}$ | Binary variable, $\alpha_{k,b,t}^{fx/sw} = 1$ if the FCB/SCB of capacity $b$ is installed at node $k$ in period $t$, $\alpha_{k,b,t}^{fx/sw} = 0$ otherwise. |
| $\alpha c_{k,t}$ | Binary variable equal to 1 if the storage installed unit at node $k$ is being charged in period $t$, and equal to 0 otherwise. |
| $\alpha d_{k,t}$ | Binary variable equal to 1 if the storage installed unit at node $k$ is being discharged in period $t$, and equal to 0 otherwise. |

| $\alpha_{k,t}^{es}$ | Binary variable equal to 1 if storage unit is installed at node $k$ in period $t$, and equal to 0 otherwise. |
| --- | --- |
| $\alpha_{k,v,t}^{pv}$ | Binary variable equal to 1 if PV module $v$ is installed at node $k$ in period $t$, and equal to 0 otherwise. |
| $\alpha_{k,w,t}^{wt}$ | Binary variable equal to 1 if WT unit $w$ is installed at node $k$ in period $t$, and equal to 0 otherwise. |
| $\alpha_{km,c,t}^{cr}$ | Binary variable equal to 1 if conductor in branch $km$ is replaced by conductor $c$ in period $t$, and equal to 0 otherwise. |
| $n_{k,t}^{cb}$ | Integer variable that define the CB modules installed at node $k$ in period $t$. |
| $n_k^{\max}$ | Integer variable that define the maximum CB modules to be installed at node $k$. |

# References

1. Abdelouadoud, S., Girard, R., Neirac, F., Guiot, T.: Optimal power flow of a distribution system based on increasingly tight cutting planes added to a second order cone relaxation. Int. J. Electr. Power Energy Syst. **69**, 9–17 (2015)
2. Agalgaonkar, Y.P., Pal, B.C., Jabr, R.A.: Stochastic distribution system operation considering voltage regulation risks in the presence of PV generation. IEEE Trans. Sustain. Energy **6**(4), 1315–1324 (2015)
3. Ahmadigorji, M., Amjady, N., Dehghan, S.: A robust model for multiyear distribution network reinforcement planning based on information-gap decision theory. IEEE Trans. Power Syst. **33**(2), 1339–1351 (2018)
4. Alsaidan, I., Khodaei, A., Gao, W.: A comprehensive battery energy storage optimal sizing model for microgrid applications. IEEE Trans. Power Syst. **33**(4), 3968–3980 (2018)
5. Amjady, N., Attarha, A., Dehghan, S., Conejo, A.J.: Adaptive robust expansion planning for a distribution network with DERs. IEEE Trans. Power Syst. **33**(2), 1698–1715 (2018)
6. Baharvandi, A., Aghaei, J., Niknam, T., Shafie-Khah, M., Godina, R., Catalão, J.P.S.: Bundled generation and transmission planning under demand and wind generation uncertainty based on a combination of robust and stochastic optimization. IEEE Trans. Sustain. Energy **9**(3), 1477–1486 (2018)
7. Baran, M.E., Wu, F.F.: Network reconfiguration in distribution systems for loss reduction and load balancing. IEEE Trans. Power Delivery **4**(2), 1401–1407 (1989)
8. Ben-Tal, A., Nemirovski, A.: Robust convex optimization. Math. Oper. Res. **23**(4), 769–805 (1998)
9. Ben-Tal, A., Nemirovski, A.: Robust solutions of uncertain linear programs. Oper. Res. Lett. **25**(1), 1–13 (1999)
10. Ben-Tal, A., Nemirovski, A.: Robust solutions of linear programming problems contaminated with uncertain data. Math. Program. **88**(3), 411–424 (2000)
11. Ben-Tal, A., Nemirovski, A.: Robust optimization - methodology and applications. Math. Program. **92**(3), 453–480 (2002)
12. Ben-Tal, A., Goryashko, A., Guslitzer, E., Nemirovski, A.: Adjustable robust solutions of uncertain linear programs. Math. Program. **99**(2), 351–376 (2004)
13. Bertsimas, D., Sim, M.: Robust discrete optimization and network flows. Math. Program. **98**(1–3), 49–71 (2003)
14. Bertsimas, D., Sim, M.: The price of robustness. Oper. Res. **52**(1), 35–53 (2004)

15. Bertsimas, D., Brown, D.B., Caramanis, C.: Theory and applications of robust optimization. SIAM Rev. **53**(3), 464–501 (2011)
16. Bertsimas, D., Litvinov, E., Sun, X.A., Zhao, J., Zheng, T.: Adaptive robust optimization for the security constrained unit commitment problem. IEEE Trans. Power Syst. **28**(1), 52–63 (2013)
17. Chiradeja, P., Ramakumar, R.: An approach to quantify the technical benefits of distributed generation. IEEE Trans. Energy Convers. **19**(4), 764–773 (2004)
18. Conejo, A.J., Baringo, L., Kazempour, S.J., Siddiqui, A.S.: Investment in Electricity Generation and Transmission. Springer, Berlin (2016). https://doi.org/10.1007/978-3-319-29501-5
19. Dehghan, S., Amjady, N.: Robust transmission and energy storage expansion planning in wind farm-integrated power systems considering transmission switching. IEEE Trans. Sustain. Energy **7**(2), 765–774 (2016)
20. Dell, R., Rand, D.: Energy storage – a key technology for global energy sustainability. J. Power Sources **100**(1), 2–17 (2001). https://doi.org/10.1016/S0378-7753(01)00894-1. Journal of Power Sources Volume 100
21. Denholm, P., Hand, M.: Grid flexibility and storage required to achieve very high penetration of variable renewable electricity. Energy Policy **39**(3), 1817–1830 (2011). https://doi.org/10.1016/j.enpol.2011.01.019
22. Ding, T., Liu, S., Yuan, W., Bie, Z., Zeng, B.: A two-stage robust reactive power optimization considering uncertain wind power integration in active distribution networks. IEEE Trans. Sustain. Energy **7**(1), 301–311 (2016)
23. Evangelopoulos, V.A., Georgilakis, P.S., Hatziargyriou, N.D.: Optimal operation of smart distribution networks: a review of models, methods and future research. Electr. Power Syst. Res. **140**, 95–106 (2016)
24. Falugi, P., Konstantelos, I., Strbac, G.: Planning with multiple transmission and storage investment options under uncertainty: a nested decomposition approach. IEEE Trans. Power Syst. **33**(4), 3559–3572 (2018)
25. Fanzeres, B., Street, A., Barroso, L.A.: Contracting strategies for renewable generators: a hybrid stochastic and robust optimization approach. IEEE Trans. Power Syst. **30**(4), 1825–1837 (2015)
26. Farahani, V., Sadeghi, S.H.H., Abyaneh, H.A., Agah, S.M.M., Mazlumi, K.: Energy loss reduction by conductor replacement and capacitor placement in distribution systems. IEEE Trans. Power Syst. **28**(3), 2077–2085 (2013)
27. Florez, H.A.R., Carreno, E.M., Rider, M.J., Mantovani, J.R.S.: Distflow based state estimation for power distribution networks. Energy Syst. **9**(4), 1055–1070 (2018)
28. Fourer, R., Gay, D.M., Kernighan, B.W.: AMPL: A Modeling Language for Mathematical Programming. Boston, Duxbury Press (2002)
29. Franco, J.F., Rider, M.J., Lavorato, M., Romero, R.: A mixed-integer LP model for the optimal allocation of voltage regulators and capacitors in radial distribution systems. Int. J. Electr. Power Energy Syst. **48**, 123–130 (2013)
30. Frank, S., Rebennack, S.: An introduction to optimal power flow: theory, formulation, and examples. IIE Trans. **48**(12), 1172–1197 (2016)
31. Ghaoui, L.E., Oustry, F., Lebret, H.: Robust solutions to uncertain semidefinite programs. SIAM J. Optim. **9**(1), 33–52 (1998)
32. IBM: IBM ILOG CPLEX V12.1 Users Manual for CPLEX (2009)
33. Jabr, R.A., Džafić, I., Pal, C.B.: Robust optimization of storage investment on transmission networks. IEEE Trans. Power Syst. **30**(1), 531–539 (2015)
34. Ji, H., Wang, C., Li, P., Ding, F., Wu, J.: Robust operation of soft open points in active distribution networks with high penetration of photovoltaic integration. IEEE Trans. Sustain. Energy **10**(1), 280–289 (2019)
35. Jiang, R., Zhang, M., Li, G., Guan, Y.: Benders' decomposition for the two-stage security constrained robust unit commitment problem. In: IIE Annual Conference, Proceedings, pp. 1–10 (2012)

36. Levron, Y., Shmilovitz, D.: Optimal power management in fueled systems with finite storage capacity. IEEE Trans. Circuits Syst. I Regul. Pap. **57**(8), 2221–2231 (2010). https://doi.org/10.1109/TCSI.2009.2037405

37. López, J., Pozo, D., Contreras, J.: Static and Dynamic Convex Distribution Network Expansion Planning, pp. 41–63. Singapore, Springer (2018). https://doi.org/10.1007/978-981-10-7056-3_2

38. Macedo, L.H., Franco, J.F., Rider, M.J., Romero, R.: Optimal operation of distribution networks considering energy storage devices. IEEE Trans. Smart Grid **6**(6), 2825–2836 (2015)

39. Melgar-Dominguez, O.D., Pourakbari-Kasmaei, M., Mantovani, J.R.S.: Adaptive robust short-term planning of electrical distribution systems considering siting and sizing of renewable energy based DG units. IEEE Trans. Sustain. Energy **10**(1), 158–169 (2019)

40. Montoya-Bueno, S., Muñoz-Hernández, J., Contreras, J.: Uncertainty management of renewable distributed generation. J. Cleaner Prod. **138**, 103–118 (2016)

41. Muñoz-Delgado, G., Contreras, J., Arroyo, J.M.: Multistage generation and network expansion planning in distribution systems considering uncertainty and reliability. IEEE Trans. Power Syst. **31**(5), 3715–3728 (2016)

42. Mwakabuta, N., Sekar, A.: Study of the application of evolutionary algorithms for the solution of capacitor deployment problem in distribution systems. In: 2008 40th Southeastern Symposium on System Theory (SSST), pp. 178–182 (2008)

43. Nikmehr, N., Najafi-Ravadanegh, S.: Optimal operation of distributed generations in microgrids under uncertainties in load and renewable power generation using heuristic algorithm. IET Renew. Power Gener. **9**(8), 982–990 (2015)

44. Available: https://ewh.ieee.org/soc/pes/dsacom/testfeeders/. Accessed Dec 3, 2018

45. Ortiz, J.M.H., Pourakbari-Kasmaei, M., López, J., Mantovani, J.R.S.: A stochastic mixed-integer conic programming model for distribution system expansion planning considering wind generation. Energy Syst. **9**(3), 551–571 (2018)

46. Pereira Junior, B.R., Cossi, A.M., Mantovani, J.R.S.: Multiobjective short-term planning of electric power distribution systems using NSGA-II. J. Control Autom. Electr. Syst. **24**(3), 286–299 (2013)

47. Pozo, D., Contreras, J., Sauma, E.E.: Unit commitment with ideal and generic energy storage units. IEEE Trans. Power Syst. **29**(6), 2974–2984 (2014)

48. Ravichandran, A., Sirouspour, S., Malysz, P., Emadi, A.: A chance-constraints-based control strategy for microgrids with energy storage and integrated electric vehicles. IEEE Trans. Smart Grid **9**(1), 346–359 (2018)

49. Santos, S.F., Fitiwi, D.Z., Bizuayehu, A.W., Shafie-khah, M., Asensio, M., Contreras, J., Cabrita, C.M.P., João, P.S.C.: Novel multi-stage stochastic DG investment planning with recourse. IEEE Trans. Sustain. Energy **8**(1), 164–178 (2017)

50. Tan, S., Xu, J., Panda, S.K.: Optimization of distribution network incorporating distributed generators: an integrated approach. IEEE Trans. Power Syst. **28**(3), 2421–2432 (2013)

51. Thiele, A., Terry, T., Epelman, M.: Robust linear optimization with recourse. Rapport technique, pp. 4–37 (2009)

52. Wang, Z., Chen, B., Wang, J., Kim, J., Begovic, M.M.: Robust optimization based optimal DG placement in microgrids. IEEE Trans. Smart Grid **5**(5), 2173–2182 (2014)

53. Wang, R., Wang, P., Xiao, G.: A robust optimization approach for energy generation scheduling in microgrids. Energy Convers. Manag. **106**, 597–607 (2015)

54. Xiang, Y., Liu, J., Liu, Y.: Robust energy management of microgrid with uncertain renewable generation and load. IEEE Trans. Smart Grid **7**(2), 1034–1043 (2016)

55. Xing, H., Cheng, H., Zhang, Y., Zeng, P.: Active distribution network expansion planning integrating dispersed energy storage systems. IET Gener. Transm. Distrib. **10**(3), 638–644 (2016)

56. Yanıkoğlu, I., Gorissen, B.L., Hertog, D.D.: A survey of adjustable robust optimization. Eur. J. Oper. Res. **27**, 799–813 (2019)

57. Zeng, B., Zhang, J., Ouyang, S., Yang, X., Dong, J., Zeng, M.: Two-stage combinatory planning method for efficient wind power integration in smart distribution systems considering uncertainties. Electr. Power Compon. Syst. **42**(15), 1661–1672 (2014). https://doi.org/10.1080/15325008.2014.913735
58. Zhao, L., Zeng, B.: Robust unit commitment problem with demand response and wind energy. In: 2012 IEEE Power and Energy Society General Meeting, pp. 1–8 (2012)
59. Zeng, B., Zhao, L.: Solving two-stage robust optimization problems using a column-and-constraint generation method. Oper. Res. Lett. **41**(5), 457–461 (2013)
60. Zheng, Y., Zhao, J., Song, Y., Luo, F., Meng, K., Qiu, J., Hill, D.J.: Optimal operation of battery energy storage system considering distribution system uncertainty. IEEE Trans. Sustain. Energy **9**, 1051–1060 (2018)

# Phase Balancing in Power Distribution Grids: A Genetic Algorithm with a Group-Based Codification

**Alejandro Garcés, Juan Camilo Castaño, and Miguel Angel Rios**

**Abstract** Phase balancing is an optimization problem which can reduce power losses in modern power distribution grids. The problem consists on phase swapping of the loads at the feeder level in order to reduce the unbalance of the grid. Despite being a classic problem, it is still relevant since unbalance is a common phenomena in power distribution grids and can be intensified by the uncoordinated use of distributed resources such as renewable energies and electric vehicles, among other single phase loads. Being a combinatorial problem, phase balancing requires heuristic algorithms whose codification must be carefully designed. In addition, high penetration of renewable energies makes the problem stochastic. This chapter shows a genetic algorithm which solves efficiently the problem, considering a detailed model of the power flow. A novel codification is proposed based on the identification of symmetries on the intrinsic structure of the problem by using the concept of group, an algebraic structure that can be easily combined with the conventional genetic algorithm. Simulations results on the IEEE test systems demonstrate the efficiency of the proposed method.

## 1 The Phase Balancing Problem

Power distribution networks are usually unbalanced due to the presence of single phase loads. Consequently, grid operators require to define right placement of each single phase load in order to reduce technical losses, in a process known as phase balancing [1]. This is a classic problem in power distribution optimization, being more important in modern systems, due to the introduction of single-phase renewable resources such as small photovoltaic systems and slow-charging electrical vehicles [2]. The problem has been also identified in aircraft electric systems [3].

A. Garcés (✉) · J. C. Castaño · M. A. Rios
Universidad Tecnologica de Pereira, Pereira, Colombia
e-mail: alejandro.garces@utp.edu.co

Power distribution systems are composed of three phases with three voltage and current signals, which are equal in magnitude and phase shifted from each other by 120°, if balanced conditions are satisfied. Nevertheless, it is common to find single phase loads connected to single-phase transformers as well as renewable energy generation such as solar panels, and low-power wind turbines which can be single-phase; it is also common to find unbalance loads connected to a three-phase transformer. These situations cause power quality degradation, high power losses, asymmetry in the voltage and current values and electricity costs rising. Slow-charging electric vehicles are also single-phase loads that can have great impact on the unbalance of the grid. As consequence of this, zero sequence currents are created which increase power losses and can result in damages for the grid infrastructure as the operational and physical constraints of the electrical components might be exceeded.

Challenges related to renewable energies, electric vehicles and specially micro-grids make the phase balance an important problem in modern power distribution grids, despite being a problem relatively unnoticed in scientific literature. This promotes the necessity of introducing new algorithms, with a stronger mathematical formulation, to solve the phase balancing in micro-grids and power distribution networks [4], considering the impact on the system given by the massive integration of distributed resources. Authors in [5], considered a probabilistic operational planning in order to optimally minimize phase unbalance in a distribution system with a large number of single phase solar generators. As presented in [2] electric vehicles chargers can be also subject to phase-balancing. Furthermore, in the internal electric grid of airplanes [3] and ships [6] the phase balancing problem has also been identified.

## 1.1 Mathematical Model

The phase balancing problem is closely related to the power system reconfiguration [7]. These two methodologies modify the topology of the network improving voltage profiles and balancing current values. However, as mentioned in [1], the former approach has a more direct effect on the balance of the grid, since it provides a direct way to balance a feeder in terms of phases. By considering the loads swapping this problem can be represented as follows:

$$\text{minimize} P_L(v, \theta, x) \tag{1}$$

$$\text{subject to } f(v, \theta, x) = 0 \tag{2}$$

$$x \in \Omega \subseteq \mathscr{B} \tag{3}$$

where, $P_L$ is the power losses function, $f$ are the expressions for the power flow, $\theta$, $V$ are the angles and nodal voltages, respectively, and $x$ are the suitable swapping actions to minimize $P_L$. $\Omega$ represents all feasible swapping actions.

The problem is clearly combinatorial since $f$ is a non-linear/non-convex constraint and $x$ include discrete variables. The main difficulty of this model lies not only in its combinatorial nature, but also in the representation of the set $\Omega$, in order to avoid restricted actions as changes on the sequence for industrial loads or to place two loads on the same phase. In that case, a large set of additional binary constraints are required for representing $\Omega$. These contraints must be included in the objective function in order to use conventional metaheuristics. An indication function $I_\Omega(x)$ as the one defined in (4) is commonly used for this task and included directly on the objective function as a penalization factor.

$$I_\Omega(x) = \left\{ \begin{array}{l} 0 \ x \in \Omega \\ \infty \ x \notin \Omega \end{array} \right\} \tag{4}$$

This approach has several disadvantages, despite being computationally feasible. On the one hand, the size of the binary set is $|\mathcal{B}| = 2^{9n}$ where $n$ is the number of nodes of the system. Nonetheless, the size of the feasible set is only $|\Omega| = 6^n$. It can be obtained that $|\Omega|/|\mathcal{B}| = \ln(6)/(9 \times \ln(2)) = 0.287$ by using a logarithmic measure. This means that the feasible connections are less than 30% of the binary solutions.[1] On the other hand, the algebraic properties of the genetic operators under a binary representation, can result in unfeasible solutions after crossover, even from feasible population. This is due to there is not a system of measurement for establishing the level of "infeasibility". The problem is clearly characterized by its algebraic and not geometric nature. Hence, an algebraic construction is necessary in order to have an efficient codification.

## 2   What is a Group?

The concept of group is the central object of abstract algebra which is basic to the development of more complex abstractions such as rings and fields (see for example [8] and [9] for more details). The main contribution that group theory adds to heuristic techniques, is the possibility to reduce the feasible solution space. In the following, a general introduction to the group concept is presented. More details about the abstract presentation of the concept can be studied from [10] and [11].

Formally, a Group is a non-empty set $G$ and a binary operation $(\circ) : G \times G \rightarrow G$ called group product which fulfills the following axioms for any $x, y, z \in G$

- Associativity: $x \circ (y \circ z) = (x \circ y) \circ z \in G$
- Existence of an identity: there exists an element $e \in G$ such that $e \circ x = x \circ e = x$ for all $x \in G$

---

[1]In section IV, it is shown that this relation is even smaller for industrial feeders.

- Existence of inverse: for every $x \in G$ there exists an element $x^{-1} \in G$ such that $x \circ x^{-1} = x^{-1} \circ x = e$

Note that ($\circ$) represents a function which combines two elements of the original set and gives as result, an element which is part to the set too. This is defined as a binary operation. As an example, consider the sum of real numbers: this operations takes two real numbers and returns a real number. Hence, the real numbers with the conventional sum as the binary operation composes a group. On the contrary, the dot product on a linear space is not a group, since it takes two objects of the set (vectors) and returns an object which is not a vector but a real number. Indubitably, the elements belonging to a linear space could form a group, notwithstanding it is necessary to establish a suitable group product. The main characteristic of groups for genetic algorithms applications is the closure, that is, the operation between two feasible solutions returns a feasible solution. This is made without any penalization or artificial procedure, but by the intrinsic characterization of the algebraic structure.

## 2.1 The Three-Phase Group

A useful group in the engineering field is the symmetric or permutation group $G_3$: consider a set conformed by all different ways that an equilateral triangle can be picked up, rotated and flipped (Fig. 1 shows the elements of this set). The element ($e$) remains the triangle unchanged (it is the identity). The second and third elements ($x_1, x_2$) move clockwise and counter-clockwise each vertex respectively, while the fourth to sixth elements ($y_1, y_2, y_3$) interchange the vertexes. It is not difficult to see that this set is finite since there are only six possibilities. Additionally, a group
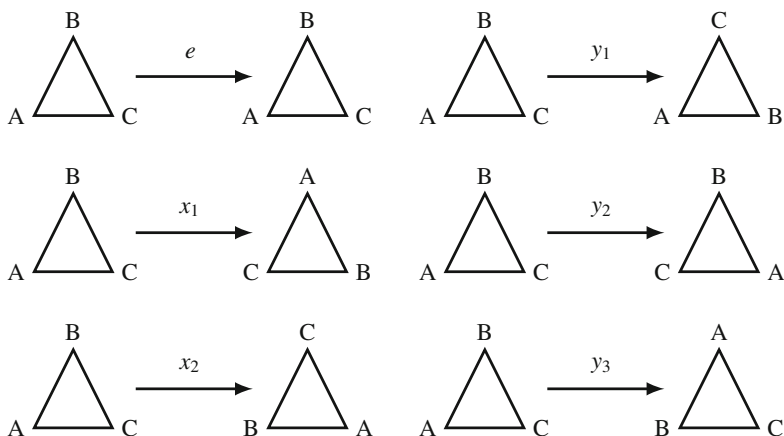


**Fig. 1** Example of a group formed by the symmetries of a triangle

**Table 1** Caley table for the symmetric group $G_3$

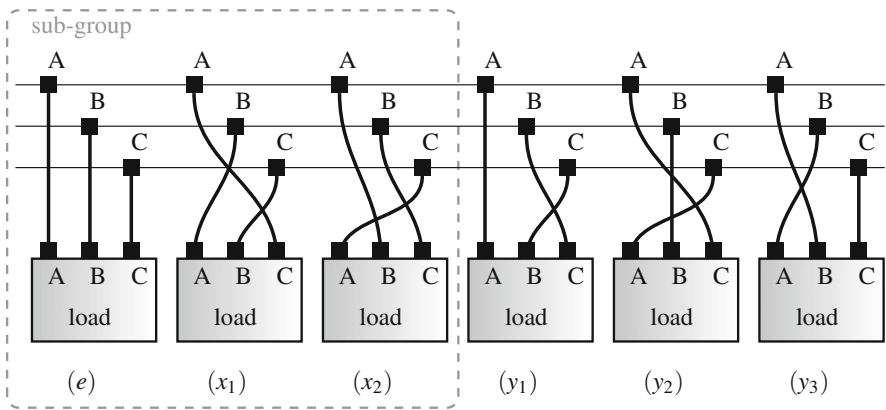| $\circ$ | $e$ | $x_1$ | $x_2$ | $y_1$ | $y_2$ | $y_3$ |
|---|---|---|---|---|---|---|
| $e$ | $e$ | $x_1$ | $x_2$ | $y_1$ | $y_2$ | $y_3$ |
| $x_1$ | $x_1$ | $x_2$ | $e$ | $y_3$ | $y_1$ | $y_2$ |
| $x_2$ | $x_2$ | $e$ | $x_1$ | $y_2$ | $y_3$ | $y_1$ |
| $y_1$ | $y_1$ | $y_2$ | $y_3$ | $e$ | $x_1$ | $x_2$ |
| $y_2$ | $y_2$ | $y_3$ | $y_1$ | $x_2$ | $e$ | $x_1$ |
| $y_3$ | $y_3$ | $y_1$ | $y_2$ | $x_1$ | $x_2$ | $e$ |



**Fig. 2** Example of a group formed by the symmetries of phase balancing problem

operation (product) can be defined as the application of each transformation. Notice that this set, with this product, fulfills all the axioms of a group.

All operations of a group can be represented by Caley's table as given in Table 1 for the group $G_3$. This table gives all the possible outcomes from two different inputs, which can be implemented computationally as a function in any programming language. In this way, the binary operation can be translated into a function that can be used by a heuristic algorithm.

The symmetric group is equivalent to the group of permutations of the phases in a transformer as depicted in Fig. 2. This is equivalent relation is called a homomorphism. In principle, all the properties of the group $G_3$ are shared with this group despite being quite different objects. Section 4 shows a third homomorphism of the same group, based on a matrix representation. This allows high flexibility in the implementation of the algorithms preserving the same mathematical structure.

On the other hand, the group can be extended to all the nodes of the grid generating a new group. This can be interpreted mathematically as a Cartesian product of the group. In practice, it means that the binary operation is executed point-wise from two arrays of the same size, as follows:

$$(x_1, x_2, \ldots, x_n) \circ (y_1, y_2, \ldots, y_n) = (x_1 \circ y_1, x_2 \circ y_2, \ldots, x_n \circ y_n) \tag{5}$$

This group is called the *Three-phase group* ($\Gamma_3$ henceforth) and will be the main structure for the proposed algorithm.

Now, let us return to the analysis of the group operation for a single load. It is important to highlight that the set $S = \{e, x_1, x_2\}$ under the same group operation constitutes a group in its own, this is called a subgroup. In the example above, the subgroup $S \subset G_3$ is composed of rotations exclusively. This subgroup has additional characteristics, for example, after three times the application of the group operation to any element of the group, this element remains unchanged, that is $x_i \circ x_i \circ x_i = x_i^3 = x_i$. Due to this characteristic, $S$ is called a cyclic group.

The commutative law is not one of the axioms of groups; Since, in general, the relation $x \circ y = y \circ x$ is not true for all $x, y \in G$. However, if this commutative law holds in a group $S$, such a group is called a commutative group or Abelian group. These are named after the mathematician Niels Abel who made several remarkable discoveries and was a pioneer in the study of groups [12]. In general, cyclic groups are Abelian. This property can be easily established on $S = \{e, x_1, x_2\} \subseteq G_3$ by noticing the symmetry of the subgroup in Table 1.

# 3 Phase Balancing Problem with Group Theory Representation

In contradistinction to the group codification, a binary representation of the problem is possible by setting a value of 1 the case in which one load is swapped from a phase $i \in \{A, B, C\}$ to a new phase $j \in \{A, B, C\}$, and 0 if it is not swapped (see Fig. 3). This representation has a major drawback for a heuristic algorithm, since it can lead easily to an unfeasible solution. Notice for example that in Fig. 3, the load in phase A is swapped simultaneously to new phase A and phase B. Nevertheless, this representation of the problem has been used in most of the heuristics applied to the phase balancing problem, see for example [4].

In other words, binary representation gives $9^n$ solutions but most of the solutions are unfeasible. In addition, an unfeasible solution can appears from two feasible solutions after the conventional genetic operators such as crossover or mutation. As aforementioned, additional constraints on the binary variables are required with a penalization function which can deteriorate the performance of the genetic algorithm.

**Fig. 3** Binary representation of the swapping action

| A | A | A | B | B | B | C | C | C |
|---|---|---|---|---|---|---|---|---|
| A | B | C | A | B | C | A | B | C |
| 1 | 1 | 0 | 1 | 0 | 0 | 0 | 1 | 0 |
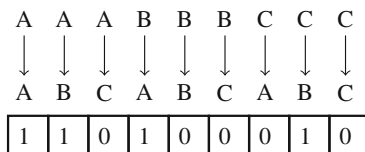
In a group-based heuristic, the representation is made as function of the group structure, in this case the three-phase group $\Gamma_3$ as follows:

$$\underset{x,v,\theta}{\text{Minimize}}\ P_L(v, \theta, x) \tag{6}$$

$$f(v, \theta, x) = 0 \tag{7}$$

$$x \in \Gamma_3 \tag{8}$$

where $\Gamma_3$ represents the Three-phase group depicted in Fig. 2 and $f$ represents the power flow equations. Now, notice that the power flow can be solved efficiently by a three-phase backward forward sweep load flow for each configuration $x$. In fact, we can define this as a function (both from the mathematical and computational point of view) such that $(v, \theta) = \phi(x)$. Consequently, the optimization problem becomes an unconstrained minimization on a group:

$$\underset{x}{\text{Minimize}}\ P_L(\phi(x), x) \text{ with } x \in \Gamma_3 \tag{9}$$

This is done in a natural way without any penalization factor. On the other hand, changing the sequence of the loads of industrial feeders could produce a change in the rotation direction of motors and other industrial components. Therefore, switching the sequence of the loads is not recommended in those cases. Notice that the problem is reduced to $\Psi_S = \{e, x_1, x_2\}$ which is a cyclic Abelian group; the size of this group is reduced to $3^n$ since for each node $x_i^3 = x_i$. Once more, the size of the problem is reduced from $2^{9n}$ to $3^n$. The combinatorial nature of the problem does not change but the size of the solution space decreases considerably.

The group operation can be used in the genetic algorithm to move in the feasible solution space. The indicator function is not required which implies that the structure of the solution space is smoother (i.e the algorithm moves in $\Gamma_3$ and not in $\mathbb{B}^{9n}$).

On the other hand, the objective function can be modified maintaining the same group structure. For example, a different approach can be considered to solve the phase balancing problem by considering the energy losses of the systems during an interval of 24 h, therefore the optimization problem is represented as follows:

$$\underset{x}{\text{Minimize}}\ \sum_{i=1}^{24} P_{Li}(\phi(x), x) \text{ with } x \in \Gamma_3 \tag{10}$$

This problem has a better physical meaning since it can include the load curve (as depicts Fig. 4) and the expected variations on the distributed generation. However, the complexity of the problem is the same since the set $\Gamma_3$ is always the same.
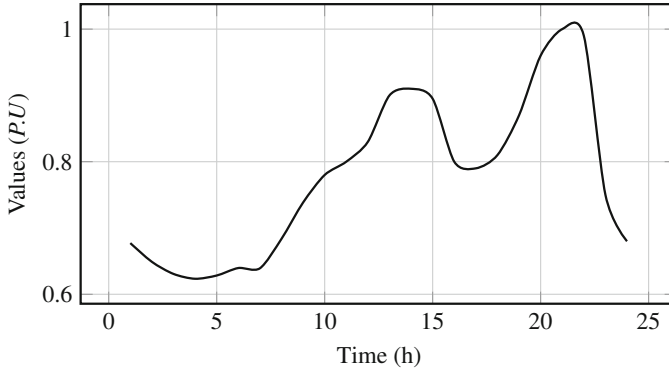
**Fig. 4** Example of a load curve for a typical residential load

## 4  Genetic Algorithm with a Group Codification

Genetic algorithms are optimization techniques inspired by the evolutionary theory of Charles Darwin, presented in his seminal book *On The Origin of Species* in 1859. In those algorithms, each feasible solution of the studied problem is represented by a vector arrays named pseudo chromosome, which are submitted to an evolutionary process that determines which individual is 'fitter' in relation to the environment. For the phase balancing problem the environment that the individuals must be adapted to is represented by the function that minimize the system losses obtained by a three-phase power flow. The proposed genetic algorithm incorporates the following steps:

- Fitness function: Finding the optimal solution of unconstrained problems is an approach that majority of meta-heuristic algorithm are designed to. In this context, the fitness function measures the adaptability of the solution if a constrained problem is considered. However, it is necessary to incorporate the problem constraints into the objective function which is a task carried out by the indicator function. In the group theory approach the aforementioned indicator function is not required since the group codification allows the algorithm moves into the feasible zone. In this way, the problem can be represented as (10)
- Selection operator: In all genetic algorithms selecting what characteristics of the good solutions will be duplicated while the size of the population keeps constants is a fundamental step, that is why a selection operator is required. In this algorithm a tournament selection is proposed.
- Variation operator: Creating new solutions is a task carried out by this operator. Its aim is incorporating diversity to the optimization process, by building unique offsprings that inherit partially characteristics of their parents. The population individuals submitted to this operator are created using the group codification. Here, every feasible connection between loads and phases for every $k$ node, given by each element of the $\Gamma_3$ group, can be formulated as an homorphism given by

the following matrix representation:

$$S^{(k)} = R^{\alpha(k)} \cdot P^{\beta(k)} \cdot \tilde{S}^{(k)}, \ \forall \ k \in \mathscr{L} \tag{11}$$

where matrices $R^\alpha$ and $P^\beta$ are shown in (12) and (13) respectively.

$$R^\alpha = \begin{pmatrix} 0 & 1 & 0 \\ 0 & 0 & 1 \\ 1 & 0 & 0 \end{pmatrix}^\alpha \tag{12}$$

$$P^\beta = \begin{pmatrix} 0 & 1 & 0 \\ 1 & 0 & 0 \\ 0 & 0 & 1 \end{pmatrix}^\beta \tag{13}$$

The $\Gamma_3$ group elements will be represented by tensor $M$ for every feasible combination between $\alpha$ and $\beta$, where $\alpha = \{0, 1, 2\}$ and $\beta = \{0, 1\}$. Then, equality (14) can be formulated for every node $k$.

$$M^{(k)} = R^{\alpha(k)} \cdot P^{\beta(k)} \tag{14}$$

Furthermore, Fig. 5 depicts every feasible connection represented by a group element as a result of combination between $\alpha$ and $\beta$ in (14).

In the same way, the crossover and mutation operators are defined by the elements of the $\Gamma_3$ group, which implies that the offspring is going to belong to the aforementioned group and those operators are closed under the binary operation defined by the symbol $\circ$.

- Crossover operator: Its function is creating new offspring from two individuals of the previous generations as it is shown Fig. 6
- Mutation operator: Producing a variation of pseudo chromosome characteristics is a function carried out by this operator.
- Elitist operator: The aim of this operator is keeping the good solutions. The most well known way to do this is preserving the best solution so far passing from



**Fig. 5** Group elements represented for every feasible $\alpha - \beta$ combination
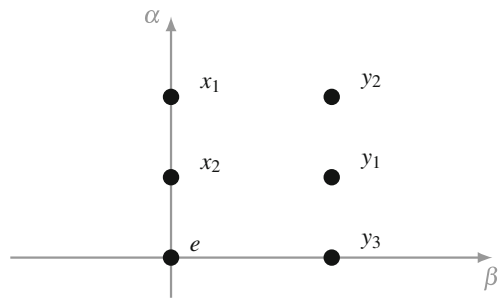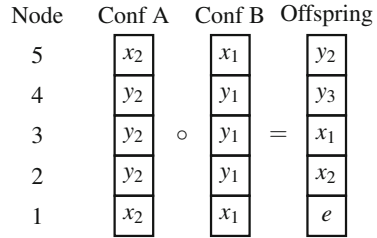
**Fig. 6** Crossover operator
using group representation.
For each node, the offspring
is given by the group
operation ∘ between each
Configuration A and
Configuration B

| Node | Conf A | | Conf B | | Offspring |
|------|--------|---|--------|---|-----------|
| 5 | $x_2$ | | $x_1$ | | $y_2$ |
| 4 | $y_2$ | | $y_1$ | | $y_3$ |
| 3 | $y_2$ | ∘ | $y_1$ | = | $x_1$ |
| 2 | $y_2$ | | $y_1$ | | $x_2$ |
| 1 | $x_2$ | | $x_1$ | | $e$ |

---

**Algorithm 1** Genetic algorithm for phase-balancing

---

1:  **procedure** GENETIC(Feeder)
2:      $i \leftarrow 0$                                                                ▷ generation counter
3:      $\rho \leftarrow \text{Rand}(\Gamma_3)$                              ▷ Initialize population randomly
4:      $f \leftarrow P_L(\rho)$                                                  ▷ Evaluate objective function
5:      $f_{opt}, \rho_{opt} \leftarrow \text{Best}(f)$
6:      **while** $i \leq$ Number of generations **do**
7:          $\partial\rho \leftarrow \text{Tournament}(\rho)$                      ▷ Selection
8:          $\rho \leftarrow \text{Crossover}(\partial\rho, \Gamma_3)$
9:          $\rho \leftarrow \text{Mutation}(\rho, \Gamma_3)$
10:         $f \leftarrow P_L(\rho)$
11:         $f_{opt}, \rho_{opt} \leftarrow \text{Best}(f)$
12:         $\rho \leftarrow \text{Variation}(\rho)$
13:         $\rho \leftarrow \text{Elitism}(\rho)$
14:         $f \leftarrow P_L(\rho)$
15:         $f_{opt}, \rho_{opt} \leftarrow \text{Best}(f)$
16:     **return** $f_{opt}, \rho_{opt}$                                          ▷ Optimal solution

---

the current generation to the next. Here, the best solution is represented by a chromosome which includes all nodes represented by an $\alpha - \beta$ combination.

The steps of the algorithm are summarized in Algorithm 1. The algorithm is basically the same when the subgroup $\Psi_S$ is used instead $\Gamma_3$.

## 5 Examples

The aforementioned genetic algorithm, under the group theory codification, was carried out several times for the energy optimization approach. Tests were performed for the IEEE-test-systems of 13, 37 and 123 nodes. All parameters of these feeders can be found in [13]. Notwithstanding, meta-heuristic algorithms were used to solve the problem, which means that the number of iterations and the computing time varied every time that the algorithm was carried out, therefore, results are presented in average. Each individual of the initial population was represented by a combination of $\alpha - \beta$ for each node. Then, the optimal point is given by the $\alpha - \beta$ combination that produces the minimum value of losses. Furthermore, unbalance indices for line currents in every node $k$ for all study cases, were calculated by using

Eq. (15) as follows:

$$\xi_k = \max_i \left\{ \frac{|I_{a_k} - I_{m_k}|}{|I_{m_k}|}, \frac{|I_{b_k} - I_{m_k}|}{|I_{m_k}|}, \frac{|I_{c_k} - I_{m_k}|}{|I_{m_k}|} \right\} \tag{15}$$

with

$$I_{m_k} = \frac{I_{a_k} + I_{b_k} + I_{c_k}}{3} \tag{16}$$

Where, $I_{a_k}$, $I_{b_k}$ and $I_{c_k}$ are the line current of each phase on node $k$, while $I_{m_k}$ in (16) corresponds to the mean value for the line current of the node $k$. Notice that for balanced conditions the value of $\xi$ must be equal to zero, i.e. the line currents are all equal to the mean value.

## 5.1 IEEE 13 Nodes Test Feeder

The IEEE 13 Nodes test feeder is a small grid with spot loads in 8 of his 13 buses(see Fig. 7). Even though this feeder is a relatively small circuit, the proposed algorithm produces a considerable reduction of losses. Table 3 presents the value of the losses when the systems is unbalanced and when this is balanced, among other important results considering energy losses reduction. Furthermore, Table 2 shows the new configurations, phase shifting, and unbalance indices for each load of the system.

Figure 8 depicts the reduction of the unbalance indices during the peak load, in all nodes considering energy losses. It is noticed that the unbalanced index is improved in most of the nodes, except in Node 11. However, the total effect on the system is reduction of energy losses. This is because Node 11 has the lowest load value and consequently, the minimum effect on the total energy losses (Table 3).

Additionally, Fig. 9 shows the energy losses reduction for the system in every hour of one day, following the load curve of Fig. 4.
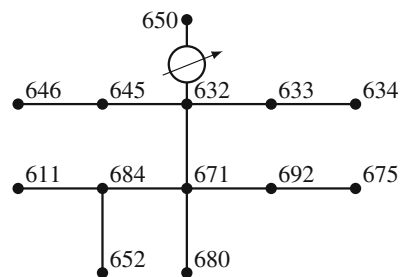


Fig. 7 IEEE 13 nodes test feeder

**Table 2** IEEE 13 Nodes test feeder optimized configurations and unbalance indices

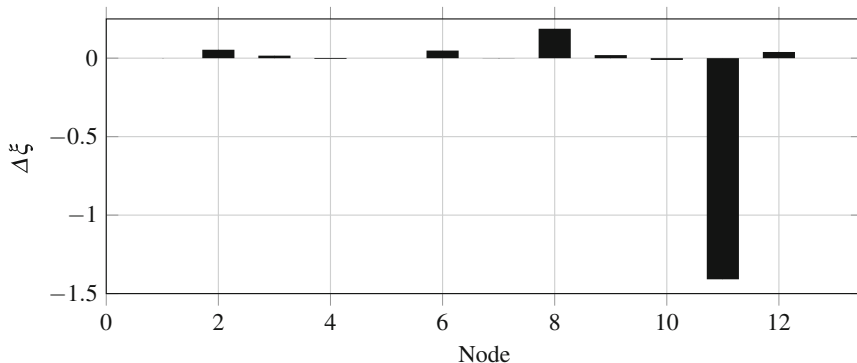| Node | Configuration | Phase shifting | Unbalance indices | |
|---|---|---|---|---|
| | | | Unbalanced system | Optimized system |
| 633 | x2 | BCA | 0.1847 | 0.1686 |
| 645 | x2 | BCA | 0.1381 | 0.0845 |
| 646 | y3 | BAC | 1.0605 | 1.0655 |
| 652 | x1 | CAB | 2.0000 | 1.9992 |
| 692 | y2 | CBA | 0.5902 | 1.9992 |
| 611 | x2 | BCA | 0.0704 | 0.0818 |
| 671 | y1 | ACB | 0.2328 | 0.0454 |
| 675 | y2 | CBA | 0.4617 | 0.4223 |



**Fig. 8** Change on the unbalance index during the peak load for the IEEE13 nodes test feeder. Positive values indicate an improvement in the unbalance index

**Table 3** IEEE 13 test feeder results considering energy losses

| | Unit | Value |
|---|---|---|
| Unbalanced system losses | kWh | 1579.035 |
| Balanced system losses | kWh | 1379.065 |
| Total reduction | % | 12.664 |
| Iterations to find the best approximation | n | 4 |
| Time to find the best approximation | s | 250.214 |

## 5.2   IEEE 37 Nodes Test Feeder

A real underground feeder located in California is represented by the IEEE 37 Nodes test system. It has an operating voltage of 4.8 kV, and its substation voltage regulation is two single-phase open-delta regulators, besides 25 of its 37 nodes are highly unbalanced (see Fig. 10). Results are shown in Table 4. Also, Fig. 11 depicts the unbalance indices reduction for the energy losses reduction. The analysis is similar to the IEEE 13 nodes. The algorithm can increase locally the unbalance
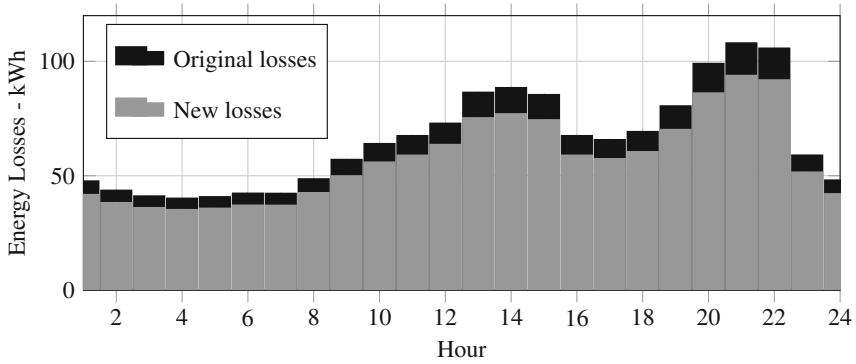
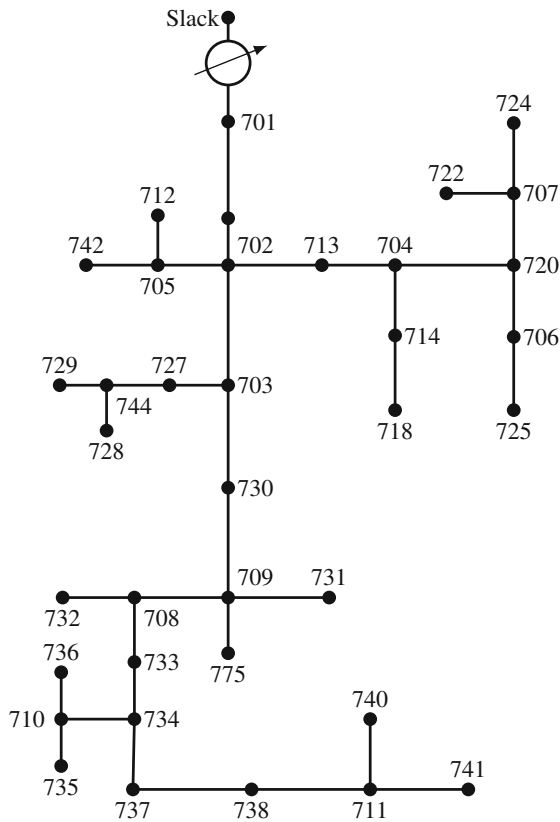**Fig. 9** Daily energy losses improvement for IEEE 13 nodes test feeder



**Fig. 10** The IEEE 37 nodes test system

**Table 4** IEEE 37 test feeder results considering energy losses

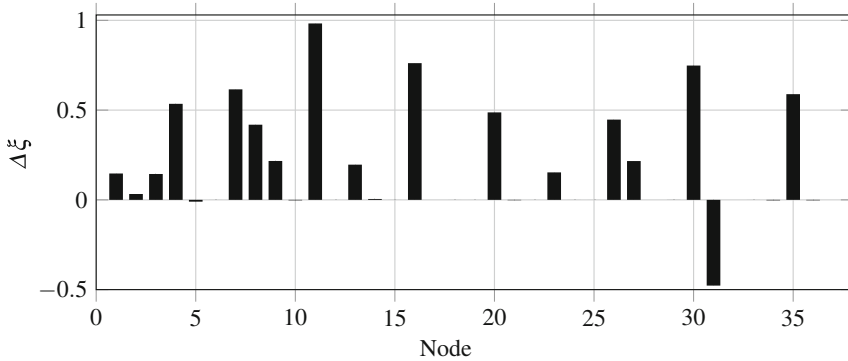|                                                | Unit | Value   |
|------------------------------------------------|------|---------|
| Unbalanced system losses                       | kWh  | 488.600 |
| Balanced system losses                         | kWh  | 443.040 |
| Total reduction                                | %    | 9.324   |
| Iterations to find the best approximation      | n    | 12      |
| Time to find the best approximation            | s    | 298.215 |



**Fig. 11** Change in the unbalance index for the IEEE 37 nodes test feeder considering energy losses. Positive values indicate an improvement in the unbalance index
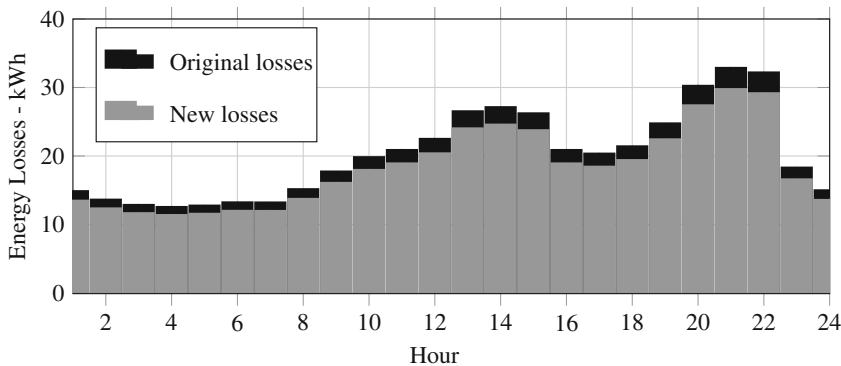


**Fig. 12** Daily energy losses improvement for IEEE 37 nodes test feeder

in a particular node or in a particular time, in order to decrease the total unbalance of the grid and, consequently, the energy losses.

Also, Fig. 12 shows the improvement of the energy losses every hour for one day, using the load curve shown in Fig. 4.

## 5.3 IEEE 123 Nodes Test Feeder

With loads in 89 out of his 123 nodes, the IEEE 123 nodes test feeder consists on overhead and underground lines; unbalance loading with constant current, impedance and power; four voltage regulators and shunt capacitor banks (see Fig. 13). Table 5 shows the numerical results for energy losses improvement. In addition, Fig. 14 presents the unbalance indices reduction and Fig. 15 the energy losses before and after implementing the algorithm, for every hour in one day.

The obtained results show that the unbalancing of all studied test feeders was considerable reduced (positive values) in spite of the unbalancing was minimally increased in some nodes (negative values) . Notice that for nodes with two phase-loads, nodes that have a single-phase, or even terminals without loads, the reduction
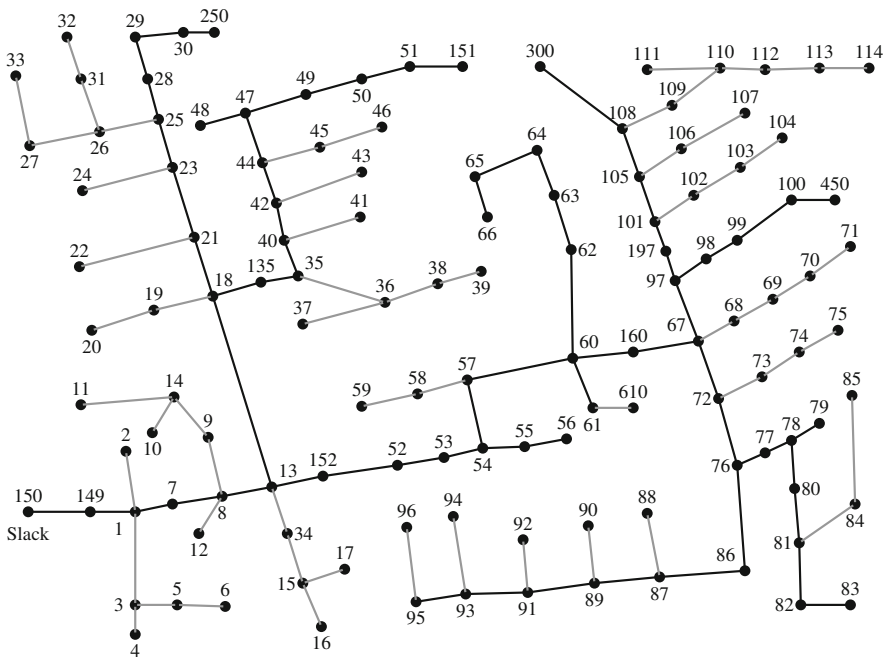


**Fig. 13** IEEE123 test distribution system

**Table 5** IEEE 123 test feeder results considering energy losses

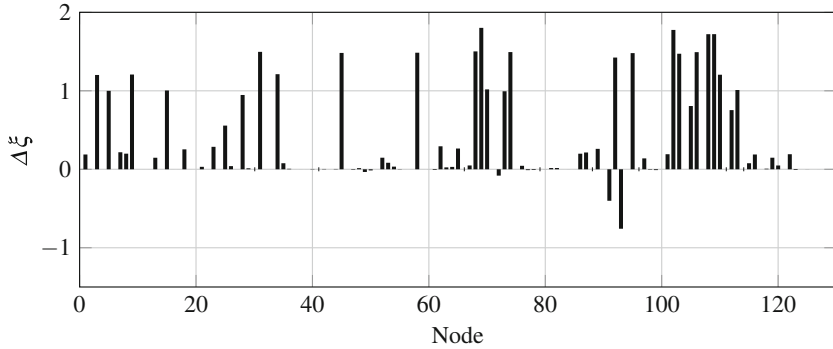|  | Unit | Value |
|---|---|---|
| Unbalanced System Losses | kWh | 1371.674 |
| Balanced System Losses | kWh | 1284.484 |
| Total reduction | % | 6.356 |
| Iterations to find the best approximation | n | 24 |
| Time to find the best approximation | s | 234.836 |

**Fig. 14** Change in the unbalance index for the IEEE 123 nodes test feeder considering energy losses. Positive values indicate an improvement in the unbalance index
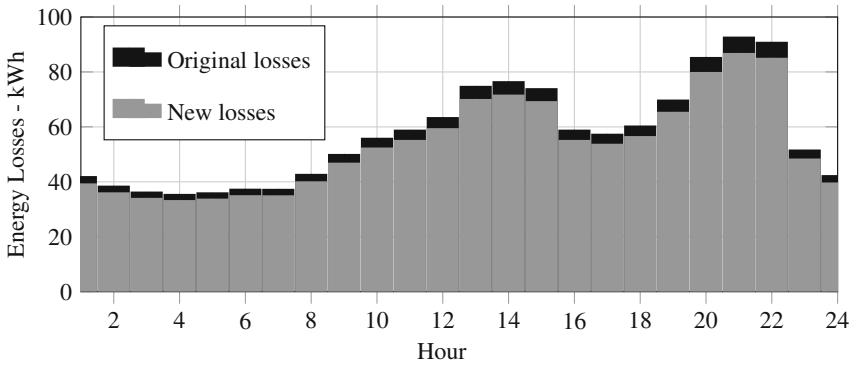


**Fig. 15** Daily energy losses improvement for the IEEE 123 nodes test feeder

value is zero since the swapping of the loads have negligible effect on the unbalance index. However, it can have effect in the total energy losses.

## 6   Comparison Between Optimization in $\Gamma_3$ and $\Psi_S$

As mentioned in previous sections, the proposed methodology can be applied for any type of feeders. Notwithstanding, the constraint related to the change of sequence of the loads must be considered for industrial feeders. In this way, the set of the feasible solution is reduced to the symmetric-Abelian subgroup that was presented in Sect. 2. Simulations were performed again, looking for a decrease on the power losses and considering the new feasible solution space. Results are presented in Table 6.

**Table 6** Comparison on the phase-balancing problem in the three-phase group and the three-phase subgroup for industrial feeders

| Solution space | Feeder | Reduction [%] | Iterations | Time [s] |
|---|---|---|---|---|
| $\Gamma_3$ | IEEE 13 | 13.3458 | 1494 | 33.0036 |
| | IEEE 37 | 10.1026 | 9601 | 492.7682 |
| | IEEE 123 | 7.3929 | 8487 | 1422.325 |
| $\Psi_S$ | IEEE 13 | 11.7830 | 1143 | 20.4441 |
| | IEEE 37 | 9.8908 | 5525 | 301.5133 |
| | IEEE 123 | 7.2785 | 8823 | 1333.903 |

From Table 6, It is easy to see that the algorithm optimizing in $\Gamma_3$ reduces the losses more than the algorithm optimizing in $\Psi_S$. This happens because the size of the solution space of $\Gamma_3$ is wider and allows changes of sequence. On the other hand, the size of the solution space of $\Psi_S$ is smaller since this subgroup represents the industrial feeders where a change of sequence is not recommended. The algorithm moving in $\Psi_S$ implies the iterations reduction and CPU time reduction. In addition, the sizes of the solutions space of the aforementioned groups are reduced by comparison to the traditional approach where an indicator function is required, this is because under this approach many unfeasible solutions are considered, something that does not happen when group codification is applied.

## 7  Conclusions

The use of group theory for the codification of phase-balancing problem in power distribution grids was studied by using two different objective functions (power losses and energy losses). Even though a modified genetic algorithm is proposed, the presented methodology can be applied for other kinds of algorithms for other types of algorithms. This codification allows to reduce the size of the solution space since the algorithm moves from feasible to feasible solution, without requiring penalization barriers or an indicator function as the conventional methodologies. In addition, crossover and mutation operators are easily codified under this representation.

It was proposed a direct method for the phase balancing of industrial feeders, where changes of sequence are not desired. A special subgroup representation is obtained in these cases where the commutative law holds, which seems to improve the convergence of the algorithm. Depth research is required for the purpose of understanding better this property. The size of the solution space was effectively reduced which is not possible when traditional approaches are used since they use an indicator function that only penalizes some zones of the solution space.

The group theory embraces many concepts that can be used in power systems. More research is required in order to explore the advantage that symmetries have in this field. The phase-balancing problem can be described in terms of finite-semigroups and in particular in terms of Monoids since the inverse operation is

not really used in the genetic algorithm. Several methodologies such as particle swarm can be used to solve the phase balancing problem with group codification. Finally, the model can be improved by including some stochastic effects on the current grids such as wind and solar resources. A suitable codification is required for these stochastic effects in order to maintain the group structure of the model.

# References

1. Zhu, J., Chow, M.-Y., Zhang, F.: Phase balancing using mixed-integer programming [distribution feeders]. IEEE Trans. Power Syst. **13**(4), 1487–1492 (1998)
2. Weckx, S., Driesen, J.: Load balancing with EV chargers and PV inverters in unbalanced distribution grids. IEEE Trans. Sustain. Energy **6**(2), 635–643 (2015)
3. Terorde, M., Wattar, H., Schulz, D.: Phase balancing for aircraft electrical distribution systems. IEEE Trans. Aerosp. Electron. Syst. **51**(3), 1781–1792 (2015)
4. Soltani, S., Rashidinejad, M., Abdollahi, A.: Stochastic multiobjective distribution systems phase balancing considering distributed energy resources. IEEE Syst. J. **12**, 2866–2877 (2018)
5. Mostafa, H.A., El-Shatshat, R., Salama, M.M.A.: Multi-objective optimization for the operation of an electric distribution system with a large number of single phase solar generators. IEEE Trans. Smart Grid **4**(2), 1038–1047 (2013)
6. Feng, X., Butler-Purry, K.L., Zourntos, T.: A multi-agent system framework for real-time electric load management in MVAC all-electric ship power systems. IEEE Trans. Power Syst. **30**(3), 1327–1336 (2015)
7. Schweickardt, G., Alvarez, J.M.G., Casanova, C.: Metaheuristics approaches to solve combinatorial optimization problems in distribution power systems. An application to phase balancing in low voltage three-phase networks. Electr. Power Energy Syst. **76**, 1–10 (2016)
8. Hungerford, T.W.: Algebra. Berlin, Springer (2000)
9. Clark, A.: Elements of Abstract Algebra. New York, Dover (1971)
10. Armstrong, M.: Groups and Symmetry. Berlin, Springer (1988)
11. Kurzweil, H., Stellmacher, B.: The Theory of Finite Groups: An Introduction. Berlin, Springer (2004)
12. Pinter, C.C.: A Book of Abstract Algebra. New York, Dover (1990)
13. Kersting, W.H.: Radial distribution test feeders. IEEE Trans. Power Syst. **6**(3), 975–985 (1991)

# Deterministic and Probabilistic Models for Energy Management in Distribution Systems

**Milad Kabirifar, Niloofar Pourghaderi, Ali Rajaei, Moein Moeini-Aghtaie, and Amir Safdarian**

**Abstract** Distribution network conventionally have been designed and operated as some passive and radial networks. However, the presence of distributed energy resources (DERs) has changed these networks' vision into some active ones. In this regard, new operational studies in the distribution level such as energy management problem has brought into existence. In this regard, this chapter mainly investigates the problem of energy management in distribution systems penetrated by DERs. To reach this goal, different classes of energy management problem, i.e., deterministic and stochastic models are carefully put under investigation. Extracting the mathematical model of these algorithms, it has been discussed that which algorithms should be applied to effectively solve the associated optimization problem. At the end, two examples associated with stochastic modeling of energy management problem, implemented on a sample case study, are provided to show how this problem can be applied in active distribution networks.

**Nomenclature**
**Indices**

| | |
|---|---|
| $b$, $w$ | Network nodes |
| $e$ | Storage units |
| $i$ | Distributed generation (DG) units |
| $l$ | Loads |
| $s$ | Scenarios |

M. Kabirifar · N. Pourghaderi · A. Rajaei
Sharif University of Technology, Tehran, Iran
e-mail: milad.kabirifar@ee.sharif.edu; pourghaderi_n@ee.sharif.edu; rajaei_ali@ee.sharif.edu

M. Moeini-Aghtaie (✉)
Faculty of Energy Engineering Department, Sharif University of Technology, Tehran, Iran
e-mail: moeini@sharif.edu

A. Safdarian
Faculty of Electrical Engineering Department, Sharif University of Technology, Tehran, Iran
e-mail: safdarian@sharif.edu

343

| $sp$ | Upstream suppliers |
|------|---------------------|
| $t$ | Time steps |
| $v$ | Electric vehicles |
| $\omega$ | Wind turbines |
| $p$ | Photovoltaic(PV) units |

**Parameters**

| | |
|------|---------------------|
| $C_{DG}^{U}$ | DG units' start up/shut down cost |
| $C_{GCP}$ | DG units' curtailment cost |
| $C_{LoadDR}$ | Cost of load reduction |
| $C_{NSD}$ | Cost of nonsupplied demand |
| $C_{Supplier}$ | Cost of external suppliers |
| $E_{BatCap}$ | ESSs/EVs batteries capacity |
| $E_{Min\text{Charge}}$ | Minimum stored energy in ESSs/EVs |
| $MP$ | Electricity price of market |
| $UP$ | Utility price |
| $N_i$ | Number of DG units |
| $N_e$ | Number of storage units |
| $N_l$ | Number of loads |
| $NL$ | Number of feeders |
| $N_s$ | Number of upstream grids |
| $N_v$ | Number of EVs |
| $P_{ChargeLimit}$ | ESSs/EVs' maximum rate of charge |
| $P_{DGScenario}$ | Non-dispatchable DG's forecasted generation |
| $P_{DGMinLimit}$ | Dispatchable DG's minimum active power |
| $P_{DGMaxLimit}$ | Dispatchable DG's maximum active power |
| $P_{DischargeLimit}$ | ESSs/EVs' maximum discharge rate |
| $P_{LoadDRMaxLimit}$ | Loads' maximum power reduction |
| $P_{MarketOfferMax}$ | Maximum allowed offer |
| $P_{MarketOfferMin}$ | Minimum allowed offer |
| $P_{MarketBuyMax}$ | Maximum allowed bid |
| $P_{MarketBuyMin}$ | Minimum allowed bid |
| $P_{SMinLimit}$ | Suppliers' minimum active power |
| $P_{SMaxLimit}$ | Suppliers' maximum active power |
| $T$ | Number of time periods |
| $Z$ | Number of scenarios |
| $\lambda^{m-1}$ | Lagrangian from slave in $m-1$ iteration |
| $\Delta t$ | Duration of time $t$ |
| $\pi$ | Scenarios' probability |
| $\eta_c$ | ESSs/EVs' charging efficiency |
| $\eta_d$ | ESSs/EVs' discharging efficiency |
| $\alpha, \beta, \delta$ | DG units cost functions' coefficients |

**Variables**

| | |
|------|---------------------|
| $C_{DG}$ | DG units' generation cost |
| $C_{\text{Discharge}}$ | ESSs/EVs' discharging cost |

| $E_{Stored}$ | Energy stored in ESS/EVs |
|---|---|
| $P_{Buy}$ | Power bid |
| $p_{Charge}$ | ESSs/EVs' charging power |
| $p_{Discharge}$ | ESSs/EVs' discharging power |
| $p_{DG}$ | Dispatchable DGs' power |
| $p_{LoadDR}$ | Loads' power reduction |
| $p_{GCP}$ | DGs' generation curtailment power |
| $p_{NSD}$ | Non-served demands' power |
| $P_{Sell}$ | Offer power |
| $p_{Supplier}$ | Upstream grid power |
| $P_{Utility}$ | Active power transacted with utility grid |
| $P_{Wind}$ | Active power generated by wind turbines |
| $P_{PV}$ | Active power generated by PV units |
| $C_{Utility}$ | Cost of power transacted with utility grid |
| $x_{DG}$ | State of DG units |
| $x_{ESS/EV}$ | Discharge state of ESSs/EVs |
| $x_{Market}$ | Choice of markets |
| $x_{Supplier}$ | Choosing suppliers |
| $y_{ESS/EV}$ | Charge state of ESSs/EVs |

**Sets**

| $\Omega_{DG}^d$ | Dispatchable DG units |
|---|---|
| $\Omega_{DG}^{nd}$ | Non-dispatchable DG units |
| $\Omega_{DG}^b$ | DG units in bus $b$ |
| $\Omega_E^b$ | Storage units in bus $b$ |
| $\Omega_L^b$ | Loads in bus $b$ |
| $\Omega_{SP}^b$ | Upstream suppliers in bus $b$ |
| $\Omega_V^b$ | EVs in bus $b$ |

# 1  Introduction

Distribution systems are going under vast changes in structure, players and customers. Conventional distribution networks are designed as passive systems in which the energy is delivered to customer only through upstream networks. However presence of DERs will change the future vision of these networks into active ones. In these systems, there are new ways to supply the loads via different technologies of DGs and also utilizing demand response (DR) programs.

Due to growth of the new energy resources in distribution systems, the operational characteristics of these systems have been changed. Power flow reversals toward upstream networks, fluctuations in loading of distribution feeders and also variations in voltage of different nodes are some operational constraints which active power distribution systems will face in near future. These call for new operational

mechanisms and energy management strategies to effectively operate these new systems. This chapter is mainly devoted to investigate different energy management algorithms in distribution systems.

To better understand the problem of energy management in distribution systems, the modeling algorithms for this problem are categorized into deterministic and stochastic models. The modeling procedure of different elements including electricity load, different technologies of DGs and charging/discharging profiles of EVs are explained. Then, mathematical models of energy management problem for both of deterministic and stochastic classes are extracted. Discussing the features of these optimization problems, different algorithms for solving these optimization problems are addressed. Finally, the main steps for running an energy management problem are explained by providing an example that implements this problem on a case study. In addition, the associated results of example are discussed.

In the remained parts, Sect. 2 covers the problem of deterministic energy management in distribution systems. By explaining the concept of this problem, main steps for running this study is explained. Section 3 is mainly devoted to stochastic modeling procedure of energy management problem. In this regard, modeling procedure of renewable-based DGs along with new demands such as EVs are discussed. After addressing main algorithms for dealing with different uncertainties in operational studies, different stochastic algorithms for solving the associated optimization problems are covered. Finally, the implementation procedure of two examples is in detail addressed in Sect. 4.

## 2 Energy Management Deterministic Modeling

### 2.1 Problem Definition

The leading goal of energy management in distribution system is to find the optimal way to utilize various DERs in the system to efficiently supply the electricity demand of customers taking into account operational constraints of these resources, the underlying network, and customers' preferences.

In the literature, various deterministic approaches have been investigated to solve the energy management problem in distribution system. Reviewing these methods, the deterministic energy management problem can be grouped into three main layers as depicted in Fig. 1. The input is the first layer where system's characteristics, customer's preferences, renewable energy sources (RESs) output profile, and network and DER's operational constraints are specified. The second layer comprises mathematical modeling of the problem and selecting a suitable solution algorithm to solve the optimization problem. Finally, in the third layer, decision variables including output profile of DGs, usage profile of customers, charge/discharge rate of batteries, along with operational state of the system and the objective function(s) value(s) is reported.
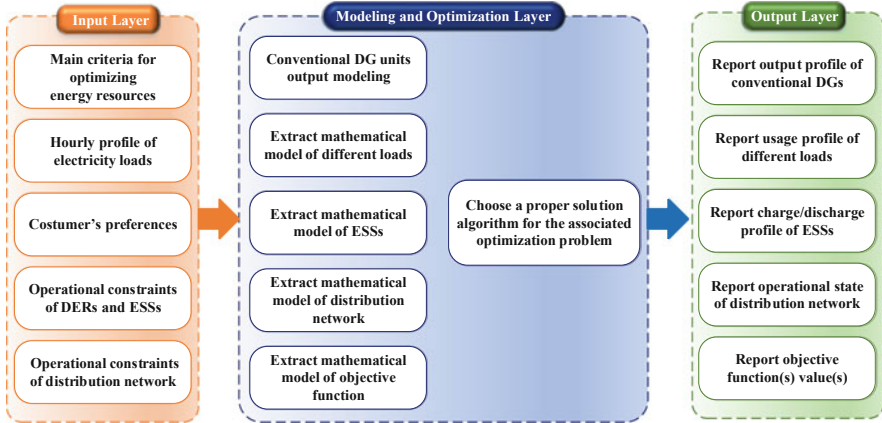
**Fig. 1** Steps to deterministic energy management

In the following, common energy resources in distribution system are discussed and modeled. Moreover in Sect. 2.4, mathematical model of energy management problem in distribution system with a deterministic point of view is presented.

## 2.2 Modeling of Energy Resources in Distribution Networks

### 2.2.1 Conventional DGs Modeling

Conventional DG (CDG) units such as diesel generators and gas turbines are counted as dispatchable sources in the grid and their active/reactive output powers denoted as $P_{i,t}^G/Q_{i,t}^G$, respectively, are variables determined by the system operator. The both active and reactive generated powers of CDGs must be between minimum and maximum allowed amounts as described by Eq. (1). $U_{i,t}^G$ represents the ON/OFF status of $i^{th}$ CDG.

$$U_{i,t}^G \underline{P_{i,t}^G} \leq P_{i,t}^G \leq U_{i,t}^G \overline{P_{i,t}^G} \tag{1}$$

$$U_{i,t}^G \underline{Q_{i,t}^G} \leq Q_{i,t}^G \leq U_{i,t}^G \overline{Q_{i,t}^G} \tag{2}$$

The fuel costs of CDGs are their major cost. This cost is mainly modeled by a quadratic function according to Eq. (3).

$$C_{i,t}^G \left( P_{i,t}^G \right) = a_i^G \left( P_{i,t}^G \right)^2 + b_i^G P_{i,t}^G + c_i^G \tag{3}$$

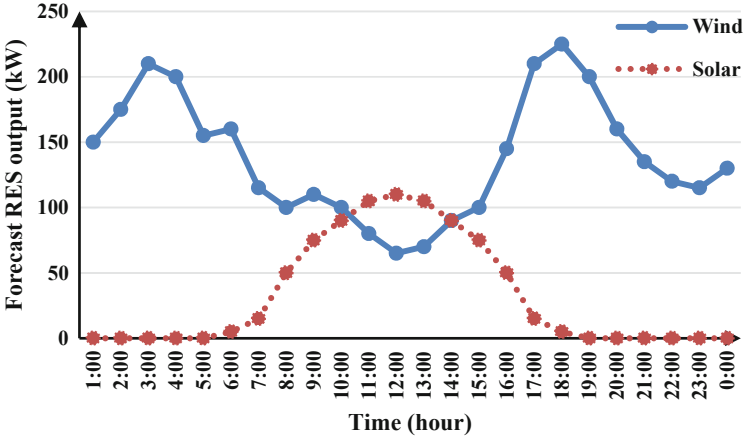Where, $a_i^G$, $b_i^G$, and $c_i^G$ are constants.

**Fig. 2** Output power for wind and solar generation

### 2.2.2 Model of Renewable Energy Resources

Electricity power generated by RESs is usually a function of meteorological data with high uncertainty: irradiation, temperature, wind speed and so forth. For instance, power produced by a photovoltaic (PV) panel depends on the sun path, temperature and cloud coverage, or a wind turbine's generated power depends on speed of wind. These parameters and their probability distributions have to be estimated everyday based on historical data. However, in case of deterministic modeling, it is assumed that the forecasted data has no error. Therefore, the electricity power produced by renewable sources in deterministic modeling is often modeled by a given output profile [1]. An example for solar and wind power generation in a summer day and in a distribution network located in Iran is depicted in Fig. 2 [2]. A more comprehensive modeling of RESs respecting their intermittent nature is presented in Sects. 3.2.1 and 3.2.2. Here, power produced by a PV panel and a wind turbine is denoted as $P_{PV}$ and $P_W$, respectively.

Moreover, power electronic inverters are utilized to connect RESs to the grid in order to convert the DC electrical output into an AC output. These inverters are usually, also capable of generating or consuming reactive power by themselves. Thereby, if this option is available, the reactive power produced or consumed by these inverters can also be considered as a decision variable for system operator to maintain voltage regulation [3]. As an example, the reactive constraint of a PV inverter can be modeled as follows:

$$P_{PV}^2 + Q_{PV}^2 \leq S_{PV}^{max} \tag{4}$$

where, $S_{PV}^{max}$ is the maximum capacity of the PV inverter.

### 2.2.3 Electricity Loads Modeling

As mentioned before, the leading goal of an energy management system is to supply the electricity demands of its customers efficiently and securely. Nowadays, with advent of DR programs, demand side is counted as an important resource in managing the energy of modern distribution systems. Therefore, a detailed modeling of electrical loads in distribution system is crucially important.

Some loads such as commercial establishments and office buildings have limited flexibility and it is not possible to be scheduled in acceptable ranges. These groups of loads can be modeled as time-varying non-deferrable loads. However, there are flexible loads in different sectors that can participate in DR programs. Industrial loads can participate in direct load control programs. Equation (5) formulates the direct load control. $\overline{P_{l,t}^{DLC}}$ is the maximum reducible amount of load $l$ at time interval $t$.

$$P_{l,t}^{DLC} \leq \overline{P_{l,t}^{DLC}} \tag{5}$$

Residential and commercial sectors consume considerable amount of power in distribution system and therefore they are counted as effective participants of DR programs. These sectors' loads are classified into three types: Type 1 includes appliances which consume fixed amount of power when they are ON, otherwise, they don't consume power. These loads are so-called on/off loads. Controllable loads, such as heater and air conditioner are counted as Type 2 appliances; the consumed power of these loads is between their minimum and maximum limits [4]. Type 3 includes deferrable loads like dishwasher and washing machine. The model of Type 1 and Type 2 loads are presented in the following:

$$\underline{P_{a,t}^{DR}} \leq P_{a,t}^{DR} \leq \overline{P_{a,t}^{DR}} \tag{6}$$

The minimum and maximum powers in the Eq. (6) are the same for Type 1 of loads whereas these two parameters are different for Type 2 appliances. The model of Type 3 appliances is presented in the following equations [5]:

$$P_{a,t} = \sum_{i=1}^{k_a} z_{a,t-k_a+i} \cdot p_{a,k_a-i+1} \tag{7}$$

$$Z_{a,t} = 0, \ \forall t \in T - [\alpha_a, \beta_a - k] \tag{8}$$

$$\sum_{t \in T} z_{a,t} = 1 \tag{9}$$

The set of expressions (7) ensures that the energy required for a complete operation cycle of all appliances is provided, in which $z_{a,t}$ is the binary variable

denoting startup status of appliance *a* at period *t*. The total required energy of each appliance is equal to the surface under its energy consumption profile (ECP) and nominal power of appliance *a* at each time step *t* is obtained from the related ECP. This power is denoted by $p_{a,t}$. Moreover, it should be mentioned that $k_a$ is the number of required time steps for complete operation of appliance *a*. Customers who participate in the DR programs specify allowed start and ending times of their responsive appliances. Responsive appliances must operate just during this time interval, i.e. during interval $\left[\alpha_a^n, \beta_a^n\right]$, which is guaranteed by Eq. (8). Finally, to ensure the continuous operation of each appliance, set of constraints (9) are defined. $z_{a,t}$ is 1 if the appliance is on at the associated time interval. It should be noted that electric vehicles (EVs) can be counted as another responsive load in distribution system and its control model is fully described in Sect. 2.3. It is worth mentioning that the mentioned approaches typically fall in incentive based DR programs. On the other hand, in price based DR programs, load behavior is analyzed with respect to electricity price. The model of load behavior in price based DR programs can be expressed by elasticity factors according to:

$$P_{l,t}^{DR} = P_{l,t} + \xi \left(\pi_t^{'} - \pi_t\right) \tag{10}$$

In Eq. (10), $\xi$ represents price elastic coefficient, and $\pi_t^{'}$, $\pi_t$ are real time and reference electricity prices, respectively.

In addition to active power, reactive power management is also of great importance in an energy management system, particularly when operational constraints such as voltage regulation are considered. Reactive power consumption of different kinds of loads can be modeled using a given power factor for each load. In other words, reactive power consumption level of each load can be assumed to be proportional to its active power consumption level. It is worth noting that loads' power factor can vary; however considering a given fixed power factor for each load simplifies the modeling procedure, especially in the cases in which linearization is conducted.

## *2.3 Modeling of Dispersed Energy Storages*

Energy storage system (ESS) is another solution to accommodate uncertainties and variabilities caused by high integration of renewable energies in the system. By integrating ESS into the system, redundant energy produced by renewable energies could be stored during low demands and in the peak periods it is injected to network. Moreover, ESS can also provide other benefits such as alleviating the RESs uncertainty, frequency regulation and improving the reliability of the system [6].

Operation model of an ESS is formulated in the following [7]:

$$SoC_{ESS,t+1} = SoC_{ESS,t} + \frac{1}{E_{ESS}} \left( \eta^c_{ESS} P^c_{ESS,t} - P^d_{ESS,t}/\eta_d \right) \tag{11}$$

$$0 \leq P^c_{ESS,t} \leq \overline{P^c_{ESS,t}} \tag{12}$$

$$0 \leq P^d_{ESS,t} \leq \overline{P^d_{ESS,t}} \tag{13}$$

$$\underline{SoC_{ESS}} \leq SoC_{ESS,t} \leq \overline{SoC_{ESS}} \tag{14}$$

where,

$SoC_{ESS,t}$ : State of the charge of ESS at $t$ ($0 \leq SOC_{ESS,t} \leq 1$).
$E_{ESS}$ : Energy capacity of ESS.
$P^c_{ESS,t} \left( P^d_{ESS,t} \right)$: Charge (Discharge) rates of ESS at $t$.
$\eta^c_{ESS} \left( \eta^d_{ESS} \right)$: ESS efficiency of charging (discharging).
$\overline{SOC_{ESS}} \left( \underline{SOC_{ESS}} \right)$: Maximum (Minimum) allowable $SoC$ of ESS.
$\overline{P^c_{ESS,t}} \left( \overline{P^d_{ESS,t}} \right)$: Maximum allowable charging (discharging) of ESS.

Equation (11) represent the state of charge (SoC) balance between time intervals, while charging rate, discharging rate and SoC limits are enforced in Eqs. (12)–(14), respectively.

In addition to ESSs, due to environmental reasons, electric vehicle (EV) penetration level in distribution system have increased dramatically in recent years. Thus, it is required to propose an energy management model that can satisfy vehicle owners' preferences and requirements. EVs and particularly those with vehicle-to-grid (V2G) system are in many ways similar to ESSs. EVs' owners can utilize their vehicle as an efficient storage device in the periods that the vehicles are parked in the parking lot [7].

Technical constraint of an EV with V2G can be formulated as bellow:

$$SoC_{EV,t} = SoC^{Ini}_{EV} + \frac{1}{E_{EV,t}} \left( \eta^c_{EV} P^c_{EV,t} - \eta^d_{EV} P^d_{EV,t} \right) \qquad t = t_s \tag{15}$$

$$SoC_{EV,t} = SoC_{b,t-1} + \frac{1}{E_{EV}} \left( \eta^c_{EV} P^c_{EV,t} - \eta^d_{EV} P^d_{EV,t} \right) \qquad t_s < t \leq t_f \tag{16}$$

$$SoC_{EV,t} = SoC^{Rq}_{EV} \qquad t = t_f \tag{17}$$

$$0 \leq P^c_{EV,t} \leq \overline{P^c_{EV}} \tag{18}$$

$$0 \leq P_{EV,t}^d \leq \overline{P_{EV}^d} \tag{19}$$

$$\underline{SoC_{EV}} \leq SoC_{EV,t} \leq \overline{SoC_{EV}} \tag{20}$$

where,

$SoC_{EV,t}$ : State of the charge of EV at $t$ ($0 \leq SoC_{EV,t} \leq 1$).
$t_s$ : Arrival (Plug-in) time of EV.
$t_f$ : Departure time of EV.
$E_{EV}$ : Energy capacity of EV.
$SoC_{EV}^{Ini}$: Initial $SoC$ of EV at arrival (plug-in) time.
$SoC_{EV}^{Rq}$: Required $SoC$ of EV at departure time.
$E_{EV}$ : Energy capacity of EV.
$P_{EV,t}^c \left( P_{EV,t}^d \right)$: Charge (Discharge) rate of EV at time t.
$\eta_{EV}^c \left( \eta_{EV}^d \right)$: Charging (Discharging) efficiency of EV.
$\overline{SoC_{EV}} \left( \underline{SoC_{EV}} \right)$: Maximum (Minimum) allowable $SoC$ of EV.
$\overline{P_{EV}^c} \left( \overline{P_{EV}^d} \right)$: Maximum allowable charging (discharging) rate of EV.

Equation (17) represents vehicle owner's preference that the battery has to be charged to a certain level before the specified departure time. Battery's technical constraints are expressed in Eqs. (18)–(20). It is important to mention that if the EV is not available for V2G application, $\overline{P_{EV}^d}$ is simply considered zero.

## 2.4 Mathematical Model of Energy Management Optimization Problem

### 2.4.1 Objective Function

Various objectives for an energy management system can be considered. The most common objective criteria is probably operational cost of the system. In this case, fuel cost of CDGs and cost of energy purchased from transmission system are generally used to calculate operational cost of the grid. The objective function can be presented by:

$$\text{Min} \quad \pi_t P_t^{Tr} + \sum_{DG} C\left(P_G\right) \tag{21}$$

where, $\pi_t$ and $P_t^{Tr}$ is the market energy price and power purchased from transmission system, respectively. It is noteworthy to mention that distribution system can inject its additional power into upstream network. In this condition $P_t^{Tr}$ is negative.

Another common objective for energy management is to minimize power loss of the network as in [8]. Power loss in distribution network is modeled as a function of active and reactive power (or simply squared current magnitude) flowing in branches.

Moreover, short term peaks and variations in the net load of the system (i.e., the actual system demand minus the RESs output) can cause serious challenges in balancing supply and demand in real time and require fast responding power generators which increases system's cost. Therefore, in [9, 10], an energy management system for peak load shaving and ramp reduction has been presented, respectively. Net load of the system ($NL_t$) and ramp in net load ($R_t$) can be calculated according to Eq. (22).

$$NL_t = D_t - P_{Ren,t} \tag{22}$$

$$R_t = NL_t - NL_{t-1} \tag{23}$$

Where, $D_t$, and $P_{Ren,t}$ represent aggregated load demand and renewable-based generation in the system, respectively. A linear or quadratic cost function is often utilized to model the imposed cost by the peak/ramp of/in the net load to the system.

Further, maximizing social welfare of customers is also a reasonable objective for an energy management system. A concave utility function can be utilized to model the social welfare of customers. The mentioned utility function is usually a quadratic function of power consumption level of the associated customer [11]. Such a utility function can also be used to model discomfort cost of customers participating in DR programs.

Additionally, multi-criteria objectives are formed based on a linear combination of weighted individual objectives such as the work done in [12]. In this case, a proper weight selection is an important factor affecting the final result.

### 2.4.2 DER's Constraints

Operational constraints of DERs available in the system must be considered in the optimization problem. So, Eqs. (1)–(2) for CDGs, (4) for RESs, (5)–(10) for loads, (11)–(14) for ESSs, and (15)–(20) for EVs, if available, are added to optimization problem.

### 2.4.3 Network's Constraints

As mentioned earlier, one of the leading goals of energy management system is the secure and reliable operation of the network. To achieve this goal, technical issues of distribution network must be addressed. The most common way to do so is to solve the classic power flow (PF) to attain the operational state of the system.

Depending on inherent characteristics of the network such as size of the network or network's power loss, different methods with different degree of accuracy have been utilized to embed the power flow equations in distribution network. In many works such as [13], only power supply-demand balance is considered, i.e., it is assumed that all generation and loads are connected to one bus and the underlying distribution network has been ignored. In [14], a linear approximation of AC-PF has been developed to calculate power flows and voltage magnitudes. Since the AC-PF problem is nonlinear, in [15, 16], second order cone programming (SOCP) and semidefinite programming (SDP) relaxations, respectively, are used to convexify the AC-PF problem for a single-phase distribution network. Moreover, in [17], the AC-PF with SDP relaxation for an unbalanced three-phase network has been formulated. As an example, branch flow model with SOCP relaxation for a radial single-phase network which has been widely used in the literature is presented in this section [18].

A radial distribution network is mathematically modeled by a tree graph $G := (N, \varepsilon)$, where $N := \{0, 1, \ldots, N\}$ represents the set of nodes and $\varepsilon$ represents the set of lines. Node 0 is the substation connected to transmission network, and the remaining $N$ nodes represent load points in medium voltage level. Each node except the substations has just one parent node $A_n$ and a set of child nodes of $C_n$. The line connecting node $n$ to its parent node $A_n$ is named as line $n$ and have $\varepsilon := \{1, \ldots, N\}$. The branch flow model [18] for a given radial distribution network, is as follow:

$$v_{Ai} = v_i - 2(r_i P_i + x_i Q_i) + l_i \left( r_i^2 + x_i^2 \right) \qquad \forall i \in \varepsilon \qquad (24)$$

$$\sum_{j \in C_i} \left( P_j - l_j r_j \right) + p_i = P_i \qquad \forall i \in \mathcal{N} \qquad (25)$$

$$\sum_{j \in C_i} \left( Q_j - l_j x_j \right) + q_i = Q_i \qquad \forall i \in \mathcal{N} \qquad (26)$$

$$P_i^2 + Q_i^2 = v_i l_i \qquad \forall i \in \mathcal{N} \qquad (27)$$

$$\underline{v_i} \leq v_i \leq \overline{v_i} \qquad \forall i \in \mathcal{N} \qquad (28)$$

$$\underline{l_i} \leq l_i \leq \overline{l_i} \qquad \forall i \in \varepsilon \qquad (29)$$

Where,

$v_n$ : Square of node $n$ voltage magnitude
$l_i$ : Squared line current magnitude of line $n$
$P_i$ ($Q_i$): Active (Reactive) power flow on line $n$
$p_i$ ($q_i$): Active (Reactive) power injection at node $n$
$r_i$ ($x_i$): Resistance (Reactance) of line $n$
$\overline{v_i}$ ($\underline{v_i}$): Upper (Lower) bounds of squared voltage magnitude of node $n$
$\overline{l_i}$ ($\underline{l_i}$): Upper (Lower) bound of squared line current magnitude of line $n$.

Due to quadratic equality constraint (28), the power flow problem (Eqs. 25–30) is non-convex. Second order cone programming (SOCP) can be used to convexify this problem as below:

$$P_i^2 + Q_i^2 \leq v_i l_i \qquad i \in \mathcal{N} \tag{30}$$

It is shown in [19] that under some mild conditions for networks with tree topology, SOCP relaxation is exact.

### 2.4.4 Solution Method

The solution method of energy management problem is firmly dependent on the problem's mathematical model. Therefore, it is crucial to recognize the structure of the optimization problem of energy management in order to efficiently solve it. First, the objective function must be defined. As mentioned earlier, for energy management problem there can be different objectives. Second, technical constraints of components considered in the study must be added to the optimization. Finally, a PF model need to be utilized to address technical issues of the underlying network.

Now, according to the mathematical form of problem, an appropriate optimization method needs to be applied. Problems with continuous linear objective and constrains are pretty straightforward and various fast linear programming (LP) approaches can be utilized to solve them. In continuous quadratic problems, quadratic constrained programing (QCP) approaches are implemented to obtain optimal solution. If optimization problem has nonlinear constraints, nonlinear programming (NLP) methods should be used. However, since NLP approaches do not guarantee global optimal solution and suffer poor convergence rates, convexification and/or linearization methods might be necessary to convert the nonlinear problem into a quadratic/linear optimization.

Optimization problems, including integer variables, form mixed-integer problems. Integer variables are utilized to involve on/off status of components and/or transformer tap settings in the optimization problem. The problems can be grouped into mixed-integer linear programing (MILP), mixed-integer quadratic constrained programming (MIQCP) or mixed-integer nonlinear programming (MINLP) in the case that the optimization objective and constraints are linear, quadratic or nonlinear, respectively.

Additionally, when variables in different time slots are coupled together (e.g. Eq. (11) in ESS model), instead of optimizing for a single snapshot, multiple time periods should be optimized simultaneously, resulting in a multi-period (MP) optimization problem.

Apart from many centralized methods to solve energy management optimization, there are also distributed algorithms which do not need a central coordinator [1]. In centralized algorithms, a coordinator should collect associated information of DERs to form the inputs of optimization problem. However, some customers may be reluctant to inform data due to privacy concerns. In this case, distributed approaches

can be utilized to solve the problem. Distributed algorithms are more scalable and privacy preserving, nonetheless, they use iterative methods which need more time for convergence.
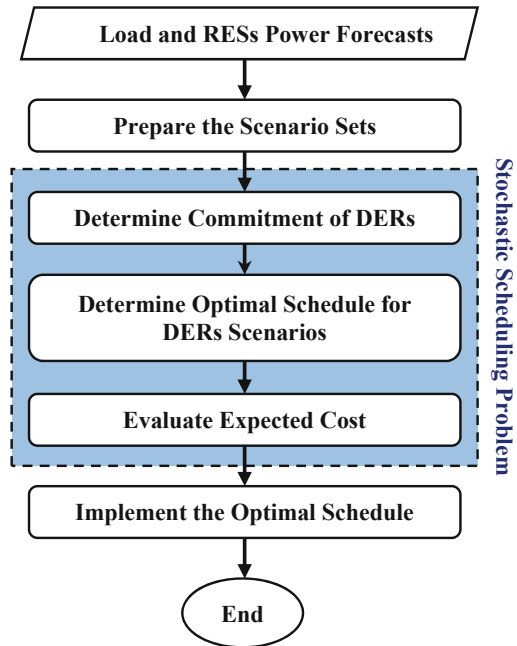
## 3 Energy Management Stochastic Modeling

### 3.1 Problem Description

During the last years, RESs penetration in power networks has considerably increased due to environmental concerns. However, due to the high variability and intermittency of the primary sources (i.e., solar irradiation and wind) the high penetration level of RESs generation could pose several problems to the operation aspects of network [20]. Meanwhile the load demand also has great uncertainty which will affect the reliability and operational stability of the system. As these uncertainties significantly affect the operation of the power system, the optimization results based on deterministic models tend to be less reliable and therefore, the uncertainties must be addressed in the problem [21]. These uncertainties have represented as worst case scenarios in the scheduling studies. Although the process of data gathering and mathematical optimization are simplified in this approach, a realistic result has not been provided which results in a conservative and costly schedule of network. To address this issue, stochastic optimization is investigated in this chapter to establish power system effective energy management strategy.

Figure 3 presents the typical steps for stochastic energy management of a system comprised of DERs. DERs can be dispatchable distributed generation (DG) units, RESs, flexible loads, and energy storage systems (ESSs) [22]. According to the figure, in the first step required data are gathered. These data usually include the forecasts of load and RESs' generation and underlying network characteristics. After that, the set of scenarios that appropriately represent the uncertainties of DERs over the operating intervals should be created by scenario generation tools. Possible realization of uncertain parameters and the corresponding occurrence probabilities are included in a scenario set.

A stochastic optimization problem is addressed in the next step to determine the optimal schedule of DERs for all operating intervals. The decision variables can be grouped as two types. The first group of optimization variables represents the commitment of DERs over the total time horizon, and the second types include schedule of DERs such as generated power of dispatchable DGs, charge/discharge patterns of storage units and load response of flexible loads for each scenario. It should be noted that commitment plan is usually assumed to be unchanged for defined scenarios. On the other hand, for each possible scenario, the second category's variables should be specified. It is worth mentioning that the schedule of DERs should be optimized through all realized scenarios. As the result, the optimal amount of both variable types should be determined simultaneously and

**Fig. 3** Steps of stochastic
energy management

```
┌────────────────────────────────────┐
│   Load and RESs Power Forecasts     /
└────────────────────────────────────┘
                 │
                 ▼
┌────────────────────────────────────┐
│      Prepare the Scenario Sets       │
└────────────────────────────────────┘
                 │
                 ▼
┌────────────────────────────────────┐
│    Determine Commitment of DERs      │
└────────────────────────────────────┘
                 │
                 ▼
┌────────────────────────────────────┐
│    Determine Optimal Schedule for    │
│           DERs Scenarios             │
└────────────────────────────────────┘
                 │
                 ▼
┌────────────────────────────────────┐
│        Evaluate Expected Cost        │
└────────────────────────────────────┘
                 │
                 ▼
┌────────────────────────────────────┐
│    Implement the Optimal Schedule    │
└────────────────────────────────────┘
                 │
                 ▼
              ( End )
```

Stochastic Scheduling Problem

in an integrated manner. The expected cost of each optimal plan through realized scenarios would be calculated as the amounts of all variables have been set. The DERs' operation costs are the main part of system operation costs. Hence, minimization of the total expected costs can be defined as the objective of the scheduling problem.

Once the above mentioned stochastic programming problem is solved, the optimal plan is attained with respect to the materialized scenarios of DERs.

## 3.2 Modeling of Renewable Energy Resources in Distribution Networks

Various DERs, such as CDGs, RESs, ESSs, and demand response (DR) resources might feed an active distribution network. To consider various models of different resources, DERs are modeled based on the associated uncertainty and dispatchability. DERs with uncertainty, such as wind farms and PV units, have intermittent power production [23]. Dispatchable DERs like CDGs are utilized to balance demand-supply. It should be noted that some dispatchable DERs can also be uncertain, e.g., DR resources are controllable however the available demand for control would be uncertain.
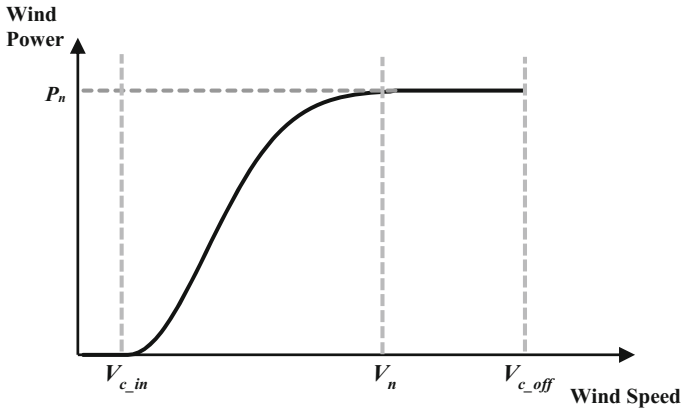
**Fig. 4** Generated power of WT with respect to wind speed

RESs, mainly solar and wind have been increasingly utilized around the network due to various advantages. However their stochastic nature cause challenges to both system operation and planning; therefore, in order to effectively utilize these resource the associated uncertainty should be accurately modeled. The uncertainty modeling of the aforementioned resources is addressed in Sect. 3.3. Three main resources including wind, solar and flexible loads are investigated in this section. The model describing each resource is described in the following.

### 3.2.1 Wind Resources Modeling

Wind turbine (WT) is used to convert the kinetic energy of an air mass in motion to electrical energy. The energy is generated if the wind speed exceeds a minimum amount, called cut-in value. On the other hand, the rotor should be stopped in the case that wind speed exceeds a cut-off value, in order to avoid turbine damage. The produced power $P_W$ is the function of wind speed between cut-in and cut-off speeds as depicted in Fig. 4. $V_n$ is the nominal turbine speed, over which the maximum nominal power is attained by utilizing pitch control system. In addition, cut-in and cut-off speeds are respectively represented by $V_{c\_in}$ and $V_{c\_off}$ [24]. The relationship between produced power of WT and wind speed is presented as follows:

$$P_W = \begin{cases} 0, & V < V_{c\_in} \text{ or } V > V_{c\_off} \\ P_m(V), & V_{c\_in} \leq V < V_n \\ P_n, & V_n \leq V < V_{c\_off} \end{cases} \tag{31}$$

where maximum achievable power of wind speed for the values lower than $V_n$ is denoted by $P_m(v)$, and $P_n$ denotes the nominal power. For the wind speed values

between cut-in and cut-off speeds, the generated power with respect to the wind speed can be expressed by a continuous function, denoted by $P_m(v)$. This continues function can be accurately approximated by fitting different mathematical functions like using a polynomial function as represented in Eq. (32) [24]. Considering the wind turbine characteristics, the wind farm's equivalent output that considers performance can be calculated by Eq. (33), in which $\eta_{WT}$ is the efficiency of wind turbine and $N$ represents the number of WTs located in the wind farm.

$$P_m(v) = P_n \times \left( \frac{V - V_{c\_in}}{V_n - V_{c\_in}} \right)^3 \tag{32}$$

$$P_{total} = N \times P_W \times \eta_{WT} \tag{33}$$

### 3.2.2 Solar Resources Modeling

PV power plant system is also an important source of output in active distribution network. The produced power of a PV power plant is dependent on the irradiance and the operating temperature at its mounting location. According to the location of PV power plant site, the annual solar radiation intensity can be obtained using available database. The total output of PV power plant can be calculated using:

$$P_{PV} = N \, \eta \, A_{PV} \, G_T \, \left( 1 + k \, \left( T_C - T_{avg} \right) \right) \tag{34}$$

where $N$ is the number of installed arrays, $\eta$ is the photoelectric conversion efficiency of PV array, $A_{PV}$ is the total array area, $G_T$ is the solar radiation incident on the panels, $T_C$ and $T_{avg}$ are the panels' operating temperature and mean temperature in daytime, respectively, and $k$ is the temperature coefficient [25]. Although the photoelectric conversion efficiency of PV is dropped gradually, its variation is ignorable during the PV life time and can be supposed to be constant.

### 3.2.3 Electricity Loads Modeling

The flexible loads can be utilized to address the fluctuations in day-ahead market prices, created by fluctuating renewable energies. The absolute forecasting error of renewable power production is expected to increase, even if relative forecasting errors decrease. As the result, the demand can be effectively utilized for reserve power. Activating DR programs in active distribution network add a new entity to the distribution system. The power flow between existing entities is depicted in Fig. 5. The remote energy management unit (REMU) schedules the flexible loads and other DERs to efficiently operate the distribution network. In this figure $D_t$ is the net generated power of DGs and $L_t$ is the net consumed power of flexible loads at each
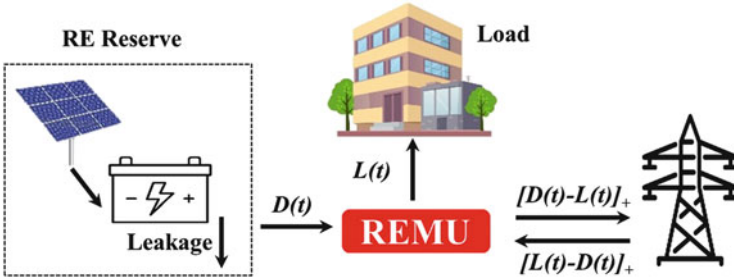
**Fig. 5** Power flows between DERs and transmission network

time step $t$. Based on the amount of generation and consumption, REMU is able to export/import electricity to/from upper level network.

A detailed model of electricity loads in distribution system is presented in Sect. 2.2.3.

## 3.3 Uncertainty Modeling

In contrast to the conventional power generators the produced power of PV and wind power plants are non-dispatchable due to intermittency and variability. Generated power of PV and wind power plants depend on the stochastic solar radiation and wind speed, respectively. The generated power of these renewable energy resources is exposed to significant uncertainties because of the stochastic nature of wind speed and sun irradiance. Therefore, the energy management of distribution networks with RESs becomes more challenging because of several types of uncertainties, such as energy demand, wind and solar generation, and electricity price. Dealing with these uncertainties in active distribution networks is crucial to solve possible issues and reach the optimal management.

There are several different methods for modeling uncertainty of DERs. In general, the methods can be categorized in to three groups. The first group is stochastic (probabilistic) approach. This approach is based on probability distribution functions (PDFs) derived from the statistical data of the variables with uncertainty. In this regard, a set of scenarios are generated by utilizing PDF and then a scenario reduction method is applied to realize a tradeoff between computational burden and the accuracy of the solution. To handle the random variables, analytical methods based on convolution form the second group. In this regard, cumulant-based methods are the methods used to reduce the computational burden associated with convolution [26]. Point estimate method (PEM) [27] and chance constrained programming [28] methods are computationally more efficient in which derivatives are applied. The third group includes interval [29], affine [30] and fuzzy arithmetic

[31] approaches. Interval arithmetic (IA) includes all possible values associated with the percentage uncertainties. In interval analysis technique for the output variables the feasible bounds are obtained by considering a probable range for uncertain parameters. In order to evaluate the noise terms, AA method considers sensitivities of uncertain parameters [32]. Fuzzy method assigns a membership function (MF) to parameters with uncertainty. The occurrence frequency of the random variables has not been considered by introduced approaches in the third group; hence these methods couldn't model the probabilistic nature of the renewable power injections. It should be noted that probabilistic approaches are among the most widely utilized approaches. These methods are classified in two groups, namely numerical and analytical. Monte Carlo Simulation (MCS) methods are categorized as numerical approaches. In addition, PDF approximation and linearization techniques are the basis of analytical methods. Section 3.4 provides more information around these approaches.

In summary, one of the strongest approaches is stochastic programming [33]. In this method, several scenarios represent parameters with uncertainty and their associated probabilities. The PEM, MCS, time series or scenario tree techniques can generate scenarios by utilizing the associated PDFs. The goal of stochastic programming is to find the problem's optimal solution by considering obtained scenarios.

### 3.3.1   Stochastic Uncertainty Modeling in DERs

Randomness in uncertain parameters including load and output generated power of WTs and PV units follow a certain distribution, such as uniform normal distribution, Weibull, Rayleigh, among others. For modeling the error of forecasted parameter, a term which would be negative or positive is added to the forecasted parameter as follows, in which $\overline{x}(t)$ is the forecasted value and $\tilde{x}(t)$ is the error term.

$$x(t) = \overline{x}(t) + \tilde{x}(t) \tag{35}$$

Three steps are handled to model the uncertainty:

1. **Forecasting:** The historical data records are utilized to realize the statistics regarding the volatile characteristic of solar and wind energy resources. In order to forecast uncertainty behavior of renewable resources statistical methods are applied and prediction information is assumed as typical probability distribution function. Based on the meteorological characteristics of energy source under study, in order to fit a function into the historical data various PDFs can be utilized. Errors between the forecasted and actual data of various PDFs represent the goodness of fit criteria. Goodness of fit criteria can be utilized to evaluate the efficiency of the methods and determine the mostly fitted distribution function for each set of data [34].

2. **Scenario generation:** In the stochastic approaches, by utilizing the PDFs of uncertain parameters a finite number of scenarios are generated to evaluate energy management problem. In order to generate adequate scenarios for describing parameters with uncertainty (e.g. solar irradiation, wind speed, load, and wholesale market prices), MCS technique is mostly used [22]. MCS utilize the associated PDFs of uncertain parameters for scenario generation. By combining the generated scenario sets of each uncertain parameter a scenario vector can be formed for optimizing energy management problem. Generated scenarios by MCS in each time slot form a time-series stochastic scenario. A scenario which is described by a time series (e.g. the generated power of a PV unit during a day) has a self-correlation during the time.

   In order to combine generated scenarios of different uncertain parameters and find the optimal management during time stages the scenario tree concept is utilized. In order to combine the discrete outcome of each stochastic input to form the larger set of scenarios, the scenario tree concept is utilized. The nodes of scenario show the states of the random variable at particular time points. On the other hand, branches represent various realizations of the variable, and a root denotes the beginning point where the first-stage decisions are made. The model of scenario tree which represents a scenario-based stochastic programming model is depicted in Fig. 6 [35].

3. **Scenario reduction:** Considering all combinations of the generated scenarios in the solving process imposes a considerable computational burden and makes the optimization intractable to solve many scenarios [36]. In order to trade-off between computation speed and model accuracy it is essential to reduce generated scenarios and choose the most generic scenarios that appropriately describe the behavior of parameters with uncertainty. There are various scenario reduction methods, such as fast forward and backward reductions which are
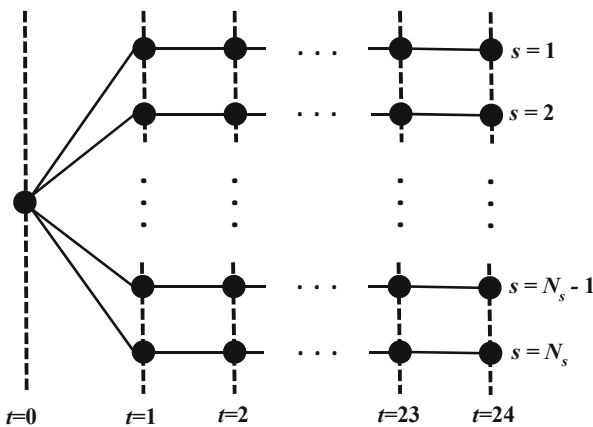


**Fig. 6** Scenario tree representation [35]

presented in [37]. The best scenario reduction technique can be chosen according to its performance accuracy and reduction time. In these techniques the low probability scenarios are excluded. In addition, scenarios which are similar from statistic metrics perspective are combined. The selected scenarios are similar to the primary distribution from a probability metrics perspective. By using scenario reduction techniques, the size of problem is significantly reduced because of the reduced number of equations and variables. Consequently, in this condition, the solution is efficiently obtained. Furthermore, the main features of the initial scenario set will not be lost. It should be noted that, introducing imprecision in the final solution can be the side effect of applying scenario generation techniques.

Various reduction algorithms have different performance in accuracy and computation speed aspects. These techniques are grouped to fast backward, fast backward/forward, and fast backward/backward methods. The methods can be selected based on the size of optimization problem required accuracy level [37]. For instance, the fast backward technique is used for problems with large scenario tress and it has the high computational speed but low accuracy. In addition, high accuracy but low speed of computation is provided by the forward method. Hence, this method is used for small size problems [37].

As described above, scenarios that are similar from statistic metrics perspective are combined. In order to combine the scenarios, clustering is an efficient tool that can be utilized. Two main clustering approaches are hierarchical clustering and partitional clustering. K-means algorithm is a general partitional algorithm used for clustering. In this algorithm, the clusters are constructed around the centers of predefined number of clusters. A various distance functions can be utilized to map the points to the different clusters [38].

(a)  Wind speed uncertainty modeling

Statistical tests have proved that the pattern of wind speed mainly closes to the Rayleigh or Weibull distributions [39]. Among these two distributions, Rayleigh distribution is mostly utilized to model stochastic nature of wind speed data [40].

It should be mentioned that the stochastic parameters can be correlated in time and space. In this regard, correlation of wind farms within an area is modeled spatially and this model would affect the uncertainties. However, a general assumption is that in the time horizon around 3 of 4 days, the weather systems are independent. In particular, wind farms that are located in far distances from each other are mostly subject to independent environmental conditions and hence their produced energies are independent.

(b)  Solar radiation uncertainty modeling

Historical data of sun irradiance mainly fit to Beta distribution. The associated PDF for solar irradiance $s$, is characterized as follows where $\alpha$, $\beta$, $\mu$, $\sigma$ are shape

parameter, scale parameter, mean value, and standard deviation respectively [41]:

$$F\,(s) = \begin{cases} \frac{\Gamma(\alpha+\beta)}{\Gamma(\alpha)\Gamma(\beta)}(s)^{\alpha-1}(1-s)^{\beta-1} \,, 0 \leq s \leq 1, \alpha \geq 0, \beta \geq 0 \\ 0, \qquad\qquad\qquad\qquad\qquad , O.W \end{cases} \tag{36}$$

$$\alpha = \frac{\mu\beta}{1-\mu} \tag{37}$$

$$\beta = (1-\mu)\left(\frac{\mu\,(1+\mu)}{\sigma^2} - 1\right) \tag{38}$$

Based on Eq. (35) in Sect. 3.2.2 the uncertainty of ambient temperature can be modeled by considering standard normal distribution as follow. It should be noted that *randn* in Eq. (46) is a random number that is subject to standard normal distribution.

$$P_{PV} = N\,\eta\,A_{PV}\,G_T\,\left(1 + k\,\left(\,T_C + \sigma.randn - T_{avg}\,\right)\right) \tag{39}$$

Other sources of uncertainty in distribution system include load, demand response and energy price that may exist in a distribution network [33]. The general approach for modeling the uncertainties in above mentioned parameters is to implement appropriate PDF based on statistical data. It is worthwhile noting that charge/discharge control of electric vehicles is counted as a demand response resource and its associated uncertainty is caused by the randomness in the driving pattern of the EV drivers. The EVs uncertainty can be modeled by normal PDF.

## 3.4 Stochastic Model of Energy Management Problem

Defining the optimal energy management in a distribution system while considering the sources of uncertainties by adopting stochastic optimization, in the following, stochastic model of energy management problem is at first described generally as its outline is depicted in Fig. 7 and then, investigated in detail and solution methods are described.

In order to efficiently utilize the DERs underlying the distribution network, the associated DERs' uncertainties should be considered. The stochastic energy management problem is an optimization problem that obtains the optimal strategy of the DERs' operation in the underlying distribution system, considering different sources of uncertainties such as loads, RESs output power, market electricity prices, and DR resources. Stochastic methods based on PDFs are the most widely used technique for modeling associated uncertainties of DERs. Methods based on approximate sampling and simulation, like PEM [27], MCS [23], and scenario trees [35], are used with the PDFs to analyze the optimization problem probabilistically. Based on the uncertainty modeling and the determined energy management problem,
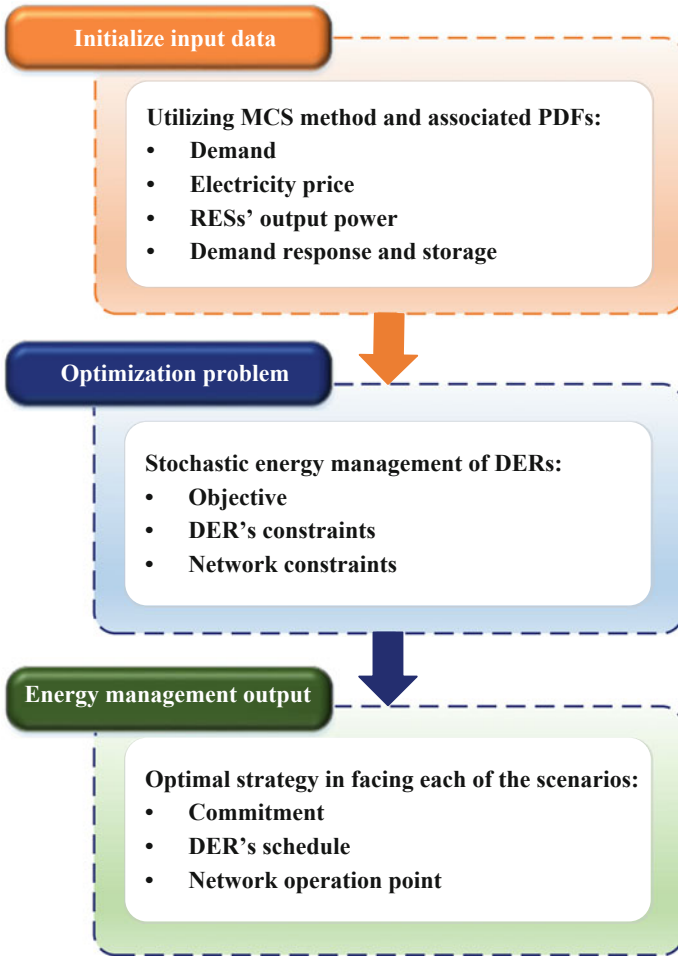
**Fig. 7** Stochastic energy management problem overview

optimization methods based on heuristic or analytic approaches can be adopted to determine the optimal solution.

The problem aims at optimizing an objective function, subjected to the DERs constraints and the network limits. The energy management problem usually attempts to minimize the system operating costs as an objective; however various criteria, such as risk, revenue attained from participating in market, system reliability and environmental factors can be considered in the objective function. Depending on the DERs in the network, the objective function and associated constraints would vary. In the following, the mathematical model of a stochastic energy management problem of a system, including RESs, CDGs, ESSs, and various loads is investigated.

### 3.4.1 Stochastic Formulation of Energy Management Problem

(a) Objective Function

As discussed in Sect. 2.4.1, in a stochastic problem modeling the associated objective function can be defined on the basis of operating cost, revenue, environmental effects, reliability, and so forth. In a stochastic problem the objective function is a sum of optimization criteria which is weighted over all scenarios. As an example, the energy management's objective function based on profit is presented in the following:

$$\max \sum_{s=1}^{NS} \sum_{t=1}^{T} \rho_s Profit_{s,t} \tag{40}$$

where,

$\rho_s$ : Probability of $s^{th}$ scenario
$Profit_{s,t}$ : Objective function of $s^{th}$ scenario at $t$.

It should be noted that profit is mostly dependent to the schedule of DERs with respect to associated uncertainties. Furthermore, all variables are scenario-based because of the uncertainty in parameters.

(b) Constraints

As discussed in Sects. 2.4.2 and 2.4.3, various operation constraints including technical aspects of DERs and characteristics of underlying network can be considered in the optimization problem. The key point here is that for each realization of scenarios, constraints need to be satisfied.

Due to space limitation, only power balance constraint as an example for stochastic formulation is presented in Eq. (41).

$$\sum_{i=1}^{N_G} P_{s,t}^{G,i} + \sum_{i=1}^{N_B} P_{s,t}^{B,i} + \sum_{i=1}^{N_{WT}} P_{s,t}^{WT,i} + \sum_{i=1}^{N_{PV}} P_{s,t}^{PV,i} = \sum_{i=1}^{N_D} P_{s,t}^{PL,i} \tag{41}$$

Equation (41) ensures that injected power to network by DERs is equal to the consumed power in each scenario $s$ at time $t$.

### 3.4.2 Probabilistic Optimization Method

The solution methodology for energy management problem by considering associated mathematical model is addressed in Sect. 2.4. In contrast to the deterministic method presented in Sect. 2, stochastic model considers several realizations of the stochastic parameters in form of scenarios with their associated probabilities. Therefore, based on the problem structure, the problem could be stochastic NLP
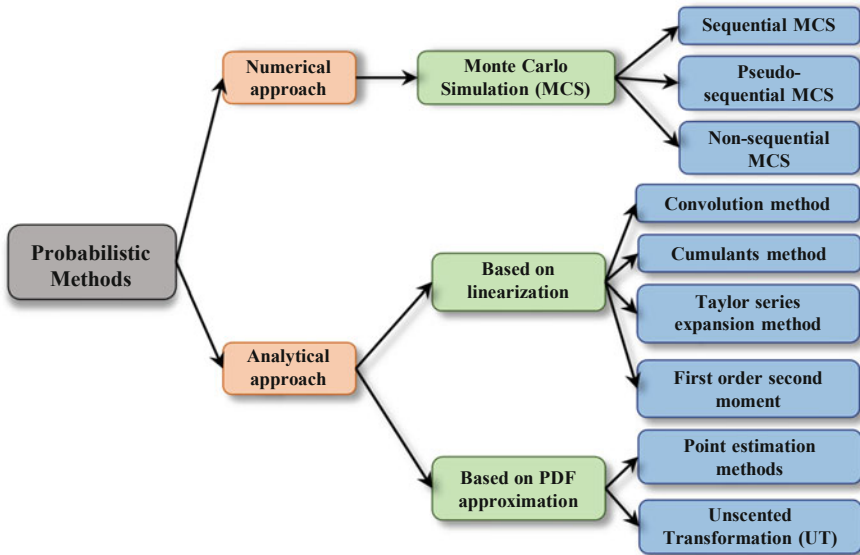
**Fig. 8** Different categories of probabilistic methods [42]

(SNLP), SMINLP, SMILP, or SMIQCP. Stochastic energy management problem described in Sect. 3.4.1 is a stochastic MINLP and the solution space is non-convex, because of the nonlinearity in equality constraints. To achieve the global optimum of this non-convex problem, either nonlinear constraints is required to be linearized or heuristic methods need to be applied. To linearize the constraints, someone may neglect the effect of distribution network in managing DERs or linearize the non-linear equations. In this condition the problem is converted to stochastic MILP with a convex solution space [42].

Various probabilistic methods can be utilized for solving the stochastic optimization problem and address associated uncertainties in operation parameters. As depicted in Fig. 8, probabilistic approaches are grouped in two common categories described as follows [42]:

1. **Numerical methods:** These methods are mainly used for stochastic and nonlinear problems. The most common numerical optimization method is MCS which is applied in three types of non-sequential, pseudo-sequential, and sequential MCSs. Sequential MCS is used to keep the features of time dependent variables. It should be noted that non-sequential MCS is based on state sampling method. Furthermore pseudo-sequential MCS is better than sequential MCS from the speed point of view.

2. **Analytical Methods:** In these methods, mathematical equations express output results and inputs variables. In these methods output results are related to the stochastic input variables by handling PDFs' arithmetic. To do so, linearization or approximation tools are utilized. In approximation based approaches, instead

of non-linear transformation function approximation, they approximate PDFs associated with variables. This is due to the fact that approximating PDFs is easier. Thus, the input variables should be appropriately sampled in order to obtain the samples with adequate information of the input variable's PDF [42].

## 4  Examples for Energy Management Problem

In this section two examples are comprehensively presented in which the energy management of DERs in active distribution network is addressed. In the first example, a two-stage stochastic framework for scheduling large scaled energy sources of aggregators in an active network is proposed [35]. The second example addresses the stochastic problem for distribution network energy scheduling in presence of intermittency and variability of renewable energy sources [43].

The outcomes of both models are compared with the corresponding deterministic models and critical analysis represents the efficacy of energy management of active networks with diverse DERs by appropriate handling of associated uncertainties.

### 4.1  Two-Stage Stochastic Framework for Scheduling Large Scaled Energy Sources of Aggregators

In this example a two-stage stochastic framework for scheduling large scaled energy sources of aggregators in an active network is proposed. The proposed model handles associated uncertainties in smart grids and considers the inherent variability of demand, RESs, EVs, and wholesale electricity price with the aim of minimizing the total operation cost. In this reference, an energy aggregator aggregates diverse energy resources like DG units, DRs, ESSs and EVs around the distribution network and attain the optimal energy resource management, considering different sources of uncertainty. Implementing the proposed model on a real distribution network, the outcome of the model is compared with the deterministic model. This example is based on the proposed framework and evaluations presented in [35]. In the following, the approach used for uncertainty modeling is introduced and the two-stage stochastic formulations are represented. Furthermore, it should be noted that the nomenclature for the following applied parameters are presented in Appendix.

(a) Uncertainty Representation

In the proposed model, the aggregator deals with various sources of uncertainty, such as EVs charging/discharging power, demands, and the output power of the renewable based generators. The model considers associated uncertainties of parameters using stochastic scenario-based optimization model. In this regard, to represent power system uncertainties the MCS is applied to create a big size dataset of scenarios. PDFs of the predict errors attained from the historical data are the
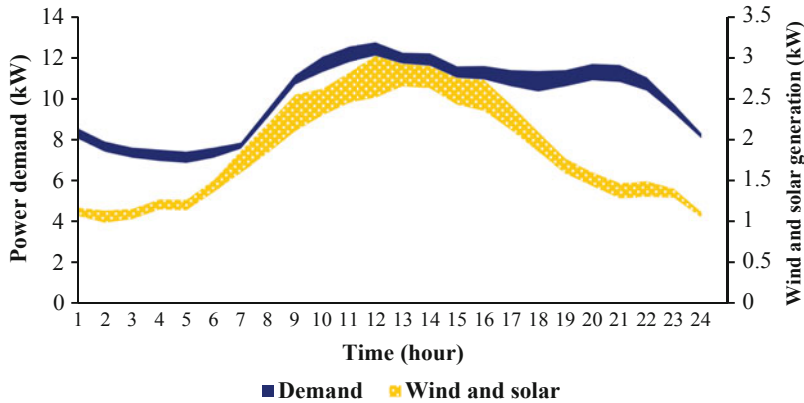
**Fig. 9** Wind, solar, and demand forecast, considering their uncertainty [35]

parameters of MCS. A positive/negative term is added to the forecasted parameter ($x^{forecasted}$) to consider the forecast error. The error term ($x^{error,\,s}$) is a noise with zero-mean and standard deviation $\sigma$. Scenarios are depicted by $x^s$ in Eq. (42). In this model, normal distribution functions are utilized to represent the forecast errors of the uncertain inputs.

$$x^s(t) = x^{forecasted}(t) + x^{error,\,s}(t), \quad \forall t, \forall s \tag{42}$$

The created scenarios in the energy management problem cause the problem to present many parameters and variables. In order to reduce the problem size with no lost in the main features of primary set of scenarios, the standard scenario reduction techniques are used in the example. In these techniques the low probability scenarios are excluded and the scenarios which are similar from statistic metrics perspectives are combined. In this regard, a subset of scenarios is defined. This subset is the most similar one to the primary PDF from the probability metric perspective.

As an example, considering uncertainty of resources, including forecasted solar and wind generated power and forecasted load is depicted in Fig. 9. 5000 primary scenarios are created and then 4850 scenarios are excluded by utilizing GAMS. As depicted in the figure, based on the generated scenarios, the forecasted generation of solar and wind units at 12 PM is between 2.6 and 3.0 MW.

(b)  Two-Stage Stochastic Model

The objective of the optimization problem is to minimize the total expected operation cost for the day-ahead operation, represented in Eq. (43). In the equation, $OC^1$, $OC^2$ and *MT* represent the first-stage operation costs, second-stage operation costs and market transactions, respectively.

$$Minimize \; E\left(OC_{Total}^{D+1}\right) = OC^1 + E\left(OC^2 + MT\right) \tag{43}$$

$OC^1$ is the first stage expected operation cost which is defined in Eq. (44). It contains two main parts; the first part is associated with the dispatchable generators' costs and the second part describes the cost of energy supplied from external source.

$$OC^1 = \sum_{t=1}^{T} \left[ \left( \begin{array}{c} \sum_{I \in \Omega_{DG}^d} p_{DG}(i,t).C_{DG}(i,t) + \\ \sum_{sp=1}^{N_{sp}} p_{Supplier}(sp,t).C_{Supplier}(sp,t) \end{array} \right).\Delta t \right] \quad (44)$$

The second stage is the expected operation cost, $OC^2$, expressed by Eq. (45). It contains the cost of non-dispatchable generators, demand response, EVs and ESS discharge power, non-served demand (NSD), and curtailed power of generation.

$$E\left(OC^2\right) = \sum_{s=1}^{S} \sum_{t=1}^{T} \left[ \left( \begin{array}{c} \sum_{i \in \Omega_{DG}^{nd}} p_{DG}(i,t,s).C_{DG}(i,t) \\ + \sum_{l=1}^{N_l} p_{LoadDR}(l,t,s).C_{LoadDR}(l,t) \\ + \sum_{e=1}^{N_e} p_{Discharge}(e,t,s).C_{Discharge}(e,t) \\ + \sum_{v=1}^{N_v} p_{Discharge}(v,t,s).C_{Discharge}(v,t) \\ + \sum_{l=1}^{N_l} p_{NSD}(l,t,s).C_{NSD}(l,t) \\ + \sum_{i=1}^{N_i} p_{GCP}(i,t,s).C_{GCP}(i,t) \end{array} \right).\pi(s).\Delta t \right]$$
$$\quad (45)$$

The expected transaction cost of the market, $MT$, is defined as follows:

$$E(MT) = \sum_{s=1}^{S} \sum_{t=1}^{T} \left[ \left( p_{Buy}(t).MP(t,s) - p_{Sell}(t).MP(t,s) \right).\pi(s).\Delta t \right] \quad (46)$$

The main decision variables of the problem are the scheduling of the dispatchable sources' generation and the optimal day-ahead market transactions (first stage). These variables are made considering second stage decisions. The second stage variables are the variation in generated power of solar and wind units and charging/discharging pattern of EVs. It is worth mentioning that the decisions variables in first stage remain unchanged for the defined scenarios of the second stage.

The optimization is subject to different constraints described in the following:

- Operational constraints of the network

The DC PF constraints are modeled in problem as described in Eq. (47), assuming that the distribution network is equipped with voltage regulators and

capacitor banks for keeping nodes' voltage in the desired level. It is assumed that the distribution network is connected to upstream network at $b = 1$.

$$
\begin{aligned}
\sum_{i \in \Omega_{DG}^b} (p_{DG}(i, t) - p_{GCP}(i, t)) + \sum_{sp \in \Omega_{SP}^b} p_{Supplier}(sp, t) \\
+ \sum_{l \in \Omega_L^b} (p_{NSD}(l, t, s) + p_{LoadDR}(l, t, s) - p_{Load}(l, t, s)) \\
+ \sum_{i \in \Omega_E^b} \left( p_{Discharge}(e, t, s) - p_{Charge}(e, t, s) \right) \\
+ \sum_{i \in \Omega_V^b} \left( p_{Discharge}(v, t, s) - p_{Charge}(v, t, s) \right) \\
- \sum_{b,w=1}^{NL} (p(b, w, t, s) - p(w, b, t, s)) = 0 \qquad \forall b, t, s
\end{aligned}
\tag{47}
$$

Furthermore, the allowable line currents are retained by the following equation.

$$
p(b, w, t, s) \leq p_{(b,w)}^{Max} \qquad \forall t, s
\tag{48}
$$

- Dispatchable generators and the upstream grid

Allowable limits for generated active power of DG units in each period $t$ are formulated as Eq. (49). Moreover, the active power of external grid is limited at each time $t$, which is expressed in Eq. (50).

$$
\begin{aligned}
x_{DG}(i, t) . P_{DGMinLimit}(i, t) \leq p_{DG}(i, t) \\
\leq x_{DG}(i, t) . P_{DGMaxLimit}(i, t) \qquad \forall t, \forall i \in \Omega_{DG}^d
\end{aligned}
\tag{49}
$$

$$
\begin{aligned}
x_{Supplier}(sp, t) . P_{SMinLimit}(sp, t) \leq p_{Supplier}(sp, t) \\
\leq x_{Supplier}(sp, t) . P_{SMaxLimit}(sp, t) \quad \forall t, \forall sp
\end{aligned}
\tag{50}
$$

- ESS Constraints

The ESS's state of charge is represented in the following:

$$
\begin{aligned}
E_{Stored}(e, t, s) = E_{Stored}(e, t\text{-}1, s) + \eta_{c(e)} . p_{Charge}(e, t, s) . \Delta t \\
- \frac{1}{\eta_{d(e)}} . p_{Discharge}(e, t, s) . \Delta t \quad \forall t, \forall e, \forall s
\end{aligned}
\tag{51}
$$

The maximum charge and discharge limits for each ESS is represented by Eqs. (52) and (53), respectively.

$$
p_{Charge}(e, t, s) \leq P_{ChargeLimit}(e, t) . y_{ESS}(e, t, s) \qquad \forall t, \forall e, \forall s
\tag{52}
$$

$$
p_{Discharge}(e, t, s) \leq P_{DischargeLimit}(e, t) . x_{ESS}(e, t, s) \qquad \forall t, \forall e, \forall s
\tag{53}
$$

Moreover, charging/discharging cannot occur at the same time:

$$x_{ESS}(e, t, s) + y_{ESS}(e, t, s) \leq 1 \qquad \forall t, \forall e, \forall s \qquad (54)$$

The limit for each ESS's maximum battery capacity is presented by Eq. (55).

$$E_{Stored}(e, t, s) \leq E_{BatCap}(e) \qquad \forall t, \forall e, \forall s \qquad (55)$$

At the end of time $t$ the ESS should be charged until the minimum stored limit which is retained by Eq. (56).

$$E_{Stored}(e, t, s) \geq E_{MinCh\arg e}(e, t) \qquad \forall t, \forall e, \forall s \qquad (56)$$

• Constraints of EVs

The technical constraints associated with EVs are the same with the ESSs' constraints. It should be noted that some parameters are uncertain due to randomness behavior of EVs' drivers. The complete formulation associated with EV constraints can be found in [35].

• DR Constraints

The proposed model for DR is based on direct load control in which, the allowable reduction of each load is formulated as Eq. (57).

$$p_{LoadDR}(l, t, s) \leq P_{LoadDRMaxLimit}(l, t) \qquad \forall t, \forall l, \forall s \qquad (57)$$

• Constraints of Electricity Market

The market bids/offer may be constrained by the allowable amounts.

$$P_{MarketOfferMin}(t).x_{MarketSell}(t) \leq p_{Sell}(t)$$
$$\leq P_{MarketOfferMax}(t).x_{MarketSell}(t) \qquad \forall t \qquad (58)$$

$$P_{MarketBuyMin}(t).x_{MarketBuy}(t) \leq p_{Buy}(t)$$
$$\leq P_{MarketBuyMax}(t).x_{MarketBuy}(t) \qquad \forall t \qquad (59)$$

Furthermore, according to Eq. (60), market only accept a bid or offer at each time $t$.

$$x_{MarketBuy}(t) + x_{MarketSell}(t) \leq 1 \qquad \forall t \qquad (60)$$

- Non-served demand constraint

The curtailed load at each scenario $s$ should be lower than the existing load.

$$p_{ENS}(l, t, s) \leq p_{Load}(l, t, s) - p_{LoadDR}(l, t, s) \qquad \forall t, \forall l, \forall s \qquad (61)$$

- Curtailed power of generating units

The curtailed power of non-dispatchable generators should be lower than fore-casted generation.

$$p_{GCP}(i, t, s) \leq P_{DGScenario}(i, t, s) \qquad \forall t, \forall i \in \Omega_{DG}^{nd}, \forall s \qquad (62)$$

The proposed optimization problem is solved using Benders' decomposition approach. Utilizing Benders' decomposition enhances computational efficiency. The details around the master and slave problems can be found in [35]. Solving the problem, the optimal stochastic solution of the problem, which represents the total expected cost (Eq. 43) is expressed by $Z^{S*}$ and is obtained using the proposed stochastic programming approach. On the other hand, $Z^{D*}$ is the optimal solution of the deterministic type of the original problem. It should be noted that the inputs of the deterministic problem are the optimal decision variables of the original stochastic problem. The value of stochastic solution (VSS) and the expected value of perfect information (EVPI) indices evaluate the efficacy of the stochastic programming. The benefits of stochastic programming versus deterministic model can be determined by utilizing the VSS index. In addition, EVPI give information about the lost profit of decision maker because of uncertainty presence. The formulation for calculating these indices is explained in [35].

Implementing the model on a real distribution network from Portugal, the optimal energy resource management is obtained for the following four cases to represent the effect of utilizing DR and storage in the energy management, considering uncertainty alleviation. The resources that are considered in each case are:

– Case A: DR and ESS;
– Case B: Neither DR nor ESS;
– Case C: ESS but no DR;
– Case D: DR but no ESS.

Figure 10 represent the generation of dispatchable DGs for the case studies. On the other hand, the market transaction powers are depicted in Fig. 11. For controllable DGs, in the periods 1 to 2, 8 to 9, and 23 to 24 the most changes can be observed. For the upstream grid in the cases B & D (i.e., with no ESS) the changes can be seen. Since the ESS is not charged in these cases, the variations are in the form of reducing produced power.

Figure 12 shows the values of the quality indices. The cost of stochastic and deterministic models is also shown in this figure. It can be concluded that when ESS and DR are available the lower cost is verified. In the case B (i.e. with no DR and ESS) the higher costs in stochastic (47,208 m.u.) and deterministic (48,668 m.u.)
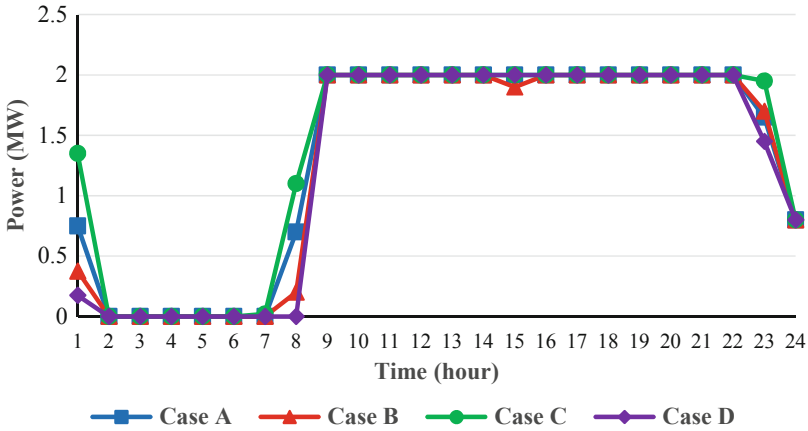
**Fig. 10** Generated power of dispatchable DGs for case studies [35]
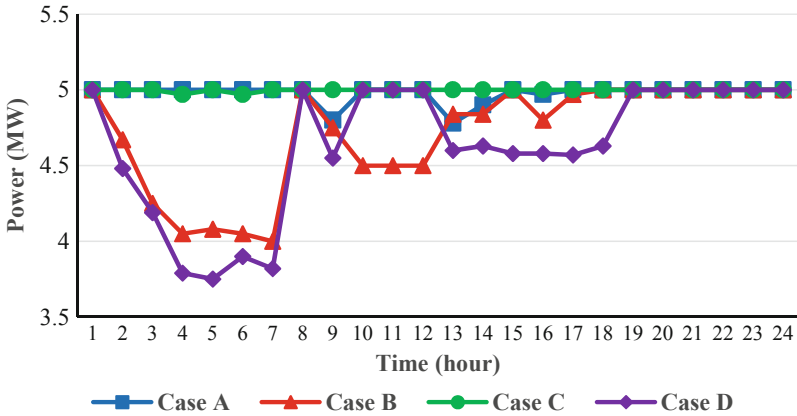


**Fig. 11** Generated power of upstream grid for the case studies [35]

models are imposed. The costs of stochastic model are the same for both cases of C & D; however, the costs are 8.9% higher in the absence of ESS in deterministic model. It can be concluded from case C that ESS leads to bypass a higher cost when the deterministic approach is applied. Comparing case D to C results that the DR is not as effective as ESS. It is because that the VSS is 11.75% higher in case D. Therefore, the stochastic model can obtain lower expected costs without ESS.

The outcomes of energy resources' stochastic scheduling for the cases A and B are depicted in Fig. 13. For these cases the quantified uncertainty is equal to 6.4 MWh. This amount is the most probable value of the variable. The ESS, discharging power of DR and EVs in case A offer an uncertainty equal to 11.3, 1.2,
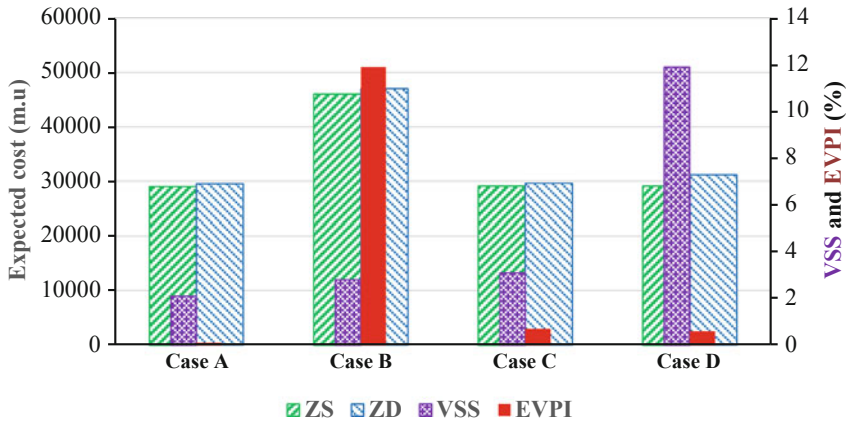
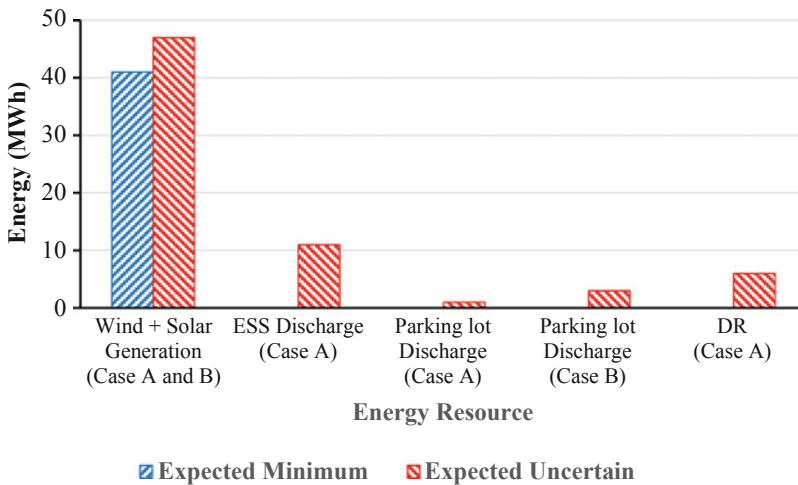**Fig. 12** VSS and EVPI for the case studies [35]



**Fig. 13** Energy resources' stochastic scheduling in the cases A and B [35]

and 7.8 MWh, respectively. For ESS discharge, the minimum expected amounts are 0.5 MWh, whereas it is zero for the other two resources. The uncertainty associated with the discharge power of parking lot in case B is 2.8 MWh and the minimum expected amount is zero. This case study verifies that the there is no change in market results. The market bid is equal to 2 MW during each time. This amount is equal to the maximum bidding amount to market.

## 4.2 Stochastic Energy Management with Intermittent Resources

This example addresses the stochastic problem for distribution network energy scheduling in presence of intermittency and variability of renewable energy sources [43]. Moreover, the proposed model considers controllable loads and distributed generators as well as distributed energy storage sources in the energy scheduling problem. The model is defined as a two-stage problem with the aim of minimizing the expected day-ahead operational cost of the network in the first stage while considering the real-time intermittencies of renewable resources in the second stage. Renewable energy sources are considered as wind and solar resources and their uncertainties are modeled using scenario-based approaches. The scenarios of uncertainties are related to the second stage and the decision variables in the first stage are independent on the scenarios.

The objective function of the model is described in Eq. (63) which represents the expected operational cost of the distribution network for each hour of the next day which should be minimized. In the formulation, the scenarios associated with the uncertainties of wind turbines' and PV units' output powers are addressed through $s_1$ and $s_2$, respectively.

$$
\begin{aligned}
F = &\sum_i \sum_t c_{DG}^U (i, t) + \sum_{s_1} \sum_{s_2} \pi (s_1) . \pi (s_2) . \\
&\left[ \sum_t c_{Utility} \left( P_{Utility}(t) \right) + \sum_i \sum_t c_{DG} \left( P_{DG} (i, t, s_1, s_2) \right) \right]
\end{aligned}
\tag{63}
$$

Based on the formulation, the operational cost is comprised of the cost of starting up/shutting down the DG units, power transaction payment with the utility as well as operating cost of DGs. It is supposed that the operational cost of renewable energy sources, ESSs and EVs would be negligible. The cost of power transaction with the utility is attained from the quantity of power transaction and the electricity price of the utility based on Eq. (64). Furthermore, the DG units' operational cost is calculated using a piecewise linear cost function defined in Eq. (65). In this relation, $\alpha(i)$, $\beta(i)$ and $\delta(i)$ represent the cost function's coefficients.

$$
C_{Utility}(t) = P_{Utility}(t).UP(t)
\tag{64}
$$

$$
C_{DG} (i, t, s_1, s_2) = \alpha(i) + \beta(i).P_{DG} (i, t, s_1, s_2) + \delta(i).P_{DG}^2 (i, t, s_1, s_2)
\tag{65}
$$

The objective function is optimized considering the constraints addressed in the following.

The system's power balance should be considered as Eq. (66). Based on this equation, the production power of wind, PV, DG and ESS units should be equal to the consumption power of loads and EVs.

$$
\begin{aligned}
&\sum_{\omega} P_{Wind}\left(\omega, t, s_1, s_2\right) + \sum_{p} P_{PV}\left(p, t, s_1, s_2\right) + \sum_{i} P_{DG}\left(i, t, s_1, s_2\right) + \\
&\sum_{e}\left[P_{Discharge}\left(e, t, s_1, s_2\right) - P_{charge}\left(e, t, s_1, s_2\right)\right] + P_{Utility}(t) \quad = \\
&\sum_{l} P_{Load}\left(l, t\right) + \sum_{v} P_{Charge}\left(v, t\right), \qquad \forall t, \forall s_1, \forall s_2
\end{aligned}
\tag{66}
$$

The voltage of each bus should be in its allowable limits using the following constraint.

$$
V_{MinLimit}(b) \leq V\left(b, t, s_1, s_2\right) \leq V_{MaxLimit}(b), \qquad \forall t, \forall s_1, \forall s_2
\tag{67}
$$

The technical constraints of DG units, ESSs and EVs should be taken into account through the constraints (68), (69)–(72) and (73), respectively.

$$
P_{DGMinLimit}(i) \leq P_{DG}\left(i, t, s_1, s_2\right) \leq P_{DGMaxLimit}(i), \qquad \forall t, \forall s_1, \forall s_2
\tag{68}
$$

$$
0 \leq P_{Charge}\left(e, t, s_1, s_2\right) \leq P_{ChargeLimit}(e), \qquad \forall t, \forall s_1, \forall s_2
\tag{69}
$$

$$
0 \leq P_{Discharge}\left(e, t, s_1, s_2\right) \leq P_{DischargeLimit}(e), \qquad \forall t, \forall s_1, \forall s_2
\tag{70}
$$

$$
SoC_{MinLimit}(e) \leq SoC\left(e, t, s_1, s_2\right) \leq SoC_{MaxLimit}(e), \qquad \forall t, \forall s_1, \forall s_2
\tag{71}
$$

$$
SoC_{Required}(e) \leq SoC\left(e, T, s_1, s_2\right), \qquad \forall s_1, \forall s_2
\tag{72}
$$

$$
0 \leq P_{Charge}\left(v, t\right) \leq P_{ChargeLimit}\left(v, t, s_1, s_2\right), \qquad \forall t, \forall s_1, \forall s_2
\tag{73}
$$

In order to verify the effectiveness of the proposed model, the model is implemented on a modified IEEE 37-bus test feeder. Figure 14 shows the proposed test system and different distributed energy resources dispersed along it. Taking the uncertainties of wind turbine into account, wind turbine's output power is forecasted, after that, different scenarios are generated using Monte Carlo simulations and some scenario reduction techniques are utilized. Furthermore, PV units' output power is forecasted and different scenarios are generated using a normal distribution function with a forecasted error. In this regard, for wind turbines and PV units output power 100 independent scenarios are defined, where each has a probability of 0.01. As an example, Fig. 15 shows 10 scenarios for PV units output power.
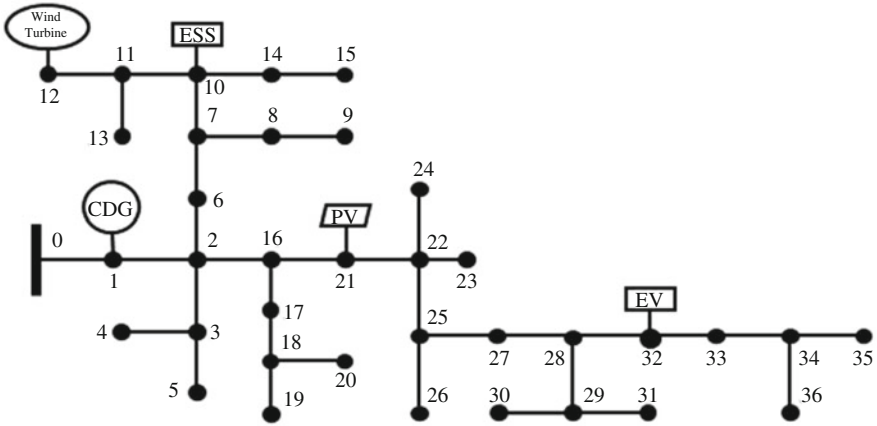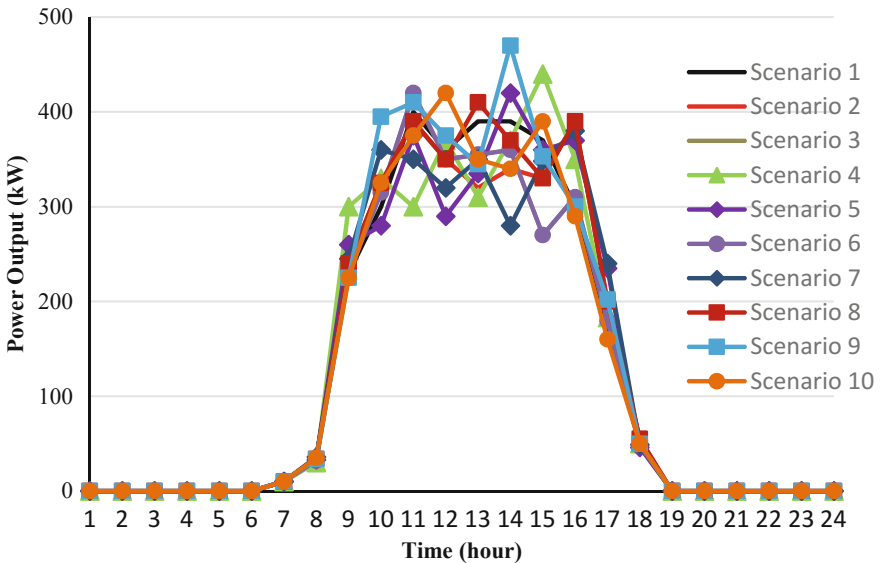
**Fig. 14** The proposed test system



**Fig. 15** PV units output power profile for different scenarios [43]

In order to compare the proposed stochastic model with the deterministic one, wind turbines' and PV units output powers are considered as the forecasted amount for the deterministic model, i.e. no uncertainty scenario is considered. Implementing the stochastic and deterministic model on the test system, the results are as follows. The expected operational cost of the network (objective function) is achieved equal to \$23,500 and \$22,276 for the cases of applying deterministic and stochastic approaches, respectively. Therefore, it can be seen that the stochastic model leads
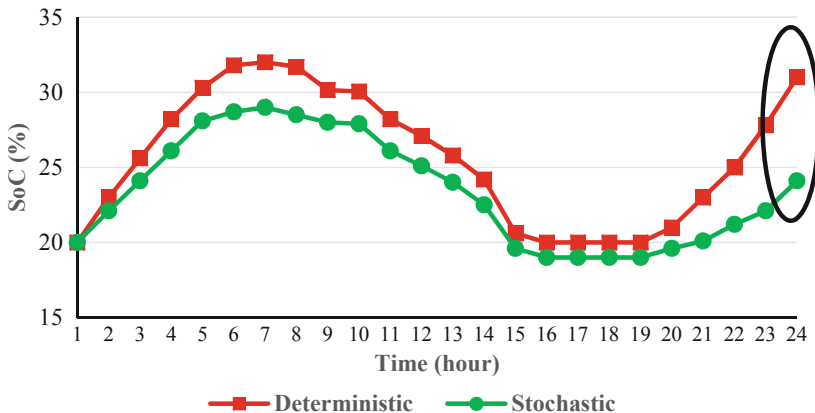
**Fig. 16** State of charge of ESS unit for each hour of a day [43]

to the lower operational cost and is more effective than the deterministic one. It is because that in the deterministic approach, the wind turbine and PV unit output power are considered as the forecasted amount; therefore, the results are more affected from the uncertainty of wind and solar resources than the stochastic approach.

Figure 16 shows the state of charge of ESS unit for each hour of the next day, attained from the scheduling problem. As it is shown in the figure, the difference between the states of charge at the first hour and last hour of the day ($\Delta SoC$) is much higher in the case of deterministic approach than the case of stochastic approach. $\Delta SoC$ is equal to 15.08% in the case of deterministic approach and 6.14% in the case of stochastic approach. It is while the smaller $\Delta SoC$ leads to get closer to the optimal solution. Therefore, the stochastic model provides more effective and accurate solution.

For more analysis, the simulation is executed for a weak and the expected operational cost of the network is attained for each day of the week as Fig. 17. It can be observed from the figure that for all the days, the expected operational cost in stochastic approach is lower than the deterministic one.

## 5  Conclusion

In this chapter, the problem of energy management in distribution systems was put under investigation. At first, different classes of this problem, i.e. deterministic and stochastic classes were introduced. Then, models of different elements in active distribution networks were addressed. Based on these models, the mathematical model of energy management optimization problem was extracted and their solution algorithms from different aspects were discussed. Two examples about implementa-
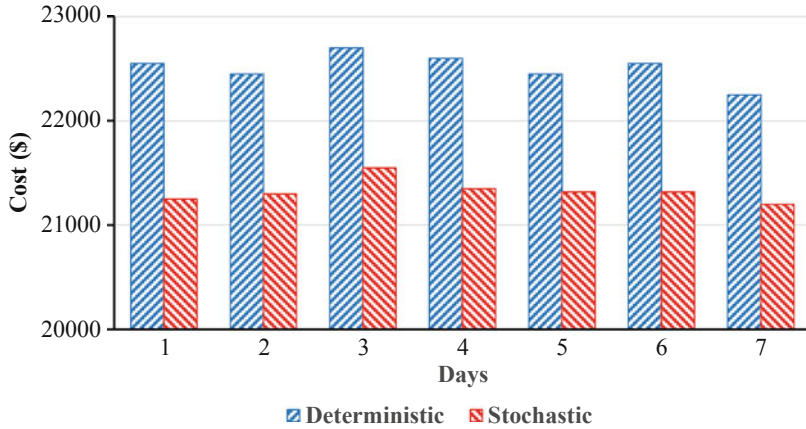
**Fig. 17** Expected operational cost of network for each day of a week [43]

tion procedure of energy management problem were covered. The results confirmed that such optimization problems in active distribution networks is inevitable and the system operators are forced to utilize such algorithms to optimally apply different energy resources by appropriate modeling of associated scenarios.

# References

1. Shi, W., Xie, X., Chu, C., Gadh, R.: Distributed optimal energy management in microgrids. IEEE Trans. Smart Grid. **6**(3), 1137–1146 (2015)
2. Renewable energy and energy efficiency organization (SATBA) [Online]. http://satba.gov.ir
3. Turitsyn, K., Sulc, P., Backhaus, S., Chertkov, M.: Options for control of reactive power by distributed photovoltaic generators. Proc. IEEE. **99**(6), 1063–1073 (2011)
4. Patnam, B.S.K., Pindoriya, N.M.: Centralized stochastic energy management framework of an aggregator in active distribution network. IEEE Trans. Ind. Inform. (2018)
5. Kabirifar, M., et al.: Centralized framework to coordinate residential demand response potentials. In: Proceeding of International Smart Grid Conference, Gwangjo, Korea, pp. 243–248 (2015)
6. Zhang, C., Xu, Y., Dong, Z.Y., Ma, J.: Robust operation of microgrids via two-stage coordinated energy storage and direct load control. IEEE Trans. Power Syst. **32**(4), 2858–2868 (2017)
7. Igualada, L., Corchero, C., Cruz-Zambrano, M., Heredia, F.: Optimal energy management for a residential microgrid including a vehicle-to-grid system. IEEE Trans. Smart Grid. **5**(4), 2163–2172 (2014)
8. Nafisi, H., Agah, S.M.M., Abyaneh, H.A., Abedi, M.: Two-stage optimization method for energy loss minimization in microgrid based on smart power management scheme of PHEVs. IEEE Trans. Smart Grid. **7**(3), 1268–1276 (2016)
9. Mahmud, K., Hossain, M.J., Town, G.E.: Peak-load reduction by coordinated response of photovoltaics, battery storage, and electric vehicles. IEEE Access. **6**, 29353–29365 (2018)

10. Nguyen, H.K., Khodaei, A., Han, Z.: Incentive mechanism design for integrated microgrids in peak ramp minimization problem. IEEE Trans. Smart Grid. **9**(6), 5774–5785 (2018)
11. Meng, W., Wang, X.: Distributed energy management in smart grid with wind power and temporally coupled constraints. IEEE Trans. Ind. Electron. **64**(8), 6052–6062 (2017)
12. Carpinelli, G., Mottola, F., Proto, D., Russo, A.: A multi-objective approach for microgrid scheduling. IEEE Trans. Smart Grid. **8**(5), 2109–2118 (2017)
13. Zhang, Y., Gatsis, N., Giannakis, G.B.: Robust energy management for microgrids with high-penetration renewables. IEEE Trans. Sustain. Energy. **4**(4), 944–953 (2013)
14. Bolognani, S., Zampieri, S.: On the existence and linear approximation of the power flow solution in power distribution networks. IEEE Trans. Power Syst. **31**(1), 163–172 (2016)
15. Jabr, R.A.: Radial distribution load flow using conic programming. IEEE Trans. Power Syst. **21**(3), 1458–1459 (2006)
16. Bai, X., Wei, H., Fujisawa, K., Wang, Y.: Semidefinite programming for optimal power flow problems. Int. J. Electr. Power Energy Syst. **30**(6–7), 383–392 (2008)
17. Gan, L., Low, S.H.: Convex relaxations and linear approximation for optimal power flow in multiphase radial networks. In: 2014 Power Systems Computation Conference, pp. 1–9 (2014)
18. Farivar, M., Low, S.H.: Branch flow model: relaxations and convexification—Part I. IEEE Trans. Power Syst. **28**(3), 2554–2564 (2013)
19. Farivar, M., Low, S.H.: Branch flow model: relaxations and convexification—Part II. IEEE Trans. Power Syst. **28**(3), 2565–2572 (2013)
20. Kardakos, E.G., Simoglou, C.K., Bakirtzis, A.G.: Optimal offering strategy of a virtual power plant: a stochastic bi-level approach. IEEE Trans. Smart Grid. **7**(2), 794–806 (2016)
21. Kou, P., Liang, D., Lin, G.: Stochastic energy scheduling in microgrids considering the uncertainties in both supply and demand. IEEE Syst. J. **12**(3), 2589–2600 (2018)
22. Farzin, H., Fotuhi-Firuzabad, M., Moeini-Aghtaie, M.: Stochastic energy management of microgrids during unscheduled islanding period. IEEE Trans. Indus. Inform. **13**(3), 1079–1087 (2017)
23. Pourghaderi, N., et al.: Commercial demand response programs in bidding of a technical virtual power plant. IEEE Trans. Indus. Inform. (2018)
24. Belloni, A., Piroddi, L., Prandini, M.: A stochastic optimal control solution to the energy management of a microgrid with storage and renewables. IEEE American Control Conference (ACC), 2016
25. Pourghaderi, N., et al.: Energy scheduling of a technical virtual power plant in presence of electric vehicles. IEEE Iranian Conference on Electrical Engineering (ICEE), 2017
26. Schellenberg, A., Rosehart, W., Aguado, J.: Cumulant-based probabilistic optimal power flow (P-OPF) with Gaussian and gamma distributions. IEEE Trans. Power Syst. **20**(2), 773–781 (2005)
27. Geidl, M., Andersson, G.: Optimal power flow of multiple energy carriers. IEEE Trans. Power Syst. **22**(1), 145–155 (2007)
28. Zhang, Y., et al.: Chance-constrained two-stage unit commitment under uncertain load and wind power output using bilinear benders decomposition. IEEE Trans. Power Syst. **32**(5), 3637–3647 (2017)
29. Mohan, V., et al.: Microgrid energy management combining sensitivities, interval and probabilistic uncertainties of renewable generation and loads. IEEE J. Emerg. Selected Topics Circ. Syst. **7**(2), 262–270 (2017)
30. Mohan, V., Singh, J.G., Ongsakul, W.: An efficient two stage stochastic optimal energy and reserve management in a microgrid. Appl. Energy. **160**, 28–38 (2015)
31. Vaccaro, A., Pisani, C., Zobaa, A.F.: Affine arithmetic-based methodology for energy hub operation-scheduling in the presence of data uncertainty. IET Gener. Transm. Distrib. **9**(13), 1544–1552 (2015)
32. Vaccaro, A., Canizares, C.A.: An affine arithmetic-based framework for uncertain power flow and optimal power flow studies. IEEE Trans. Power Syst. **32**(1), 274–288 (2017)
33. Vahid-Pakdel, M.J., et al.: Stochastic optimization of energy hub operation with consideration of thermal energy market and demand response. Energy Convers. Manag. **145**, 117–128 (2017)

34. Abdulkarim, A., Abdelkader, S.M., Morrow, D.J.: Statistical analyses of wind and solar energy resources for the development of hybrid microgrid. In: 2nd International Congress on Energy Efficiency and Energy Related Materials (ENEFM2014). Springer, Cham (2015)
35. Soares, J., et al.: Two-stage stochastic model using benders' decomposition for large-scale energy resource management in smart grids. IEEE Trans. Ind. Appl. **53**(6), 5905–5914 (2017)
36. Ghazvini, M.A.F., et al.: Incentive-based demand response programs designed by asset-light retail electricity providers for the day-ahead market. Energy. **82**, 786–799 (2015)
37. Wu, H., et al.: Thermal generation flexibility with ramping costs and hourly demand response in stochastic security-constrained scheduling of variable energy sources. IEEE Trans. Power Syst. **30**(6), 2955–2964 (2015)
38. Jain, A., Dubes, R.: Algorithms for Clustering Data. Prentice Hall, Upper Saddle River, NJ (1998)
39. Etesami, S.R., et al.: Stochastic games for the smart grid energy management with prospect prosumers. IEEE Trans. Autom. Control. **63**(8), 2327–2342 (2018)
40. Dolatabadi, A., et al.: Optimal stochastic design of wind integrated energy hub. IEEE Trans. Indus. Inform. (2017)
41. Gazijahani, F.S., Salehi, J.: Stochastic-based optimal daily energy management of microgrids in distribution systems. arXiv preprint arXiv:1708.04880 (2017)
42. Aien, M., Hajebrahimi, A., Fotuhi-Firuzabad, M.: A comprehensive review on uncertainty modeling techniques in power system studies. Renew. Sust. Energ. Rev. **57**, 1077–1089 (2016)
43. Su, W., Wang, J., Roh, J.: Stochastic energy scheduling in microgrids with intermittent renewable energy resources. IEEE Trans. Smart Grid. **5**(4), 1876–1883 (2014)